https://doi.org/10.1070/RCR5011

Functional supramolecular systems: design and applications

Igor S. Antipin,[a, b] Mikhail V. Alfimov,[c] Vladimir V. Arslanov,[d] Vladimir A. Burilov,[a] Sergey Z. Vatsadze,[e] Yan Z. Voloshin,[f] Konstantin P. Volcho,[g] Valery V. Gorbatchuk,[a] Yulia G. Gorbunova,[d, f] Sergey P. Gromov,[c, e] Semyon V. Dudkin,[h] Sergei Yu. Zaitsev,[i] Lucia Ya. Zakharova,[b] Marat A. Ziganshin,[a] Anna V. Zolotukhina,[e, j] Maria A. Kalinina,[d] Eduard A. Karakhanov,[e] Ruslan R. Kashapov,[b] Oskar I. Koifman,[k, l] Alexander I. Konovalov (deceased),[b] Vladimir S. Korenev,[m] Anton L. Maksimov,[e, j] Nugzar Zh. Mamardashvili,[k] Galina M.Mamardashvili,[k] Alexander G. Martynov,[d] Asiya R. Mustafina,[b] Ramil I. Nugmanov,[a] Alexander S. Ovsyannikov,[b] Pavel L. Padnya,[a] Andrei S. Potapov,[m] Sofiya L. Selektor,[d, n] Maxim N. Sokolov,[m] Svetlana E. Solovieva,[a, b] Ivan I. Stoikov,[a] Pavel A. Stuzhin,[l] Evgenii V. Suslov,[g] Evgeny N. Ushakov,[c, o] Vladimir P. Fedin,[m] Svetlana V. Fedorenko,[b] Olga A. Fedorova,[h] Yury V. Fedorov,[h] Sergei N. Chvalun,[n, p] Aslan Yu. Tsivadze,[d, f] Sergei N. Shtykov,[q] Dmitriy N. Shurpik,[a] Maxim A. Shcherbina,[p, r] Luidmila S. Yakimova [a]

[a] *A.M.Butlerov Institute of Chemistry, Kazan (Volga region) Federal University, ul. Kremlevskaya 18, 420008 Kazan, Russian Federation*
[b] *Arbuzov Institute of Organic and Physical Chemistry, FRC Kazan Scientific Center, Russian Academy of Sciences, ul. Akademika Arbuzova 8, 420088 Kazan, Russian Federation*
[c] *Photochemistry Center of RAS, FSRC 'Crystallography and Photonics', Russian Academy of Sciences, ul. Novatorov 7a, stroenie 1, 119421 Moscow, Russian Federation*
[d] *Frumkin Institute of Physical Chemistry and Electrochemistry, Russian Academy of Sciences, Leninsky prosp. 31, korp. 4, 119071 Moscow, Russian Federation*
[e] *Department of Chemistry, Lomonosov Moscow State University, Leninskie Gory 1, stroenie 3, 119991 Moscow, Russian Federation*
[f] *Kurnakov Institute of General and Inorganic Chemistry, Russian Academy of Sciences, Leninsky prosp. 31, 119991 Moscow, Russian Federation*
[g] *N.N.Vorozhtsov Novosibirsk Institute of Organic Chemistry, Siberian Branch of the Russian Academy of Sciences, prosp. Akademika Lavrentieva, 9, 630090 Novosibirsk, Russian Federation*
[h] *A.N.Nesmeyanov Institute of Organoelement Compounds, Russian Academy of Sciences, ul. Vavilova 28, 119991 Moscow, Russian Federation*
[i] *Federal Research Center for Animal Husbandry named after Academy Member L.K.Ernst, Dubrovitsy 60, 142132 Podolsk Municipal District, Moscow Region, Russian Federation*
[j] *A.V.Topchiev Institute of Petrochemical Synthesis, Russian Academy of Sciences, Leninsky prosp. 29, 119991 Moscow, Russian Federation*
[k] *G.A.Krestov Institute of Solution Chemistry of the Russian Academy of Sciences, Akademicheskaya 1, 153045 Ivanovo, Russian Federation*
[l] *Ivanovo State University of Chemistry and Technology, prosp. Sheremetevskii 7, 153000 Ivanovo, Russian Federation*
[m] *Nikolaev Institute of Inorganic Chemistry, Siberian Branch of the Russian Academy of Sciences, prosp. Academika Lavrentieva 3, 630090 Novosibirsk, Russian Federation*

Received 5 October 2020
© 2021 Uspekhi Khimii, ZIOC RAS, Russian Academy of Sciences and IOP Publishing Limited

[n] *Enikolopov Institute of Synthetic Polymeric Materials, Russian Academy of Sciences, ul. Profsoyuznaya 70, 117393 Moscow, Russian Federation*
[o] *Institute of Problems of Chemical Physics, Russian Academy of Sciences, prosp. Academika Semenova 1, 142432 Chernogolovka, Moscow Region, Russian Federation*
[p] *National Research Center 'Kurchatov Institute', pl. Akademika Kurchatova 1, 123182 Moscow, Russian Federation*
[q] *Saratov State University, ul. Astrakhanskaya 83, 410012 Saratov, Russian Federation*
[r] *Moscow Institute of Physics and Technology (National Research University), Instststitutskii per. 9, 141701 Dolgoprudnyi, Moscow Region, Russian Federation*

The interest in functional supramolecular systems for the design of innovative materials and technologies, able to fundamentally change the world, is growing at a high pace. The huge array of publications that appeared in recent years in the global literature calls for systematization of the structural trends inherent in the formation of these systems revealed at different molecular platforms and practically useful properties they exhibit. The attention is concentrated on the topics related to functional supramolecular systems that are actively explored in institutes and universities of Russia in the last 10 – 15 years, such as the chemistry of host – guest complexes, crystal engineering, self-assembly and self-organization in solutions and at interfaces, biomimetics and molecular machines and devices.
The bibliography includes 1714 references.

Contents

1. Introduction 898
2. Host – guest chemistry and crystal engeneering 898
2.1. Supramolecular chemistry of tetrapyrrole macrocycles 898
2.1.1. Supramolecular assemblies formed by π – π and electrostatic interactions 898
2.1.2. Cation-induced formation of supramolecular assemblies based on crown-substituted tetrapyrroles 901
2.1.3. Supramolecular assembly of tetrapyrroles *via* hydrogen bonding 905
2.2. Functional supramolecular coordination cages 912
2.2.1. Main approaches to the fabrication of functional metal-organic polyhedra 912
2.2.2. Cages based on V-shaped metallic connecting nodes and polytopic ligands with monodentate coordination sites 912
2.2.3. Cages based on tetragonal metal connecting nodes and polytopic ligands with monodentate coordination sites 914
2.2.4. Cages based on V-shaped and trigonal metal connecting nodes and polytopic ligands with chelating sites 916
2.2.5. Cages based on bidentate tetragonal metal connecting nodes and polycarboxylic ligands 920
2.3. Supramolecular aspects of hydrocarbon separation on metal-organic frameworks 922
2.3.1. Separation of xylene isomers 922
2.3.2. Separation of benzene and cyclohexane 925
2.4. Coordination cages, supramolecular assemblies, polynuclear systems based on metal clathrochelates and reactivity of encapsulated ions 927
2.4.1. Coordination cages 927
2.4.2. Coordination polymers 929
2.4.3. Hybrid systems 930
2.4.4. Supramolecular associates with protein macromolecules and their macromolecular chelators 933
2.4.5. Reactivity and physical properties of encapsulated metal ions 936
2.5. Inorganic nanosized spherands — keplerates 937
2.5.1. Keplerates with mononuclear bridges 938
2.5.2. Keplerates with binuclear bridges 940
2.5.3. Properties of keplerates 942
2.6. Supramolecular analytical chemistry 945
2.6.1. Development of approaches to understanding of the subject of supramolecular analytical chemistry 945
2.6.2. Supramolecular objects in different stages of chemical analysis 946
2.6.3. Role of solubilization in chemical analysis 947

2.6.4. Chemical analysis methods using supramolecular effects 948
2.6.5. Miscellaneous examples of using supramolecular effects in analysis 948
3. Self-assembly and self-organization in solution and at the interface 949
3.1. Amphiphilic (thia)calix[4]arenes: synthesis and functional colloidal systems based on them 949
3.1.1. Amphiphilic calix[*n*]arene derivatives bearing anionic polar head groups 949
3.1.2. Amphiphilic derivatives of calix[***n***]arene bearing cationic polar head groups 955
3.1.3. Click chemistry modular approach in the synthesis of amphiphilic derivatives of calix[***n***]arenes 959
3.2. Self-assembly of supramolecular and hybrid systems at the interface 966
3.2.1. Self-assembled monolayer method 967
3.2.2. Langmuir – Blodgett method 970
3.2.3. Layer-by-layer assembly technique 974
3.3. Structures and phase transitions of low-dimensional self-organizing systems with different symmetry 978
3.4. Supramolecular design of functional nanosystems based on amphiphilic compounds: fundamental aspects and prospects for biomedical applications 985
3.4.1. Supramolecular systems based on cationic surfactants: self-assembly, construction and modification of nanocontainers and complex formation with biopolyanions 985
3.4.2. Micellar and vesicular drug delivery systems based on non-ionic surfactants 992
3.5. Supramolecular catalysis 995
3.5.1. Hydrogen bonding and other non-covalent interactions 997
3.5.2. Catalytic systems based on receptor molecules 998
3.6. Co-self-assembly of macrocyclic compounds: new prospects for the design of supramolecular systems 1005
3.6.1. Supramolecular assemblies based on host – guest complexes 1006
3.6.2. Layer-by-layer assembly of supramolecular assemblies through ion – ion interactions 1008
3.7. Self-organization and self-assembly of nanostructures based on short-chain oligopeptides 1011
3.7.1. Oligopeptides and nanostructures based on them 1011
3.7.2. Methods for producing nanostructures based on oligopeptides 1011
3.7.3. Factors affecting the self-association of oligopeptides 1012
4. Biomimetics 1018
4.1. Dye – DNA complexes: interaction principles, biological and medical applications 1018
4.2. Supramolecular biochemical systems based on proteins and nanoparticles for bionanotechnology and fundamental medicine 1024
4.2.1. Systems based on albumins and nanoparticles 1024
4.2.2. Systems based on lipase and nanoparticles 1028
4.2.3. Systems based on bacteriorhodopsin and nanoparticles 1030
4.3. Development of multifunctional nanoparticles for biomedical applications on the basis of silica nanoplatforms 1032
4.3.1. Methods for producing silica nanoparticles 1033
4.3.2. Effect of the dopant on the size and polydispersity of silica nanoparticles 1035
4.3.3. Mutual influence of components in composite silica nanoparticles considered for nanoparticles of iron oxide, silver(0) and metal complexes 1035
4.3.4. Covalent and non-covalent surface modification of silica nanoparticles 1037
4.3.5. Correlation between cellular internalization and surface properties of of silica nanoparticles 1038
4.4. Calixarenes and pillararenes containing amino acid moieties: from supramolecular self-assembly to biomimetics 1039
4.4.1. Amino acid derivatives of calix[*n*]arenes and their applications 1039
4.4.2. Amino acid derivatives of pillar[*n*]arenes and their applications 1044
4.5. Supramolecular recognition in the chemistry of 3,7-diazabicyclo[3.3.1]nonanes: design of biologically active molecules, functional materials and catalysts 1046
4.5.1. Coordination compounds of bispidines: general issues 1046
4.5.2. Application of bispidine complexes as bioimaging materials 1047
4.5.3. The use of bispidine derivatives in catalytic transformations 1048
4.5.4. The use of bispidine derivatives and their complexes with metals to interact with biological targets 1049
4.6. Suprampolecular systems based on macrocyclic meroterpenoids: biological activity and membranotropic properties 1052
5. Molecular machines and devices 1055
5.1. Development of photoactive supramolecular machines and devices 1055
5.2. Dendrimer porphyrin-based supramolecular devices: synthesis and practical applications 1060
5.2.1. Types of porphyrin dendrimers and methods for their synthesis 1061
5.2.2. Possible practical applications of supramolecular devices based on porphyrin dendrimers 1062
6. Conclusion 1071
7. List of acronyms and abbreviations 1071
8. About authors 1073

1. Introduction

Supramolecular chemistry, that is, the chemistry of molecular assemblies and intermolecular bonds,[1,2] is one of the dynamically developing areas of experimental and theoretical chemistry. Supramolecular systems have rapidly burst into modern scientific research and technology, with a wide range of scientists from various branches of knowledge, including chemists, biochemists, physicists, engineers and so on, being involved in their creation. First of all, this is caused by the unique properties of these structures, which are capable of spontaneous formation and easy transformation under the action of external stimuli such as temperature, composition of the environment, light, *etc.*, caused by the dynamic nature of intermolecular interactions underlying their formation. It is difficult to disagree with Academician M.V.Alfimov, who stated that a supramolecular system is the place where properties of the material are born.[3]

The universality of these interactions allows one to say that almost 'everything around seems to be supramolecular'.[4] This is not a joke any more. Indeed, virtually in any of the objects or processes around us, we can find supramolecular interactions endowing them with unique features, ranging from the amazing properties of one of the simplest molecules, water molecule, to the processes that occur in living organisms and involve huge biomolecules demonstrating fantastic molecular recognition abilities. Therefore, Academician A.I.Konovalov redefined supramolecular chemistry as 'a bridge between nonliving and living matter'.[5] Indeed, according to Academician A.Yu.Tsivadze, 'The concepts and notions borrowed from biology have played a significant role in the formation of supramolecular chemistry as a separate field of science. The most important of such concepts are the molecular recognition and cooperativity'.[6]

Supramolecular interactions appeared in the Universe billions of years ago, when its temperature after the Big Bang dropped to values at which such rather weak intermolecular contacts could occur. However, the field of science studying supramolecular systems is quite young, being formed in the 1960–1970s. It was based on the works of D.Cram, C.Pedersen and J.-M.Lehn in the field of macrocyclic compounds, which gave impetus to the creation of structures capable of highly selective specific intermolecular interactions, enabling the construction of supramolecular assemblies on the principles of molecular recognition and multi-site binding. For their pioneering work in this field, these scientists were awarded the Nobel Prize in Chemistry in 1987 with the formulation 'for their development and use of molecules with structure-specific interactions of high selectivity'.

In recent years, particular interest has been drawn to the design of self-organizing, functional supramolecular systems that have become the basis for advanced materials, in particular smart materials with controlled and adaptive properties.[7–9] A new and very important research area stemmed from supramolecular chemistry, namely, the design and synthesis of molecular machines, which was acknowledged in 2016 by the Nobel Prize in Chemistry, awarded to J.-P.Sauvage, J.Stoddart and B.Feringa.[10–12] Indeed, a large number of molecular devices have been developed based on various classes of chemical compounds the motion of which can be controlled by external stimuli of various nature: irradiation with light, changes in temperature and pH, redox transformations, *etc.*[13] Furthermore, the development of nanotechnology cannot be imagined without the well-known bottom–up approach, where highly organized nanosystems are formed spontaneously from single atoms and molecules through supramolecular self-assembly. The design and properties of such supramolecular systems are the subject of this review. The review was not intended to cover all works on this topic that have appeared recently in the scientific literature all over the world. The authors limited themselves to the most relevant areas in which intensive research has been carried out over the past 10–15 years, in particular, by scientific organizations and universities in Russia. The material of this review is grouped into four Sections reflecting the most actively developed areas of modern supramolecular chemistry: chemistry of host–guest complexes and crystal engineering, self-assembly and self-organization in solutions and at the interface, biomimetics and molecular machines and devices.

2. Host–guest chemistry and crystal engeneering

2.1. Supramolecular chemistry of tetrapyrrole macrocycles

From the point of view of developing functional supramolecular materials, tetrapyrrole compounds, such as porphyrins, porphyrazines, phthalocyanines and related macrocycles, are among the most promising building blocks. These compounds possess a number of unique physicochemical properties that lead to their wide practical application as dyes, photosensitizers for bio-visualization and photodynamic therapy, catalysts, magnetic materials and photo(or redox)-active and conductive components in various optoelectronic devices. Control over the supramolecular level of organization of tetrapyrrole compounds is the basis for expanding the scope of their applicability. This research is largely inspired by the high level of ordering of porphyrinoids in natural objects, for example in photosynthetic plant systems. The possibility of using supramolecular assembly as a tool for fine-tuning the properties of tetrapyrrole compounds opens up great opportunities for creating materials with controllable properties, including molecular switches, as the basis for new high-density information storage technologies, development of sensing and biomimetic systems, *etc.*[13,14]

The interest in the controlled supramolecular assembly of porphyrins, phthalocyanines and related compounds emerged almost simultaneously with the concept of supramolecular chemistry. This assembly is based on the use of various types of non-covalent interactions, such as $\pi-\pi$ stacking, electrostatic and donor–acceptor interactions, hydrogen and coordination bonds, *etc*. Numerous examples of the formation of supramolecular assemblies with participation of these interactions have been systematized in several reviews of the past decade, devoted mainly to the formation principles of the assemblies and studying of their structure (see, for example, Refs 15, 16). The aim of this Section is to survey the results obtained mainly in the last decade on functional supramolecular materials based on tetrapyrrole compounds with a focus on their practical applications.

2.1.1. Supramolecular assemblies formed by $\pi-\pi$ and electrostatic interactions

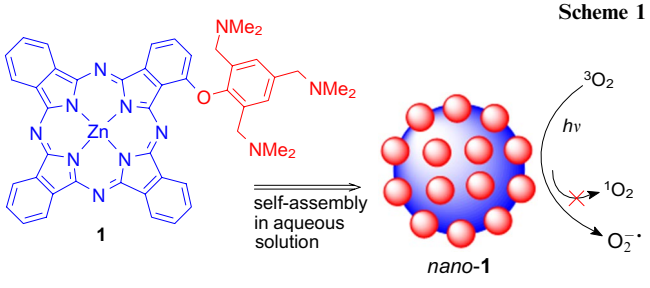
Tetrapyrroles are directly involved in the supramolecular self-assembly through aggregation induced by intermolecular $\pi-\pi$ interactions, which first of all decrease the solubil-

ity of the compounds. In terms of practical applications, aggregation of tetrapyrroles has long been viewed as an adverse phenomenon that deteriorates the functional characteristics of materials based on them, such as quantum yields of luminescence and singlet oxygen generation. Thus, the use of porphyrins, phthalocyanines and related compounds as agents for photodynamic therapy and diagnosis of cancer, and for photoinactivation of pathogenic microorganisms [17] is largely limited by the ability of these molecules to aggregate in aqueous media, which affects their photophysical properties. In this regard, numerous efforts of researchers were aimed at obtaining water-soluble compounds that do not tend to aggregate.[18]

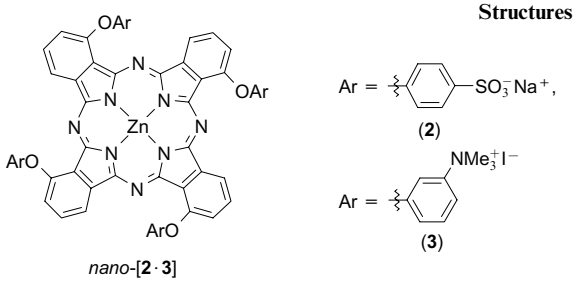
Nevertheless, it was found that phthalocyanine-based aggregates stable in aqueous solutions could be used for biomedical purposes by implementing other mechanisms of relaxation of excited states. For example, photochemical properties of amphiphilic zinc phthalocyanine complex **1** containing one tris(dimethylaminomethyl)phenoxy group have been studied (Scheme 1).[19] It was shown that this complex, when transferred from DMF to water or phosphate buffer, forms stable colloidal solutions. According to dynamic light scattering and transmission electron microscopy (TEM) data, molecules in these solutions form spherical aggregates, nanodots *nano*-**1** with a narrow size distribution (55 ± 20 nm at a concentration of 20 μmol L^{-1}). The surface of the nanodots bears hydrophilic tris(dimethylaminomethyl)phenoxy groups, which ensure stability in aqueous solutions, while their interior consists of hydrophobic phthalocyanine moieties bound by stacking interactions. This architecture of nanodots causes fluorescence quenching, restricts the excited state vibrational relaxation and completely inhibits singlet oxygen generation. However, these aggregates acquire the ability to generate another reactive oxygen species, the superoxide radical anion ($O_2^{-\bullet}$). The formation of this species was confirmed using hydroethidine, a blue fluorescent dye, as a chemical probe. A study of the possibility of using *nano*-**1** particles for photoinactivation of pathogenic microorganisms showed their high efficiency: even at a concentration of 50 nmol L^{-1}, they suppressed the growth of both Gram-positive (*Staphylococcus aureus*) and Gram-negative (*Escherichia coli*) antibiotic-resistant microorganisms.

Controlled aggregation of tetrapyrrole compounds can also be induced by using electrostatic interactions. Thus, the interaction of anionic and cationic water-soluble phthalocyanines **2** and **3** gave nano-aggregates *nano*-[**2**·**3**] of 30–100 nm in size, which, unlike the initial phthalocyanines, possess neither fluorescence nor singlet oxygen generation capability.[20] However, these aggregates exhibited a photothermal effect: their colloidal aqueous solution with a concentration of 5.6 μmol L^{-1} warmed up from 22 to 43 °C under laser irradiation (with a wavelength of 655 nm and a power density of 0.6 W cm^{-2}) for 5 min, whereas

Scheme 1



Structures 2, 3



solutions of the initial phthalocyanines warmed up to no more than 35 °C under the same conditions. Based on this observation, the possibility of using *nano*-[**2**·**3**] assemblies for photothermal therapy was demonstrated *in vivo* with a 4T1 murine mammary carcinoma. In addition, these structures exhibited a pronounced optoacoustic effect under laser irradiation (Fig. 1), which allowed their accumulation and distribution in the tissues to be monitored by optoacoustic microscopy.

Electrostatic interactions between differently charged porphyrins have been used to create binary ionic materials.[21,22] Thus, the interaction of cationic tin porphyrin complexes **4a**,**b** with anionic porphyrin **5** produces either crystalline plate aggregates *nano*-[**4a**·**5**] or X-ray amorphous clover-like structures *nano*-[**4b**·**5**] (Fig. 2). The deposition of such nanoparticles on the platinum surface

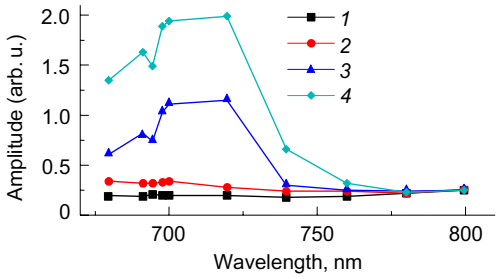
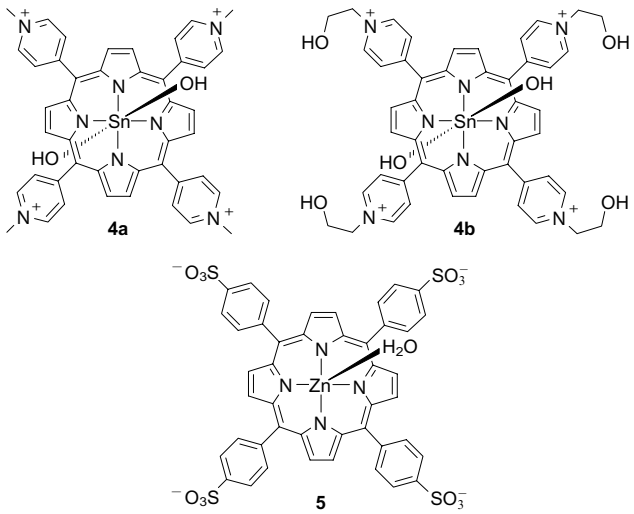


Figure 1. Amplitude of the optoacoustic signal obtained in water (*1*) and in aqueous solutions containing phthalocyanines **2** (*2*), **3** (*3*) and *nano*-[**2**·**3**] (*4*).[20] Reproduced with permission from Wiley.

Structures 4, 5



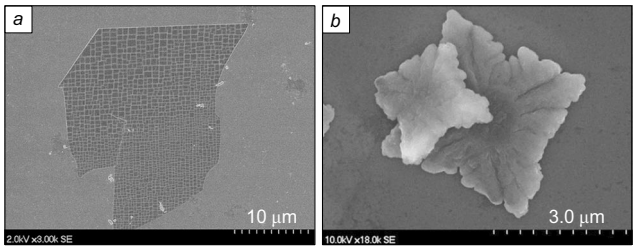


Figure 2. Scanning electron microscopy (SEM) images of *nano*-[**4a**·**5**] (*a*) and *nano*-[**4b**·**5**] (*b*). Reproduced with permission from Tian *et al.*[22]

produced hybrid nanomaterials, which were used for the photodegradation of water in the presence of methyl viologen and triethanolamine.[22] The efficiency of these photocatalysts was determined by the structure of the aggregates: a significantly higher rate of hydrogen evolution was observed in the case of a photocatalyst based on *nano*-[**4b**·**5**] (Fig. 3). This effect was explained on the basis of X-ray crystallography data, indicating the absence of intermolecular interactions in the structure of *nano*-[**4a**·**5**], which are necessary for the appearance of electronic conductivity. At the same time, the conclusion about the presence of such interactions in *nano*-[**4b**·**5**] was made on the basis of electron absorption spectroscopy data.

A number of studies are devoted to self-assembly of tetrapyrrole systems *via* electrostatic interactions. For example, the self-assembly mechanisms of protonated tetrakis(4-sulfonatophenyl)porphyrin (H_4TSPP^{2-}, **6**) to form porphyrin nanotubes due to electrostatic interaction of zwitter ions were discussed in a review of Sheinin *et al.*[23] and a similar controlled formation of J- and H-aggregates was also studied[24] for its analogue **6′** with an inverted porphyrin macrocycle (Fig. 4).[25]

The presence of an extended aromatic system allows tetrapyrrole macrocycles to form supramolecular assemblies with other polyunsaturated compounds, including carbon nanomaterials, such as fullerenes, graphene, nanotubes, *etc.*, through intermolecular stacking interactions. In these

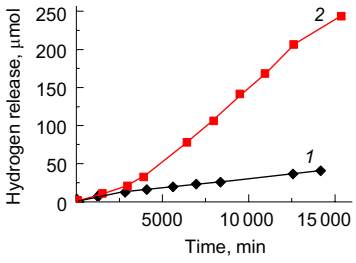
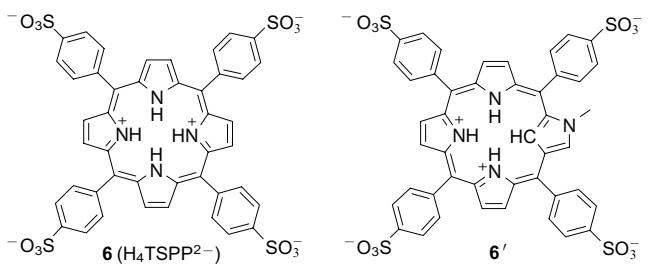


Figure 3. Dependences of the amount of released hydrogen on time in the presence of *nano*-[**4a**·**5**] (*1*) and *nano*-[**4b**·**5**] (*2*) aggregates coated with platinum nanoparticles as photocatalysts.[22] Reproduced with permission from the RSC.

Structures 6, 6′



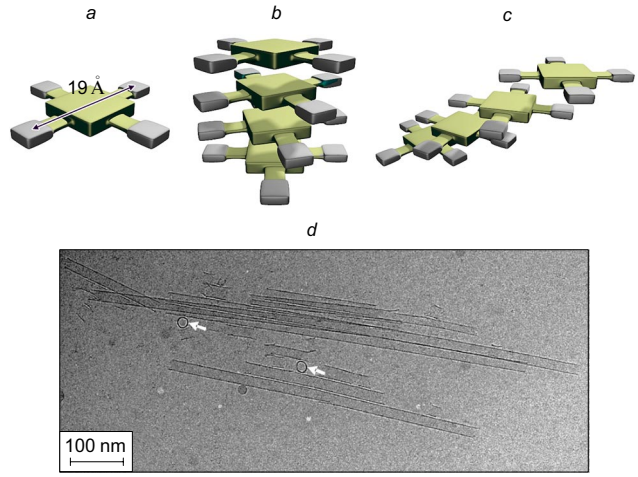


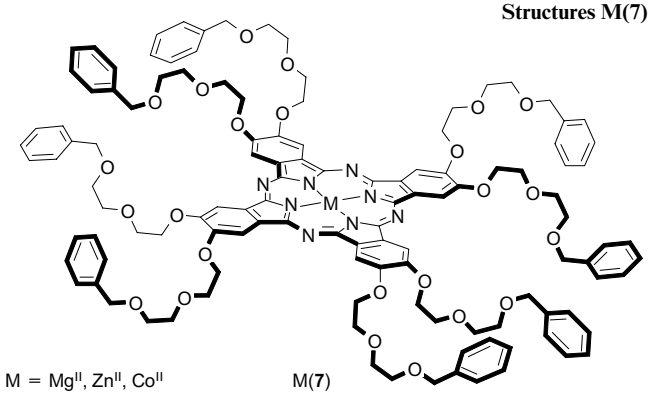
Figure 4. Schematic representation of **6** (*a*) and H- (*b*) and J-aggregates (*c*) it forms; and cryo-electron micrograph of single-walled nanotubes formed by H_4TSPP^{2-} (*d*). White arrows indicate tubes oriented perpendicular to the surface.[25] Image *d* is reproduced with permission from the American Chemical Society.

hybrid systems, tetrapyrroles act as electron donors, while carbon components act as acceptors.[26] As a result, under the action of light, they efficiently generate charge separated states and, hence, they are considered as promising components of photovoltaic materials. A significant advantage of supramolecular assembly of these systems compared to covalent bonding is that the conjugation chain of the carbon components is not broken and their unique photophysical properties are preserved.

The introduction of additional receptor groups to the periphery of tetrapyrrole compounds increases the efficiency of their binding to carbon nanomaterials. Thus, M(**7**) complexes containing eight conformationally flexible *O*-benzyldiethylene glycol residues are capable of forming supramolecular complexes with fullerenes C_{60} and C_{70}, and the receptor molecules behave like octopuses capturing spherical guest molecules by tentacles.[27] It was shown that the interaction of phthalocyanine derivatives of magnesium Mg(**7**) and zinc Zn(**7**) is accompanied by quenching of fluorescence of phthalocyanines due to the formation of charge transfer complexes in the excited state.

Analysis of the fluorescence quenching curves using the Stern–Volmer equation made it possible to determine the stability constants of these assemblies.[27] It turned out that the stability of the supramolecular complex with C_{70} is 1.5–2.5 times higher than that for the complex formed with

Structures M(7)



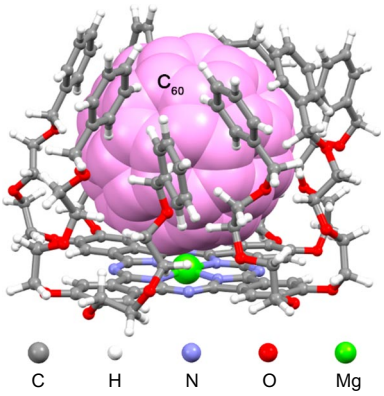


Figure 5. Structure of the supramolecular assembly formed by complex of Mg(**7**) with fullerene C_{60} according to the data of quantum chemical calculations (PM6-DH2). Reproduced from Ref. 28 with permission of Wiley.

fullerene C_{60}. This selectivity to C_{70} is also consistent with the results of quantum chemical calculations using the PM6-DH2 Hamiltonian parameterized for the study of non-covalent systems (Fig. 5). Based on the EPR data, it was concluded that cobalt(II) complex Co(**7**) binds to C_{70} *via* dipole – dipole interactions without changes in the spin density distribution.[27]

An increase in the selectivity of binding of various fullerenes can be used to develop methods for the separation of fullerene mixtures.[29] For example, palladium acetate-induced assembly of zinc *meso*-tetrakis(4-carboxyphenyl)-porphyrin **8** with macrocyclic ligand **9** in acetonitrile yielded macrocyclic capsule $[(\mathbf{8})_2\cdot(\mathbf{9})_4\cdot(PdOAc)_8]^{8+}$. This capsule was capable of binding fullerenes C_{60} and C_{70} in a homogeneous solution; after being dissolved in acetonitrile, it can extract solid fullerenes (Fig. 6).[30] X-Ray diffraction data indicate that, upon binding of fullerenes to this receptor, the size of the cavity decreases to better adjust to the guest molecule. The binding constants ($\log K_a$) of this capsule with C_{60} and C_{70} found by spectrofluorimetric titration were 7.47 ± 0.03 and 8.60 ± 0.30 L mol^{-1}, respectively, which is consistent with a significant increase in selectivity of binding of fullerene C_{70}. Such a high difference between the $\log K_a$ values made it possible to develop a chromatographic method for isolation of C_{60} from a mixture of fullerenes containing also C_{70} and C_{82}.

2.1.2. Cation-induced formation of supramolecular assemblies based on crown-substituted tetrapyrroles

One of the most successful solutions to the problem of controlling the assembly of tetrapyrrole compounds was the synthesis of their crown-substituted analogues, from which

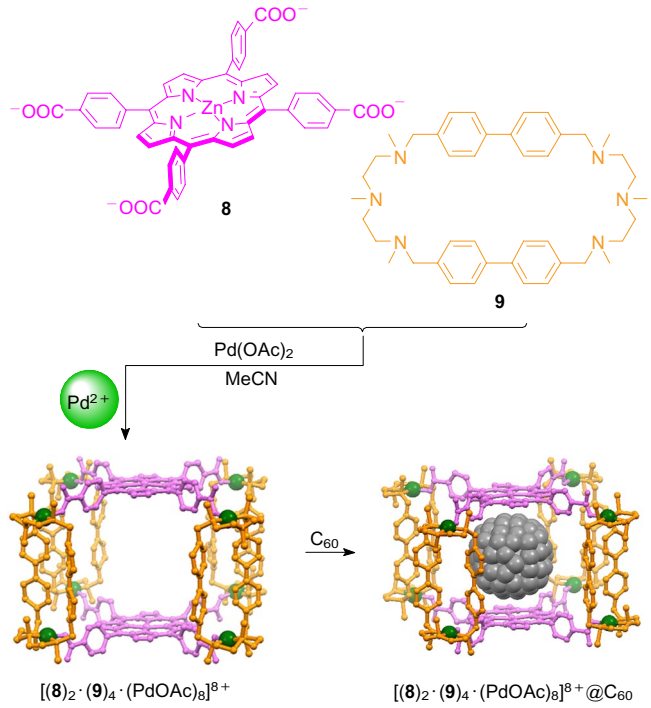


Figure 6. Scheme of the formation of the capsule $[(\mathbf{8})_2\cdot(\mathbf{9})_4\cdot(PdOAc)_8]^{8+}$ and the host – guest complex with fullerene C_{60} according to X-ray diffraction data. The figure was created by the authors using the Cambridge Crystallographic Data Centre (CCDC 1027669 and 1027670) and data of Ref. 30.

supramolecular assemblies of a given architecture can be obtained using the cation-induced assembly method. In addition, binding of alkali metal cations to crown-substituted tetrapyrroles directly affects the physicochemical properties of these heterotopic receptors, which makes them applicable for the fabrication of materials with controlled properties.

Thus, porphyrazines (Pz) modified with azacrown groups were proposed as fluorescent sensors for alkali metal cations (Fig. 7).[31] These sensors have no intrinsic fluorescence because of the nonradiative deactivation of their excited states *via* charge transfer from the azacrown ether nitrogen atom to the tetrapyrrole macrocycle. However, binding to alkali metal cations blocks the conjugation of the nitrogen lone pair with the porphyrazine ring, thereby preventing the photoinduced charge transfer, which results in the observed enhancement of the receptor fluorescence. Thus, when receptor **10** interacts with potassium and sodium cations, the fluorescence intensity increases by a factor of 10.5 and 11.5, respectively; however, the presence

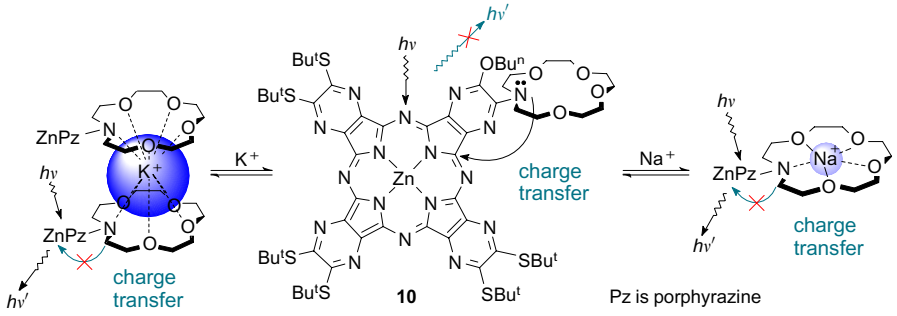
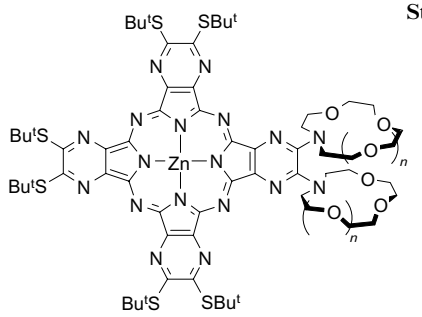


Figure 7. Operation principle of crown-substituted porphyrazine **10** as a fluorometric sensor for the detection of alkali metal ions.[31]

of ions of other alkali, alkaline earth and heavy metals does not increase fluorescence.

To exhibit a selective fluorescence response to potassium or sodium cations, pincer receptors **11a**,**b** containing a pair of azacrown ether groups were synthesized.[32] In this case, the method of binding the cations depended on which crown ether groups were introduced into the receptor molecule and gave rise to selectivity.

Structures 11



n = 1 (**a**), 2 (**b**) **11a**,**b**

The fluorescence intensity of receptor **11a** based on 12-azacrown-4 in the presence of sodium cations was selectively enhanced 291-fold, whereas receptor **11b**, containing 15-azacrown-5 ether moieties exhibited selectivity to potassium cations, enhancing fluorescence 22-fold (Fig. 8). Importantly, the introduction of macrocycles **11a,b** into SiO_2 nanoparticles made it possible to obtain hybrid materials in which the receptors retained a selective fluorescence response toward sodium and potassium cations.

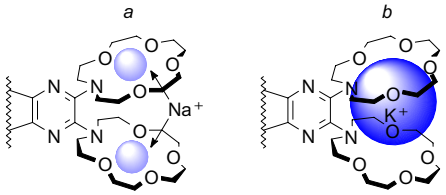


Figure 8. Coordination modes of alkali metal cations depending on the size ratio of the ion and the crown ether moiety in macrocycle **11b**.[32]

The above example emphasizes the importance of structural compliance and cooperative interaction between the receptor (crown ether) and the substrate (alkali metal cation) for the formation of supramolecular assemblies of a given architecture and obtaining the required analytical response.

Using these ideas, a highly sensitive sensor system for detecting and determining the concentration of beryllium salts was fabricated on the basis of zinc tetra(9-crown-3)-substituted phthalocyanine complex Zn[(9C3)$_4$Pc] (where 9C3 is 9-crown-3 ether, and Pc is phthalocyanine) (Fig. 9).[33] It was shown that in the presence of Be^{2+} cations, this complex forms J-aggregates (Scheme 2), which leads to significant changes in the absorption and fluorescence spectra even at an analyte concentration of 10^{-9} mol L^{-1}. Other cations (Li^+, Na^+, K^+, Cs^+, Mg^{2+}, Ca^{2+}, Ba^{2+}, Al^{3+}, Co^{2+}, Hg^{2+}, Ni^{2+}, Pb^{2+}, Zn^{2+}) cause no changes in the absorption/fluorescence spectra of the sensor.

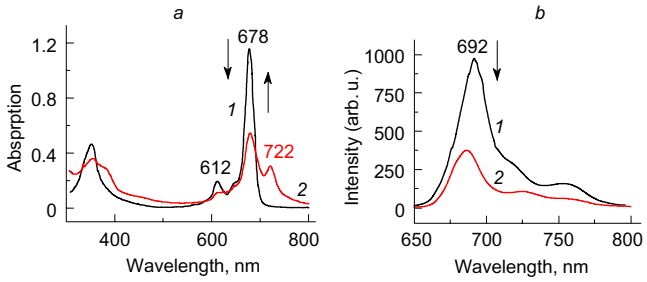
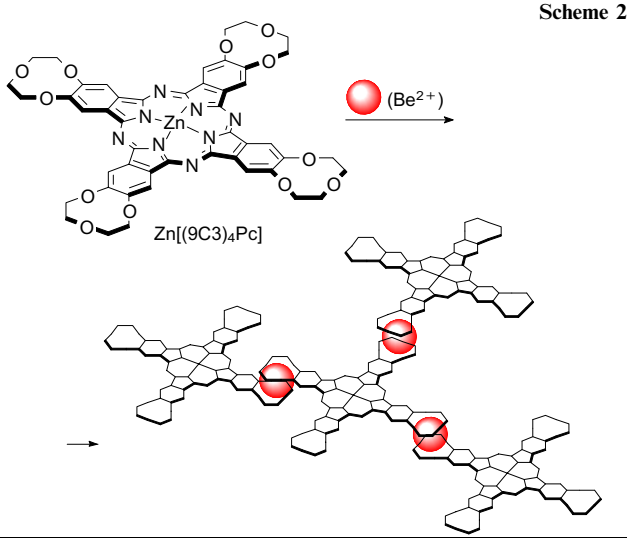


Figure 9. Changes in the absorption (*a*) and fluorescence (*b*) spectra of Zn[(9C3)$_4$Pc] (*1*) upon the formation of J-aggregates with Be^{2+} cations (*2*). The figure was created by the authors using data of Ref. 33, with permission from the American Chemical Society.

Scheme 2

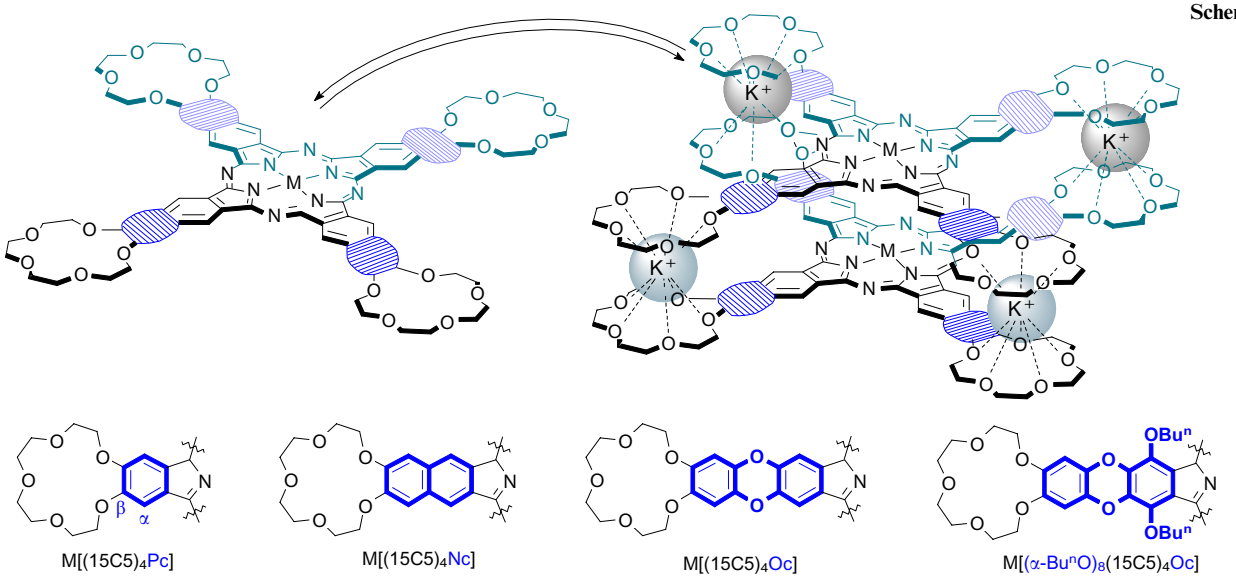


On going to 15-crown-5-substituted (15C5) complexes, it was found that aggregation can be caused by cations with large ionic radii, K^+, Rb^+ and Cs^+. In contrast to Zn[(9C3)$_4$Pc], the M[(15C5)$_4$Pc] complexes in the presence of these cations form cofacial supramolecular dimers with effective intramolecular exciton interaction between the aromatic systems.[34] The formation of these dimers in solutions was confirmed by various physicochemical methods not only for phthalocyanines, but also for their analogues with extended aromatic systems such as naphthalocyanines (Nc)[35] and oxanthrenocyanines (Oc)[36,37] (Scheme 3).

Only in 2018, the structure of supramolecular assemblies formed by crown-substituted phthalocyanines in the presence of alkali metal cations was established using X-ray diffraction analysis in relation to the dimer $\{[Rb_4(NicAl(15C5)_4Pc)_2(\mu\text{-}O)]^{2+}(Nic^-)_2\}$, where Nic is a nicotinate (Fig. 10).[38] This dimer was obtained by the reaction of a hydroxy aluminium tetra(15-crown-5)-substituted phthalocyanine complex [(15C5)$_4$Pc]Al(OH) with rubidium nicotinate. It was shown that the supramolecular assembly is accompanied by the formation of an μ-oxo-bridge between aluminium atoms. The Al–O–Al moiety formed in this case has a linear structure and is located perpendicular to the plane of phthalocyanine macrocycles, with the Al–Al distance being 3.762 Å.

The analogy between the architecture of these supramolecular dimers and the structure of dimers formed by

Scheme 3



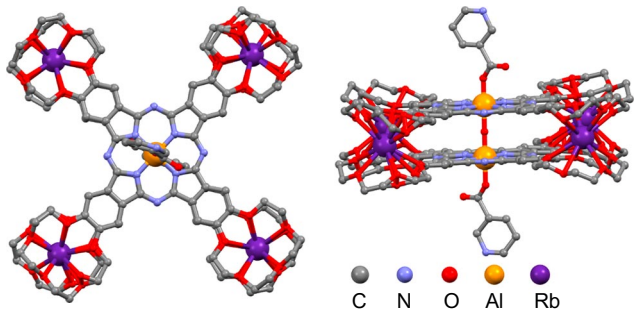


Figure 10. Crystal structure of $\{[Rb_4(NicAl(15C5)_4Pc)_2(\mu\text{-}O)]^{2+}(Nic^-)_2\}$ dimer according to X-ray diffraction data. The figure was created by the authors using the Cambridge Crystallographic Data Centre (CCDC 1566600) and data of Ref. 38.

chlorophyll *a* molecules in plant photosynthetic systems made it possible to fabricate a donor – acceptor biomimetic system, which formed a long-lived charge-separated state upon photoexcitation. For this, an electron-donor zinc crown-substituted phthalocyanine complex Zn[(15C5)$_4$Pc] was used as a donor, while 2-(4-pyridyl)-5-(5-ammoniopentyl)pyrrolidino[3.4:1.2][60]fullerene served as an acceptor (Fig. 11).[39] The lifetime of charge-separated state of $ZnPc^{+\bullet} - C_{60}^{-\bullet}$ was 4.8 μs, and it increased to 6.7 μs on going from the dyad with a monomeric donor to the tetrad in which a supramolecular dimer acted as the donor.

Indium(III) tetra(15-crown-5)-substituted phthalocyanine complex ([(15C5)$_4$Pc]In(OH)) was used to demonstrate the possibility of targeted and reversible cation-induced control of photophysical properties of compounds such as luminescence, singlet oxygen generation and photostabil-

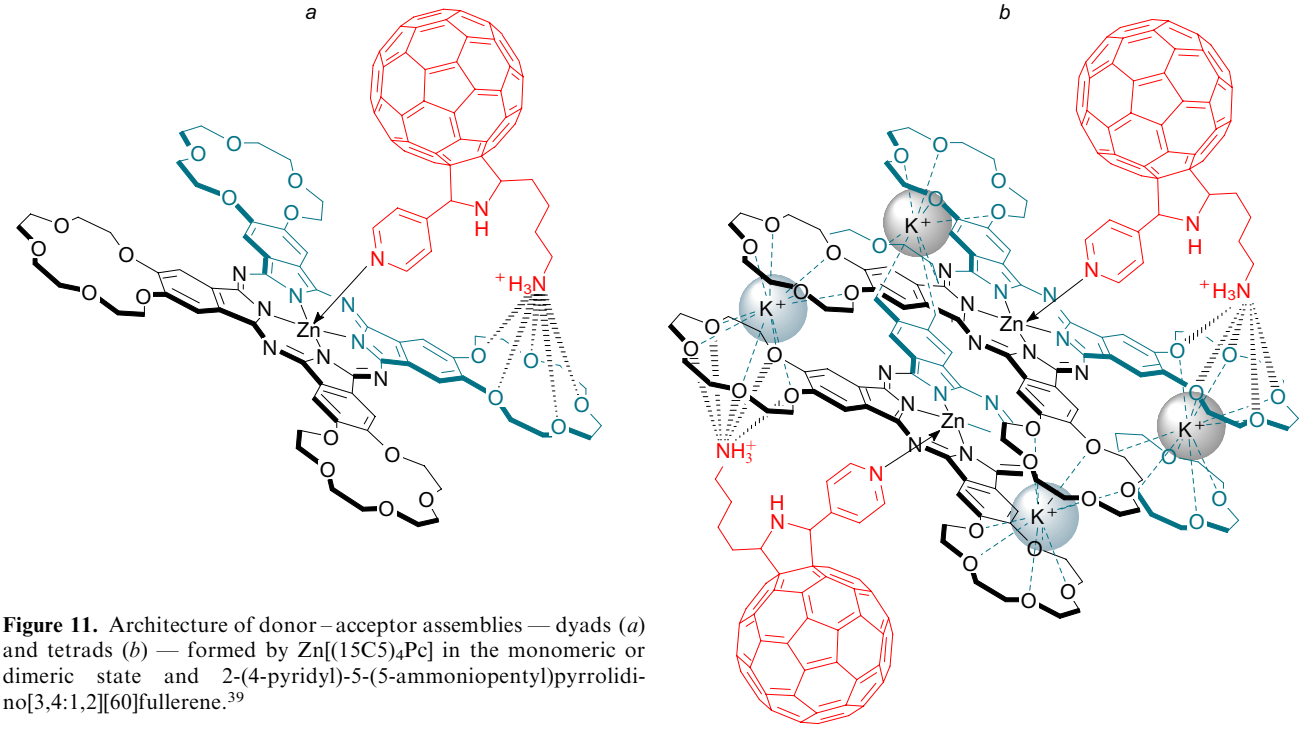


Figure 11. Architecture of donor – acceptor assemblies — dyads (*a*) and tetrads (*b*) — formed by Zn[(15C5)$_4$Pc] in the monomeric or dimeric state and 2-(4-pyridyl)-5-(5-ammoniopentyl)pyrrolidino[3,4:1,2][60]fullerene.[39]

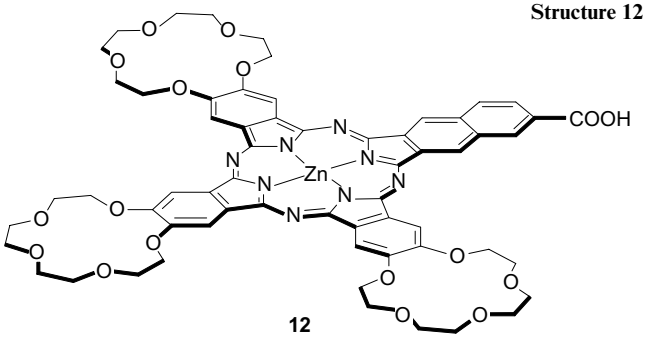
ity.[40] In the monomeric state, this complex had low photostability due to its ability to generate singlet oxygen, whereas supramolecular dimerization resulted in inhibition of $^1O_2$ generation and increased the photostability.

Reversible cation-induced supramolecular assembly was also used to control the aggregation and photophysical properties of crown-substituted macrocycles exhibiting an increased propensity for intermolecular π–π interactions, tetra(15-crown-5)naphthalocyanines M[(15C5)$_4$Nc], where M = 2H, Mg, Zn,[35] and tetra(15-crown-5)oxanthrenocyanines M[(15C5)$_4$Oc], where M = Mg, Zn.[36]

Using UV-vis spectroscopy, it was shown that naphthalocyanines M[(15C5)$_4$Nc] exist in an aggregated state in a $CHCl_3$ + MeOH mixture.[35] However, under the action of potassium acetate, these aggregates are converted to soluble supramolecular dimers 2 M[(15C5)$_4$Nc]·4 K^+. The removal of potassium cations from the dimers in the presence of [2.2.2]cryptand leads to the formation of monomeric forms of complexes, which do not re-aggregate. It is important to note that solutions containing supramolecular dimers and aggregated forms of M[(15C5)$_4$Nc] remained photostable upon irradiation with white light. At the same time, solutions of monomeric naphthalocyanines underwent rapid photodegradation due to the generation of singlet oxygen, which causes the destruction of tetrapyrrole macrocycles. The photostability of crown naphthalocyanines M[(15C5)$_4$Nc] decreased in the M series as follows: 2H > Mg > Zn, which is consistent with the increase in the quantum yields of singlet oxygen generation on going from the naphthalocyanine ligand to metal complexes.

Tetra(15-crown-5)oxanthrenocyanines M[(15C5)$_4$Oc], structurally related to crown naphthalocyanines,[36] also formed soluble supramolecular dimers 2 M[(15C5)$_4$Oc]·4 K^+ in the presence of potassium cations. However, in contrast to naphthalocyanine analogues, the destruction of these dimers in the presence of [2.2.2]cryptand did not lead to the formation of monomeric forms of complexes. Instead, repeated aggregation of the complexes was observed with the formation of nanoparticles characterized by panchromatic absorption in the 250–900 nm range.[41]

Structure 12



12

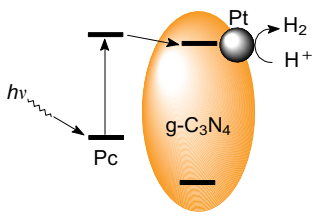


Figure 12. Functioning principle of the hybrid material [Pt/g-C_3N_4·**12**]. The figure was created by the authors based on the data of Ref. 42.

A hybrid material with graphite-like carbon nitride modified with platinum nanoparticles was obtained using an asymmetric photosensitizer, zinc 4-carboxybenzoannulated tri(15-crown-5)phthalocyanine complex **12** (Pt/g-C_3N_4), (Fig. 12).[42]

This material showed the ability to photocatalytically form hydrogen from an aqueous solution of triethanolamine with a turnover number (TON) of 3105 h^{-1} due to photoinduced electron transfer from phthalocyanine molecules **12** to an inorganic matrix with subsequent reduction of protons to molecular hydrogen. It was shown that binding of alkali metal cations to crown ether substituents has different effects on the quantum yield, the rate of hydrogen evolution, and the TON of the catalytic system. These characteristics virtually did not depend on binding of lithium cations, while in the presence of sodium and especially potassium cations, a significant increase in the rate of hydrogen evolution was observed (Fig. 13). In the latter case, the TON value reached 9067 h^{-1}. The authors used a wide range of methods, including time-resolved fluorescence spectroscopy and quantum chemical calculations, to study the processes of electron transfer from a photosensitizer to Pt/g-C_3N_4.

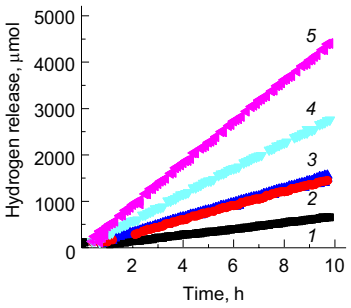


Figure 13. Dependences of the amount of released hydrogen on the composition of the hybrid material Pt/g-C_3N_4 (*1*); Pt/g-C_3N_4·**12** (*2*); Pt/g-C_3N_4·**12**(Li^+) (*3*); Pt/g-C_3N_4·**12**(Na^+) (*4*); Pt/g-C_3N_4·**12**(K^+) (*5*).[42] Reproduced with permission from Elsevier.

In relation to the heteroleptic double-decker terbium(III) phthalocyanine complex [(15C5)$_4$Pc]Tb(Pc), which behaves as single-molecule magnet (SMM), it was shown that the formation of a supramolecular dimer (Fig. 14*a*) leads to a 1000-fold decrease in the relaxation rate of magnetization at 2 K, and the temperature range in which the hysteresis of magnetization is observed expands from 7 to 15 K.[43] Such an improvement in the magnetic properties is primarily due to ferromagnetic interaction between the terbium ions. The distance between the Tb^{3+} cations (6.2 Å), estimated from NMR spectroscopy data, is in line with the value of 6.249 Å found by X-ray diffraction for a structurally similar six-decker dimer obtained by supramolecular dimerization of the complex [(15C5)$_4$Pc]Y(Pc)Y(Pc) in the presence of $KBPh_4$ (see Fig. 14*b*).[44] This structure is the first direct evidence for the architecture of supramolecular dimers based on sandwich crown-substituted phthalocyanine complexes of rare earth elements.

It should be noted that the nature of the solvent and heat treatment of crown phthalocyanines can also lead to the formation of assemblies with new physicochemical properties due to numerous non-covalent interactions involving crown ether groups, aromatic moieties and solvent molecules. Thus, it was shown that the supramolecular self-assembly of the [(15C5)$_4$Pc]Ru(Pyz)$_2$ (**13**) (Pyz is pyrazine) complex in a mixture of tetrachloroethane and polymer composites with polyvinylcarbazole induced by repeated heat treatment with heating the solution to 70 °C

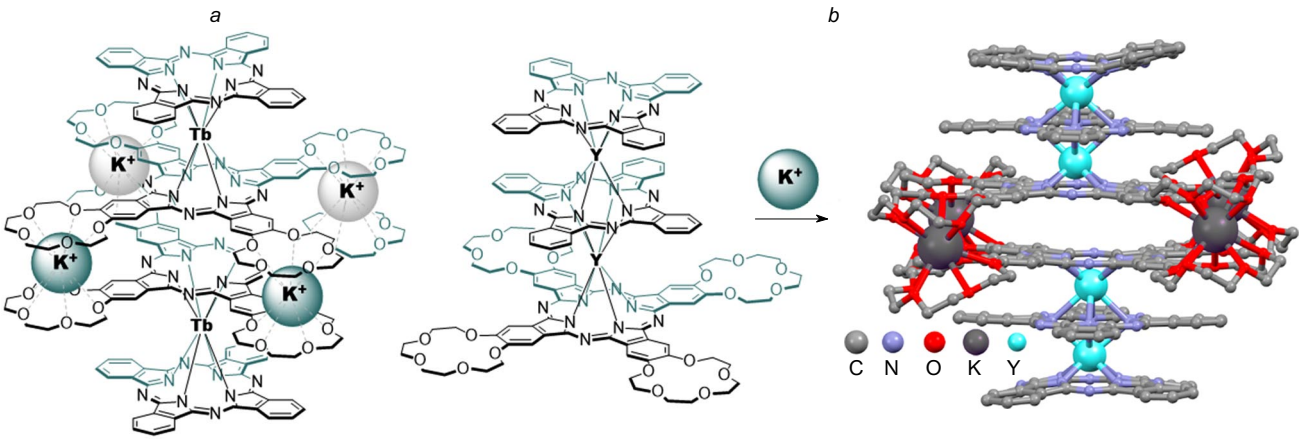
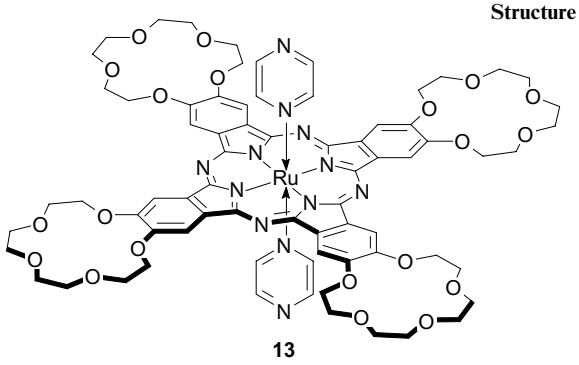


Figure 14. Structure of the supramolecular dimer $2[(15C5)_4Pc]Tb(Pc)\cdot 4K^+$ (*a*),[43] scheme of supramolecular dimerization of the complex $[(15C5)_4Pc]Y(Pc)Y(Pc)$ and crystal structure of the six-decker dimer according to X-ray diffraction data (*b*).[44] The figure was created by the authors using the Cambridge Crystallographic Data Centre (CCDC 1994699).

Structure 13



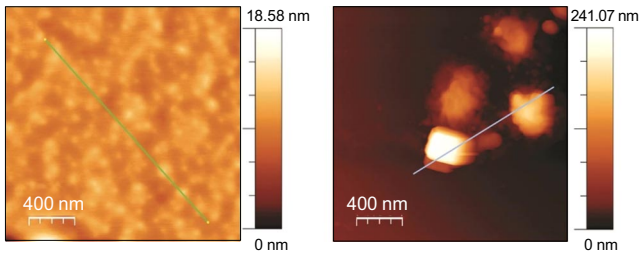


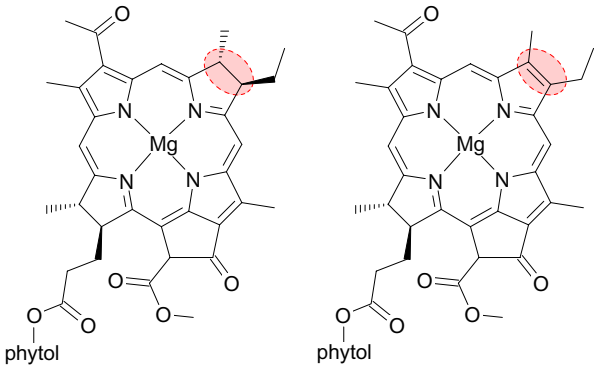
Figure 15. AFM photomicrographs of films obtained from a solution of complex **13** in tetrachloroethane before (*a*) and after (*b*) heat treatment.[45] Reproduced with permission from the Royal Society of Chemistry.

and subsequent cooling to 5 °C gives rise to a nonlinear optical response of the material, which is absent in the case of the monomeric complex (Fig. 15).[45]

2.1.3. Supramolecular assembly of tetrapyrroles *via* hydrogen bonding

Hydrogen bonds (H-bonds) play a crucial role in the formation of supramolecular structures based on natural tetrapyrrole macrocycles, providing their high activity and exceptional selectivity in various biochemical processes in life (chlorophyll in photosynthesis, haem proteins in oxygen transport and in enzymatic processes). These structures can arise *via* the formation of intermolecular hydrogen bonds

Chlorophyll structures



between appropriate functional groups at the periphery of the tetrapyrrole complex or *via* axial coordination of proton-donating small molecules to the complex-forming metal, or *via* a combination of both types of binding.[46, 47]

Figure 16 shows the hydrogen bonding between bacteriochlorophyll *a* molecules and tryptophan (Trp) or tyrosine (Tyr) residues in light-harvesting complex II from Gram-negative purple non-sulfur bacteria *Rhodoblastus Acidophilus*.[46] Recently, model studies[47] showed that H-bond formation involving the keto group of chlorophyll *a* (see Fig. 16) as a part of supramolecular complex with protein in photosystem II of higher plants allows smooth changes of the energy of electronic transitions in a supramolecular assembly, providing high efficiency of cascade energy transfer by a light harvesting antenna.

Hydrogen-bonded supramolecular structures also play a key role in haem protein structure and function. Participation of a distal water molecule coordinated to the haem in the H-bonding to the tyrosine residue Tyr107 (Fig. 17 *a*) was shown to regulate H_2O_2 binding and activation in model myoglobins,[48] while H-bonding to histidine His29 (see Fig. 17 *b*) determines their hydrolytic activity.[49]

Similar principles of the assembly of supramolecular systems *via* hydrogen bonding are used in the case of synthetic porphyrins and their *meso*-aza-substituted analogues (porphyrazines and phthalocyanines). Over the last decade, this approach has been actively used for the

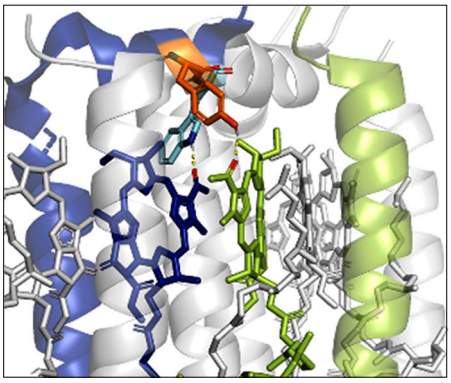


Figure 16. Formation of hydrogen bonds in the structure of light-harvesting complex II from *Rhodoblastus Acidophilus* between residues Trpα44 and Tyrα45 and molecules of the αβ-heterodimer of bacteriochlorophyll *a* (B850).[47] Reproduced with permission from Elsevier.

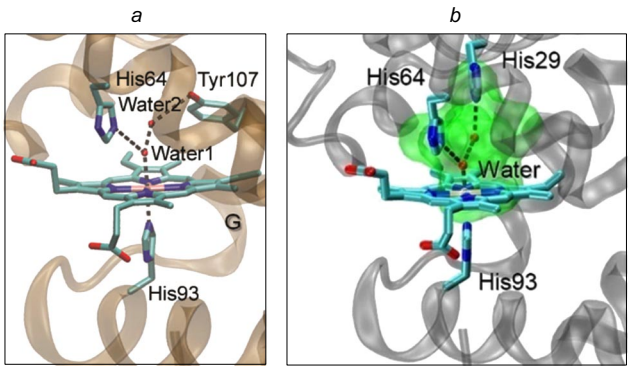
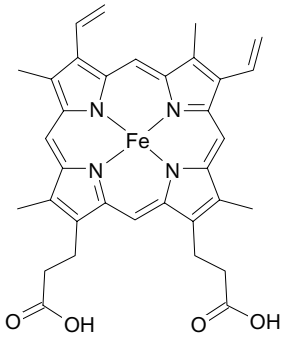


Figure 17. Formation of hydrogen bonds with the distal water molecule in model myoglobin structure with tyrosine (*a*) and histidine (*b*). The figure was created by the authors using data of Refs 48 and 49.

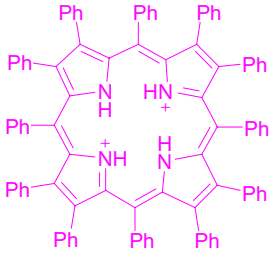
development of both biomimetics and new functional materials. These issues are addressed using the same types of interactions that occur in nature, and the porphyrin macrocycle can serve as both a donor and an acceptor of H-bonds, thus forming dimeric, oligomeric or polymeric framework structures, which have been named hydrogen-bonded organic frameworks (HOFs).

Free porphyrin bases generally have a planar structure, their pyrrole NH groups form intramolecular H-bonds with pyrrolenine nitrogen atoms and are incapable of intermolecular interactions. However, protonation of these molecules usually disrupts the planarity of the macrocycle and

Haem structure



Structure 14a



14a

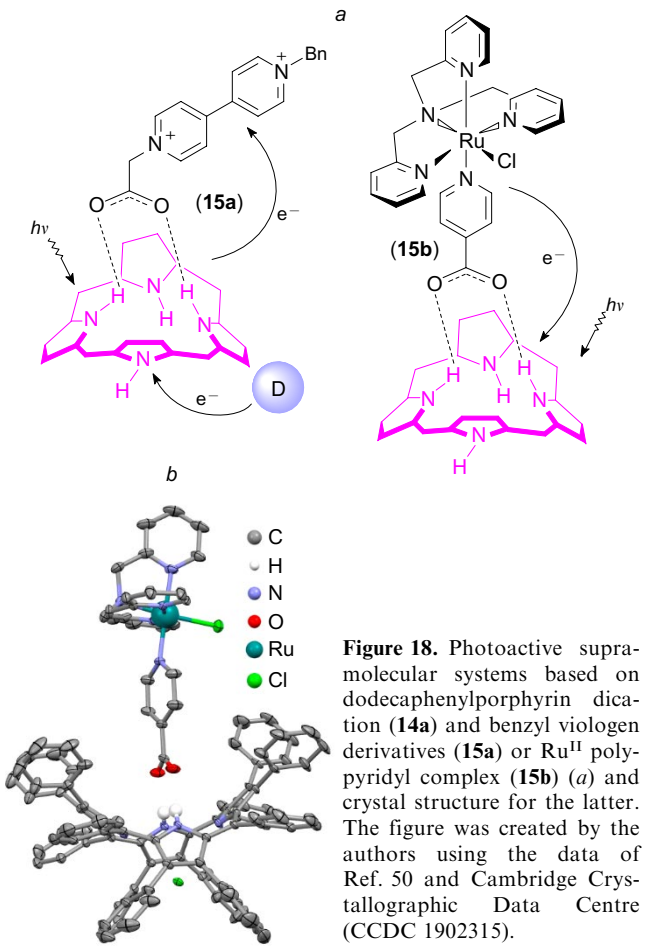


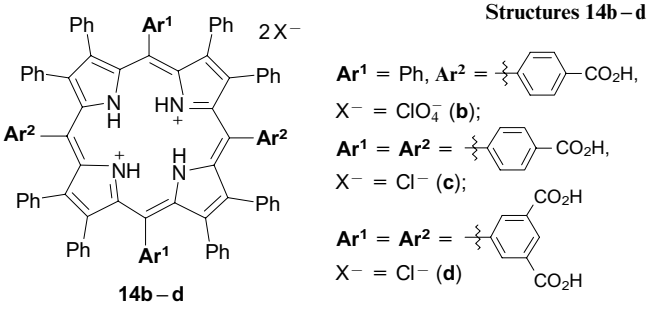
Figure 18. Photoactive supramolecular systems based on dodecaphenylporphyrin dication (**14a**) and benzyl viologen derivatives (**15a**) or Ru^{II} polypyridyl complex (**15b**) (*a*) and crystal structure for the latter. The figure was created by the authors using the data of Ref. 50 and Cambridge Crystallographic Data Centre (CCDC 1902315).

changes the H-bonding capacity. For example, due to the saddle-shaped distortion of the macrocycle in the diprotonated forms of porphyrins, especially in the case of dodecasubstituted derivatives, NH groups become good H-bond donors and can form supramolecular structures *via* intermolecular hydrogen bonding to various anions. Thus, various photoactive supramolecular systems with carboxyl-containing redox-active guest molecules capable of photoinduced electron transfer (H_4DPP^{2+}, **14a**) were derived from dodecaphenyl-substituted porphyrin dication (Fig. 18).[50] Using benzyl viologen derivative **15a** as an electron acceptor, the H_4DPP^{2+} porphyrin mediated the photoinduced electron transfer from decamethylferrocene (indicated by the blue circle with the letter D in Fig. 18 *a*) to the acceptor molecule. In the case of H_4DPP^{2+} binding to the ruthenium(II) polypyridyl complex **15b**, intramolecular photoinduced electron transfer was observed. This is the first example of application of protonated porphyrins as

photoactive platform for the creation of charge transfer systems *via* hydrogen bonding.

Extended two- and three-dimensional supramolecular structures based on tetrapyrrole macrocycles formed *via* H-bonds have recently attracted particular interest. Thus, supramolecular assemblies of various dimensionalities were obtained from dodecaaryl-substituted porphyrins **14b – d**.[51]

Structures 14b – d



A self-assembly process involving porphyrin **14b** containing two *p*-carboxyphenyl groups in the opposite *meso*-positions resulted in one-dimensional chains (Fig. 19 *a*). Upon the introduction of four *p*-carboxyphenyl groups, porphyrin **14c** forms supramolecular 2D networks (see Fig. 19 *c*). The presence of 3,5-dicarboxyphenyl groups in the *meso*-positions of porphyrin macrocycle **14d** results in the formation of H-bonded ladder-type structures (see Fig. 19 *d*). An interesting feature of these supramolecular structures is the presence of nanochannels containing anions (see Fig. 19 *b*).

It has recently been shown that the self-assembly of *meso*-tetrakis(4-carboxyphenyl)porphyrin-based HOF (H_2TCPP) can be finely tuned by kinetically and thermodynamically controlled blocking of a portion of the carboxyl groups upon interaction with DMF at various temperatures.[52] Thus, HOFs with porphyrin – DMF stoichiometric ratios of 1 : 2, 1 : 4 and 1 : 6 were obtained at 120, 130 and 140 °C, respectively. X-Ray diffraction analysis was used to elucidate the nature of the non-covalent interactions responsible for the formation of each type of HOF (Fig. 20). The resulting supramolecular structures were used for the photocatalytic decomposition of 9,10-diphenylanthracene, with the 1 : 6 assembly being the most active. The same assembly showed the highest intrinsic photostability.

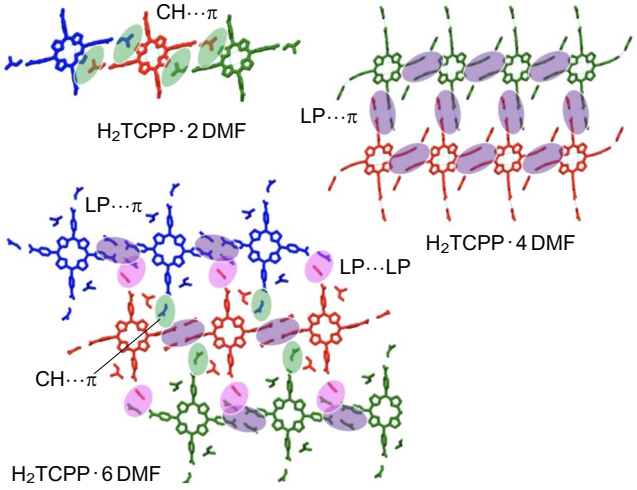


Figure 20. Nature of non-covalent interactions in HOF formed by *meso*-tetrakis(4-carboxyphenyl)porphyrin and DMF. LP is lone pair.[52] Reproduced with permission from the American Chemical Society.

Three-dimensional HOF-type supramolecular structures can also be obtained by simultaneous introduction of two types of functional groups, *e.g.*, pyridyl and carboxy groups, into the porphyrin molecule. For example, in the Mn^{II} and Zn^{II} complexes with 5,15-di(4-pyridyl)-10,20-bis(4-carboxyphenyl)porphyrin (**16**), HOF structures are formed through interaction of carboxyl groups among themselves and with the pyridine moieties not involved in coordination with metal cations (Fig. 21).[53]

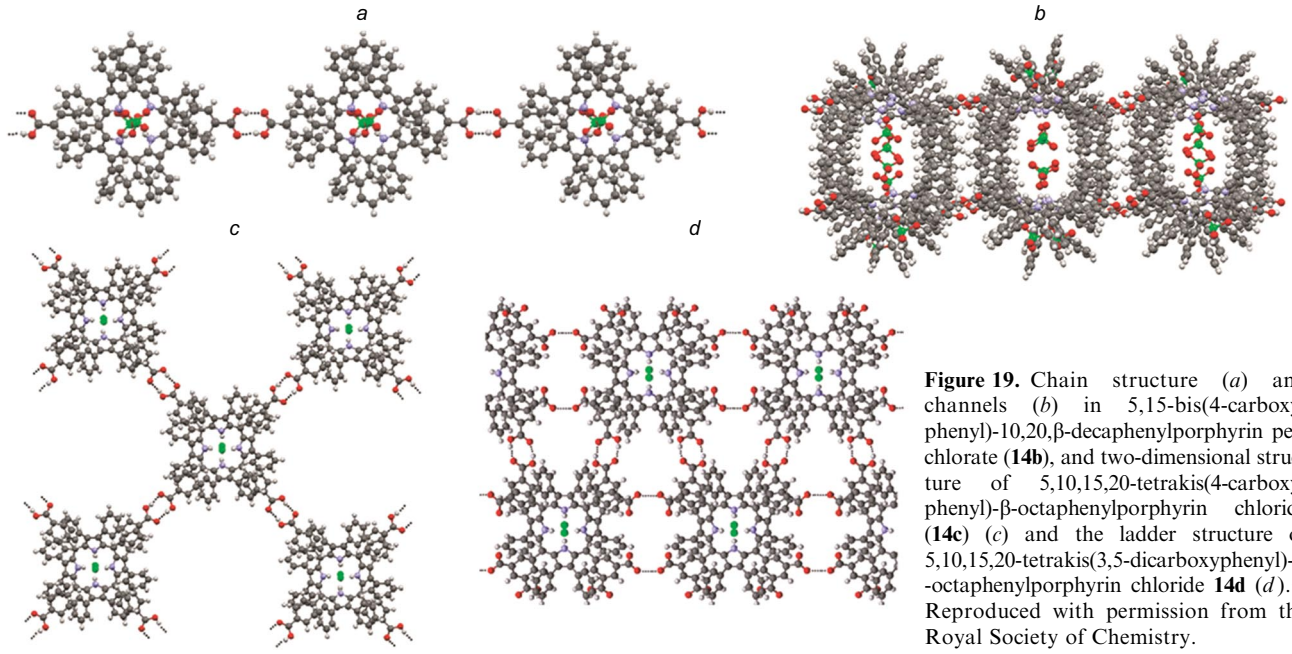


Figure 19. Chain structure (*a*) and channels (*b*) in 5,15-bis(4-carboxyphenyl)-10,20,β-decaphenylporphyrin perchlorate (**14b**), and two-dimensional structure of 5,10,15,20-tetrakis(4-carboxyphenyl)-β-octaphenylporphyrin chloride (**14c**) (*c*) and the ladder structure of 5,10,15,20-tetrakis(3,5-dicarboxyphenyl)-β-octaphenylporphyrin chloride **14d** (*d*).[51] Reproduced with permission from the Royal Society of Chemistry.

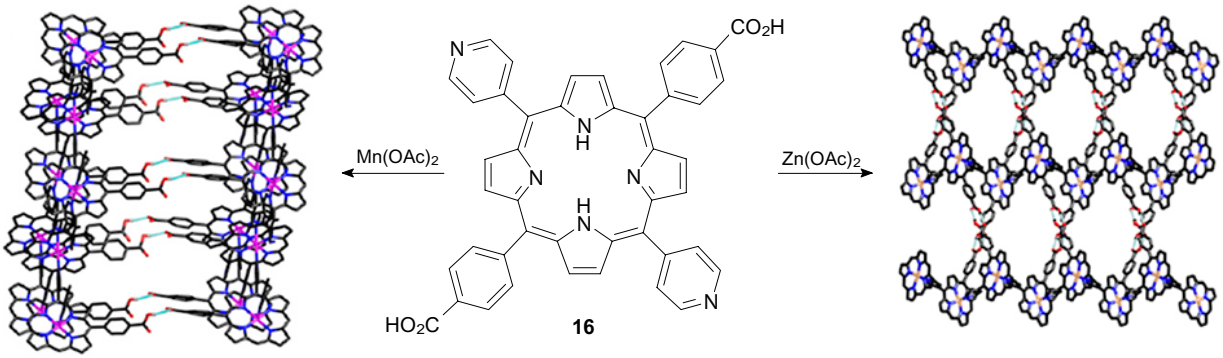
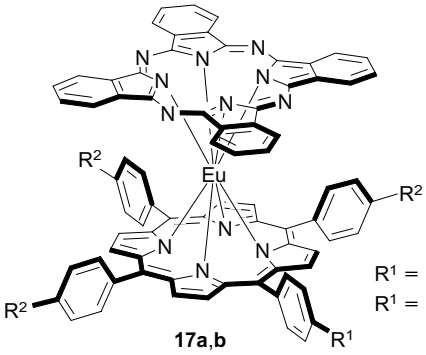


Figure 21. 3D supramolecular HOF structures based on 5,15-di(4-pyridyl)-10,20-bis(4-carboxyphenyl)porphyrin (**16**).[53] Reproduced with permission from Elsevier.

The formation of supramolecular structures through hydrogen bonding is also possible upon the interaction of tetrapyrrole macrocycles of various types. Thus, heteroleptic sandwich complexes of Eu^{III} (**17a**,**b**) containing octylamine-substituted tetraphenylporphyrin and phthalocyanine ligands were used to form nanoaggregates of various architectures *via* the formation of *meso*-N···NHC_8H_{17}-n hydrogen bonds.

Complex **17a** containing one octylaminophenyl group forms nanorods organized into J-type aggregates (Fig. 22 *a*), while its analogue **17b** with four aminoalkyl groups forms extended nanolayers which assemble into H-aggregates (see Fig. 22 *b*). It was shown that H-aggregates based on complex **17b** have higher conductivity as compared to that of J-aggregates of complex **17a**.[54]

Structures 17



R^1 = H, R^2 = NHC_8H_{17}-n (**a**);
R^1 = R^2 = NHC_8H_{17}-n (**b**)

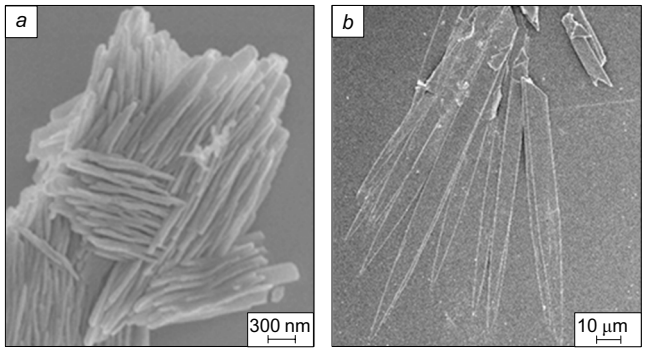
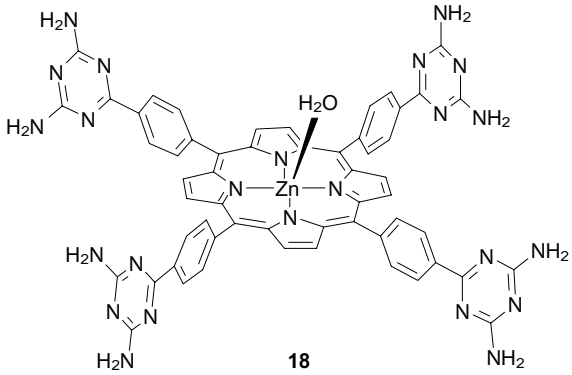


Figure 22. SEM images of the assemblies formed by complexes **17a** (*a*) and **17b** (*b*).[54] Reproduced with permission from Elsevier.

Porphyrin **18** containing 2,4-diaminotriazine rings in *meso*-positions was employed to obtain a highly porous supramolecular HOF structure due to several types of noncovalent interactions.[55] First of all, molecules **18** form dimers *via* hydrogen bonding between axially coordinated

Structure 18



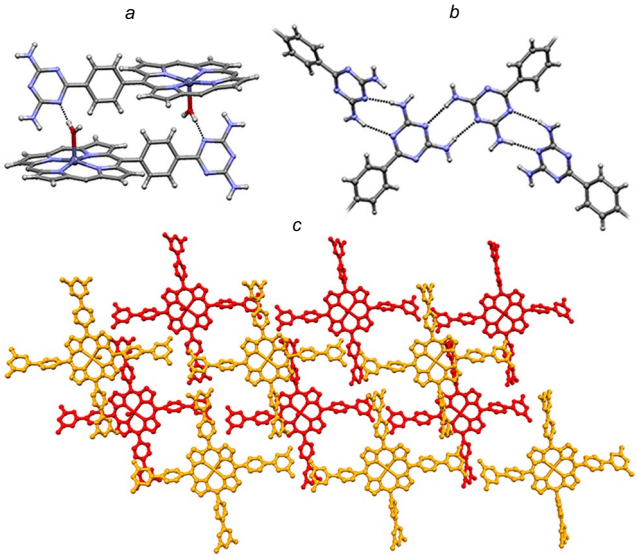


Figure 23. Hydrogen bonds formed in compound **18** upon interaction of 4-(2,6-diaminotriazinyl)phenyl groups with a coordinated water molecule (*a*) and with each other (*b*), leading to a porous supramolecular structure 3D-HOF (*c*). The figure was created by the authors using the Cambridge Crystallographic Data Centre (CCDC 1044789) and data of Ref. 55.

water molecules and the nitrogen atoms of triazine heterocycles (Fig. 23 *a*). Further, these dimers form intermolecular hydrogen bonds involving diaminotriazine moieties (shown in relation to 2,6-diamino-4-phenyltriazine; see Fig. 23 *b*), which gives rise to a porous structure (see Fig. 23 *c*). Due to specific structural features, this HOF system is capable of selective sorption of CO_2.

Intermolecular hydrogen bonds play a paramount role in the formation of supramolecular structures of tetrapyrrole metal complexes with an axially coordinated water molecule. The formation of H-bonded assemblies with participation of water molecules is particularly characteristic of Mg^{II} and Zn^{II} complexes, which efficiently adsorb traces of water from solvents. For example, a recent study [56] demonstrated the formation of supramolecular dimers based on magnesium(II) and zinc(II) aqua complexes with unsubstituted phthalocyanine *via* hydrogen bonding between the coordinated water molecule and *meso*-nitrogen atoms of the adjacent phthalocyanine molecule; simultaneously, an H-bond was formed with the 4-methylmorpholine solvation molecules (Fig. 24).

In the case of *meso*-aza-substituted porphyrins, in particular porphyrazines **19a – c**, *meso*-nitrogen atoms can also

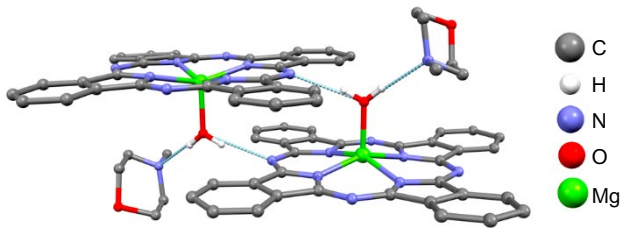
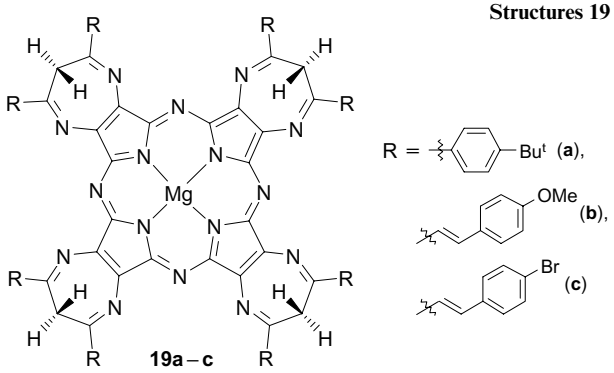


Figure 24. Supramolecular dimer of magnesium phthalocyanine aqua complex with 4-methylmorpholine solvation molecules. The figure was created by the authors using the Cambridge Crystallographic Data Centre (CCDC 1872453) and data of Ref. 56.

Structures 19



participate in the formation of intermolecular H-bonds. Thus, for porphyrazines with annulated 1,4-diazepine moieties, a unique complementary H-bonds were found to arise between the *meso*-nitrogen atoms of one molecule and the hydrogen atom of the methylene group having enhanced acidity in the diazepine ring of another molecule, which gives rise to stable dimers (Fig. 25).[57, 58]

It was found that the tendency of tetrakis(1,4-diazepino)porphyrazines to form dimers is influenced by the nature of both the substituent in the diazepine rings and the solvent.[57 – 59] Thus, complex **19a** with a 4-*tert*-butylphenyl

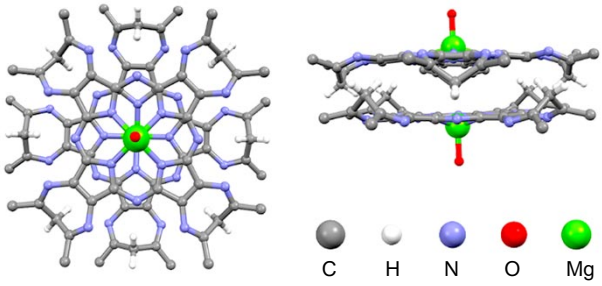


Figure 25. Structure of the dimer formed by **19c** by means of complementary intermolecular H-bonds. Only the carbon atoms of the substituents and the hydrogen atoms of the CH_2 groups are shown. The figure was created by the authors using the Cambridge Crystallographic Data Centre (CCDC 1489687) and data of Ref. 58.

group in aprotic solvents (DMF, DMSO) exists in the monomeric form, and upon the addition of water, dimers are formed, which is accompanied by characteristic changes in the absorption spectra.[57] Additional stabilization of the dimeric form can occur due to the π – π interactions of the peripheral styryl substituents; therefore, the styryl-substituted complex **19b** also exists as dimers in DMSO.[58, 59] However, the addition of fluoride anions as strong H-bond acceptors to the solution leads to the transformation of the dimer into a monomer. Since the dimeric form, unlike the monomeric form, does not show fluorescence, diazepinoporphyrazines can be used as responsive fluorescent sensors, for example, to detect water or fluoride anions in aprotic solvents (Fig. 26).

Interestingly, the nature of the complexing metal also plays a key role in the formation of H-bonded supramolecular assemblies involving water molecules. Thus, for magnesium(II) and zinc(II) complexes with oxanthrenocyanine $M[(\alpha\text{-}Bu^nO)_8(15C5)_4Oc]$, containing n-butoxy groups in the α-position (see Scheme 3), single crystals were obtained. X-Ray diffraction analysis showed that the magnesium complex additionally contains two axially coordinated water molecules, while the zinc complex contains only one such molecule (Fig. 27).[37] The oxanthrene moieties in the complexes have an almost flat structure, with the crown ether moieties participating in the formation of the crystal packing *via* hydrogen bonding with the water molecules

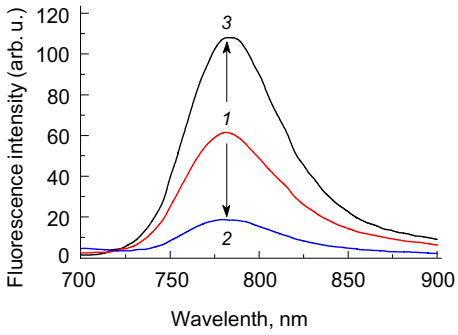


Figure 26. Changes in the fluorescence spectrum (*1*) of the styryl-substituted complex **19b** in DMSO: fluorescence quenching upon the addition of water, which shifts the equilibrium towards the dimer (*2*), and fluorescence enhancement upon addition of Bu^n_4F, which shifts the equilibrium towards the monomer (*3*). The figure was created by the authors using data of Ref. 59.

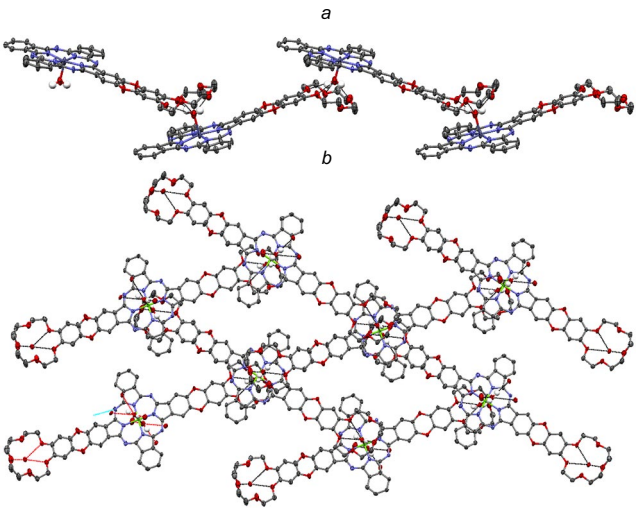


Figure 27. Fragments of the crystal packing of the complexes $M[(\alpha\text{-}Bu^nO)_8(15C5)_4Oc]$, where $M = Zn^{II}$ (*a*) and Mg^{II} (*b*).[37] Reproduced with permission from the American Chemical Society.

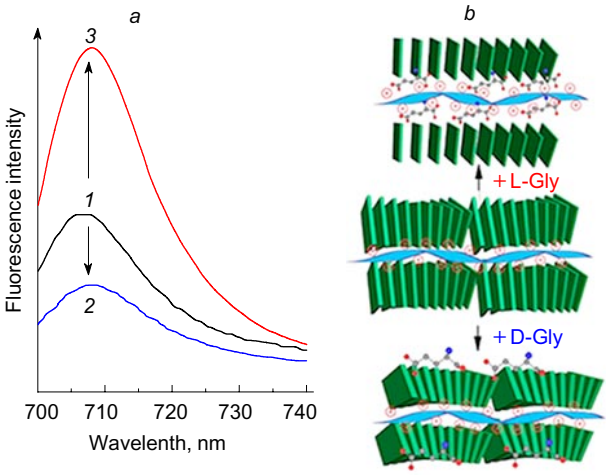


Figure 28. Changes in the fluorescence intensity (*1*) of the supramolecular assembly formed by tetrakis(15-crown-5)phthalocyanine and poly(L-lysine) in the presence of D- (*2*) and L-forms (*3*) of glutamic acid (*a*) and schematic representation of change in the degree of aggregation of $H_2[(15C5)_4Pc]$ upon binding to different enantiomers (*b*).[60] Reproduced with permission from the American Chemical Society.

axially coordinated to the metal cations. In the case of the zinc complex, 1D coordination polymer is formed (see Fig. 27 *a*), while for the magnesium complex, 2D network arises (see Fig. 27 *b*).

It is noteworthy that the number of axially coordinated water molecules determines the type of supramolecular assembly and leads to different participation of these crown-containing molecules in the formation of cation-induced supramolecular assemblies.

The ability of crown ether macrocycles to form hydrogen bonds with ammonium ions enables the development of functional multicomponent assemblies of various architectures. The deposition of a solution of tetrakis(15-crown-5)phthalocyanine ($H_2[(15C5)_4Pc]$) on the surface of an aqueous solution of poly(L-lysine) and subsequent transfer of the assemblies to a quartz surface gave rise to fluorescent sensors capable of detecting chiral substrates, sugars and amino acids (Fig. 28).[60] The analytical signals used to distinguish between enantio- and diastereomers were either changes in fluorescence intensity (enhancement, quenching) for amino acids containing additional carboxy groups (Glu, Asp) or changes in fluorescence quenching rate for aromatic amino acids (Phe, His) or D-monosaccharides (glucose, galactose, mannose). The authors explained the observed patterns by changes in the degree of aggregation of the $H_2[(15C5)_4Pc]$ fluorophore applied on the chirality-inducing poly(L-lysine) upon interaction with different stereoisomers. Thus, the degree of aggregation increased upon interaction with D-enantiomer

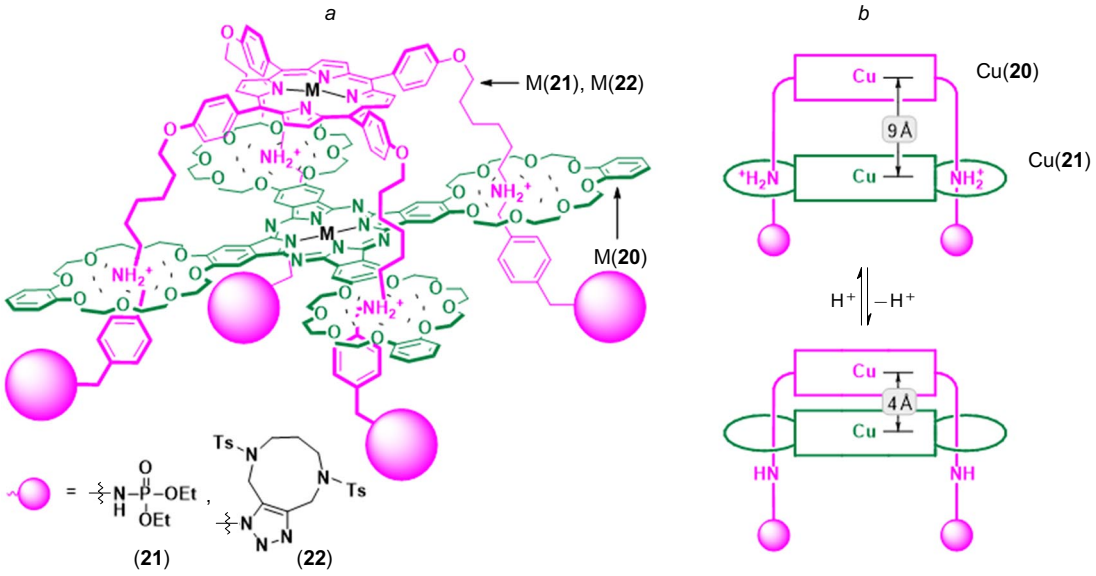


Figure 29. Structure of rotaxanes based on tetrakis(benzo-24-crown-8)phthalocyanines M(**20**) and porphyrins M(**21**), M(**22**) (*a*) and principle of controlling the distance between rotaxane components [Cu(**20**)·Cu(**21**)] under the action of reversible protonation–deprotonation (*b*).[61] Ts is *p*-toluenesulfonyl (tosyl).

of glutamic acid, leading to fluorescence quenching, while in the case of L-enantiomer, a decrease in the degree of aggregation was observed and the fluorescence intensity increased. This conclusion was based, in particular, on atomic force microscopy data.

Disubstituted ammonium cations are able to pass through fairly large crown ether macrocycles to form assemblies with the rotaxane topology. This approach was used to prepare rotaxanes based on tetrakis(benzo-24-crown-8) phthalocyanine M(**20**) and porphyrins M(**21**), M(**22**) complexes containing four dialkylammonium substituents with terminal azide groups (Fig. 29 *a*). For the introduction of bulky stoppers preventing the dissociation of rotaxanes, click reactions of azide groups with triethyl phosphite [61] or with a cyclic strained alkyne were used;[62] this gave supramolecular structures [M(**20**)·M(**21**)] or [M(**20**)·M(**22**)].

It was shown that the reversible deprotonation of ammonium and amidodiester groups in rotaxane [Cu(**20**)·Cu(**21**)] makes it possible to control the intramolecular distance between the porphyrin and phthalocyanine components, which affects the photophysical and magnetic properties of the material.[61] According to EPR and magnetochemical studies performed for a complex containing two copper(II) ions, the amplitude of motion was about 5 Å (see Fig. 29 *b*).

The presence of positively charged ammonium groups in rotaxane leads to interaction with anionic porphyrins to form heteronuclear supramolecular assemblies with a strictly defined arrangement of metal centres.[63, 64] The architectural control achieved in this way made it possible to develop a catalyst with tunable properties based on rotaxane [Fe(**20**)·(μ-N)·Fe(**22**)] containing a (μ-N)Fe_2 catalytic site for the ethane oxidation reaction (Fig. 30 *a*).[65] The original rotaxane showed TON of 195 for ethane oxidation by hydrogen peroxide (60 °C, 24 h), whereas supramolecular assemblies Cu(**23**) and Ni(**23**) formed by rotaxane with copper and nickel *meso*-tetrakis(4-sulfophenyl)porphyrin complexes (MTSPP) had TONs of 376 and 394 respectively (see Fig. 30 *a*,*b*). These values surpass those found for iron μ-nitridobis(tetra-*tert*-butylphthalocyanine) (TON = 289), which reported earlier to be the most efficient catalyst for this reaction.[66] An electrochemical study showed that the interaction of rotaxane with porphyrin M(**23**) leads to a decrease in the oxidation potential of the complex. This indicates the electron-donating nature of MTSPP with respect to rotaxane, and the enhanced catalytic activity is presumably due to facilitation of the heterolytic cleavage of the O – O bond in hydroperoxy complex **A** to form the highly reactive oxo complex **B** (see Fig. 30 *c*).

Thus, the presented results demonstrate a great potential of tetrapyrrole compounds as components of supramolecular materials. Prospects for the development of this research area include the molecular design of novel macrocycles and their complexes, development of synthetic approaches related to the preparation of compounds with desired properties, and investigation of supramolecular assembly processes that determine the architecture and properties of the resulting assemblies. Each of these stages contributes to the development of all fields of modern chemistry, and the functional diversity of the resulting materials includes both biomimetic systems (catalysts and photosensitizers) and

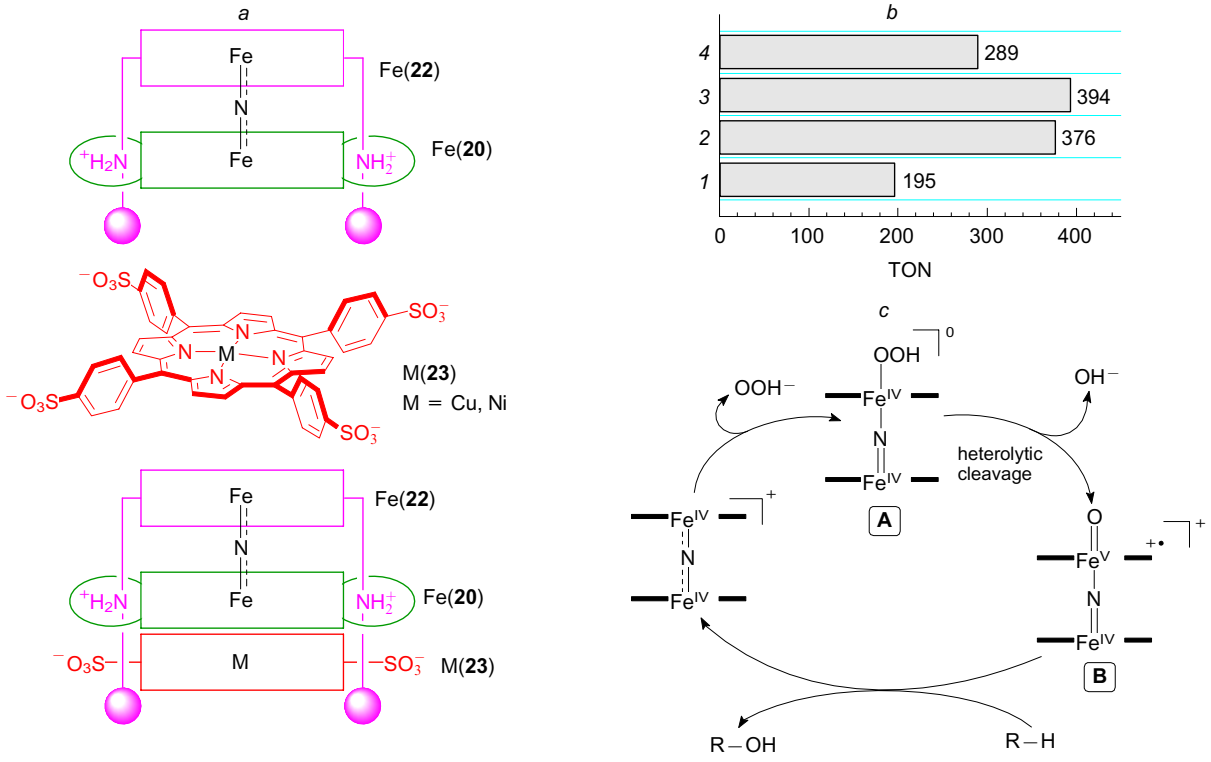


Figure 30. Scheme of fabrication of a trinuclear supramolecular assembly based on ionic interaction between cationic rotaxane [Fe(**20**)·(μ-N)·Fe(**22**)] and anionic complexes M(**23**) (*a*); characteristics of various catalytic systems for the oxidation of ethane with hydrogen peroxide (60 °C, 24 h): rotaxane [Fe(**20**)·(μ-N)·Fe(**22**)] (*1*), rotaxane + Cu(**23**) (*2*), rotaxane + Ni(**23**) (*3*) and $[Bu^t_4PcFe]_2$(μ-N) (*4*) (*b*); schematic mechanism of oxidation of organic substrates by hydrogen peroxide with the participation of μ-nitride complexes of diiron with tetrapyrrole ligands (*c*). The figure was created by the authors using data of Refs 65, 66.

assemblies that exhibit properties not found in nature, such as molecular magnetism and optical confinement. Finally, the molecular recognition underlying the supramolecular assembly of tetrapyrroles enables the development of highly selective sensor systems and smart materials.

2.2. Functional supramolecular coordination cages

Coordination cages, metal-organic cages (MOCs), metal-organic capsules or metal-organic polyhedra (MOPs) are hollow supramolecular discrete structures of hybrid nature, formed as a result of interaction of organic ligands containing at least two sites for coordination to metal cations or to metal complexes that have vacancies in the coordination sphere. Coordination cages differ from their extended structural analogues, coordination polymers, or metal-organic frameworks (MOFs), which are also formed as a result of binding of metal atoms to organic linkers giving periodic structures of different dimensionality (1D–3D) in the crystalline phase, by the presence of a limited number of pores and solubility with preservation of the coordination motif, which opens up additional opportunities for practical applications.[67,68]

Over the last decades, a large number of MOPs have been synthesized and studied, which made it possible to reveal the main regularities of their formation[69] and to formulate the main design principles of these supramolecular architectures[70] in order to obtain new functional and multifunctional materials with targeted properties. Direct control over the size and nature of the pores can be achieved by rational selection of appropriate molecular building blocks, *i.e.*, ligands and the metal cation (metal connecting node).[71] It was found that the ability of MOPs to selectively bind certain substrates, guest molecules, depends on their constituent components. As a result of research, great successes have been achieved in the preparation of various MOPs, which have found application in the catalysis of chemical reactions,[72–79] adsorption,[80–82] separation,[83] storage,[84] transport and delivery of drug molecules[85,86] and anticancer therapy,[87,88] as well as in the development of sensor materials.[89]

This Section addresses current trends in MOP design with the aim of obtaining new functional materials.

2.2.1. Main approaches to the fabrication of functional metal-organic polyhedra

It is known that the properties of any material are determined by the nature of its constituent components and by the spatial arrangement of these components relative to each other within the material. In this regard, the methods of supramolecular chemistry as a science that studies the processes of self-organization of molecules at the nanoscale represent an effective modern tools for solving various applied problems, in particular, owing to the development of sequential self-assembly of molecules according to the bottom-up approach with a built-in recognition programme. This gives rise to smart materials with unique properties due to control over the spatial organization of molecules.

Several basic approaches to the targeted design of homoleptic (consisting of ligands of the same type) and heteroleptic (consisting of ligands of different types) MOPs have been developed as a result of studying the self-organization of supramolecular systems.[90] The formation of structures with different topologies depends on the arrangement of binding centres in both organic (ligand) and inorganic (metal cation, metal complex) complementary molecular building blocks.

Various methods for the synthesis of functional MOPs based on different types of molecular recognition between certain functional groups and metal centres have been described in the literature.[91] There are known MOPs that have been obtained by combining one metal cation with a rigid coordination sphere and complex metal ligands containing another type of metal. This approach was utilized to prepare novel heterometallic coordination cages.[92] The use of ligands and metal complexes based on cavitands such as calix[4]arenes,[93] calix[4]resorcinarenes[94–97] and pyrogallol[4]arenes[98,99] displaying a pre-organized macrocyclic structure, served for studying the regularities of formation of macrocyclic coordination cages and coordination polymers based on them.[100–105]

The data available from the literature on the formation of the most common motifs of homometallic coordination cages (and their complexes) based on spatially pre-organized acyclic structurally rigid (aromatic) polytopic ligands are analyzed below. Such ligands contain several (two to four) homogeneous coordination sites that participate in the molecular recognition with metal cations due to their mutual complementarity in terms of spatial and electronic factors. The selected models of molecular self-assembly of coordination cages are classified according to increasing coordination capacity of ligands containing monodentate or bidentate (chelating) coordination sites and metal centres (metal connecting nodes).

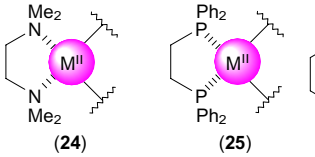
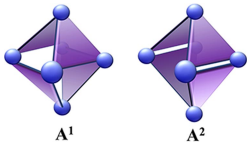
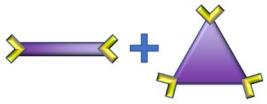
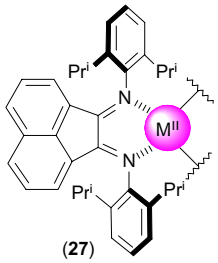
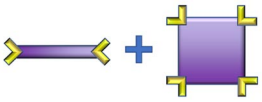
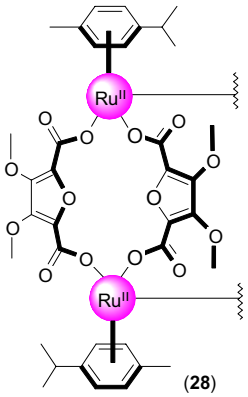
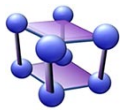
2.2.2. Cages based on V-shaped metallic connecting nodes and polytopic ligands with monodentate coordination sites

One of the first types of molecular recognition forming the basis for a large number of coordination cages was the interaction of cations (metal complexes) that have two (angular, or V-shaped metal connecting node) or four (tetragonal metal connecting node) vacant sites for coordination to ligands containing monodentate coordination sites (Table 1) in their coordination sphere. The V-shaped metal connecting nodes usually include cations with a square or octahedral coordination sphere (Pd^{2+}, Pt^{2+}, Ru^{2+}, Ir^{2+}, Rh^{2+}). In this sphere, two or four sites are occupied by bidentate chelating co-ligands coordinated in the *cis*-position (ethylene-1,2-diamine, ethylene-1,2-diphosphine, cyclohexane-1,2-diamine, 2,2′-dipyridine, *etc.*), while the remaining two (or four) sites in the coordination sphere are available for coordination of other ligands (Fig. 31). By combining V-type metal connecting nodes **24**–**28** with three or four monodentate ligands, usually having a rigid structure (angular, trigonal or tetragonal geometry, respectively), and pyridyl- or imidazolyl-containing ligands, one can generate coordination cages of different geometries.

One of the first coordination cages was obtained using intermolecular recognition of this type: interaction of tri(4-pyridyl)triazine **29** with metal connecting node **24** afforded cationic octahedral structure $[(\mathbf{24})_6\text{-}(\mathbf{29})_4]^{12+}$ (type $\mathbf{A}^1$, see Table 1) (Fig. 32). This electron-deficient structure was subsequently used to adsorb water molecules, nitrate ions and perfluorinated hydrocarbon molecules.[106] The size of the inner cavity can be characterized by the distance between the palladium atoms at the opposite vertices of the octahedron: $d_{Pd-Pd} = 18.8$ Å.

Other ways of obtaining similar cages based on ligand **29** with various metal connecting nodes to fabricate new functional materials have also been described in the literature. In

Table 1. Geometry of the coordination cage based on V-shaped (angular) metal connecting nodes and polytopic ligands with monodentate binding sites.[106–113]

Cage type	Ligand geometry	V-shaped metal connecting node	Coordination cage geometry
A			
B			
C			

Note. Here and in Tables 2–5, the yellow and red triangles denote the complementary binding sites of the ligand and the metal connecting node. Tildes in structures **24**–**27** show the attachment site of the binding polytopic ligands.

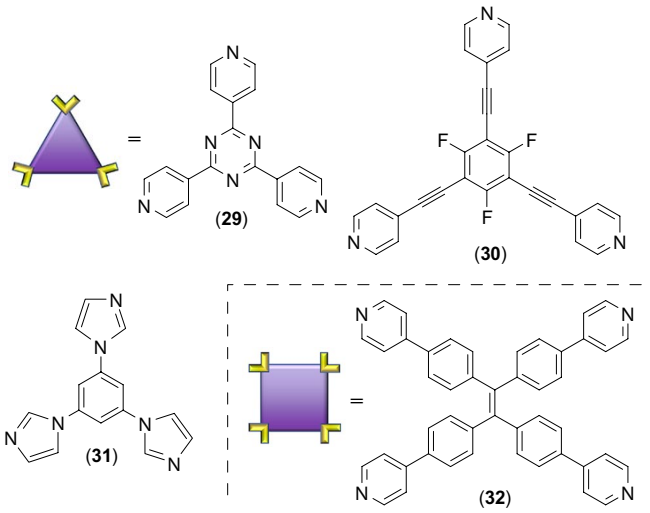


Figure 31. Examples of tri- and tetrasubstituted monodentate ligands **29**–**32** used to produce coordination cages with V-shaped metal connecting nodes. The figure was created by the authors using data of Refs 106–113.

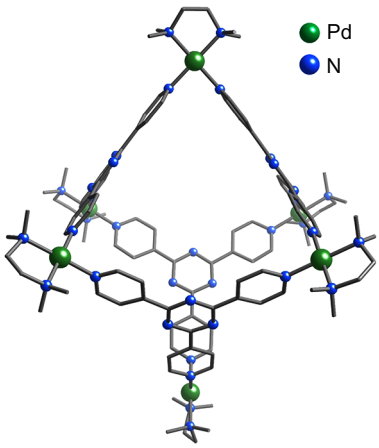


Figure 32. Crystal structure of the cationic octahedral coordination cage $[(\mathbf{24})_6\text{-}(\mathbf{29})_4]^{12+}$. The figure was created by the authors using Cambridge Crystallographic Data Centre and data of Ref. 106.

particular, mention should be made of redox-active cage $[(\mathbf{27})_6\text{-}(\mathbf{29})_4]^{12+}$ (type $\mathbf{A}^1$, see Table 1) with a potential between 0 and −2 V, which was obtained from complex **27** as the V-shaped metal connecting node. This system is of interest as a promising electron-switchable supramolecular container in an organic medium for binding–release processes of various substrates.[107]

A similar supramolecular structure was obtained from 1,3,5tris(4-pyridylethynyl)trifluorobenzene **30** and complex **25**. Compared with cage $[(\mathbf{24})_6\text{-}(\mathbf{29})_4]^{12+}$, the analogue $[(\mathbf{25})_6\text{-}(\mathbf{30})_4]^{12+}$ (type $\mathbf{A}^1$, see Table 1) (Fig. 33), as expected, had a larger inner cavity (d_{Pd-Pd} = 24.1 Å). This fact demonstrates the possibility of controlling the size of the inner cavity of the cage by varying the ligand used to bind certain guest molecules.[108]

Using 4,4′-bipyridine (bpy) as a co-ligand, cationic cage $[(\mathbf{26})_6\text{-}(\mathbf{29})_2(bpy)_3]^{12+}$ (Fig. 34) was obtained as a trigonal prism (type **B**, see Table 1). In this structure, two parallel faces, represented by molecules **29** coordinated to the metal centre of complex **26**, were spatially separated by three 4,4′-bipyridine molecules due to interaction at the second vacant site in the metal coordination sphere. This cage was successfully used for the selective recognition of mononucleotides in an aqueous medium and for the synthesis of dinucleotides.[109] In addition, a similar cage based on the tetramethyl derivative of 4,4′-bipyridine, ligand **29** and complex 1,2-ethylenediamine-coordinated Pd^{II} cations was used for the formation of an inclusion complex of naph-

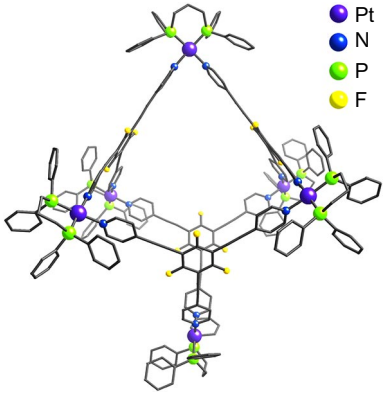


Figure 33. Crystal structure of the cationic octahedral coordination cage $[(\mathbf{25})_6\text{-}(\mathbf{30})_4]^{12+}$. The figure was created by the authors using Cambridge Crystallographic Data Centre and data of Ref. 108.

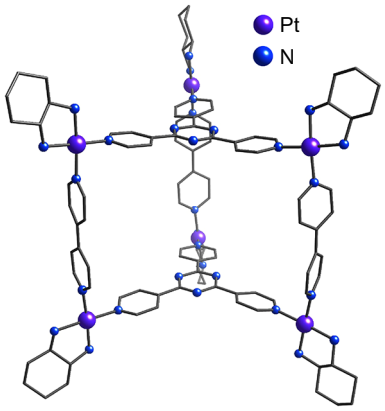


Figure 34. Crystal structure of the cationic octahedral coordination cage $[(\mathbf{26})_6\text{-}(\mathbf{29})_2(\text{bpy})_3]^{12+}$. The figure was created by the authors using Cambridge Crystallographic Data Centre and data of Ref. 109.

thalene diimide with corannulene, which was accompanied by flattening of the bowl-like structure of the latter.[110]

Coordination cages are easily formed when the pyridine ligands are replaced with molecules containing imidazole binding groups. Thus, an octahedral supramolecular structure of type $\mathbf{A}^2$ (see Table 1) was obtained *via* molecular recognition of the tris(imidazole) derivative **31** and complex **24**. The cage $[(\mathbf{24})_6\text{-}(\mathbf{31})_4]^{12+}$ (Fig. 35) is more flexible than $[(\mathbf{24})_6\text{-}(\mathbf{29})_4]^{12+}$, which makes it adaptable to binding of particular substrates. For example, it was shown that this cage is capable of accomodating molecules of photosensitive compounds such as azobenzene and a spiropyran derivative, which can be reversibly uptaken and released from the cage surface under the action of light; this was used for the design of data storage media.[111, 112]

Using this method of molecular recognition, it s possible to obtain, apart from octahedral structures, neutral coordi-

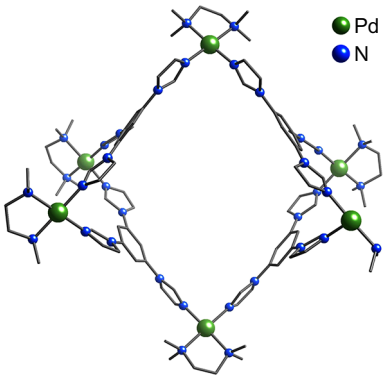


Figure 35. Crystal structure of the cationic octahedral coordination cage $[(\mathbf{24})_6\text{-}(\mathbf{31})_4]^{12+}$. The figure was created by the authors using Cambridge Crystallographic Data Centre and data of Ref. 111.

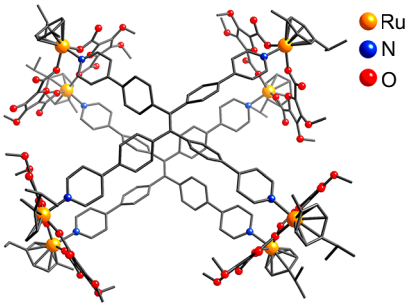


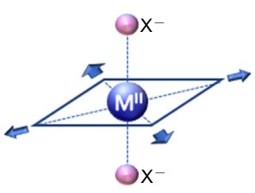
Figure 36. Crystal structure of neutral cubic coordination cage $[(\mathbf{28})_4\text{-}(\mathbf{32})_2]$. The figure was created by the authors using Cambridge Crystallographic Data Centre and data of Ref. 113.

nation cage $[(\mathbf{28})_4\text{-}(\mathbf{32})_2]$ (Fig. 36) with a cubic geometry (type **C**, see Table 1). This was demonstrated for metal complex **28** and tetragonal planar tetrasubstituted monodentate organic linker **32** containing four pyridine moieties. It should be noted that complex **28**, used as a metallic bis-connecting node, was prepared in advance by the reaction of $[(\text{cymene})\text{RuCl}_2]_2$ (cymene is 4-isopropyltoluene) with 3,4-dimethoxyfuran-2,5-dicarboxylate. Crystallization experiments carried out in various solvents showed that cage $[(\mathbf{28})_4\text{-}(\mathbf{32})_2]$ is converted to dimer $[(\mathbf{28})_2\text{-}(\mathbf{32})]$ upon recrystallization from a solution.[113]

2.2.3. Cages based on tetragonal metal connecting nodes and polytopic ligands with monodentate coordination sites

One more method of obtaining cages based on polytopic monodentate ligands is based on molecular recognition between cage-forming monodentate ligands and metal cations with a characteristic square coordination sphere (Pd^{II}, Pt^{II}) in which all four sites are free for coordination or octahedral cations in which two coordination sites in the *trans* position are occupied by solvent molecules or anions (Table 2). By varying the geometry of the monodentate

Table 2. Geometry of coordination cage based on tetragonal metal connecting nodes and polytopic ligands with monodentate binding sites.[114–121]

Cage type	Ligand geometry	Geometry of the tetragonal metal connecting node	Coordination cage geometry
			
A		 M = Pd, Pt	
B		 M = Pd, Pt  M = Cu; X = Cl, Br, OH	

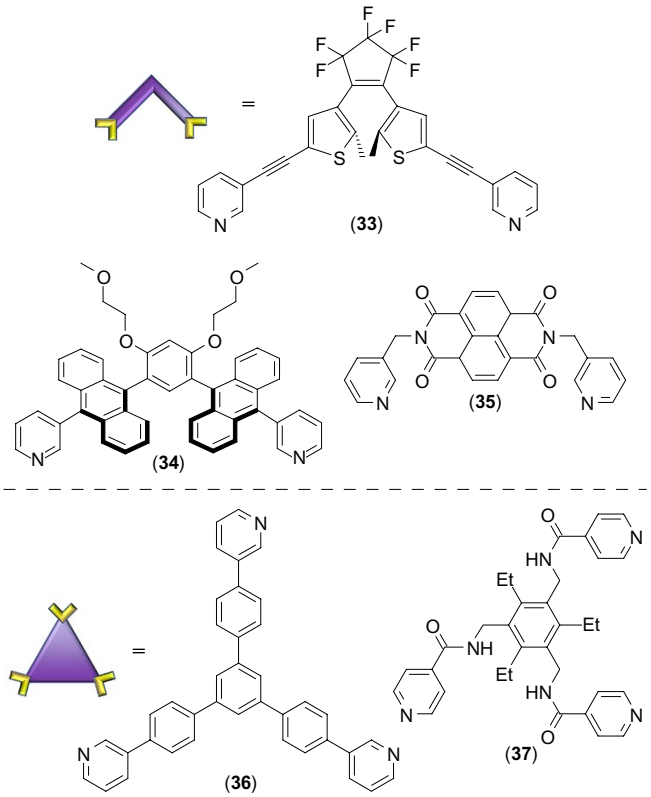


Figure 37. Examples of angular (**33**, **34**, **35**) and trisubstituted (**36**, **37**) monodentate ligands used to obtain coordination cages with tetragonal metal connecting nodes. The figure was created by the authors using data of Refs 114–121.

binding sites of the ligand (Fig. 37) and the type of tetragonal planar metal connecting node, it is possible to obtain dimeric, octahedral and cuboctahedral coordination cages.

The coordination of Pd^{II} to bis(3-pyridylethynyl) ligand **33**, which is capable of reversible photoisomerization under the action of light owing to the bis(thienyl)ethene moiety, leads to the cationic cage $[Pd_2^{II}\text{-}(\mathbf{33})_4]^{4+}$ (Fig. 38) of a capsular dimeric structure (type **A**, see Table 2). This cage can be used for controlled binding and release of guest molecules.This was demonstrated, in particular, in relation to photocontrolled adsorption–desorption of the spherical $[B_{12}F_{12}]^{2-}$ anion.[114, 115]

Molecular recognition between molecules containing polyaromatic substituents and pyridyl binding sites and palladium(II) cations afforded coordination cages. The cages were used for the adsorption of aromatic pigments

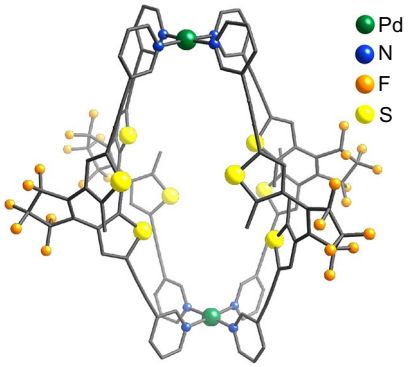


Figure 38. Crystal structure of the cationic dimeric coordination cage $[Pd_2^{II}\text{-}(\mathbf{33})_4]^{4+}$. The figure was created by the authors using the Cambridge Crystallographic Data Centre and data of Ref. 114.

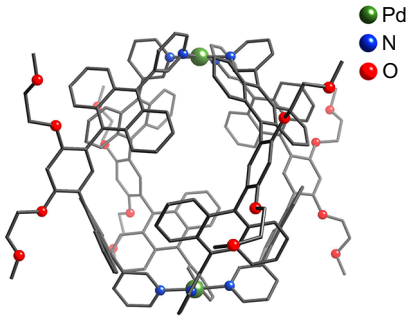


Figure 39. Crystal structure of the cationic dimeric coordination cage $[Pd_2^{II}\text{-}(\mathbf{34})_4]^{4+}$. The figure was created by the authors using the Cambridge Crystallographic Data Centre and data of Ref. 116.

and dyes from water, which is a relevant problem related to environmental protection.[81] Cages with anthracene moieties, for example $[Pd_2^{II}\text{-}(\mathbf{34})_4]^{4+}$ (type **A**, see Table 2) (Fig. 39) are capable of luminescent response depending on the guest adsorbed in their cavity. The presence of coumarin molecules leads to increase in the fluorescence of this system.[116, 117] In addition, this system was used as a matrix for MALDI-TOF mass spectrometry experiments for the detection of single sulfur clusters $[S_6]$, $[S_8]$ and $[S_{12}]$.[118]

When naphthalene diimide derivative **35** acts as a V-shaped cage-forming dipyridyl ligand, supramolecular cage $[Pd_2^{II}\text{-}(\mathbf{35})_4]^{4+}$ is obtained, which has a similar structural motif (type **A**, see Table 2). When dissolved in DMSO, it forms a gel and exhibits selective sensing activity towards pyrene and many anionic dyes (methylene blue and methyl orange).[119]

The reaction of Pd^{II} and Pt^{II} cations with tripyridyl derivative **36** with trigonal binding centres produced coordination cages $[M_6^{II}\text{-}(\mathbf{36})_8]^{12+}$(Fig. 40) of octahedral struc-

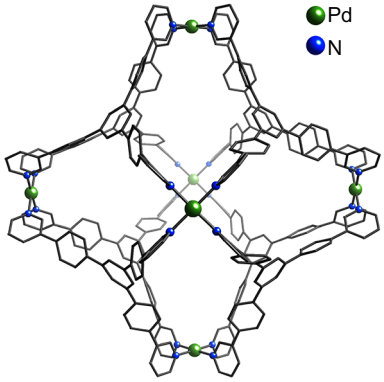


Figure 40. Crystal structure of the cationic dimeric octahedral coordination cage $[Pd_6^{II}\text{-}(\mathbf{36})_8]^{12+}$. The figure was created by the authors using the Cambridge Crystallographic Data Centre and data of Ref. 120.

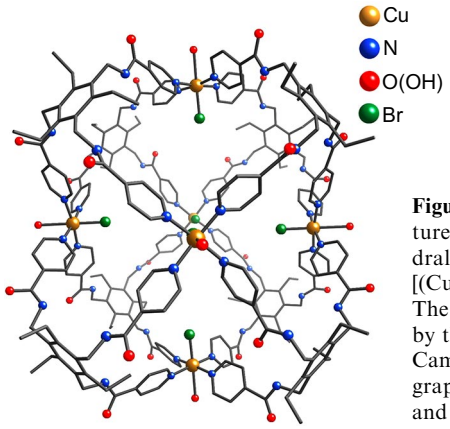


Figure 41. Crystal structure of neutral octahedral coordination cage $[(Cu^{II}(OH)Br)_6\text{-}(\mathbf{37})_8]$. The figure was created by the authors using the Cambridge Crystallographic Data Centre and data of Ref. 121.

ture (type **B**, see Table 2). These cages were used for binding to neutral aromatic molecules such as anthracene, pyrene and 1,8-naphthalimide. They are also able to bind selectively to the anionic guest, *p*-toluenesulfonate, due to spatial complementarity.[120]

Neutral coordination cage $[(Cu^{II}(OH)Br)_6\text{-}(\mathbf{37})_8]$ (Fig. 41) of octahedral shape (type **B**, see Table 2), in which the octahedral Cu^{II} cation acts as a square metal connecting node, was obtained using a relatively flexible tridentate ligand based on tripyridyl derivative **37**. The resulting cage was found to form smart multifunctional vesicles and to participate in controlled delivery of anticancer drugs, such as doxorubicin (DOX), to living cells. Control of the drug release from the vesicle can be achieved by switching the pH of the medium. In addition, these vesicles have demonstrated high stability in biological media, allowing them to be used as biomembrane models.[121]

2.2.4. Cages based on V-shaped and trigonal metal connecting nodes and polytopic ligands with chelating sites

Coordination cages obtained *via* complementary intermolecular interaction of this type can be divided into two groups, depending on the number of metal cations in the metal centres: mononuclear and polynuclear ones.

Cages with mononuclear metal connecting nodes provide recognition between ligands having two, three or four terminally located chelating moieties and transition metal cations, usually $Fe^{II/III}$, Co^{II}, Zn^{II}, Ga^{IV}, Sn^{IV}, Ti^{IV}, with an octahedral coordination sphere. This results in the formation of either a trigonal metal binding centre (upon reaction with bidentate functional groups) or a V-shaped metal connecting node (when a tridentate chelating moiety is used by the ligand to bind to a metal) (Table 3). Ligands with N-donor centres, such as Schiff bases, bipyridyl or similar bidentate moieties, can then act as chelates (Fig. 42). Among chelating ligands containing O-donor cavities, catechols are most encountered. Mixed-type chelating cavities containing both O- and N-donor atoms have also been described in the literature.[122] Thus, depending on the number and geometry (linear, V-shaped, trigonal or tetragonal) of the chelating cavities they have, ligand molecules can form a dimeric, tetrahedral or cubic coordination cage upon interaction with a trigonal metal connecting node. It should be noted that due to the chelating type of ligand binding to the metal cation possessing octahedral geometry, both D and L enantiomers can be formed (Fig. 43).[123, 124]

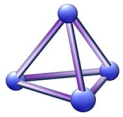
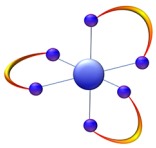
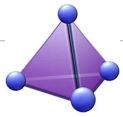
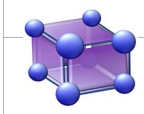
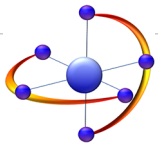
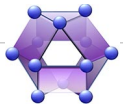
For ligands **38** and **40**, containing two and three catechol chelating moiety, respectively, anionic tetrahedral coordination cages $[M^{IV}_4\text{-}(\mathbf{38})_6]^{8-}$ (Fig. 44) and $[M^{IV}_4\text{-}(\mathbf{40})_4]^{8-}$ were obtained (Fig. 45), in which hard octahedral cations M^{IV} = Ga, Ti, Sn were used as the metal coordination centres. Whereas in the cages formed by dicatechol derivative **38**, organic ligands are located along the edges of tetrahedra (type **A**, see Table 3),[125, 126] in the supramolecular structure based on ligand **40** with a rigid trigonal arrangement of catechol binding sites, organic moieties of the cage occupy the positions of faces of the supramolecular tetrahedron (type **C**, see Table 3).[127] It was shown that such hollow structures can act as catalysts for organic reactions,[73] in particular, the cage $[Ga^{IV}_4\text{-}(\mathbf{38})_6]^{8-}$ accelerates the formation of a C–C single bond in the reductive elimination (cross-coupling reaction) taking place in the coordination sphere of gold cations.[125]

The coordination cages of the cationic type were obtained using ligands containing N-donor chelating moieties. The most common examples of coordination cages reported in the literature are systems constructed using molecular recognition between ligands with pyridine pyrazolyl coordination sites. For example, ligand **39a** in combination with Co^{II} cations forms cage $[Co^{II}_8\text{-}(\mathbf{39a})_{12}]^{16+}$ (Fig. 46) of cubic geometry (type **B**, see Table 3), which showed catalytic properties in the Kemp elimination reaction (synthesis of cyanophenolates from benzoxazoles).[128] It should be noted that the hydrophobic cavity of the cubic cage $[Co^{II}_8\text{-}(\mathbf{39a})_{12}]^{16+}$ demonstrated selective adsorption properties towards carbon dioxide in the presence of nitrogen,[129] as well as towards alkylphosphonates[130] and isoquinoline N-oxide.[131]

At the same time, Piper *et al.*[132] found that a similar cage $[Cd^{II}_8\text{-}(\mathbf{39b})_{12}]^{16+}$ is able to provide photoelectron charge transfer from naphthalene substituents to the guests adsorbed inside the cavity, which can be used in photocatalysis. In addition, the possibility of obtaining isostructural cages $[M^{II}_8\text{-}(\mathbf{39b})_{12}]^{16+}$ (type **B**, see Table 3) with different metal cations (M = Ru, Os), meant for enhancing the photoadsorption properties and consequently improving the photoelectron transfer function, was shown.

Upon the interaction of ligand **41**, which has a trigonal arrangement of dipyridyl coordinating moieties, with Fe^{II} cations, coordination cage $[Fe^{II}_4\text{-}(\mathbf{41})_4]^{8+}$ of tetrahedral geometry (type **C**, Table 3) was obtained. It exhibits distinct electron-deficient properties, which was utilized for selective binding of the triflate anion (triflate is trifluoromethanesul-

Table 3. Geometry of the coordination cage formed by trigonal and linear metal connecting nodes and polytopic ligands with bidentate and tridentate chelating binding sites.[122–138]

Cage type	Ligand geometry	Trigonal metal connecting node	Coordination cage geometry
			
A			
B			
C		 $Fe^{II/III}$, Co^{II}, Zn^{II}, Ga^{IV}, Sn^{IV}, Ti^{IV}	
D			
E		 Co^{II}	

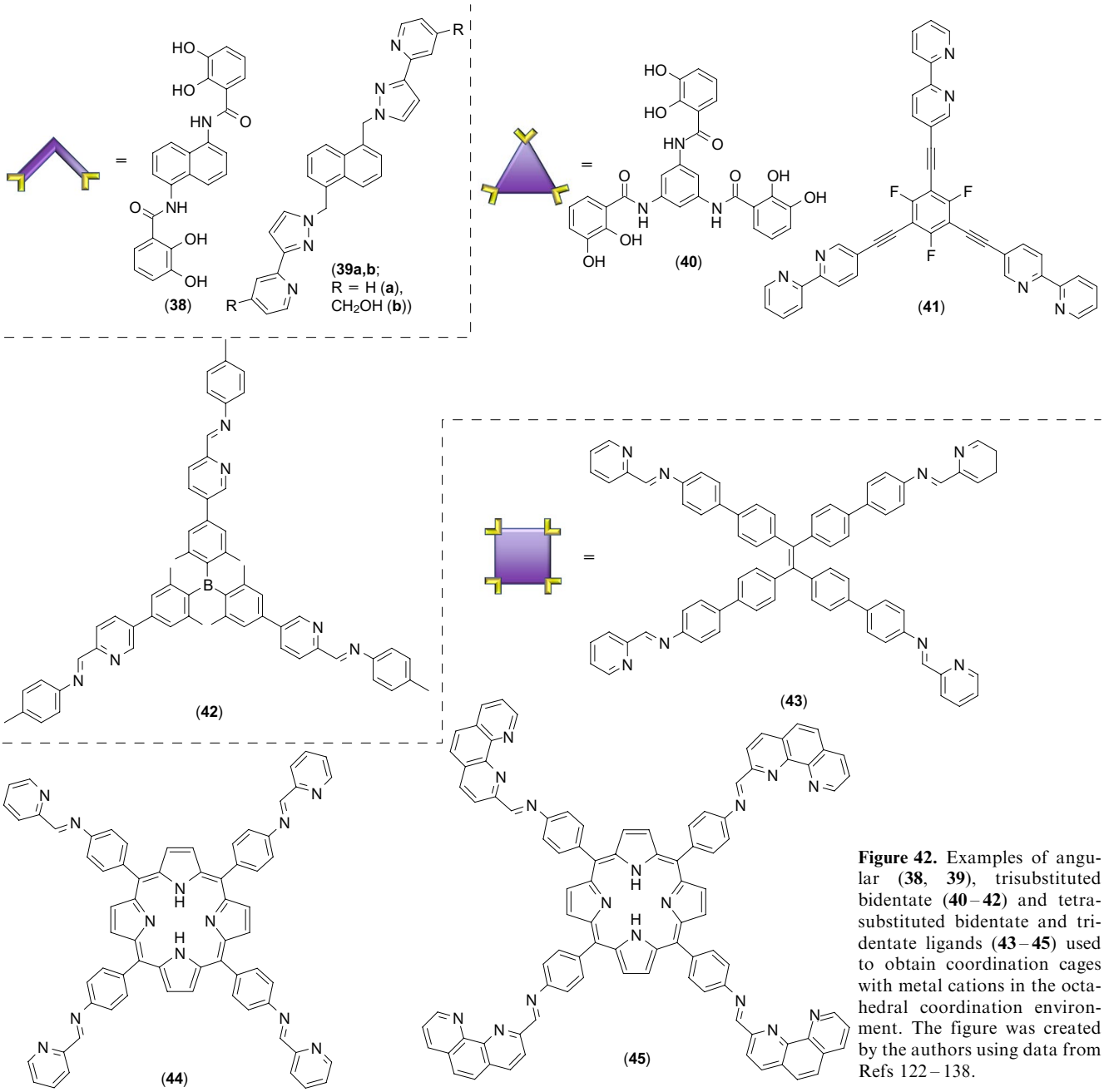


Figure 42. Examples of angular (**38**, **39**), trisubstituted bidentate (**40**–**42**) and tetrasubstituted bidentate and tridentate ligands (**43**–**45**) used to obtain coordination cages with metal cations in the octahedral coordination environment. The figure was created by the authors using data from Refs 122–138.

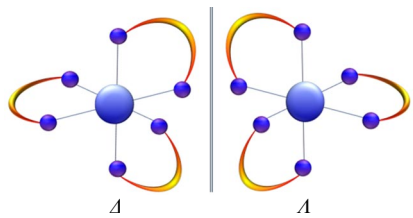


Figure 43. Formation of two enantiomers in the case of chelate complexes of M^{n+} metal cations in the octahedral coordination environment.

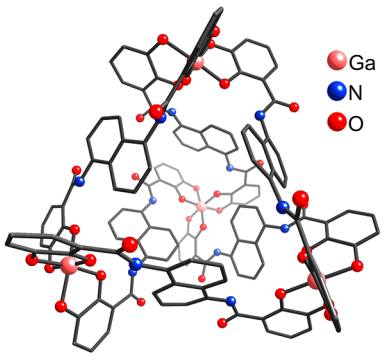


Figure 44. Crystal structure of the anionic tetrahedral coordination cage $[Ga_4^{IV}\text{-}(\mathbf{38})_6]^{8-}$. The figure was created by the authors using the Cambridge Crystallographic Data Centre and data of Ref. 125.

fonate). In addition, such systems are capable of adsorbing polyaromatic contaminants from aqueous media.[81] Importantly, many Fe^{II}-based cages demonstrate spin-crossover properties.[134]

Another effective and common recognition model used to produce coordination cages is the interaction of octahedral cations with bidentate N-donor groups (analogues of dipyridyl and pyridyl pyrazolyl moieties) that contain iminopyridyl binding sites (pyridine Schiff bases). The advantages of this approach include the ease of formation of such functional groups *in situ* and the ability to design

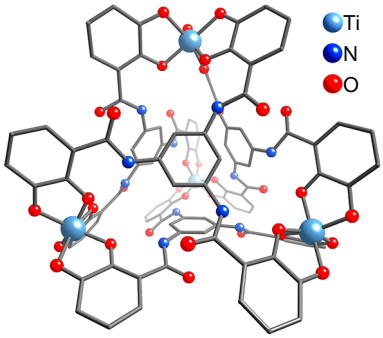


Figure 45. Crystal structure of the anionic tetrahedral coordination cage $[Ti_4^{IV}\text{-}(\mathbf{40})_4]^{8-}$. The figure was created by the authors using the Cambridge Crystallographic Data Centre and data of Ref. 127.

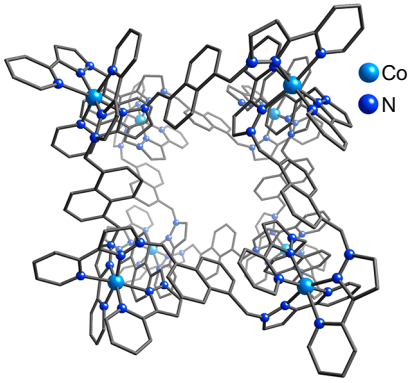


Figure 46. Crystal structure of the cationic cubic coordination cage $[Co_8^{II}\text{-}(\mathbf{39a})_{12}]^{16+}$. The figure was created by the authors using the Cambridge Crystallographic Data Centre and data of Ref. 128.

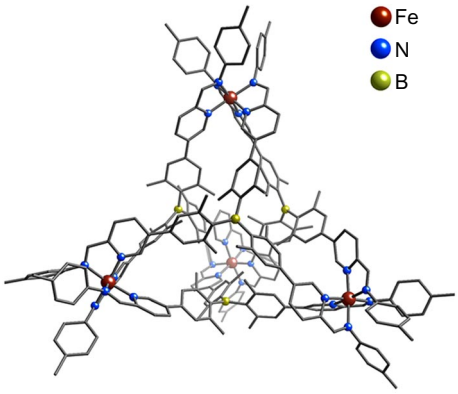


Figure 47. Crystal structure of the cationic tetrahedral coordination cage $[Fe_4^{II}\text{-}(\mathbf{42})_4]^{8+}$. The figure was created by the authors using the Cambridge Crystallographic Data Centre and data of Ref. 135.

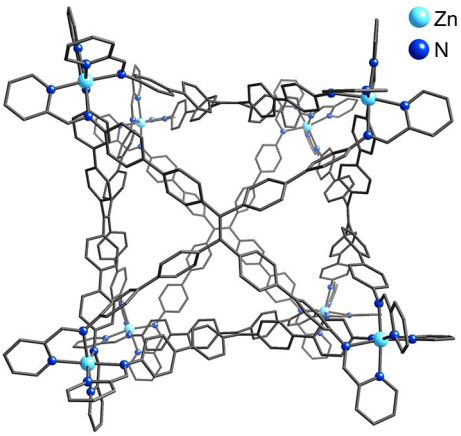


Figure 48. Crystal structure of the cationic cubic coordination cage $[Zn_8^{II}\text{-}(\mathbf{43})_6]^{16+}$. The figure was created by the authors using the Cambridge Crystallographic Data Centre and data of Ref. 136.

supramolecular cages by varying both the amine and aldehyde components.

Compound **42**, containing three iminopyridyl groups and an electron-deficient boron atom, was shown to be an excellent cage-forming ligand. It reacts with Fe^{II} cations to give cage $[Fe_4^{II}\text{-}(\mathbf{42})_4]^{8+}$ (Fig. 47) with tetrahedral structure (type **C**, see Table 3) capable of selective binding of fluoride anions.[135]

The use of ligand **43**, which has a rigid structure with a tetragonal arrangement of iminopyridyl coordinating moieties, and Zn^{II} cations yielded supramolecular cage $[Zn_8^{II}\text{-}(\mathbf{43})_6]^{16+}$ (Fig. 48), which has a cubic geometry (type **D**, see Table 3). Owing to CH–π and hydrophobic interactions, this structure is able to effectively encapsulate anthranilamides and aromatic aldehydes, as well as to accelerate successive condensation–amino addition reactions of guests adsorbed in the cavity of the cage with participation of 2,3-dihydroquinazolinone.[136]

In addition, similar cubic cages were synthesized by using porphyrin **44** and its complexes with Ni^{II} and Zn^{II} as building blocks. In this case, Fe^{II} cations behaved as metal connecting nodes. The hollow positively charged structures $[Fe_8^{II}\text{-}(\mathbf{44})_6]^{16+}$, enclosed by electron-rich porphyrin moieties, demonstrated high selective adsorption capacity towards polyaromatic guests, such as coronene and higher fullerenes (C_{70}–C_{84}).[138]

An excellent result was obtained in the formation of coordination cages using tridentate iminophenanthrolyl binding sites located at the terminal positions of *meso*-substituents in porphyrin **45**. The interaction of compound **45** with zinc(II) cations gives a pseudo-cuboctahedral coordination cage $[Zn_{12}^{II}\text{-}(\mathbf{45})_6]^{24+}$ (Fig. 49) (type **E**, see Table 3). In this cage, metal atoms act as V-shaped (angular) metal connecting nodes, which are coordinated to two tridentate moieties of iminophenanthrolyl substituents incorporated in two adjacent porphyrin molecules **45**. A study of the receptor properties of the resulting cage demonstrated its affinity for fullerene molecules with efficient formation of stable 1 : 2 inclusion complexes. This cage was also found to bind various spherical anions $CB_{11}H_{12}^-$, BPh_4^- and $B_{12}F_{12}^{2-}$.[137]

Polynuclear species can be considered as one more example of trigonal metal connecting nodes that have been used to prepare MOPs with polytopic ligands containing chelating groups. In particular, it was shown that the complex $Cp_2Zr^{IV}Cl_2$ (Cp is cyclopentadienyl) is hydrolyzed

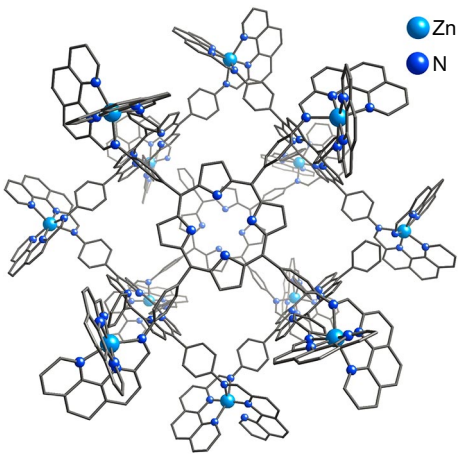


Figure 49. Crystal structure of the cationic cuboctahedral coordination cage $[Zn_{12}^{II}\text{-}(\mathbf{45})_6]^{24+}$. The figure was created by the authors using the Cambridge Crystallographic Data Centre and data of Ref. 137.

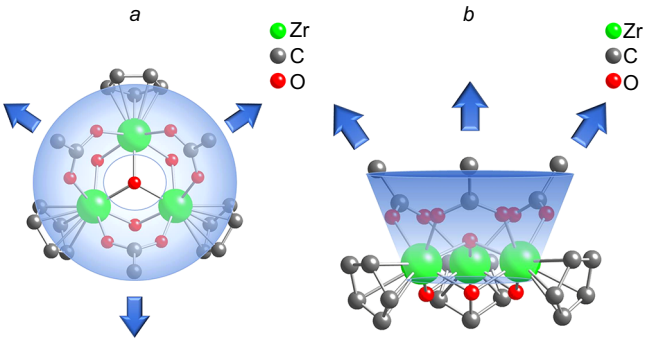


Figure 50. Structure of the cone-shaped trigonal building block $[Cp_3Zr_3^{IV}(\mu^3\text{-}H_2O)(\mu^2\text{-}O)_3]^{3+}$: top view (*a*) and side view (*b*). The figure was created by the authors using the Cambridge Crystallographic Data Centre and data of Ref. 139.

in situ in the presence of carboxylates to give triuclear cluster $[Cp_3Zr_3^{IV}(\mu^3\text{-}H_2O)(\mu^2\text{-}O)_3]^{3+}$ (denoted by $[Zr_3]^{3+}$), in which three carboxy groups point outwards, thus forming a conical trigonal metal connecting node (Fig. 50).[139] As the organic counterparts, dicarboxyl ligands are often used (Fig. 51), leading to the formation of capsular dimeric and tetrahedral coordination cages (Table 4).

One of the first coordination structures obtained by molecular recognition of this type was the neutral coordination cage $[(Zr_3)_4\text{-}(\mathbf{46})_6]$ (Fig. 52) with a tetrahedral geometry (type **A**, see Table 4).[139] This structure was subsequently modified by introducing amino groups into the edge positions of the cage involving 2-aminoterephthalic acid (**47**), resulting in the cage $[(Zr_3)_4\text{-}(\mathbf{47})_6]$ of a similar structure (type **A**, see Table 4). This cage was found to exhibit pronounced photocatalytic properties in the hydrogen evolution reactions.[140] Besides, the possibility of post-synthetic modification was demonstrated: two cages were cross-linked by the acylation reaction with a dicarboxylic acid chloride containing a flexible hydrocarbon spacer.[141] This gave a new polymeric material with a microporous structure. Thus, by covalent cross-linking of coordination cages, it is possible to design new materials with controlled porosity, and also to obtain new adsorbents with tunable properties by varying the building blocks (coordination cages and cross-linking reagents). Moreover, this strategy allowed the synthesis of a microporous polyfunctional hybrid membrane based on imine binding groups, which had water permeability and antibacterial properties.[142]

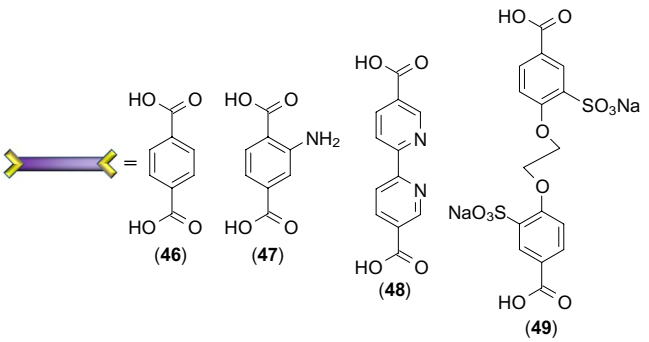


Figure 51. Examples of dicarboxylate ligands **46** – **49** used to obtain coordination cages with complex trigonal $[Zr_3]^{3+}$ connecting node. The figure was created by the authors using data of Refs 139 – 144.

Table 4. Geometry of the coordination cage based on $[Zr_3]^{3+}$ trigonal metal connecting nodes and linear ligands containing carboxyl binding sites.[139 – 144]

Cage type	Ligand geometry	Geometry of the complex trigonal metal connecting node	Coordination cage geometry
A		$[Zr_3]^{3+}$	
B			

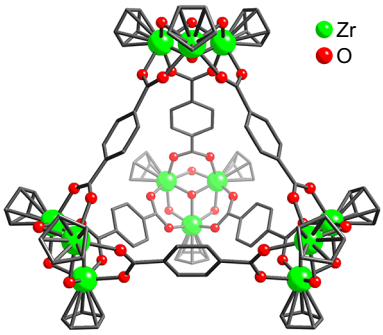


Figure 52. Crystal structure of the neutral tetrahedral coordination cage $[(Zr_3)_4\text{-}(\mathbf{46})_6]$. The figure was created by the authors using the Cambridge Crystallographic Data Centre and data of Ref. 139.

Another method of functionalization of cages of this type consists in the introduction of additional binding sites into the structure of the organic cage-forming ligand. Coordination cage $[(Zr_3)_4\text{-}(\mathbf{48})_6]$ of tetrahedral geometry (type **A**, see Table 4) has been obtained; the structure was based on dipyridine chelating moieties capable of coordination to d-element cations. The use of $Re(CO)_3Cl^+$ complex cations gave rise to nanoreactors, which were successfully used for photocatalytic reduction of carbon dioxide.[144]

Coordination capsules $[(Zr_3)_2\text{-}(\mathbf{49})_3]$ (Fig. 53) (type **B**, see Table 4) showed an interesting result in terms of selective adsorption and also proton conductivity. It was

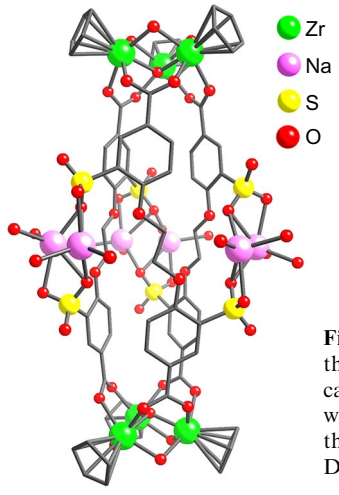


Figure 53. Crystal structure of the neutral dimeric coordination capsule $[(Zr_3)_2\text{-}(\mathbf{49})_3]$. The figure was created by the authors using the Cambridge Crystallographic Data Centre and data of Ref. 143.

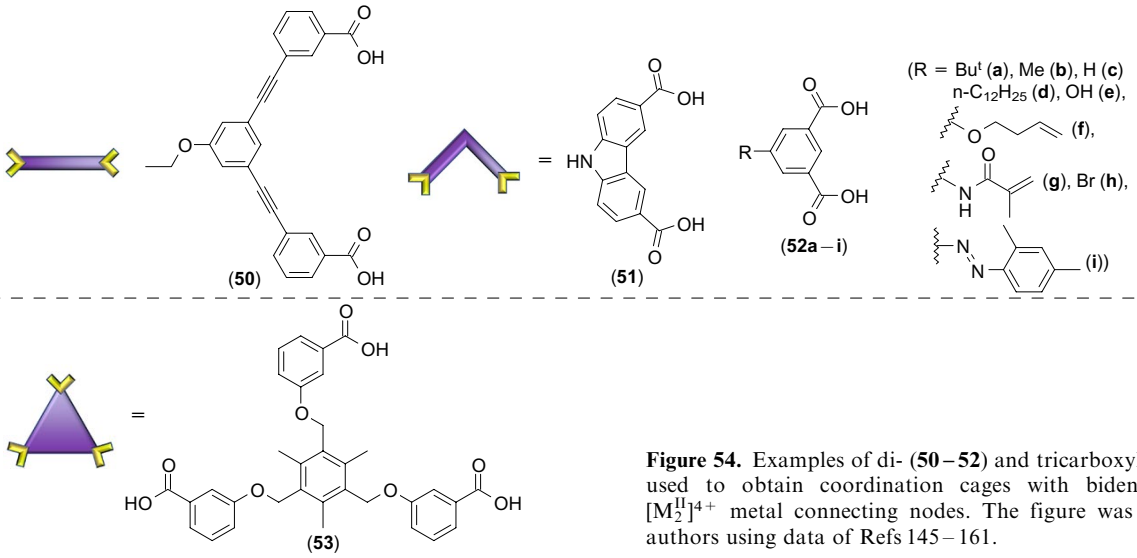


Figure 54. Examples of di- (**50 – 52**) and tricarboxylate ligands (**53**) used to obtain coordination cages with bidentate tetragonal $[M_2^{II}]^{4+}$ metal connecting nodes. The figure was created by the authors using data of Refs 145 – 161.

found that the above complexes are capable of selective binding of carbon dioxide in the presence of nitrogen and oxygen molecules; owing to the presence of sulfonate groups, they can adsorb a large number of water molecules (*via* hydrogen bonding) promoting proton conductivity.[143]

2.2.5. Cages based on bidentate tetragonal metal connecting nodes and polycarboxylic ligands

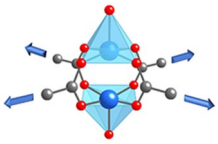
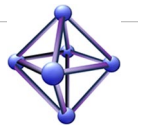
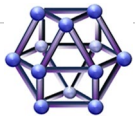
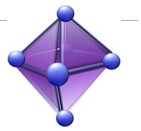
It was shown that in some cases, the interaction of d-element cations, such as Cr^{II}, Co^{II}, Fe^{II}, Cu^{II}, Mo^{II}, Rh^{II}, with carboxyl ligands under solvothermal conditions leads to bidentate tetragonal paddle wheel-like metal connecting nodes $[M_2^{II}]^{4+}$. They consist of two metal cations that are in a pentagonal pyramidal coordination sphere and are linked together at the base of the pyramids by four carboxylate groups of adjacent organic linkers (Fig. 54). A number of dimeric, octahedral and cuboctahedral coordination cages have been synthesized based on molecular recognition of this type (Table 5). Li *et al.*[145] analyzed the effect of the angle between the coordination sites of the V-shaped organic linker and its size on the volume and supramolecular motif of the resulting coordination cage.

It has been established that dimeric capsules (type **A**, see Table 5) were formed most often when the carboxylate sites of the ligands were located parallel to each other in the molecule. In particular, the reaction of ligand **50** with Cu^{II} cations gave neutral coordination capsule $[(Cu_2^{II})_2$-(**50**)$_4]$ (Fig. 55), capable of displaying the so-called gate opening effect. It consists in the proneness of a crystalline material to exhibit a strong cooperative increase in the adsorption capacity, accompanied by a reversible solid-phase transition in which the crystallinity is preserved. It was found that this dimeric coordination cage is indifferent with respect to adsorption of nitrogen molecules, but shows a gate opening effect in the case of CO_2, allowing the adsorption of 12 CO_2 molecules per molecule of the metal-organic complex in the crystalline phase.[146]

While coordination cages based on metal connecting nodes consisting of coordinatively unsaturated Cu^{II} cations exhibit adsorption properties towards carbon dioxide molecules, for octahedral $[(M_2^{II})_6$-(**51**)$_{12}]$ (M = Cu, Cr, Mo; type **B**, see Table 5 and Fig. 56)[147] and cuboctahedral systems $[(M_2^{II})_{12}$-(**52a**)$_{24}]$ (M = Cr, Mo, Ru; type **C**, see Table 5 and Fig. 57),[148] a pronounced affinity towards methane molecules was found. Moreover, the adsorption properties of the material were improved by binding the cuboctahedral cages $[(M_2^{II})_{12}$-(**52b**)$_{24}]$ (M = Fe, Co) *via* additional coordination of metal connecting nodes to 1,4-diazabicyclo[2.2.2]octane (DABCO), which resulted in coordinated cross-linked molecular cages.[148]

The cages of similar cuboctahedral structure $[(M_1^{II}M_2^{II})_{12}$-(**52a**)$_{24}]$ (type **C**, see Table 5) containing two types of d-elements (M_1 = Cu, Ni, Zn; M_2 = Pd) in the metal connecting node behave as efficient adsorbents for binding hydrogen molecules due to the presence of coor-

Table 5. Geometry of the coordination cage based on tetragonal binuclear metal connecting nodes and angular and trigonal ligands containing carboxyl binding sites.[145 – 161]

Cage type	Ligand geometry	Geometry of the complex trigonal metal connecting node	Coordination cage geometry
			
A		 $[M_2^{II}]^{4+}$ M = Cr, Co, Fe, Cu, Mo, Rh	
B			
C			
D			

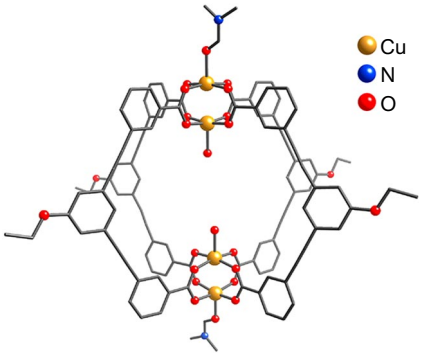


Figure 55. Crystal structure of the neutral coordination capsule $[(Cu_2^{II})_2$-(**50**)$_4]$. The figure was created by the authors using the Cambridge Crystallographic Data Centre and data of Ref. 146.

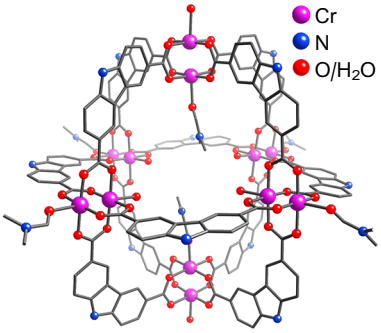


Figure 56. Crystal structure of the neutral octahedral coordination cage $[(Cr_2^{II})_6$-(**51**)$_{12}]$. The figure was created by the authors using the Cambridge Crystallographic Data Centre and data of Ref. 147.

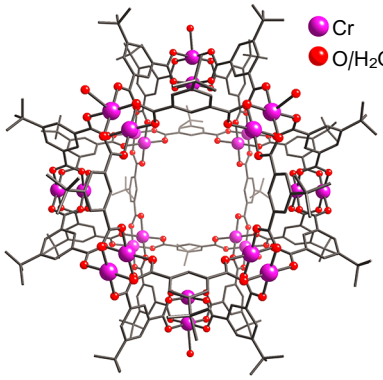


Figure 57. Crystal structure of the neutral cuboctahedral coordination cage $[(Cr_2^{II})_{12}$-(**52a**)$_{24}]$. The figure was created by the authors using the Cambridge Crystallographic Data Centre and data of Ref. 148.

dinatively unsaturated metal cations in the desolvated (activated) coordination cage structure.[150] The use of ligand **52c** also resulted in a similar cuboctahedral structure $[(Cu_2^{II})_{12}$-(**52c**)$_{24}]$ (type **C**, see Table 5), capable of absorbing organic dye molecules and iodine molecules from aqueous and ethanol solutions.[151]

Examples of coordination cage-based systems obtained by post-synthetic modification to enhance their adsorption properties and develop new polymeric functional materials with controlled porosity are often encountered in the literature. Two strategies are employed for this purpose. The first one is to use the possibilities associated with the additional coordination to coordinatively unsaturated metal cations; the second one is based on covalent bonding of cages to form a stable membrane with controlled porosity. In both cases, the coordination cages play the role of secondary building blocks. The coordination cage $[(Rh_2^{II})_{12}$-(**52d**)$_{24}]$ (type **C**, see Table 5) was shown to form coordination-bonded aggregates with constant porosity upon the reaction with a bis(imidazolyl) derivative containing a phenyl spacer.[152] The adsorption properties of this solid phase material towards methyl orange dye were superior to those of the initial coordination cage monomer.[153]

It should be noted that the indicated molecular cage $[(Rh_2^{II})_{12}$-(**52d**)$_{24}]$ was used to fabricate ultra-thin membranes (2.5 nm) for carbon dioxide extraction from gas mixtures by the Langmuir – Blodgett method.[154] Binding by relatively labile sites in the coordination sphere of metal cations in the metal connecting node of $[(Rh_2^{II})_{12}$-(**52e**)$_{24}]$ (type **C**, see Tabel 5) was applied to separate thiophene and thiophane molecules in heterogeneous liquid systems (water – organic solvent).[155]

The possibility of depositing cages of this type on the surface of graphene and a single-walled carbon nanotube has been demonstrated. It was found that the thus obtained composite cage-based material $[(Cu_2^{II})_{12}$-(**52e**)$_{24}]$ (type **C**, see Table 5) shows catalytic properties in the synthesis of propylene carbonate from propylene oxide and CO_2.[156]

As noted above, covalent binding of coordination cages to one another was used to create new polymeric membranes. Cages $[(M_2^{II})_{12}$-(**52f**)$_{24}]$, where M = Cu, Rh, and $[(Cu_2^{II})_{12}$-(**52g**)$_{24}]$ (type **C**, see Table 5) were copolymerized with each other and with n-butyl methacrylate[157] and styrene.[158] The resulting microporous materials had enhanced adsorption properties towards carbon dioxide and methylene blue dye compared to the initial monomer cages. This is probably due to the increased structural stability of the cage pores in the covalently bonded polymer matrix and to the appearance of new pores as a result of copolymerization.

An important achievement in the development of systems simulating physiological processes was the synthesis of the cage $[(Cu_2^{II})_{12}$-(**52h**)$_{24}]$ (type **C**, see Table 5). It showed high efficiency as a catalyst for hydrogen peroxide decomposition at a pH of the medium close to that of a living cell.[159]

It is worth noting that varying the nature of the substituent in the isophthalic acid makes it possible to obtain coordination cages with photo-switchable adsorption properties. Coordination cage $[(Cu_2^{II})_{12}$-(**52i**)$_{24}]$ (type **C**, see Table 5) based on a ligand containing a photoisomerizable azophenyl moiety is capable of controlled adsorption of methylene blue dye (in solid form) from solutions and release of the dye upon irradiation with UV light.[160] In addition, deposition of this cage on a mesoporous silica gel surface enhances its photo-switchable adsorption properties towards propylene molecules and brilliant blue dye. This is due to the fact that aggregation, which decreases the adsorption capacity, is less pronounced for the cages deposited on silica gel.[161]

In addition to the dicarboxylate ligands, ligand **53**, which has a triangular geometry of the carboxyl binding sites, was also used to produce a cage-based molecular recognition of the indicated type. This resulted in the octahedral supramolecular structure $[(Cu_2^{II})_6$-(**53**)$_8]$ (type **D**, see Table 5 and Fig. 58). The study of its adsorption properties in the crystalline phase showed that this structure efficiently adsorbs carbon dioxide molecules under ambient conditions.[149]

Thus, in this Section, we summarized the main types of molecular recognition using different building blocks to produce supramolecular functional coordination cages. It was shown that by varying the geometry and nature of the binding sites of both the ligand and the metal connecting node, their structure and properties can be specifically tuned up. The use of molecular recognition principles

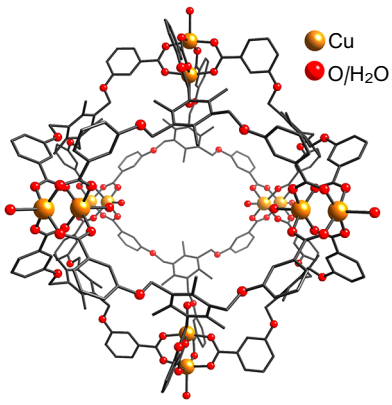


Figure 58. Crystal structure of the neutral octahedral coordination cage $[(Cu_2^{II})_6$-(**53**)$_8]$. The figure was created by the authors using the Cambridge Crystallographic Data Centre and data of Ref. 149.

makes it possible to control the spontaneous molecular self-assembly of MOPs and produce new materials with specific adsorption, catalytic, sensing and biological properties.

In recent years, the annual number of publications focusing on metal-organic cages has been increasing. The authors pay special attention to the description of possible ways to stabilize these nanoscale structures in order to find the optimal balance between their kinetic stability and the potential for use as materials for various applications with a controlled porosity. In this regard, approaches to the search for new models of molecular recognition are actively developing, new building blocks are involved in the process, for example, calixarenes [162–165] and resorcinarenes,[166, 167] which expands the possibilities of the design of discrete nanoporous structures in order to endow them with the desired functional properties combined with increased stability. One of the possible options for increasing the porosity of such materials is fabrication discrete multicage structures based on a combination of the presented types of molecular recognition.[168]

Covalently bonded polymeric functional membranes, micelles, gels and nanoscale films have been obtained using modern methods of post-synthetic modification of MOPs.[169] In the future, coordination cages could become parts of many new smart materials based on molecular host–guest recognition and constructed using the bottom-up approach, namely, membrane reactors, efficient molecular transport systems for drug delivery to the cells, film molecular separators, selective adsorbents, *etc*.

2.3. Supramolecular aspects of hydrocarbon separation on metal-organic frameworks

Metal-organic frameworks (MOFs) are porous structures consisting of metal ions and organic ligands binding them along two or three directions.[170–173] Owing to the presence of pores, the size and surface properties of which can be finely tuned by varying the structure of the organic ligand and the nature of the metal ion, MOFs are fairly promising materials for the storage and adsorption separation of gases,[174–178] liquid organic compounds [179–181] and ions and molecules in solutions.[182, 183] This Section addresses the supramolecular aspects of sorption and separation of industrially important xylene isomers and cyclohexane–benzene mixtures using MOFs.

2.3.1. Separation of xylene isomers

Mixtures of xylene isomers (molecular formula C_8H_{10}) are formed in catalytic reforming and toluene disproportionation processes; xylenes are also present in light petroleum coke products and pyrolysis gasoline. The world production output of xylene isomers is ~40 million tons per year.[184] The separation of these isomers is considered to be highly important for modern chemical industry.[185] Xylenes are separated from other accompanying aromatic hydrocarbons (mainly benzene and toluene) by fractional distillation [186] and then single isomers are isolated, of which *p*- and *o*-xylenes are most valuable for industry. *p*-Xylene is then oxidized to terephthalic acid or dimethyl terephthalate, which are used as monomers to produce polyesters, first of all, poly(ethylene terephthalate) (PETP). *o*-Xylene is oxidized to phthalic anhydride, which serves for the production of phthalates, used as plasticizers for polymers. *m*-Xylene is converted to isophthalic acid — a monomer for the synthesis of polyesters — and can also be isomerized to *p*- and *o*-xylenes. Xylene isomers have similar physicochemical properties (*e.g.*, the boiling points of *o*-, *m*- and *p*-xylenes are 144.4, 139.1 and 138.4 °C, respectively);[187] therefore, separation of these isomers is a challenge. The difference of 5 °C between the boiling points of *o*-xylene and the other two isomers allows separation of *o*-xylene by distillation on high-performance columns with high reflux ratios. The similarity of the boiling points of *m*- and *p*-xylenes makes their separation by distillation virtually impossible; therefore, pure *para*-isomer is isolated by crystallization (the melting points of *ortho*-, *meta*- and *para*-isomers amount to −25.2, −47.9 and 13.3 °C, respectively) [187] or by adsorption. The natural mineral Faujasite [188, 189] and synthetic zeolites ZSM-5,[190] SMZ-100 [191] and HZSM-5 [192] were used as sorbents. High industrial significance of *p*-xylene stimulates further search for new methods for separating this isomer from the mixture; therefore, extractive distillation [193] and simulated moving bed chromatography [194, 195] procedures were recently proposed.

The possibility of wide variation of the pore size and topology of metal-organic frameworks and the nature of functional groups on their surface can be used to tune MOFs for supramolecular recognition of a desired molecule, which makes them fairly promising sorbents for the separation of xylene isomers. The results of the first studies of inclusion of *p*-xylene molecules into MOF based on zinc ions and napthalene-2,6-dicarboxylic acid (H_2ndc) were reported in 2004.[196] The authors demonstrated selective inclusion of the *para*-isomer in the framework pores in the presence of an equivalent amount of *ortho*- or *meta*-isomer and determined the crystal structure of the *p*-xylene inclusion compound described by the formula $\{[Zn_2(ndc)_2(DMF)_2]\cdot C_8H_{10}\}_n$. Quantum chemical calculations showed that inclusion of *p*-xylene into the framework causes the least structural rearrangement of the unit cell, which accounts for the selectivity to this particular isomer.

The inclusion compounds of *o*-, *m*- and *p*-xylenes into the complex $\{[Cd(ClO_4)_2(L^1)_2]\cdot H_2O\}_n$ (L^1 is 4-amino-3,5-bis[3-(4-pyridyl)phenyl]-1,2,4-triazole) were studied by X-ray crystallography.[197] It was found that the guest molecules interact with the framework *via* the C–H···π-contacts with interatomic distances in the range of 2.9–3.2 Å. A study of the selectivity of formation of inclusion compounds with three xylene isomers being present simultaneously demonstrated that *o*- and *m*-xylenes are adsorbed in approximately equal amounts, whereas *p*-xylene does not enter the framework pores under these conditions.

The complex $[VO(bdc)]_n$ (commercial code MIL-47, bdc is the terephthalate anion) was studied most comprehen-

sively as applied to the liquid-phase separation of xylenes.[198] This framework demonstrates selective adsorption of *p*-xylene from mixtures with other isomers and with ethylbenzene with a selectivity coefficient of ~3. A powder X-ray diffraction study of inclusion compounds formed by xylenes and MIL-47 with Rietveld refinement showed that encapsulation of the guest (xylene) into framework pores almost does not change the unit cell parameters, although each unit cell accommodates two xylene molecules The *p*-xylene molecules are located in parallel planes, with methyl groups being shifted relative to each other, which ensures most efficient π–π interactions. Somewhat weaker interactions are found for *o*-xylene, and the interactions involving *m*-xylene are the weakest because of steric hindrance, which prevents molecules from being arranged in parallel planes.[198] Finsy *et al.*[199] studied the adsorption of xylenes with the MIL-47 framework from the gas phase and demonstrated that virtually no selectivity is observed at low partial pressures, but with increasing degree of filling of the sorbent channels with xylene molecules, the selectivity increases. As a result, it was found that the adsorption selectivity can be controlled by varying pressure or temperature. The adjustment of sorbent activation conditions makes it possible to attain the selectivity coefficient of 14 for a *p*-xylene—*m*-xylene binary mixture.[200]

Chromium terephthalate $[Cr_3O(OH)(H_2O)_2(bdc)_3]_n$ (MIL-101) was used as the stationary phase for the analytical separation of xylenes by gas chromatography[201,202] and high-performance liquid chromatography.[203] Analysis of adsorption isotherms showed that aromatic hydrocarbons are more strongly adsorbed by the MIL-101 framework than aliphatic hydrocarbons, with the highest Henry constant being inherent in *o*-xylene.[202] This framework also demonstrated record-high uptake capacity of xylenes equal to ~120 mass %.[202]

Huang *et al.*[204] investigated sorption of xylene from an equimolar liquid mixture of the three isomers by zinc biphenyl-3,5-dicarboxylate $[Zn(\mu_4\text{-}L^2)]_n$, which had extended one-dimensional channels with a diameter of ~1.7 nm. A predominant inclusion of *p*-xylene into this framework was observed.

Causes for the selective adsorption of *p*-xylene by the boron imidazolate framework $[Zn_2(BH(mim)_3)_2(obb)]_n$, where mim is 2-methylimidazolate, obb is 4,4′- oxybis(benzoate), (BIF-20), were addressed by Lyndon *et al.*[205] Despite high and nearly equal uptake capacities of *o*- and *p*-xylene (~30 mass %), the *p*-xylene adsorption had a selectivity coefficient of ~3 due to the smaller size of its molecule compared with the *ortho*-isomer, which was characterized by faster diffusion. The crystal structures of *p*- and *o*-xylene inclusion compounds in the cavities of this framework were determined. According to the results, the *ortho*-isomer molecules are disordered to a much higher degree, which indicates that they weakly interact with the framework. The molecules of *p*-xylene are located near the imidazole borate linkers and are involved in π–π interactions with the imidazole rings and boron atoms (Fig. 59). It is noteworthy that the aperture of framework pores (~3 Å) is markedly smaller than the kinetic diameter of xylene molecules (~6 Å). Nevertheless, xylene molecules can enter the pores. This is attributable to structural mobility of the framework, enabling conformational changes of the imidazole rings, which depart from the equilibrium conformation, and hence xylene molecules can slip into the pores.[205]

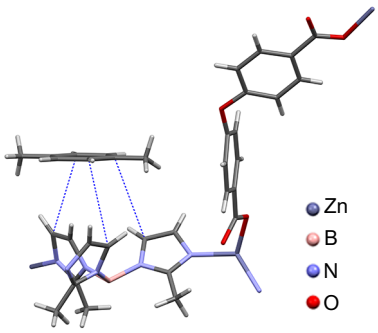


Figure 59. Fragment of the crystal structure of the inclusion compound of *p*-xylene into the $[Zn_2(BH(mim)_3)_2(obb)]_n$ framework (BIF-20). The dashed lines show π–π interactions. The figure was created by the authors using data of Ref. 205.

The $[Zn(mpba)]_n$ framework (MAF-X8), where mpba is the 4-(1*H*-3,5-dimethylpyrazol-4-yl)benzoic acid dianion, showed a selectivity towards *p*-xylene, which was only slightly inferior to the selectivity of BaX zeolite currently used in industry, while the uptake capacity of MAF-X8 was markedly higher, which increased the operating life of the sorbent between regenerations.[206] Molecular modelling demonstrated that the channels of MAF-X8 match *p*-xylene molecules almost perfectly.

Experimental and theoretical study of selective sorption of *p*-xylene from an isomer mixture with the $[Cu(ndc)(DABCO)_{0.5}]_n$ framework [DUT-8(Cu)] was reported by Kim *et al.*[207] DUT-8(Cu) is a 3D metal-organic framework with 1D channels with a square cross-section of 9.6 Å side. In the adsorption of xylenes from a three-component mixture, the selectivity coefficient for the *p*-isomer was ~2. Molecular dynamics simulation showed that *p*-xylene molecules are packed in the channels in an ordered manner and mainly in the vicinity of DABCO linkers, whereas the other two isomers fill the channels in a random manner.

An interesting 'molecular imprinting' effect in the synthesis of MOFs was demonstrated by Yang *et al.*[208] The reaction of 4-(1*H*-pyrazol-4-yl)pyridine (Hpypz) with copper(II) ions in the presence of *p*-xylene results in the formation of the layered metal-organic framework $[Cu_2(pypz)_2]\cdot 0.5\,pX$, where pX is *p*-xylene, (MAF-36) in which zigzag-like channels are filled with the *para*-isomer molecules. The removal of *p*-xylene molecules affords a metal-organic framework, which retains high selectivity for the *p*-xylene over other xylene isomers, despite the structural rearrangement taking place upon removal of the guests. The adsorption of an equimolar liquid mixture with MAF-36 demonstrated the record-high selectivity for *p*-xylene, amounting to 51, which was several times as high as that exhibited by other MOFs (7 to 10) and by the commercially used BaX zeolite (~7).

Selective sorption of *p*-xylene, which has the smallest kinetic diameter of the molecule among xylenes, can be attained by using flexible ligands for MOF fabrication. Mukherjee *et al.*[184] described the layered metal-organic framework $[Zn_4O(L^3)_3(DMF)_2]_n\cdot x\,G$ (L^3 is 4,4′-[(4-*tert*-butyl-1,2-phenylene)bis(oxy)]dibenzoate with two flexible ester groups, G is the guest molecule). The removal of guests from the MOF pores leads to a considerable contraction of the framework: the fraction of free space in the unit cell decreases from 34 to 12%. The repeated immersion of the MOF into the medium of a guest with the appropriate size of molecules, in particular *p*-xylene, leads to restoration of the crystal structure and uptake of a considerable amount of guest molecules into the framework (up to 4 *p*-xylene

molecules per formula unit). Meanwhile, in the case of *o*- and *m*-xylenes, only 0.08 and 0.34 molecules per formula unit, respectively, are adsorbed.[184]

The conformational mobility of the ligand with amide groups played an important role in the selective encapsulation of xylene into the linear MOF $\{[Cu(L^4)_2(H_2O)](ClO_4)_2\}_n$, [$L^4$ is N^1,N^4-bis(4-pyridylmethyl)fumaramide].[209] Upon crystallization, polymer chains are assembled into layers through hydrogen bonding, while the layers are stacked to form 19.3×11.3 Å channels. The synthesis of such a metal-organic framework in the presence of binary or ternary mixtures of xylene isomers leads to competitive inclusion of only one of them, particularly, only *o*-xylene is adsorbed from a ternary mixture and only the *m*-xylene is adsorbed when a mixture of *m*- and *p*-xylenes is used. It is worth noting that, depending on the adsorbed xylene isomer, the dimensionality of the resulting MOF bearing the guest molecules changes. Particularly, the presence of *o*- and *p*-xylenes induced crystallization of 2D MOF (Fig. 60), while the *meta*-isomer caused crystallization of 1D MOF.

There are also MOFs that demonstrate adsorption selectivity not only for *p*-xylene, but also for other isomers. Nicolau *et al.*[210] investigated the adsorption of xylene and ethylbenzene vapours for binary and quaternary mixtures. The authors showed that the $[Zn(bdc)(DABCO)_{0.5}]_n$ framework exhibits selectivity for *o*-xylene with a selectivity coefficient of 1.88 due to stronger interaction of this isomer with the framework surface.

The layered metal-organic framework $[Co(bpy)_2(NCS)_2]_n$ showed high uptake capacities towards *o*- and *p*-xylene (85 mass %), which are inferior only to those of MIL-101.[211] Powder X-ray diffraction of the inclusion compounds $[Co(bpy)_2(NCS)_2]_n \cdot x\,C_8H_{10}$ demonstrated that xylene vapour fills the space between MOF layers (Fig. 61), the uptake being four xylene molecules per formula unit. This is in line with the observed adsorption capacity. The nature of the intermolecular interactions between the guests and the framework is somewhat different over the series of isomeric xylenes. The shortest distance (4.003 Å) between the xylene molecule and the pyridine rings of the linker is characteristic of the *ortho*-isomer. In addition, the hydrogen atoms of the aromatic ring of *o*-xylene are involved in the C–H···π interactions, whereas the *meta*- and *para*-isomers form contacts only by their methyl groups. Finally, this MOF shows high selectivity (~10) for *o*-xylene over *p*-xylene.[211]

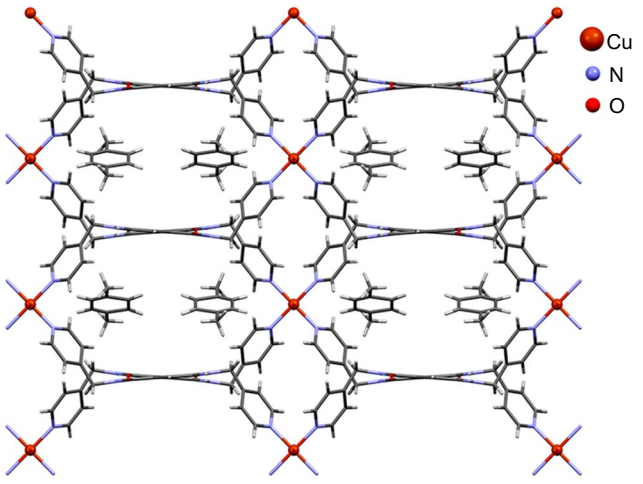


Figure 60. Layer of the coordination polymer $\{[Cu(L^4)_2(H_2O)](ClO_4)_2\}_n$ [L^4 is N^1,N^4-bis(4-pyridylmethyl)fumaramide] with encapsulated *p*-xylene molecules. The ClO_4^- counterions are omitted for the sake of simplicity. The figure was created by the authors using data of Ref. 209.

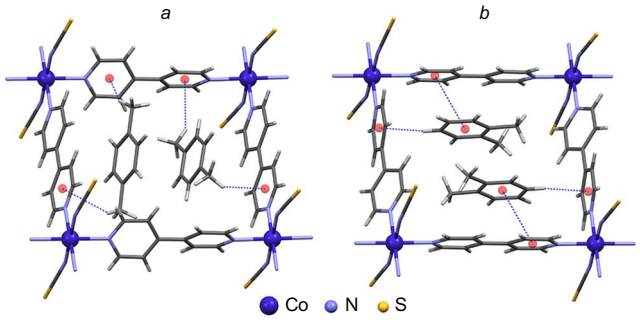


Figure 61. Fragment of the crystal structure of the layered MOF $[Co(bpy)_2(NCS)_2]_n$ with encapsulated *p*-xylene (*a*) and *o*-xylene (*b*) molecules. The dashed lines show π–π and C–H···π interactions. Hydrogen atoms are omitted for the sake of simplicity. The figure was created by the authors using data of Ref. 211.

A very high selectivity for *o*-xylene was found for chromium terephthalate $[Cr(OH)(bdc)]_n$ [MIL-53(Cr)]. The *o*-xylene–*p*-xylene selectivity for sorption from a liquid isomer mixture (13.75) makes this material a promising alternative to zeolites in the industrial sorption processes using a simulated moving bed.[212]

Among the factors affecting the selectivity of adsorption of a particular xylene isomer is the presence of coordinatively unsaturated sites in the MOF structure. Gonzalez *et al.*[213] carried out a structural study of the compounds formed upon encapsulation of xylenes into the $[Co_2(dobdc)]_n$ framework (dobdc is 2,5-dihydroxybenzene-1,4-dicarboxylate). The framework contains hexagonal channels, the inner surface of which has coordinatively unsaturated cobalt(II) sites. It was found that encapsulation of *o*-xylene induces a substantial distortion of three out of each four framework pores and that each distorted pore accommodates four *o*-xylene molecules, while the undistorted pores contain three such molecules (Fig. 62). In the case of *para*- and *meta*-isomers, characterized by lower adsorption capacity, no framework distortions were

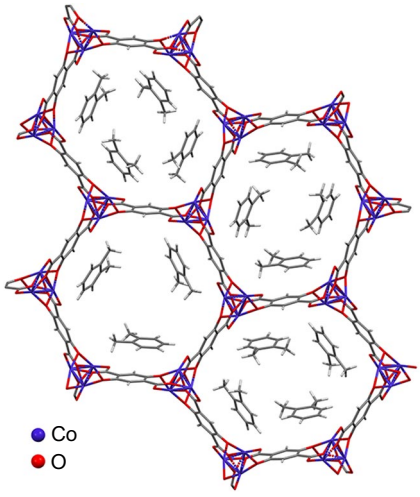


Figure 62. Crystal structure of the MOF $[Co_2(dobdc)]_n$ with channels filled with *o*-xylene molecules. The figure was created by the authors using data of Ref. 213.

detected. Three cobalt(II) cations can be identified as binding sites for *o*-xylene molecules, whereas only two such sites are present for *m*-xylene and only one site is found for *p*-xylene. As a result, the *o*-xylene–*p*-xylene selectivity is 3.9, while the volumetric capacity of this framework (3.8–4.2 mmol cm^{-3}) exceeds those of zeolites that are currently used in industrial processes of xylene separation.[213]

2.3.2. Separation of benzene and cyclohexane

Cyclohexane is a large-scale product of chemical industry, used as a raw material for the production of cyclohexanol, cyclohexanone and caprolactam, which are, in turn, used for the production of polyamide fibres and threads. Cyclohexane is produced by catalytic hydrogenation of benzene, and the unreacted benzene has to be separated in order to isolate a pure product. Separation of small amounts of benzene from cyclohexane is an energy-demanding task complicated for implementation.[185] Due to close boiling points (80.1 °C for benzene and 80.7 °C for cyclohexane), conventional distillation is inapplicable. Therefore, azeotropic and extractive distillation processes are used,[214–216] which decreases the environmental and economic efficiency of the processes. The methods of benzene separation from cyclohexane by pervaporation using polymer membranes appear relatively promising from the engineering standpoint.[217–220] In recent years, considerable attention of researchers has been devoted to the adsorption separation of benzene and cyclohexane using silica gels,[221] mesoporous carbon [222] and also organic cavitands.[223, 224]

The first studies dealing with inclusion compounds formed upon encapsulation of benzene into MOF pores appeared rather long ago. In 2007, Shimomura *et al.*[225] reported the results of an X-ray diffraction study of the compound $\{[Zn(\mu_4\text{-TCNQ-TCNQ})(bpy)]\cdot 1.5\,PhH\}_n$ (TCNQ-TCNQ is 1,2-bis[4-(dicyanomethylene)cyclohexa-2,5-dien-1-yl]ethane-1,1,2,2-tetracarbonitrile), which showed that benzene molecules are strongly held by C–H···π interactions (Fig. 63).

One of the first examples of comparative study of MOF adsorption of benzene and cyclohexane was reported by Tan *et al.*[226] in 2012. For the three-dimensional MOF $\{[Cu_2(obb)_2(bpy)_{0.5}(DMF)]\cdot 2\,DMF\}_n$, the uptake capacity for benzene adsorption from the gas phase was 20.6 mass % and that for cyclohexane was 14.9 mass %. As specific features of the process, the authors noted a wide hysteresis in the adsorption isotherms and incomplete desorption related to the lock effect of the framework pores towards the adsorbed molecules.

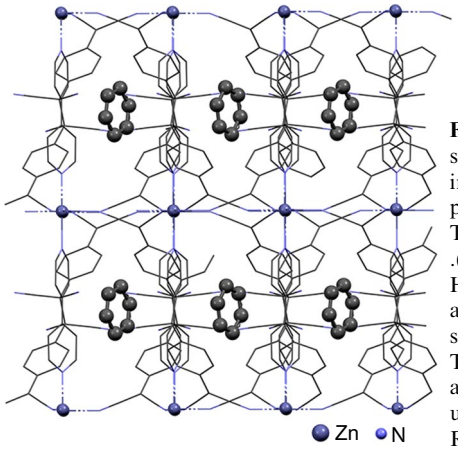


Figure 63. Crystal structure of the inclusion compound $\{[Zn(\mu_4\text{-TCNQ-TCNQ}).(bpy)]\cdot 1.5\,PhH\}_n$. Hydrogen atoms are omitted for the sake of simplicity. The figure was created by the authors using data of Ref. 225.

Basic amide groups and C–H···π and π–π interactions were considered [227] to be responsible for the increased benzene–cyclohexane selectivity of $[Cu_2(L^5)_4(NO_3)_4(H_2O)]_n$ MOF [L^5 is di(4-pyridyl)-5-*tert*-butylisophthalamide). The sorbent can take up ~2 benzene molecules per formula unit when adsorbed from the gas phase, with the selectivity over cyclohexane being 8.

Zhou *et al.*[228] made an attempt to separate benzene and cyclohexane by sorption under dynamic conditions with the hcp-UiO-66 MOF based on $\{Zr_{12}O_8(OH)_{14}\}$ clusters and terephthalic acid. The sorbent more efficiently retains benzene with the selectivity coefficient of 2.39, which is sufficient for separation of cyclohexane from mixtures with relatively low contents of benzene.

Some MOFs exhibit inverse selectivity, that is, they better retain cyclohexane than benzene. For example, the $[Zn(eim)_2]$ metal azolate framework, where eim is 2-ethylimidazolate anion, (MAF-6) has a high concentration of ethyl groups on the pore surface, which make it highly hydrophobic. As a result, during gas chromatographic separation, more lipophilic cyclohexane (lipophilicity: $\log P = 3.6$) is held more strongly than benzene ($\log P = 2.2$).[229]

Logvinenko *et al.*[230] compared the thermal stability of benzene and cyclohexane inclusion compounds into $\{[Zn_2(bdc)_2(DABCO)]\cdot 4\,PhH\}_n$ and $\{[Zn_2(bdc)_2(DABCO)]\cdot 3.5\,C_6H_{12}\}_n$ MOFs. The compound with cyclohexane was thermally more stable, despite the fact that the boiling point and the enthalpy of vaporization of cyclohexane are virtually equal to those of benzene. The higher kinetic stability of the cyclohexane inclusion compound was attributed to the entropy factor, related to the conformational flexibility of the cyclohexane molecule.

As in the case of xylene adsorption, the presence of coordinatively unsaturated sites in MOF often has a crucial effect on the selectivity of benzene sorption. Liu *et al.*[231] investigated sorption of benzene by the $[Mg(dobdc)]_n$ framework (Mg-MOF-74). This framework has channels with a hexagonal cross-section with an inscribed circle diameter of ~15 Å; each magnesium atom coordinates five oxygen atoms in a square-pyramidal environment. Studying the adsorption isotherms of benzene from a vapour revealed a high uptake capacity (8.2 mmol g^{-1}) and adsorbed benzene density of 815 kg m^{-3}, which is comparable with the density of liquid benzene (870 kg m^{-3}) and attests to a liquid-like state of the adsorbed benzene molecules. When sorption was carried out from an equimolar mixture of benzene and cyclohexane vapour, only benzene was shown to be sorbed, and the diffusion coefficient of pure cyclohexane in the sorbent was 1–3 orders of magnitude higher than that for benzene. The molecular dynamics simulation of the intermolecular interactions of benzene and cyclohexane with the framework surface indicates that benzene molecules are mainly adsorbed near magnesium ions, with the average distance from the centre of mass of the molecule to the nearest magnesium ion being 3.78 Å. Meanwhile, the low-polarity cyclohexane molecules have a low affinity to coordinatively unsaturated magnesium ions, with the average distance between them being 4.65 Å.[231]

Benzene and cyclohexane sorption was studied for a series of frameworks with various coordinatively unsaturated sites $[M(dobdc)]_n$, where M = Mn, Ni, Mg, Cu, Zn,

Co, Fe (the codes are M-MOF-74). The benzene adsorption capacity decreased in the series from manganese(II)- to iron(II)-containing framework; this series coincides with the order of decreasing ionization potentials of the metals. For the Mn-MOF-74 framework, the saturation capacity for benzene reached 9.38 mmol g^{-1}, while that for cyclohexane was only 0.25 mmol g^{-1}. The calculation of the benzene–cyclohexane selectivity using the ideal absorbed solution theory (IAST) for Mn-MOF-74 gives a very high value of about 10^5.[232]

Kondo *et al.*[233] reported the MOF $[Cu(bpp)_2(BF_4)_2]_n$ [bpp is 1,3-di(4-pyridyl)propane], capable of solvent-induced reversible transformation from the close-packed non-porous 3D structure into a porous 1D structure. For sorption from the gas phase, the uptake capacity for benzene was 248 mg g^{-1} ($\sim$2 benzene molecules per formula unit), while the uptake of cyclohexane was negligibly low. It is noteworthy that the adsorbed benzene molecules are held very strongly by the MOF and are not released even when the relative pressure drops to 10^{-2}.

Modification of the inner surface of channels in the two-dimensional MOF $\{[CuI(L^6)]\cdot(DMF)\cdot H_2O\}_n$ [L^6 is 4′-(anthacene-9-yl)-4,2′:6′,4″-terpyridine] by anthracene moieties provided high selectivity of benzene sorption from the gas phase with the benzene–cyclohexane selectivity of $\sim$42.[234]

The polar groups on the pore surface of the $[Zn(pbda)(dpni)]_n$ framework (pbda is 4,4′-[(2-*tert*-butyl)-1,4-phenylene)bis(oxy)]dibenzoic acid, dpni is *N*,*N*′-di(4-pyridyl)napthalene-1,4,5,8-tetracarboxydiimide) were indicated[235] to be responsible for the selectivity of benzene sorption (uptake capacity of $\sim$4.5 mmol g^{-1}) over cyclohexane sorption (the uptake is negligibly low).

With the goal of generating π-electron-deficient sites on the surface of MOF channels, Manna *et al.*[236] proposed a new ligand, 4-(4,6-diamino-1,3,5-triazin-2-yl)benzoic acid. The reaction of this ligand with copper nitrate gave a 2D MOF, the layers of which were combined into a three-dimensional structure with 6.71 × 7.08 Å channels through hydrogen bonding. Due to the π–π stacking with electron-deficient triazine rings, the π-electron density-rich benzene molecules were efficiently adsorbed by the obtained MOF with an uptake capacity of 1.5 mmol g^{-1}, whereas the uptake of cyclohexane was only 0.2 mmol g^{-1}. The IAST calculation of the sorption selectivity for an equimolar benzene–cyclohexane mixture resulted in the value of $\sim$200.[236, 237]

The role of π-acceptor 1,3,5-triazine moieties in increasing the benzene–cyclohexane adsorption selectivity *via* π–π interactions was also demonstrated in relation to the frameworks $\{(Et_4N)_3[In_3(tatb)_4]\cdot(DEF)_{16}\cdot(H_2O)_{11}\}_n$, where tatb is 4,4′,4″-*s*-triazine-2,4,6-triylbenzoate, DEF is diethylformamide,[238] (code FJI-C1) and $\{[Cd(ataia)]\cdot 4\,H_2O\}_n$, where ataia is 5-[(4,6-diamino-1,3,5-triazin-2-yl)amino]isophthalate.[239] When adsorption was carried out from saturated vapour at 298 K, the uptake capacity of FJI-C1 for benzene was about 13.4 mass %, which was 111 times higher than the capacity of the same MOF for cyclohexane.[238] For the cadmium-organic framework the selectivity coefficient was 6.5.[239]

The ligand flexibility and the presence of Lewis π-acid sites on the pore surface of the three-dimensional MOF $[Zn_2(L^7)_2(DMF)_2]_n$ [L^7 is 2,2′-(1,3,5,7-tetraoxo-5,7-dihydropyrrolo[3,4-*f*]isoindole-2,6(1*H*,3*H*)-diyl)dipropiolate] with one-dimensional channels provide selective adsorption of benzene, although the uptake capacity is moderate (one benzene molecule per formula unit). Cyclohexane is virtually not adsorbed by this framework.[240]

The competing sorption of benzene and cyclohexane from liquid and gaseous equimolar mixtures was studied[241] in relation to a series of isostructural MOFs described as $[Zn_{12}(tdc)_6(gly)_6(DABCO)_3]_n$ (H_2tdc is thiophene-2,5-dicarboxylic acid, gly is alkane-1,2-diol dianion). These MOFs contain channels with a diameter from 1.4 to 4.8 Å, depending on the alkyl chain length of the diol. The alkyl chain length also affects the selectivity for benzene over cyclohexane; it is maximum for ethane-1,2-diol and amounts to 20 : 1 for sorption from the gas phase and 92 : 1 for sorption from the liquid phase. Elongation of the alkane-1,2-diol chain is accompanied by a decrease in the selectivity and, in the case of butane-1,2- and pentane-1,2-diols, the selectivity is reversed, *i.e.*, cyclohexane is adsorbed predominantly. The MOF with the pentane-1,2-diolate anion had a cyclohexane selectivity over benzene equal to 5 for the gas phase and 2.5 for the liquid phase.[241]

The sorption selectivity can be controlled by changing the pore size in MOFs. Wang *et al.*[242] investigated the adsorption of benzene and cyclohexane from their equimolar liquid mixture by a series of MOFs obtained by ion exchange: NH_4@ZnPzC, Me_3NH@ZnPzC and Et_3NH@ZnPzC (PzC is 1*H*-pyrazole-4-carboxylate). On going from the trimethylammonium cation to the triethylammonium cation, the adsorption selectivity for benzene, which has a smaller molecular size than cyclohexane, increased from 3.1 to 14, which is consistent with decreasing pore size of the framework.[242] A similar trend was observed for a MOF based on copper(II) ions, $CAT@[Cu_3\text{-}(\mu_3\text{-}OH)(\mu_3\text{-}PzC)_3]_n$ (where CAT = NH_4^+, Et_3N^+, Li^+): the selectivity coefficient increased from 5 to 12 on going from the ammonium cation to the lithium cation.[243]

The correlation between the kinetic diameter of the benzene molecule (5.85 Å) and the pore size of MOF $[Zn(ip)(bpa)]_n$, where ip is isophthalate, bpa is 1,4-di(4-pyridyl)acetylene, (CID-23) endows the framework with an enhanced selectivity for benzene; the benzene–cyclohexane selectivity coefficient for adsorption from an equimolar gas-phase mixture is 25.[244]

The possibility of template tuning of MOF for attaining high sorption properties was demonstrated.[245] It is known that the reaction of 4-(3,5-dimethyl-1*H*-pyrazol-4-yl)benzoic acid (H_2mpba) with zinc(II) ions may give diverse metal-organic frameworks. In the presence of benzene, the MOF $\{[Zn_2(Hmpba)_2(mpba)]\cdot 2\,PhH\}_n$ is formed with zig-zag-like channels filled with benzene molecules. Guest exchange may allow the preparation of inclusion compounds with other guests, particularly cyclohexane. X-Ray diffraction data indicate that the framework undergoes a substantial restructuring as one guest is replaced by another one. The obtained MOF was used as the stationary phase for gas chromatographic separation of benzene and cyclohexane with a selectivity coefficient of 2.85.[245]

The first example of using MOFs for separating benzene and cyclohexane (or other hydrocarbons) by liquid chromatography was reported by Nuzhdin *et al.*,[246] who used a composite sorbent based on the framework HKUST-1 and aerogel SiO_2 as the stationary phase. In this sorbent, MOF ensures the selectivity towards unsaturated hydrocarbons and silica gel improves the hydrodynamic properties of the column.

Thus, the diversity of MOF building blocks allows for the fabrication of porous materials with high selectivity for the desired xylene isomer or benzene, while the high porosity of MOFs ensures the uptake capacity values that cannot be attained for traditional sorbents. The progress in the methods of MOF synthesis makes the frameworks more and more economically accessible, and some of them can even now compete with materials applied in the existing industrial processes of hydrocarbon separation.

2.4. Coordination cages, supramolecular assemblies, polynuclear systems based on metal clathrochelates and reactivity of encapsulated ions

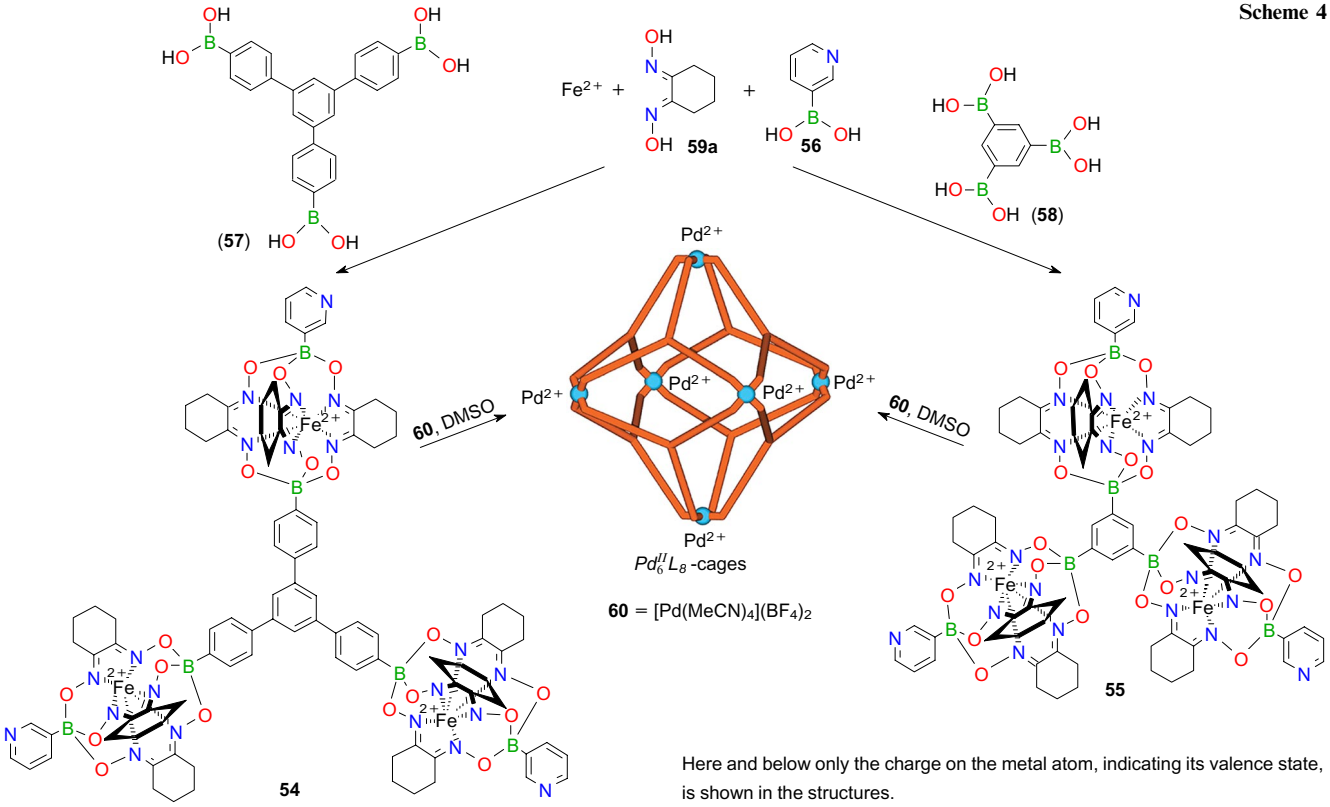
The state-of-the-art studies in the title area of supramolecular chemistry up to the end of 2014 is described in detail in the monographs *The Encapsulation Phenomenon: Synthesis, Reactivity and Applications of Caged Ions and Molecules*[247] and *Cage Metal Complexes: Clathrochelate Revisited*,[248] published by Springer in 2016 and 2017, respectively. Later, these monographs were translated into Russian. A number of recent reviews [249–254] address particular areas of the chemistry and application prospects of metal clathrochelates and systems based on them. In particular, two reviews [249, 250] are devoted to the prospects of using clathrochelate ligands in supramolecular chemistry and modern materials science. It was shown that, with minor synthetic effort, clathrochelate ligands can form nanosized molecular assemblies, including coordination cages with unusual geometry such as digonal gyrobicupola (gyrobifastigium) or square orthobicupola and also large (>3 nm) supramolecular associates and linear or cross-linked clathrochelate polymers with permanent porosity.[250] Since the clathrochelate cages decorated with functional groups in lateral and apical positions are multimodal compounds, they can form metal-organic frameworks and are also promising monomers for the production of metallopolymers and conductive coatings of electrodes. The advances in the use of 3d metal clathrochelates in the controlled radical polymerization of vinyl monomers are reflected in the reviews [251, 252] published in 2011 and 2016, respectively. The achievements and prospects of biological and medicinal applications of cage metal complexes and their supramolecular assemblies with biomacromolecules are described in detail in the review of Voloshin *et al.*[253] The most recent achievements in the studies of d-metal tris(dioximate) clathrochelates and functional hybrid materials based on them as promising electro- and pre-catalysts for the production of molecular hydrogen and synthesis gas were surveyed by Voloshin *et al.*[254]

2.4.1. Coordination cages

The tritopic clathrochelate ligands **54**, **55** based on arylboronic acids **56**–**58** and dioxime **59a** shown in Scheme 4 [255] were used to prepare two larger-size $Pd_6^{II}L_8$ type coordination cages with Pd···Pd distances of up to 4.2 nm in the presence of palladium complex **60**.

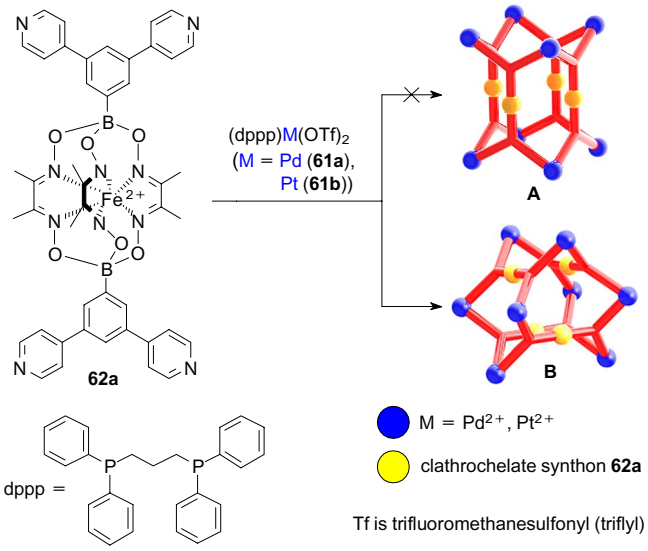
The effect of the size and geometry of clathrochelate ligands on the coordination-controlled association of $M_{2n}^{II}L_n$ coordination cages of various types was studied both theoretically and experimentally.[256, 257] It was found that, instead of the tetragonal barrel-like (**A**) cages, the reaction of mononuclear clathrochelate synthons with 2 equivalents of (dppp)M(OTf)$_2$ [**61**: M = Pd (**a**), Pt (**b**)] gives gyrobifastigium-like (**B**) $M_8^{II}L_4$ type cages, which are shown in Scheme 5 [257] in relation to synthon **62a** as an example. Meanwhile, analogous synthons **62b**–**e** and complexes **61b**–**e** were converted to both barrel-like $Pt_{2n}^{II}L_n$ cages and $Pt_{16}^{II}L_8$ assemblies with molecular weight of >23 kDa and diameter of ~4.5 nm. The geometry of compounds obtained in this way depends on the structure of complexes

Scheme 4



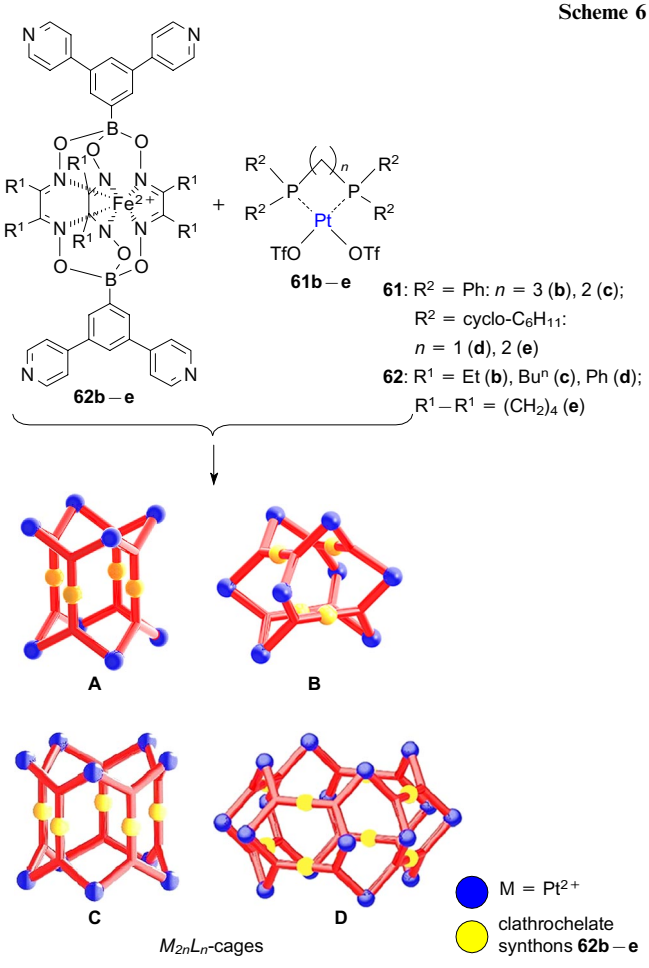
Here and below only the charge on the metal atom, indicating its valence state, is shown in the structures.

Scheme 5

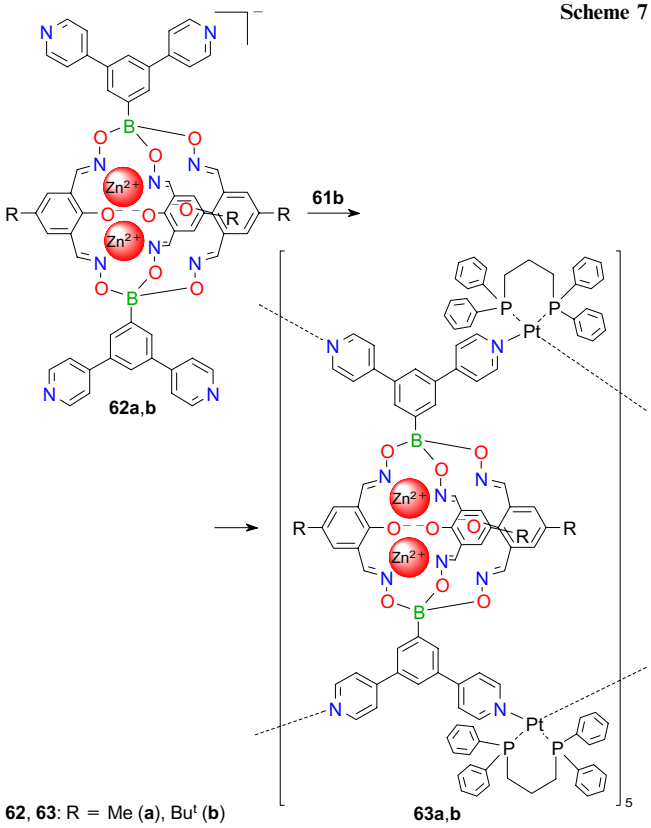


61b–e. Indeed, when synthons **62d**,**e** react with complexes **61d**,**e**, the tetragonal barrel-like $Pt_8^{II}L_4$ cages **A** are formed; synthons **62b**,**c**,**e** and complex **61b** react to give gyrobifastigium-like $Pt_8^{II}L_4$ cages **B**; pentagonal barrel-like $Pt_{10}^{II}L_5$ cages **C** are formed in the reaction of synthon **62c** with complex **61d**; and the reaction of synthon **62c** with complex **61c** affords $Pt_{16}^{II}L_8$ assembly **D** (Scheme 6).[257] The binuclear

Scheme 6



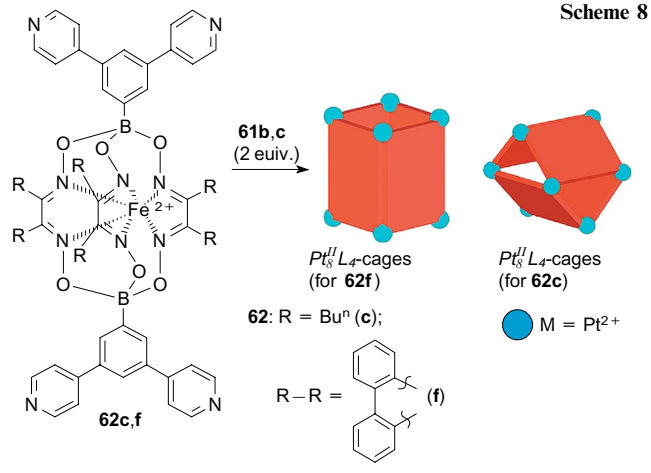
Scheme 7



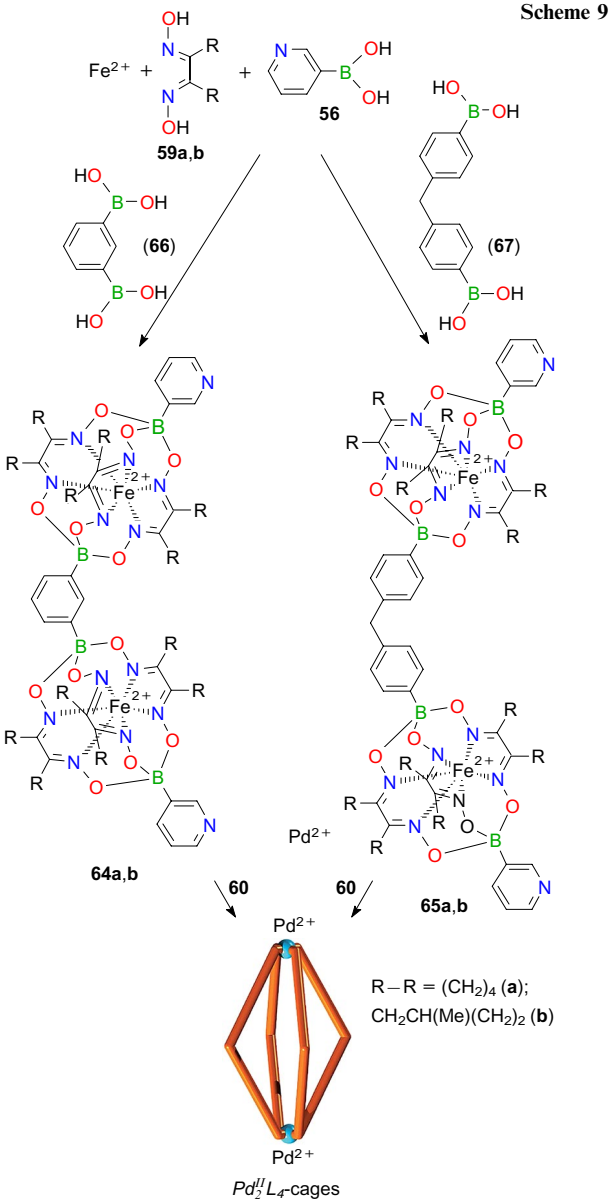
clathrochelate ligands **62a**,**b** react with complex **61b** to give pentagonal $Pt_{10}^{II}L_5$ barrels **63a**,**b** (Scheme 7).[257]

Cecot *et al.*[258] showed that during the formation of $Pt_8^{II}L_4$ coordination cages, lateral groups can direct the coordination-controlled self-assembly of clathrochelate ligands by promoting the formation of a structure that enables energetically favourable (*i.e.*, associated with minor steric restrictions) packing of bulky groups. Clathrochelate ligand **62f**, containing four pyridyl groups in the apical positions and three phenanthrene groups in the lateral chelating moieties, was reacted with complexes **61b**,**c** to give $Pt_8^{II}L_4$ coordination cages with a tetragonal prismatic geometry (Scheme 8).[258] In the case of clathrochelate ligand **61c** with aliphatic n-butyl lateral groups, gyrobifastigium-like $Pt_8^{II}L_4$ cages were obtained.[258]

Scheme 8



Scheme 9



Jansze *et al.*[259] reported the synthesis of bent ditopic clathrochelate ligands **64a**,**b** and **65a**,**b** with terminal 3-pyridyl groups. They were obtained by template condensation of a mixture of the corresponding aryldiboronic (**66**, **67**) and 3-pyridylboronic (**56**) acids on an iron(II) ion as the template (Scheme 9).[259] These macrobicyclic synthons were used for the coordination-controlled self-assembly of $Pd_2^{II}L_4$ cages in the presence of palladium complex **60**. It was shown[257] that cages with nioxime (cyclohexane-1,2-dione dioxime) substituents [R–R = $(CH_2)_4$] in the lateral chelating moieties are more stable than their dimethylglyoximate analogues (R = Me).

2.4.2. Coordination polymers

Binuclear zinc and cobalt(II) clathrochelates **68**–**71**, containing cyano groups at the periphery of encapsulating ligands (Scheme 10), were prepared[260] by two pathways:

— using the template polycondensation of CN-containing arylboronic acids (*e.g.*, compound **72**) and the appropriate phenoldioximate ligand synthons **73a**,**b** on zinc or cobalt(II) ion as the template (for complexes **68**, **69**);

— post-synthetic cross-coupling of polybrominated zinc(II) clathrochelates **74a**,**b**, obtained from bromides **75a**,**b**, with 4-cyanophenylboronic acid (**72**).

The reactions of clathrochelate ligands **68**–**71**, containing terminal cyano groups, with silver salts resulted in the formation[260] of heterometallic (Zn^{2+}, Ag^+ and Co^{2+}, Ag^+) coordination polymers.

Bila *et al.*[261] reported the formation of microporous thermally and hydrolytically stable polymer networks with permanent porosity based on ligands **76a**–**79a** (Fig. 64). These ligands were obtained in two ways. The first method was based on the Suzuki–Miyaura covalent cross-coupling of pre-synthesized iron(II) dibrominated clathrochelates **80a**,**b** with reactive halogen atoms of compound **75b** and the corresponding diboronic acids **81**, **82** (Scheme 11) and the other method comprises Sonogashira–Hagihara polycross-coupling of clathrochelate precursors **83a**,**b**, containing terminal C≡C bonds in the apical substituents, with 1,3,5-tribromobenzene (Scheme 12). The clathrochelate precursor **80b**, derived from enantiomerically pure α-dioximate ligand **59c**, was used[261] to prepare chiral polymeric products, one of which adsorbed mainly D- tryptophan in comparison with the L-epimer.

Fe^{II},Fe^{III}-heterobinuclear clathrochelates were obtained by template condensation of 4-pyridylboronic acid (**84**) with the corresponding phenol dioxime ligand synthon **73** in the presence of iron(III) and/or iron(II) ions (Scheme 13). Their macrobicyclic ligands can encapsulate iron ions in two redox states to give either homobinuclear clathrochelates **85a**,**b** with two encapsulated iron(II) cations or their heterobinuclear Fe^{II},Fe^{III}-analogues **86a**,**b**, which easily undergo reversible chemical or electrochemical oxidation or reduction.

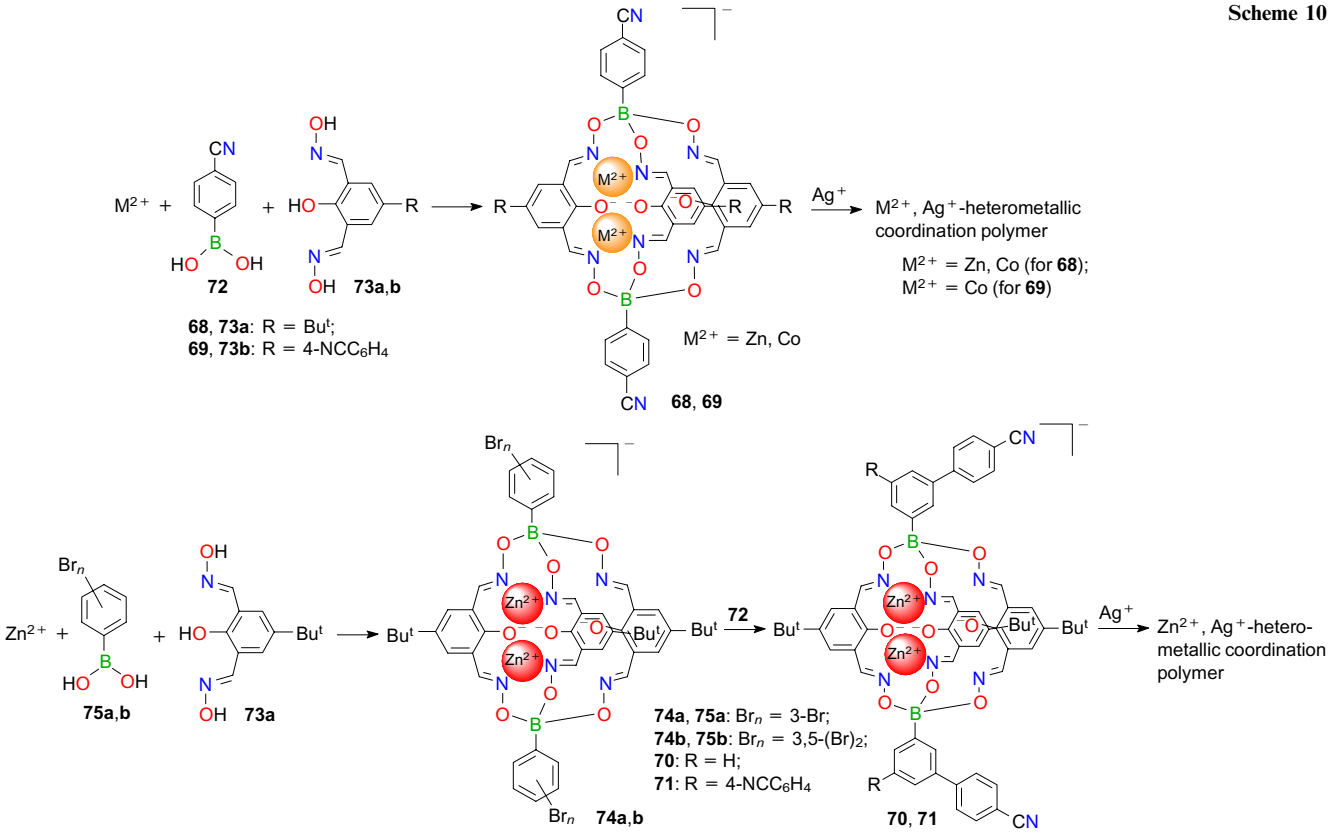
Using a mixture of zinc or iron salts, Bila *et al.*[262] prepared Zn^{II},Fe^{III}-heterobinuclear clathrochelate **87** (Scheme 14). Studying ion exchange reactions of encapsulated metal cations in these binuclear clathrochelates showed[262] that Fe^{II},Fe^{III}-heterobinuclear cage complexes **86a**,**b** are thermodynamically more stable than analogous binuclear complexes of zinc (**88**) and cobalt(II) (**89**) (Scheme 15).

Palladium-catalyzed polycross-coupling of Fe^{II},Fe^{III}-heterobinuclear clathrochelate **90** with the terminal bromine atoms in the encapsulating ligand and benzene-1,4-diboronic acid (**81**) afforded[262] thermally and hydrolytically stable coordination polymer with permanent porosity (Scheme 16).

The template condensation of the corresponding phenol dioxime ligand synthon with 3-(acrylamidophenyl)- or 3-(methacrylamidophenyl)boronic acids on cobalt or manganese(II) ion templates yields binuclear boron-containing macrobicyclic complexes **91a**,**b** with reactive apical substituents.[263] It was found that the type of supramolecular clathrochelate network in the crystals of the product depends on the nature of terminal groups at the cross-linking boron atoms and that transition from 2D to 3D supramolecular assemblies can be accomplished using appropriate guests (Fig. 65).[263]

Iron(II) clathrochelates **92a**–**d** with terminal 4-pyridyl groups are converted[264] to paddle-wheeled metal-organic frameworks with *N*,*N*′-di(4-pyridyl)napthalene-tetracarboxydiimides *via* ligand exchange reactions.

Scheme 10



Scheme 11

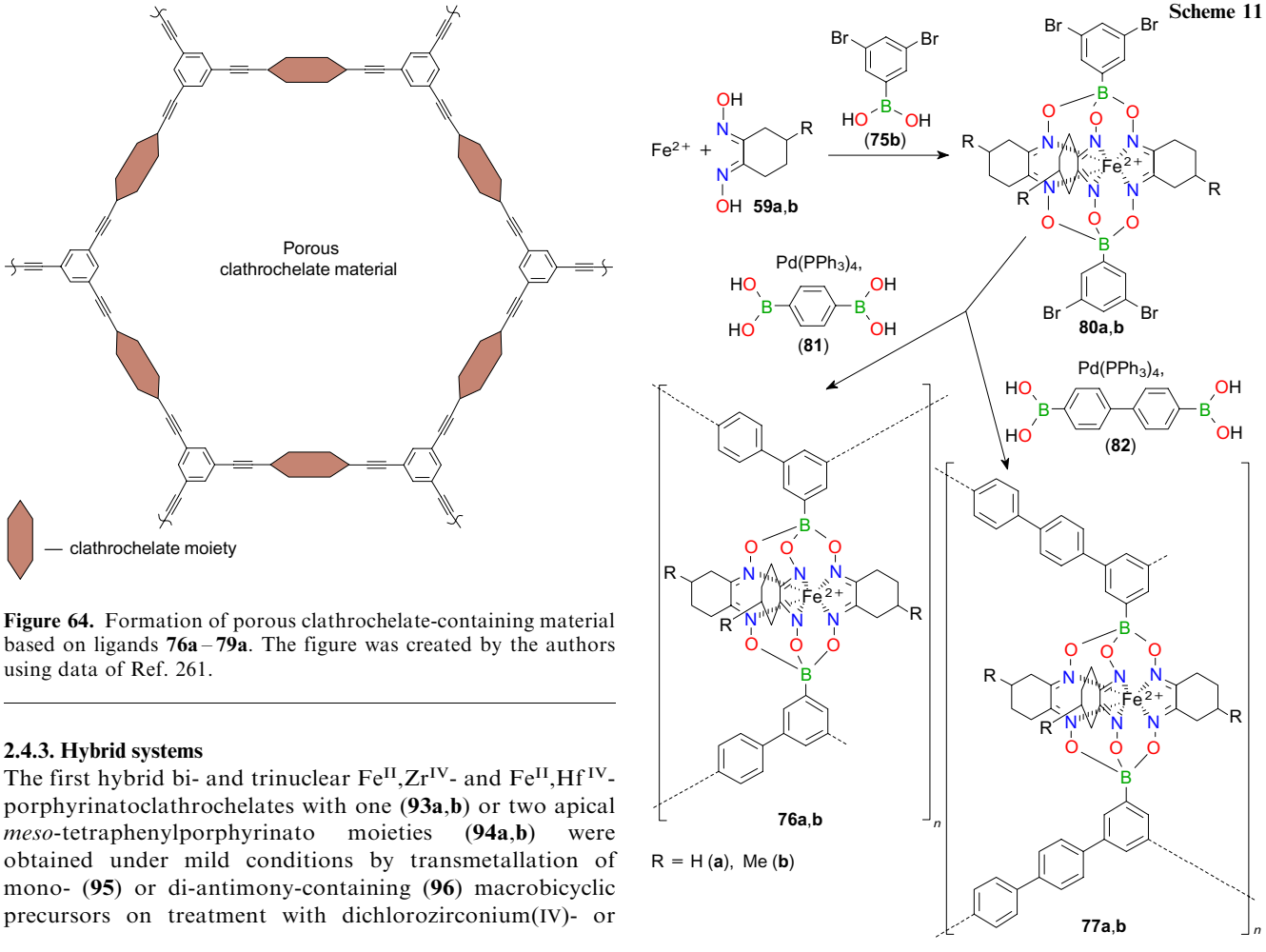
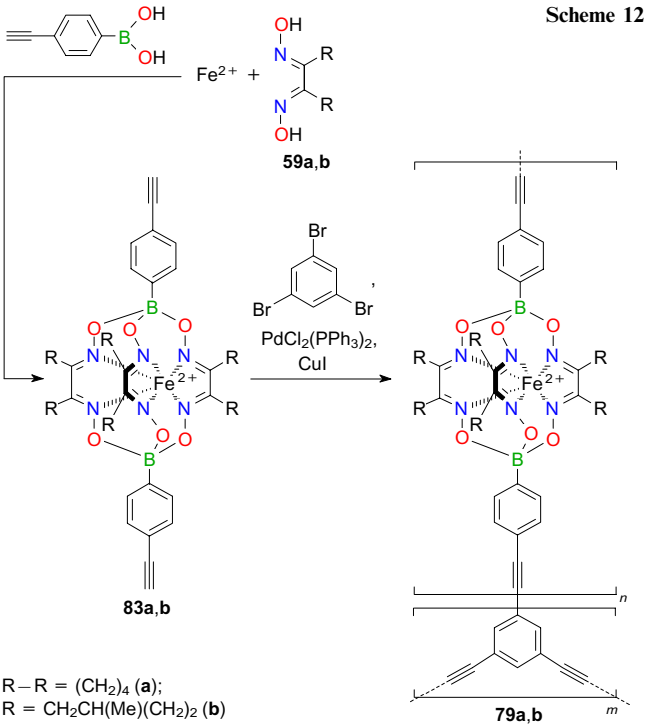


Figure 64. Formation of porous clathrochelate-containing material based on ligands **76a** – **79a**. The figure was created by the authors using data of Ref. 261.

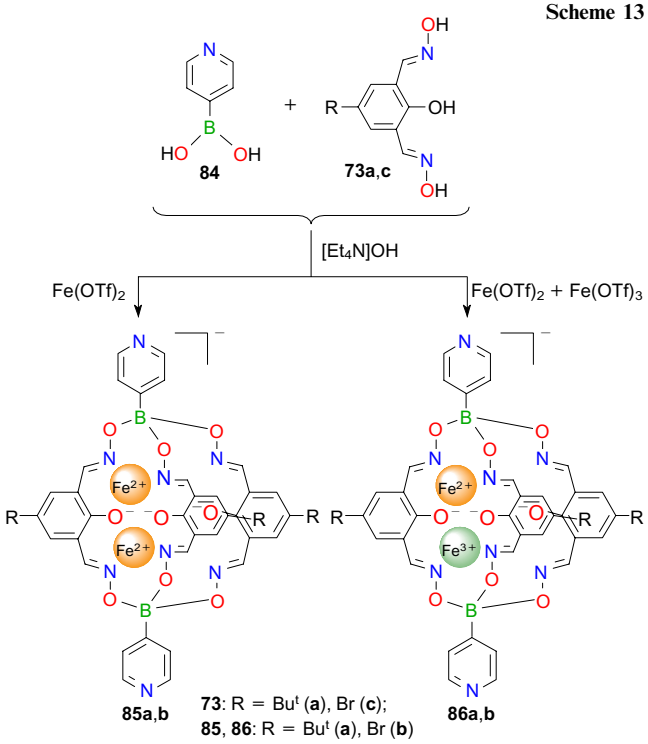
2.4.3. Hybrid systems

The first hybrid bi- and trinuclear Fe^{II},Zr^{IV}- and Fe^{II},Hf^{IV}-porphyrinatoclathrochelates with one (**93a**,**b**) or two apical *meso*-tetraphenylporphyrinato moieties (**94a**,**b**) were obtained under mild conditions by transmetallation of mono- (**95**) or di-antimony-containing (**96**) macrobicyclic precursors on treatment with dichlorozirconium(IV)- or

Scheme 12

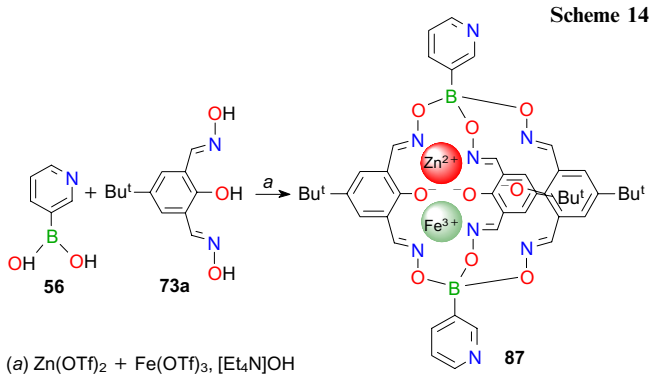


Scheme 13

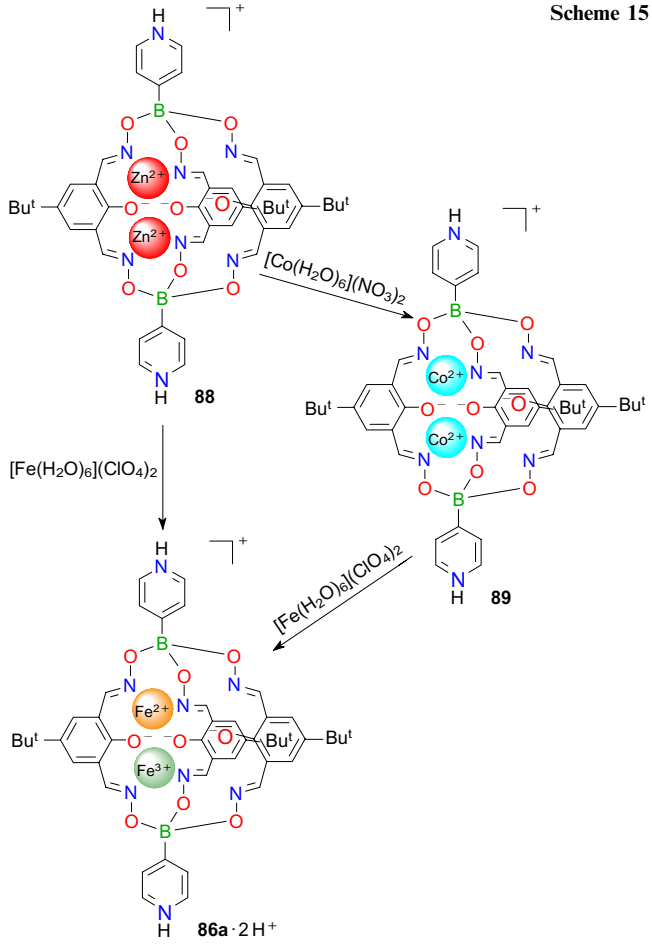


dichlorohafnium(IV)-*meso*-tetraphenylporphyrins **97a,b** as Lewis acids (Scheme 17).[265] It was reported [266] that the reactive antimony-containing iron(II) clathrochelate **98** with a terminal vinyl group shown in Scheme 18 also undergoes exchange reaction of the cross-linking group (transmetallation) under the action of the hafnium(IV) phthalocyanine complex (HfPc, **99a**) as a stronger Lewis acid to give hybrid binuclear HfPc-cross-linked iron(II) phthalocyaninoclathrochelate **100**.

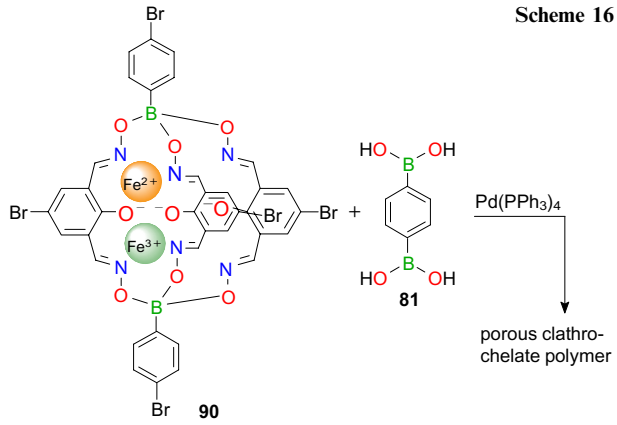
Scheme 14



Scheme 15



Scheme 16



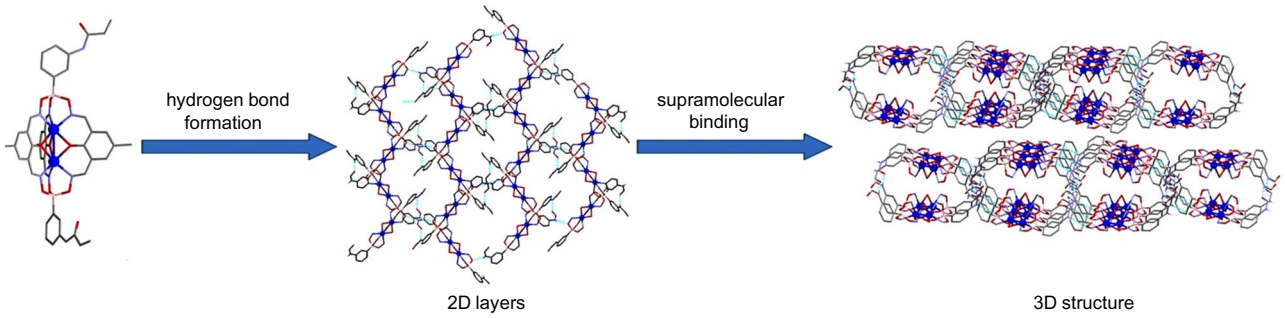
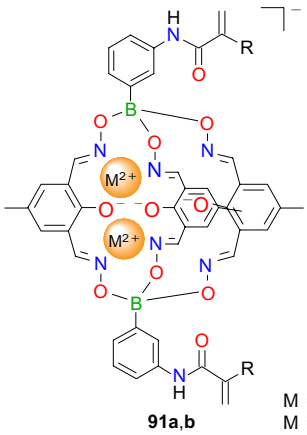


Figure 65. Formation of supramolecular clathrochelate-containing 2D layer networks and their conversion to 3D supramolecular assemplies. The figure was created by the authors using data of Ref. 263.

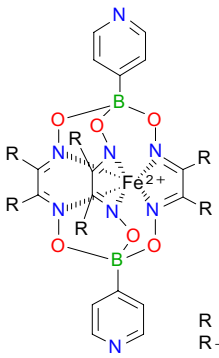
Structures 91



91a,b

M = Co, R = H (**a**);
M = Mn, R = Me (**b**)

Structures 92

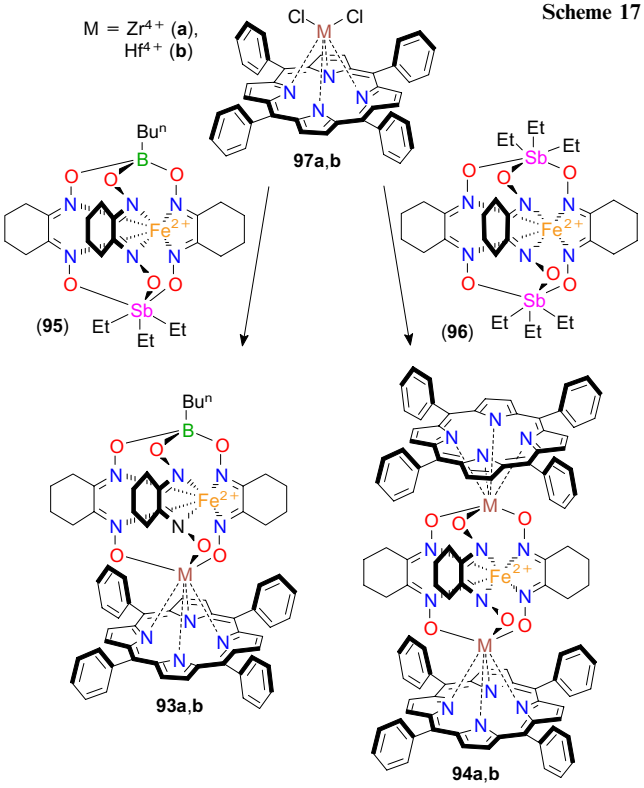


92a–d

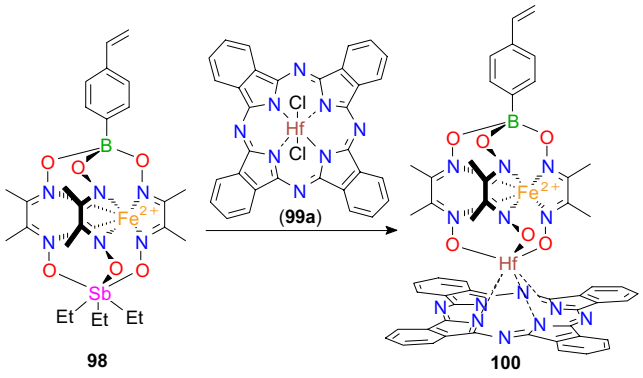
R = H (**a**), Et (**b**);
R–R = $(CH_2)_4$ (**c**);
$CH_2CH(Me)(CH_2)_2$ (**d**)

Antimony-containing iron and nickel(II) tris(pyridineoximates) **101a**,**b** with the reactive triethylantimony cross-linking group were prepared by template condensation of 2-acetylpyridineoxime and triethylantimony(V) dibromide using the corresponding metal ion as the template.[267] These labile complexes were readily transmetallated on treatment with zirconium and hafnium(IV) phthalocyanine complexes **99a**,**b** as Lewis acids to give binuclear iron (**102a**,**b**) and nickel(II) (**102c**,**d**) tris(pyridineoximates) with a phthalocyanine cross-linking group (Scheme 19, pathway *a*). Subsequently, Dudkin *et al.*[268] proposed a more convenient and efficient one-step preparation method of hybrid complexes **102a–d** in high yields, which consists in template condensation of 2-acetylpyridineoxime with phthalocyanines **99a**,**b** in the presence of 3d metal salts (pathway *b* in Scheme 19).

Scheme 17

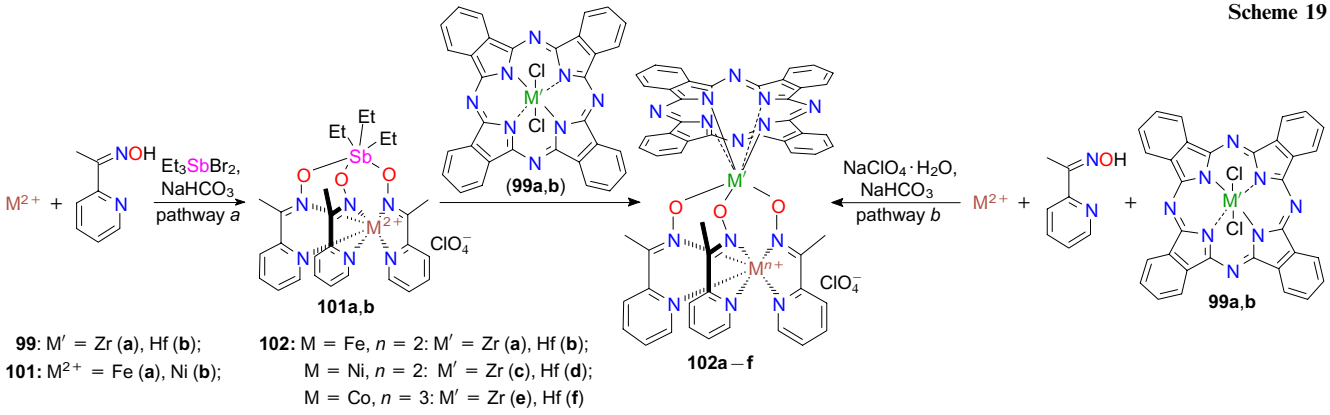


Scheme 18



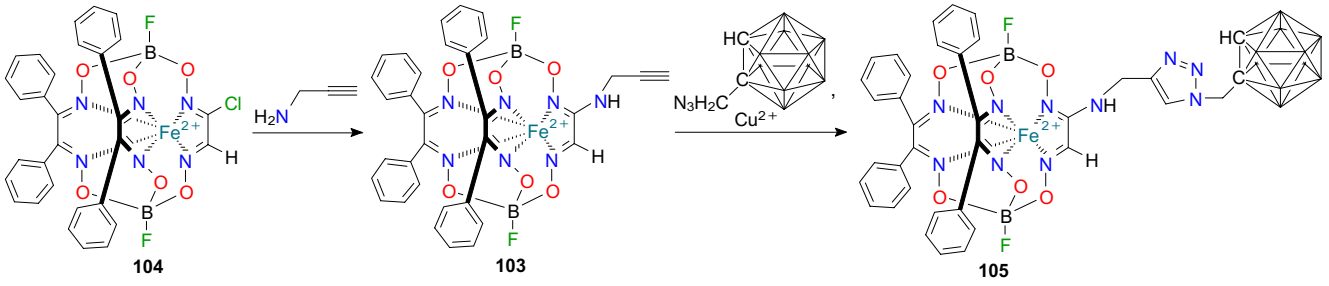
The aggregation of four hybrid binuclear iron and nickel(II) tris(pyridineoximates) shown in Scheme 19 with metal phthalocyanine cross-linking moieties **102a–d** was studied by spectral methods both in solutions and in fluoro-

Scheme 19



99: M′ = Zr (**a**), Hf (**b**);
101: M^{2+} = Fe (**a**), Ni (**b**);
102: M = Fe, *n* = 2: M′ = Zr (**a**), Hf (**b**);
M = Ni, *n* = 2: M′ = Zr (**c**), Hf (**d**);
M = Co, *n* = 3: M′ = Zr (**e**), Hf (**f**)

Scheme 20



plastic thin films.[269] It was shown that these complexes form H-type dimers in solutions or in poly(vinylidene fluoride)–hexafluoropropylene (PVDF-HFP) copolymer matrix, while the complexes immobilized on the surface of polymers exist mainly as single molecules.

Similar pseudo-macrobicyclic cobalt(III) tris(pyridineoximates) **102e**,**f** with phthalocyanine cross-linking moieties were prepared[270] according to Scheme 19 (pathway *b*) by direct template reaction of 2-acetylpyridineoxime with zirconium and hafnium(IV) phthalocyanine complexes **99a**,**b** and cobalt(II) salt. During this reaction, the central cobalt(II) ion was oxidized to Co^{3+}. According to single crystal X-ray diffraction,[270] the CoN_6 polyhedron of the cross-linked binuclear ZrPc complex has a truncated trigonal pyramidal geometry. The encapsulated cobalt(III) ion occurs nearly at the centre of this polyhedron, which is typical of low-spin cobalt(III) complexes: this cation is only slightly shifted along the molecular Co···Zr pseudo-C_3 symmetry axis of the semiclathrochelate cation.

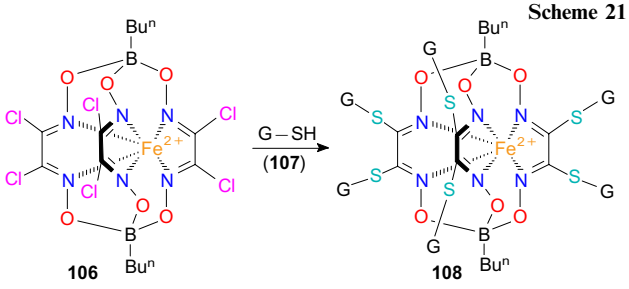
The monopropargylamine iron(II) cage complex **103**, obtained in a high yield by nucleophilic substitution reaction of monochlorinated clathrochelate precursor **104** with propargylamine, was introduced in the copper-catalyzed click-reaction with *o*-carborane-12-methyl azide, resulting in the formation of hybrid iron(II) monocarborane clathrochelate **105** (Scheme 20; BH groups are located at the dodecahedron vertices).[271]

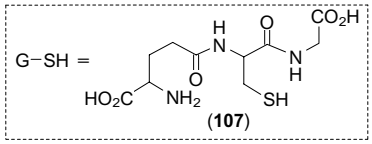
2.4.4. Supramolecular associates with protein macromolecules and their macromolecular chelators

Iron(II) n-butylborate hexachloroclathrochelate **106** showed[272] high cytotoxicity *in vitro* against human promyelocytic leukemia (HL-60) cell line [the half-maximal inhibitory concentration (IC_{50}) was 6.5 μmol L^{-1}]. This result was correlated with the substantial (17-fold with respect to the control) increase in the intracellular oxidative stress. Relying on the reported results,[272] this effect can be attributed to the alkylation (shown in Scheme 21) of glutathione (**107**) with highly reactive electrophilic clathrochelate **106**. This led to inhibition of the antioxidant defense system in cells and to catalytic generation of reactive oxygen species by the products of alkylation of this macrobicyclic complex, *e.g.*, compound **108**.

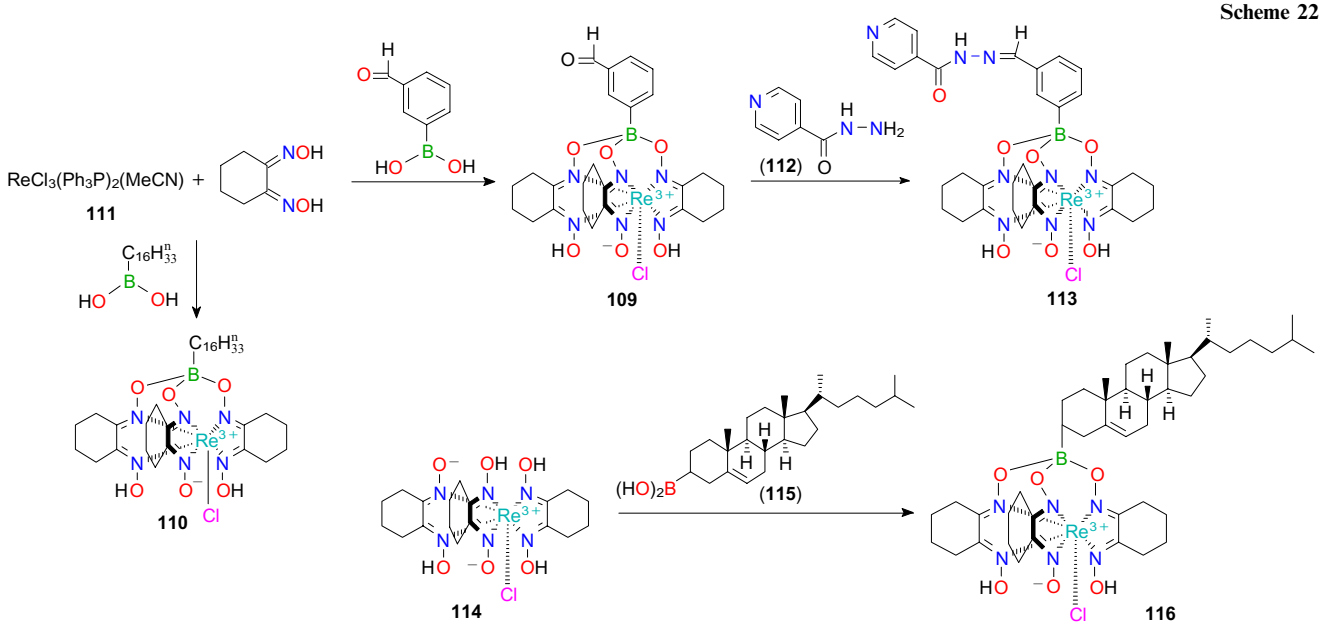
A number of iron and cobalt(II) mono- and bis-clathrochelates were tested *in vitro* in the transcription system of Taq DNA polymerase (DNAP), which uses polymerase chain reaction.[273] All of these complexes were found to be micromolar transcription inhibitors in this system, but only a few clathrochelates with terminal biorelevant groups showed IC_{50} values in a low micromolar range (5 to 40 μmol L^{-1}). The highest *in vitro* inhibitory activity was found[273] for homodifunctionalized iron(II) dicarboxyl monoclathrochelates. Meanwhile, their analogues such as C–C conjugated bis(clathrochelates) and heterofunctionalized morpholine-containing cage complexes with one termi-

Scheme 21





Scheme 22



nal carboxyl group and iron(II) monoclathrochelates with two carboxyl-terminated alkyl sulfide groups and alkylamine ribbed substituents containing terminal pyridine or morpholine groups are much less active transcription inhibitors of the DNAP system.

Rhenium(III) semiclathrochelates **109** and **110**, containing a biorelevant apical substituent, were synthesized from rhenium(III) solvate complex **111** (Scheme 22).[274] The template condensation of **111** with nioxime and 3-formylphenylboronic acid gives rise to rhenium(III) tris(nioximate) **109** with a terminal formyl group, which is subsequently subjected to H^+-catalyzed condensation with isoniazid (**112**) to give rhenium(III) semiclathrochelate **113** with an apical functionalizing vector substituent. Rhenium(III) semiclathrochelate **110** with an apical hexadecyl group at the bridging boron atom was prepared[274] by template condensation of nioxime and hexadecylboronic acid, with rhenium(III) ion serving as the template. In addition, cross-linking of pre-synthesized non-macrocyclic rhenium(III) tris(nioximate) **114** on treatment with cholesteryl boronic acid **115** resulted in the synthesis of rhenium(III) semiclathrochelate **116** with a cholesterol apical moiety (see Scheme 22).

Zelinskii *et al.*[275] described monoribbed-functionalized iron(II) cage complexes, the molecular design of which implied their efficient supramolecular binding to nucleic acids, and determined their biologically important ADMET characteristics.†

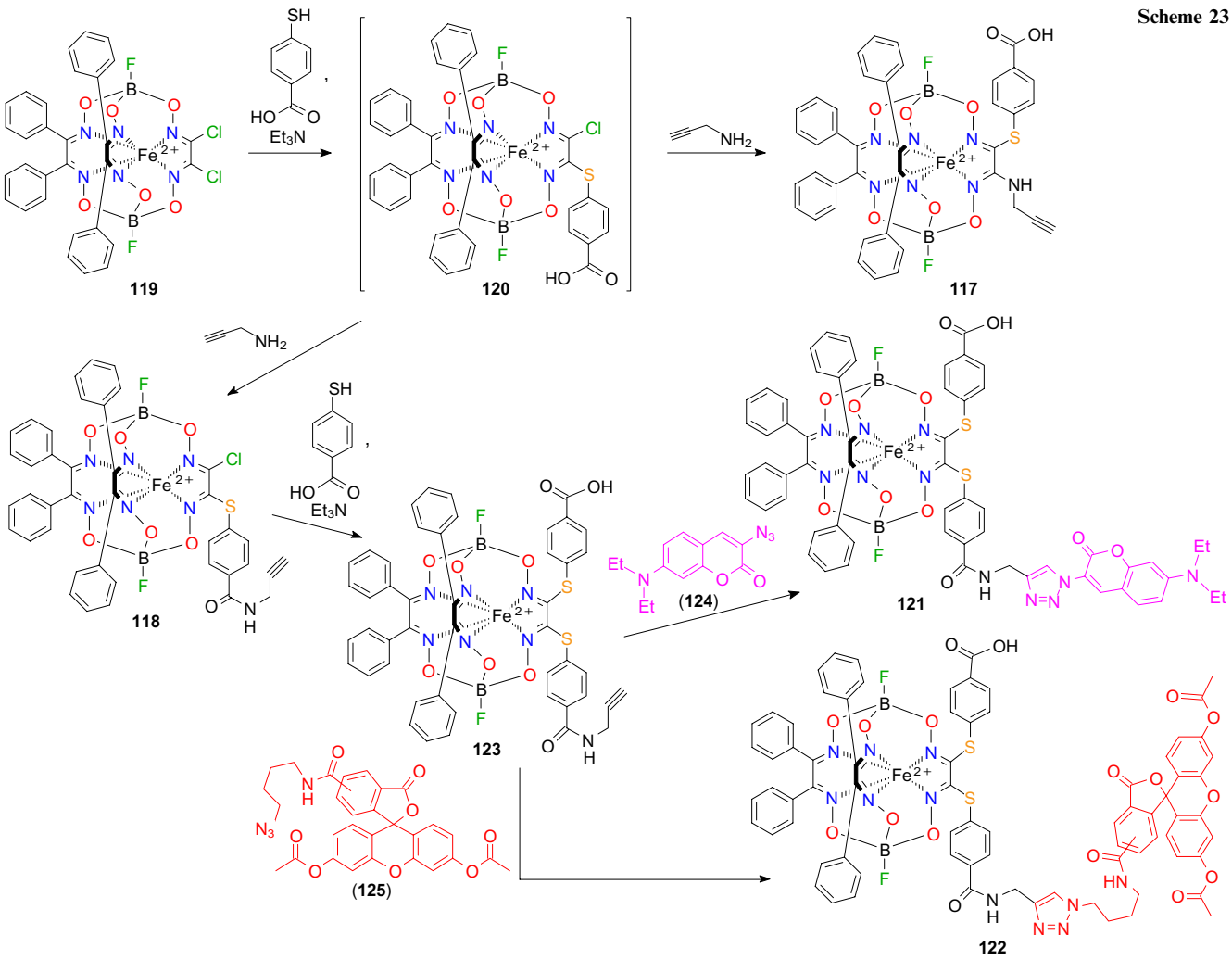
Heterodifunctionalized iron(II) clathrochelates **117** and **118**, containing terminal biorelevant carboxyl groups and reactive C≡C bonds, were obtained as depicted in Scheme 23.[276] The two-step synthetic procedure included stepwise nucleophilic substitution of dichloro clathrochelate precursor **119** under the action of *p*-carboxyphenylthiolate anion (to give intermediate **120**) and the subsequent treatment with 2-propargylamine. Clathrochelates **121** and **122**, prepared by the click reaction between alkyne **123** and azides **124** and **125**, were proposed as promising precursors of macrobicyclic iron(II) complexes.[276] These molecules contain an optically active (first of all, luminescent) reporter group or a radioactive label to visualize their cellular uptake and/or biodistribution in a specified biological system.

Kovalska *et al.*[277] discovered the appearance of induced chirality of metal clathrochelates **126a–m** and **127**, caused by their supramolecular or covalent binding to both biological macromolecules and optically active organic molecules, chirality inducers. In particular, ribbed-functionalized iron(II) clathrochelates, when acting as guests, were found to suppress the CD response (CD is circular dichroism) upon the supramolecular binding to an appropriate protein macromolecule as the host. Metal tris(dioximate) clathrochelates have a Russian doll-like structure (shown in Fig. 66): owing to the distorted trigonal prismatic (TP)–trigonal antiprismatic (TAP) geometry, the MN_6 coordination polyhedra have no inversion centre and possess chirality, but due to equal probabilities of the formation of levo- (Λ) and dextrorotatory (Δ) forms, they give no CD signal. The selective fixation of one of C_3-distorted conformations produces a CD signal in the visible region, where intense charge transfer bands (CTBs), $d(M) \rightarrow \pi^*(L)$, are also observed. The supramolecular interaction of the initially CD-inactive iron(II) clathrochelates containing terminal carboxyl groups with bovine serum albumin (BSA) induces[277] molecular asymmetry. Hence, the CD spectra of these clathrochelate-centred assemblies exhibit intense signals in the 350–600 nm range, whereas their methyl esters and amide derivatives remain virtually CD-inactive. It was shown that the supramolecular interaction of carboxyl-containing clathrochelates with BSA, or their covalent binding to (*R*)-(+)-1-phenylethylamine depend both on the solvent polarity and on the structural isomerism of the clathrochelate CD reporter.

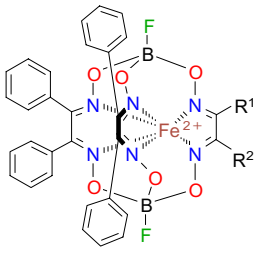
The induced circular dichroism (ICD) spectra of clathrochelate-centred isomeric macrobicyclic iron(II) complexes with six terminal carboxyl groups was used[278] to determine the structural and conformational changes of serum albumins. These clathrochelate CD reporters are able to discriminate between transport albumins with similar structure such as BSA and human serum albumin

† ADMET means absorption, distribution, metabolism, excretion and toxicity.

Scheme 23

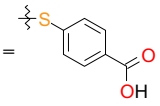


Structures 126, 127

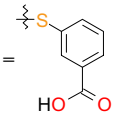


126a – m

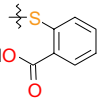
126a: R^1 = H, R^2 =



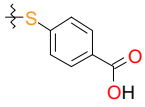
126b: R^1 = H, R^2 =



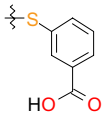
126c: R^1 = H, R^2 =



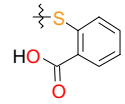
126d: R^1 = R^2 =



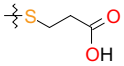
126e: R^1 = R^2 =



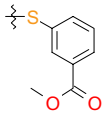
126f: R^1 = R^2 =



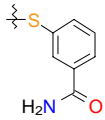
126g: R^1 = R^2 =

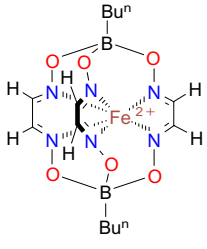


126h: R^1 = R^2 =



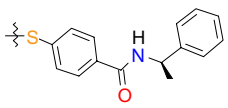
126i: R^1 = R^2 =



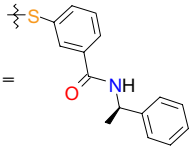


127

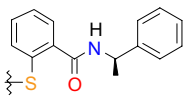
126j: R^1 = R^2 =



126k: R^1 = R^2 =



126l: R^1 = R^2 =



126m: R^1 = R^2 =



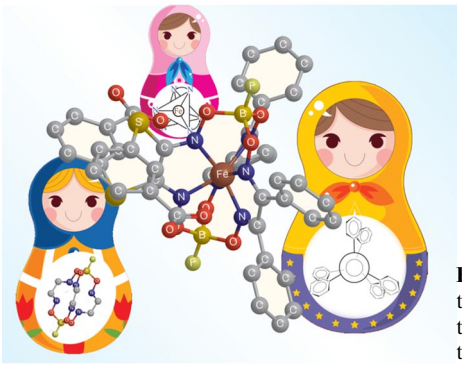


Figure 66. Schematic image of metal tris(dioximate) clathrochelates.[277]

(HSA), the binding to which gives clathrochelate-centred structures with intense ICD spectra. Variation of the shape and intensity of the bands in these spectra was also used to detect[278] changes in the tertiary structure of albumin macromolecules. It was shown that the structural isomerism of CD-inducing hexcarboxyl clathrochelates significantly affects both the ICD response upon binding to the above-mentioned proteins and the thermodynamic parameters of the clathrochelate–albumin supramolecular assembly. These iron(II) clathrochelates were proposed[278] as promising three-dimensional molecular platforms for the design and synthesis of sensitive CD reporting molecules able to efficiently recognize specific elements on the surface of protein macromolecules.

Iron(II) clathrochelates with two terminal carboxyl groups were tested[279] as potential CD reporters for studying the structures of various proteins. The authors obtained structural isomers of heterodifunctionalized iron(II) clathrochelate with two non-equivalent ribbed carboxyphenyl sulfide groups. They studied the interaction of these clathrochelates and their homodifunctionalized isomers with serum albumins, lysozyme, β-lactoglobulin (BLG), trypsin and insulin using quenching of intrinsic fluorescence of the protein and ICD spectra of clathrochelate-centred structures. High-intensity ICD signals were observed upon the formation of 1 : 1 supramolecular assemblies of these clathrochelates with albumins. In the presence of BLG, various structural isomers of dicarboxyl-containing iron(II) clathrochelate demonstrated ICD bands with opposite signs, which indicates that opposite (Λ or Δ) configurations are stabilized in these assemblies upon the supramolecular binding to the mentioned globular proteins.

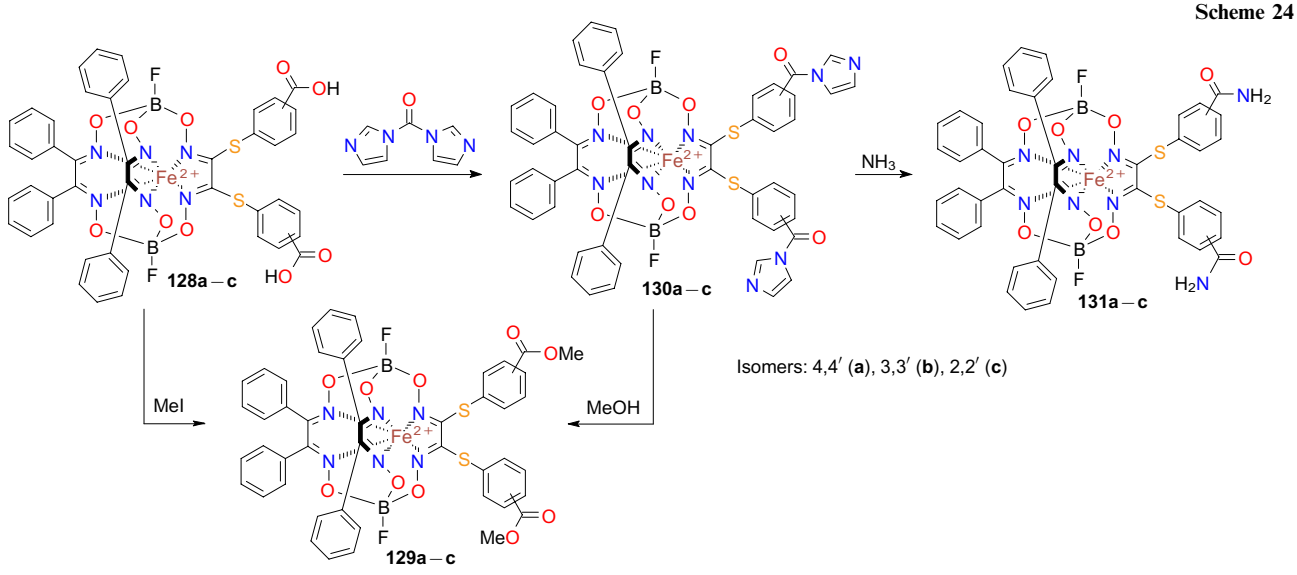
Functionalization of terminal carboxyl groups in iron(II) carboxyaryl sulfide clathrochelate isomers **128a–c** was used to prepare their macrobicyclic carboxymethyl (**129a–c**) and carboxyamide (**130a–c**, **131a–c**) derivatives (Scheme 24).[280] Quenching of the intrinsic luminescence of the protein was used to investigate the reaction of compounds **129** and **130** with BSA. It was shown that this modification of the terminal groups of iron(II) clathrochelates reduces quenching of the intrinsic luminescence of this protein by an order of magnitude and also alters the type of influence of the clathrochelate isomerism on the quenching of the BSA intrinsic luminescence. The most pronounced luminescence quenching was observed for complexes **128** and, among them, by isomer **128c**, which quenches the intrinsic luminescence of BSA 16 times more strongly than **128a**,**b**. The complexes with ester (**129**) and amide (**131**) substituents affect to a much lesser extent the protein luminescence intensity. In the case of amide-containing clathrochelates **131**, the most pronounced quenching is observed for the *ortho*-isomer **131c**, which quenches the protein luminescence almost two times more efficiently than complexes **131a**,**b**.[280]

2.4.5. Reactivity and physical properties of encapsulated metal ions

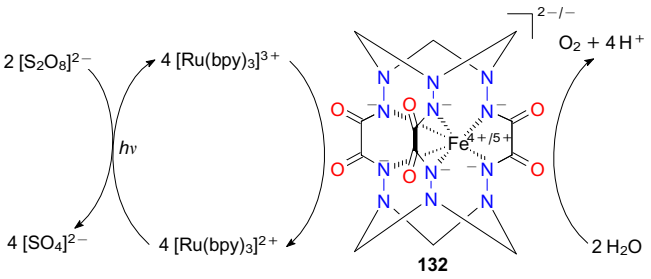
Shykin *et al.*[281,282] reported efficient photochemical splitting of water on exposure to visible light catalyzed by iron(IV) oxalyl hydrazonate clathrochelate **132**. The possible catalytic cycle for this fast and efficient homogeneous photochemical decomposition of water to O_2 is depicted in Scheme 25 and includes the formation of Fe^{V}-containing intermediate under catalytic conditions.

The first 'classical' iron(I) dioximate **133** was prepared as shown in Scheme 26[283] and was characterized by X-ray diffraction. The chemical reduction of the macrobicyclic precursor — iron(II) hexachloroclathrochelate **106** — with potassium graphite in the presence of 18-crown-6 ether (**134**) results in a clathrochelate with an encapsulated iron(I) ion. Complex **133** and its cobalt(I)-encapsulating analogues were highly chemically stable to strong H-acids such as trifluoroacetic acid.

Scheme 24

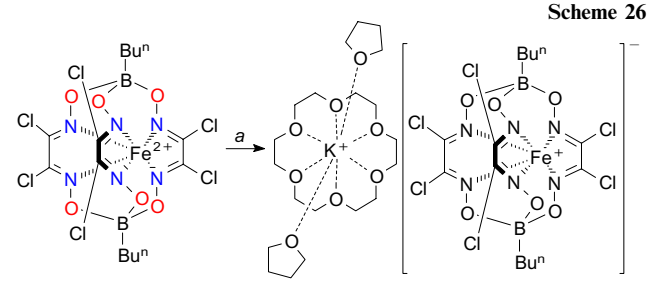


Scheme 25



132

Scheme 26



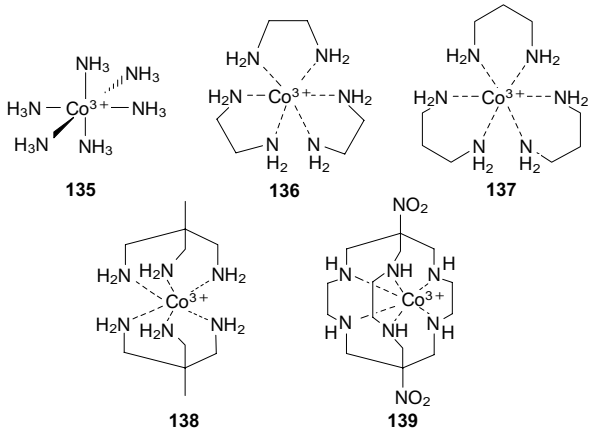
106 **133**

(*a*) C_8K, 18-crown-6 (**134**), THF

Ozvat *et al.*[284] studied the effect of encapsulation of the cobalt(II) ion by the dinitrosarcophagine ligand on the temperature dependence of the ^{59}Co NMR chemical shifts; this chemical shift can be used to determine the local temperature (so-called NMR thermometry). It was shown that encapsulation of this low-spin ion ($s = 1/2$) increases its temperature sensitivity. The temperature dependence of the chemical shift (δ) in the ^{59}Co NMR spectrum ($\Delta\delta/\Delta T$ ratio) for the series of low-spin cobalt(II) complexes **135** – **139** increases with increasing degree of encapsulation of cobalt(II) ion: hexaammoniate **135** with monodentate ligands had a value of 1.44(2) ppm $°C^{-1}$, while the value for macrobicyclic dinitrosarcophagine complex **139** was 2.04(2) ppm $°C^{-1}$.[284]

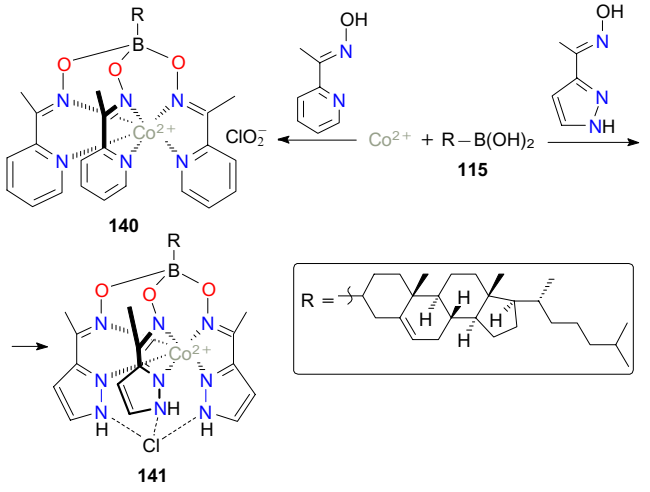
The temperature-dependent NMR spectroscopy can serve for highly accurate determination of the anisotropy of the magnetic susceptibility tensor ($\Delta\chi$) for paramagnetic d-metal complexes. This approach was successfully implemented[285] to study cholesteryl-containing cobalt(II) pseudo-clathrochelates **140**, **141** with a high anisotropy of the magnetic susceptibility tensor (Scheme 27). The conformational rigidity and large size of the apical cholesterol moiety, which contains a large number of magnetically nonequivalent nuclei of hydrogen and carbon, ensured a high convergence of the obtained experimental and theoretically calculated ^1H and ^{13}C NMR chemical shifts. This allowed for highly accurate determination of $\Delta\chi$ and the zero-field splitting energy for cobalt(II) complexes of this type.

Structures 135 – 139



135 **136** **137** **138** **139**

Scheme 27



140 **115** **141**

Paramagnetic complexes **140** and **141** were also proposed[285] as promising single-molecule magnets and paramagnetic labels for determining the structure of biological macromolecules (in particular, cholesterol-binding proteins) and as model compounds for determining chirality using NMR spectroscopy.

2.5. Inorganic nanosized spherands — keplerates

Spherical polyoxometallates called keplerates were discovered by Professor A.Müller and co-workers[286] in Germany in 1998. The first keplerate, $[Mo^{IV}_{72}Mo^{V}_{60}O_{372}(AcO)_{30}(H_2O)_{72}]^{42-}$ (**142**), was obtained by hydrazine reduction of an ammonium molybdate solution in an acetate buffer. The keplerate anions have an icosahedral symmetry and are composed of twelve pentagonal $\{(M^{VI})M^{VI}_5\}$ units (M = Mo, W), which occupy the vertices of an icosahedron and are linked by thirty bridging moieties (Fig. 67). The $\{(M)M_5\}$ building blocks are composed of the

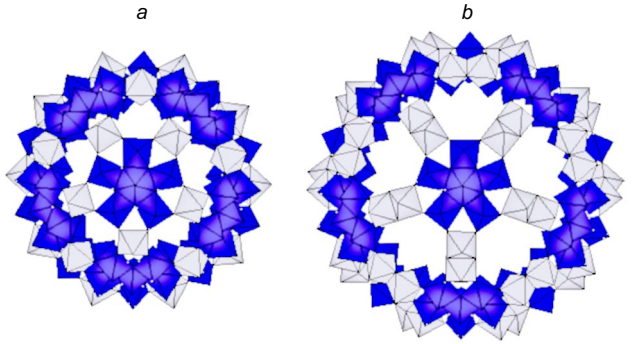


Figure 67. Keplerate with mononuclear (*a*) and binuclear (*b*) bridges. Blue colour designates the $\{M_6O_{21}(H_2O)_6\}$ groups and gray colour shows the bridges. The figure was created by the authors using data of Ref. 289.

central pentagonal bipyramid $\{MO_6(H_2O)\}$ and five $\{MO_6\}$ octahedra connected to the central bipyramid at the equatorial edges. Single metal ions or dimolybdenum groups form the bridges (B). The general formula of the keplerate anion has the form $[\{M_6O_{21}(H_2O)_6\}_{12}B_{30}]^{n-}$. It is of interest that all aqua ligands point inside the spherical shell, while the terminal oxo ligands are located on the outer surface of the sphere.[287, 288]

The keplerate anions possess a relatively large internal cavity with a diameter of up to 17 Å. An important feature of the keplerate structure is the presence of 20 pores opening the access into this cavity, the pore size being determined by the type of bridges. In the case of keplerates with dimolybdenum bridges, the pore diameter is 7–8 Å, while for the keplerate with mononuclear linkers, the maximum pore size is 6 Å. Through these pores, small molecules and ions are free to both enter the shell and return back to the solution. The cavity of keplerates isolated from aqueous solutions usually accommodates 60 to 150 water molecules.

2.5.1. Keplerates with mononuclear bridges

2.5.1.1. Keplerates containing {(Mo)Mo$_5$} type pentagonal units

The reaction of keplerate **142** with a solution of $FeCl_3 \cdot 6\,H_2O$ at pH 3 is accompanied by replacement of the dimolybdenum $\{Mo_2O_4\}^{2+}$ bridges by the $\{Fe(H_2O)\}^{3+}$ groups, This gives rise to compound $[Mo_{72}Fe_{30}O_{252}(AcO)_{12}\{Mo_2O_7(H_2O)\}_2\{H_2Mo_2O_8(H_2O)\}(H_2O)_{91}] \cdot 150\,H_2O$ (**143**) (the condensed formula is $\{Mo_{72}Fe_{30}\}$), which contains neutral discrete spherical molecules. The $\{Mo_2O_7(H_2O)\}$ and $\{H_2Mo_2O_8(H_2O)\}$ moieties (Fig. 68), which are coordinated in the keplerate cavity in the tetradentate fashion, are disordered.[289]

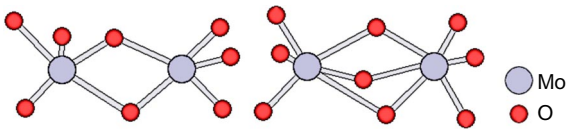


Figure 68. Structures of the $\{Mo_2O_7(H_2O)\}$ and $\{H_2Mo_2O_8(H_2O)\}$ groups. Hydrogen atoms are omitted for the sake of simplicity. The figure was created by the authors using data of Ref. 289.

The Raman spectra for the solution and crystals of compound **143** are identical, which attests to the stability of the spherical shell upon dissolution. Magnetochemical measurements reveal weak antiferromagnetic exchange interactions between the high-spin Fe^{3+} ions.[289] Owing to the high spin ordering and high total magnetic moment, the molecule of keplerate **143** is one of the most highly symmetrical magnetic bodies.[290] In dilute aqueous solutions, the molecules of **143** are rapidly assembled into large spherical aggregates with a hydrodynamic radius of 34 nm, comprising approximately 600 $\{Mo_{72}Fe_{30}\}$ spherical molecules (Fig. 69). The aggregate size can be controlled by varying the keplerate concentration.[291, 292] The influence of the solution pH on the assembly was studied. When pH < 2.9, keplerate **143** is neutral and exists in solution as single species, whereas in the pH range of 2.9–6.6, self-assembly takes place.[293] Complexes of nanosized aggregates with dimethyldioctadecylammonium (DODA) cation were prepared; this allowed the aggregates to be transferred into organic phase without degradation. Upon the coordination

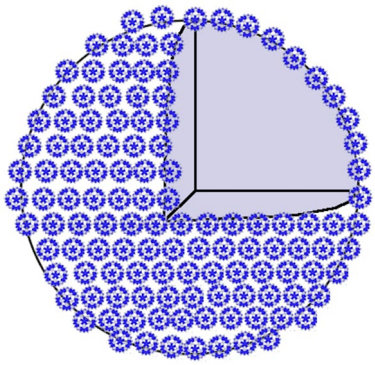


Figure 69. Hollow spherical aggregate formed by molecules of keplerate **143**. The figure was created by the authors using data of Ref. 292.

of DODA, the hydrodynamic radius of the spherical aggregates increases to 60 nm.[294]

A decrease in the pH is accompanied by the formation of the neutral keplerate $[Mo_{72}Fe_{30}O_{252}(AcO)_{10}\{Mo_2O_7(H_2O)\}.\{H_2Mo_2O_8(H_2O)\}_3(H_2O)_{91}] \cdot 140\,H_2O$ (**144**), which has two acetate ligands less and the charge of which is counterbalanced by an additional $\{H_2Mo_2O_8(H_2O)\}^{2-}$ oxomolybdate unit. When the crystals of keplerate **144** are dried in air, the solid-state condensation reaction takes place to give Fe–O–Fe bonds between the keplerates (Fig. 70). The compound thus formed has a network structure with the general formula $\{[H_4Mo_{72}Fe_{30}O_{254}(AcO)_{10}\{Mo_2O_7(H_2O)\}.\{H_2Mo_2O_8(H_2O)\}_3(H_2O)_{87}] \cdot 80\,H_2O\}_n$ (**145**).[295, 296]

The reaction of iron(II) sulfate with a sodium molybdate solution acidified with sulfuric acid gives rise to the partially reduced keplerate $Na_9K_3[K_{20}\subset Mo^{VI}_{70}Mo^{V}_{2}Fe^{III}_{30}O_{252}(SO_4)_{24}(H_2O)_{75}] \cdot 140\,H_2O$ (**146**).[297] The cavity of anion **146**, unlike that of keplerate **143**, is occupied by sulfate ligands, while the 20 keplerate pores confined by the $\{Fe_3Mo_3O_6\}$ rings are occupied by the K^+ ions.

The reaction of a sodium molybdate solution acidified with a considerable amount of glacial acetic acid with iron(III) chloride gives the keplerate $Na_4[\{Mo_6O_{19}\}\subset\{Mo_{72}Fe_{30}O_{252}(AcO)_{20}(H_2O)_{92}\}] \cdot 120\,H_2O$ (**147**).[298] Unlike keplerates **143** and **144**, complex **147** contains, in the internal cavity, the hexamolybdate $[Mo_6O_{19}]^{2-}$ with the Lindqvist structure, which is not linked to the

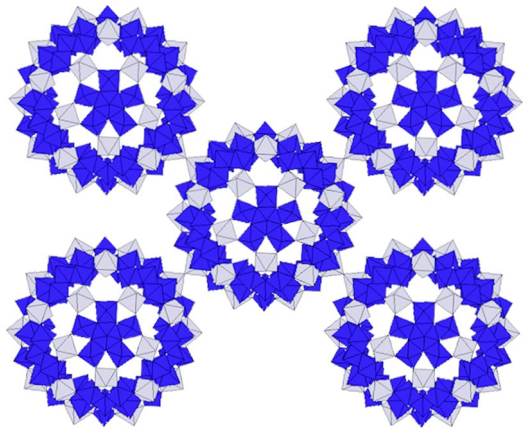


Figure 70. Formation of infinite layers by condensation of keplerate **144**. Blue colour designates $\{Mo_6O_{21}(H_2O)_6\}$ groups and gray colour shows the $\{FeO_6\}$ bridges. The figure was created by the authors using data of Ref. 295.

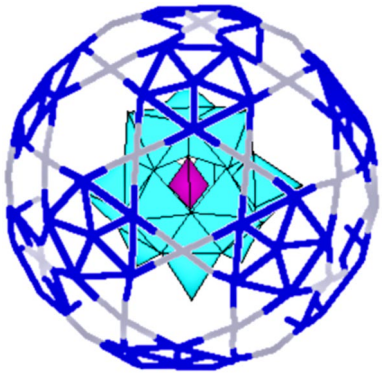


Figure 71. Schematic image of keplerate **148**. Blue lines designate the $\{Mo_6O_{21}(H_2O)_6\}$ groups and gray lines correspond to the $\{FeO_6\}$ bridges. Pink colour corresponds to the $\{PO_4\}$ tetrahedron and light blue colour marks the $\{MoO_6\}$ octahedra. The figure was created by the authors using data of Ref. 299.

keplerate shell by covalent bonds. The addition of salts $FeCl_2 \cdot 4H_2O$ or $FeCl_3 \cdot 6H_2O$ to an aqueous solution containing $[PMo_{12}O_{40}]^{3-}$ in air, some of Keggin anions are destroyed to give the $\{Mo_6O_{21}(H_2O)_6\}$ building blocks, which react with iron ions.[299, 300] The remaining Keggin anions act as templates for the assembly, resulting in the $O_{Keggin} \cdots O_{keplerate}$ shortest distances of approximately 2.6 Å, which is typical of hydrogen bonding (Fig. 71).

When $FeCl_2 \cdot 4H_2O$ is used, the reaction gives $[H_xPMo_{12}O_{40} \subset Mo_{72}Fe^{III}_{30}(AcO)_{15}O_{252}(H_2O)_{102}] \cdot 120H_2O$ (**148**), which is a keplerate molecule with the encapsulated partially reduced $[H_xPMo_{12}O_{40}]^{3-}$ anion. In the case of $FeCl_3 \cdot 6H_2O$, fully oxidized keplerate $[PMo_{12}O_{40} \subset \subset Mo_{72}Fe^{III}_{30}(AcO)_{15}O_{252}(H_2O)_{102}] \cdot 120H_2O$ (**149**) is formed. Similar compounds, $Na_6[SiMo_{12}O_{40} \subset \subset Mo68^{VI}Mo^{V}_4Fe^{III}_{30}O_{252}(AcO)_{16}(H_2O)_{100}] \cdot 120H_2O$ (**150**)[297] and $Na_3K_4[BW_{12}O_{40} \subset Mo^{VI}_{68}Mo^{V}_4Fe^{III}_{30}O_{252}(AcO)_{16}(H_2O)_{100}] \cdot 120H_2O$ (**151**),[301] were obtained with the Keggin anions $[SiMo_{12}O_{40}]^{4-}$ and $[BW_{12}O_{40}]^{5-}$.

When iron(II) reacts with a solution of sodium molybdate in the presence of acetic acid, the compound $Na_2[Mo^{VI}_{72}Mo^{V}_6Fe^{III}_{24}(AcO)_{20}O_{258}(H_2O)_{84}] \cdot 150H_2O$ (**152**) is formed.[302] The $\{Fe^{III}(H_2O)_2\}$ and $\{Mo^{V}O(H_2O)\}$ bridges in this product are randomly distributed over thirty positions.

The partial oxidation of keplerate **142** with air oxygen in a solution with pH 2.5 in the presence of NaCl gives dark blue crystals of $[\{Mo_6O_{21}(H_2O)_4(AcO)\}_{12}\{Mo^{V}O(H_2O)\}_{30}] \cdot \cdot 150H_2O$ (**153**). Apart from the thirty Mo^{V} metal centres, which constitute the $\{MoO(H_2O)\}^{3+}$ bridges, the structure contains six more Mo^{V} atoms, which are delocalized and fall within the $\{Mo_6O_{21}(H_2O)_6\}$ pentagonal units. The presence of 36 Mo^{V} centres was confirmed by the results of cerimetric titration. An interesting feature of the $O{=}Mo^{V}(H_2O)$ bridge is that the terminal oxygen atoms point inside the spherical anion.[303]

The reaction of chromium(III) chloride with sodium molybdate in acidified aqueous solution with high acetic acid concentration gave the keplerate $[\{Na(H_2O)_{12}\} \subset \subset \{Mo_{72}Cr^{III}_{30}O_{252}(AcO)_{19}(H_2O)_{94}\}] \cdot 150H_2O$ (**154**).[304] An interesting feature of this complex is the occurrence of the $\{Na(H_2O)_{12}\}^{+}$ associate in the keplerate anion cavity, with the oxygen atoms of $\{Na(H_2O)_{12}\}^{+}$ forming an icosahedron. The associate is stabilized owing to the hydrophobic environment formed by acetate ligands inside the shells. The behaviour of complex **154** in solution resembles that of the iron-containing keplerate **143**: at low pH (< 2.7) the compound exists as discrete species, while the self-assembly occurs in the pH range from 2.7 to 7.0.[305]

The addition of vanadyl sulfate to an acidified solution of sodium molybdate in the presence of potassium cations results in the formation of the keplerate anion $[K_{10} \subset \{Mo_6O_{21}(SO_4)(H_2O)_3\}_{12}\{(V^{IV}O)_{30}(H_2O)_{20}\}]^{26-}$ ($\{Mo_{72}V_{30}\}$) (**155**), which was isolated as the mixed salts $K_{14}Na_8(VO)_2 \cdot$ [**155**] $\cdot 150H_2O$ (Ref. 306) and $Na_8K_{16}(VO)(H_2O)_5 \cdot$ [**155**] $\cdot 150H_2O$.[307] The assembly of keplerate anions **155** in solution was studied by Kistler *et al.*[305] Unlike neutral keplerates **143** and **154**, the keplerate $\{Mo_{72}V_{30}\}$ has a high negative charge and exists in aqueous solutions as discrete anions. The addition of acetone to a solution of anion **155** induces the formation of spherical aggregates, the size of which increases with increasing concentration of acetone. The reduction of aqueous solutions of sodium molybdate and vanadyl sulfate with sodium dithionite in the presence of potassium cations gave the product $K_2Na_6[K_{20} \subset \{Mo_6O_{21}(SO_4)(H_2O)_3\}_{12} \cdot \{V^{IV}O(H_2O)\}_{22}\{Mo^{V}O(H_2O)\}_8] \cdot 140H_2O$ (**156**).[308] Each $\{(Mo)Mo_5\}$ pentagonal unit coordinates the sulfate anion in the tridentate mode, while twenty potassium cations plug the keplerate pores, being linked to six oxygen atoms.

Two mixed-metal keplerate complexes, $K_{23}Na_4[\{Mo^{V/VI}_6O_{21}(H_2O)_3(SO_4)\}_{12}(V^{IV}O(H_2O))_{15}(Mo^{V}O(H_2O))_8 \cdot (Fe^{III}(H_2O)_2)_7] \cdot 150H_2O$ (**157**) and $K_{21}Na_2[\{Mo^{V/VI}_6O_{21} \cdot (H_2O)_3(SO_4)\}_{12}(V^{IV}O(H_2O))_{11}(Mo^{V}O(H_2O))_8(Fe^{III}(H_2O)_2)_{11}] \cdot \cdot 150H_2O$ (**158**), were prepared by adding vanadyl and iron(II) sulfates to an acidified solution of sodium molybdate.[309] The $[Fe^{III}(H_2O)_2]^{3+}$, $[V^{IV}O(H_2O)]^{2+}$ and $[Mo^{V}O(H_2O)]^{3+}$ bridges present in this structure are statistically disordered over 30 positions.

It was shown that Fe^{3+} ions in keplerate **143** can be partly replaced by larger cations, such as Ce^{3+} and Pr^{3+}. The addition of the corresponding lanthanide chlorides resulted in the synthesis of $[\{Mo_{18}O_{66}Ln_2(H_2O)_n\} \subset \subset \{Mo_{72}Fe_{24}Ln_6O_{252}(H_2O)_{105}\}] \cdot 200H_2O$, where Ln = Ce (**159**) and Pr (**160**).[310] The six lanthanide bridging ions are disordered over 12 positions and are slightly elevated above the keplerate surface. The structure of the moiety designated as $\{Mo_{18}O_{66}Ln_2(H_2O)_n\}$ and encapsulated in the keplerate cavity could not be reliably determined because of its high disorder.

2.5.1.2. Keplerates containing {(W)W$_5$} type pentagonal units

The keplerate anion $[(NH_4)_{20} \subset \{W_6O_{21}(SO_4)\}_{12}\{Fe(H_2O)\}_{30} \cdot (SO_4)_{13}(H_2O)_{34}]^{12-}$ (**161**) is formed upon the reaction of sodium tungstate with iron(II) sulfate in the presence of ammonium chloride.[311] The pores of keplerate **161** confined by the $\{Fe_3W_3O_6\}$ rings are occupied by twenty ammonium cations.

The reaction of a tungstate solution acidified with sulfuric acid with vanadyl sulfate in the presence of potassium cations affords the keplerate $K_{14}(VO)_2[K_{20} \subset \subset \{W_6O_{21}(SO_4)\}_{12}(VO)_{30}(SO_4)(H_2O)_{63}] \cdot 150H_2O$ (**162**).[312] Twelve out of the thirteen sulfate ligands located in the internal cavity are coordinated to twelve $\{(W)W_5\}$ units in the tridentate fashion, while one more sulfate ligand links one V atom and two W atoms and is disordered over eight positions. Each of the 20 pores confined by the $\{V_3W_3O_6\}$ rings accommodates a potassium cation (Fig. 72).

One more method that can be used to prepare keplerate anions $\{W_{72}(VO)_{30}\}$ comprises the reaction of sodium tungstate with ammonium vanadate in the presence of potassium sulfite and hydrazine sulfate. The vanadyl cations are formed in solution *in situ* and constitute the structure of keplerate **163**, which was isolated as the complex $K_2Na_{14}[Na_{14}K_6 \subset \{W_6O_{21}(H_2O)_3(SO_4)\}_{12}\{VO(H_2O)\}_{30}] \cdot \cdot 90H_2O$. In this case, no additional disordered sulfate

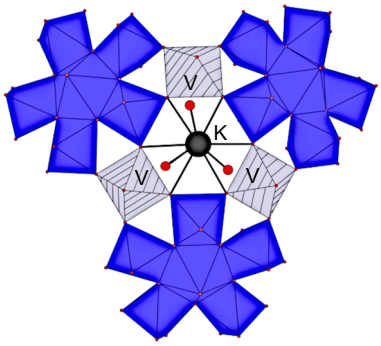


Figure 72. Position of a potassium cation in the pores of keplerate **162**. Blue colour designates the $\{W_6O_{21}(H_2O)_6\}$ groups and gray colour shows the $\{VO_6\}$ bridges. Black colour corresponds to the potassium atom and red colour shows the oxygen atoms of the coordinated water molecules. The figure was created by the authors using data of Ref. 312.

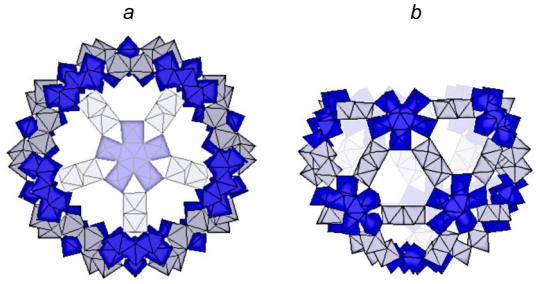


Figure 73. Structure of the anion in compound **165**, top view (*a*) and side view (*b*). Blue colour designates the $\{Mo_6O_{21}(H_2O)_6\}$ groups and gray colour corresponds to the $\{Mo_2O_{10}\}$ bridges. The figure was created by the authors using data of Ref. 317.

ligand is present in the cavity, and the pores are occupied by sodium and potassium cations.[313]

2.5.2. Keplerates with binuclear bridges

2.5.2.1. Keplerates containing {(Mo)Mo$_5$} type pentagonal units

As has already been noted, the first known keplerate $[Mo^{VI}_{72}Mo^{V}_{60}O_{372}(AcO)_{30}(H_2O)_{72}]^{42-}$ (**142**) was obtained from a solution of ammonium molybdate in the presence of acetate ligands.[286] An important role in this reaction belongs to pH of the solution, because it is necessary to create conditions for the formation of the $\{Mo^{VI}O_7\}$ pentagonal bipyramidal groups, which form the basis for the pentagonal $\{(Mo^{VI})Mo^{VI}_5\}$ building blocks. Upon the addition of hydrazine sulfate, molybdenum centres are partly reduced and are converted to bridging $\{Mo^{V}_2O_4(AcO)\}$ groups, which are stabilized due to the high concentration of bidentate acetate ligands. The assembly of keplerate **142** was studied in a water–acetone solvent mixture. It was shown that the presence of counter ions is of crucial importance, because both the assembly and destruction of aggregates depend on the absolute magnitude of the charge of keplerate: neutral species and highly charged anions do not form aggregates. The aggregate size can be controlled by changing the component ratio in the water–acetone system.[314] The reaction of an aqueous solution of keplerate **142** with a solution of DODA gives the corresponding salt $(DODA)_{40}(NH_4)_2[(H_2O)_{50}\subset Mo_{132}O_{372}(AcO)_{30}(H_2O)_{72}]$ (**164**), which immediately migrates to the organic phase.[315, 316]

When a solution of keplerate **142** is kept in air in the presence of Na^+ cation, the product $Na_{46}[Mo^{VI}_{66}Mo^{V}_{50}O_{331}(AcO)_{30}(H_2O)_{56}]\cdot 300\,H_2O$ (**165**) is formed.[317] The basket-shaped structure of the $[Mo^{VI}_{66}Mo^{V}_{50}O_{331}(AcO)_{30}(H_2O)_{56}]^{46-}$ anion can formally be derived from the structure of anion **142** by removing one $\{Mo_{16}\}\equiv\{(Mo^{VI})(Mo^{VI}_5)(Mo^{V}_2)_5\}$ group (Fig. 73). Compound **165** is substantially more readily soluble in water than complex **142**, owing to the easy access of solvent molecules into the cavity.

The keplerate anions $[Mo_{132}O_{372}(HCO_2)_{30}(H_2O)_{72}]^{42-}$ (**166**),[318] $[Mo_{132}O_{372}(ClCH_2CO_2)_{30}(H_2O)_{72}]^{42-}$ (**167**)[318] and $[Mo_{132}O_{372}(EtCO_2)_{30}(H_2O)_{72}]^{22-}$ (**168**)[319] were prepared by reaction of hepta-ammonium molybdate with formic, monochloroacetic and propionic acids in the presence of hydrazine sulfate. When butyric acid was used, the $[Mo_{132}O_{372}(Pr^nCO_2)_{24}(H_2O)_{84}]^{16-}$ keplerate anion (**169**) was formed, with 24 butyrate ligands being coordinated in the cavity, which is caused by steric reasons.[320] In the inner cavity of anion **166**, self-organization of water molecules takes place to form onion type hydrogen-bonded cluster. Six H_2O molecules form a nearly trigonal antiprism with a 3.5 Å distance from the centre of the onion. The second shell (with 6.2–6.9 Å size) contains approximately 35 closely packed H_2O molecules. The third shell (8.2–8.7 Å) consists of a smaller number of water molecules, which occupy positions between bidentate ligands in the pore region. This unusual arrangement is obviously possible only in the presence of relatively small formate ligands, which coordinate the $\{Mo^{V}_2\}$ groups.

A specific feature of anions **168** and **169** is that the $\{H_2O+NH_4^+\}$ associate with the O–N distance of 2.7 Å, disordered over nine possible positions, is incorporated in each of the twenty pores of the shell. These keplerates were shown to encapsulate molecules of hydrophobic alcohols into the cavity.

One more method for preparing new keplerate anions is replacement of labile acetate ligands in the cavity of keplerate **142**. For example, the reaction with oxalic acid ($H_2C_2O_4$) yielded keplerate $(NH_4)_{42}[\{Mo_6O_{21}(H_2O)_6\}_{12}.\{Mo_2O_4(O_2CCO_2H)\}_{30}]\cdot\{300\,H_2O+2\,H_2C_2O_4\}$ (**170**), in which the acetate ligands have been replaced by oxalate ligands.[321] When a solution of compound **170** is kept at room temperature, partial deprotonation and dissociation of oxalate ligands take place to give the $[\{Mo_6O_{21}.(H_2O)_6\}_{12}\{Mo_2O_4(O_2CCO_2H)\}_8\{Mo_2O_4(O_2CCO_2)\}_{16}\{Mo_2O_4.(H_2O)_2\}_6]^{52-}$ keplerate anion (**171**). X-Ray diffraction data confirm the presence of 24 partially deprotonated oxalate ligands, which are statistically distributed over thirty positions, and six $\{Mo_2O_4\}^{2+}$ linkers each containing two water molecules as ligands.

The introduction of a reactive azide group into the keplerate cavity was attained by replacing the acetate ligands in compound **142** in the presence of excess azidoacetic acid, which gave $[\{Mo_6O_{21}(H_2O)_6\}_{12}\{Mo_2O_4.(N_3CH_2CO_2)\}_{13}\{Mo_2O_4(H_2O)_2\}_{17}]^{25-}$ (**172**).[322] The reaction of complex **172** with excess propiolic acid at room temperature afforded a mixed-ligand keplerate with coordinated azidoacetate and propiolate groups over a period of several minutes.[322] On standing of the solution, the Huisgen reaction product, keplerate $[Mo_{132}O_{372}(triazole)_{11}(H_2O)_{110}]^{23-}$ (**173**), where triazole-H is 4-carboxy- or 5-carboxy-1,2,3-triazole-1-acetic acid, was isolated in a quantitative yield. The NMR spectrum of compound **173** exhibited no signals for the coordinated azidoacetic or propiolic acid, but showed signals for free 4-carboxy- and 5-carboxy-1,2,3-triazole-1-acetic acids in 4 : 1 ratio relative to the keplerate.

The possibility of replacing acetate groups in the keplerate anion with isobutyrate, pivalate and benzoate ligands was studied by ^1H NMR spectroscopy.[323] For this purpose,

keplerate **142** was several times treated with a 4 M solution of sodium acetate buffer; this gave compound **174**, which was described as $Na_{34}[\{Mo_6O_{21}(H_2O)_6\}_{12}\{(Mo_2O_4)_{30}.(AcO)_{22}(H_2O)_{16}\}]\cdot 300\,H_2O$ according to the data of elemental analysis. The data of ^1H NMR spectroscopy also confirmed the presence of 22 acetate ligands per each keplerate. When aliquot portions of acids RCO_2D (R = Pr^i, Bu^t, Ph) were added to a solution of compound **174** in D_2O, the substitution took place only in the case of isobutyric and pivalic acids, but not with benzoic acid. Whereas for R = Pr^i, the equilbrium in the substitution reaction is attained as soon as within 17 min, in the case of R = Bu^t, this requires 45 days. This is attributable to the size of substituent at the carboxyl group, which is smaller than the keplerate pores in the former case. For larger Bu^t group, entering the cavity requires a minor change in the bond lengths and angles in the $\{Mo_9O_9\}$ group and/or other reversible changes in the coordination environment of the Mo metal centres.

The acetate ligands can also be replaced by other oxygen-containing anion groups. The reaction of keplerate **142** with sodium hypophosphite at pH 2 resulted in the isolation of product $(NH_4)_{42}[\{Mo_6O_{21}(H_2O)_6\}_{12}\{Mo_2O_4(H_2PO_2)\}_{30}]\cdot \cdot 300\,H_2O$ (**175**), in which the keplerate core was preserved without changes, except that all thirty acetate groups have been replaced by hypophosphite groups.[317] The addition of keplerate **142** to a solution of a mixture of sodium dihydrogen phosphate and ammonium chloride at pH 5 afforded the anionic complex $[\{Mo_6O_{21}(H_2O)_6\}_{12}\{Mo_2O_4(HPO_4)_{30}\}]^{72-}$ (**176**).[324] It is of interest that in this case, the solution pH had to be increased (by adding, *e.g.*, NH_4OH) rather than decreased, as in other cases. If this reaction is carried out at pH 2, partial decomposition of keplerate **142** takes place, giving rise to some free molybdate. The latter enters the cavity as $\{Mo^{VI}O_3H\}$ groups, each being bonded to three phosphate ligands surrounding the $\{Mo_9O_9\}$ pores from the inside. In view of geometric considerations, up to eight molybdenum groups can be accommodated in the cavity; however, only five $\{MoO_3H\}$ groups were actually found, which corresponds to the formation of $[\{Mo_6O_{21}(H_2O)_6\}_{12}\{Mo_2O_4(HPO_4)_{30}\}(MoO_3H)_5]^{67-}$ (**177**).[324]

Refluxing of a solution of keplerate **142** in the presence of excess $(NH_4)_2SO_4$ at pH 1 is accompanied by replacement of the acetate ligands by thirty sulfate groups, thus giving keplerate $[(H_2O)_{81-n}+(NH_4)_n\subset\{Mo_6O_{21}(H_2O)_6\}_{12}.\{Mo_2O_4(SO_4)\}_{30}]^{(72-n)-}$ (**178**).[325] A similar reaction at pH 3 leads to partial replacement of acetate ligands to yield the anionic complex $[\{Mo_6O_{21}(H_2O)_6\}_{12}\{Mo_2O_4(SO_4)\}_{18}.\{Mo_2O_4(AcO)\}_{12}]^{60-}$ (**179**).[325] The addition of $CeCl_3$ during the synthesis of anion **178** induces the formation of keplerate $Ce_3(NH_4)_{54}[Ce_3\subset\{Mo_6O_{21}(H_2O)_6\}_{12}\{Mo_2O_4(SO_4)\}_{30}]\cdot \cdot 300\,H_2O$ (**180**).[324] Three cerium cations reside in the cavity of this compound, each of them being bound to the coordinated sulfate ligand in the bidentate fashion. In the presence of excess urea and sodium chloride, $[\{(NH_2C(O)NH_3)_{20}+Na_{13}\}\subset\{Mo_6O_{21}(H_2O)_6\}_{12}\{Mo_2O_4(SO_4)\}_{30}]^{39-}$ (**181**) is formed.[324] In this compound, 20 protonated urea cations can fit inside the $\{Mo_9O_9\}$ rings, which confine the pores, and they are hydrogen-bonded to the oxygen atoms, while each of the 13 sodium cations inside the cavity is linked to six oxygen atoms, three of which belong to sulfate groups and the other three belong to the aqua ligands (Fig. 74).

When keplerate **142** reacts with sodium sulfate at pH 2.5 and at room temperature, the acetate ligands are not completely replaced, but the process stops after the formation of the $[Na_6+(H_2O)_n\subset\{Mo_6O_{21}(H_2O)_6\}_{12}\{Mo_2O_4(SO_4)\}_{24}.\{Mo_2O_4(AcO)\}_6]^{60-}$ anion (**182**).[325] Meanwhile, if the reaction is carried out at pH 4.5 with long-term holding of the reaction mixture at 30 °C, the $[\{Mo_6O_{21}(H_2O)_6\}_{12}.\{Mo_2O_4(HSO_4)\}_{18}\{Mo_2O_4(AcO)\}_{12}]^{42-}$ keplerate anion (**183**), containing hydrogen sulfate groups, is formed.[317]

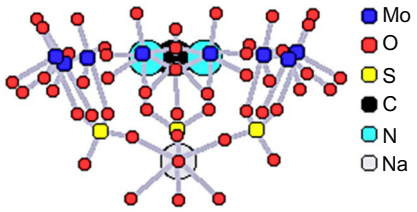


Figure 74. Positions of urea and sodium cations in the pores of keplerate **181**. The figure was created by the authors using data of Ref. 324.

The reaction of keplerate **142** with Cs_2SO_4 carried out with heating (80 °C) gives the product $Cs_{10}(NH_4)_{52-n}.[\{Cs_{10}+(H_2O)_{81-n}+(NH_4)_n\}\subset\{Mo_6O_{21}(H_2O)_6\}_{12}\{Mo_2O_4(SO_4)\}_{30}]\cdot 200\,H_2O$ (**184**).[324] The caesium cations are coordinated to keplerate pores, but due to too small size, they are not located at the centre, but are slightly shifted towards the sides. The reaction of complex **178** with calcium chloride resulted in the synthesis of $Ca_{16}\{Ca_{20}(H_2O)_{60}\}\subset\subset\{Mo_6O_{21}(H_2O)_6\}_{12}\{Mo_2O_4(SO_4)\}_{30}]$ (**185**).[326] Twenty Ca^{2+} cations are arranged in the inner cavity of the keplerate, being bound to the pores from the inside, while the other are coordinated in the pores and on the outer surface of the shells.

When CO_2 is bubbled through a neutral solution of keplerate **142** in the presence of formamidinium chloride, the anion $[(HC(NH_2)_2)_{20}\subset\{Mo_6O_{21}(H_2O)_6\}_{12}.\{Mo_2O_4(CO_3)\}_{30}]^{52-}$ (**186**) is formed.[327] In compound **186**, all 20 pores are plugged with formamidinium cations, which are hydrogen-bonded to the oxygen atoms of the $\{Mo_9O_9\}$ rings. The ammonium salt of the same anion — $(NH_4)_{72}[\{Mo_6O_{21}(H_2O)_6\}_{12}\{Mo_2O_4(CO_3)\}_{30}]\cdot 260\,H_2O$ (**186′**) — was prepared in a similar way. At room temperature, salts **186** and **186′** gradually decompose, which is associated with the release of coordinated CO_2; salt **186** decomposes much more slowly due to the stabilizing effect of closed pores.

It was demonstrated that the hypophosphite ligands in $(NH_4)_{42}[\{Mo_6O_{21}(H_2O)_6\}_{12}\{Mo_2O_4(H_2PO_2)\}_{30}]\cdot 300\,H_2O$ (**175**) can be partially substituted.[317] On short-term heating (90 °C) of a solution of compound **175** with guanidinium

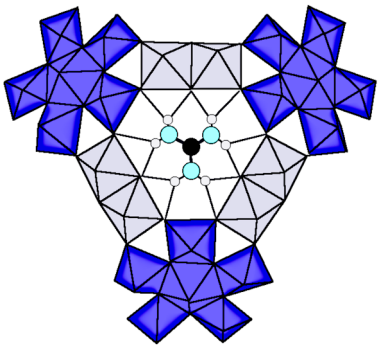


Figure 75. Position of the guanidinium cation in the pores of keplerate **187**. Blue colour designates the $\{Mo_6O_{21}(H_2O)_6\}$ groups and gray colour corresponds to the $\{Mo_2O_{10}\}$ bridges. Black colour corresponds to the carbon atom, blue colour marks the nitrogen atoms, and light gray shows the hydrogen atoms. The figure was created by the authors using data of Ref. 328.

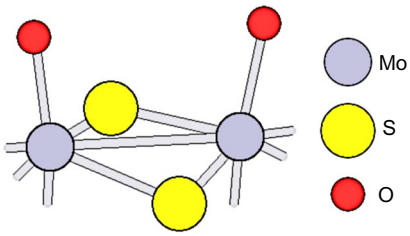


Figure 76. Structure of the $\{Mo_2O_2S_2\}$ unit. The figure was created by the authors using data of Ref. 330.

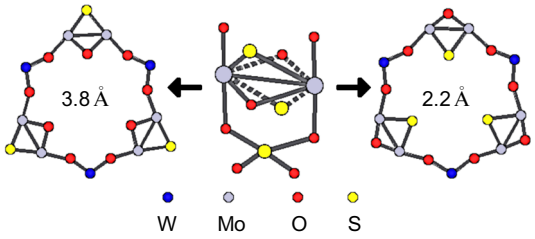


Figure 77. Disorder of the bridging ligands in the $\{Mo_2O_2(\mu\text{-}O)(\mu\text{-}S)\}$ moiety and two boundary types of the pores formed in keplerate **195**. The figure was created by the authors using data of Ref. 335.

sulfate, the guanidinium salt of the keplerate anion $[\{[(NH_2)_3C]\}_{20}\subset\{Mo_6O_{21}(H_2O)_6\}_{12}\{Mo_2O_4(SO_4)\}_{10}.\{Mo_2O_4(H_2PO_2)\}_{20}]^{32-}$ (**187**) is formed in a nearly 100% yield.[328] In this product, 20 guanidinium cations are coordinated to keplerate pores *via* hydrogen bonds (Fig. 75).

Apart from the dimolybdenum bridging group $\{Mo_2O_2(\mu\text{-}O)_2\}^{2+}$, there are other known examples of binuclear linkers. A sulfide analogue — keplerate $Na_{38}K_{3.5}(NMe_4)_{3.5}[\{Mo_6O_{21}(H_2O)_6\}_{12}\{Mo_2O_2S_2(AcO)\}_{30}]\cdot\cdot(AcO)_3\cdot 200\,H_2O$ (**188**) [329] — was obtained by the reaction of ammonium molybdate with a source of the $\{Mo_2O_2(\mu\text{-}S)_2\}^{2+}$ cations (Fig. 76).[330] A similar reaction carried out in the presence of sulfate anions yielded the keplerate $(NMe_2H_2)_{27}(NH_4)_{15}[\{Mo_6O_{21}(H_2O)_6\}_{12}\{Mo_2O_2S_2\}_{30}.(SO_4)_{15}(H_2O)_{30}]\cdot 90\,H_2O$ (**189**),[331] in which the sulfate ligands were disordered over thirty possible positions in the $\{Mo_2O_2S_2\}$ groups. Recrystallization of compound **188** gave a structure with the $[\{Mo_6O_{21}(H_2O)_6\}_{12}\{Mo_2O_2S_2\}_{30}(AcO)_{15}(H_2O)_{30}]^{27-}$ anion (**190**) characterized by a similar disorder of the coordinated acetate ligands.[329]

2.5.2.2. Keplerates containing $\{(W)W_5\}$ type pentagonal units

The first keplerate with dimolybdenum bridges containing $\{(W^{VI})W_5^{VI}\}$ type pentagonal units was reported in 2009.[332] It was synthesized by adding a slight excess of the binuclear complex $(NH_4)_2[Mo_2^{V}O_4(C_2O_4)_2(H_2O)_2]\cdot 3\,H_2O$ to a solution of sodium tungstate acidified with acetic acid. Apart from thirty acetate ligands coordinated to the dimolybdenum bridging moiety, the structure contains six disordered acetate ligands, which are coordinated to pentagonal units and bind the central W atom to a peripheral one. Thus, the keplerate anion has the formula $[\{W_6O_{21}(H_2O)_5(AcO)_{0.5}\}_{12}\{Mo_2O_4(AcO)\}_{30}]^{48-}$ (**191**). In solutions of compound **191** containing 30–75% acetone, spherical aggregates are formed, and their size increases with increasing acetone concentration. This result is consistent with the data that were obtained earlier for analogous molybdenum keplerate **142**.[314]

When an acidified solution of keplerate **191** reacts with ammonium selenate, thirty coordinated acetate ligands are replaced by selenate ligands.[333] Six additional acetate ligands are also substituted, but by water molecules. On the basis of elemental analysis data, this keplerate was described by the formula $(NH_4)_{72}[\{W_6O_{21}(H_2O)_6\}_{12}.\{Mo_2O_4(SeO_4)\}_{30}]\cdot 150\,H_2O\cdot 6\,(NH_4)_2SeO_4$ (**192**). Recrystallization of compound **192** in the presence of dimethylammonium cations affords the keplerate $(NH_4)_{20}(NH_2Me_2)_{32}[\{W_6O_{21}(H_2O)_6\}_{12}\{Mo_2O_4\}_{30}(SeO_4)_{20}.(H_2O)_{20}]\cdot 150\,H_2O$ (**193**). Some of the selenate ligands are lost during recrystallization, with their sites being occupied by coordinated water molecules.

Using dimolybdenum monosulfide building block, $[Mo_2O_2(\mu\text{-}O)(\mu\text{-}S)]^{2+}$ (Ref. 334), the keplerate $[\{W_6O_{21}(H_2O)_6\}_{12}\{Mo_2O_3S(AcO)\}_{30}]^{42-}$ (**194**) was prepared. [335] When a solution of this anion was acidified with sulfuric acid to pH 2 in the presence of methylammonium chloride, the product $Na_4(MeNH_3)_{68}[\{W_6O_{21}(H_2O)_6\}_{12}.\{Mo_2O_3S(SO_4)\}_{30}]\cdot 230\,H_2O$ (**195**), containing sulfate ligands, was obtained. Each of the thirty dimolybdenum moieties is disordered with 50% probability between the bridging oxide and sulfide ligands; this gives rise to four types of pores on the keplerate surface — $\{W_3Mo_6O_9\}$, $\{W_3Mo_6O_8S\}$, $\{W_3Mo_6O_7S_2\}$ and $\{W_3Mo_6O_6S_3\}$ — differing in both the size and reactivity (Fig. 77).

The reaction of sodium tungstate with the $\{Mo_2O_2(\mu\text{-}S)_2\}^{2+}$ cation [330] gives rise to $[\{W_6O_{21}(H_2O)_6\}_{12}\{Mo_2O_2S_2(AcO)\}_{20}\{Mo_2O_2S_2(H_2O)_2\}_{10}]^{32-}$ (**196**).[336] Upon the addition of $CoCl_2\cdot 6\,H_2O$ to a solution of anion **196**, the crystals of $[\{W_6O_{21}(H_2O)_6\}_{11}\{W_6O_{21}.(H_2O)(H_2Mo_2O_8(H_2O))\}(Mo_2O_2S_2)_{30}(AcO)_{10}(H_2O)_{40}]^{24-}$ (**197**) are formed. The $\{H_2Mo_2O_8(H_2O)\}$ inner group, which was detected previously in keplerate **143**,[289] is coordinated to five oxygen atoms of the $\{(W)W_5\}$ unit and is disordered over four pentagonal units of this type.

2.5.3. Properties of keplerates

The diversity of keplerates is notable '...not only from an aesthetic point of view, but also because they show properties of interest for different areas of science',[332] and this will be clear from the examples given below.

2.5.3.1. Conduction of chemical reactions within the shell

It was shown that keplerate shell can affect the reactions that take place inside the cavity. An example is the above-described synthesis of keplerate **172**,[322] containing azidoacetate ligands, followed by Huisgen cycloaddition of internal azide groups to propiolic acid. In the resulting keplerate anion **173**, the cavity accommodates coordinated triazole ligands. It is noteworthy that the reaction within the shell is markedly faster and more regioselective than this reaction without the shell.

One more example concerns the possibility of controlled removal of the internal acetate ligands of the $[Mo_{132}O_{372}(AcO)_{30}(H_2O)_{72}]^{42-}$ anion (**142**). This gives rise to the $\{Mo_2O_4(H_2O)_2\}^{2+}$ bridges with labile water molecules. These bridging groups are both Lewis and Brønsted acids and show catalytic activity. This was demonstrated for model reaction: reversible cleavage and formation of *tert*-butyl methyl ether in water under mild conditions.[337]

2.5.3.2. Catalytic reactions involving keplerates

Catalytic properties of iron-containing keplerate **143** were studied in the selective liquid-phase oxidation of thioethers to sulfoxides.[338] With hydrogen peroxide and *tert*-butyl

hydroperoxide as oxidants, the compound exhibited high catalytic activity and good selectivity. The catalytic properties of the iron-containing keplerate **143** and also chromium- ($[\{Na(H_2O)_{12}\}\subset\{Mo_{72}Cr_{30}O_{252}(AcO)_{19}(H_2O)_{94}\}]$, **154**) and vanadium-containing ($K_{14}Na_8(VO)_2[K_{10}\subset\subset\{Mo_6O_{21}(SO_4)(H_2O)_3\}_{12}\{(VO)_{30}(H_2O)_{20}\}]$, **155**) keplerates were tested in olefin epoxidation with hydrogen peroxide.[339] All these keplerates catalyze this reaction; the lowest activity was found for keplerate **143**, while the highest conversion and selectivity were observed for **154**. Their activity did not change over several catalytic cycles. The same keplerates were studied in the catalytic oxidation of various sulfides with hydrogen peroxide.[340] The highest activity in this reaction was found for chromium-containing keplerate **154**, although compounds **143** and **155** were also relatively active.

The keplerate $[H_xPMo_{12}O_{40}\subset Mo_{72}Fe_{30}.(AcO)_{15}O_{252}(H_2O)_{102}]$ (**148**), bearing the phosphomolybdate $\{H_xPMo_{12}O_{40}\}$ within the shell, catalyzes the oxidation of alcohols to aldehydes and ketones by hydrogen peroxide.[341] A total of 19 alcohols were studied in this work. The activity of keplerate **148** and the other two keplerates $Na_6[SiMo_{12}O_{40}\subset Mo_{72}Fe_{30}O_{252}(AcO)_{16}(H_2O)_{100}]$ (**150**) and $Na_3K_4[BW_{12}O_{40}\subset Mo_{72}Fe_{30}O_{252}(AcO)_{16}(H_2O)_{100}]$ (**151**) with encapsulated Keggin anions was studied in olefin epoxidation reactions with hydrogen peroxide.[342] The catalytic activity of these keplerates proved to be appreciably higher than that of the free Keggin anions or the 'empty' keplerate **143**. The highest conversion and selectivity were inherent in compounds **150** and **151**. Keplerates **148**, **150** and **151** were also used in the catalytic oxidation of sulfides to sulfoxides or sulfones and oxidative desulfurization of dibenzothiophene.[343] The utilization of keplerates proved to be more efficient than the use of free Keggin anions, with the highest activity being inherent in compound **151**.

The catalytic properties of the $[Mo_{132}O_{372}(AcO)_{30}(H_2O)_{72}]^{42-}$ (**142**) keplerate anion were tested in the aerobic epoxidation of various olefins taking place in an aqueous solution in the absence of radical initiators.[344] Most reactions gave the expected epoxides in high yields and with good chemo- and stereoselectivity. The keplerate stability over 10 catalytic cycles was confirmed by Raman spectroscopy. It was also shown that the catalytic reaction does not proceed if keplerate is replaced by MoO_3 or common molybdenum(VI) salts — $Na_2MoO_4\cdot 2H_2O$ or $(NH_4)_6Mo_7O_{24}\cdot 4H_2O$.

2.5.3.3. Production of materials based on keplerates

In the reaction of an aqueous solution of keplerate **142** with an excess of a chloroform solution of dimethyldioctadecylammonium chloride, the compound $(DODA)_{36}(NH_4)_6[Mo_{132}O_{372}(AcO)_{30}(H_2O)_{72}]\cdot 75H_2O$,[345] differing only slightly in the cationic composition from the above-described keplerate **164**, is extracted into the organic phase. This salt exhibits liquid crystalline properties between room temperature and the temperature of the loss of a water molecule (260 °C). A phase with liquid crystalline properties were also obtained using the $[\{Mo_6O_{21}(H_2O)_6\}_{12}\{Mo_2O_2S_2\}_{30}(SO_4)_{15}(H_2O)_{30}]^{42-}$ keplerate anion (**189**).[346] Anion **189** was initially treated with a solution of ammonium sulfate in order to replace water molecules by SO_4 groups, and then the keplerate was extracted with a DODA-Cl solution in chloroform. The products thus formed had the following compositions: $(DODA)_{44}(NH_4)_{14}[Mo_{132}S_{60}O_{312}(SO_4)_{23}(H_2O)_{86}]$ (**198**) and $(DODA)_{56}(NH_4)_{16}[Mo_{132}S_{60}O_{312}(SO_4)_{30}(H_2O)_{72}]\cdot 15H_2O$ (**199**). Polarized light microscopy shows the formation of a liquid birefringent uniform texture, which suggests a liquid crystalline nature of the samples.

In 2013, Jin *et al.*[347] reported for the first time the use of spherical keplerates in photoelectric systems. A composite film consisting of the $[K_{20}\subset\{W_6O_{21}(SO_4)\}_{12}(VO)_{30}(SO_4)(H_2O)_{63}]^{18-}$ keplerate anion (**162**) and a water-soluble poly(*p*-phenylenevinylene) derivative was obtained by layer-by-layer self-assembly. The photocurrent response in this system is attributable to the photoinduced electron transfer from the polymer part to keplerate **162**. This result indicates that $\{W_{72}V_{30}\}$ type keplerate could be a promising electron-withdrawing material.

The interfacial contact and control of morphology are highly significant for the fabrication of high-performance planar photodetectors. It is supposed that substrates coated by a perovskite film would direct the growth of a perovskite crystal and would ensure an appropriate energy level for efficient capture of photoelectrons. Recently, a film based on keplerate **162** and polyethyleneimine was used for substrate modification;[348] furthermore, the amount of keplerate was controlled *via* layer-by-layer self-assembly. The results indicate that keplerate can not only facilitate the electron transfer, but can also affect the crystal growth rate. The film-modified sample demonstrated a twofold increase in the photocurrent in comparison with the control sample, from 4.5 to 9.1 μA.

In 2020, the possibility of aggregation of rhodamine B, a xanthene dye, on the surface of the keplerate anion $[Mo_{132}O_{372}(AcO)_{30}(H_2O)_{72}]^{42-}$ (**142**) was reported.[349] By using the Langmuir isotherms and Stern–Volmer complete model, the authors were able to identify the thermodynamic causes for adsorption on the keplerate surface of both monomer mixture and H- and J-aggregated dye forms, which can either coexist or be interconverted (UV and fluorescence spectroscopy data). A method for switching between H- and J-aggregates by functionalization of keplerate **142** and rhodamine B associates was proposed; this can be used in photovoltaics or bioimaging.

2.5.3.4. Potential biomedical applications of keplerates

In 2013, the acute toxicity of the neutral keplerate $[Mo_{72}Fe_{30}O_{252}(AcO)_{12}\{Mo_2O_7(H_2O)\}_2\{H_2Mo_2O_8(H_2O)\}.(H_2O)_{91}]\cdot 150H_2O$ (**143**) as a candidate for targeted drug delivery into the body was studied for the first time.[350] No considerable deviations of biochemical characteristics of the functional state of liver, kidney and pancreas from normal values was detected. Study of the subacute toxicity did not reveal accumulation of compound **143** or deviation of any characteristics from normal values. Then the possibility of transport of keplerate **143** through the rat skin was revealed. The transport efficiency considerably increased in an electric field.[351] As a result, the authors selected the optimal conditions of electrophoresis and established the absence of changes in the biochemical values used in clinical laboratory diagnosis to assess the functional state of the heart, liver, kidneys and pancreas, which indicates the possibility of clinical use of this compound. The ability of keplerate **143** associates with polyvinylpyrrolidone and lanthanum cations to penetrate the skin membrane was studied in a similar way.[352] Polyvinylpyrrolidone is a biocompatible polymer, which serves for hiding nano-sized keplerate **143** from the immune system. Presumably, lan-

thanum cations can be used in these systems as ion tracers to monitor the keplerate migration and distribution in the body tissues. The diffusion coefficient of the associates was found to be much lower than that for pure keplerate. This effect seems to be related to the ability of keplerates to be assembled into spherical associates, while the lanthanum cations and polyvinylpyrrolidone can accelerate this process by functioning as bridges between the anions. In turn, increase in the size of associates retards their transport across the skin membrane.

The electrophoretic transport of keplerate **143** through the skin was simulated on the basis of experimental data.[353] The physicochemical model of the keplerate transport under the action of an electric field gives close values for calculated and experimental diffusion coefficients of keplerates in the skin. This model implies an empirical concentration dependence of the specific electrical conductivity of keplerates in the skin membrane, which allows estimation of the intrinsic electrical conductivity of the membrane. Thermodynamic approach provided data that can be used to predict the penetration depth of keplerates into the skin and the possibility of their accumulation with time.

Further *in vitro* studies of the physicochemical aspects of the electric transport of keplerate **143** made it possible to determine the optimal operating conditions and to examine polarization phenomena on native skin membranes. New experimental data on the layer-by-layer distribution of keplerates in the skin were obtained by X-ray fluorescence spectroscopy.[354] Using a model setup, Ostroushko *et al.*[355] explored the possibility of electrophoretic transport of keplerate-associated biologically active compounds across native membranes and determined the relevant diffusion coefficients. Thiamine chloride (vitamin B_1) and insulin were chosen as parts of associates to model the membrane transport. Additionally, features of formation of ionic associates of keplerate **143** with biologically active molecules such as thiamine chloride, insulin and albumin were investigated and the arrangement of the thiamine molecules on the keplerate surface was determined.[356]

Danilova *et al.*[357] studied the effect of keplerate **143** on the content of histone proteins and heat shock proteins in the peripheral blood and in the liver of rats after single and multiple administration. The keplerate injection did not induce a decrease in the amount of histone proteins in the peripheral blood lymphocytes, which may indicate the absence of pro-inflammatory factor gene expression. An increase in the content of heat shock proteins (Hsp60 and Hsp70) in the liver was detected; the magnitude of this increase was found to depend on the duration of exposure to compound **143**. The assumption of the absence of pro-inflammatory lymphocyte phenotype and the protective action of heat shock proteins was confirmed by the fact that the values characterizing the state of liver remain normal throughout the keplerate exposure. The introduction of keplerates was also accompanied by increasing number of cells containing heat shock proteins Hsp60 and Hsp70 in the spleen and thymus, despite the presence of blood–thymus barrier.[358,359] No changes of blood values indicating an inflammatory process or anaemia were detected, and no significant morphological disorders were found in the spleen or thymus.

The wide occurrence of anaemia and the presence of side effects of the use of existing iron-containing drugs stimulate the search for new therapeutic agents. The intramuscular administration of iron molybdenum keplerate **143** (in a dose of 1.5 mg kg^{-1}) in anaemic rats promoted faster recovery of the red blood count and hematocrit, haemoglobin level and serum iron in blood plasma, and also the number of red blood cell precursors in bone marrow in comparison with the values measured for the control group of animals.[360]

The biological activities of the $[Mo_{132}O_{372}(AcO)_{30}(H_2O)_{72}]^{42-}$ keplerate anion (**142**) and neutral keplerate **143** were compared on normal and transformed fibroblast cultures.[361] The dermal fibroblasts were more resistant to keplerate **143**, while anion **142** caused extensive disorders of membrane organelles in both normal and transformed fibroblasts. This result indicates that keplerate **143** could be used in biomedicine, and keplerate **142** may be applicable for the therapy of cancer. In 2020, Ostroushko *et al.*[362] summarized the results of studying keplerates **142** and **143** in biological systems. The authors evaluated their toxicity and the ability to bind to proteins, drugs (*e.g.*, insulin and antibiotic kanamycin A) and vitamins (vitamin B_1). They also demonstrated the possibility of electrophoretic transport of associates through the skin.

Sorption of nitric oxide and nitrogen dioxide by keplerate **143** was studied under environmental conditions and in an air–argon atmosphere.[363] The composition of the product was found to be $[\mathbf{143}-(NO_2)_x]\cdot(NO_2)_y$ (where $x = 6$, $y = 14 \pm 3$). Thermal analysis revealed the effect of NO_x coordination on the release of water molecules and decomposition of acetate ligands in keplerate **143**. Complex $[\mathbf{143}-(NO_2)_x]\cdot(NO_2)_y$ has a relatively high NO_2 uptake capacity, water solubility and pH-dependent decomposition and is a potential donor of nitrogen oxides, which may find use in biology and medicine.

In 2017, Elistratova *et al.*[364] showed the possibility of obtaining colloidal particles based on the $[Mo_{132}O_{372}(AcO)_{30}(H_2O)_{72}]^{42-}$ anions (**142**) and Gd^{3+} cations. The idea of this study was to obtain contrast agents for magnetic resonance imaging (MRI). An additional stabilization of particles in dilute aqueous solutions was attained using triblock copolymers based on polyethylene oxide and polypropylene oxide moieties. It was shown that the rates of magnetic relaxation of keplerate-based particles are much higher than those of most other Gd^{3+}-based colloids. Colloidal particles have low toxicity. Also, the interaction of $[\{Mo_6O_{21}(H_2O)_6\}_{12}.\{Mo_2O_4(HPO_4)_{30}\}]^{72-}$ (**176**) and $[\{Mo_6O_{21}(H_2O)_6\}_{12}\{Mo_2O_2S_2(AcO)\}_{30}]^{42-}$ (**188**) anions with Gd^{3+} was studied.[365] Upon replacement of keplerate **142** by **188**, which differs only in the nature of the binuclear bridge, the relaxivity of the resulting colloidal particles markedly decreased. In the case of compounds **176**, which has a markedly higher negative charge, the relaxivity also proved to be somewhat lower than that for keplerate **142**. It is important that the obtained colloids were non-toxic in concentrations necessary for high-quality magnetic resonance imaging. In addition, the magnetic relaxation of colloids remains at a fairly high level in buffer solutions of bovine serum albumin. The differences between the behaviours of keplerates **142** and **176** towards Gd^{3+} ions were studied by NMR relaxometry with fast cycling of magnetic field.[366] Analysis of longitudinal relaxivity data showed that $[Gd(H_2O)_8]^{3+}$ ions interact, in both cases, with the oxygen atoms of the $\{Mo_9O_9\}$ pores. However, in the case of keplerate **142**, the number of bound Gd^{3+} cations proved to be $\sim$3.5 times higher, which accounts for the high relaxivity of the colloids. In 2019, Elistrativa *et al.*[367] studied the complex formation with gadolinium cations and aggregation of three more keplerates: neutral

(**143**) and two anionic ones — $[K_{10}\subset\{(Mo)Mo_5O_{21}(SO_4)(H_2O)_3\}_{12}\{(VO)_{30}(H_2O)_{20}\}]^{26-}$ (**155**) and $[\{W_6O_{21}(H_2O)_5(AcO)_{0.5}\}_{12}\{Mo_2O_4(AcO)\}_{30}]^{48-}$ (**191**). The magnetic relaxivity of the complex of **191** with Gd^{3+} proved to be markedly higher than those for complexes formed by **143** and **155**. The structure of keplerate **191** also affects the stability of gadolinium complexes, protecting them from the oxidative degradation in solutions. The optimal compositions possessing low cytotoxicity and high stability and relaxivity in the range suitable for MRI applications were determined in this study.

In conclusion, it is noteworthy that, despite the high diversity of keplerates prepared over twenty and a few years, it is still early to consider that synthetic chemists have solved all the problems in this field. The search for new possible mono- and binuclear bridges is in progress; ideas of using longer linkers are being put forward for increasing the size of the internal cavity and the sizes of pores of spherical shells. It is possible to modify the internal cavity by introducing ligands containing various functional groups. The examples considered in the last Section give the idea of modern applications of keplerates, but the applied potential of these readily available, stable and easily tunable structures is far from being exhausted. In our opinion, the most interesting facts concerning this class of compounds, called keplerates, which is new on the scale of chemistry, are still to be discovered.

2.6. Supramolecular analytical chemistry

Recognition of inorganic, organic and bioorganic ions and molecules based on spontaneous and selective binding of an analyte (guest molecule) to an analytical reagent (host molecule) is a common subject of supramolecular and analytical chemistry, which are interdisciplinary fields of chemistry. In the 21st century, integration of these two fields gave rise to 'supramolecular analytical chemistry'.[368, 369] However, for a number of reasons, both this term itself and the relevant area of analytical chemistry have so far attracted attention of only a small number of analytical chemists. Therefore, currently, the potential of supramolecular chemistry cannot be fully implemented in the practice of chemical analysis.

Many publications of supramolecular chemists, especially when supramolecuar chemistry was in its infancy, were aimed at demonstrating the selectivity of interaction of a synthesized molecule with a substrate, high stability of host–guest systems and the possibility of designing chemical sensors. Usually, it did not come to the real design of sensors or development of procedures for determination of compounds, which is customary for analytical chemists. Meanwhile, recognition makes it possible to detect and, in some cases, identify a chemical compound, *i.e.*, to carry out qualitative analysis, which should logically be followed by the next stage, that is, development of a procedure for quantitative determination of this compound. Thus, the possible integration of these branches of science stopped at achieving the selectivity of detection, since this was the goal of studying for supramolecular chemistry, but analytical chemistry did not catch up the discovered effects and did not bring the research to a procedure for determination of a particular analyte in a sample. This can be seen when considering the early monographs in supramolecular chemistry (see, for example, an encyclopaedia [370]), which present numerous examples of self-assembly, studying the properties and application prospects of the products of synthesis in diverse molecular devices (wires, switches, rectifiers, capsules) and also in catalysis, photochemistry and nonlinear optics; in the development of new functional polymers, gels and molecular machines; in biomimetics; and as drug delivery vehicles, but only rarely in chemical sensors. Furthermore, the authors barely used the terms 'analytical chemistry' or 'chemical analysis'. The same conclusion can be drawn from analysis of reviews [371–373] on this subject. Hence, close cooperation between scientists specializing in supramolecular and analytical chemistry has not yet been widespread, and analytical chemists, in turn, have not always paid attention to the nature of systems and phenomena used in analytical procedures.

Among other factors, the lack of large-scale interest of analytical chemists in the unique results obtained by supramolecular chemists is due to the fact that the synthesized molecules possessing recognition ability are, most often, exotic and difficult to obtain and, hence, they are relatively expensive. For example, the practice of chemical analysis does not utilize the unique effects of binding of sodium and potassium ions to some spherands, cavitands and carcerands with $\log K_{st} = 10-14$ (K_{st} is the stability constant).[4, 374] The unprecedented Na^+/K^+ selectivity, amounting to 10^{10} (Ref. 374), which cannot be attained by other methods, is not utilized in any way either. Nevertheless, some researchers made attempts to apply the achievements of supramolecular chemistry for solving analytical problems and deemed this approach to be well-timed.[368] The opinion that self-assembly and recognition phenomena are most appropriate for the design of chemical sensors has been widely accepted.[368, 369] In this case, by sensor is meant a receptor that interacts with an analyte in the dynamic mode to give a product generating a definite analytical signal.

2.6.1. Development of approaches to understanding of the subject of supramolecular analytical chemistry

Actually, an attempt to find ways for real integration of analytical and supramolecular chemistry initiated the formation of a new branch of analytical chemistry.[368] Simultaneously, the fundamental questions related to supramolecular analytical chemistry were formulated as follows:

— which types of chemical reactions should be classified as supramolecular interactions and whether the general definition proposed by J.M.Lehn [1] fully covers this subject;

— whether there is any threshold in energy or in the time of intermolecular interaction to distinguish between supramolecular and other types of interactions, for example, covalent exchange interactions;

— whether the supramolecular nature is inherent in spontaneous selective reactions of complex formation (Werner coordination) between metal ions and organic reagents, widely used by analytical chemists, and whether these reactions should be assigned to supramolecular chemistry;

— whether dynamic covalent interactions based on the formation and exchange of reversible covalent bonds can be assigned, together with the classical non-covalent supramolecular interactions, to supramolecular analytical chemistry;[369]

The pioneering publication of Anslyn [368] presents a lot of examples of applying host–guest pH systems, some metal ions, inorganic and organic anions and various uncharged organic compounds and enantiomers as optical and electrochemical sensors. The use of arrays of non-

selective sensors such as electronic nose and electronic tongue, in particular for the recognition of the odour and taste of food and other volatile products, was quite rightly attributed to supramolecular processes.

More appropriate definition of the term 'supramolecular analytical chemistry', further development of this concept and classification and analysis of recent achievement in this field were surveyed by Anslyn and co-workers.[369] The supramolecular analytical chemistry is defined as a field that explores the molecular recognition and self-assembly of chemical structures using dynamic interactions that create assemblies which result in signal modulations upon addition of analytes.[369] The authors proposed to subdivide sensory interactions into three types: sensing of single analytes, sensing based on competing interactions of substances and chirality sensing. For each of these types, several practical approaches to the design of supramolecular sensors are distinguished:

— direct detection based on the selective interaction of the host (receptor) and analyte (substrate) molecules;

— indirect detection associated with displacement of the indicator (probe) molecule by analyte molecule from the cavity of the host;

— competitive detection requiring an array of nonselective sensors functioning as an electron nose or electron tongue and subsequent use of chemometric methods for the processing of analytical signal with a complex geometric shape.

Spanish researchers[375–379] paid attention to another aspect of analytical application of host–guest systems and self-organized assemblies formed mainly by diphilic micelle-forming surfactant molecules, that is, their application in the separation and preconcentration and in determination methods coupled to them. The interaction of receptor molecules and polymolecular assemblies with an analyte is of supramolecular nature, *i.e.*, it is based on self-assembly *via* non-covalent electrostatic, hydrophobic and donor–acceptor interactions and hydrogen bonding. Analysis of the literature shows that cyclodextrins and calixarenes, which are much more readily available and less expensive than spherands, cavitands or carcerands, are used most often in chromatographic analysis, capillary electrophoresis and extraction with receptor molecules acting as hosts.

The so-called micellar nanosized objects or systems are used even more widely as analytical reagents for separation, preconcentration and determination of compounds. These reagents include direct and reverse micelles and microemulsions, liposomes and vesicles formed by surfactant molecules and even Langmuir–Blodgett films.[380–383] The term 'micellar systems' covering all these objects was derived from the name of the simplest representatives of these self-organized systems, that is, surfactant micelles.[382, 383] Indeed, the presence of diphilic surfactant molecules as the major constituent of a supramolecular assembly, the way of their spontaneous formation and similarity of their properties are common features of all organized systems of this type.[382, 383] Generally, the media in which the major solvent contains receptor molecules or micellar systems are called organized media.[380–383] These media are usually transparent, optically isotropic solutions in which the major bulk of the solvent (aqueous or non-aqueous one) contains nanosized pseudophase systems able to solubilize (co-dissolve) substances insoluble in this solvent.[383] Thus, liquid organized media are homogeneous and are single-phase on a macroscale, but are nanoheterogeneous and two-phase on a nanoscale.

Extensive use of supramolecular organized media started back in the 1980s.[380, 381] In the 21st century, Spanish researchers[375–379, 384] proposed to call these systems supramolecular solvents (SUPRAS), because, from the standpoint of the authors, they replaced the classical aqueous, aqueous organic and non-aqueous media by biosimilar ones. According to these views, supramolecular analytical chemistry was redefined as 'an emergent science covering the study and application of supramolecular systems (host molecules and molecular aggregates) in analytical processes'.[375–379, 384]

It should be also borne in mind that the supramolecular chemistry is closely connected with nanochemistry and nanotechnologies, which are also based on bottom-up self-organization processes, and, hence, with nanoanalytical chemistry, which uses both nano-objects and self-assembly in various stages and in various fields of chemical analysis.[385–388]

The classical chemical analysis is not reduced to mere detection and quantitative determination of substances, but also includes the preceding sequence of interdependent processes (operations). Therefore, supramolecular analytical chemistry also should not be restricted to the recognition effect, *i.e.*, qualitative analysis, use of host–guest systems and studying supramolecular assemblies as solvents of a new type[375–379] or nanoreactors.[383] It is necessary to consider all stages of analysis that involve supramolecular effects and that provide data for qualitative and quantitative determination of a sample component. These operations include sampling, sample conservation and preservation of the sample composition, sample preparation (including separation of components of a complex mixture and analyte preconcentration), conduction of the analytical reaction (process) under supramolecular conditions and calculation of the content of the analyte. In some cases, *e.g.*, in strip tests and sensors, some of the indicated stages may be absent.

This part of the review is meant to briefly consider the role of supramolecular effects in particular stages of chemical analysis on the basis of both literature data and our own research. Examples of using supramolecular effects and systems for sample preparation, separation and preconcentration, as media for conducting chemical reactions or as nanoreactors are presented. In addition, we describe self-assembly phenomena that underlie the generation of the analytical signal (effect) and are implied in the procedures of quantitative determination in various methods of chemical analysis. We did not claim to cover all phenomena, systems, approaches and methods that can be attributed to supramolecular analytical chemistry, but we intended to outline the main trends, goals and achievements of this new, emerging field of analytical chemistry. The number of publications in which supramolecular effects and systems were utilized for the development of analytical procedures is several thousand, some of the original papers were integrated in reviews and monographs.[368, 369, 375–383, 389–398]

2.6.2. Supramolecular objects in different stages of chemical analysis

Analysis of the literature shows that two types of supramolecular objects (systems) are employed in the stages of chemical analysis (sample preparation, separation, preconcentration and determination). The first type are solutions

of pre-organized receptor molecules (cyclodextrins, calixarenes, cavitands, cyclophanes, cyclopeptides, *etc.*), which act as hosts with respect to analytes. The second type includes solutions of self-organized micelle-like assemblies, which serve as new media for solubilization, assembly and bring together the components of analytical reactions, *i.e.*, like receptor molecules, they actually function as nanoreactors.[383] Micellar systems can also be formed in non-aqueous solvents and on solid surfaces, being organized as hemimicelles and admicelles (adsorption bilayers).

Thus, supramolecular analytical chemistry, unlike nanoanalytics, is rather a new tool for conducting analytical reactions than a new branch of analytical chemistry. This tool is based on the use of receptor molecules and self-assembled molecular aggregates (micellar systems) as media (nanoreactors) for reaction components to approach each other and for changing local properties of the microenvironments of analytical systems, *i.e.*, for creating conditions for the whole sequence of reactions to occur. It is noteworthy that both the analytical reactions and processes taking place in supramolecular media (cavities of receptor molecules) have supramolecular nature, because components interact according to the self-assembly principle and serve as sources of the analytical signal. In this connection, we will give a number of examples of supramolecular interactions and reactions of the supramolecular nature that have been widely used in analytical chemistry for approximately 40 years.

2.6.3. Role of solubilization in chemical analysis

The simplest example of a supramolecular process used in chemical analysis is solubilization, *i.e.*, an analyte migrates from the main bulk of the solvent into the receptor cavity or into the nanosized space of the micellar assembly. Solubilization results in increased solubility of poorly water soluble hydrophobic organic reagents and analytes and changes the polarity of their environment and their physicochemical properties even at the stage of sample preparation for the analysis and then throughout the whole analytical determination process.[380, 383, 387] Solubilization extends the range of compounds that can be determined in aqueous solutions by titrimetric,[380 – 382] photometric,[380 – 383, 389] luminescence,[389 – 391, 399] electrochemical,[392] chromatographic[394, 395, 400 – 403] and electrophoretic[403 – 405] methods and by atomic absorption and atomic emission spectrometry.[406] The solubilization of participants of an analytical process in the nanopseudophase of an organized system (micelle, microemulsion, liposome, vesicle or cyclodextrin/calixarene cavity) considerably changes their hydrophobic properties, hydration, hardness and conformation of the molecule, which modifies physicochemical, spectroscopic, electrochemical, adsorption, protolytic, tautomeric, complexing, redox and other properties.[383, 385, 387, 388, 407, 408] This also changes the pattern of charge distribution in the molecule, the efficiency of intra- and intermolecular transfer of the electronic excitation energy and electron transfer, particle distribution among the phases, solubility and also the rate, route and equilibrium state of analytical reactions. As a result, the analytical signal intensity markedly increases, the spectroscopic, electrochemical and chromatographic parameters of the signal and conditions of electrophoretic separation are optimized and, as a consequence, the sensitivity and selectivity of analytical determination is enhanced.

A fundamental difference of microheterogeneous organized media from common homogeneous solutions (aqueous, aqueous organic and non-aqueous solutions) is that local effects play the crucial role in this case.[383] This means that changes in the properties of compounds solubilized in organized systems are caused by changes only in the state of their microenvironment, *i.e.*, in their solvation shell, but not in the whole bulk of the solution.[409]

It is possible to distinguish a number of consequences of solubilization and formation of ionic associates of organic reagents with surfactant counter-ions that are common to analytical systems:[381 – 383, 389, 409, 410]

— the ability to bring together and preconcetrate components of an analytical reaction in the nanopseudophase of an organized system, even if the components substantially differ in hydrophobicity;

— multicentre and multifunctional interactions (electrostatic, donor – acceptor, van der Waals and hydrophobic interactions and hydrogen bonding) of components or parts of the nanopseudophase with the solubilized substrate, with hydrophobic interactions being predominant;

— clear-cut oriented sorption and cavity effect, in which the nature and geometric matching between the host and the guest are the decisive factors for analyte binding to the substrate;

— significant microheterogeneity of the medium within the nanopseudophase along the direction from the interface with water (solvent) towards the centre, manifested as a sharp change in the dielectric constant, microviscosity, micropolarity, microacidity and other physicochemical properties of the medium.

An important advantage of micellar systems and receptor molecules is the possibility of controlling their composition and the properties of assemblies formed in solution (charge, hydrophobicity, micropolarity, *etc.*), and, hence, solubilization of reagents and analytes. This control is directly related to the supramolecular nature of assemblies and can be accomplished in several ways:[383]

(1) targeted choice of the type of organized system: direct or reverse micelles, cyclodextrins, microemulsions [oil-in-water (o/w) and water-in-oil (w/o)];

(2) adjusting the nature of surfactants that form the organized systems, in particular varying the hydrophilic group (cation, anion, oxyethylene chain length) or hydrophobic moiety (aliphatic, aromatic, oxypropylene); varying the hydrophilic – lipophilic balance of surfactant molecules and analytes and the sizes of receptor cavity and the analyte;

(3) adjusting the properties of the organized nanosized assemblies, in particular:

— charge density and surface potential of the micelle,

— hydration and hydrophobic properties of the micelle interface,

— micropolarity and microviscosity of the micelle nanopseudophase,

— size and aggregation number of micelles and microemulsions,

— distance between the reactants,

— degrees of electronic excitation energy transfer and electron transfer,

— substrate exchange kinetics in the micelle – solvent system,

— concentration of oxygen and other gases in micelles,

— charge and hydrophobicity of the groups grafted at the entrance of the receptor molecule.

2.6.4. Chemical analysis methods using supramolecular effects

The occurrence of solubilization not only considerably improves characteristics of the known methods for separation, preconcentration and determination of many inorganic and organic compounds, but has also resulted in the development of some new methods. The most well known among them is micellar extraction (called also 'cloud point extraction' or 'supramolecular solvents'), proposed in 1977 by Ishii and Watanabe.[411] It is successfully combined with determination of compounds, by, for example, gas[412] and liquid[394,413] chromatography and capillary electrophoresis[406,413] and with photometric,[380,381,406,414] luminescence,[393,415] atomic absorption and atomic emission[406] determination methods. There are two dozens of reviews dealing with the micellar extraction alone in sample preparation, spectrometric determination of metal ions and inorganic anions, organic compounds and biomolecules.

Other examples of the effective use of supramolecular effects include micellar liquid chromatography (MLC)[416] and micellar thin layer chromatography,[417] which were proposed by Armstrong and co-workers. Micellar TLC has been widely used in Russia and in Ukraine.[400,418–422] One of the numerous reviews on MLC including analysis of both author's own works and studies of foreign colleagues[401] was published in 1999. The most widespread among these methods are micellar electrokinetic chromatography (MEKC), developed by Terabe *et al.*,[423] and its microemulsion version (MEEKC), proposed by Watarai.[424] The use of micelles and microemulsions provided an unusually high separation efficiency for both ionic and neutral compounds, because the number of theoretical plates reached in some cases 3–5 million.[425] The results of application of MEKC, MEEKC and capillary electrophoresis with cyclodextrin mobile phases are comprehensively integrated in a monograph.[425] The use of micelles and cyclodextrins allowed simultaneous separation of hydrophilic and hydrophobic, charged and neutral, optically active and inactive molecules, eliminated the necessity of regeneration of chromatographic column and made it possible to use electrochemical detector with gradient elution and to perform direct injection of biological fluids as micellar solutions into the column.

Organized media have found use almost in all types of luminescence spectrometry employed in chemical analysis: fast, photoinduced, sensitized fluorescence, room temperature phosphorescence (RTP) and sensitized RTP (s-RTP), immunofluorescence and chemiluminescence; this is reflected in a number of books and fundamental reviews.[380,381,426,427,382,383,389–391,393,399,415] Spectral changes and analytical effects were found to be more significant in luminescence than in photometry. In some cases, 100- and 1000-fold increase in the analytical signal intensity was attained, and the limit of detection decreased to a nano-, pico- or femtogramme level.[390,391,426,427] New results were obtained in phosphorimetric analysis, because it became possible to observe an analytical signal in micelles, microemulsions and cyclodextrins at room temperature rather than at liquid nitrogen temperature (77 K).[390,391,426] The main conditions for observing phosphorescence at room temperature are the presence of a heavy atom and removal of oxygen from the solution.[428–430] The sensitized RTP based on the triplet–triplet (T–T) transfer of the electron excitation energy proposed in our study appears most interesting. This procedure substantially increased the selectivity of the phosphorimetric determination of polycyclic aromatic hydrocarbons; this was the first implementation of the idea of using analytical organic reagents in the triplet state.[431–433]

One more type of luminescence based on the supramolecular transfer of electron excitation energy that is affected by organized media is the sensitized fluorescence of lanthanides. In this case, upon light absorption, a chromophoric chelating ligand passes from a singlet to a triplet excited state *via* intersystem crossing, and the energy transfer from the triplet level of the ligand to the lower-energy resonance level of the lanthanide ion is accompanied by characteristic sensitized fluorescence. This conversion of the energy absorbed by one or several ligands to lanthanide ion emission as a result of intramolecular transfer of the excitation energy was called 'antenna effect'.[390,399,427,434,435] The chelate formation brings about one more effect, namely, displacement of lanthanide-coordinated water molecules by organic ligands, which results in quenching of the metal excitation energy by these water molecules. Therefore, mixed-ligand complexes are often used instead of complexes with one ligand. This allows displacement of more lanthanide-coordinated water molecules. The use of micellar media is favourable for the removal of coordinated water, increases the stability constant of chelates, changes the rates of photophysical processes and increases the efficiency of energy transfer and the sensitized fluorescence intensity. This is associated with the change in the microenvironment of the solubilized chelate and brings together the reaction components in a nanosized space.[436–438] A combination of mixed-ligand complex formation and introduction of a second lanthanide ion into the micellar system (sensitized co-fluorescence effect) proved to be especially efficient, resulting in an almost 1000-fold increase in the fluorescence intensity.[439] An unusually high 3800-fold enhancement of the sensitized fluorescence signal was found for a system containing warfarin, an anticoagulant used in agriculture as a rodenticide and pesticide.[440] It is noteworthy that supramolecular nature is inherent in not only micellar media employed for increasing the luminescence intensity, but also in the processes of energy transfer from the excitation energy donor to an emitting acceptor in a micelle.[390]

2.6.5. Miscellaneous examples of using supramolecular effects in analysis

Chemical sensors make use of dynamic interaction of a sensing element with an analyte in solution or in the gas phase. Their major benefit is the possibility of obtaining direct information (detection and recognition) about the presence and amount of one (pH of the solution, contents of glucose, oxygen, biogenic amine, *etc.*) or several components using an array of electrochemical or optical sensors. The reversibility of interaction between the receptor layer and the analyte is the main factor of supramolecular nature. The number of publications on chemical sensors is a few tens of thousands; some examples can be found in reviews.[368,369,441–443] The sensors that appeared in the last 10–15 years comprise, as a rule, various nanoparticles, which participate in supramolecular reactions.[369,444,445] Supramolecular nature is characteristic of numerous immune and enzymatic reactions meant for determining biologically active compounds.[446]

Thus, it can be stated that analytical chemistry would further extend the range of supramolecular systems and interactions that would be utilized to develop methods of

analysis of various specimens, especially new materials and biological fluids.

3. Self-assembly and self-organization in solution and at the interface

3.1. Amphiphilic (thia)calix[4]arenes: synthesis and functional colloidal systems based on them

Supramolecular chemistry is one of the youngest and extensively developing fields of modern chemistry. Owing to the ability to self-assemble, supramolecular structures can be used in the development of biomimetic systems, molecular receptors, nanoreactors, catalysts, molecular machines, *etc*. Of special attention are amphiphilic molecules forming highly ordered assemblies in water, starting from traditional micelles and vesicles to more complex morphologies such as nanotubes, nanotapes, nanofibres, nanosheets and other.[447] The morphology of such molecular assemblies can be tuned by appropriately modifying the structure of the elementary unit, *i.e*. an amphiphilic molecule, and also by varying reaction conditions such as concentration, temperature, ionic strength and pH of the medium.[448]

Among the diversity of amphiphilic molecules, an important role belongs to amphiphilic macrocycles. Like traditional linear amphiphilic molecules, they comprise hydrophobic and hydrophilic sites enabling their self-assembly in aqueous solutions. A particular feature of amphiphilic macrocycles is molecular recognition. According to the definition of Shinkai *et al*.,[449] amphiphilic macrocycles are amphiphilic molecules containing host–guest type recognition sites. Owing to high concentration of the binding sites on the surface of their aggregates, amphiphilic macrocycles acquire the ability for multisite binding of guests, which in turn can enhance their sensitivity (selectivity) to molecular recognition in aqueous solutions.

Among amphiphilic macrocycles, calix[*n*]arenes and their thia analogues have a special place (Fig. 78).

Calixarenes are unique in the possibility of chemical modification of their upper and lower rims, the diversity of their stereoisomeric forms, the possibility of attaching more than one receptor moiety for multisite binding, *etc*. These factors rendered them a very convenient macrocyclic platforms to construct amphiphilic structures with receptor properties, which has been described in detail in several recent reviews.[450–455] Even being unmodified with polar groups, a calix[*n*]arene molecule can display amphiphilic properties. Thus, as early as 1989, it was found [456] that calix[6]arene **200** can form vesicles having an average diameter of 50–100 nm and produce stable 10 Å monolayers. Later, it was demonstrated that tetra-*O*-dodecyl-substituted calix[4]arene **201** bearing no ionized moieties can also form stable monolayers at the water/air interface and produce submicrometre-sized particles of 400 nm diameter in solution.[457]

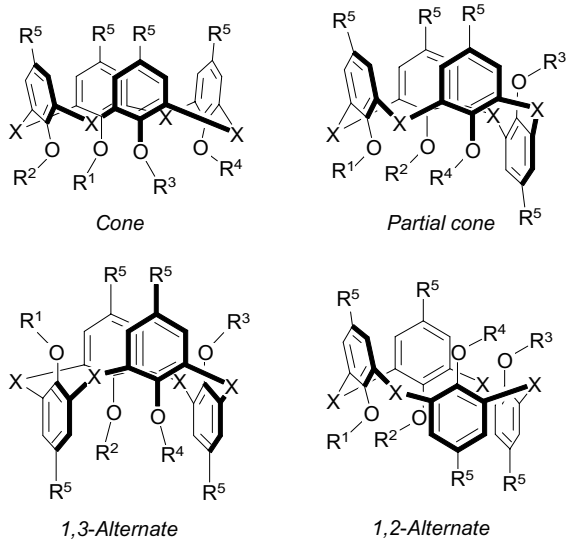
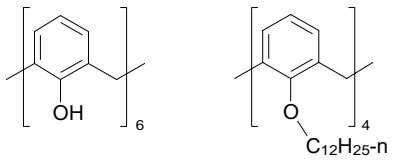


Figure 78. Structures of calix[4]arenes and their thia analogues.

Structures 200, 201



200 **201**

Nevertheless, to improve their solubility in water and endow them with amphiphilic properties, calix[*n*]arene molecules are most often functionalized with polar ionic and non-ionic groups to construct amphiphilic macrocycles in the *cone* and *1,3-alternate* stereoisomeric forms (Fig. 79).

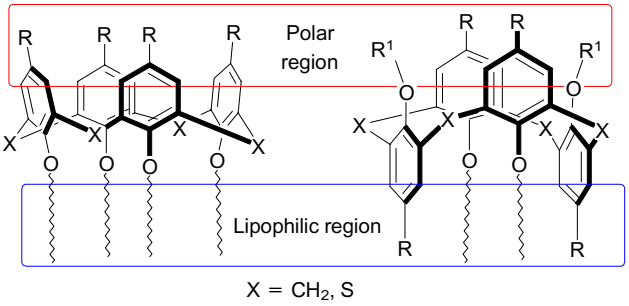


Figure 79. Structures of amphiphilic macrocycles in the *cone* and *1,3-alternate* stereoisomeric forms.

These stereoisomeric forms provide optimal spatial separation of hydrophilic and lipophilic parts of the molecule.

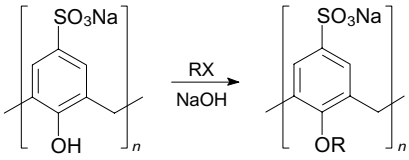
In this Section, special attention will be given to the synthetic approaches to construct amphiphilic macrocycles based on both classical calix[*n*]arenes and their thia analogues, thiacalix[*n*]arenes. The prospects of the click chemistry modular approach for designing amphiphilic structures based on (thia)calix[*n*]arenes are discussed, and examples of the application of colloidal systems derived based on them are provided.

3.1.1. Amphiphilic calix[*n*]arene derivatives bearing anionic polar head groups

3.1.1.1. Synthesis and properties of amphiphilic sulfonate calix[*n*]arenes

The first calixarene **202** with surface-active properties was synthesized by Shinkai *et al*.[458] in 1984 by alkylation of

Scheme 28



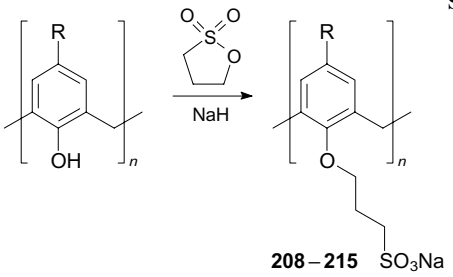
202–207

Compound	*n*	R	Yield (%)	Compound	*n*	R	Yield (%)
202	6	n-C_6H_{13}	58	**205**	4	Bu^n	76
203	6	Me	62	**206**	6	Bu^n	20
204	6	n-$C_{12}H_{25}$	96	**207**	8	Bu^n	20

sulfonate calix[6]arene with n-hexyl bromide in the presence of NaOH (Scheme 28). In 1986, a series of amphiphilic sulfonate calix[6]arenes was complemented with hexamethyl- and hexadodecyl-substituted macrocycles **203**, **204**,[449] and two years later, n-butyl-substituted calix[4(6,8)]arenes **205–207** were prepared (see Scheme 28).[459, 460]

Several novel derivatives of calix[*n*]arene **208–215** bearing propyl sulfonate groups at the lower rim and various alkyl groups in the *para*-position of the aromatic ring were synthesized by Shinkai *et al.*[460] in 1989. Calix[*n*]arenes unsubstituted at the lower rim reacted with propane sultone in the presence of sodium hydride (Scheme 29).

Scheme 29



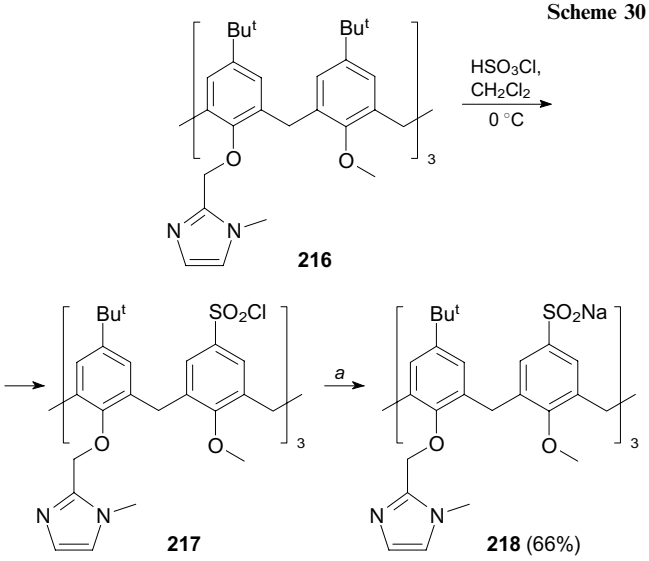
208–215

Compound	*n*	R	Yield (%)	Compound	*n*	R	Yield (%)
208	6	Bu^n	75	**212**	6	H	30
209	6	n-C_6H_{13}	86	**213**	8	H	23
210	6	n-$C_{12}H_{25}$	60	**214**	6	Bu^t	75
211	4	H	10	**215**	8	Bu^t	76

The pioneering works of Shinkai and co-workers concerning sulfonate calixarenes were continued by other researchers. Thus, Reinaud and co-workers[461] proposed an original method to use precursors **216**, **217** in the synthesis of sulfonate calixarene **218** (Scheme 30) *via* the regioselective *ipso*-chlorosulfonylation followed by alkaline hydrolysis. Imidazole moieties deactivated the electrophilic attack, due to their ability to be protonated; as a result, the reaction proceeded selectively on the anisole moieties of the macrocycle.

A study of the aggregation of macrocycle **218** in water showed that despite the absence of the typical amphiphilic architecture, it can form polydisperse multilamellar vesicles of the pH-dependent size (450 nm at pH 8.5 and 50 nm at pH 6.5).[462] The addition of Ag^I ions was found to affect the

Scheme 30



(*a*) NaOH, DMSO, H_2O, 80 °C

aggregation process, resulting in the formation of compact micelles of 2.5 nm diameter; this was related to a change in the macrocycle packing parameter as a result of complex-induced contraction of the macrocycle lower rim (Fig. 80).

Modification of calix[*n*]arenes with propane sultone was proposed by Puntoriero and co-workers,[463] who succeeded in reacting *p-tert*-butylcalix[5]arene (**219**) with 1,4-butane sultone in the presence of sodium hydride to obtain water-soluble sulfonate **220** (Scheme 31). Using the diffusion-ordered NMR studies and fluorescence spectroscopy, it was demonstrated that macrocycle **220** can form a supramolecular amphiphilic structure with n-dodecylammonium chloride, due to encapsulation of the latter into the macrocyclic cavity, and also to form micelles of 2.6 nm diameter (Fig. 81).

Liu and co-workers[464] carried out chlorosulfonylation of calixarene **221** with chlorosulfonic acid followed by the treatment with NaOH in anhydrous ethanol and thus obtained the tetrasodium salt of *p*-sulfonatocalix[4]arene tetraheptyl ether **222** in a good yield (Scheme 32).

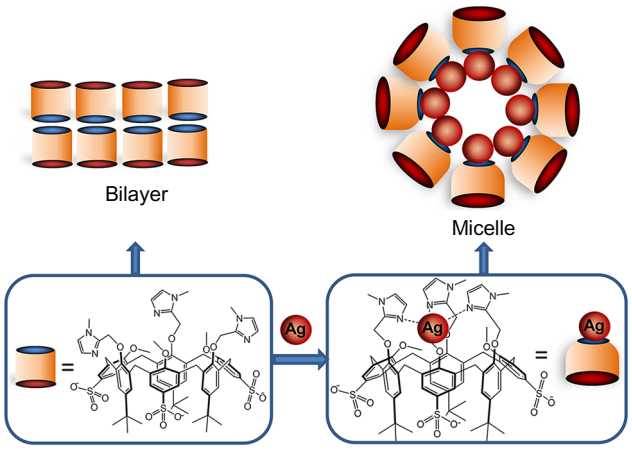
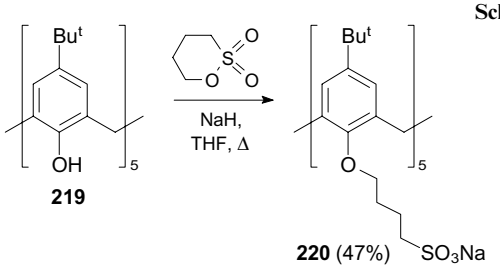
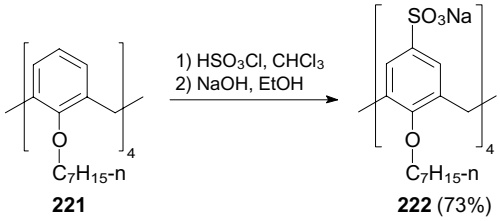


Figure 80. Aggregation of macrocycle **218** in water in the presence and in the absence of silver(I) ions. The Figure was created by the authors using data of Ref. 462.

Scheme 31



Scheme 32



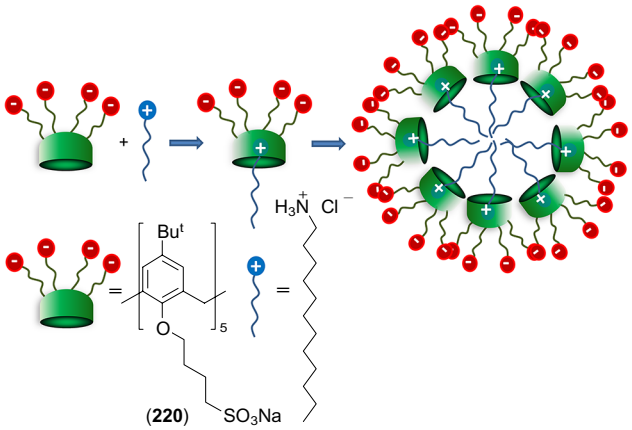


Figure 81. Scheme for the formation of an amphiphilic structure from compound **220** and n-dodecylammonium chloride and micelles based on this structure. The Figure was created by the authors using data of Ref. 463.

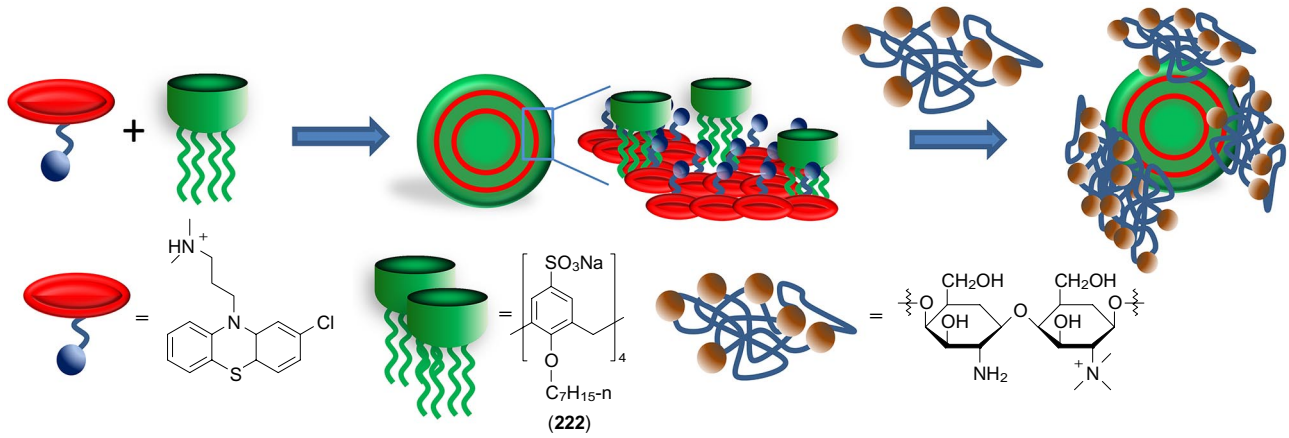


Figure 82. Scheme for the formation of aggregates based on calixarene **222**. The Figure was created by the authors using data of Ref. 464.

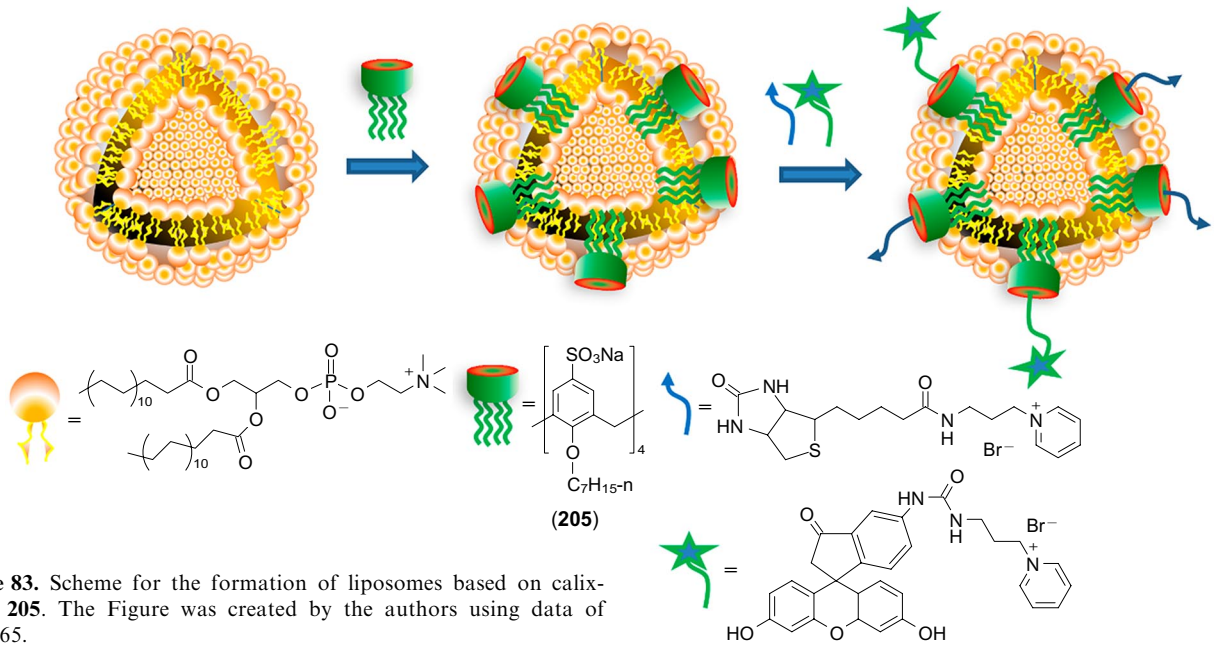


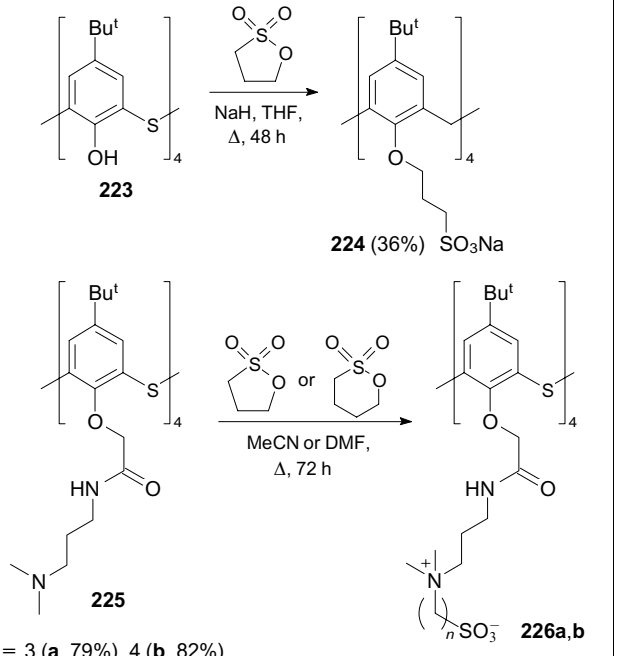
Figure 83. Scheme for the formation of liposomes based on calixarene **205**. The Figure was created by the authors using data of Ref. 465.

Macrocycle **222** can co-assembly with high amounts (46%) of antipsychotic drug Chlorpromazine to afford joint nanoaggregates in aqueous solutions (Fig. 82). Moreover, due to electrostatic interactions, the resulting aggregates successively react with trimethylated chitosan, which can actively transfer nanoparticles across the blood – brain barrier *via* absorption-mediated transcytosis.

The same research team [465] prepared functional liposomes from tetra-*O*-butyl-substituted sulfonylated calix[4]arene **205** and a zwitterionic phospholipid, dipalmitoyl phosphatidylcholine (DPPC), for living cell imaging and targeted drug delivery (Fig. 83). Due to electrostatic interactions, the liposome was functionalized with biotinylated pyridinium salt as a targeting agent and a fluorescein-containing pyridinium salt as a fluorescent probe. The liposomes thus obtained were internalized into the MCF-7 cancer cells through the receptor-mediated endocytosis, thus demonstrating great prospects for their therapeutic and diagnostic applications.

Stoikov and co-workers [466] successfully implemented Shinkai's approach to modification of calix[*n*]arenes with propane sultone to functionalize *p*-*tert*-butylcalix[4]arene (**223**). Propanesulfonate **224** (Scheme 33) proved to be able to form colloidally stable fractal hybrid nanodendrites of 95 nm size with silver ions. Later, the same research team [467] carried out the reaction of 1,3-propane sultone or 1,4-butane sultone with calix[4]arene **225** bearing tertiary amino groups to produce sulfobetaines **226a**,**b** (see Scheme 33) in high yields. These macrocycles can form stable submicron-sized aggregates with silver ions.

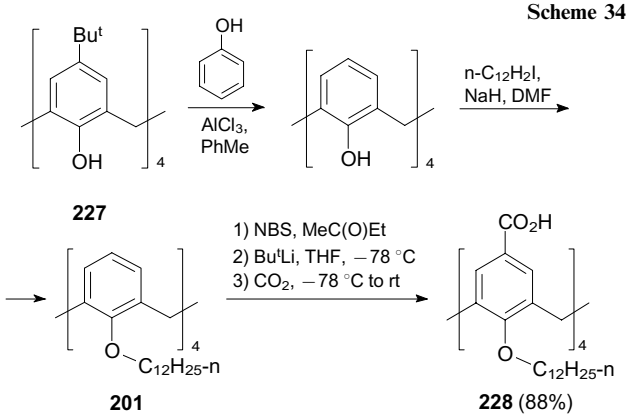
Scheme 33



3.1.1.2. Synthesis and properties of amphiphilic carboxylate calix[*n*]arenes

Meier and co-workers [468] carried out consecutive removal of the *tert*-butyl groups in *p*-*tert*-butylcalix[4]arene **227**, alkylation with dodecyl iodide and bromination followed by replacement of the bromine atom with lithium and direct carboxylation to produce tetra(carboxyl)-substituted calixarene **228** (Scheme 34).

Scheme 34



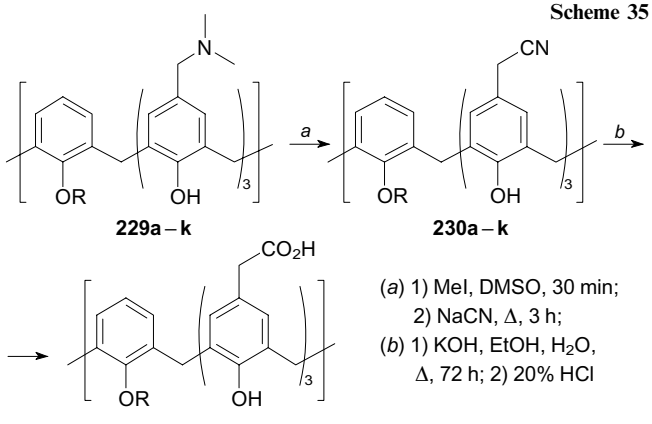
NBS is *N*-bromosuccinimide

Using the data from dynamic and static light scattering and cryogenic transmission electron microscopy, macrocycle **228** was shown to form vesicles in aqueous solutions and stable bilayers at the water/air interface.

Shahgaldian and co-workers [469] revealed that Langmuir films obtained from macrocycle **228** can react with drugs such as salicylic acid, acetylsalicylic acid and acetaminophen.

Suwinska *et al.*[470] used a quinone methide approach, which had been earlier developed by Gutsche and co-workers,[471] to replace the trimethylammonium moiety in calix[4]arenes **229a** – **k** with sodium cyanide with subsequent hydrolysis of intermediate tricyano derivatives **230a** – **k**. As a result, a series of tri(carboxymethyl)-containing calix[4]arenes **231a** – **k** was synthesized in high yields (Scheme 35).

Scheme 35

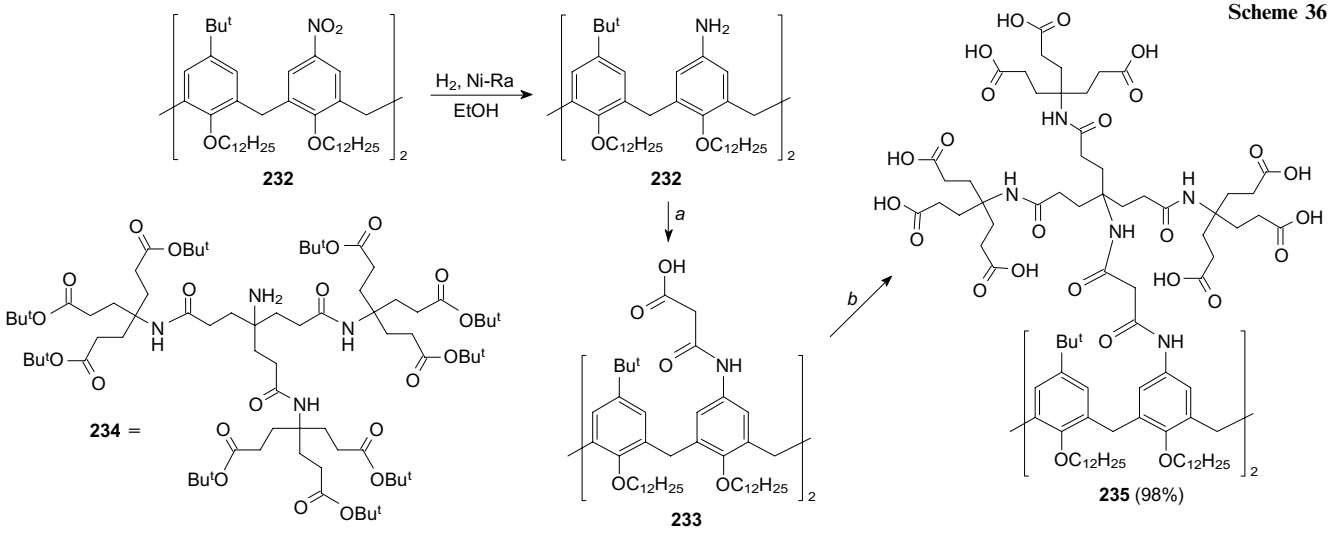


R = Me (**a**, 70%), Et (**b**, 73%), Pr^n (**c**, 78%), Bu^n (**d**, 75%), n-C$_5$H$_{11}$ (**e**, 72%), n-C$_6$H$_{13}$ (**f**, 79%), n-C$_7$H$_{15}$ (**g**, 78%), n-C$_8$H$_{17}$ (**h**, 80%), n-C$_9$H$_{19}$ (**i**, 79%), n-C$_{10}$H$_{21}$ (**j**, 82%), n-C$_{11}$H$_{23}$ (**k**, 85%)

It was demonstrated that macrocycles **231a** – **k** form micelles in aqueous solutions at pH > 6, when a significant part of the carboxyl groups are ionized, and the critical aggregation concentration (CAC) decreases with the elongation of the hydrophobic alkyl substituent in the macrocycle.

Hirsch and co-workers [472] carried out reduction of dinitrocalix[4]arene **232**, decorated with four dodecyl substituents at the lower rim, followed by the reaction with

Scheme 36



(*a*) 1) ClC(O)CH_2CO_2Me, THF, 5 h; 2) NaOH, THF, H_2O; 3) HCl; (*b*) 1) **234**, DCC, HOBT, DMF, 48 h; 2) CF_3CO_2H, PhMe, 24 h; $C_{12}H_{25}$ is n-dodecyl; Ni-Ra is Raney nickel, DCC is dicyclodecylcarbodiimide, HOBT is 1-hydroxybenzotriazole

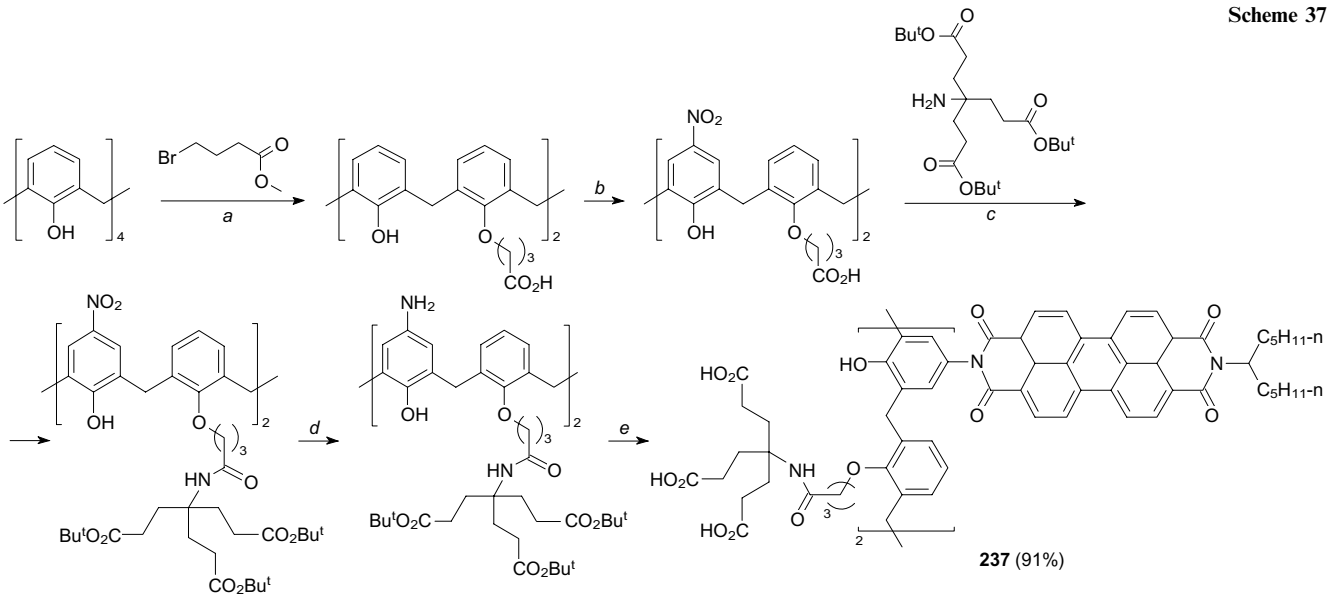
methyl malonyl chloride, hydrolysis of the resulting compound **233**, and carbodiimide cross-linking of the intermediate diacid with amino-substituted dendrimer **234** to afford amphiphilic dendrocalix[4]arene **235**, containing 18 carboxyl moieties in the polar part of the molecule (Scheme 36).

Using cryo-TEM and 3D reconstruction techniques, it was found that dendrocalix[4]arene **235** forms 7.5 nm micelles composed of seven macrocycle molecules. Later, the same research team employed a similar synthetic strategy to prepare a macrocycle containing a terephthalic spacer instead of the malonic one. This derivative possessed intrinsic fluorescence and was able to form micelles comprising 12 macrocycle molecules at pH 7.[473]

In a follow-up study,[474] a fundamentally different approach was implemented to construct amphiphilic macrocycles by introducing carboxyl groups into the lower rim of the macrocycle, and functionalizing the upper rim with perylene moieties **236**, prone to intensive π–π stacking (Scheme 37).

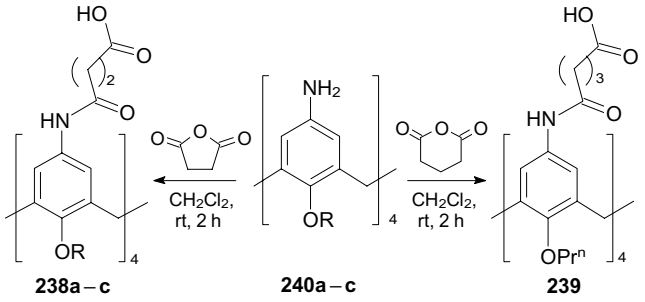
In a tetrahydrofuran–water mixture, macrocycle **237** tends to form nanowires having a diameter of 6.5–8.4 nm and a length of a few hundred nanometres. By molecular dynamics calculations, it was demonstrated that the conformation of this molecule changes from tetrahedral (perylene moieties are remote from each other) to a closed one (two perylene moieties approach each other due to π–π stacking).

Scheme 37



(*a*) 1) K_2CO_3, MeCN, Δ, 12 h; 2) KOH, Me_2CO, rt, 4 days; 3) HCl;
(*b*) 65% HNO_3, 100% AcOH, CH_2Cl_2, 0 °C, 15 min; (*c*) DMT-MM, THF, rt, 4 h;
(*d*) $NH_2NH_2 \cdot H_2O$, Pd/C, EtOH, Δ, 12 h; (*e*) 1) **236**, $Zn(OAc)_2$, quinoline, 120 °C, 2 h;
2) HCO_2H, $CHCl_3$; DMT-MM is 4-(4,6-dimethoxy-1,3,5-triazin-2-yl)-4-methylmorpholinium chloride

Scheme 38



238a – c **240a – c** **239**

R = Pr^n (**a**, 93%), Bu^n (**b**, 90%), n-C_5H_{11} (**c**, 89%)

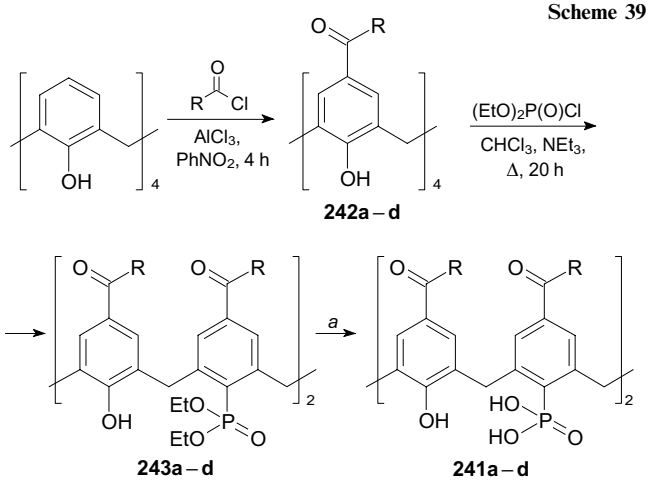
A convenient and facile method for the synthesis of acylamino calix[4]arene derivatives **238a – c** and **239** from readily available calixarene amines **240a – c** was proposed by Song *et al.*[475] The reaction with succinic or glutaric anhydride at room temperature gave the corresponding products in high yields within 2 h (Scheme 38).

It was found that in aqueous solutions, macrocycles **238a – c** and **239** can change their morphology over time: the nanospheres formed initially are transformed into nanofibres, which induce gelation of the solution. The hydrogel thus formed was utilized as a template for the preparation of silica nanotubes.[475]

3.1.1.3. Synthesis and properties of amphiphilic phosphorus-containing calix[*n*]arenes

p-Phosphonylmethylcalix[4]arenes obtained by Ungaro and co-workers[476] by the classical Arbuzov reaction from *p*-chloromethylcalix[4]arenes and trialkyl phosphites represented early examples of phosphorylated calix[4]arenes. However, amphiphilic structures **241a – d** bearing long-chain alkyl substituents were first synthesized by Kalchenko and co-workers.[477] The parent calix[4]arene was functionalized with long-chain acyl moieties, then intermediates **242a – d** were treated with diethyl chlorophosphate in the presence of triethylamine (Scheme 39). The diethoxyphosphoryl groups were successfully converted to phosphoric acid moieties by the treatment of compounds **243a – d** with trimethylsilyl bromide followed by refluxing in methanol.

Scheme 39



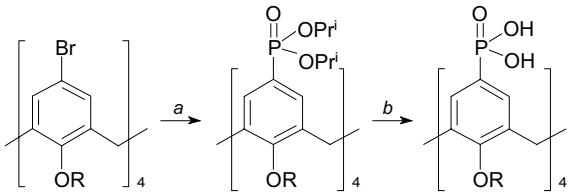
242a – d **243a – d** **241a – d**

(*a*) 1) Me_3SiBr, $CHCl_3$, rt, 48 h; 2) MeOH, Δ 24 h;
R = Bu^n (**a**), n-C_6H_{13} (**b**, 90%), n-C_8H_{17} (**c**, 89%), n-$C_{10}H_{21}$ (**d**, 90%)

Dihydroxyphosphoryloxy-containing macrocycles **241a – d** were established to form stable Langmuir films, and elongation of the acyl moiety induced an increase in the collapse pressure of the monolayer in this series of compounds.

Phosphorylation of the upper rim of *p*-tetrabromo-substituted calix[4]arenes **244a**,**b** with triisopropyl phosphite in the presence of $NiBr_2$ (Scheme 40) followed by the treatment of intermediates **245a**,**b** with trimethylsilyl bromide and methanol gave dihydroxyphosphoryloxy-containing macrocycles **246a**,**b**.[478]

Scheme 40



244a,**b** **245a**,**b** **246a**,**b**

(*a*) P(OPr^i)$_3$, $NiBr_2$, PhCN, 170 °C, 1 h;
(*b*) 1) Me_3SiBr, $CHCl_3$, rt, 30 h; 2) MeOH, 50 °C, 2 h;
R = n-$C_{10}H_{21}$ (**a**, 95%), n-$C_{12}H_{25}$ (**b**, 92%)

Using dynamic light scattering and atomic force microscopy, it was found that macrocycles **244a**,**b** assemble into submicron-sized aggregates with a diameter of 130 – 170 nm with a low polydispersity index.

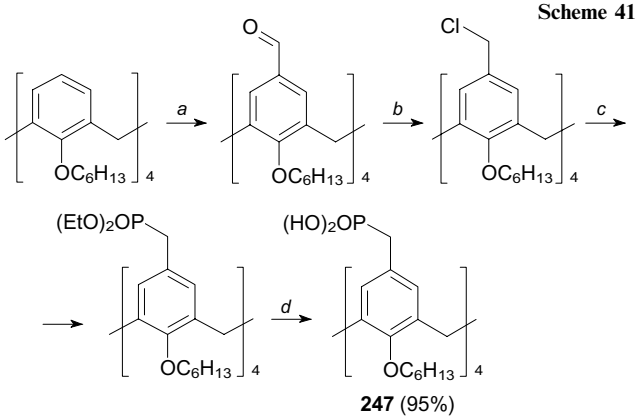
Martin *et al.*[479] substantially expanded the range of dihydroxyphosphoryloxy-containing macrocycles. They prepared derivatives bearing hexyl, octyl, and tetradecyl substituents at the lower rim of the macrocycles using triethyl phosphite in place of triisopropyl phosphite. A study of the toxicity of the prepared series of dihydroxyphosphoryloxy-substituted macrocycles in the PC12 cell line showed that the lowest toxicity was achieved for a calixarene bearing no alkyl groups at its lower rim. Also, it was demonstrated that octyl-substituted macrocycle can form micelles of 4 – 5 nm in diameter, which were stable in a wide range of pH values and can enclose curcumin as a model antioxidant into their cavities, with the micelle toxicity decreasing significantly as compared to that of the monomeric form of the same macrocycle. Later, in relation to the oxidative stress of PC12 cells under the action of H_2O_2, menadione and glutamate, the same research team[480] found that dihydroxyphosphoryloxy-containing calix [4]arenes *per se* are potent antioxidants, which is a great advantage for development of safe carriers for drug delivery.

Using a modified procedure of Ungaro and co-workers,[476] Mo *et al.*[481] synthesized a phosphonomethyl calix[4]-arene derivative **247** (Scheme 41).

According to dynamic light scattering and TEM data, macrocycle **247** forms vesicles of ~100 nm diameter. Using a set of physical methods including NMR spectroscopy and mass spectrometry, it was shown that this compound forms an inclusion complex with carboplatin, opening up prospects for the targeted delivery of this drug to the cancer cells.

An effective nano composition was prepared on the basis of associates formed by macrocycle **247** with paclitaxel and carboplatin anticancer drugs.[482] The composition inhibited the invasion and migration of HT-29 cells more

Scheme 41



(*a*) hexamethylenetetramine, CF_3CO_2H, Δ, 96 h;
(*b*) 1) $NaBH_4$, THF, rt, 18 h; 2) $SOCl_2$, rt, 18 h;
(*c*) $P(OEt)_3$, Δ, 16 h; (*d*) Me_3SiBr, MeCN, Δ, 15 h;
C_6H_{13} is n-hexyl

effectively than these free drugs taken separately and also inhibited the tumour growth in mice.

3.1.2. Amphiphilic derivatives of calix[*n*]arene bearing cationic polar head groups

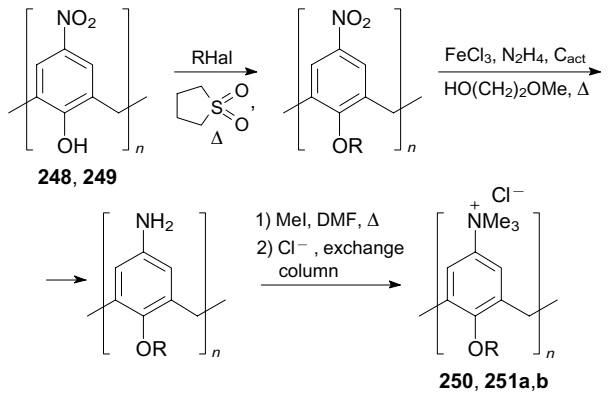
3.1.2.1. Synthesis and properties of amphiphilic amino(ammonio)-containing calix[*n*]arenes

A pioneering work of Shinkai *et al.*[460] described amphiphilic calixarenes with cationic head groups (Scheme 42).

These compounds were synthesized by alkylation of nitro-substituted calix[4]- (**248**) and calix[6]arenes (**249**) with alkyl halides in refluxing sulfolane, and the corresponding *O*-alkylated nitro calixarenes were then reduced with hydrazine hydrate in the presence of iron(III) chloride and activated charcoal. Alkylation with methyl iodide followed by subjecting the products to the Cl^--type ion-exchange column furnished chlorides **250** and **251a**,**b** in 29, 45 and 76% yields, respectively. It was shown that only calixarene **251b** bearing long-chain octyl substituents forms micelles in aqueous solutions.

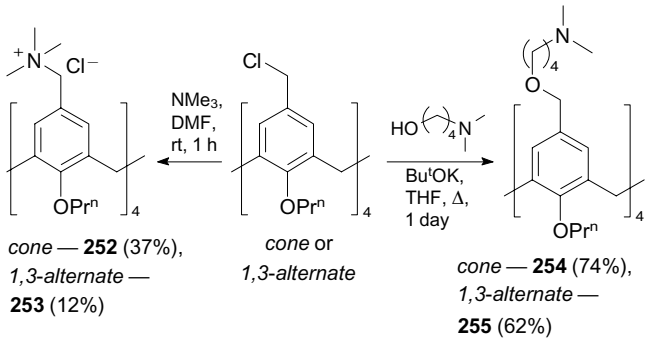
Shinkai and co-workers[483] also prepared a series of macrocycles **252**–**255** substituted with cationic groups in the *cone* and *1,3-alternate* stereoisomeric forms by the reaction of a chloromethyl calix[4]arene derivative with triethylamine and *N*,*N*-dimethylaminobutanol (Scheme 43).

Scheme 42



n = 4 (**248**, **250**), 6 (**249**, **251**); R = Me (**250**, **251a**), n-C_8H_{17} (**251b**); C_{act} is activated charcoal

Scheme 43



The authors demonstrated that a stereoisomeric form affects the shape and type of aggregates generated by amphiphilic compounds. The amphiphile shape depends on the critical packing parameter (N_s) representing the ratio of volumes of the hydrophobic and hydrophilic units of the molecule. The N_s value determines the aggregate shape: $N_s < 1/3$ for spheric micelles, $1/3 < N_s < 1/2$ for rod-like micelles, and $1/2 < N_s < 1$ corresponds to formation bilayer structures.

As illustrated in Fig. 84, calixarenes in the *cone* stereoisomeric form preferably form micelles, while those in the *1,3-alternate* conformation, assemble into bilayer structures, including vesicles.

In addition to the synthesis of tetracarboxy-calix[4]arene **228**, Meier and co-workers[468] carried out chloromethylation of tetra(octyloxy)- (**256**) and tetra(dodecyloxy)-containing calix[4]arenes (**201**), which was followed by the treatment with trimethylamine and gave ammonium calixarenes **257a**,**b** (Scheme 44).

Macrocycles **257a**,**b** were established to form 5 nm micelles, unlike their carboxylate analogue **228**, which self-assembled into vesicles. The authors explained this fact by the existence of a hydrogen bond between carboxyl groups in **228** and the absence of this bond or the presence of electrostatic repulsion between the ammonium moieties in **257a**,**b**; this alters the packing of molecules and results in the formation of micelles.

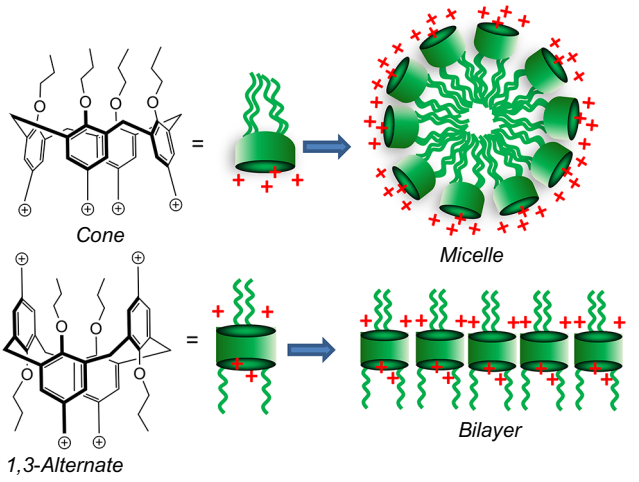
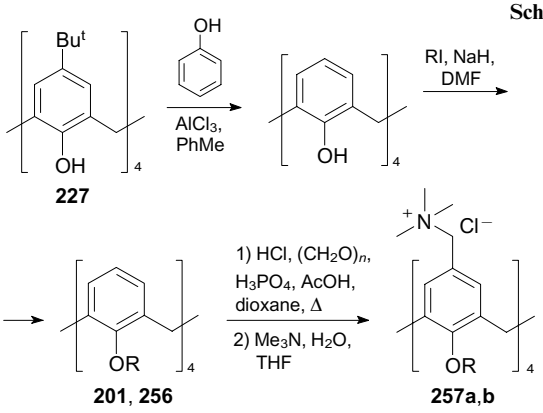


Figure 84. Dependence of the shape and type of aggregates on the stereoisomeric forms of the starting amphiphilic macrocycles.

Scheme 44



R = n-C_8H_{17} (**256**; **257a**, 74%), n-$C_{12}H_{25}$ (**201**, **257b**, 67%)

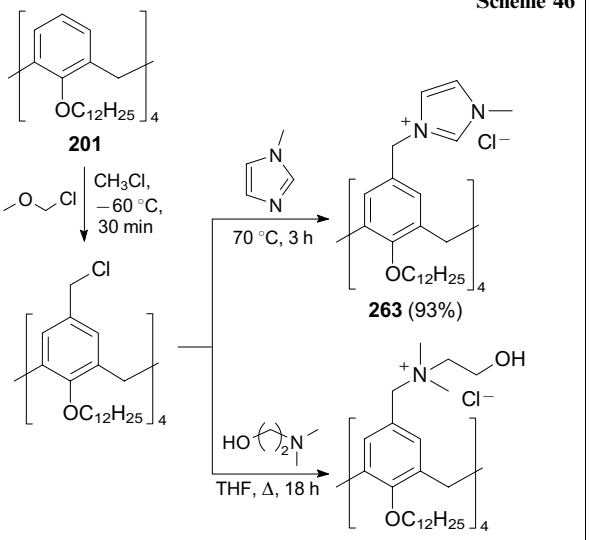
Schatz and co-workers[484] prepared a number of imidazolium macrocycles **258a–e** in high yields (Scheme 45). Derivative **227** was used as the starting compound, and the multistep reaction proceeded *via* the formation of functionalized calixarenes **259–262**. Products **258** can form stable palladium N-heterocyclic carbene complexes, which are reactive towards the Suzuki cross-coupling, and also act as receptors for anions such as sulfates, phosphates, chlorides and bromides.[485]

Kalchenko and co-workers[486] synthesized macrocycles **263** and **264** bearing cationic groups at the upper rim and dodecyl groups at the lower rim (Scheme 46). According to dynamic light scattering (DLS), atomic force microscopy and polyacrylamide gel electrophoresis data, the produced macrocycles can form micelles of 3–6 nm diameter in aqueous solutions and effectively condense the model calf thymus DNA into nanoparticles with average diameters of 55 and 65 nm for **263** and **264**, respectively (Fig. 85).

Liu and co-workers[487] alkylated tetra(chloromethyl)-substituted calixarene with trimethylamine to afford macrocycle **265**. The complex of this macrocycle with adenosine triphosphate (ATP) (Fig. 86) proved to be a very promising system for the targeted drug delivery. Upon complexation of compound **265** with ATP, its critical micelle concentration (CMC) significantly decreases, as the positive charges of the macrocycle head groups are counterbalanced by the negative charge of ATP. When this system is treated with phosphatase, adenosine diphosphate (ADP) is formed, the surface charge neutralization decreased, thus causing the disassembly of the aggregates.

Stoikov and co-workers[488] synthesized thiacalixarenes **266a–e** in the *cone* conformation (Scheme 47). The parent *p-tert*-butylcalix[4]arene (**267**) was first converted to tetra-

Scheme 46



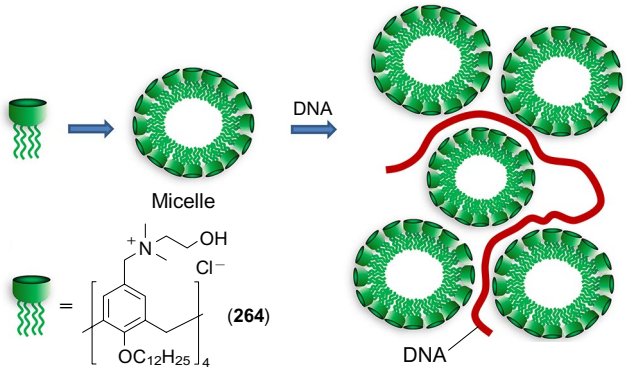
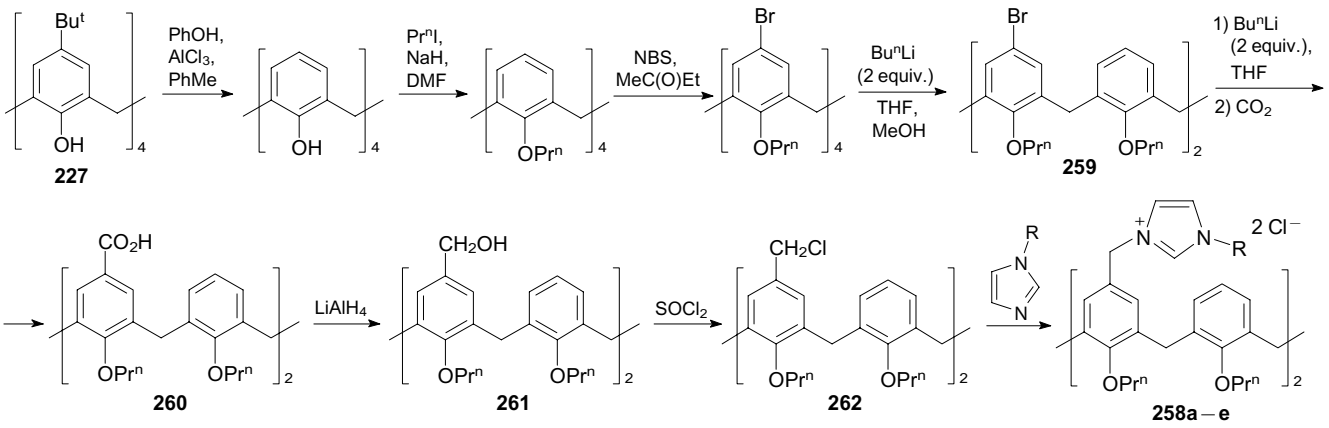


Figure 85. Micellization of calixarene **264** and condensation of the micelles with the model DNA to form nanoparticles. The Figure was created by the authors using data of Ref. 486.

Scheme 45



R = Me (**a**, 96%), Pr^i (**b**, 98%), 2,4,6-$Me_3C_6H_2$ (**c**, 91%), 2,6-$Pr^i_2C_6H_3$ (**d**, 91%), cyclo-C_6H_{11} (**e**, 96%)

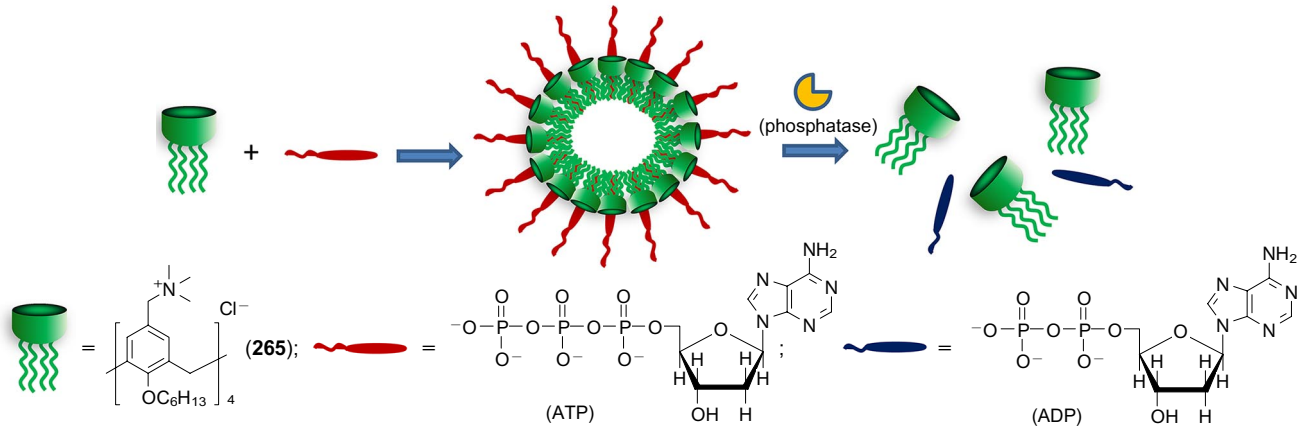
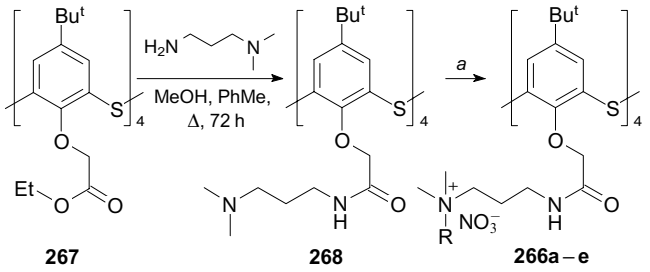


Figure 86. Aggregation of calixarene **265** with ATP and destruction of the aggregates under the action of phosphatase. The Figure was created by the authors using data of Ref. 487.

Scheme 47



(*a*) 1) RX, MeCN, Δ, 72 h; 2) $AgNO_3$, MeCN, rt, 27 h;
R = Me (**a**, 95%), Et (**b**, 98%), CH_2CO_2Et (**c**, 94%), Bn (**d**, 90%), $(CH_2)_2Pht$ (**e**, 96%); Pht is phthalimido

amidoamine derivative **268**, which was quaternized under the action of various alkylating agents in acetonitrile. The subsequent replacement of the counterion with a nitrate ion *via* the reaction of the intermediates with $AgNO_3$ gave the target products **266**.

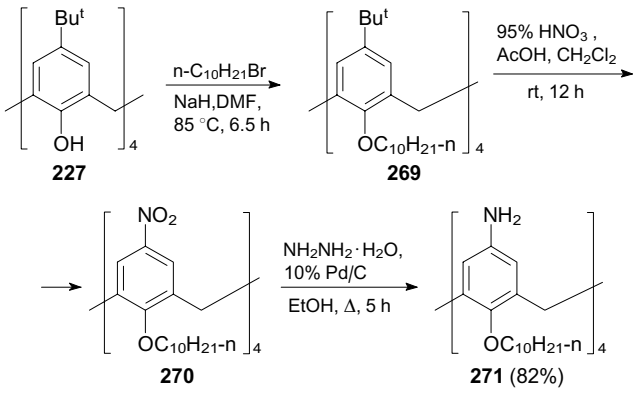
These amphiphilic derivatives effectively react with silver nitrate, while macrocycles **266a**,**e** form 1 : 1 complexes with fluorescein. As shown by DLS and spectrophotometry, the complexes of macrocycles **266a**,**e** with fluorescein react with BSA to produce a structure of 6–8 nm in size.

Using a similar approach, the same research team[489] introduced chiral L-tryptophan residues into the *p-tert*-butylthiacalix[4]arene molecule to obtain macrocycles both in the *cone* and *1,3-alternate* conformations. According to TEM and DLS data, these macrocycles form aggregates with diameters of 86–134 nm. Also, the aggregates were found to be chiral and to possess intrinsic fluorescence depending on the solvent polarity.

Recently, Ma and co-workers[490] used a traditional approach of calixarene chemistry, namely, *ipso*-nitration of calixarene **269** followed by the reduction of tetranitro derivative **270**, to obtain tetraaminocalix[4]arene **271** (Scheme 48).

The authors deposited macrocycle **271** onto the inner surface of a capillary chromatographic column and obtained excellent characteristics for the separation of both aromatic amines and traditional aliphatic analytes of various polarities. The column demonstrated good reproducibility of results and was thermally stable up to 240 °C.

Scheme 48



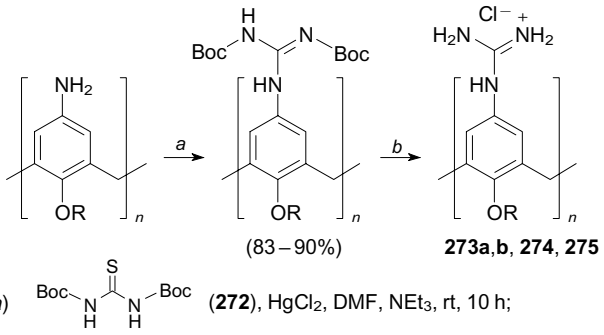
3.1.2.2. Synthesis and properties of amphiphilic guanidinium-containing calix[*n*]arenes

Guanidinium-containing calix[*n*]arenes are of special interest since this functional group can be effective in binding anionic guests (carboxylates, phosphates, sulfates, nitrate, *etc.*) and is particularly relevant in DNA binding. The synthesis and systematic studies of amphiphilic guanidinium-containing calix[*n*]arenes were carried out by Ungaro and co-workers.[491] The reaction of appropriate *p*-aminocalix[*n*]arenes with *N*,*N*-di(*tert*-butoxycarbonyl)thiourea (**272**) in the presence of catalytic amounts of $HgCl_2$ and the subsequent Boc-deprotection (Boc is *tert*-butoxycarbonyl) on treatment with hydrochloric acid affords macrocycles **273**–**275** in high yields (Scheme 49).

All newly formed macrocycles were found to exhibit low cytotoxicity and bind to plasmid DNA, and lipophilic macrocycle **273b** forms aggregates in water. In the follow-up studies, a similar synthetic route was used to prepare a series of calix[4]arenes in the *cone* (**276**) and *1,3-alternate* (**277**) conformations and conformationally mobile macrocycle **278**.[492]

The authors studied in detail the interaction of calixarenes with plasmid DNA and found (Fig. 87) that lipophilic macrocycles **273b** and **276** condense DNA to form a dense core and facilitate the cell transfection, whilst conformationally mobile macrocycles bearing methyl substituents at the lower rim form large gorgon-like structures, which do not condense DNA and do not promote transfection.

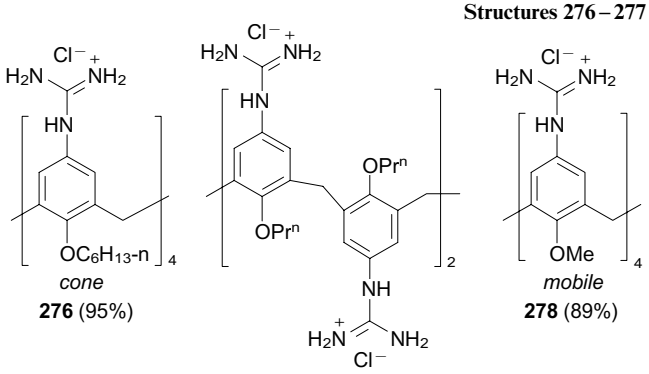
Scheme 49



(*a*) (**272**), $HgCl_2$, DMF, NEt_3, rt, 10 h;

(*b*) HCl, dioxane, rt, 24 h; *n* = 4: R = Pr^n (**273a**), n-C_8H_{17} (**273b**); R = Me: *n* = 6 (**274**), 8 (**275**)

Structures 276–277



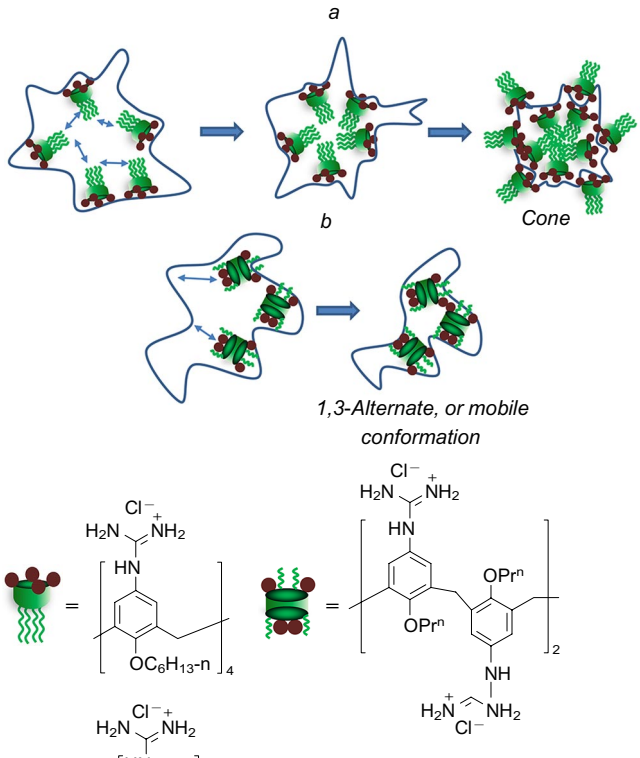


Figure 87. Scheme for the interaction of calixarenes **276**–**278** in various conformations such as *cone* (*a*) and mobile, or *1,3-alternate* (*b*) with plasmid DNA. The Figure was created by the authors using data of Ref. 492.

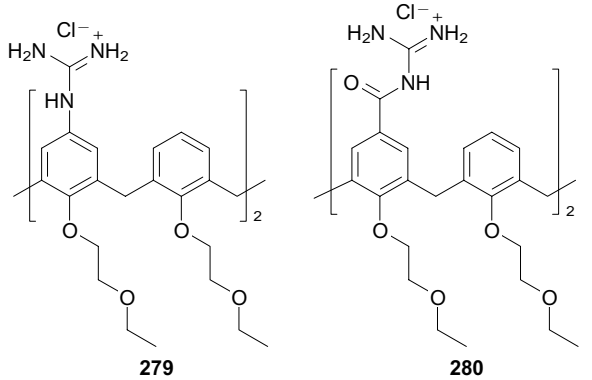
Macrocycle **277** in the *1,3-alternate* conformation occupies an intermediate position, as it condenses DNA into more compact structures, but this occurs only due to the electrostatic interactions and, hence, does not promote transfection.

It was further established that being incorporated into the phospholipid membrane, macrocycle **273b** exhibited a ionophoric activity and enabled the selective transfer of chloride ions due to binding to guanidinium moieties.[493]

The same research team [494] found that macrocycle **279** containing two guanidinium moieties at the upper rim and four ethoxyethoxy units at the lower rim can act as a synthetic phosphodiesterase effectively hydrolyzing 2-hydroxypropyl *p*-nitrophenyl phosphate taken as a RNA model. In addition, in the recently obtained [495] macrocycle **280** containing a carbonyl spacer between the macrocyclic platform and guanidinium moieties, the mobility of guanidinium groups is increased, which promotes cleavage of the phosphodiester bonds.

Guo and co-workers,[496] employing the synthetic approach similar to that applied by Ungaro s team, synthesized calix[5]arene **281** bearing five guanidinium units at the

Structures 279, 280



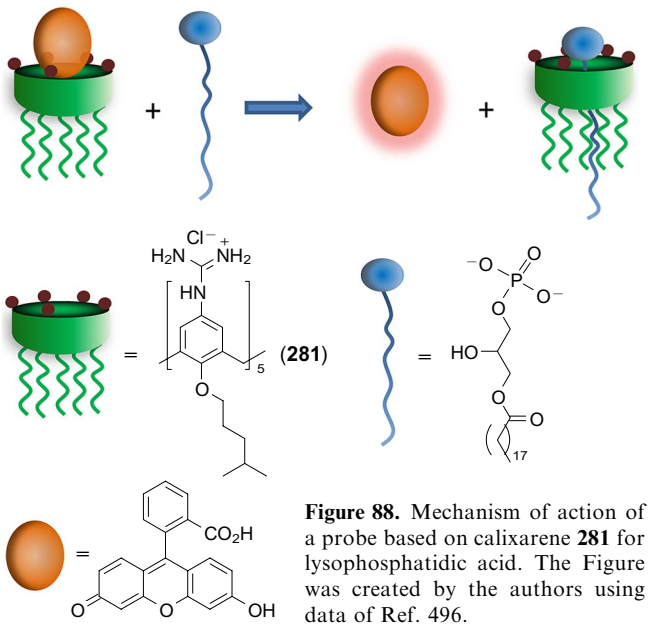


Figure 88. Mechanism of action of a probe based on calixarene **281** for lysophosphatidic acid. The Figure was created by the authors using data of Ref. 496.

upper rim and isopentyloxy moieties at the lower rim. This macrocycle has been successfully used in the design of an ultrasensitive fluorescent sensor for lysophosphatidic acid (Fig. 88), a biomarker for early diagnosis of ovarian cancer and other gynaecological malignant neoplasms, which operates on the principle of displacing the fluorophore (fluorescein) from the calixarene complex. The unique feature of this system is that the untreated blood serum can be used as a raw material.

3.1.3. Click chemistry modular approach in the synthesis of amphiphilic derivatives of calix[*n*]arenes

In 2001, Sharpless and co-workers [497] first introduced the term click chemistry. According to the proposed classification, click reactions should meet the following criteria: be stereospecific, versatile and atom-economic, provide high yields of the products and proceed under mild conditions to afford only safe by-products. Azide – alkyne cycloaddition catalyzed by copper salts (CuAAC) and furnishing 1,4-disubstituted triazoles under particularly mild conditions and in high yields became most popular among the click reactions. However, later several research teams (*e.g.*, Ref. 498) showed that these reactions can be successfully catalyzed by ruthenium, gold, silver, iridium, nickel, zinc or lanthanum salts or metal complexes. In this case, both 1,4- and 1,5-disubstituted triazoles can be produced depending on the metal nature. A key advantage of the CuAAC reaction is an exceptional functional group tolerance as allowing the straightforward introduction of even ionized moieties without the use of protecting groups. These reactions open access to libraries of various compounds, including amphiphilic ones, by varying azide- or alkyne-containing units (Fig. 89).[499, 500]

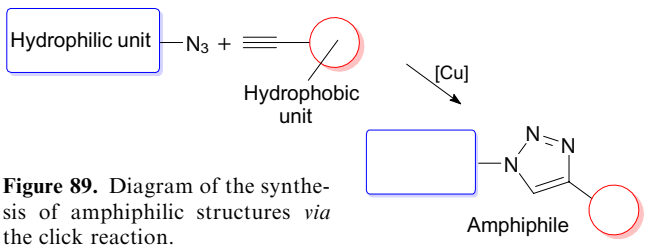
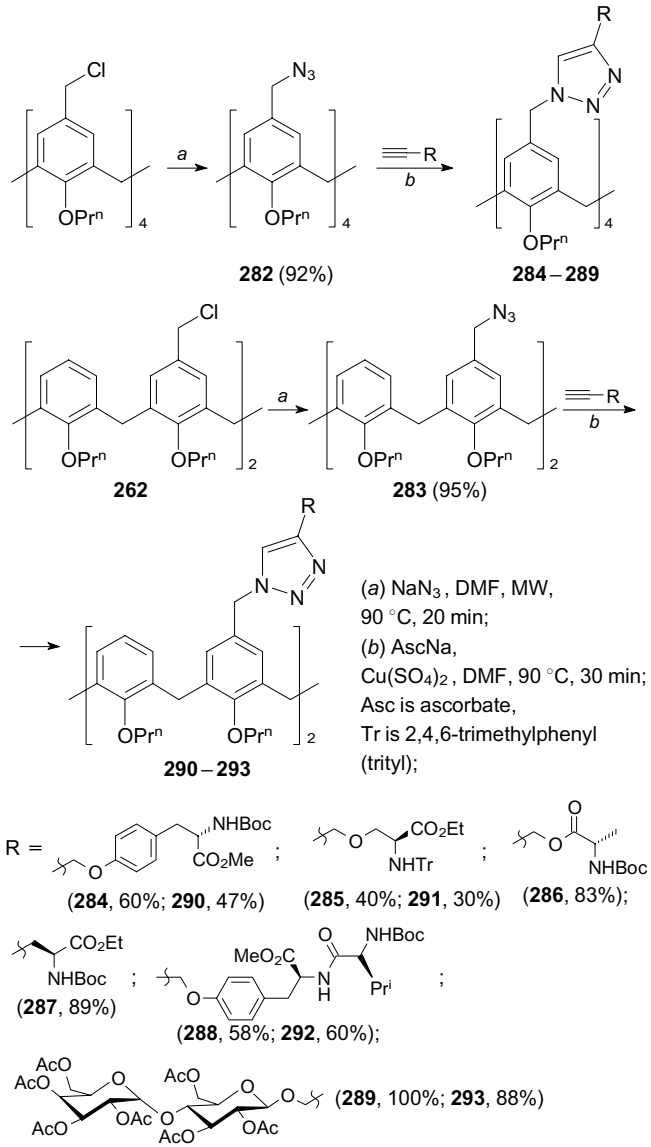


Figure 89. Diagram of the synthesis of amphiphilic structures *via* the click reaction.

One of the earliest studies that made use of the modular approach and provided a variety of amphiphilic calix[4]arenes was performed by Sharma and co-workers.[501] By the reaction of readily available tetra- and dichloromethyl calix[4]arene derivatives (**262**) with sodium azides under microwave (MW) irradiation, they synthesized the corresponding tetra- and diazides **282** and **283** over a period of 20 min in almost quantitative yields (Scheme 50). Such azides were employed in the CuAAC reaction with amino acids, dipeptides and disaccharides bearing a propargyl moiety. The reaction was also carried out under microwave heating, and products **284** – **293** were isolated in moderate to quantitative yields.

Later, Shen and co-workers [502] implemented the CuAAC reaction to prepare amphiphilic star copolymers. For this purpose, the starting *p-tert*-butylcalix[4]arene was successively functionalized with two propargyl and two methyl acetateoxyl moieties, which were then reduced to give alcohol **294** (Scheme 51). Compound **294** was polymerized with ε-caprolactone in the presence of $SnOct_2$ (Oct is 2-ethylhexanoate) as a catalyst to yield macrocycles **295** with a polymerization degree from 11 to 40. In these macrocycles, polyoxyethylated moieties composed of 25 or 45 units were introduced *via* the CuAAC reaction.

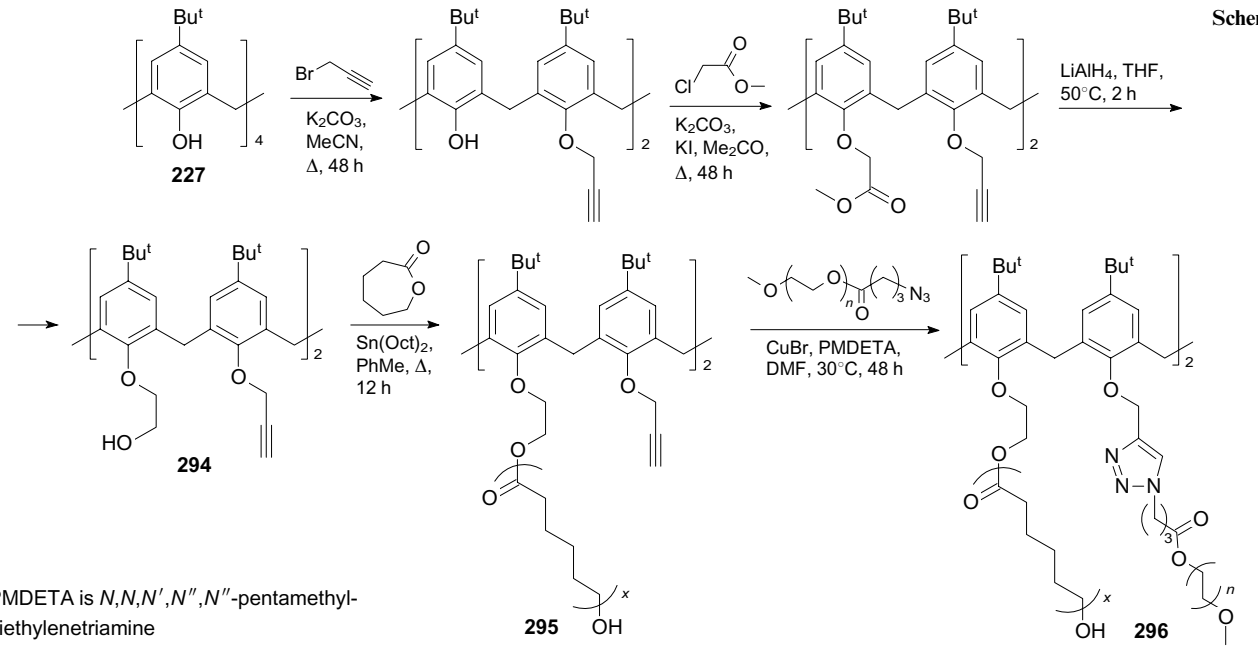
Scheme 50



Macrocycles **296** form aggregates in aqueous solutions; by varying the length of oxyethyl arms, one can affect the aggregate size. Thus, with decreasing the content of polyoxyethylated units, the aggregate size increased from 10 to 30 nm, while further decrease resulted in the formation of vesicles ranging in size from 100 to several hundred nanometres.

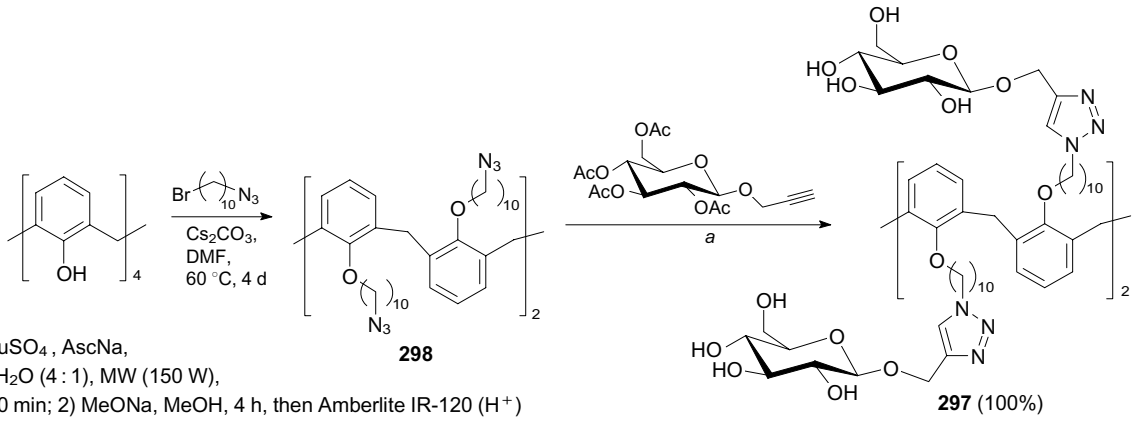
Sansone and co-workers [503] applied the click chemistry modular approach to prepare bolaamphiphile **297** substituted with four glucose residues. Tetraalkylazide-containing calix[4]arene **298** in the *1,3-alternate* conformation (Scheme 52) formed initially was reacted with 2,3,4,6-tetra-*O*-acetyl-1-propargyl-β-D-glucopyranoside under microwave heating. The reaction product was treated with sodium methoxide and deacetylated by being passed through ion exchange resin to afford macrocycle **297** in a quantitative yield.

Scheme 51



PMDETA is *N*,*N*,*N*′,*N*″,*N*″-pentamethyldiethylenetriamine

Scheme 52



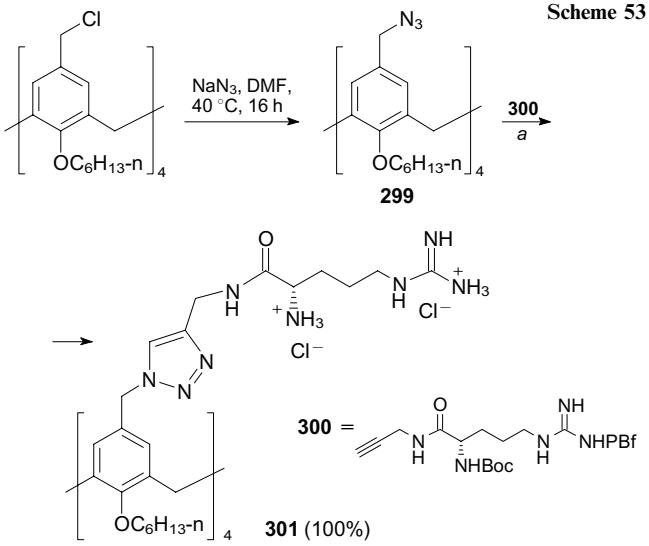
(*a*) 1) $CuSO_4$, AscNa, DMF–H_2O (4 : 1), MW (150 W), 80°C, 40 min; 2) MeONa, MeOH, 4 h, then Amberlite IR-120 (H^+)

Mixed liposomes composed of macrocycle **297** and 1,2-bis[(9*Z*)-octadecenoyl]-*sn*-glycero-3-phosphocholine (DOPC) were obtained. This compound was found to decrease the permeability of liposomes by rigidifying the lipid bilayer. Also, mixed liposomes were found to interact with the glucose binding protein concanavalin A, which is promising for the targeted drug delivery.

The same research team[504] used tetraazidomethylcalix[4]arene **299** and alkyne **300** to obtain macrocycle **301** decorated with four guanidinium moieties in a quantitative yield (Scheme 53).

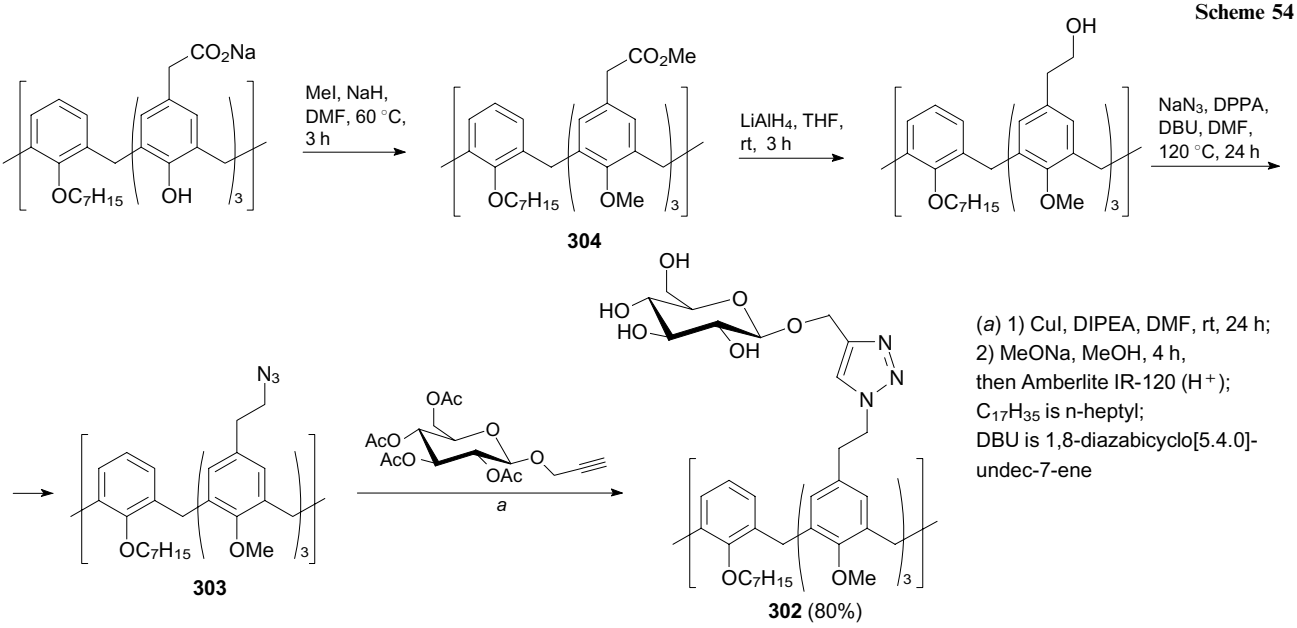
The authors compared the efficiency of DNA transfection for macrocycle **301** and its analogue bearing an amide spacer in place of the triazole one and found that the amide-spacered compound is slightly more efficient. In this case, the transfection efficiency for macrocycles containing amide or triazole units between the macrocyclic platform and guanidine residue proved to be significantly higher than that for calix[4]arenes containing four guanidinium moieties directly attached to the aromatic rings. An increase in the transfection efficiency was attributed to the presence of additional nitrogen atoms, which, due to their ability to be reversibly protonated, impart a certain buffering ability to the macrocycle and its complex with DNA,

Scheme 53



(*a*) 1) CuI·$P(OEt)_3$, DIPEA, Me_2CO, Δ, 24 h; 2) TFA–TIS–H_2O (95 : 2.5 : 2.5), 0.1 M HCl; PBf is 2,2,4,6,7-pentamethyldihydrobenzofuran-5-sulfonyl, DIPEA is diisopropylethylamine, TFA is trifluoroacetic acid, TIS is triisopropyl silane

Scheme 54



thus facilitating the endosome release *via* the 'proton sponge' mechanism.

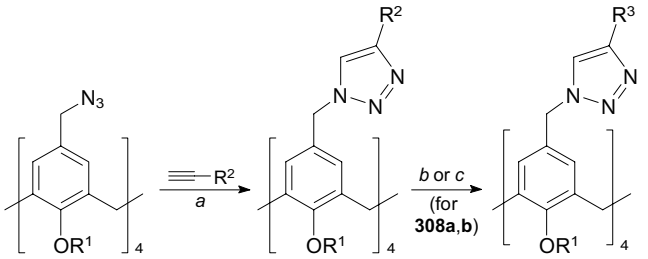
Recently, Jawhari and co-workers [505] synthesized calix[4]arene **302** bearing three glucose residues. Tri(azidoethyl)-containing precursor **303** is formed through the exhaustive methylation of tri(carboxymethyl)calix[4]arene **304** followed by the reduction of ester groups and replacement of hydroxyl groups with diphenyl phosphoryl azide (DPPA) (Scheme 54). The CuAAC reaction was carried out using the CuI – DIPEA catalytic system, and deacetylation was accomplished by treatment with sodium methoxide in methanol, thus providing product **302** in high yield.

In aqueous solutions, compound **302** forms monodisperse micelles of 6 nm average hydrodynamic diameter, composed of 20 macrocycles. This compound can stabilize membrane proteins for a long period of time (more than 45 days) with a negligible loss in their activity, significantly outperforming other known surfactants.

During the last decade, a series of amphiphilic triazoles bearing cationic (**305a**,**b**), zwitterionic (**306a**,**b**) and nonionic (**307a** – **c**) head groups have been prepared [506 – 511] (Scheme 55). As a basic molecular platform, azidomethyl-containing calix[4]arenes in the *cone* configuration with alkyl chains of various lengths at the lower rim were used, and the target amphiphilic macrocycles were formed in high (including quantitative) yields. In the case of salts **305a**,**b**, amido derivatives **308a**,**b** were initially obtained.

Considerable work was undertaken to study physicochemical properties of the newly synthesized triazoles. Thus, it was shown [506] that calixarene **305a** forms micelles in the acidic pH region, while with increasing pH, the micelles transform into cylindrical structures as a result of deprotonation. At the same time, for a macrocycle with longer-chain alkyl substituents (*e.g.*, hexyl), micelles transform into vesicles. More lipophilic calixarene bearing nonyl substituents formed cylinders even at low pH values. Calixarene **305b** containing cysteine residues was used as a template in the synthesis of monomodal gold nanoparticles of 2 nm diameter, which exactly matches the size of the cavity formed by the adjacent cysteine moieties attached to the calix[4]arene platform.[507] Calixarenes **306a**,**b** bearing a

Scheme 55



(*a*) $CuSO_4$, AscNa, DMF or DMSO, 90 or 80 °C, 24 – 38 h;
(*b*) CH_2Cl_2, 0 °C, 2 h (for **308a**); (*c*) TFA, Et_3SiH, HCl,
2 h (for **308b**); $R^2 = CH_2NMe_2^+(CH_2)_2OP(=O)(OMe)O^-$:
$R^1 = Pr^n$ (**306a**, 76%), n-C_6H_{13} (**306b**, 70%);
R^1 = n-C_5H_{11}: $R^2 = CH_2O(CH_2CH_2O)_nMe$ (*n* = 11 (**307a**, 74%),
22 (**307b**, 80%), 42 (**307c**, 70%)); $R^1 = Pr^n$: $R^2 = CH_2NHBoc$ (**308a**);
$R^3 = CH_2NH_3^+Cl^-$ (**305a**);
$R^1 = Bu^n$: $R^2 = CH_2NHC(O)CH(NHBoc)CH_2STr$ (**308b**),
$R^3 = CH_2NHC(O)CH(CH_2SH)NH_3^+Cl^-$ (**305b**)

choline phosphate moiety proved to be able to form monodisperse micelles having diameters of 1.9 and 26 nm, respectively. Moreover, mixed micelles based on macrocycles and phospholipid DOPC were actively taken up by the cells *via* endocytosis, which is a significant advantage for the design of carriers for drug delivery systems.[508] A unique ability of macrocycles **307a**,**b** with polyethylene glycol arms to form micelles with a stationary aggregation number corresponding to the number of vertices of regular polyhedra, the so-called Platonic micelles, was demonstrated.[511] Thus, macrocycle **307a** forms only dodecameric particles, while macrocycle **307b** with longer-chain polyethylene glycol arms assembles into octamers. It is noteworthy that macrocycle **307c** with the longest polyethylene glycol moieties is unable to form stable micelles due to a strong shift of the hydrophilic – lipophilic balance.

During the last decade, active studies of amphiphilic derivatives of calix[4]arene have been pursued in the Kazan Federal University (KFU). For example, the stepwise modification of the starting *p-tert*-butylthiacalix[4]arene (**223**) *via* the Mitsunobu reaction led to a series of distally disubstituted *p-tert*-butylthiacalix[4]arenes **309a–c** bearing alkyl substituents of various lengths.[512–514] By the Mitsunobu reaction or Williamson alkylation under microwave heating, the corresponding macrocycles were successfully functionalized with various bromoalkyl moieties, and the resulting macrocycles **310a–i** were obtained in the *1,3-alternate* stereoisomeric form (Scheme 56).

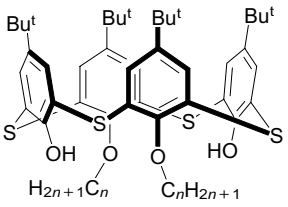
Thiacalixarenes **310** proved to be versatile precursors for the synthesis of amphiphilic macrocycles both *via* reactions with various nitrogen-containing nucleophiles (amines, heterocycles) and *via* conversion of **310** to azides **311–313**. Using the click chemistry modular approach, the latter compounds gave rise to macrocyclic amphiphiles decorated with anionic and cationic head groups (Scheme 57).

The azide–alkyne cycloaddition with acetylene dicarboxylic acid gave tetra(carboxyl)-containing macrocycles **314–316** (see Scheme 57).[513]

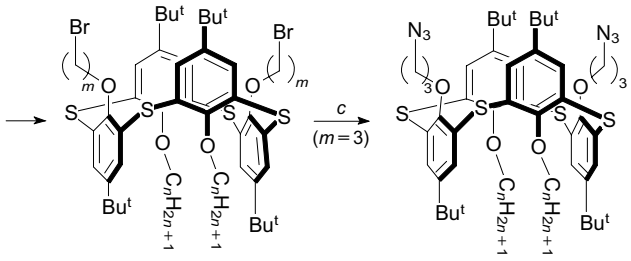
To improve their colloidal stability, macrocycles **314–316** were embedded into phospholipid vesicles of DPPC (Fig. 90). The mixed DPPC–**316** vesicles proved to be effective sensitizing antennas for terbium ion, exhibiting intense luminescence. The DPPC–**316**–Tb^{III} ternary system was used do design a fluorescence probe for pyridoxine [4,5-bis(hydroxymethyl)-2-methylpyridin-3-ol], which functioned through the competitive binding and stripping terbium ions from the surface of vesicles, thus quenching the luminescence. This sensor can detect pyridoxine at a concentration of 7 mol L^{-1} in the presence of a 100-fold excess of other biomolecules.

Macrocycles **317–319** bearing two ammonium moieties were obtained in high yields *via* the CuAAC reaction of azide-containing calixarenes **311–313** with *N*-propargyl-

Scheme 56



309a–c

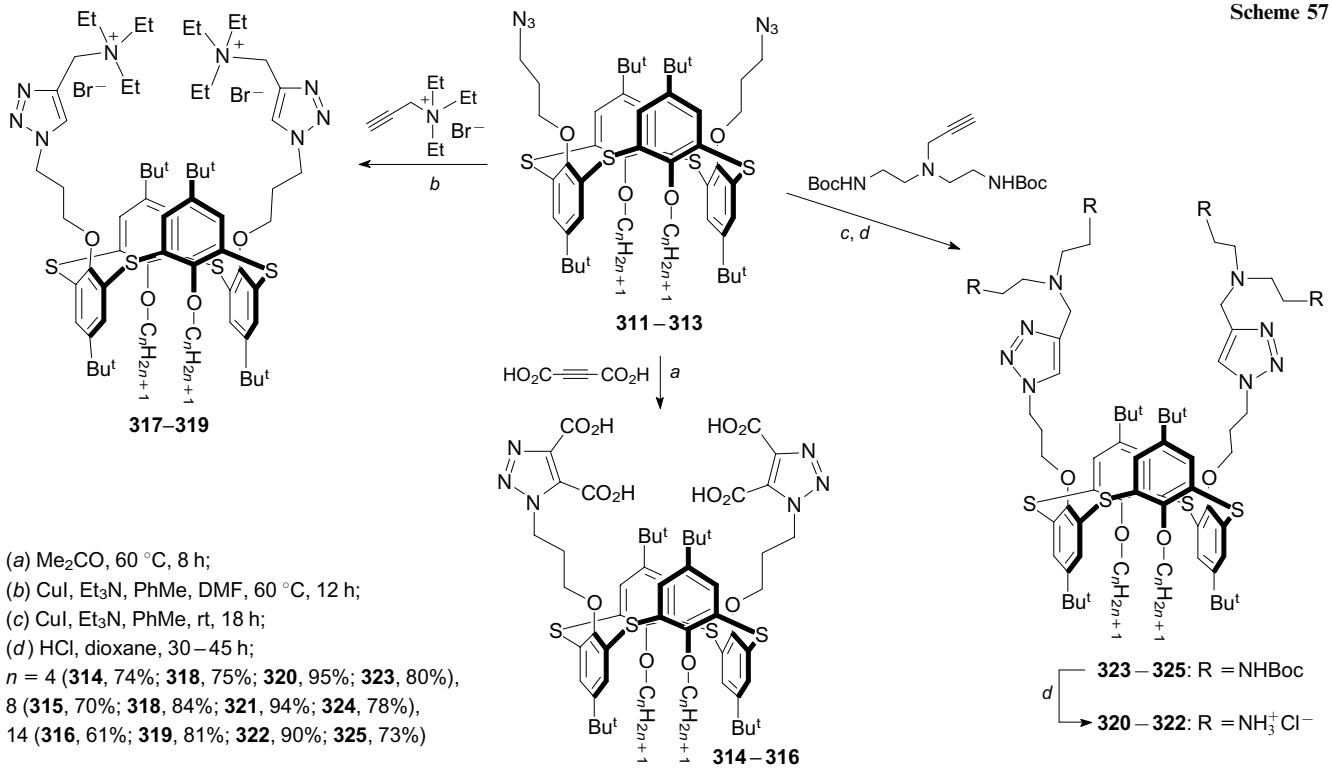


310a–c **311–313**

(*a*) $Br(CH_2)_3OH$, DEAD, PhMe, 70 °C, 24 h;
(*b*) $Br(CH_2)_mBr$, K_2CO_3, Me_2CO, MW (400 W), 130 °C;
(*c*) NaN_3, DMF, 110 °C, 3–8 h; *n* = 4 (**309a**; **311**, 52%), 8 (**309b**; **312**, 69%), 14 (**309c**; **313**, 72%);
DEAD is diethylacetylene dicarboxylate

Compounds **310**	*n*	*m*	Time, h	Yield (%)
a	4	3	24	76
b	8	3	24	87
c	14	3	24	85
d	4	4	8	64
e	8	4	8	60
f	14	4	8	63
g	4	5	12	55
h	14	5	12	57
i	4	6	15	40

Scheme 57



317–319 **311–313** **314–316**

(*a*) Me_2CO, 60 °C, 8 h;
(*b*) CuI, Et_3N, PhMe, DMF, 60 °C, 12 h;
(*c*) CuI, Et_3N, PhMe, rt, 18 h;
(*d*) HCl, dioxane, 30–45 h;
n = 4 (**314**, 74%; **318**, 75%; **320**, 95%; **323**, 80%), 8 (**315**, 70%; **318**, 84%; **321**, 94%; **324**, 78%), 14 (**316**, 61%; **319**, 81%; **322**, 90%; **325**, 73%)

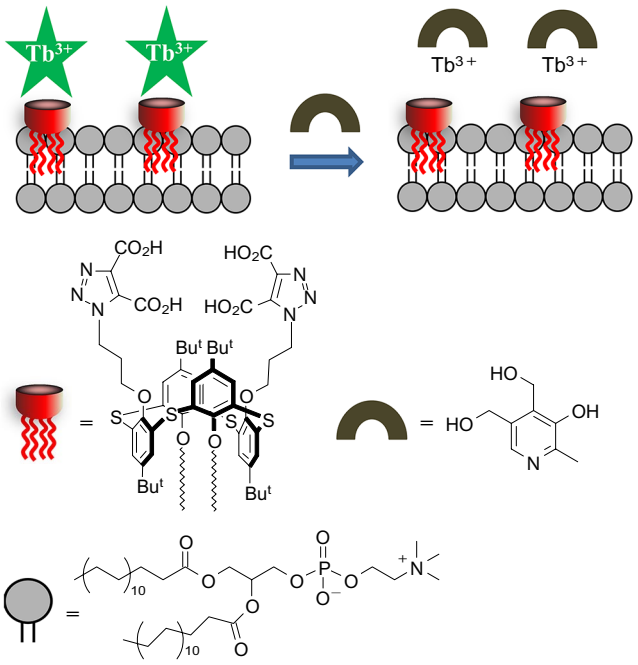


Figure 90. Scheme for the embedding of amphiphilic structures **314**–**316** into vesicles of dipalmitoyl phosphatidylcholine (DPPC). The Figure was created by the authors using data of Ref. 513.

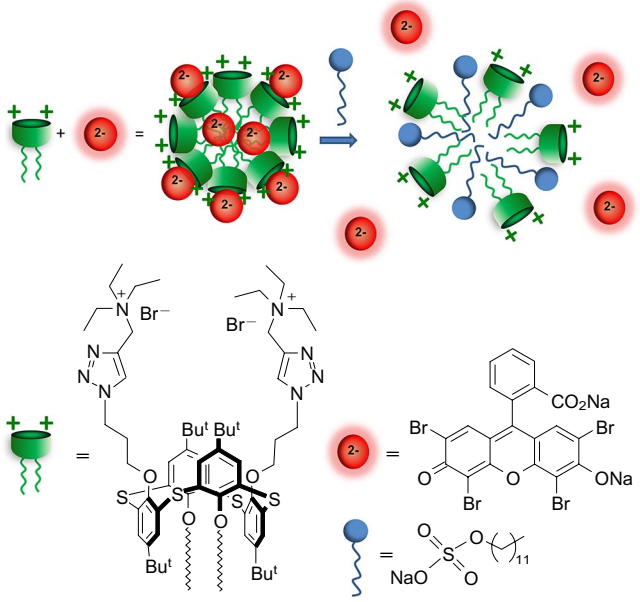


Figure 91. Mechanism of action of a fluorescence probe based on macrocycles **317**–**319**. The Figure was created by the authors using data of Ref. 516.

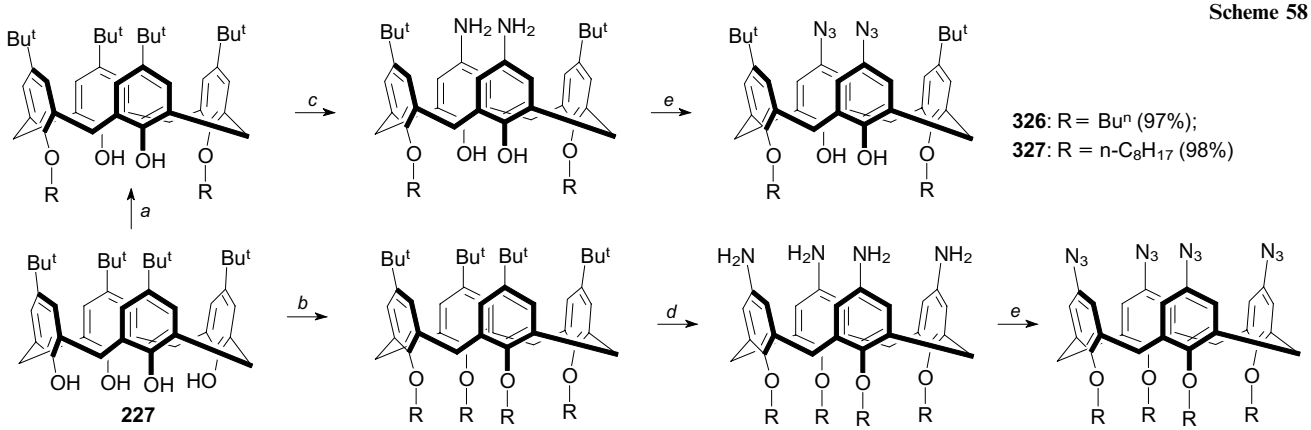
N,*N*,*N*-triethylammonium bromide[515] (see Scheme 56). It was found that macrocycles **317**–**319** can react with BSA and that the logarithm of the stability constant doubled with increasing macrocycle hydrophobicity, due to the ability of more lipophilic macrocycle **319** to interact both with the negatively charged BSA surface and with its hydrophobic pocket.

Macrocycles **317**–**319** were employed to prepare a fluorescent probe capable of determining alkyl sulfate surfactants (Fig. 91).[516] In aqueous solutions, they form 130 nm aggregates, with the critical aggregation concentration decring on moving to more hydrophobic macrocycle **319** containing tetradecyl substituents. When macrocycles reacted with the anionic dye eosin, the CAC value significantly decreased (> 15 times), and the aggregate sizes were reduced to 90 nm, which is associated with a partial neutralization of the charge of ammonium moieties and, as a result, with a decrease in the repulsion between the neighbouring macrocycles.

It was found that the addition of alkyl sulfate surfactants leads to eosin displacement from the joint aggregates with calixarene, while the addition of other surfactants (anionic, cationic and zwitterionic) does not produce such an effect. This is due to the tetrahedral structure of the sulfate ion and, consequently, to the possibility of more effective electrostatic interactions to occur with ammonium groups of calixarene as compared, *e.g.*, with carboxylate ion.

Polyammonium macrocycles **320**–**322** were synthesized using the click chemistry modular approach from azides **311**–**313** followed by deprotection of Boc derivatives **323**–**325**. These calixarenes proved to form stable aggre-

Scheme 58



(*a*) RBr, K_2CO_3, Me_2CO, 130 °C, MW (400 W); (*b*) RBr, NaH, DMF, rt; (*c*) 1) HNO_3, CH_2Cl_2, 0 °C; 2) NH_2NH_2, $Ni/SiO_2/Al_2O_3$, EtOH, Δ; (*d*) 1) 100% HNO_3, AcOH, CH_2Cl_2, 0 °C; 2) NH_2NH_2, $Ni/SiO_2/Al_2O_3$, EtOH, Δ; (*e*) NaN_3, $NaNO_2$, AcOH, DMF, 0 °C

326: R = Bu^n (97%);
327: R = n-C_8H_{17} (98%)

328: R = Bu^n (93%);
329: R = n-C_8H_{17} (85%)

gates of 50–150 nm in size in aqueous solutions and to interact with the model calf thymus DNA to displace the DNA intercalator such as the fluorescent ethidium bromide dye.[517] It was found that with increasing lipophilicity of the macrocycle, the efficiency of the displacement of ethidium bromide increases twofold. Macrocycles **320**–**322** lead to condensation of DNA and reduce the DNA size in water up to 5 times.

Chemists from the KFU developed a method for the synthesis of calix[4]arene derivatives bearing azide moieties at the upper rim. Copper-catalyzed aryl substitution of bromo derivatives of calix[4]arene with sodium azide[518] and diazotization of available di- and tetraamino calix[4]-arene derivatives in a DMF–acetic acid medium[519] furnished aryl azides **326**–**329** in almost quantitative yields (Scheme 58).

With the use of click chemistry, these azides served as a platform for the synthesis of amphiphilic polyamine macrocycles (compounds **330**–**333**), containing 6 or 12 amino moieties,[519] and amphiphilic octaacids **334**–**336** (Scheme 59).[520]

Eosin H complex with aggregated calix[4]arene **331** was used to develop an optical sensor for adenosine diphosphate in aqueous solutions, which functioned through the competitive dye displacement.[519] It was found that the selectivity to adenosine diphosphate results from its complementarity to the cavity of macrocycle **331**. Macrocycle **331** and *N*-(2-aminoethyl)pentacosa-10,12-diamide were employed to obtain polydiacetylenic vesicles, which allowed for the naked-eye sensing of adenosine diphosphate in aqueous solutions *via* the colour change (Fig. 92).

Studies of the aggregation characteristics of macrocycles **334**–**336** in aqueous solutions showed that their CAC values decrease with increasing lipophilicity.[520] Macrocycles **334** and **335** containing octyl and tetradecyl moieties can form compact micelles of 20–30 nm in diameter, whilst

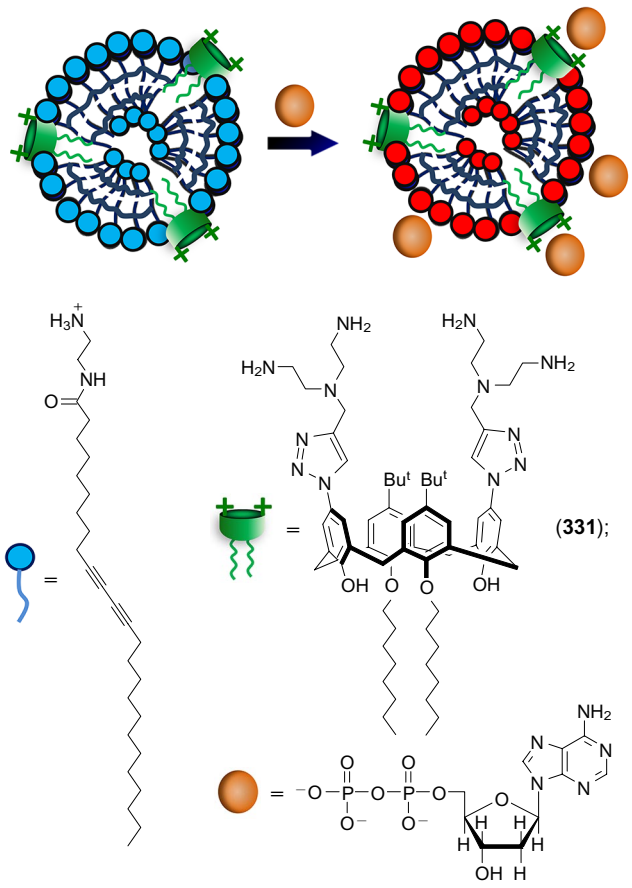


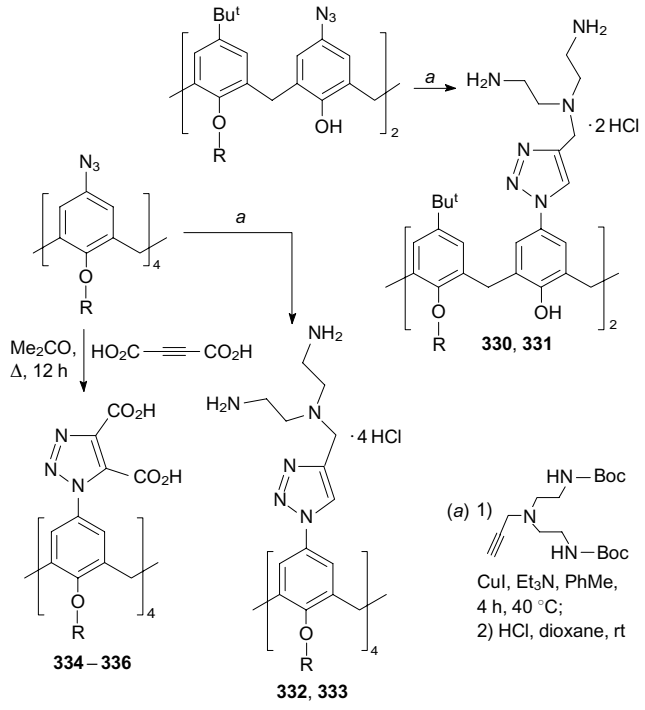
Figure 92. Operating principle of the optical sensor based on macrocycle **331**. The Figure was created by the authors using data of Ref. 519.

more lipophilic macrocycle **336** forms submicron-sized aggregates. When macrocycle **336** was used as a micellar catalyst for the Suzuki cross-coupling reaction of phenylboronic acid with various iodo-, bromo-, and chloroarenes, the conversion turned out to be high even with inactive aryl chlorides.

In addition to the non-covalently bound functional polydiacetylenic species, the authors of this part of the review and co-workers[521, 522] obtained thiacalix[4]arene derivatives containing photopolymerized pentacosa-10,12-diynamide moieties. For this purpose, propyl azide and polyphthalimide moieties were successively introduced into the starting *p*-*tert*-butylthiacalix[4]arene **223**, after which tetrasubstituted macrocycle **337** was subjected to hydrazinolysis and acylation with pentacosa-10,12-diynoyl chloride to afford azide **338** in a good yield (Scheme 60). The azide–alkyne cycloaddition produced peripheral triazole rings in thiacalixarenes decorated with carboxyl (compound **339**), sulfonate (**340a**)[522] and diethylenetriamine (**340b**)[523] moieties.

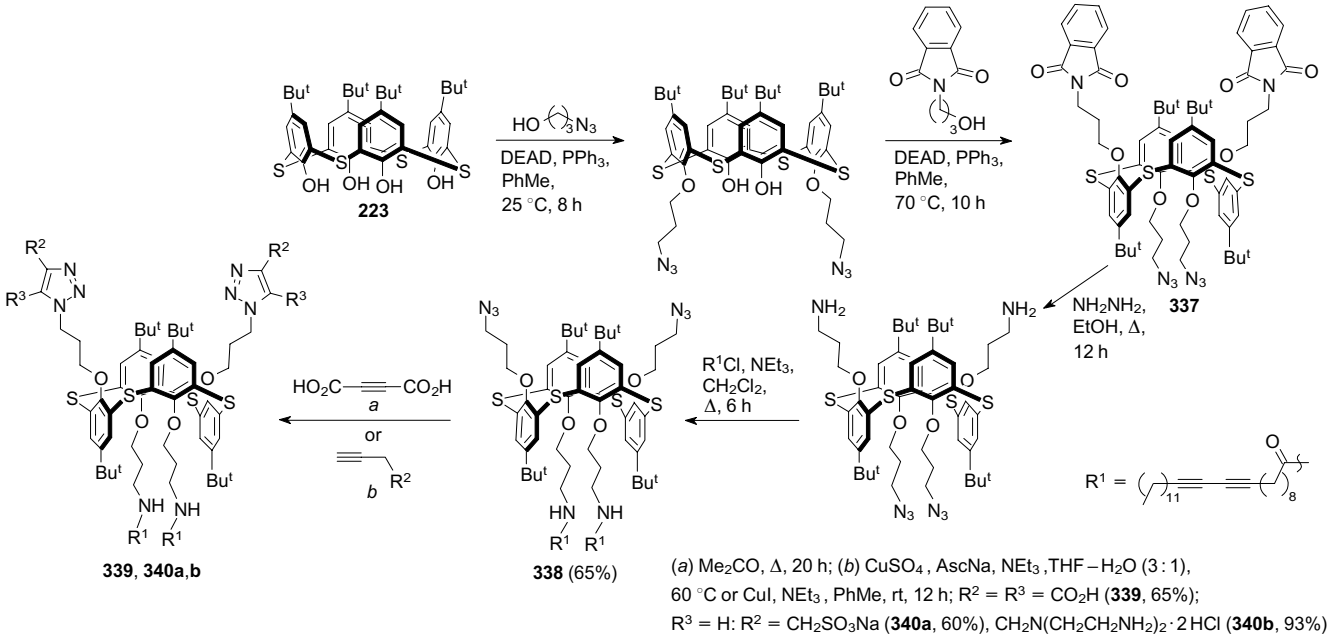
It was shown that embedding of macrocycles **339** and **340a** into vesicles formed by pentacosa-10,12-diynoic acid led to stable submicron-sized particles having a diameter of ~300 nm.[522] An increase in the content of calixarene in the vesicles caused a slight decrease in the polymerization degree of diynoic acid; however, the addition of calixarene promoted the appearance of a colorimetric response of photopolymerized vesicles to lanthanide ions with a detection limit of down to 8 mmol L^{-1}. The colorimetric

Scheme 59



R = Bu^n (**330**, 93%; **332**, 92%; **334**, 88%), n-C_8H_{17} (**331**, 86%; **333**, 92%; **335**, 86%), n-$C_{14}H_{29}$ (**336**, 92%)

Scheme 60



(*a*) Me_2CO, Δ, 20 h; (*b*) $CuSO_4$, AscNa, NEt_3, THF – H_2O (3 : 1), 60 °C or CuI, NEt_3, PhMe, rt, 12 h; $R^2 = R^3 = CO_2H$ (**339**, 65%); R^3 = H: $R^2 = CH_2SO_3Na$ (**340a**, 60%), $CH_2N(CH_2CH_2NH_2)_2 \cdot 2HCl$ (**340b**, 93%)

response of a series of lanthanides is dependent of the ionic radius, with the highest response being found for the La^{III} ion.

Macrocycle **340b** proved to be capable of forming submicron-sized particles with a 200 nm size and surface potential of +43 mV.[523] With the use of ethidium bromide, it was found that this compound intercalates into the calf thymus DNA to give a lipoplex with a surface potential of −30 mV. Macrocycle **340b** was used to synthesize mixed polydiacetylene species with *N*-(2-aminoethyl)pentacosa-10,12-diynamide (Fig. 93). These species responded to DNA, which was visible to the naked eye at 20 mol L^{-1} concentration of the calf thymus DNA.

As noted above, thiacalix[4]arene-containing dibromides **310a** – **i** are versatile precursors to obtain amphiphilic macrocycles due to the possibility of not only replacement of the bromine atom with the azide group and subjecting the latter to click reactions but also the direct alkylation of *N*-heterocycles. Some of these bromines were reacted with amines [triethylamine, *N*-methylmorpholine (NMM)] and nitrogen-containing heterocycles such as pyridine (Py) and *N*-methylimidazole (NMI) to give products **341** – **348** (Scheme 61).[524]

It turned out that steric hindrance caused by bulky *tert*-butyl substituents hampers the reaction of simple tertiary amines, whilst planar heterocycles afforded the expected products in high yields. Elongation of the linker between the bromine atom and the macrocycle decreased the steric hindrance, thereby enabling the reaction with *N*-methylmorpholine.

Having this procedure in hand, Burilov *et al.*[525] prepared a series of (benz)imidazolium salts of calixarenes **344**, **346**, **348** – **355** with various substituents at the heterocyclic nitrogen atom (Scheme 62, Table 6).

Heating these salts with palladium acetate in dioxane gave rise to a series of bis(*N*-heterocyclic) (NHC) chelate complexes **356** – **365**. The structure of these complexes was established by the X-ray diffraction analysis, which confirmed the *trans* arrangement of ligands relative to the

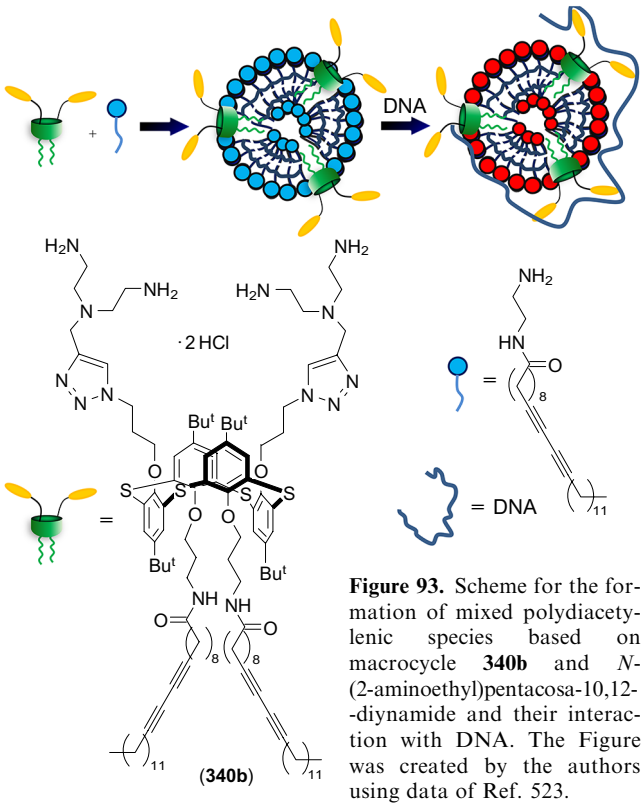
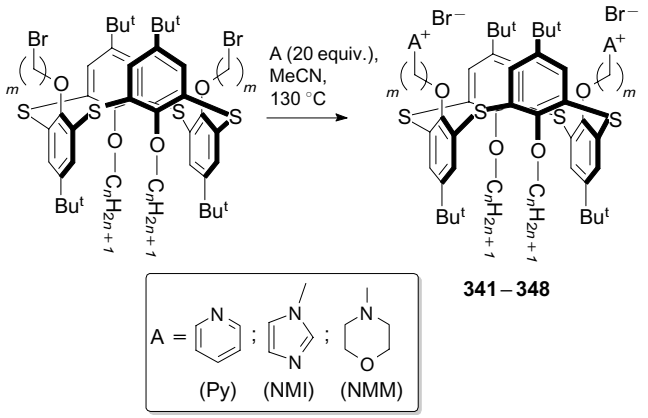


Figure 93. Scheme for the formation of mixed polydiacetylenic species based on macrocycle **340b** and *N*-(2-aminoethyl)pentacosa-10,12-diynamide and their interaction with DNA. The Figure was created by the authors using data of Ref. 523.

palladium ion. The catalytic activity of the obtained Pd^{II} – NHC complexes in the Suzuki – Miyaura cross-coupling reaction involving aryl halides and phenylboronic acid was studied. A twofold increase in the conversion of 4-bromoanisole was observed when moving from pure DMF to a water – DMF (3 : 1) mixture due to the combination of micellar and transition metal catalysis. The resulting NHC complexes demonstrated high activity in a model reaction of *p*-nitrophenol hydrogenation with sodium bor-

Scheme 61



Compound	Nucleophile (A)	n	m	Time, h	Yield (%)
341	Py	4	3	37	88
342	NMI	4	3	34	87
343	Py	4	4	12	84
344	NMI	4	4	10	85
345	NMM	4	4	45	81
346	Py	14	4	25	79
347	NMI	14	4	23	75
348	NMM	14	4	31	73

ohydride. It was established that the apparent rate constant increases by a factor of 2.5 when switching from complex **357** to a more lipophilic complex **358**, which can be explained by the additional concentration of nitrophenol in the aggregates due to the higher hydrophobic capacity.

Scheme 62

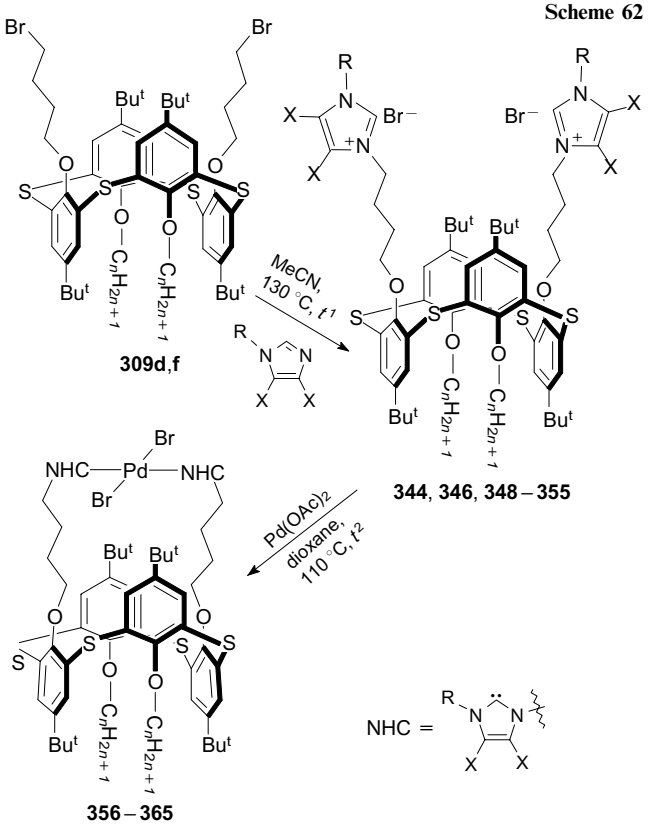


Table 6. Synthesis of (benz)imidazolium salts of thiacalix[4]arenes and palladium complexes with N-heterocyclic ligands (see Scheme 62).

Compounds	*n*	R	t^1, h	Yield of the salt (%)	t^2, h	Yield of the complex (%)
344, **356**	4	Me	10	85	27	99
346, **357**	14	Me	23	75	30	86
348, **358**	4	Bu^n	27	82	28	70
349, **359**	14	Bu^n	27	70	31	84
350, **360**	4	Pr^i	27	87	48	70
351, **361**	14	Pr^i	48	70	48	67
352, **362**	4	Bu^t	50	74	50	70
353, **363**	4	Mes	50	87	38	52
354, **364**	4	2,6-$Pr^i_2C_6H_3$	50	60	60	50
355, **365**	4	Me [a]	50	50	30	50

Note. Mes (mesyl) is 2,4,6-trimethylphenyl. [a] X – X is benzo, otherwise X = H.

Thus, the material presented above demonstrates that the scope of applicability of amphiphilic macrocycles is indeed enormous, and the amphiphilic calix[*n*]arenes *per se* fully correspond to the felicitous definition of Shinkai *et al.*,[449] since they have host – guest sites of molecular recognition. Nevertheless, the synthesis of amphiphilic macrocycles decorated with anionic and cationic head groups is accomplished by quite different synthetic procedures, which are often multistep and require the use of starting macrocycles with various functionalities. In this regard, the click chemistry approach, which involves the modular design of the target molecule from single building blocks prepared in advance, opens up great opportunities for the rapid variation of polar groups and hydrophobic moieties. In this way, by changing the configuration of the macrocyclic platform, one can directly affect the geometry of the resulting amphiphile.

3.2. Self-assembly of supramolecular and hybrid systems at the interface

A promising area of research in supramolecular chemistry is the design of molecular devices, defined as structurally organized and functionally integrated chemical systems. Components and the devices that they constitute perform their functions at molecular and supramolecular levels. These devices containing supramolecules or assemblies are generally used as functional layers and coatings deposited on to a solid substrate. Currently, 2D systems are extensively studied in order to elucidate the factors that control the supramolecular 2D ordering, which finally should provide a more stringent control of the self-assembly and allow the application of new functional molecules and particles for the design of complex smart devices.

Supramolecular chemistry of surface systems significantly differs from traditional supramolecular chemistry dealing primarily with the assembly of aggregates in solutions and crystal engineering.[526] The surface-based self-assembly can occur *via* both physical adsorption and chemisorption of molecules. The self-organization at the interface results in 2D structures organized to a certain extent. The thickness and degree of order of these structures depend on a lot of factors, such as the physical (aggregation) state and composition of the substrate, the material, the way of deposition of modifying layers, *etc*. As opposed to more common 3D systems, the manipulations with 2D

structures limit the number of possible mutual orientations of the molecules and functional groups and interactions between them. On the other hand, the substrate surface provides not only the geometric specificity of adsorption layers but also, due to interfacial interactions, the occurrence of effects, which are not typical of 3D systems. These interactions are often the key factors responsible for strong adhesion of the molecules to the substrate. If high adhesion is not required, the final result of self-assembly depends on the competition between lateral and orthogonal (interfacial) intermolecular interactions. These interactions can lead to a change in the structure of not only the film but also the surface layer of the substrate due to its reconstruction. The self-assembly process and the properties of the fabricated supramolecular systems are determined by interactions of the solvent, serving as the basis for the film formation, with the building blocks (tectons) and the substrate, thermodynamic and kinetic factors and many other parameters.

At least two assembly modes should be considered: the formation of functional films, which, together with the substrate, are an indispensable component of the manufactured devices, and the deposition of auxiliary templates, which initiate the subsequent assembly of the target supramolecular structures. The molecular assembly on the surface is used to address relevant practical issues (this approach was applied to design such devices as sensors and biochips, photovoltaic cells, fuel cells and biomimetic materials) and provides a tool for the formation of single- and multilayer supramolecular structures to study the energy and electron transfer and control surface reactions. The selection of an optimal method for the self-assembly of well-organized functional supramolecular architectures on the surface is essential for the success in addressing these challenges.

Three main approaches are currently used to fabricate thin films: the self-assembled monolayer (SAM) method, the Langmuir – Blodgett (LB) method and the layer-by-layer (LbL) assembly. This Subsection considers the principles of formation of each type of systems, areas of their application and characteristic features of molecules and substrates providing the functional potential of the resulting coatings and films.

3.2.1. Self-assembled monolayer method

In essence, self-assembled monolayers, like those prepared by the layer-by-layer assembly of films, are adsorption layers formed by adsorbate/substrate pairs with a certain combination of characteristics. In 1946, Zisman and coworkers [527] prepared ad-layers by adsorption of surfactants from solutions onto metal surfaces, which are the most similar to modern SAMs. The distinguishing feature of these films, mentioned by the authors, was their high molecular ordering achieved due to the self-assembly of amphiphilic molecules (aliphatic carboxylic acids, amines). Modern SAMs are characterized by much higher stability provided by special terminal functional groups of unsymmetrical molecules. Therefore, self-assembled monolayers are ultrathin films of one molecule thick that are self-assembled through the immersion of an appropriate solid substrate into a solution of a surfactant.

3.2.1.1. Organosilane self-assembled monolayers

Organosilane monolayers on the silicon dioxide surface (and other hydroxylated surfaces) belong to the earliest type of self-assembled monolayers. Haller [528] was the first to use alkylsilanes to fabricate films on silicon and gallium arsenide surfaces. Sagiv [529] contributed significantly to the development of research on stability of alkylsilane films.[530] The author fabricated these films by the reaction of trichloro- or trialkoxysilanes with the hydroxylated silica (SiO_2) surface.

Such films can be prepared on substrates, the surface of which contains hydroxyl groups, such as glass, aluminium, zinc oxide, indium – tin oxide (ITO), polyvinyl alcohol, mica, graphene oxide, *etc*. The properties of the films, including the chemical composition, thickness, orientation and lateral order of alkyl chains, as well as stability in an aqueous medium were characterized in the publications.[531 – 533]

An important step in the fabrication of high-quality SAMs on a silica surface is the preparation of the surface, including its cleaning and the formation of the maximum possible number of silanol active sites. As rightly pointed out in the study,[531] it is difficult to determine the precise localization of the interface between SAMs and silica. The chemical nature of the interface depends on such factors as the surface hydration and the presence of water trace in a solution of the organosilicon precursor. The silane/silica interface is schematically presented in Fig. 94. It is assumed that only 10 – 20% of the chains are bonded to the surface.

Parker *et al.*[534] noted that investigations of supramolecular interactions between SAMs attached to the planar surface and the guest distributed in the solution are important for an understanding of the behaviour of complex dynamic supramolecular systems. Photocontrolled supramolecular interactions between α-cyclodextrin and an azobenzene derivative covalently attached to a self-assembled monolayer of (3-aminopropyl)triethoxysilane were studied using an integrated optical Bragg grating sensor (Fig. 95).

Yan *et al.*[535] investigated the effect of three important characteristics of alkylsiloxane SAMs on the structural dynamics of alkyl chains using 2D infrared vibrational echo spectroscopy:

— the mode of attachment of the alkyl chain to the amorphous silica surface,
— the chain length,
— the packing density.

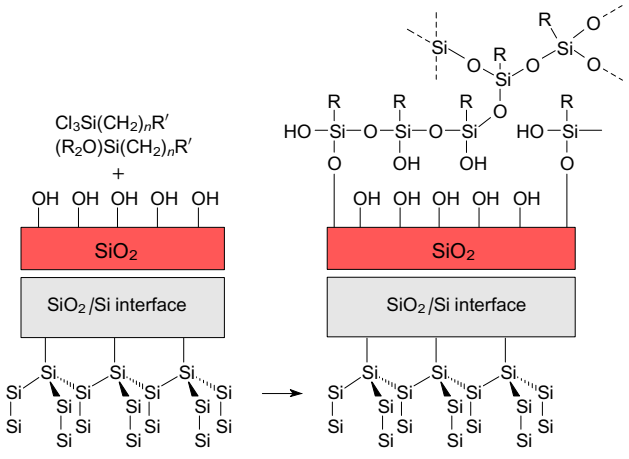


Figure 94. Schematic of the interaction between hydrocarbon chains and Si – O bonds of adjacent silanol groups as a driving force for the self-assembly of organosilane SAMs.[531] Published with the permission of Royal Society of Chemistry.

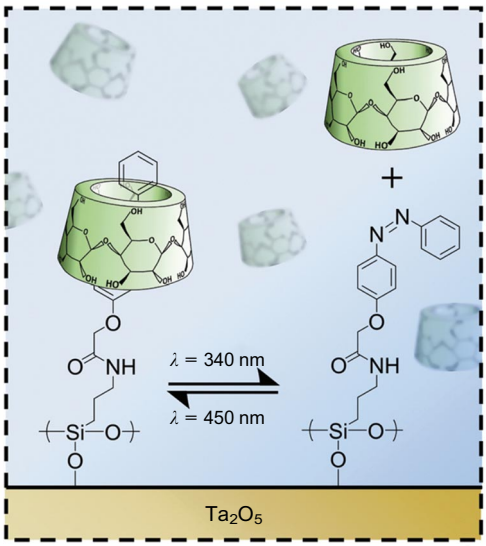


Figure 95. Schematic of the azobenzene-modified self-assembled monolayer on the surface of an integrated optical Bragg grating sensor. The formation of the guest–host inclusion complex between azobenzene attached to the surface and an aqueous solution of α-cyclodextrin is dynamically triggered through photoisomerization of the azobenzene moiety.[534] Published with the permission of Royal Society of Chemistry.

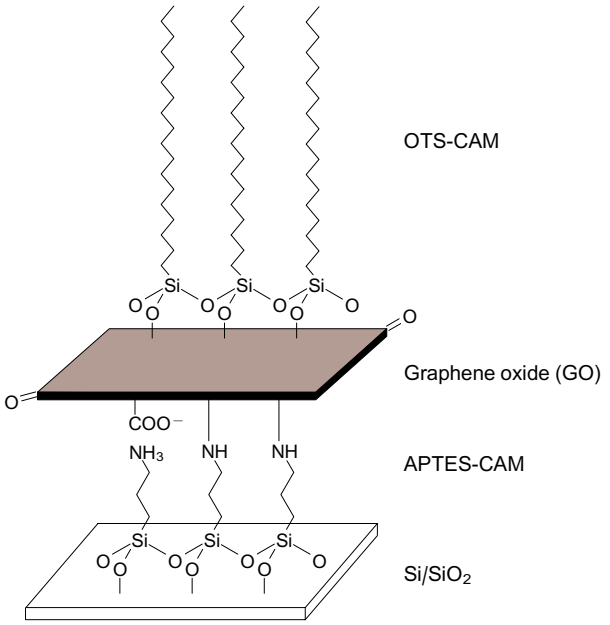


Figure 96. Schematic illustration of an APTES/GO/OTS three-layer film on a Si wafer.[536] Published with the permission of American Chemical Society.

Alkylsiloxane monolayers on the SiO_2 surface were formed using two procedures. In one case, dialkylmonochlorosilane was utilized to fabricate monolayers, in which independent chains were directly linked to the silica surface *via* a single bond. In another case, trichlorosilane served as the precursor to form a network of siloxane bonds. To study the effect of the alkyl chain length, the authors used alkylsilanes containing three, four and eleven CH_2 groups. Finally, the chain density (φ) was varied by preparing samples ranging from ~15% to the maximum coverage (100%). It was found that the manner of attachment of the chains to the substrate has no significant effect on the structure of alkylsilane monolayers on the silica surface. The investigation of the dependence of the chain dynamics on the distance to the substrate showed that motions of the chains near the substrate are significantly slower than those further away and that the structural fluctuations for sufficiently long chains are little sensitive to the chain length. For SAMs containing 11 CH_2 groups, the reduction from full coverage (φ = 100%) to 50% has an insignificant effect on the structural dynamics of the monolayer. However, for the 25% and 15% coverage, the dynamic characteristics of SAMs radically changed. Thus, a single-exponential time dependence is observed for 100% coverage, whereas two regions exist for substrates with φ = 25 and 15%. One of them corresponds to a fast process with a time constant much smaller than that for the monolayer with 100% chain density, while another one corresponds to an exceptionally slow process, the time constant of which cannot be measured in the experimental time window determined by the vibrational lifetime. It was suggested that the observed changes in the chain dynamics for monolayers with a low chain density are due to the collapse and entanglement of alkyl chains.

Ou *et al.*[536] used the condensation between Si–OH bonds of hydroxylated octadecyltrichlorosilane (OTS) and C–OH bonds on the graphene oxide (GO) surface to graft OTS onto the GO-based dual-layer film, which was composed of a GO outerlayer and a (3-aminopropyl)triethoxysilane (APTES) self-assembled underlayer, on a Si substrate (Fig. 96). It was shown that this three-layer film exhibits much better tribological behaviour compared with APTES — GO- or APTES — stearic acid-based films, which have been studied previously ‡ as lubricant films in nano- or microelectromechanical systems (NEMS or MEMS, respectively).

3.2.1.2. Self-assembled monolayers based on sulfur-containing compounds

The second type of SAMs is based on sulfur-containing compounds, most often alkanethiols. These systems were first proposed by Nuzzo and Allara[537] in 1983. They prepared ordered dialkyl disulfide monolayers on gold surfaces. Once the fundamental issues concerning the substrate/S-sublayer interface have been mainly addressed, a new era of the assembly of complex systems using supramolecular chemistry methods has begun.

Depending on the destination, SAMs can contain hydrocarbon chains of different lengths. It is assumed that in the case of saturation of all adsorption sites on the surface, which provides rather dense initial structure of the film, weak van-der-Waals forces between the chains result in the 2D crystallization of alkyl groups. It should be noted that a small number of CH_2 groups ($n < 9$) does not ensure a sufficient integrated force for stabilization of a two-dimensional quasicrystal. At $n > 24$, there is a higher probability of preparing 2D crystals with an excessive number of defects. Molecules containing from 9 to 24 methylene groups are optimal for the assembly of ordered structures. Along with supramolecular interactions, the molecular mobility plays an important role in the formation of surface

‡ See J.Ou, J.Wang, S. Liu, B.Mu, J.Ren, H.Wang, S.Yang. *Langmuir*, 26, 15830 (2010).

crystals. Thus, the molecules should have sufficient time for terminal thiolate groups to occupy proper sites in the dense packing on the surface and for alkyl chains to form a quasicrystal.[538]

A high degree of SAM organization, provided by supramolecular interactions, is essential also for topochemical reactions on the surface of films containing terminal functional groups [539] and for self-healing mechanisms.[540]

Ermakova *et al.*[541] reported the fabrication of a responsive layer of a chemical sensor based on surface plasmon resonance (SPR sensor). The authors prepared a SAM1/LBF-C12 bilayer film consisting of a rarefied self-assembled monolayer (SAM1) of octanethiol on a gold substrate topped with a Langmuir – Blodgett monolayer of the amphiphilic ligand 1,8-diaminoanthraquinone modified by two [(acetylamino)methyl]diethoxyphosphoryl groups and two dodecyloxy groups (LBF-C12, where LBF is a Langmuir – Blodgett film). In each step of the formation of the SAM1/LBF-C12 bilayer, the transfer of monolayers to the gold substrate was controlled by cyclic voltammetry and electrochemical impedance spectroscopy. The electrochemical data are indicative of the formation of a dense nanostructured defect-free film, which restricts the access of the electrolyte to the surface of the gold electrode. These SPR sensors can selectively detect and determine mercury cations in aqueous solutions at concentrations down to 10^{-11} mol L^{-1} inclusive. High stability of the responsive bilayer allows its use for at least five times without loss of analytical performance.

The application of SAMs makes it possible not only to significantly increase the activity of conventional catalysts but also to gain a deeper insight into the mechanisms of catalytic processes using monolayers with a certain architecture.[542] Schoenbaum *et al.*[543] used SAMs on platinum and palladium surfaces to create a more favourable surface environment, providing the specific pathway of the heterogeneous catalytic reaction. The data obtained for SAMs with different surface densities showed that the hydrogenation of furfural affords target products primarily at the edges and steps of surface inhomogeneities, whereas undesirable products are formed on terraces. An increase in the density of alkanethiolate SAMs restricts the access to active sites located on terraces of catalysts, while leaving the access to the sites at particle edges and steps largely unaffected.

Another route for controlling the catalytic activity is based on the tuning of the structural and chemical parameters of the tail moiety of the thiol molecule in order to position reactant molecules in a desired orientation. This approach was applied for the catalytic hydrogenation of cinnamaldehyde containing an aromatic phenyl moiety. The use of a phenyl-containing thiol with a sufficiently long tether group made it possible to achieve >90% selectivity towards the reaction of the aldehyde group. On the contrary, the utilization of a modifier, in which the phenyl moiety was closer to the catalyst surface increased the selectivity towards the hydrogenation of the C=C double bond due to the reorientation of the molecule to form a face-on structure. It was also demonstrated that SAMs facilitate the hydrogenation of polyunsaturated fatty acids giving monounsaturated fatty acids but inhibit further hydrogenation to completely saturated acids due to the formation of a sterically hindered kink shape.

In recent years, supramolecular chemistry and nanochemistry have shown increasing interest in biological molecules, such as proteins, peptides and nucleic acids as building blocks in the design and construction of materials, the structural features of which allow their use to address challenging functional issues to. The tendency of these molecules to undergo self-assembly leads to a great diversity of nanoscale functional structures. Due to the development of supramolecular chemistry methods, an insight was gained into the principles of the control of assembly of such complex molecules to functional structures. Protein monomers are assembled through oligomerization to form systems of different scales and complexity, such as viral capsids, filaments and regulatory complexes. Owing to the structural diversity, these proteins are attractive candidates as building scaffolds.[544]

An example is the enzyme peroxiredoxin with antioxidant properties (Fig. 97). The proteins of this family are prone to undergo self-assembly to form a wide range of well-ordered quaternary structures, ranging from dimers and toroids to stacks and tubes, catenanes and (under certain conditions) cages.[545]

Domigan *et al.*[545] used SAMs for the adsorption of different structures of human peroxiredoxin III (HsPrx3-6His) onto gold substrates. Two types of SAMs were prepared. For this purpose, the gold surface was modified with 4-mercaptobenzoic acid (4-MBA) or the nitrilotriacetic acid (NTA) – thiol (SH) system conjugated to Ni^{2+} ions. In the former case (Fig. 98 *a*), the protein is covalently bound to the surface *via* interactions between carboxyl groups of the modifier and amino groups of the protein in the presence of 1-(3-dimethylaminopropyl)-3-ethylcarbodiimide (EDC) and *N*-hydroxysuccinimide (NHS) mediating the amide bond formation. In the latter case, histidine residues form chelates with nickel cations located on the outer side of SAMs (see Fig. 98 *b*).

Therefore, self-assembled monolayers, provided by supramolecular chemistry, immobilized on substrates are widely used as thin-film coatings in various areas of science and technique, ranging from surface templating, corrosion inhibition, sensorics and catalysis to bioengineering. Self-assembled monolayers have a great potential in nanoscale optical and electronic devices. The stability of SAMs and their functional potential are increased by means of constructing special molecules, which exhibit strong adhesion

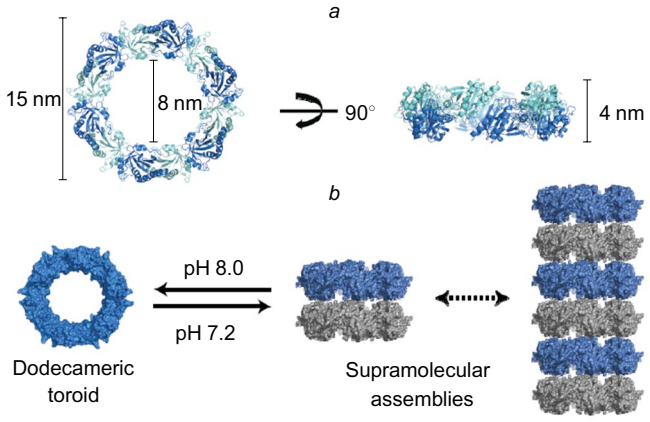


Figure 97. The pH-triggered assembly of the protein in solution: the structure of the dodecameric protein HsPrx3-6His (see the text) formed by the monomers highlighted in alternate colours (blue and teal) (*a*) and the self-association of HsPrx3-6His existing as a dodecameric torroid at pH 8.0 to form stacked toroids at pH 7.2 (*b*).[545] Published with the permission of AIP Publishing.

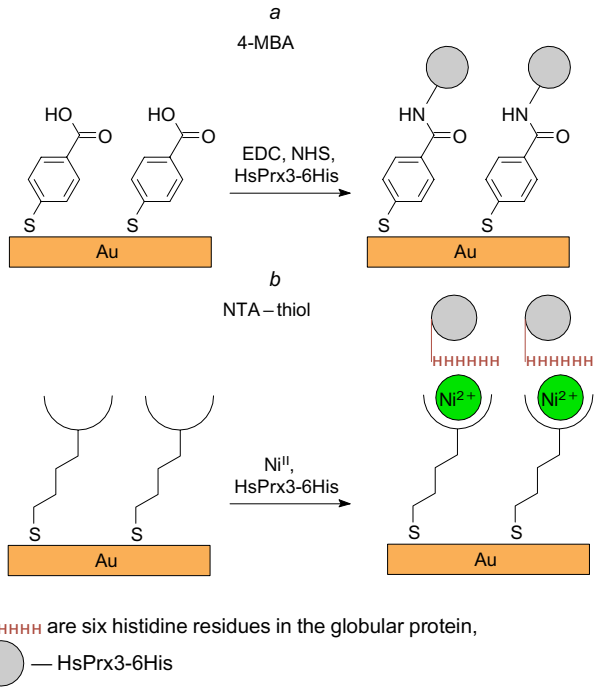


Figure 98. Schematic illustration showing two modes of SAM formation on Au surfaces for the binding of the protein HsPrx3-6His (for more detail see the text).[545] Published with the permission of AIP Publishing.

(in particular, multidenticity) to substrates and contain peripheral groups capable of undergoing controlled structural and chemical transformations.

3.2.2. Langmuir – Blodgett method

The history of the development of the Langmuir – Blodgett method dates back to 1774, when Benjamin Franklin published a prominent paper.§ In this paper, he described an experiment performed in 1765 on the surface of the Mount Pond at Clapham Common, London, resulting in stilling of waves over a large area by means of a small volume of oil. This was the first description of a surface chemistry experiment. More than a century later, lord Rayleigh repeated Franklin's experiment, calculated the film thickness and evaluated the size of oil molecules (~2 nm). Agnes Pockels made a great contribution to the development of tools to study oil films on water. At the end of the 19th – beginning of the 20th century, she was the first to devise a surface balance and used it to measure pressure – area isotherms.

Outstanding contributions of Irving Langmuir to theoretical and experimental fundamentals led to the birth of this interesting area of research. In his famous work 'The Constitution and Fundamental Properties of Solids and Liquids' published in 1917, Langmuir described a balance for determining the surface tension, currently known as 'Langmuir surface balance', and demonstrated the application of this device to determine the size and shape of molecules and their orientation on the surface in different two-dimensional phase states. In 1932, Langmuir was awarded a Nobel Prize for his discoveries and investigations in surface chemistry. Monomolecular films of insoluble amphiphilic substances on liquid surfaces are called Langmuir films. In 1919, Langmuir reported on the transfer of a monomolecular film of fatty acid from the water surface to a solid substrate (the vertical deposition method). In conclusion to the paper, Langmuir expressed appreciation to Katherine Blodgett for help in experiments. In 1934, Blodgett published a paper showing that multilayer films can be built up by repeated dipping of a plate in and out of a monolayer-covered liquid. These multilayer films are called Langmuir – Blodgett films. Vincent Joseph Schaefer, an apprentice of Langmuir, proposed another method for the transfer of films onto a solid substrate from the liquid surface (the horizontal deposition method). Langmuir and Schaefer applied this method for the first time to prepare protein films.[546]

The Langmuir – Blodgett technique is a synergistic combination of two powerful techniques of surface chemistry — the Langmuir monolayer technique and the Langmuir – Blodgett (Schaefer) film technique. The Langmuir monolayer technique at the air/water interface (Langmuir film technique) can not only be used to pre-organize molecules for their subsequent transfer as monolayers onto solid substrates but also serves as a tool for investigating and controlling the structure and properties of monolayers. Apart from conventional techniques such as Langmuir surface balance, surface potential methods, Brewster angle microscopy and rheology, state-of-the-art tools for studying monolayers on the liquid surface include optical spectroscopic methods and X-ray diffraction with synchrotron radiation.[547 – 549] Methodological possibilities are significantly expanded in studies of LB films on solid substrates.

The monolayer technique is a unique tool for investigating the supramolecular assembly because the air/water interface provides an experimental situation strictly specified with respect to the energy and geometry, thereby allowing one to consider individual steps of the self-assembly of 2D systems. Currently, systematic studies of monolayers at the air/water interface are commonly carried out in relation to characterization and rational design of target molecular structures capable by themselves of performing certain functions in particular devices. Langmuir monolayers are successfully employed as model structures to investigate physicochemical properties of ordered 2D structures, in particular vitally important bilayer membranes.[550 – 552]

Taking into account the importance and prospects of the use of 2D colloidal systems containing metal nanoparticles, quantum dots, 2D layered materials of different nature or their mixed monolayers bearing functional molecules, it is particularly relevant that the monolayer technique can be used not only to study interactions between molecules (particles) at precisely controlled distances from each other and in a strictly set mutual orientation but also to perform the synthesis (assembly) of such low-dimensional hybrid structures. The possibility of performing chemical reactions in a limited volume, under anisotropic conditions or involving molecules fixed in a specially chosen template allows the preparation of unique materials and the functional modeling of complex supramolecular and biological systems.

The second component of the LB methodology is the Langmuir – Blodgett (Schaefer) film technique. Langmuir – Blodgett films are ordered single- or multilayer molecular structures fabricated *via* successive transfer of monolayers

§ For the history of the discovery, see R.F.De Oliveira, A.De Barros, M.Ferreira. In *Nanostructures*. (Amsterdam: William Andrew Publishing, Elsevier, 2017). P. 105.

of insoluble compounds from the air/liquid subphase interface to solid substrates. These films are used in different areas of science and technique, such as electronics, optics, applied chemistry, micromechanics, biology, medicine, *etc.*[553]

The LB method has found broad applicability in recent years because it allows researchers to study relevant issues and address challenges using new compounds and to employ new and known molecules and particles for the design of desired functional systems.

An important problem is to control the alignment of liquid crystals on transparent conducting substrates (most often, on ITO-coated glass plates). Choudhary *et al.*[554] addressed this issue using the LB method and a new type of surfactants, bent-shaped liquid-crystal (LC) molecules or bent-core liquid crystals (BCLCs). Langmuir monolayers, serving as precursors of orienting sublayers, were fabricated from asymmetrically nitro-substituted BCLC molecules containing 12 (BN1) or 18 (BN2) carbon atoms in the aliphatic chain (Fig. 99).

Studies by atomic force microscopy (AFM) and X-ray diffraction demonstrated that the vertical transfer of BN2 molecules onto a glass substrate resulted in the formation of a partial bilayer film with defects, on which nematic liquid-crystal (E-7) molecules are in a planar orientation. This orientation of LCs occurs at all surface pressures for BN2 transfer (from 2 to 20 mN m^{-1}). Monolayers of BN1 transferred at low surface pressures form defect-rich structures on solid substrates and induce a planar orientation of E-7. These monolayers transferred at high surface pressures form uniform monolayers, supporting a homeotropic orientation of the nematic LC (Fig. 100).

It is worth noting that this type of amphiphiles[555] and a new class of compounds, supra-amphiphiles[556, 557] have attracted extensive attention due to the prospects of their use for the preparation of supramolecular systems.

It is known that the limitation of the degrees of freedom of light-sensitive dyes can significantly affect both the formation of an excited state and its major relaxation pathway.[558] Hence, the optical characteristics of the system can be efficiently modulated by changing the packing of the dye molecules to form well-organized 2D films. The characteristic features of light absorption, conversion and emission in well-organized 2D systems and the role of aggregation of the molecules at the interface in these processes are considered in detail in a review.[559] The possibility of controlling the optical and receptor properties

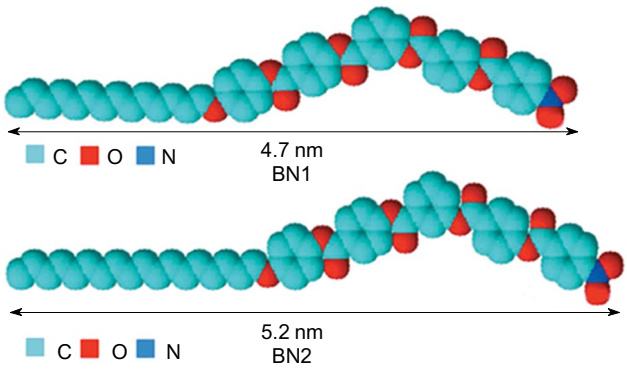


Figure 99. The 3D space-filled model for the BCLC molecules BN1 and BN2.[554] Published with the permission of Taylor and Francis.

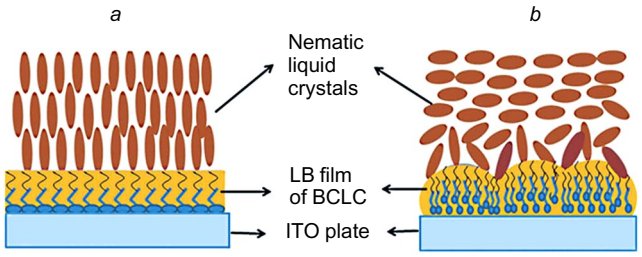


Figure 100. Schematic representation of the homeotropic (*a*) and planar (*b*) alignment of liquid crystals on Langmuir – Blodgett films of BCLCs deposited onto an ITO substrate.[554] Published with the permission of Taylor and Francis.

of LBFs through structural pre-organization of a monolayer was convincingly demonstrated in publications.[560 – 563]

The structural organization of the monolayer, the type and degree of its aggregation significantly affect also the electrophysical properties of ultrathin films fabricated from the monolayer. This effect is due to the dependence of cooperative properties of molecular conductors on intermolecular interactions, which are determined by the mutual arrangement of the molecules in 2D systems.[564 – 567]

Capabilities of the LB method, which can provide an exact ratio of components in mixed monolayers and their adsorption on a solid substrate at a particular distance from the surface determined by inert layers, are traditionally used to perform elegant studies on non-radiative transfer of excitation energy.[568 – 570]

The rapid development of physical methods of investigation of nanoscale structures made it possible to study the non-radiative energy transfer in planar systems with separated donor and acceptor monolayers at very small (down to 2 Å) distances between the components. The behaviour of such systems significantly differs from that predicted by the classical Förster theory, which describes the dependence of the efficiency of non-radiative energy transfer on the distance. It was demonstrated[571, 572] that the efficiency of light energy transfer can be controlled both in a mixed monolayer and multilayer LBFs with different structures. The authors found for the first time that the dependence of the efficiency of non-radiative energy transfer in a multilayer film with separated donor and acceptor layers on the thickness of the spacer layer has an extreme character. The most efficient energy transfer is observed in the case of a non-zero thickness of the layer separating the donor and acceptor monolayers.

Dexter[573] was the first to give an idea of silicon photosensitization using ultrathin films, suggesting that the generation of electron – hole pairs in silicon can occur *via* energy transfer from excited dye molecules deposited on the silicon surface. Light-absorbing organic layers combined with thin silicon semiconductor layers (< 1 μm) are of interest for the fabrication of solar cells due to possibility of decreasing the amount of the required semiconductor material by two orders of magnitude. The control of molecular organization and intermolecular distances is a key factor in the development of these structures. In order to achieve high efficiency of excitation energy transfer, it is essential to exclude non-radiative dissipative (quenching) side processes.

To address this issue, Fang *et al.*[574] deposited mixed Langmuir – Blodgett monolayers of the carbocyanine dye (3,3′-dioctadecyloxacarbocyanine perchlorate, DiO) and

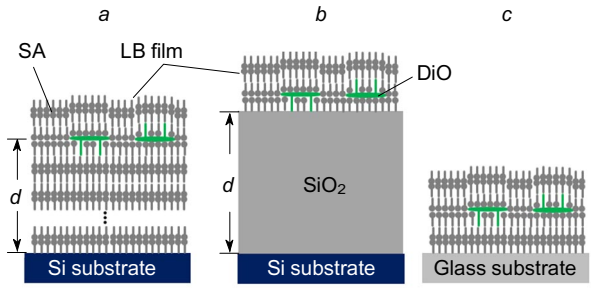


Figure 101. Langmuir – Blodgett films of mixed monolayers of the dye and stearic acid deposited onto silicon substrates with stearic acid (*a*) and silicon dioxide spacer layers (*b*) and onto the control glass substrate (*c*).[574] Published with the permission of Taylor and Francis.

stearic acid (SA) onto glass (control) and silicon substrates (Fig. 101). The spacer layers were made of pure stearic acid (LB transfer) or silicon dioxide films deposited by plasma-enhanced chemical vapour deposition. For the control glass substrate, the ratio of DiO and SA molecules in the layer was varied from 1 : 1000 to 1 : 1 in order to study the effect of this ratio on the energy transfer between the resulting particles. Monomer emission was observed at low mixing ratios of DiO and SA (at low concentrations of the dye). At high concentrations, the emission spectrum shows two broad bands assigned to two types of aggregates (dimers and higher aggregates), the excitation energy transfer from the dimers to aggregates being the major process.

In the case of silicon substrates, the SA monolayer mixed with the dye was separated from the semiconductor surface by a SA monolayer with a thickness (*d*) of up to 80 nm or a silicon dioxide monolayer (*d* up to 350 nm).

It was found that the fluorescence lifetime of the dye monolayer is significantly shortened when it is deposited close to the silicon surface, which is indicative of efficient energy transfer. The dissipation of the excitation energy of chromophore molecules deposited on the silicon surface is explained in terms of the classical Chance – Prock – Silbey theory[¶] developed for metals. This approach satisfactorily describes the behaviour of the system for the distances larger than 50 nm (far field). However, the theory does not work for small thicknesses of spacer layers (near field). At a close distance from the silicon surface, this model gives the lifetime (τ_d) as proportional to the cubic distance *d* with the constant of proportionality determined by the imaginary part of the dielectric permeability.

Danos *et al.*[575] also studied the efficiency of silicon photosensitization using dye monolayers and varying the distance to the substrate surface. The perylene derivative, bis(n-decylimido)perylene (PTCD-C10), was examined as a photosensitizer. The supramolecular assembly of a mixed monolayer of PTCD-C10 and SA, which was separated from the Si(111) surface by pure SA monolayers, was performed by the LB technique. Close distances between the photosensitizer and the silicon surface were kept through grafting of PTCD-C10 to the Si(111) surface functionalized with vinyl and allyl groups. Studies by steady-state and time-resolved fluorescence and confocal microscopy showed that the energy transfer efficiency was up to 90% for distances less than 1 nm. It was noted that the Förster resonance energy transfer (FRET) theory adequately described interactions between the dye and silicon at distances of < 5 nm, for which the estimated Förster radius was 2.5 nm (an inverse cubic dependence of the transfer rate constant on the distance). For the distances in the range from 10 to 50 nm, it is necessary to take into account other processes, in particular photon tunneling.

The Langmuir – Blodgett technique made it possible to discover and investigate an interesting phenomenon — the two-dimensional redox isomerization that is induced by molecular reorientation at the interface and controlled by the surface pressure in the monolayer. In the studies,[576 – 578] the authors fabricated ultrathin films of donor-substituted cerium ($Ce^{3+/4+}$) and europium ($Eu^{2+/3+}$) bis(phthalocyanine) complexes in a required redox isomeric state, which affects all physicochemical properties of LBFs.

In recent years, researchers engaged in chemistry and physics of supramolecular systems have focused on the design of hybrid materials.[579, 580] Hybrid materials (hybrids) are heterogeneous systems composed of several components of different kinds and classes (most often organic and inorganic) with a specific structure, giving rise to useful properties not inherent in the starting compounds. Apart from the chemical composition of the components and interactions at interfaces, the internal architecture of the hybrid plays an important role in the properties. This architecture can be considered as an additional degree of freedom used for the tuning of the functional properties of the material. Generally, such hybrid materials are not found in nature but are fabricated artificially. Many supramolecular systems, in particular metal complexes, belong to hybrid materials.[581]

Organic – inorganic hybrid materials can not only combine useful properties of both organic and inorganic components but also generate new properties and functionalities. In the past decades, various types of functional organic-inorganic hybrid structures were developed, characterized and tested. These structures showed promise in the design of materials and devices, thin-film architectures being of great importance due to their wide application. When assembling hybrid thin films, particular attention is given to the control of their structure, the distance between different layers and their total thickness. The Langmuir – Blodgett method is one of the most efficient tool for the fabrication of ordered hybrids.

Hybrid systems based on 2D materials, such as graphene, hexagonal boron nitride (hBN) and transition metal dichalcogenides (MoS_2, WS_2, *etc.*[582 – 584]), have attracted great attention in the past decade. The supramolecular organization in these systems can significantly differ from that in organic thin-film structures deposited onto conventional solid substrates. This allows the fabrication of hybrids with new properties, which appear only due to the unique characteristics of 2D materials. Graphene stands out among these materials. It possesses unique properties, such as transparency, high charge mobility, thermal conductivity and mechanical strength. Graphene is regarded as a promising candidate for transparent conducting electrodes, transistors, hydrogen storage devices, gas sensors, *etc.*

Thin-film structures composed of alternating layers of graphene nanoflakes (or nanoflakes of graphene derivatives) and an organic component are fabricated using the LB technique.[585, 586] Unlike polymer composites filled with graphene or its derivatives, in which graphene particles are randomly distributed in polymer templates, layered struc-

[¶] See R.Chance, A.Prock, R.Silbey. In *Advances in Chemical Physics*. Vol. 37. (Eds I.Prigogine, S.A.Rice).) (New York: Wiley, 1978). P. 1

tures consist of alternating layers of the polymer and carbon material nanoflakes. Graphene hybrids are utilized as membranes and thin films in photoelectric devices. These architectures were made from graphene oxide films, which were deposited by the Langmuir–Blodgett method onto films of polyelectrolytes [poly(allylamine hydrochloride) (PAH) and poly(sodium 4-styrenesulfonate) (PSS)] fabricated *via* layer-by-layer assembly (Fig. 102).[584] Micromechanical measurements demonstrated an increase in the elastic modulus by an order of magnitude, from 1.5 GPa for membranes without a graphene oxide layer to 20 GPa for 8 vol.% GO-encapsulated membranes (generally, graphene composites contain at least 50% of this filler). These reinforced nanocomposite films with a thickness of only 50 nm can be freely, without destruction, suspended over large (up to a centimetre) apertures and sustain large mechanical deformations.

To fabricate supramolecular coatings acting as templates, it is necessary to solve many problems associated primarily with the effect of interactions between the template and the substrate on the structure, stability and functional characteristics of the fabricated system. Currently, self-assembled monolayers are most commonly utilized as structure-mediating templates, which have a limited applicability.

In order to address this issue, Ermakova *et al.*[587] proposed a strategy for the design of a new type of templates consisting of two monolayers, each being functionally relevant to the neighbouring material (the substrate and the coating deposited onto the template). The fabrication of the template involves the one-step assembly of the bilayer in a Langmuir trough. For this purpose, a self-organized monolayer of functionalized porphyrin is formed on the surface of an aqueous graphene oxide solution. After the adsorption of a graphene oxide layer on a porphyrin monolayer, the bilayer is LB transferred to a solid substrate. This strategy allows the fabrication of templates on solid substrates of any nature without using self-assembled monolayers.

Interesting amphiphilic hybrid molecules were prepared[588] by click chemistry from fullerene and linear poly(ethylene oxide) (PEO) chains of different lengths: 31.6 (subscript *n*1) and 63.2 (*n*2) nm. Nanoparticles of C_{60} were linked to one end of the polymer chain (C60-PEO$_n$) and to two ends (C60-PEO$_n$-C60) (Fig. 103). Monolayers of these molecules were formed on the water surface and then transferred to solid substrates *via* the Langmuir—Blodgett method.

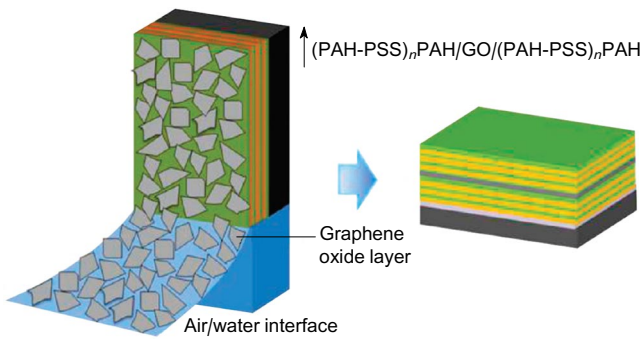


Figure 102. Schematic representation of the fabrication of the (PAH-PSS)$_n$PAH/GO/(PAH-PSS)$_n$PAH multilayer membrane.[584] Published with the permission of American Chemical Society.

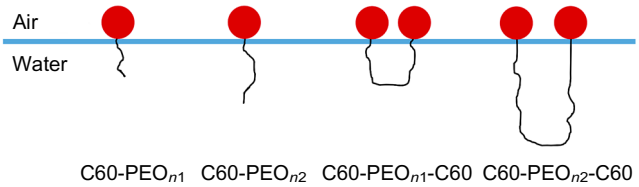


Figure 103. Schematic representation of C60-PEO$_n$ and C60-PEO$_n$-C60 monolayers with different PEO chain lengths.[588] Published with the permission of Springer Nature.

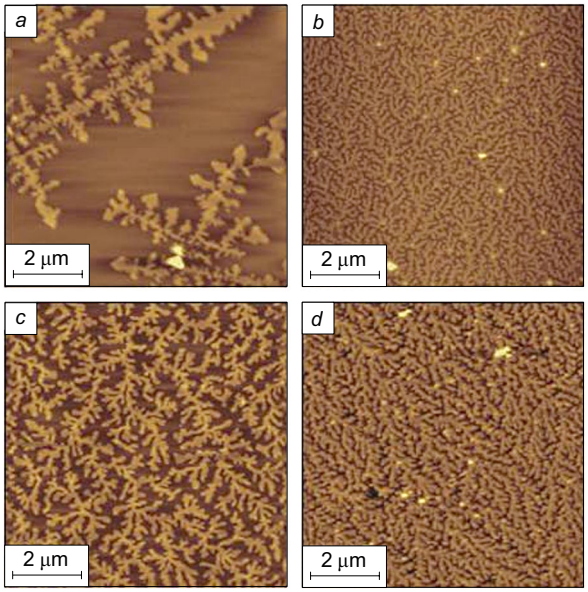


Figure 104. AFM images (8 × 8 μm) of LB films fabricated at the surface pressure of 15 mN m^{-1}: C60-PEO$_{n1}$ (*a*), C60-PEO$_{n2}$ (*b*), C60-PEO$_{n1}$-C60 (*c*) and C60-PEO$_{n2}$-C60 (*d*).[588] Published with the permission of Springer Nature.

Due to crystallization ability of PEO chains, LB films of these giant amphiphilic molecules showed fractal growth patterns (Fig. 104). The PEO chain length and the geometry of the molecules affect the fractal growth behaviour. The LB technique enables the precise control of the molecular packing on the water surface and, consequently, provides a platform for investigating the effect of the polymer chain density on the fractal growth of crystallized polymer chains at the interface.

Therefore, the LB method is an efficient tool in supramolecular chemistry. The scope of this method is extended far beyond traditional amphiphilic molecules. So far, virtually all molecules or nanoparticles have been deposited on the water surface of the Langmuir trough and, with some success, compressed and transferred to solid substrates. The advantage of this method in supramolecular chemistry is the simplicity of the determination of the receptor properties of the ligand for water-soluble substrates (analytes) introduced in the subphase. Hence, this method is of great importance for investigation of biological and medical issues.

3.2.3. Layer-by-layer assembly technique

The layer-by-layer assembly (LbL) of thin films is a universal, simple and commonly used method for the fabrication of functional supramolecular materials and devices.[589 – 593] This method is a cyclic process, in which a charged material (polyelectrolyte) is adsorbed from an aqueous solution onto a substrate and, after rinsing, an oppositely charged material is deposited on top of the first layer. This results in the formation of one bilayer with a thickness of usually a few nanometres. The process can be repeated until a multilayer film of a desired thickness is assembled. This assembly can be considered [594, 595] as a universal top – down technique (Fig. 105).

The layer-by-layer assembly technique was first proposed by Iler [597] in 1966. He deposited alternating positively and negatively charged colloidal particles from soles onto a smooth glass substrate. Based on the results of this investigation, Iler concluded that this kind of electrostatic self-assembly can be accomplished using multivalent ions, surfactants and water-soluble polymers. The assembled films were visualized using colloidal silica or polystyrene latex particles of large sizes (100 μm). This approach was described in detail for the first time by Decher,[598] who studied the electrostatic layer-by-layer self-assembly of electrolytes. He drew an important conclusion that the self-assembly can be performed using different systems, which will allow the fabrication of ordered nanoscale systems (*e.g.*, molecular machines) described by Feynman.[599, 600]

This universal approach can be applied to a wide range of materials as building components, including polymers, functional ligands, lipids, proteins, surfactants, dye molecules, nanoparticles, *etc.*, and can be used to perform the assembly on different substrates due to interactions typical of supramolecular systems, such as electrostatic, hydrogen and halogen interactions, coordination bonds, charge transfer interactions, biospecific interactions (*e.g.*, sugar – lectin), host – guest and cation – dipole interactions and their combinations.[590, 592, 601 – 603]

The removal of the substrate after the assembly of a multilayer film results in the formation of free nanostructured materials with different morphology and various functions. This approach, known as the layer-by-layer templating technique,[604] allows the fabrication of macroscopic ultrathin films, for example membranes or free micro- or nanoscale films that form hollow capsules.[605] Figure 106 presents the schematic illustration of nanostructured (supramolecular) materials fabricated *via* the layer-by-layer assembly on different templates. The central circle represents different types of templates; the medium ring, the layer-by-layer assembly (templated material); the outer circle, the results of self-assembly: free-standing films (from nonporous planar templates), nanotubes (from porous planar templates), nanoporous particles (from porous spherical templates), macroporous materials (from crystalline arrays of colloidal particles), nanotubes (from nonporous rods and fibres) and capsules (from solid spheres). Polymers, functional ligands, lipids, proteins, dye molecules and nanoparticles served as building blocks in the layer-by-layer assembly.

The enzyme immobilization in capsules and pores of metal-organic frameworks, prepared *via* layer-by-layer assembly, or on their surface significantly extended the use of enzymes due to the hundred- to thousand-fold enhancement of their stability.[607, 608] Enzymes are biological catalysts of protein nature, which accelerate chemical reactions essential for viability of organisms. Unlike chemical catalysts, enzymes exhibit much higher specificity. Thus, each

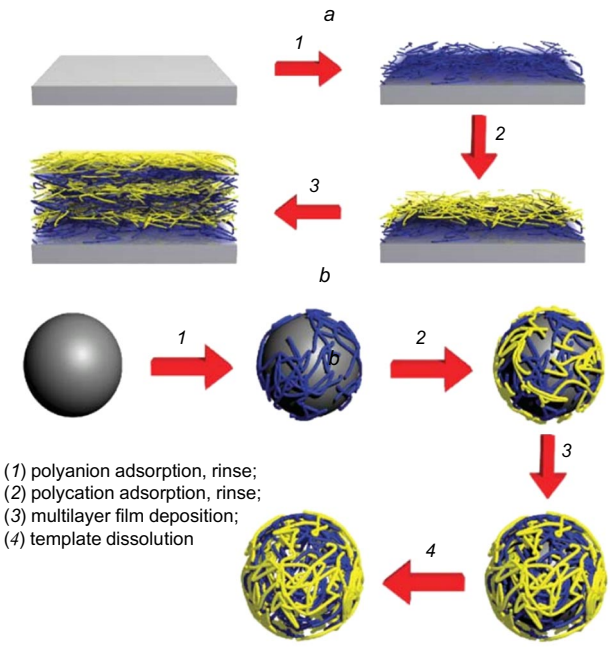


Figure 105. Layer-by-layer assembly of polyelectrolytes on planar substrates (*a*) and colloidal particles (*b*).[596] *a*: An oppositely charged polyelectrolyte is adsorbed onto a substrate with an inherent charge; after thorough rinsing, the material with a reverse charge is adsorbed onto the first layer. The process is continued until the desired thickness of the multilayer film is achieved. *b*: The core (template) is dissolved to give hollow polyelectrolyte capsules. Published with the permission of Royal Society of Chemistry.

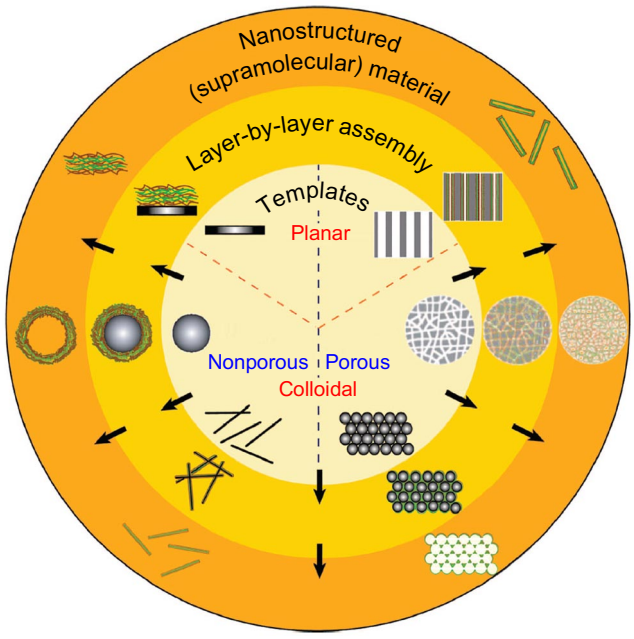


Figure 106. Schematic illustration of various nanostructured (supramolecular) materials prepared *via* the layer-by-layer templating technique (see the text).[606] Published with the permission of American Chemical Society.

enzyme catalyzes only a particular reaction or a group of reactions in the body. However, enzymes are much more sensitive to changes in the environmental conditions than chemical catalysts. In particular, enzymes function in a much narrower temperature range and are active within a definite pH range.[609] Immobilized enzymes are not only more stable but also acquire new properties, which are not typical of their free state, *e.g.*, they can function in a nonaqueous medium and exhibit activity in wider temperature and pH ranges and in the presence of heavy metal ions (Hg, Pb, Cd).

In recent years, researchers have begun to wrap up individual enzymes in single enzyme nanoparticles (SEN)[609] prepared *via* layer-by-layer assembly. By controlling the parameters of the shell, one can control the interaction of the enzyme with the environment and, consequently, its catalytic activity and access of external reactants. This elegant approach offers prospects for a significant increase in the catalytic performance and service life of enzymes under conditions intolerable for nonisolated protein molecules and also enables the switching of the activity by modulation of the outer material layer.

A glucose-sensitive multilayer film was fabricated *via* layer-by-layer assembly using positively charged star-like poly[2-(dimethylamino)ethyl methacrylate] and negatively charged insulin and glucose oxidase.[610] The unique properties of the film components and the film structure provide the switching of the response of the system for the stepwise glucose addition (insulin release only in the presence of glucose). Besides, the multilayer film continuously released a sufficient amount of insulin *in vivo* after being subcutaneously implanted in streptocozotin-induced diabetic rats and reduced the blood glucose level for at least two weeks. This system may have a considerable potential as a glucose-sensitive carrier for insulin.

Kazakova *et al.*[611] demonstrated the possibility of encapsulating enzymes (lactate oxidase, peroxidase and glucose oxidase) together with sensitive dyes to prepare capsule-based sensors with a micrometre size. Calcium carbonate nanoparticles served as the sacrificial template. The enzymes are confined to the interior of the capsule, while the fluorescent dyes [tris(4,7-diphenyl-1,10-phenanthroline)ruthenium(II) dichloride and dihydrorhodamine 123] are incorporated into multilayer shells of microcapsules of polyelectrolytes [poly(styrene sulfonate) and polyallyamine] *via* electrostatic and hydrophobic interactions with the shell material. These multicompartmentalized capsules (Fig. 107) were utilized as chemical sensors and biosensors to detect oxygen, glucose and lactate, a single capsule being able to act as a sensing element.[612] The calibration of capsule-based sensors demonstrated that millimolar concentrations of glucose and lactate are easily detected by fluorescence.

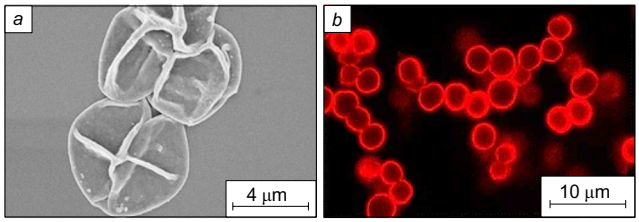


Figure 107. SEM image of capsules containing glucose oxidase (*a*) and the confocal microscopy image of capsules containing glucose oxidase and a fluorescent probe (*b*).[611] Published with the permission of Springer Nature.

Therefore, the simultaneous encapsulation of enzymes and fluorescent dyes, enabling the optical monitoring of biologically important metabolites in a single microcapsule, provides a tool for preparing unique systems to study a biological microenvironment and evaluate real-time changes in the concentration of biologically relevant compounds. Encapsulation-protected enzymes maintain sufficient activity towards the conversion of analytes, which diffuse across the semipermeable shell to the product detected by localized fluorescent dyes. The sensor should be placed at a distance of a few millimetres away from the skin in the human body, and the information is processed by optical methods. It was shown[613, 614] that capsules can be incorporated into cells in order to monitor metabolites during the cell cycle.

Electrostatically assembled films are insufficiently stable for the application under extreme conditions, such as high or low pH values and high salinity. To enhance the stability, the deposition is often followed by the chemical treatment of these films.[615, 616]

The biomimetic synthesis of nacre is an interesting example of the application of layer-by-layer assembly to fabricate layered hybrid structures.[617] Natural nacre consists of 0.5 μm-thick hexagonal-shaped aragonite tablets (crystalline calcium carbonate) with a width of 10 – 20 μm arranged in parallel layers. These inorganic layers are separated by organic matrix layers consisting of elastic biopolymers (chitin-like horn-shaped substance of protein type). The organic portion of artificial nacre was fabricated by the successive deposition of polyacrylic acid and polyvinylpyridine layers. Calcium carbonate was crystallized on the organic layer bearing receptor carboxyl groups. By carefully designing the strategy of cyclic deposition, the authors managed to prepare a structure that approximates biological nacre in both optical and mechanical properties. An investigation of the replication of nacre and the preparation of a biomimetic material are essential for an understanding of biological principles of the growth of this biomineral in nature, providing a route to the fabrication of new materials using cheap components under environmental conditions.

A considerable progress has been made in micro(nano)-capsulation. These systems have great potential in biomedicine, because they can be used for targeted drug delivery at a specified instant of time at the desired concentration.[618, 619] The capsule shell prevents the release of the cargo, making it possible to use, in particular, toxic compounds and increase the duration of drug action. The permeability of the polymer shell significantly depends on its chemical composition and thickness, the template and the chemical composition, temperature and acidity of the environment, where carriers are present. Smart shells can release their cargo in response to external stimuli.

Hammond and co-workers[620] reported the first *in vivo* application of polymer multilayer capsules built on gold nanoparticles as a core with a size of 20 nm. The authors found the key parameters responsible for stability of ten-layer capsules in the blood stream. Degradable polyelectrolytes, such as poly(L-lysine), dextran sulfate and hyaluronic acid, were utilized as components of the film. The degradation of the capsule was evaluated by measuring the concentration of poly(L-lysine) containing a fluorescent probe. It

was found that the outer layer of hyaluronic acid significantly extends the circulation time of the colloidal system. The optimization of films *via* LbL technique made it possible to fabricate stable nanoparticles for cancer applications.

Paramasivam *et al.*[621] used gold nanorods (the axial ratio varied from 3 to 16) coated with chitosane–dextran sulfate LbL multilayers. The capsules served for the immobilization of water-soluble antibacterial agents, such as ciprofloxacin hydrochloride. The efficacy of drug loading of rod-shaped capsules was 13–14% higher compared to spherical capsules. The advantages of the developed system are that it can be used for the targeted delivery of encapsulated drugs and their release in response to external stimuli and that the capsules can serve as imaging agents for near-IR biological visualization.

The assembly of ultrathin films of metal-organic frameworks, called SURMOFs (surface-mounted metal-organic frameworks), is the brightest illustration of the potential of the layer-by-layer assembly technique for the fabrication of synthetic supramolecular systems on solid substrates. These systems are extended ordered structures of nanometre thickness, perfectly oriented in the direction of the substrate. The lateral ordering of SURMOF components within a single domain may be structurally perfect, which is typical of supramolecular systems prepared by the Langmuir–Blodgett method.[622] Publications on SURMOFs are rather few in number compared to the publications on polycrystalline MOFs integrated with the solid surface. Nevertheless, SURMOF systems were fabricated based on most types of organic linkers, which are utilized for the formation of bulk MOFs derived from trimellitic, terephthalic,[623] diphenyldicarboxylic acids,[624] perylene,[625,626] porphyrins,[627] *etc*. In this field, SURMOFs based on chromophores, such as porphyrins and perylenes, and SURMOFs based on lanthanide metal clusters[628] are of particular importance due to their high practical potential for application in the catalysis, nonlinear optics, solar power and organic nano- and microelectronics.[629]

Due to high order of MOFs, resulting from an arrangement of components *via* directional coordination bonds, the LbL method was successfully adapted to the assembly of SURMOFs on different planar substrates. As applied to the fabrication of SURMOFs, this method is often called the quasiepitaxial layer-by-layer growth.[622,630,631] It allows the anchorage of the crystallographic plane of the framework that directs the growth of the latter from the substrate surface *via* layer-by-layer deposition of organic linkers and metal coordination sites (metal salts). Generally, the fabricated films are characterized by high homogeneity and low roughness.[632] The attachment of the linker to the surface limits the spatial access or reduces the reactivity of functional groups of the organic molecule. Therefore, for the subsequent formation of the coordination bond even in the first layer, the surface may significantly affect the molecular organization in SURMOFs. For a large number of SURMOF structures assembled by the epitaxial method, the observed packing of the components does not correspond to the known structures of bulk MOFs of the same composition.[633] The epitaxial layer-by-layer deposition can be applied to fabricate not only two-component highly oriented MOFs based on a linker of one type but also multicomponent layered systems combining several types of linkers. For example, these are the structures $[M_2L_2P]$, where M = Cu, Zn, L is naphthalene-1,4-dicarboxylate, P = DABCO;[634] $ML(DABCO)_{0.5}$, where M = Cu, Zn, L is naphthalene-1,4-dicarboxylic acid or tetrafluorobenzene-1,4-dicarboxylate;[635] and SURMOFs based on carboxy- and pyridyl-substituted porphyrins.[636] The opposite statement is also true. Thus, many types of coordination networks of MOFs cannot be prepared by the LbL method in a thin film on a solid substrate due to the specificity of the fabrication procedure.

The main distinguishing feature of the quasiepitaxial layer-by-layer assembly of SURMOFs is the use of an adhesive layer for the attachment of the growing network to the surface. The adhesive layer should have inherent smoothness (atomic or nearly atomic) to avoid the creation and accumulation of defects in the crystal lattice of SURMOFs and possess the functional activity towards components of SURMOFs for strong adhesion with the framework structure. These requirements are met by self-assembled thiol and silane monolayers, which are utilized in most cases for the formation of SURMOFs by means of combined application of the LbL and SAM methods representing two main approaches to the synthesis of supramolecular systems at the interface.

The first SURMOF system of the HKUST-1 type was assembled in 2007 from the metal cluster $Cu^{2+}[Cu(OAc)_2$ and benzene-1,3,5-tricarboxylic acid $(H_3BTC)]$[623] on the carboxylated octanethiol SAM surface deposited onto a gold substrate. The procedure used for the assembly remains a gold standard for the fabrication of SURMOFs. It includes the successive immersion of the substrate into solutions of inorganic and organic components in organic solvents and rinsing of each layer to remove the excess of the deposited compound at 20–50 °C. Generally, the first SURMOF layer is formed by metal centers linked to functional groups of SAM followed by the deposition of the orientation-directing layer of linkers.[635] The deposition sequence of the layers and the nature of functional groups of SAM play a key role in the packing of SURMOFs, which confirms the effect of the surface on the supramolecular self-assembly process. Thus, films grown on carboxyl-terminated SAMs are generally highly oriented along the [100] direction,[623,637] films grown on hydroxyl-terminated SAMs favour the [111] direction,[623] the growth along the [001] direction is strongly preferred for films on pyridyl-terminated SAMs,[635] whereas methyl groups completely suppress the growth of SURMOFs.[637]

The choice of the method for controlling the growth of SURMOFs of uniform thickness is determined by the nature of the linker. Electronic spectroscopy is the most convenient method for chromophore linkers, for example, porphyrins or bisperylene derivatives.[626,636] This method provides information about the relationship between the increase in absorption intensity and the amount of the deposited compound in each layer. For linkers, which do not have strong chromophoric properties, quartz-crystal microbalance (QCM)[638] and atomic force microscopy[639] can be employed. The former method provides reliable, fast and accurate measurements of the increase in the weight of SURMOFs fabricated on the surface of gold electrodes of quartz crystal resonators. Atomic force microscopy, although being more time consuming compared to spectroscopic and gravimetric methods, allows the direct evaluation of changes in the thickness and roughness of SURMOFs.

The assembly of SURMOFs can be performed using, apart from SAMs based on functionalized thiols, silane-

based SAMs functionalized with terminals, making it possible to integrate SURMOFs into optical elements.[631] The drawback of silanes is that they are not perfectly smooth as opposed to thiols with small head groups, which can lead to the formation of a defect structure of SURMOFs. The sensitivity of the packing to the roughness of the adhesive layer is most significant for bulky linkers (*e.g.*, porphyrin metal complexes) due to a large free volume for these molecules in the well-organized assembly. In particular, well-resolved diffraction patterns were not obtained for SURMOF based on the zinc tetracarboxyphenylporphyrin complex ZnTCPP and zinc acetate deposited on the surface of the (3-aminopropyl)triethoxysilane monolayer despite a uniform increase in the film thickness.[636]

Graphene oxide can serve as an alternative to silane monolayers. Due to the presence of oxygen-containing functional groups, graphene oxide can efficiently adsorb metal (Zn^{II}, Cu^{II}, Mg^{II}, *etc.*) acetates utilized for the fabrication of SURMOFs. Adhesive GO monolayers are formed *via* their transfer from the oil/water interface (GO exhibits properties of a mild surfactant and spontaneously forms adsorption interfacial layers[640]). The LbL assembly of SURMOFs on such monolayers is accomplished by a standard method.[641] The advantages of the assembly of SURMOFs on graphene oxide monolayers, formed on quartz and silicon substrates, were demonstrated for systems based on $Zn(OAc)_2$ and different types of polyaromatic linkers (*e.g.*, perylene-3,4,9,10-tetracarboxylic acid *N*,*N*′-dipropionate[626] and Zn complexes with tetrasubstituted porphyrins).[641] Well-resolved X-ray diffraction patterns obtained for these SURMOFs are indicative of their high quality, the morphology of the systems varying depending on the type of interactions stabilizing the framework. Delocalized electrostatic interactions between metal clusters and carboxyl groups give rise to roughness features due to accumulation of shear defects, and the self-assembly *via* directional coordination bonds involving pyridyl groups affords SURMOFs with exceptional surface smoothness at the atomic level (on a millimetre scale).[642]

It is worth noting that X-ray diffraction patterns collected even for high-quality SURMOFs on standard laboratory X-ray diffractometers generally show single reflections corresponding to the lattice parameters in the direction away from the substrate. The complete description of the SURMOF structure can be obtained only using synchrotron radiation. For example, for SURMOF based on deprotonated porphyrin [*meso*-tetrakis(4-carboxyphenyl)porphyrin] and cobalt(II) acetate, the formation of a hexagonal packing of porphyrins in each layer with tilting of the macrocycle plane of 60° relative to the surface of the substrate was confirmed by grazing incidence small-angle X-ray scattering and X-ray reflectivity.[643] The packing of SURMOFs can be successfully modelled using well-resolved X-ray diffraction patterns from a vertical structure, such as SURMOFs based on zinc porphyrin complexes of different structures on the GO monolayer surface, by means of analytical approaches applied to calculate the structures of layered minerals.[642]

The unique structural features of SURMOFs are responsible for the exceptional characteristics of these systems (sensitivity, selectivity, the rate of generation of optical or electrochemical response), which are important for a number of practical applications, from medicine[644] and catalysis[645] to nonlinear optics.[646] Due to porosity of SURMOFs comparable with this property of bulk MOFs[647] combined with a small thickness and a considerable potential for the directed functional design of the appropriate organic components, these systems are among the most promising nanoscale materials for the integration with sensor platforms.[629] The tuning of the structural characteristics of SURMOFs allows the creation of selective elements for monomolecular recognition, *e.g.*, zinc-based optical sensors (ZnTCPP) selective for adenosine monophosphate[648] or gravimetric MOFs based on Co(TCPP) and $Co(OAc)_2$ (PIZA-1) for the selective binding of benzene,[649] and also can be applied to assemble multisensitive gravimetric sensors. A similar electronic nose-type system was assembled from three QC resonators with deposited HKUST-1 SURMOFs for the selective detection of six types of volatile compounds (geraniol, citronellol, *etc.*).[650]

An important application of SURMOFs is in the catalysis of photochemical reactions. An increase in the rate and selectivity of these reactions is achieved *via* supramolecular control, enabling the fixation of reactants in the SURMOF structure.[651] A vivid example of the application of this strategy is the oxidative photocyclization giving phenanthrene in bilayer Zn(TPE-BDC) SURMOF (TPE-BDC is 4′,4‴-(1,2-diphenylethane-1,2-diyl)-(*E*)-bis([1,1′-biphenyl]-4-carboxylate). The reaction affords one isomer with an increase in the yield of the product by more than 70% due to hindered rotation about the C=C bond of tetraphenylethylene in the rigid framework structure.[652]

The design of SURMOFs based on organic chromophores, primarily porphyrins, which are utilized in optics and electronics, is the most rapidly growing area of research. This is associated with both photophysical properties of porphyrin molecules and the adaptive potential of the LbL method for the available manufacturing technologies of elements for microcircuits and optical chips (Fig. 108).[646, 653, 654] According to transition state absorption spectroscopy, the exciton diffusion length in some porphyrin SURMOFs can theoretically reach several micrometres and is limited in real SURMOFs only by interactions of excitons with lateral defects of the structure within crystalline domains with an average size of ~100 nm.[655] Therefore, the improvement of the procedure for assembling structurally ideal SURMOFs is related to the possibility of improving their optical properties.

Haldar *et al.*[656] showed that the computational screening of a library of compounds can be used to select appropriate porphyrin for the fabrication of SURMOFs with specified properties. The algorithm predicts the spectral characteristics of the framework depending on the composition and structure of functional substituents of the macrocycle and allows the tuning of these characteristics by changing the strength of intermolecular interactions in the framework structure. The photoelectric properties of porphyrin SURMOFs can be significantly improved by introducing strong electron acceptors, *e.g.*, fullerenes, integrated into SURMOF pores *via* layer-by-layer assembly of a ZnTCPP-based film.[657] Due to the ordered SURMOF structure, the interaction with a light beam provides the efficient separation of charge carriers, the hole transfer in organized layers of porphyrins as donors and the electron transfer through channels formed by C_{60} molecules. It is worth noting that the LbL method, which allows the control of the spatial organization of components in each layer, can be applied to achieve the functional characteristics of this type of hybrid structures.

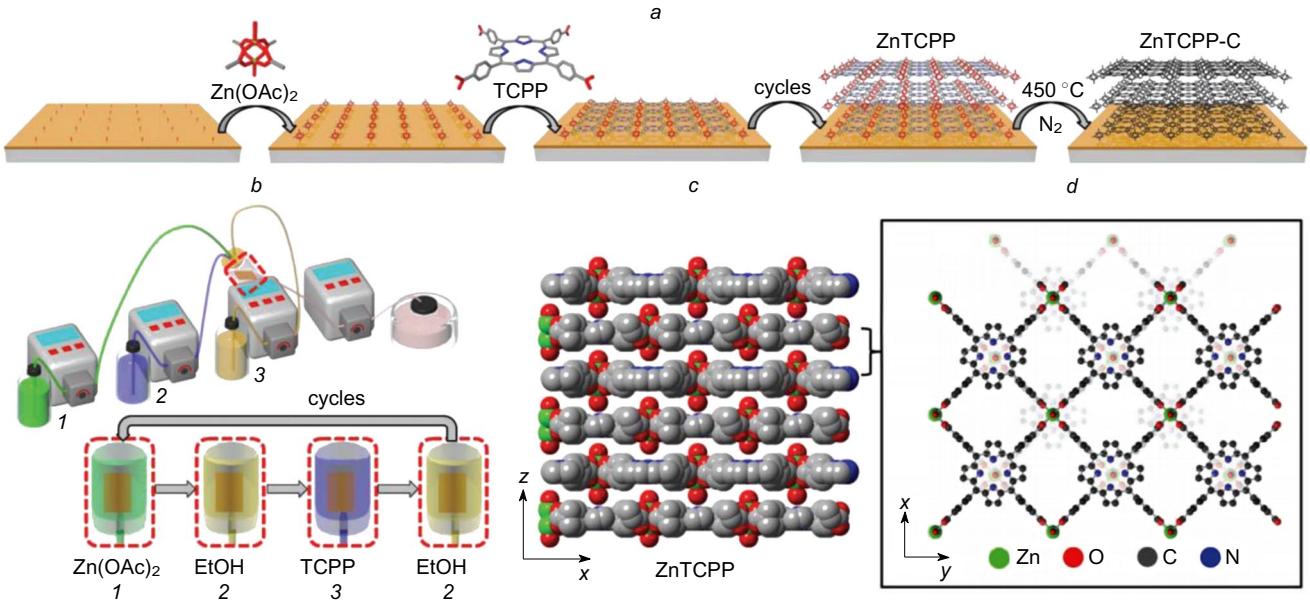


Figure 108. Schematic illustration of the integration of ITO-mounted SURMOFs into a Grätzel cell: the sequence of the quasiepitaxial assembly of ZnTCPP followed by calcination (*a*) and the experimental setup for the deposition and rinsing of layers (*b*); the normal (*c*) and lateral (*d*) structures of assembled SURMOFs.[653] Published with the permission of Wiley.

Therefore, due to simplicity, versatility and nanoscale control provided by the layer-by-layer assembly, this technology is commonly used to fabricate supramolecular and hybrid multilayer structures. This method is easily adapted to a wide range of compositions of the coatings and enables their deposition onto both planar substrates and substrates of different shapes.

Supramolecular chemistry at the interface is one of the most rapidly growing areas, which employs intermolecular interactions for the assembly of not only alike molecules but also nanoscale structures formed under the effect or with the direct involvement of surface layers of the substrate.

This Section considers three main methods of the assembly of supramolecular structures on the surface, which have been already employed to fabricate numerous nanoscale materials and devices for different applications. These methods are used for the self-assembly of layered structures with a desired thickness and sequence of layers on substrates of different nature and of various shape. A great advantage of all three methods is that the films are fabricated under mild conditions, generally in aqueous media, which is particularly important both in the case of essential biomolecules and for the solution of challenging problems of green chemistry.

3.3. Structures and phase transitions of low-dimensional self-organizing systems with different symmetry

The use of self-assembly and self-organization of supramolecular nanostructures for the fabrication of smart materials, *i.e.*, materials sensitive to external stimuli (changes in the temperature and pressure, electric or magnetic field), the chemical composition of the environment and so on, is an important area of research in materials science.[658–662] First, it is necessary to give exact definitions of the terms 'self-assembly' and 'self-organization', which are often used as synonyms in the research community. By the self-assembly we mean the formation of supramolecular aggregates *via* weak noncovalent interactions. Examples are inclusion compounds,[663–671] Langmuir monolayers,[560,672–675] lyotropic liquid-crystalline aggregates,[676–678] including colloidal systems,[679–681] *etc*. The self-organization is the formation of extended macroscopic phases (often with low symmetry, such as nematic, smectic, columnar phases with different symmetry, platelet crystals and so on) based on aggregates or molecules of a particular shape or with a specific function. The self-organization of complex systems has attracted attention of many theoretical researchers, who developed different approaches to the investigation of this phenomenon. Worthy of mention are Haken's synergetic model based on the order parameter concept and the slaving principle,[682] thermodynamic models of nonequilibrium processes (the dissipative structure theory) put forth by Prigogine,[683] self-organized criticality models (the self-organization at the edge of chaos) introduced by Bak,[684] the formation and evolution on nonstationary structures in aggravation regimes developed by Samarsky and Kurdyumov,[685–687] *etc*.

It is worth noting that both the self-assembly not accompanied by self-organization (inclusion compounds) and the self-organization not accompanied by self-assembly can occur in nature. Thus, in diblock and triblock copolymers consisting of two and three incompatible units, respectively, the mutual repulsion and induced segregation of different blocks leads to the requirement of minimization of interface energy with a constant curvature $\langle H \rangle$. The latter value is determined primarily by the composition of the block copolymer (for a diblock copolymer, it is sufficient to introduce the volume fraction (f) of one component). Symmetric diblock copolymers ($f = 1/2$) are characterized by the presence of a lamellar phase.[688,689] In the case when the number of one type of blocks is only slightly larger than the number of blocks of another type, the formation of a gyroid bicontinuous cubic phase is observed. This phase is described in detail below. If this difference is significant, the minor blocks are arranged in columns, which are surrounded by a matrix phase of the

major block and are packed in a two-dimensional hexagonal lattice. A further increase in the asymmetry results in the formation of spherical aggregates of the minor block arranged in a body-centred cubic phase. Finally, in the extreme cases ($f \to 0$ and $f \to 1$), one phase is distributed in another one in a disordered manner.

This behaviour of the systems was reported for two extreme cases: weak ($\chi N \approx 10$) [690] and strong ($\chi N \gg 10$) [691] segregation ($\chi \approx 1/T$ is the Flory – Huggins parameter, which describes the interaction between the blocks of the copolymer, N is the total degree of polymerization). The theory that combines two extreme regimes was considered by Matsen and Bates. [688] Therefore, the phase behaviour of diblock and triblock copolymers depends on the following two factors: on the one hand, the average interfacial curvature of homopolymers is dictated by the segregation of blocks (the energy contribution to the enthalpy); on the other hand, the tendency for uniform filling of the space with a polymer material (the entropy contribution) [692 – 694] leads to a deviation of the interfacial curvature (δ) from the average value. The systems, in which the entropy factor is negligible, are characterized by the following sequence of classical phase states: lamellar phase → two-dimensionally ordered columnar phase → three-dimensionally ordered cubic phase → isotropic state, for which $\delta \approx 0$. The account of the entropy contribution explains the formation of complex phases, such as gyroid and metastable hexagonally perforated lamellar phases, in the weak segregation regime. A mathematically similar mechanism of formation of liquid-crystalline aggregates and extended systems occurs in lyotropic colloidal systems.[681]

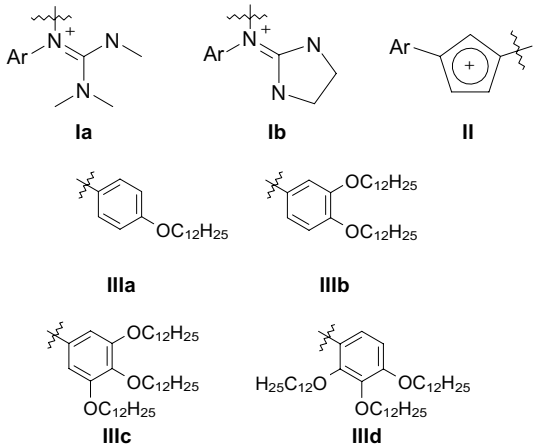
Another example of the self-organization not accompanied by self-assembly are orientationally disordered mesophases [695] having different crystal lattices. Thus, a cubic lattice is observed for plastic crystals; a two-dimensional hexagonal or rectangular lattice, for rotationally crystalline mesophase, with aggregates in the sites of the latter rather freely rotating with respect to each other. The plastic crystal state is typical of compounds with a nearly spherical molecular shape, such as neopentane (Me_4C), fullerene C_{60}, adamantane, a series of tetrasubstituted halogenated methane derivatives,[696] dicarboxylic acid nitriles or their mixtures,[697] hybrid perovskites,[698, 699] dendrimers,[700] *etc*. Rotationally crystalline mesophases in polymers are characterized by the absence of a long-range order along the chain axis and, correspondingly, the two-dimensional packing of macromolecules.[701, 702] In the case of flexible linear macromolecules [polytetrafluoroethylene (PTFE), halogenated polyethylenes, *trans*-polybuta-1,4-diene, polyethylene, poly(*p*-xylylene), *etc*.], the violation of the order along the chain axis is due to disturbance of the regularity of the polymer chain. This may be associated, for example, with the formation of conformational defects, which occupy a small volume and leave the direction of the macromolecule unchanged. Therefore, the transition to the orientationally disordered mesophase is generally accompanied by a significant increase in the entropy with small free energy changes.[703] Due to the above-described structural features, the hexagonal columnar mesophase is highly promising for the processing of polymer materials bearing a flexible chain, because a relatively low (compared with an isotropic melt) content of molecular units and connectivities provide high flexibility of the polymer chains. This fact significantly facilitates the polymer processing; in the case of high-molecular-weight materials, there is often no alternative for the processing through the formation of a rotationally disordered mesophase.[704, 705]

This Section considers the self-assembly followed by the self-organization of sector-shaped dendrons of different nature and also the practical aspects of their applications to address important technological issues. As shown below, these compounds are characterized by a great diversity of the structures of supramolecular aggregates and phase behaviour. However, their major common feature is the formation of columnar aggregates, which, in turn, form two-dimensional columnar mesophases of a certain type. Hereinafter, we will distinguish two types of columnar mesophases — ordered and disordered — depending on the presence of the order within individual columns. Generally, X-ray scattering patterns of ordered columnar mesophases show narrow small-angle peaks, which characterize a two-dimensional crystal lattice formed by cylindrical supramolecular aggregates, and broad wide-angle peaks determined by the structure of individual aggregates. It should be noted that a two-dimensional ordered columnar mesophase cannot be referred to as a crystalline one, because there is no correlation between the structures of its individual columns. Upon the transition of the ordered columnar mesophase into the disordered state, the violation of the order within the cylindres leads to the disappearance of the scattering peaks at wide angles, whereas small-angle peaks become significantly narrower due to an increase in the size of liquid-crystalline domains.[706, 707]

Several types of dendrons can be distinguished depending on the driving forces for the self-assembly of supramolecular aggregates. Ionic liquid-crystalline (ILC) dendrons consist of cation – anion pairs, in which the cation and the anion can be either of organic or inorganic nature. However, one or both ions include a rigid sector-shaped moiety and one or several aliphatic tails containing from six to eighteen carbon atoms. In turn, aliphatic substituents can be branched or linear, saturated or containing double or triple bonds.

For instance, in the past decade considerable attention has been given to ILCs based on imidazolium salts [708 – 720] and guanidinium salts.[721, 722] Thus, Butschies *et al.* [723] used cation – anion pairs composed of guanidinium cations (**Ia**,**b**) or imidazolium cations (**II**) and I^- or $ArSO_3^-$ anions; alkyl-containing phenyl groups served as sector-shaped substituents (**IIIa** – **d**). (The alkyl groups considered in this Section have a normal structure.)

Structures I – III



Ionic liquid crystals based on congruent ion pairs consisting of mesogenic cations or anions of the same shape have attracted interest because they are an attractive tool for the fine tuning of the physical and thermal properties of the resulting mesophases. A comparative analysis of the structures and properties of imidazolium and guanidinium salts was performed by differential scanning calorimetry, polarized optical microscopy and X-ray scattering.[723] It was shown that if the cation or anion bears only one dodecyloxy tail and the cation–anion pair contains no more than three these groups, such pairs form a smectic mesophase of type *A*. If the total number of alkoxy tails is equal to four or five, a columnar mesophase is formed regardless of the nature of the sector-shaped unit. However, in the case of longer aliphatic tails, their steric repulsion becomes to play an important role in the formation of supramolecular aggregates.

Guanidinium sulfonates with symmetric anions formed a hexagonal columnar mesophase, whereas no mesophases were observed for asymmetric anions. On the contrary, the formation of cubic mesophases for symmetric cation–symmetric anion and symmetric cation–asymmetric anion pairs was observed in the case of imidazolium sulfonates. Imidazolium sulfonates with asymmetric cations formed a hexagonal columnar mesophase. The detailed study of the structures of the columnar mesophases showed that individual columns in these mesophases consist of supramolecular discs. Their structural constant is the number of aliphatic tails equal to 12. As is seen in Fig. 109 *a*, a single disc can contain from six to four ions depending on the number of aliphatic tails in an individual dendron. Besides, Fig. 109 *b* represents the proposed schemes of aggregation of ions of different symmetry.

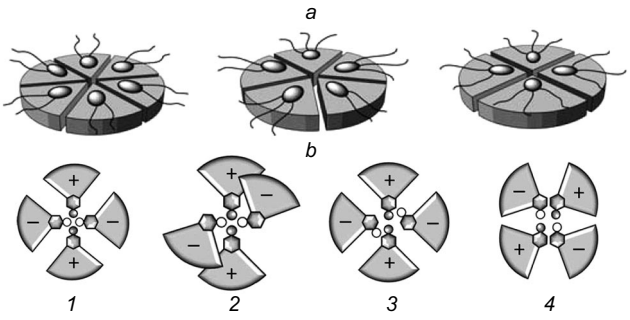
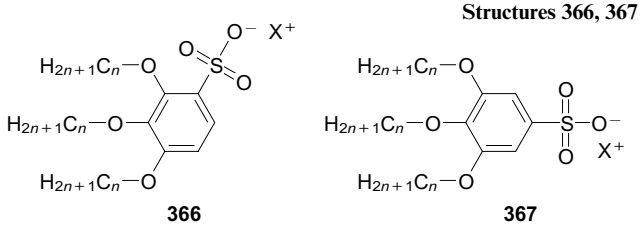


Figure 109. A model of discs consisting of six, five and four ions (*a*) and the schematic illustration of aggregation of different-symmetry ions: (*1*) two symmetric cations and two symmetric anions; (*2*) and (*3*) two symmetric cations and two asymmetric anions; (*4*) two asymmetric cations and two asymmetric anions (*b*).[723] Published with the permission of Taylor and Francis.

The structure of columnar mesophases in ILCs was studied in most detail for asymmetric and symmetric salts of tri(alkoxy)benzenesulfonic acids **366** and **367**, respectively.[724–727] Thus, the investigation of the phase behaviour of caesium 3,4,5-tri(dodecyloxy)benzenesulfonate (345-BSA-Cs, **366a**, $n = 12$, X = Cs) demonstrated that, at room temperature, this material is characterized by the presence of large domains of an ordered hexagonal columnar mesophase. Its supramolecular aggregates 4.88 nm in diameter consist of discs composed by twelve dendrons, the long axes of which are perpendicular to the

Structures 366, 367



axis of the column. Meanwhile, to overcome the steric hindrance associated with the packing of 36 aliphatic tails, on the one hand, and to facilitate π-interactions between adjacent dendrons in the layer, on the other hand, the 345-BSA-Cs molecules form a large propeller angle, *i.e.*, the rotation from the plane of the layer about the line normal to the column axis (Fig. 110).

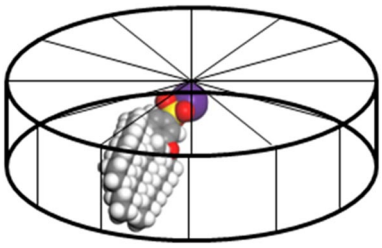


Figure 110. Structure of the layer in supramolecular aggregates of the ordered columnar mesophase formed by dendrons of caesium 3,4,5-tri(dodecyloxy)benzenesulfonate **366a** at room temperature.

Upon heating, the cylindre diameter of the columnar mesophase changes insignificantly; however, the phase transition to a disordered columnar mesophase composed of supramolecular aggregates 3.67 nm in diameter occurs at the temperature (T) ~ 120 °C. Therefore, a decrease in the cylindre diameter (D) compared to that in the ordered columnar phase is $\Delta D/D \approx 25\%$. The mechanism of this strong structural change of the material calls for a special attention. The reconstruction of electron density distribution (EDD) from the relative intensities of small-angle reflections showed that the order–disorder transitions in cylindres of the columnar mesophase causes the largest changes in the central parts of these columns. In EDD maps (Fig. 111), the highest electron density regions, coloured in red, can be assigned to the caesium cation–benzenesulfonate ion pair, whereas the low electron density

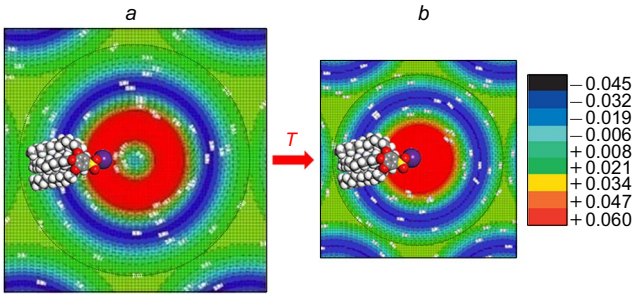


Figure 111. Electron density distribution in the plane perpendicular to the cylindre axes for a columnar mesophase formed by caesium 3,4,5-tri(dodecyloxy)benzenesulfonate **366a** ordered at room temperature (*a*) and disordered at $T = 120$ °C (*b*). The boundaries of the central supramolecular aggregates are indicated by dashed lines. The Figure was drawn by the authors of the review using data of Ref. 706.

regions (coloured in green and shades of blue) correspond to positons of aliphatic tails.

At room temperature, a relatively low electron density region ~9 Å in diameter is observed in the centres of the columns; this region is surrounded by high-density mesogenic groups and the bound caesium ions. As demonstrated in the comprehensive review,[706] the reconstruction of EDD provides a rather low resolution. Therefore, in regions neighboring the most dense regions, the interfaces are always blurred, resulting in a significant increases in the density of the adjacent regions. Hence, it can be concluded that cylindres of the ordered columnar mesophase of compound **366a** actually contain almost hollow central coaxial channels formed through a mutual alignment of the focal regions of the dendrons — cation – anion pairs.

The intensity of thermal motion increases with increasing temperature, which leads to violation of this order and, correspondingly, to the closure of the central channels in the columns. It is also worth noting that the loss of the central channel is associated with at least a 65% total decrease in the column diameter after the order – disorder transition.

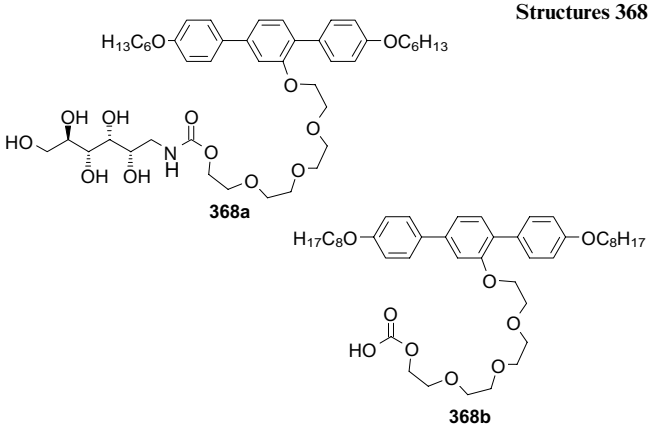
Fall *et al.*[728] made an attempt to perform a theoretical analysis of the order – disorder transition using statistical physics methods in terms of the formalism of magnetic spin chains for compounds similar to 345-BSA-Cs, namely, lithium and sodium 3,4,5-tri(dodecyloxy)benzoates (345-BCA-Li, **366b**; and 345-BCA-Na, **366c**, respectively). The authors demonstrated that this transition is driven predominantly by the entropy change of the end chains. The quantitative fitting of the expression for the energy of the column showed that the free energy of aliphatic tails is the only temperature-dependent term. The entropy of these groups increases with increasing temperature due to the accumulation of *gauche* conformers, which, in turn, leads to the ejection of one dendron from the column. This results in a decrease in the positive contribution to the free energy of the column, thereby making the attraction between the remaining dendrons sufficient for stabilization of the new column.

The expulsion of a monodendron from the cylindres of the columnar phase was experimentally confirmed in blends of 345-BCA-Li and higher alkanes.[729] For these blends, a sharp shift of X-ray reflections to the small-angle region was observed at the transition temperature due to the formation of a superlattice, which involved simultaneously columns consisting of four (stable at low temperatures) and three (stable at high temperatures) dendrons. Unfortunately, the authors did not publish the X-ray diffraction patterns for the compound 345-BCA-Li at temperatures higher than the temperature of the transition from one columnar phase to another. Hence, it cannot be ultimately stated that the order – disorder transition occurs within cylindres of the hexagonal columnar mesophase.

Another successful example of the theoretical analysis of the self-organization of complex liquid-crystalline mesophases, which is also related to the theory of magnetism, is a multicolour hexagonal-shape confetti network and its application to gain an understanding of the self-organization of T-shaped bolamphiphiles **368a**,**b** (Fig. 112).[730 – 733]

It is worth noting that the established relationships between the structure and the phase behaviour are not typical of single compounds of a particular type. The thing is that the physical chemistry of sector- and cone-shaped dendrons can use libraries of compounds, in which one structural parameter (the size of the focal group, the length

Structures 368



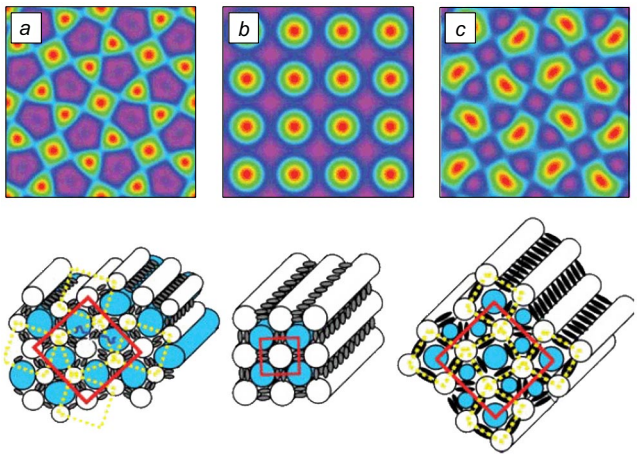


Figure 112. Electron density distribution maps for columnar mesophases formed by T-shaped amphiphiles **368**: a mixture of triangular and square columns (*a*), columns with a round cross-section (*b*) and pentagonal columns (*c*).[731] Published with the permission of American Association for the Advancement of Science.

of aliphatic tails, the symmetric or asymmetric mode of binding to mesogenic moieties) is varied in small increments with the other parameters kept constant. Thus, for tri(alkyloxy)benzenesulfonic acids, a comparative analysis of the structure and phase behaviour was performed in the following series:

— alkali salts of 2,3,4-tri(dodecyloxy)benzenesulfonic acid (investigation of the role of the counterion size);[725]

— 3,4,5-tri(dodecyloxy)benzenesulfonic acid derivatives containing bulky focal groups;[726]

— 2,3,4-tri(dodecyloxy)benzenesulfonic acid derivatives containing focal organic groups and alkali metal ions of a comparable size;[727]

— caesium 2,3,4- and 3,4,5-tri(dodecyloxy)benzenesulfonates (investigation of the role of the binding mode of the focal group);

— caesium 3,4,5-tri(alkyloxy)benzenesulfonates with aliphatic tails containing from six to eighteen carbon atoms.

It was shown that small changes in the structure of the dendrons lead to predictable changes in the phase behaviour of the material, such as the sequence of phase states, the temperature of the order – disorder transition in cylindres of the columnar mesophase, the region of existence of the columnar mesophase, *etc*. Figure 113 represents the phase diagram characterizing the dependence of the phase behav-

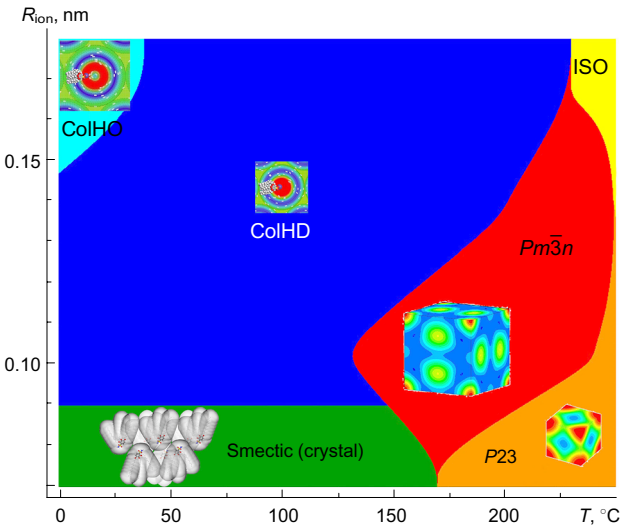


Figure 113. Dependence of the phase behaviour of alkali metal 2,3,4-tri(dodecyloxy)benzenesulfonates on the temperature and the cation size.[725] ColHO is an ordered columnar mesophase, ColHD is a disordered columnar mesophase, ISO is an isotropic melt region.

iour of alkali metal 2,3,4-tri(dodecyloxy)benzenesulfonates on the temperature and the cation size.

Consequently, 2,3,4- and 3,4,5-tri(alkyloxy)benzenesulfonic acid derivatives are characterized by the formation of an ordered hexagonal columnar phase, which undergoes a transition to a disordered hexagonal columnar mesophase upon heating. Cylindres of the ordered columnar mesophase contain coaxial channels, the sizes of which allow the use of these compounds as working substances for ion-selective membranes. The order–disorder transition leads to the closure of the pores. Hence, the fabricated membranes can be controlled by varying the temperature. Since the phase behaviour of dendrons changes in a predictable pattern upon varying a particular parameter of their structure, the performance characteristics of ion-selective membranes can be controlled by choosing an appropriate dendron.

To manufacture high-tech items from these promising materials, several conditions should be fulfilled. First, the appropriate orientation of the ion channels with respect to the membrane surface should be provided. Second, since ILCs are generally waxy substances or exist as dispersed particles, the synthesized compounds should be additionally processed to fabricate ion-selective membranes suitable for use under environmental conditions.

One approach to address these issues is the self-assembly of dendrons with unsaturated tails, the formation of a columnar mesophase in the compound and the subsequent cross-linking of the tails exposed to a certain external stimulus. Bakirov *et al.*[734] studied the phase behaviour of sodium 2,3,4-tris(11-methacryloylundecyloxy)benzenesulfonate (234-BSA-Na*, **369**). At room temperature, an ordered columnar hexagonal phase with a cylindre diameter of 3.80 ± 0.01 nm formed in this compound. Upon heating to 53 °C, this phase underwent an irreversible transition to a disordered columnar hexagonal mesophase. The distinguishing feature of the temperature behaviour of compound **369** is that the temperature dependences of the column diameter [$D(T)$] are significantly different for different samples and, what is more, the column diameter depends not only on the temperature but also on the duration of the experiments. A significant change in the solubility of the material is also worthy of note. Thus, fresh samples of 234-BSA-Na* were completely dissolved in cyclohexane, whereas samples irradiated with X-rays for ~100 h in a Kratky camera were insoluble. Therefore, since the transition to the columnar phase is irreversible, it can be suggested that the X-ray irradiation and(or) heating of compound **369** trigger the chemical linking between aliphatic substituents at methacryloyl functional groups, with the participation of dendrons both belonging to one supramolecular columnar aggregate and from different aggregates (the loss of solubility of the samples).

Let us consider the main factors responsible for the linking of methacryloyl groups in compound **369**. For this purpose, two sample of 234-BSA-Na* were used. One sample was heated to 50 °C, and then the intensity of X-ray scattering was measured for 15 min in a narrow region of the first reflection of the tenth columnar mesophase. Another sample was irradiated in an X-ray camera overnight, then heated to 50 °C and again cooled to room temperature. As a result, both samples had the same temperature history; however, the irradiation dose of the latter one was higher than that of the first one by 2.4 Gy. The cylindre diameter of the columnar phase was 3.87 nm for the initial samples, 3.85 nm for the non-irradiated sample and 3.77 nm for the irradiated sample. Therefore, the irradiation of the material plays an important role in the chemical linking of the compound.

An attempt was made to prepare a xerogel from a 2% solution of 234-BSA-Na* in styrene (see Fig. 114 *a*). The photomicrographs show thin fibres with a diameter of ~0.1 μm. Each fibre is apparently a bundle of supramolecular cylindres of the columnar mesophase. Consequently, this material holds great promise for the creation of highly oriented materials not only on a nanoscale but also at a microlevel. Besides, the stretching of the material at temperatures corresponding to the region of existence of the disordered columnar phase afforded macroscopic oriented samples. Small-angle X-ray scattering patterns of these fibres (see Fig. 114 *b*) show three reflections of the columnar phase with a cylindre diameter of 3.67 nm (see Fig. 114 *c*).

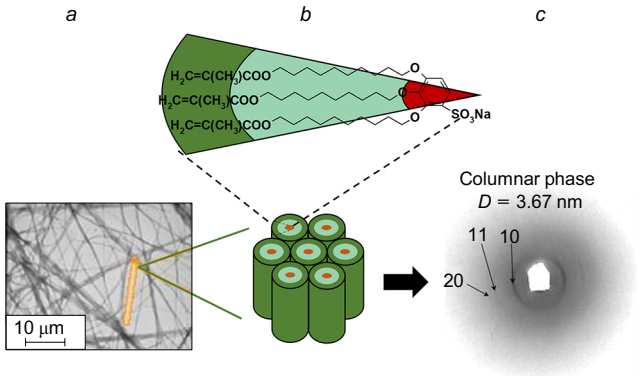


Figure 114. Photomicrograph of gel fibrils prepared from a 2% solution of compound **369** (234-BSA-Na*) in styrene (*a*), a schematic illustration of the molecular packing in columnar supramolecular structures (*b*) and the small-angle X-ray scattering pattern of an uniaxially oriented fibre (*c*).[734] In Fig. *b*, the focal group is in green, the aliphatic chain is in light green, functional tails are in dark green. Published with the permission of Springer Nature.

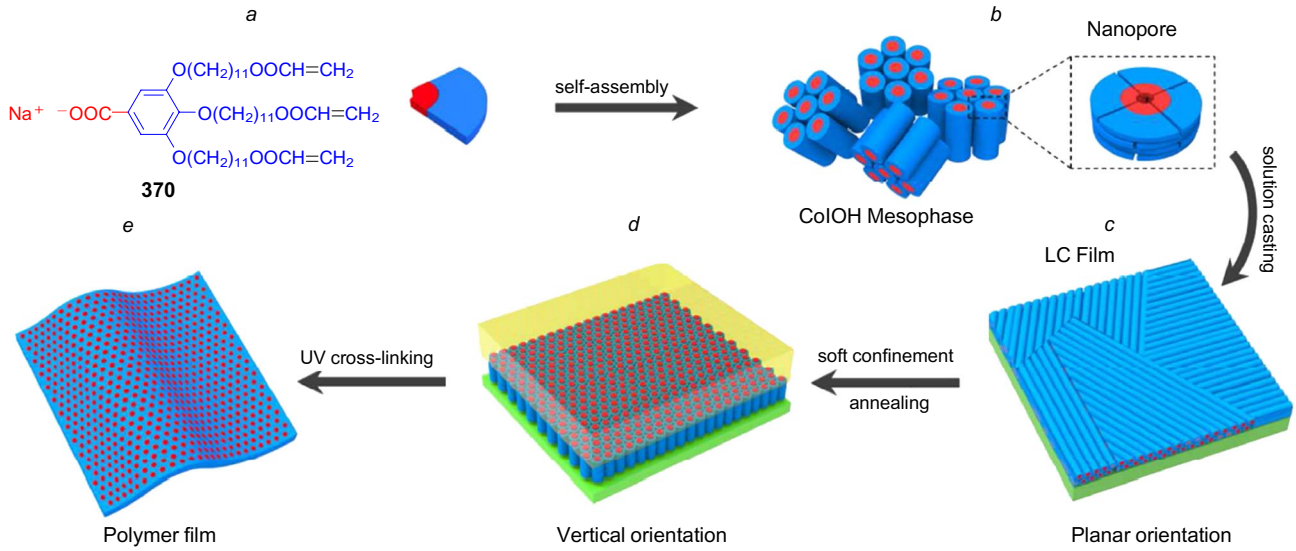


Figure 115. Schematic illustration of the self-organization of compound **370** and its use for the soft confinement-assisted fabrication of a thin film with pores aligned parallel to the layer director.[736] (*a*) The structure of conical dendrons of 245-BSA-Na*; (*b*) domains of the hexagonal columnar mesophase possessing central pores with a dimeter of ~1 nm; (*c*) a submicrometre-thick film obtained by casting a dilute solution of compound **370** in tetrahydrofuran onto a silicon substrate followed by solvent evaporation (in the film, cylindrical liquid-crystalline aggregates are aligned parallel to the surface of the substrate); (*d*) the reorientation of supramolecular columns to the vertical position by imposing a soft polydimethylsiloxane pad followed by thermal annealing; (*e*) the formation of a film, using UV-cross-linking, that can be easily detached from the substrate.

Their azimuth width does not exceed 30°, which is indicative of a relatively high fibre orientation. Therefore, the newly synthesized compounds based on the benzenesulfonic acid salt can be used to fabricate stable oriented chemically cross-linked materials characterized by the presence of functional ion channels.

A similar approach was applied for the self-assembly of films based on sodium 3,4,5-tris(11-acryloyloxyundecyloxy)benzoate (**370**, 345-BCA-Na*).[735] It was demonstrated that the magnetic-field alignment of a disordered columnar phase of this compound results in the formation of highly ordered liquid-crystalline domains with an orientational order parameter of up to 0.95 (small-angle X-ray scattering and polarized optical microscopy). The diameter of ion-selective channels in the material was ~1 nm. The ionic conductivity measurements showed at least 85-fold enhancement of the conductivity over magnetically non-aligned samples. This research group[736] developed also another approach using the same material, which was based on the soft confinement of a self-organized mesophase (Fig. 115). For this purpose, liquid-crystalline films were fabricated by casting a dilute solution of compound **370** in tetrahydrofuran onto silicon substrates and the subsequent solvent evaporation. Then a soft polydimethylsiloxane pad was imposed on an ILC film followed by thermal annealing. It was confirmed that most of columns of the hexagonal phase were in a vertical orientation. The UV-induced cross-linking of aliphatic tails of dendrons afforded a membrane, which can be easily detached from the substrate and the ionic conductivity of which is three orders of magnitude higher than that of the nonaligned material.

An interesting example is the fabrication of ion-selective membranes based on 3,4,5-tri(dodecyloxy)trimethylammonium tetrafluoroborate and hexafluorophopshate.[736] Both compounds are characterized by the following phase sequence: crystal → columnar rectangular mesophase 1 → columnar rectangular mesophase 2 → columnar hexagonal mesophase → isotropic phase. Unfortunately, the authors did not address the issue of the alignment in columnar aggregates of the observed phases. However, grazing incidence small-angle X-ray scattering patterns for the high-temperature rectangular phase show one narrow reflection corresponding to the interplanar spacing of 4.8 Å. The transition of this phase to a disordered hexagonal columnar mesophase was accompanied by an increase in the conductivity by at least three orders of magnitude.

It is also worth noting that the hexagonally ordered channels are not the only candidate for the fabrication of controlled ion-selective membranes. Another approach is based on the use of a gyroid bicontinuous cubic mesophase with symmetry $Ia\bar{3}d$.[737] This phase consists of a system of non-interpenetrating tubes, the basic units of which are composed of two tripods with planes rotated with respect to each other by 70.53° (Fig. 116).

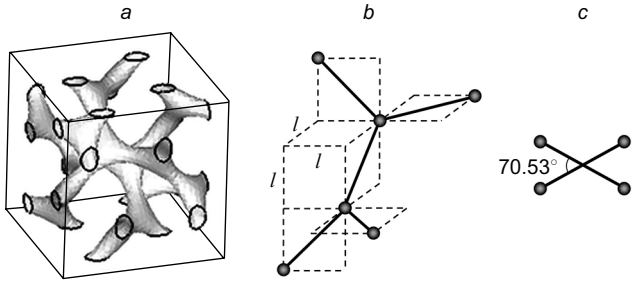


Figure 116. Structure of a gyroid cubic mesophase with symmetry $Ia\bar{3}d$ (*a*) and the schematic illustration of the basic unit of the gyroid structure consisting of two connected tripoids rotated with respect to each other by 70.53°: the lateral view (*b*) and the top view (*c*).[706, 737]

From a technological standpoint, this bicontinuous structure is more interesting for the fabrication of selective membranes than the hexagonal structure. In the latter, the charge diffusion length in the channel at a specified membrane thickness is much shorter, but the material in the gyroid phase does not require the preliminary alignment, whereas the branched system of channels can mediate ion transport in the case of any domain alignment. In this respect, the publication by Ichikawa *et al.*[738] is of particular interest. The authors demonstrated the occurrence of a gyroid phase for analogues of 3,4,5-tri(dodecyloxy)triethylammonium tetrafluoroborate with unsaturated aliphatic tails. The gyroid phase was stabilized by the UV-induced cross-linking of the tails (diene and acryloyl). In the resulting membranes, the conductivity jump at a temperature of the transition from the gyroid to hexagonal columnar mesophase was negative; however, the value of this jump was insignificant (see Fig. 8 in the publication [738]).

Approaches were developed to fabricate self-organized ILCs responsive to different external stimuli such as light,[739–743] particular chemical compounds,[744–747] mechanical pressure,[748] electric field.[749] Other applications of ILCs, both sector-shaped and linear, are reviewed by Kato *et al.*[750]

Apart from the above-mentioned ILCs, the following self-organized ILCs are known: with pyridinium, pyrimidinium and quinolinium cations,[751] isoquinolinium cations,[752] 1,10-phenanthrolinium cations,[753] 4-hydroxypyridine derivatives,[754] amino acid derivatives,[708] nanobiphasic systems based on hydrophobic phosphonium salts and hydrophilic ammonium salts,[755,756] *etc.*[757–761]

Another type of dendrons includes systems self-organized through van der Waals forces (LCWdV). Since relatively strong Coulombic interactions in ion pairs and interactions between ion pairs play a key role in the mutual alignment of dendrons, the self-assembly of ILCs generally affords flat discs, which form cylindres of a columnar phase stabilized by π-interactions between aromatic moieties. The self-assembly of LCWdV has no this limitation, the angle of rotation of the dendron being only rarely a divisor of 360°. Hence, these dendrons most often form supramolecular aggregates with helical symmetry.

In recent years, classical LCWdV based on gallic acid derivatives with long aliphatic tails (compounds **371**) [762–764] became classical compounds. Since the beginning of the 1990s, these compounds have been systematically studied.[737,765–770]

Some representatives of this class of compounds are prone to undergo self-assembly to form supramolecular cylindres. The latter, in turn, are organized in a block state to form either a two-dimensional ordered (φ_{oh}) or disordered columnar LC phase (φ_h) (Fig. 117). With increasing temperature, two phase transitions were observed in the synthesized compounds: the disorder in the columns and their subsequent melting. Besides, it was found that the order–disorder transition temperature, the isotropization temperature and, on the whole, the ability of the macromonomers and polymers containing bulky sector-shaped side groups to form a columnar phase depend on the structure of the monomer, namely, on the length and the chemical structure of the spacer and the nature of the mesogenic group and the alkyl tails.

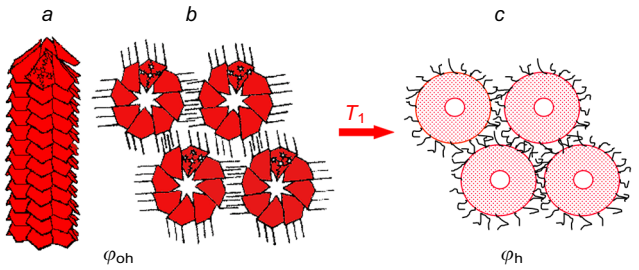


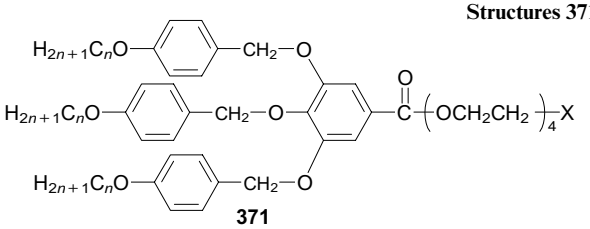
Figure 117. Model of the ordered supramolecular structure of polymethacrylates containing bulky side substituents and their macromonomers (the lateral view (*a*) and the top view (*b*)) and the schematic illustration of the transition from the ordered to disordered columnar LC phase (*c*).[737,769] Rigid columns composed of mesogenic groups (shaded rings) are located in a continuous aliphatic template.

The distinguishing structural feature of gallic acid-based supramolecular aggregates is the tilt of individual dendrons with respect to the column axis (tilt angle) to facilitate π-stacking between individual molecules in the column. The order–disorder transition within columns is a cooperative process and involves the successive melting of aliphatic tails, disorder of dendrons and an increase in the amplitude of thermal vibrations. As a result, the average tilt of dendrons with respect to the axes of supramolecular aggregates in a disordered columnar phase is 90°. Therefore, the transition to the disordered columnar phase leads to a sharp increase in the diameter of columnar aggregates rather than to a decrease in this diameter, as in the above-considered examples of ILCs. It is also worth noting that supramolecular aggregates have helical symmetry different for different dendrons (see Fig. 117 *a*).

Many biological macromolecules (proteins [771] and DNA [772,773]) require the chiral organization of their supramolecular aggregates. Hence, in recent years, researchers have paid great attention to the self-assembly and self-organization of optical stereoisomers of different nature.[774–785]

Let us consider the most interesting, in our opinion, example intermediate between the self-assembly and self-organization. Six helicoidal molecules based on [7]-heterohelicene (**372**) form helical aggregates of the first level, which, in turn, are arranged in supramolecular columns with symmetry 13_2. The helical symmetries of the aggregates

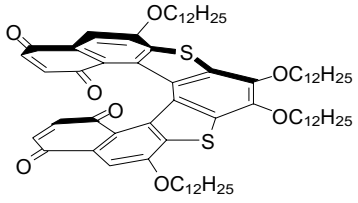
Structures 371



371

X is a focal group (*e.g.*, OH) or a polymer chain

Structure 372



372

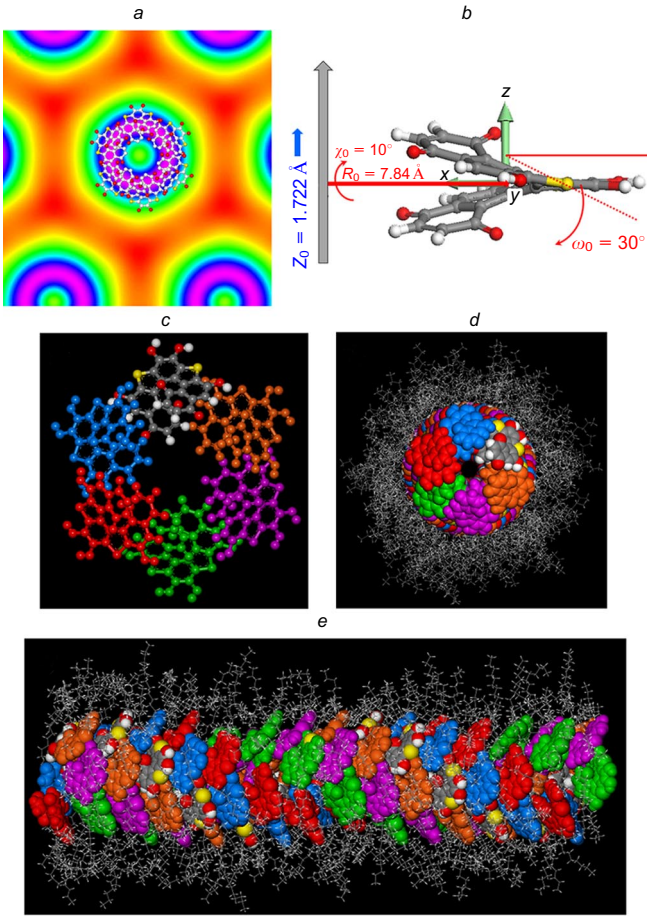


Figure 118. Electron density distribution in an ordered columnar phase composed of [7]-heterohelicene molecules **372**: the calculated model of the supramolecular aggregate composed of six molecules is superimposed on the high electron density zone (*a*); structural parameters (*b*) and the results of simulation (*c*), the top view (*d*) and the lateral view (*e*) of helical cylindres, formed by [7]-heterohelicene.[786] R_0 is the distance from the centre of gravity of the molecule to the column axis; χ_0 is the angle of rotation of the molecule around the radius of the helix (fan angle), ω_0 is the angle of rotation of the molecule around the intramolecular axis *y* (tilt angle), Z_0 is the vertical shift of two adjacent molecules with respect to each other. Published with the permission of Wiley.

of different levels are significantly different. Supramolecular columns are characterized by the presence of a rather wide axial channel with a size of 7–8 Å (Fig. 118). The self-assembly of supramolecular aggregates leads to the selection of optical isomers. Thus, each individual column is composed of molecules with the same chirality.[786, 787]

3.4. Supramolecular design of functional nanosystems based on amphiphilic compounds: fundamental aspects and prospects for biomedical applications

Supramolecular systems based on amphiphilic compounds (surfactants, lipids, polymers, macrocycles) are widely used in modern nano- and biotechnology to create drug delivery systems, modify and stabilize various dispersions in the food and cosmetics industry, agriculture, production of protective coatings, *etc.*[788, 789] The practical application of supramolecular systems is based on the amphiphilic nature of building blocks, which ensures their affinity to both hydrophilic and hydrophobic objects (molecules, surfaces, particles), as well as the related ability to self-assemble at the interfaces and in the bulk solution to form nanoscale aggregates of various morphology: micelles, microemulsions, vesicles, liquid crystals.[788, 790] An important property of such aggregates is their solubilizing activity toward poorly soluble compounds.[791] This explains the high level of interest in the use of supramolecular systems based on amphiphiles of open-chain and macrocyclic structure as nanocontainers for concentrating, stabilizing and delivering drug substances for various purposes.[792]

This part of the review focuses on two relevant areas that attract the attention of researchers at the current stage of development of supramolecular and colloidal chemistry. The first one is related to the problems of self-assembly and functional activity of cationic amphiphilic compounds, their biomedical potential in drug delivery and design of lipoplexes, micellar and microemulsion nanocontainers, liposomes and supra-amphiphilic structures involving macrocycles. The second area concerns nonequilibrium supramolecular carrier systems based on non-ionic surfactants (niosomes, nanoemulsions, transferosomes), which have broad prospects for practical use as drug delivery systems and the development of compositions based on them with improved mucoadhesive properties suitable for noninvasive drug administration.

3.4.1. Supramolecular systems based on cationic surfactants: self-assembly, construction and modification of nanocontainers and complex formation with biopolyanions

In biomedicine, cationic surfactants have received quite a lot of attention due to their high affinity to cell membranes and intracellular organelles (in particular mitochondria), biopolyanions, for example, DNA, high antimicrobial activity, *etc.*[793, 794] Despite the large number of publications, the search for new amphiphilic compounds that meet the criteria of modern technologies remains a relevant task. The main requirements are low aggregation thresholds, reduced toxicity, biodegradability and the capacity for multipoint interactions that enhance the binding of guest molecules (drugs and diagnostic probes). For this reason, the current scientific literature covering fundamental and applied aspects of supramolecular systems focuses on the design of novel amphiphilic compounds and evaluation of their characteristics.[795]

3.4.1.1. Cationic surfactants containing a pyrimidine moiety

The introduction of natural moieties into amphiphilic molecules is a pronounced trend in the design of amphiphilic compounds and is aimed at obtaining biocompatible supramolecular systems with affinity to biomolecules. Reviews of Zakharova *et al.*[796, 797] summarize the results of systematic studies of various surfactants, including pyrimidine-containing macrocyclic (pyrimidinophanes) and open-chain mono-, di- and multicationic compounds differing in hydrophobicity (the number and length of alkyl chains) and in the nature of the spacer. These publications establish the regularities of self-assembly of pyrimidine-containing surfactants characterized by the presence of a bulky pyrimidine moiety in the spacer and the macrocyclic structure of the molecule, which prevent the dense packing of the surfactant during aggregation. These factors cause rather high values of the packing parameter and a specific association pattern differing from that of the conventional cationic trimethylammonium (TMA) surfactants. Most of pyrimidine surfactants tend to form large aggregates with

diameters close to 100 nm and are capable of structural rearrangements. The loose packing of pyrimidine-containing surfactants in aggregates underlies a unique phenomenon, a shift in solution pH above the critical micelle concentration. The probable cause of this is ionization of water molecules in the head group shells due to low degree of binding of counterions and excess surface charge of the aggregates. As a consequence, a hydroxide–hydroxonium ion pair is generated, with the hydroxide ions remaining in the Stern layer due to electrostatic interaction with the positively charged head groups, and the hydroxonium ions located in the bulk phase. The controlled self-assembly ability, the morphological lability and the presence of a natural moiety complementary to the nucleotide units of DNA formed the basis for the development of supramolecular nanocontainers made of pyrimidine-containing surfactants for the delivery of gene material and hydrophobic bioactive substances, including pH-dependent low-toxic nanocontainers.[796, 797]

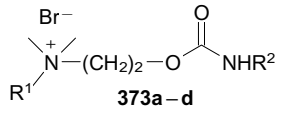
3.4.1.2. Biodegradable amphiphilic compounds

One of the most important criteria when selecting amphiphilic building blocks is their biodegradability. In this connection, much attention is paid to the design of so-called degradable surfactants, which contain groups that are detached under the action of enzymes, such as ester, amide and carbamate groups.[798] In accordance with this trend, a homologous series of carbamate-containing surfactants **373a–d** with ethyl and butyl substituents in the carbamate moiety was synthesized.[799, 800] It was shown that introduction of carbamate moiety decreases the CMC (~5-fold) and the Krafft temperature (by up to ~15 °C) in comparison with those for typical surfactants with TMA head group and increases the half-lethal dose (LD_{50}) from 27 [for cetyltrimethylammonium bromide (CTAB)] to 80–100 mg kg^{-1}. Consequently, this series of cationic surfactants belongs to the category of moderately toxic compounds. It was shown that carbamate-containing surfactants can be used as effective micellar nanocontainers for hydrophobic guest molecules. They provide higher solubilization activity in the low concentration range than conventional TMA-containing surfactants, probably due to the additional contribution of hydrogen bonds to the aggregation and binding of the guests. A significant advantage of carbamate-containing surfactants is their antimicrobial activity, which is comparable or superior to that of commercial products Norfloxacin and Ketoconazole, and also a combination of antibacterial and antifungal activities.[799]

Further improvement of the aggregation and functional properties of compounds **373b,c** was undertaken by Mirgorodskaya *et al.*[800] Mixed micellar systems and oil/water microemulsions with the addition of nonionic surfactants Tween 80, Tween 20 and Triton-X-100 were formed in order to reduce the CMC and improve the toxicity characteristics. A negative deviation of the behaviour of these binary systems from the ideal mixing behaviour was shown. In the course of the research, the mixture composition was optimized in order to achieve a balance between practically valuable characteristics of both surfactants: retention of the positive surface charge, high solubilization capacity and antimicrobial activity of cationic surfactants in combination with low CMC and low acute toxicity of nonionic amphiphiles. Low-toxicity nanocontainers of micellar and microemulsion types for the hydrophobic drug Meloxicam were obtained as a result of optimization, allowing increasing its solubility in water by a factor of 575.

Supramolecular systems based on carbamate-containing surfactants can act as selective traps for binding and concentrating polycyclic aromatic pollutants.[801] High solubilization capacity of **373b**-based systems toward naphthalene was found, exceeding that toward anthracene by two orders of magnitude. Moreover, an example of the use of carbamate-containing surfactants **373a,b** as adjuvants enhancing the efficiency of plant protection products was reported [802] (Fig. 119). Nanoscale supramolecular compositions based on the Lontrel pesticide were developed to improve its wetting effect and penetration in the treatment of plants. The main factors controlling the efficacy of such compositions are surfactant structure and concentration, treatment time and temperature. The greatest effect was detected for compound **373a**, for which a higher increase in efficacy was observed with increasing temperature.

Structures 373



373a–d

R^2 = Bu^n: R^1 = n-$C_{14}H_{29}$ (**a**), n-$C_{16}H_{33}$ (**b**), n-$C_{18}H_{37}$ (**d**); R^1 = n-$C_{16}H_{33}$, R^2 = Et (**c**)

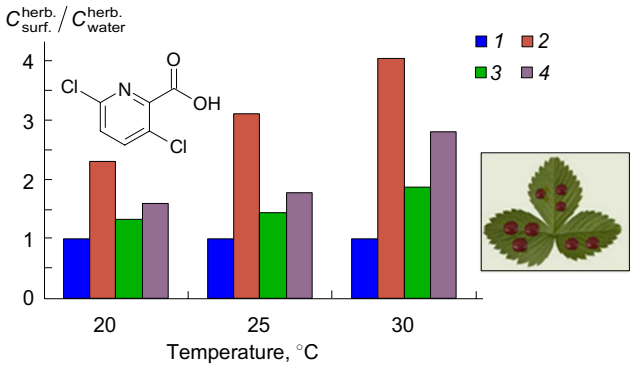
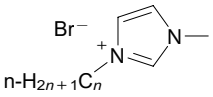


Figure 119. Structure of Lontrel and effect of temperature on its content in the plant in the absence (*1*) and in the presence of carbamate-containing surfactants **373a** (*2*) and **373b** (*3*) and CTAB (*4*). C^{herb} is the concentration of Lontrel herbicide when delivered to the plant in an aqueous or aqueous micellar solution.[802] Published with permission from Elsevier.

3.4.1.3. Cationic surfactants with imidazolium head group

Imidazolium surfactants constitute a separate class of amphiphilic compounds and ionic liquids, which is widely demanded in the design of polyfunctional supramolecular compositions and their use in synthetic and technological development of drug delivery systems.[803] Therefore, the design and study of new imidazolium surfactants is of significant interest from both theoretical and practical points of view. Samarkina *et al.*[804, 805] synthesized a homologous series of imidazolium surfactants **374a–d** and carried out a systematic study of their self-organization at the interface between phases and in the bulk solution; a significant potential of these products in the field of biomedicine was demonstrated. For imidazolium surfactants **374a–d**, the CMC was found to decrease fourfold with an increase in the length of the alkyl substituent by one methylene unit.

Structures 374



n = 12 (**a**), 14 (**b**), 16 (**c**), 18 (**d**)

374a – d

The morphological behaviour of the lower and higher homologues is significantly different. The tetradecyl derivative **374b** is characterized by the formation of small spherical micelles < 10 nm in size, and the higher homologues form large aggregates with a hydrodynamic diameter (D_h) of ~100 nm. The ζ-potential of the aggregates increases with increasing alkyl chain length in the range of 65 – 90 mV. At the same time, the solubilization activity of the systems changes little with hydrophobicity of the surfactant.

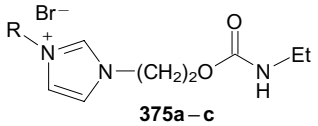
An important property of amphiphilic compounds is their membranotropic activity, *i.e.*, the ability to integrate into the lipid bilayer of cell membranes. For the homologous series of imidazolium surfactants, it was established that the membranotropic properties depend on the length of the alkyl substituent. For compounds **374b**,**c**, a significant decrease in the main phase transition temperature of dipalmitoyl phosphatidylcholine in the presence of surfactants was shown, which is associated with disordering of the bilayer due to the integration of surfactant molecules. Meanwhile, in the case of surfactant **374d**, the main phase transition temperature increases, which correlates with the stabilization of the bilayer structure. For hydrophobic drug Indomethacin, it was shown that it does not penetrate into the lipid bilayer, while the integration of the imidazolium surfactant **374b** into the liposome provides the membranotropic ability of the system.

Cationic surfactants are widely used as nucleic acid transporters.[806] The interaction of positively charged surfactant head groups with the phosphate anions of nucleotide units leads to charge neutralization and compaction of the DNA macroion, which facilitates its delivery across cell membranes. Imidazolium surfactants **374a – d** were investigated as nanocontainers for oligonucleotides. It was shown that the surfactant – oligonucleotide complexes (lipoplexes) do not exceed 250 nm in size and, in the case of higher homologues, they are formed at rather low ratios of surfactant to oligonucleotide. A specific feature of this series of homologues is the absence of recharging of lipoplexes with an increase in the surfactant concentration: in the course of complexation, a compensatory change in the ζ-potential was observed, but no change in the negative charge of phosphate anions with increasing proportion of surfactants was detected. Probably, in contrast to the TMA series, complexation occurs not only due to electrostatic interactions, but also due to alternative mechanisms, including, for example, the contribution of hydrophobic and intercalation effects.

Studies of the interaction of imidazolium surfactants with natural polyanions were continued by Samarkina *et al.*[805] in relation to the interaction of the homologous series of imidazolium surfactants **374a – d** with BSA. The surfactant – protein systems are of interest from the point of view of the effect of amphiphilic compounds on the processes of denaturation and stabilization of biopolymers, and also for studying the mechanisms underlying a number of serious diseases of the central nervous system.[807] It was found that the addition of BSA has a synergistic effect on the aggregation of imidazolium surfactants, providing a 50-fold decrease in CMC values. The formation of nanocomplexes with a hydrodynamic diameter of ~10 nm is mediated by the contribution of tryptophan moieties of the protein, which is confirmed by the data of polarization fluorescence spectroscopy. Polymer-colloidal complexes of **374a – d** with BSA exhibit improved solubilization activity toward hydrophobic spectral probes and drugs (for example, Metronidazole) in comparison with separate components, and this activity increases with increasing hydrophobicity of surfactants. Nanocontainers based on binary systems provide prolonged drug release (fourfold retardation) and the ability to penetrate the lipid bilayer.

To improve the aggregation and functional characteristics and also the biomedical potential of imidazolium surfactants, amphiphilic compounds **375a – c** containing an additional carbamate moiety were synthesized.[808] The functionalization resulted in a 2 – 3 times lower CMC and enhanced membranotropic activity of the systems compared to their imidazolium analogues. In addition, this series exhibited more diverse morphological behaviour, which was controlled by hydrophobicity and surfactant concentration. In particular, a transition takes place from small spherical micelles formed in solutions of compound **375b** at low concentrations to large aggregates (~100 nm) formed at higher concentrations.

Structures 375



R = n-$C_{14}H_{29}$ (**a**),
n-$C_{16}H_{33}$ (**b**),
n-$C_{18}H_{37}$ (**c**)

375a – c

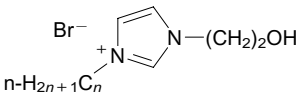
The biomedical potential of supramolecular systems based on surfactants **375a – c** was confirmed by the effective formation of lipoplexes. In contrast to imidazolium surfactants, the complexation of compounds **375a – c** with the oligonucleotide was accompanied by recharge of the system, which indicates the predominant contribution of the electrostatic mechanism. In addition, this homologous series exhibited improved antimicrobial properties against a number of bacterial and fungal strains, which are superior to those of commercial reference drugs in the concentration range characterized by a low hemolytic activity of surfactants (not more than 0.9%).

An evaluation of the surfactant complex-forming ability in relation to BSA showed a synergistic nature of the interaction, which is confirmed by a 5 – 8-fold decrease in the aggregation threshold.[809, 810] The use of a combination of fluorescence spectroscopy and circular dichroism techniques shed light on the nature of the interaction between the components. It was shown that complex formation involves tryptophan residues of the protein and occurs *via* contributions of van der Waals and electrostatic forces in combination with hydrophobic effect, with the balance between them being controlled by the length of the alkyl group of the surfactant. Using compound **375b** as an example, it was shown that the addition of a surfactant causes partial reversible destruction of α-structures and an increase in the fractions of β-structures and disordered hydrophobic domains.

An effective technique to modify the properties of amphiphilic molecules is their functionalization with hydroxy-containing moieties, which makes it possible to

change the micropolarity and involves hydrogen bonding into the processes of aggregation and binding of guest molecules. A series of imidazolium surfactants **376a–c** with a 2-hydroxyethyl moiety was synthesized.[811] The presence of OH in the head group of these surfactants somewhat reduces the CMC and enhances the solubilization activity of the systems, while maintaining a high level of antimicrobial properties. As in the case of compounds **375a–c**, the introduction of a new structural moiety increases the diversity of the morphological behaviour of supramolecular systems: transition from spherical micelles formed for lower homologues to large aggregates (~100 nm) with increasing hydrophobicity of surfactants is observed. When the particles are visualized by electron microscopy, the formation of cylindrical micelles in the system based on surfactant **376b** is detected.

Structures 376



n = 12 (**a**), 16 (**b**), 18 (**c**)

376a–c

OH-functionalization enhances the membranotropic activity of the compounds, which increases in the following surfactant series: TMA < imidazolium < hydroxyethylated imidazolium.[811,812] In the case of hydroxyethylated imidazolium surfactants **376a–c**, the effect depends on the length of the alkyl substituents. For lower members of the series, disordering of the lipid bilayer (decrease in the main phase transition temperature) with increasing surfactant : lipid ratio was observed, while compound **376c** stabilized the bilayer, contributing to the liquid crystal–gel transition.

A study of the complex formation of hydroxyethylated imidazolium surfactants with oligonucleotides[810] confirmed the regularities first established for unsubstituted imidazolium surfactants. The formation of nanosized (200–250 nm) lipoplexes was shown. Despite the high binding efficiency of the components confirmed by quenching of the fluorescence of the ethidium bromide intercalator, no recharging of the complex occurs, indicating the domination of alternative mechanisms over electrostatic interactions. Probably, the key role in this case is played by the structure of the head group (transition from TMA to imidazolium derivative), whose functionalization with hydroxyethyl moieties has no significant effect. Meanwhile, as shown above, carbamate-containing imidazolium surfactants caused not only the compensation of the negative charge of the phosphate anions, but also the transition to the region of positive ζ-potentials, as in the case of TMA analogues and some other cationic surfactants with pyrimidine and morpholinium moieties.[796,797] Fluorescence microscopy visualized the internalization of lipoplexes by M-HeLa cells,[808] which confirms the potential of the formed supramolecular systems as nanocontainers for intracellular delivery of gene material.

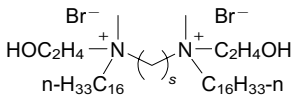
3.4.1.4. Gemini surfactants

Among the new generation of amphiphilic compounds, much attention has been paid to dimeric (gemini) surfactants, which contain two head groups linked to alkyl chains and a spacer of variable length.[813,814] Along with the key factor of hydrophobicity of amphiphilic compounds, which determines their level of aggregation activity, the properties of gemini surfactants are largely controlled by the nature, length and flexibility of the spacer and by the presence of heteroatoms and rings. Therefore, the current literature is focused on aspects related to the design of gemini surfactants and elucidation of structure–property relationships in homologous series.

In contrast to conventional gemini surfactants, their OH-functionalized counterparts have hardly been studied, although significant effects of hydroxyalkyl moieties on the aggregation properties and functional activity have been shown for monocationic surfactants.[815] This gap was partially filled by Zakharova and co-workers,[816,817] who performed a systematic study of a series of gemini surfactants **377a–d** with different spacer lengths containing a hydroxyethyl moiety in the head group. A comparison of compounds **377c** and **378**[818] shows that OH-functionalization of the spacer has less effect on surfactant properties than in the case of introduction of substituents in the head groups. This may be due to lower accessibility of the OH groups in the spacer for hydrogen bonding with guest molecules.

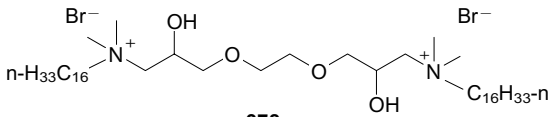
A comprehensive study of the self-assembly of a series of gemini surfactants **377a–d** was initiated by the results demonstrating a high efficiency of transfection of eukaryotic cells, which was comparable or superior to that of commercial products and was regulated by the length of the spacer, increasing in the series of compounds **377b** < **377a** < **377d**.[816] The highest level of transfection found for surfactant-based lipoplexes with a dodecamethylene spacer should have been determined by the specific structural characteristics of the systems. The set of data from diffusion-ordered NMR spectroscopy, DLS and fluorescence anisotropy showed the formation of spherical aggregates of 4–7 nm in size in all systems in the CMC region. With an increase in the surfactant concentration, an increase in the size, aggregation numbers, and ζ-potential of the particles was observed. A specific structural feature of aggregates based on compound **377d** is a looser molecular packing and labile morphological behaviour, which is consistent with the calculation of the packing parameter, fluorescence anisotropy, higher micropolarity in the site of location of the fluorescent probe and a higher degree of hydration of the peripheral region of the aggregates. In addition, compound **377d** exhibits enhanced membranotropic properties.[817] An increase in the efficiency of transfection with increasing spacer length correlates with a higher efficiency of complexation of surfactant with oligonucleotides found for surfactant **377d** by quenching of the ethidium bromide fluorescence and with neutralization of the charge of nucleotide units. However, this effect is not confirmed by the data of gel electrophoresis and docking, which attest to a low degree of electrostatic interaction of the components in the **377d**–oligonucleotide system. Probably, in this case, the key factors are hydrophobic inter-

Structures 377, 378



s = 4 (**a**), 6 (**b**), 10 (**c**), 12 (**d**)

377a–d

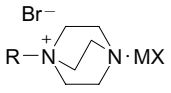


378

actions and conformational and morphological lability of the amphiphile, which allows for a favourable orientation during the formation of lipoplexes.

3.4.1.5. Metal-containing surfactants

Supramolecular systems based on an amphiphilic matrix incorporating an inorganic structural moiety can be used to design new hybrid organic-inorganic nanomaterials, which have a range of specific properties required in modern technologies. Such amphiphilic building blocks include metal-containing surfactants (metallosurfactants),[789] which are widely used in template synthesis and homogeneous catalysis, as well as in biomedical applications as non-viral vectors, diagnostic probes, antimicrobial agents, *etc*.



379a – g

Structures 379

R = n-$C_{14}H_{29}$, MX = $La(NO_3)_3$ (**a**);
R = n-$C_{16}H_{33}$: MX = $La(NO_3)_3$ (**b**),
$CuBr_2$ (**c**), $Cu(NO_3)_2$ (**d**), $Co(NO_3)_2$ (**e**),
$Ni(NO_3)_2$ (**f**); R = n-$C_{18}H_{37}$, MX = $La(NO_3)_3$ (**g**)

Despite the widespread use in practice, fundamental aspects of the formation of supramolecular systems based on metallosurfactants have been little studied. For example, a series of works[819 – 824] is devoted to the synthesis, self-organization and functional activity of complexes **379a – g** of cationic surfactants based on 1,4-diazabicyclo[2.2.2]octane

Table 7. Quantitative parameters characterizing the aggregation and solubilization activities of cationic surfactants.[799, 800, 804, 806, 808, 811, 816, 818 – 826]

Cationic surfactant	CMC (tens.), mmol L^{-1}	D_h, nm	N_{agg}	ζ-potential, mV	β	S
373a	1.0	–	69	–	0.56	0.0125 (*1*)
373b	0.24	3 – 5	35	106 [d]	0.51	0.024 (*1*)
						0.451 (*2*)
						0.007 (*3*)
						0.375 (*4*)
						0.226 (*5*)
373c	0.75	–	29	–	0.54	0.027 (*1*)
						0.186 (*5*)
373d	0.09	–	23	–	0.55	0.0207 (*1*)
374a	10	4 – 6	–	40	–	–
374b	2.7	6 – 10	–	65	0.90	0.01 (*1*)
374c	0.9	100	–	75	0.91	0.014 (*1*)
374d	0.7	118	–	90	0.94	0.019 (*1*)
375a	1.3	2 – 4	16	50	–	0.0037 (*1*)
375b	0.3	2 – 120	40	80	–	0.0021 (*1*)
375c	0.1	2 – 10	38	60	–	0.0075 (*1*)
376a	2	2 – 4	44	59	0.73	0.02 (*1*)
376b	0.6	80 – 150	142	76	0.80	0.031 (*1*)
376c	0.2	90 – 250	150	89	0.95	0.037 (*1*)
377a	0.0014	⩽10	12	–	–	0.029 (*1*)
377b	0.0045	⩽10	18	–	–	0.036 (*1*)
377d	0.008	⩽10	28	50 – 80	–	0.016 (*1*)
378	0.03	–	–	–	–	0.034 (*1*)
379a	2.37	5 – 6	21 – 46	20 – 60	0.33 – 0.4	0.028 (*1*)
379b	0.33	4 – 6;	24 – 27	–	0.85 – 0.95	0.103 (*1*)
		69 – 83; 339				0.126 (*6*)
379c	0.65	1 – 6;	20 – 29	50 – 80	0.76 – 0.90	0.0495 (*1*)
		120 – 240				0.254 (*7*)[a]
						0.0167 (*7*)[b]
379d	0.38	4 – 6;	16 – 25	37 – 75	0.85 – 0.90	0.053 (*1*)
		28 – 68				0.120 (*8*)
379e	0.60	5 – 7; 44 – 105	23 – 44	37 – 75	–	0.034 (*1*)
379f	0.56	6 – 7; 50 – 59	21 – 64	5 – 25	0.28 – 0.30	0.023 (*1*)
379g	0.097	39 – 61; 228	10 – 30	50 – 60	0.49 – 0.7	0.109 (*1*)
380d	2.0	–	11	78 [c]	0.45	0.029 (*6*)
						0.013 (*1*)
380e	0.33	1.7	6	92 [c]	0.50	0.043 (*6*)
						0.020 (*1*)
380g	0.10	3.4	2	108 [c]	0.75	0.054 (*6*)
						0.0277 (*1*)

Note. The following designations are accepted: CMC (tens.) is critical micelle concentration obtained by tensiometry; N_{agg} is the micelle aggregation number; β is degree of binding of counterions by micelles; S is solubilization capacity in relation to Orange OT (*1*), naphthalene (*2*), anthracene (*3*), Indomethacin (*4*), Meloxicam (*5*), Sudan I (*6*), Nitrofurantoin (*7*), Griseofulvin (*8*). [a] In the pre-micellar concentration range. [b] In the area above the CMC. [c] Surface potential.

derivatives (DABCO-*n*, where *n* is the number of carbon atoms in the alkyl substituent) with transition metal salts.

Complexes **379b**,**d**–**f** formed by the hexadecyl derivative with La^{III}, Cu^{II}, Co^{II}, Ni^{II} nitrates, respectively, exhibit higher aggregation activity compared with the amphiphilic ligand DABCO-16, and the CMC value changes, depending on the nature of the metal, in the series Co ~ Ni > Cu ~ La.[820,821] It was found that vesicle–micelle morphological rearrangements take place in solutions of metal complexes, which is confirmed by a decrease in the fluorescence anisotropy and decrease in the aggregate size (D_h) from ⩾100 to ⩽10 nm with increasing surfactant concentration (Table 7) and also by increasing pyrene eximerization coefficient, equal to the ratio of fluorescence intensity of the excimer and pyrene monomer in the region preceding the CMC. According to DLS data, a bimodal aggregate size distribution occurs for the majority of metallosurfactants. This probably indicates the coexistence of micelles and vesicles in the studied systems, which are in dynamic equilibrium, but micellar nanoparticles dominate as the fraction of metallosurfactants in the solution increases.

Acute toxicity assays showed 2–6 times higher LD_{50} values for metal complexes **379** compared to those of a classical surfactant, CTAB, which allowed them to be classified as moderately or low toxic. The lowest toxicity was found for complex **379b** (DABCO-16 with lanthanum nitrate). Like the parent ligand, the metal complexes have antimicrobial activity accompanied by higher selectivity and are superior to Norfloxacin against several strains (*Staphylococcus aureus*, *Bacillus cereus*).

Metallosurfactants exhibit high potential as micellar nanocontainers.[820,821] Their solubilization capacity toward the hydrophobic spectral probe Orange OT was shown to increase in the series **379f** < **379e** < **379d** < **379b** (see Table 7). These findings were used to increase the solubility of the hydrophobic antifungal agent Griseofulvin.[824] Micellar nanocontainers based on DABCO-16 complexes with Cu^{II} (**379d**) and La^{III} (**379b**) nitrates were formed, for which an even higher solubilization capacity was achieved than that of Orange OT. An additional advantage of these systems is their activity in a low concentration range: the solubilization capacity of the pre-micellar aggregates was higher than that of the micellar structures. In addition, the drug efficacy was enhanced by the antimicrobial activity of the amphiphilic metal complexes themselves.

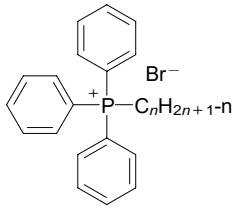
Zhiltsova *et al.*[822,823] synthesized a DABCO-16 complex with copper dibromide (**379c**), which showed a slightly lower aggregation activity than the complex with copper nitrate. DLS studies confirmed the tendency of metallosurfactants to polymorphism: transition from large vesicular-type aggregates formed in the low-concentration range to small micelles was observed as the CMC was attained. Evaluation of the solubilization capacity of such systems showed similar values for DABCO-16 complexes with copper nitrate (**379d**) and bromide (**379c**) toward Orange OT (see Table 7). Micellar nanocontainers based on **379c** were used to increase the solubility and bioavailability of the antimicrobial drug Nitrofurantoin.[823] A high solubilization capacity (S = 0.254) of this compound was found in the premicellar range, which was 15 times higher than the effect found in the concentration range above the CMC (S = 0.0167). As in the case of traditional amphiphilic compounds, the properties of metallosurfactants are largely controlled by the length of the alkyl substituent. In relation to lanthanum nitrate complexes, it was shown that the CMC values were 2.37, 0.33 and 0.097 mmol L^{-1} in the series of ligands with R = n-$C_{14}H_{29}$ (**379a**), n-$C_{16}H_{33}$ (**379b**) and n-$C_{18}H_{37}$ (**379g**).[819] The solubilization capacity increases by a factor of five on going to higher homologues.

3.4.1.6. Cationic surfactants with a phosphonium head group

Amphiphilic compounds with phosphonium head group have high potential for biomedicine. First of all, this concerns triphenylphosphonium (TPP) derivatives **380a**–**g**, which are considered as highly effective systems of drug delivery into mitochondria,.[794] The aggregation behaviour of TPP–surfactant series significantly differs from that of conventional cationic surfactants.[825,826] It was shown[825] that, although the slope of the linear dependence of log CMC on n (n is the number of carbon atoms in the alkyl group), characterizing the surfactant aggregation activity, is close to 0.3 and coincides with that for a wide range of cationic surfactants, the plot of this dependence for TPP series lies much lower than that for other surfactants. This attests to superior aggregation properties of this homologous series. Another significant advantage compared to TMA analogues is high solubilization capacity of TPP-based nanocontainers. It was suggested[825] that the additional non-polar domain formed by the benzene rings of such surfactants contributes to the solubilization process. Furthermore, the selectivity of micellar TPP containers to guest molecules of various structures, in particular the spectral probes Orange OT and Sudan I, is noteworthy (see Table 7).

Zakharova *et al.*[827] reported the first example of a study of TPP surfactants as nanocontainers for DNA decamer. A high degree of component affinity was shown, which increased with increasing surfactant hydrophobic substituent length, indicating the contribution of cooperative binding involving surfactant aggregates. The cytotoxicity assay revealed a dependence of the effect on the surfactant hydrophobicity: the highest cytotoxicity was observed for compounds **380d**,**e**, while for the terminal members of the series (**380a**,**g**), the cytotoxicity decreased. In addition, charge neutralization during formation of lipoplexes was also accompanied by a decrease in the toxicity. Thus, high aggregation activity, pronounced membranotropic properties and the ability to form lipoplexes cause a high level of scientific interest in these compounds and confirm their practical potential for the development of drug delivery systems.

Structures 380



n = 7 (**a**), 9 (**b**), 10 (**c**), 12 (**d**), 14 (**e**), 16 (**f**), 18 (**g**)

380a–**g**

3.4.1.7. Liposomes modified with cationic surfactants

Liposomes are the most demanded drug delivery systems.[828] In order to improve their properties, first of all, the efficiency of loading and encapsulation, duration of circulation and targeted delivery and to reduce side effects, several generations of liposomal systems have been devel-

oped to date. One of the effective approaches to improve the properties of liposomes is their modification aimed at increasing stability and specificity to diseased cells. The frequently applied methods include liposome pegylation, covalent functionalization with targeting moieties, *etc*. In contrast to the covalent strategy, non-covalent liposome modification is a relatively new method, little described in the literature.

The interest in cationic carriers is associated primarily with the search for systems for DNA transport and targeted drug delivery to cell organelles, in particular to mitochondria. There are only few studies dealing with the fabrication of cationic liposomes using the non-covalent strategy. Kuznetsova *et al.*[829,830] fabricated DPPC-based liposomes modified with cationic surfactants with imidazolium and TPP groups. When creating liposomal delivery systems, the authors optimized the composition in order to maintain a balance and preserve the advantages of both lipid components (low toxicity, biocompatibility) and cationic surfactants (the presence of a positive charge, providing the affinity for cell membranes and particle stability). In the case of imidazolium surfactants, liposomes of 70 – 100 nm in size and with high ζ-potential (up to 45 – 70mV) were obtained and remained stable for six months. The properties of liposomes were controlled by varying the surfactant to lipid ratio and surfactant hydrophobicity. The compositionally optimized liposomes were used to encapsulate Metronidazole; the highest encapsulation efficiency (75%) was obtained for octadecyl derivative **380g**. Prolonged release of this drug from modified liposomes was demonstrated.

Kuznetsova *et al.*[830] reported one of the first examples of non-covalent modification of liposomes with a TPP surfactant. For the first time, systematic optimization of the composition of liposomes was carried out and the influence of the structural factor on the properties and stability of systems was revealed. The best results were obtained using dodecyl (**380d**) and tetradecyl (**380e**) derivatives of TPP surfactants. Using Rhodamine B as an example, it was shown that an increase in the surfactant content promotes accelerated release of guest molecules. Successful highly efficient encapsulation of Metronidazole and Doxorubicin was performed and prolonged drug release was demonstrated. All functional parameters of modified liposomes (stability, loading and release) were higher by a large factor than those of lipid liposomes. Using the example of pancreatic tumour cells, it was for the first time reliably shown by confocal microscopy that non-covalently modified liposomes containing an amphiphilic TPP cation provide a higher degree of colocalization with mitochondria than unmodified carriers (Fig. 120).

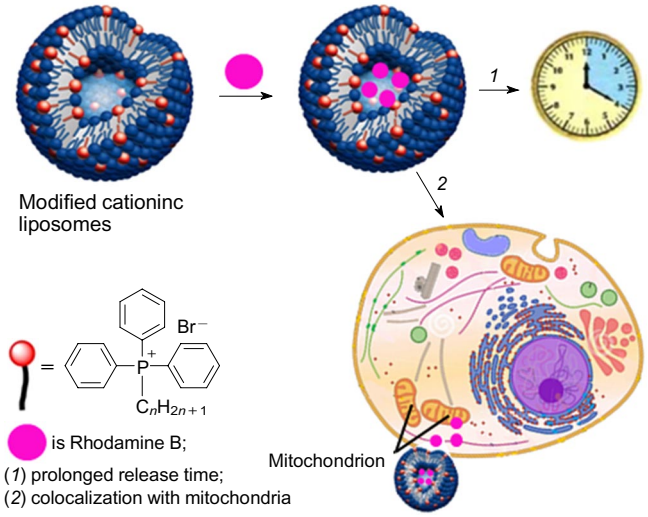


Figure 120. Mitochondria-targeted cationic liposomes modified with TPP bromides and loaded with hydrophilic substrates.[830] Published with the permission from the Royal Society of Chemistry.

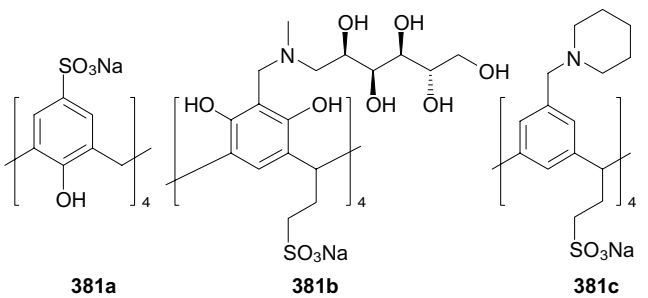
3.4.1.8. Supramolecular amphiphiles based on surfactants and macrocycles

One of the promising methods for obtaining functional assemblies is to combine various components through non-covalent interactions. This approach avoids lengthy procedures for the formation of complex nanostructures using organic solvents, which meets the criteria of green chemistry. The supramolecular amphiphiles (supra-amphiphiles) are fabricated with participation of flexible open-chain surfactant molecules and macrocyclic molecules with a rigid skeleton. Unlike traditional amphiphilic compounds, in supra-amphiphilic systems, hydrophobic and hydrophilic parts are linked *via* non-covalent interactions.[831] The dynamic nature of the formation of non-covalent bonds in supra-amphiphiles determines a reversible change in their physicochemical properties, which is important for creating smart stimuli-responsive nanomaterials. The wide opportunities of modifying the rims of the calixarene platform with various functional groups allow for the design of such systems, which is confirmed by recent reviews.[453 – 455,832]

Sulfonate derivatives of calix[4]arenes are most often used to fabricate supra-amphiphilic systems. The complexation of these macrocycles with cationic surfactants affords supra-amphiphiles, which are capable of aggregation at lower concentrations than single surfactant molecules. It should be noted that, in contrast to other macrocycles (cyclodextrins and cryptands), the CMC value of gemini surfactants can decrease 1000-fold in the presence of sulfonate calix[4]arene **381a**.[833] Moreover, a comparison of complexation of cyclodextrins, cucurbiturils and sulfonate calix[n]arenes (n = 4, 5 or 6) with ammonium derivative of tetraphenylethylene showed that, in addition to the electrostatic factor, pre-assembled cyclic scaffold and the encapsulating capacity of the inner cavity of calix[4]arene play a decisive role in the efficient co-aggregation.[834]

Supra-amphiphiles based on sulfonate calix[4]resorcinarene **381b** and a cationic viologen surfactant with a hexadecyl substituent, in turn, can aggregate into various

Structures 381



381a **381b** **381c**

assemblies that can function as nanocontainers for both hydrophobic and hydrophilic substrates.[835] Varying the ratio of the macrocycle to surfactant in these systems allows for the control over substrate binding and release by changing the morphology of assemblies,[836] which makes this supramolecular approach promising for biomedical applications. However, in the case of co-aggregation of calix[4]arenes with a cationic surfactant, it is necessary to take into account the toxicity of the latter.[837,838] Co-aggregation of sulfonate calix[4]arenes can also be realized with an anionic surfactant, sodium dodecyl sulfate (SDS), if besides sulfonate groups, pH-dependent amino groups, such as piperidine moieties, are present in the macrocycle structure at the upper rim (**381c**).[839] Acidification leads to protonation of the amino groups of the macrocycle and electrostatic interaction with negatively charged sulfo groups of the surfactant. As a result, a morphological transition from spherical surfactant micelles (Fig. 121 *a*) to mixed rod-shaped aggregates (Fig. 121 *b*) occurs, accompanied by an increase in solubilization of the hydrophobic flavonoid quercetin (Fig. 121 *c*).

Analysis of the literature data indicates a high level of interest in the design of functional supramolecular systems based on amphiphilic compounds, especially cationic surfactants, and their broad demand for targeted drug and gene delivery, increasing the solubility and bioavailability of hydrophobic compounds, prolongation of therapeutic action and overcoming biological barriers. Despite their high biotechnological potential, nanocontainers based on cationic surfactants have a number of limitations related to their toxicity, which can be overcome by targeted functionalization of the amphiphilic matrix, for example by creating metallomicelles,[819–824] mixed compositions with non-ionic surfactants[800] or hybrid liposomes.[829,830] Furthermore, micellar nanocontainers are dynamic systems capable of uncontrolled decay under biomicroenvironment conditions. The material presented below in this Section focuses on alternative systems based on non-ionic surfactants, which include nanoemulsions, liposomes, transferosomes, *etc.* Particular attention is paid to the modification of the systems to improve their mucoadhesive properties in order to increase the therapeutic effect of noninvasive drug administration.

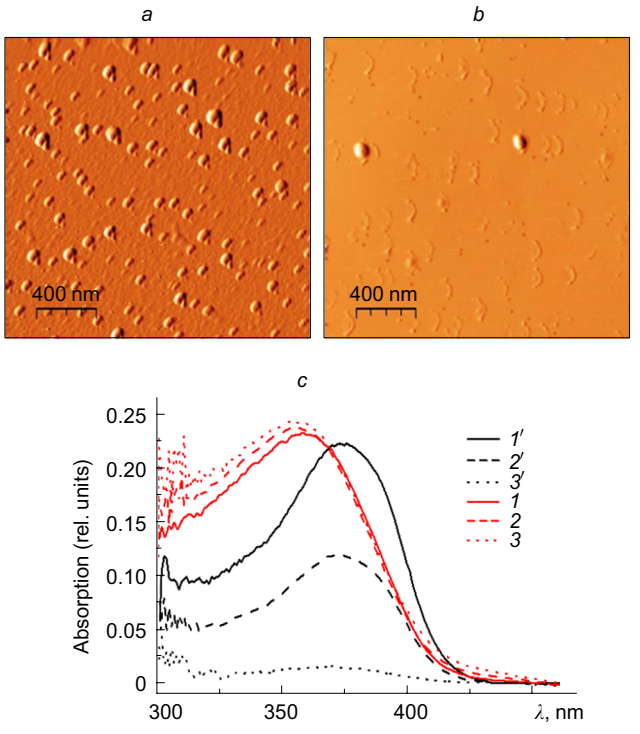


Figure 121. AFM images for solutions of the samples containing 1 mmol L^{-1} of compound **381c** and 10 mmol L^{-1} of SDS at pH 8.5 (*a*) and 1.5 (*b*); and UV spectra of rutin (red lines) and quercetin (black lines) in aqueous solution of 1 mmol L^{-1} of compound **381c** and 10 mmol L^{-1} of SDS at pH 2.7 (*1*, *1′*), 4.2 (*2*, *2′*) and 6.3 (*3*, *3′*) (T = 25 °C, light path length of 0.1 cm) (*c*).[839] Published with the permission from Elsevier.

3.4.2. Micellar and vesicular drug delivery systems based on non-ionic surfactants

Poor water solubility of drug substances, degradation under physiological conditions, short biological half-life due to extensive intestinal and hepatic metabolism and, consequently, low bioavailability of drugs are often overcome by using micellar and vesicular aggregates as carriers of the active ingredient. Since amphiphilic compounds are widely used to fabricate such aggregates, surfactant-based delivery systems play an important role in enhancing the safety and efficacy of biologically active molecules, including antitumour, antiviral, anti-inflammatory, antimicrobial drugs and proteins.[792,840–844]

Non-ionic polymeric surfactants, Pluronics (block copolymers of ethylene oxide and propylene oxide), can be used in the design of effective drug delivery systems. Curcumin solubilization in aqueous systems of such surfactants is performed by thin film hydration, presumably because the slow dynamics of micellar rearrangement processes generates obstacles to direct solubilization. Ganguly *et al.*[845] solved this problem by dissolving curcumin directly into micellar solutions of Pluronic P123 by heating these systems up to the phase separation temperature. The resulting micellar solutions containing curcumin exhibited cytotoxicity against human breast carcinoma cells with IC_{50} values similar to those of the free curcumin solution. When the mucoadhesive polymer κ-carrageenan was added, these solutions turned into gels containing curcumin. In these solutions, in the presence of NaCl, structural transitions from spherical to worm-like aggregates and from micelles to vesicles were also implemented. The curcumin-containing aggregates thus formed exhibited kinetic stability upon dilution, which is important for their use in drug delivery.

Non-phospholipid vesicles formed from non-ionic surfactants may be a promising alternative to the widely studied liposomes. Various types of nanosized vesicles based on non-ionic surfactants improve both permeability and bioavailability of poorly water soluble drugs.[846,847] Mixtures of cholesterol and non-ionic surfactants such as polyoxyethylene ethers of alcohols and phenols and polyoxyethylene esters are often used for bioadhesive drug delivery systems. Such molecules are not only capable of forming vesicular particles, niosomes, which have similar physical properties to phospholipid vesicles, but also have a number of benefits. Of particular note is their relatively low cost, which makes them attractive targets for the pharmaceutical and cosmetic industries. Moreover, the preparation of niosomes for routine and large-scale production can be done without the use of organic solvents.[848]

Niosomes can be generated from a non-ionic surfactant Span 20 and then surface-modified with chitosan gluta-

mate.[849] The added polymer is able to bind to nasal mucin, which prolongs the residence time of the niosome in the nasal cavity and facilitates drug delivery to the brain. Niosomes also showed a significant improvement in the ocular bioavailability of naltrexone hydrochloride[850] and prednisolone.[851] Abdelbary *et al.*[852] prepared vesicles by mixing three surfactant molecules, Span 20, Span 60 and Span 80, with cholesterol in three molar ratios (1 : 1, 1 : 2 and 1 : 3). The size of the obtained niosomes was 500 nm and their encapsulation efficiency toward Lomefloxacin exceeded 78%. Transcorneal permeability improved with increasing amounts of Span 20 and Span 80 in contrast to niosomes containing Span 60. The revealed transport properties may be related to the low phase transition temperatures of Span 20 and Span 80 or to the small size and polydispersity of the niosomes based on them. Despite the negative ζ-potential of these niosomes, the increase in penetration of Lomefloxacin loaded into them was more significant compared to a solution of the pure drug.

A wider range of different surfactants (Span, Tween, Pluronic, Bridge, Cremophor) was used to prepare Carbopol-based pro-niosome gels, which rapidly transformed into nanosized niosomes after oral saliva hydration.[853] The pro-niosome gel composition consisting of Span 60, lecithin and cholesterol proved optimal, as its 243 nm nanoparticles showed the highest encapsulation of Lornoxicam (99.8%). In addition, this composition demonstrated the rheological and mucoadhesive properties necessary to achieve optimal clinical efficacy and higher penetration parameters compared to Carbopol gel containing the same dose of lornoxicam.

Di Marzio *et al.*[854] assessed the possibility of using Polysorbate 20 vesicles as systems for oral drug delivery. *In vitro* stability studies showed that pH and enzymes of gastrointestinal fluids (pepsin and pancreatin) did not affect the stability of these vesicles. However, in the presence of bile salts, nanosized vesicles showed the release of a fluorescent marker: ~11% after 2 hours and ~28% after 4 hours. In addition, pegylated vesicles had the ability to adhere to mucin in the intestinal medium rather than in the stomach. Despite the fact that these results were obtained *in vitro*, the presented data may be useful in the development of innovative drug delivery systems for oral administration.

Vesicular nanoparticles can be formed from non-ionic surfactants and bile salts and then embedded in chitosan gels. Mixtures of Span 60 and sodium deoxycholate in a ratio of 80 : 20 form spherical vesicles with a diameter of 203 nm with Acetazolamide encapsulation efficiency of 90%.[855] Due to the negative ζ-potential of this composition (−38.1 mV), the resulting vesicles were embedded in chitosan nanogels, obtained by ionic cross-linking with sodium tripolyphosphate. Nanogels showed good mucoadhesion times with the least irritating effect compared to drug dispersion. Moreover, a decrease in intraocular pressure was found with the use of nanogels compared with oral administration of Acetazolamide tablets.

Another equally interesting type of vesicular aggregates are transferosomes, which are deformable and very flexible vesicles composed mainly of phospholipids and permeability enhancers that soften lipid bilayers. The deformability allows them to change their shape and easily squeeze between cells, enhancing permeation.[856, 857] Salem *et al.*[858] obtained transferosomes containing a mixture of surfactants (Cremophor RH 40 and soy lecithin), which could effectively encapsulate resveratrol. These transferosomes are non-toxic and are transported through the nasal mucosa to a greater extent than an oral suspension of this drug.

3.4.2.1. Surfactant-based emulsion compositions

Dispersed systems such as nanoemulsions are promising as a means of drug and bioactive compound delivery. Nanoemulsions stabilized with surfactants[859] have great potential for effective treatment of dry-eye diseases.[860, 861] According to existing concepts, nanoemulsions lose stability when mixed with the tear film, resulting in oil fusion with the lipid layer of the tear film, and surfactant molecules bind to the mucus layer.[862, 863] The replenishment of the lipid layer of the tear film with the appropriate lipid components by fusing with the oil droplets possibly causes the tear film to stabilize. In addition, surfactant-based nanoemulsions effectively deliver drugs with limited water solubility to the corneal segment, ensuring its delayed and sustained release.[864]

Nanoemulsions can be used to improve the bioavailability of the immunomodulator cyclosporine A (Restasis®, Allergan).[861] Various ophthalmic forms of cyclosporine-based nanoemulsions are used in the therapy of dry eye syndrome. This medication is a preservative-free anionic nanoemulsion of castor oil and water loaded with cyclosporine A, emulsified and stabilised with Polysorbate 80 and a carbomer copolymer. Lacrinmune® (manufactured by Bausch&Lomb) has a composition similar to that of Restasis®, except for the addition of sodium hyaluronate, which increases the viscosity of the composition to prolong the time it remains on the eye surface. Ikervis® (Santen Pharmaceuticals) is a cationic nanoemulsion of triglycerides emulsified and stabilized with tyloxapol, Poloxamer 188 and cetalconium chloride. The latter formulation contains cetalkonium chloride, an alkyl derivative of benzalkonium chloride, which imparts a positive charge to the oil nanodroplets and enables their electrostatic interaction with negatively charged mucins on the eye surface, improving the pre-corneal stay of the preparation.[865] The retention time of cyclosporin A on the ocular surface is longer with Ikervis® than with Restasis®.[866] Mucoadhesive chitosan can be used as a positive charge carrier in similar nanoemulsions.[867] The incorporation of chitosan into nanoemulsions is realized through electrostatic interaction with negatively charged lecithin, which is a natural lipid mixture of phospholipids, including phosphatidylcholine and phosphatidylethanolamine, which are commonly found in tears. Kolliphor®EL (non-ionic surfactant) was used as a second more hydrophilic surfactant to optimize the size and stability of this nanoemulsion.

An important characteristic of ophthalmic topical preparations is their biocompatibility with the corneal epithelium. Surfactant molecules are capable of non-specific distribution in the plasma membrane, causing its fluidization. This is not only due to a concentration-dependent increase in permeability, but also to possible abrasion of the epithelium by the surfactant.[868] Non-ionic surfactant molecules, such as polysorbates, have lipophilic and hydrophilic moieties. This structure allows them to be distributed between the lipid matrix and hydrophilic protein domains, thereby accelerating the solubilization of lipid components and thus facilitating drug penetration into intercellular areas.[869]

3.4.2.2. Fatty acid-based drug delivery systems

Fatty acids can be used as surfactants to create effective delivery systems. The effect of unsaturated fatty acids (*e.g.*, linoleic and oleic acids) on buccal absorption of salbutamol sulfate from polymeric films has been reported.[870] For films based on hydroxypropyl methylcellulose, oleic acid increased the permeability most effectively compared to films without fatty acid. According to the authors,[870] the factor promoting absorption of oleic acid is due to the presence of a double bond, which facilitates interaction with the lipid components of the buccal epithelium. The linear chain present in the structure of this surfactant has the ability to disrupt the organization of the long n-alkyl chains of ceramides, which provide the barrier function of the buccal epithelium.

Favacho *et al.*[871] studied *in vitro* the effect of a combination of biocompatible polymers (pullulan and hydroxypropyl methylcellulose K100LV) and a mixture of surfactants (oleic acid and Polysorbate 80). These polymers act as enhancers of penetration of drugs such as Prilocaine and Lidocaine hydrochlorides through the porcine esophageal epithelium and mucosa. The authors of this work observed no significant effect of the type of mucoadhesive polymer on drug release, whereas the rate of drug release from the tablets was reduced in the presence of surfactants. Moreover, surfactant molecules enhanced the mucoadhesive properties of pullulan compared to those of hydroxypropyl methylcellulose. There was also a significant synergistic effect of pullulan and surfactant on the permeability and retention time of both drugs. The improved buccal drug permeation with pullulan compared to that with hydroxypropyl methylcellulose can probably be attributed to the fact that after hydration of the polymeric matrix, pullulan does not increase its viscosity as much as the mentioned polymer. Due to the reduced viscosity of the pullulan solution, diffusion of drugs through the polymeric matrix is facilitated, their bioavailability increases, and penetration through the epithelium is enhanced due to the effect of surfactants.

3.4.2.3. Mucoadhesive systems based on macrocycles

It was noted above that among various methods of drug delivery and modification of dosage forms to increase the bioavailability, the phenomenon of mucoadhesion, *i.e.*, the ability of compositions to adhere to the mucosal surface (mucosa), is of particular importance. In order to keep the encapsulated drug in the body tissues (in the mucous membranes of the internal organs, oral cavity, digestive tract, respiratory system, urinary tract) for a long period of time, the drug nanocontainer must have mucoadhesive properties. In this regard, understanding the mechanisms of mucoadhesion is of paramount importance for the creation of effective drug delivery systems in the human body.

It is known that cyclodextrins (CDs) can increase the solubility of various lipophilic molecules by forming relatively stable inclusion complexes. Chemical modification of CD molecules makes it possible to obtain derivatives with improved physicochemical properties (good solubility, optimal size and charge) compared to natural CDs, which can positively influence their biomedical efficacy.[872] Mucosa functions are largely due to specific glycoproteins (mucins), which directly contact epithelial cells. Sialic acids, which have a negative charge at neutral pH, can act as monosaccharide moieties in mucosal glycoproteins.[873] Positively charged CD derivatives have become particularly important for oral delivery because of their affinity for negatively charged mucosal membranes. The complex formation of ethylenediamine-modified γ-CD with daidzein, a natural isoflavonoid of soybean origin, has been studied.[874] The obtained complexes penetrated well into nerve cells *in vitro* and reduced the level of cellular mucopolysaccharides (glycosaminoglycans).

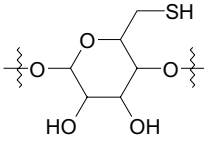
It was found[875] that the cationic derivative of γ-CD modified with propylenediamine is also mucoadhesive, resistant to α-amylase and can be an effective carrier for oral delivery of the berberine alkaloid. When complexed with the macrocycle, the alkaloid more easily penetrated into the lipid membrane than in a free form, but both dosage forms penetrated both normal and cancer cells of the mammary gland of mice. In normal cells, both free and encapsulated berberine were evenly distributed in the cytoplasm and were non-toxic up to a concentration of 131 mol L^{-1}. In tumour cells, the free alkaloid was also homogeneously dispersed, but it was toxic to 25% of the cells at a concentration of 131 mol L^{-1}, while the complex with CD was localized in lysosomes and was twice as active as free berberine.

A similar study was performed with the berberine complex with non-cationic macrocycles, β-CD (Ref. 876) and its 2-hydroxypropyl derivative.[877] In both cases, an increase in the activity of the encapsulated drug was observed due to modulation of P-glycoprotein activity. However, a significant difference was found in the distribution of berberine delivered using these two CD derivatives. The β-CD complex with the alkaloid showed increased intestinal absorption, and oral absorption of berberine was improved using 2-hydroxypropyl-β-CD. Nevertheless, the results of another study[878] indicate increased penetration of poorly soluble genipin through the intestinal mucosa due to complexation with 2-hydroxypropyl-β-CD. The complex formed with the participation of hydrogen bonds between CD and the drug is able to aggregate and interact with P-glycoprotein responsible for the absorption of pharmacological drugs in the intestine.

To improve mucoadhesion to mucosal surfaces, CD derivatives are also thiolated to provide covalent binding to mucin subdomains, thus forming disulfide bridges with cysteine. The surface of the bladder mucosa has mucin-glycocalyx domains, which can form covalent bonds with the thiol groups of CDs and thereby increase the residence time of CD-encapsulated drugs.[879] Thiolated CDs (TCD, a monomeric unit represented by structure **382**) can be used as drug carriers due to high mucoadhesive properties and due to the formation of disulfide bonds with glycoproteins of mucus enriched with cysteine.[880]

α-TCD can encapsulate almost 100 times more iodine than unmodified α-CD.[881] The resulting complex does not exhibit cytotoxicity against Caco-2 colon adenocarcinoma cells, but has antimicrobial activity against Gram-positive *Staphylococcus aureus* and Gram-negative *E. coli*. Moreover, the mucoadhesion of such a complex on freshly cut

Structure 382



382

pig intestinal mucosa was 38 times more effective than in the case of unmodified α-CD. The residence time of α-TCD on the pig intestinal mucosa increases due to the formation of covalent bonds with free thiol groups of mucus glycoproteins.[882] However, aqueous solution of α-TCD is unstable at pH > 5 due to oxidation of the thiol group if it is not stored in sealed containers.[883] Mucoadhesive interaction between α-TCD and the mucus layer decreases due to premature oxidation, which leads to a decrease in the efficacy of the thiolated macrocycle. One solution to improve the stability at higher pH values could be covalent grafting of the cysteine – 2-mercaptonicotinic acid conjugate containing disulfide bonds to the carbonyl groups of oxidized α-CD. The disulfide bonds within the macrocycle can be reduced to free thiol groups on treatment with $NaBH_4$.[884]

β-TCD and γ-TCD can also serve as platforms for mucoadhesive excipients for the preparation of oral dosage forms.[880, 885, 886] β-TCD has better water solubility compared to unmodified β-CD, it dissolves well lipophilic acyclovir and exhibits improved mucoadhesive properties.[887] 2-Hydroxypropyl-β-TCD is able to form a reversible water-soluble inclusion complex with Budesonide, increasing its adhesion to the esophageal mucosa. This composition must be prepared in an aqueous medium at pH < 5, which guarantees binding to mucosal surfaces through the formation of covalent bonds (disulfide bridges) with thiol groups of mucin cysteine residues.[888]

To create effective mucoadhesive systems, the β-CD molecule can be functionalized with diphenyl carbonate to form hyperbranched cylindrical structures with a size of 40 nm and a ζ-potential of −19 mV.[889] This system is capable of encapsulating Norfloxacin to a greater extent than individual β-CD and exhibits mucoadhesive properties with increased permeability and antibiotic activity *in vivo* as compared to the free drug.[890] Despite the negative charge of the formed drug carrier, bioadhesion is probably associated with the formation of hydrogen bonds between the chemical groups of the macrocycle and the mucus layer.

Cyclodextrin molecules can be used as excipients in ophthalmic preparations due to their ability to increase the water solubility of riboflavin[891] and econazole nitrate.[892] The water solubility of riboflavin can also be improved by combining with another class of macrocycles, crown ethers. The latter are capable of extracting calcium ions from the corneal epithelium, which weakens tight junctions of cell membranes and enhances the penetration of riboflavin into the cornea *in vitro*.[893] However, *in vivo* experiments performed on rats did not show any statistically significant increase in permeability compared to the drug without the crown ether.

Studies on the solubility of Indomethacin using sulfobutyl ester of β-CD and 2-hydroxypropyl-β-CD have shown better potential of the latter as an adjuvant agent for eye drops.[894] Nanoparticles based on γ-CD and dexamethasone provide a high concentration of drug on the surface of the eye and can deliver the drug to its posterior segment.[895] Cyclodextrin molecules are responsible for extracting cholesterol and other lipids from the ocular cell membrane, which causes increased drug permeability. However, drug crossing of different barriers does not depend only on the action of the encapsulating macrocycle, but also on the size of the drug molecule. Corneal pretreatment with a β-CD-based composition provides higher permeability for low molecular weight compounds such as sodium fluorescein, but does not improve the penetration of larger molecules.[896]

Thus, analysis of the literature data shows that supramolecular strategy aimed at the formation of nanoscale systems based on amphiphilic molecules of open-chain and macrocyclic structure and non-covalent binding of biologically active guest molecules is an effective tool to solve the problems of drug delivery, increase bioavailability of poorly soluble drugs, overcome biological barriers and reduce side effects by concentrating drugs in nanocontainers. The supramolecular approach has a high potential and versatility and can thus be successfully used for the modification of a wide range of nanocontainers for the delivery of different drugs. This makes it possible to impart the required properties (charge, membranotropic activity, affinity to various biosurfaces and sites) and to adapt such systems for a wide range of biotechnological applications.

3.5. Supramolecular catalysis

Supramolecular interactions play a key role in catalysis, determining the high selectivity and activity of the system as a whole. Supramolecular interactions supplement the conventional covalent interactions between an active site and a substrate (whether a small area of the surface of a heterogeneous or nanoscale catalyst or substrate coordination to an atom of a metal complex), thus providing specific orientation of the reacting species for an optimal course of the process.[897, 898]

'Directing' covalent interactions are well known in the asymmetric transition metal catalysis. Thus, the enantioselectivity of epoxidation and hydrogenation is provided by the pre-orientation of the substrate towards the active site due to coordination of a 'directing' group to the metal centre. Nature has demonstrated the possibility of preorganization *via* non-covalent interactions (van der Waals forces, hydrogen bonding, and also hydrophobic, π-ionic, C−H···π- or π−π-interactions, *etc.*) by the example of catalytic enzymes, which are unique in their selectivity and activity per catalytic site. This effect indicates the presence of one more way to influence the activity and selectivity of catalytic systems.[93, 899, 900] It results from additional supramolecular interactions altering the primary and secondary structures of an enzyme upon activation and thereby providing a specific binding of the reacting species and lowering the transition state energy.[901] Attempts to design novel acceptable models of artificial enzymes gave rise to a new trend in catalysis, namely, supramolecular catalysis, which implies the targeted construction of catalysts by introducing the moieties responsible for an additional non-covalent binding of substrates (Fig. 122).[902 – 904]

Hosseini and Lehn[905, 906] have defined supramolecular catalysis as a chemical transformation of a bound substrate, the main prerequisites of which are the steps of the complex formation and recognition. Due to the relationship between the specificity of non-covalent interactions for a given substrate and the reaction pathway, supramolecular catalytic systems are capable of molecular recognition. Substrates for which these interactions lower the activation energy of the catalyzed process to a greatest extent react considerably faster; therefore, the catalyst recognizes such substrates, thus providing the high reaction selectivity not only to certain products but also to the substrate itself. Specific geometry, which is set by these interactions, can also determine, in large part, the selectivity of the process to afford a particular product.[907, 908]

In addition to high selectivity, supramolecular systems are also characterized by higher reaction rate due to the pre-

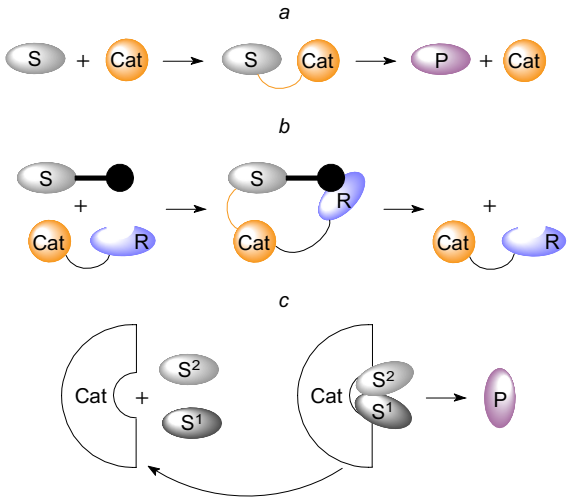


Figure 122. Examples of the molecular recognition for the substrate S *via* non-covalent interactions:[902–904] conventional catalysis (*a*); supramolecular catalysis with participation of one molecular recognizing reactant (*b*); supramolecular catalysis with participation of two substrates (*c*). Cat is catalyst, S is substrate, P is product, R is reactant.

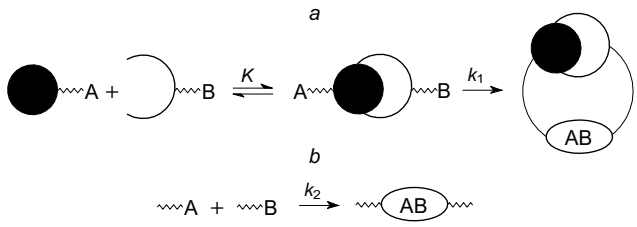


Figure 123. Definition of the effective molarity.[909,910] (*a*) Supramolecular catalysis involves non-covalent binding of substrates A and B (or substrate A and catalyst B), which contain moieties capable of molecular recognition to afford complex with the stability constant *K*. Within the resulting supramolecular complex, A and B approach each other and then react by unimolecular mechanism. (*b*) When no moieties responsible for molecular recognition are present in structures of A and B, the supramolecular complex is not formed, and the reaction occurs by bimolecular mechanism.

binding of the substrate. The increase in the reaction rate is explained primarily by the increase in the local concentration of the reactants and, simultaneously, by changing in the entropy of the system upon binding, which can be described using the concept of 'effective molarity' (Fig. 123). This notion is defined as the ratio of the rate constant or equilibrium constant k_1 for a unimolecular reaction generating supramolecular complex AB to the rate constant or equilibrium constant k_2 for a hypothetical bimolecular process involving substrates A and B, as if there were no binding.[909,910]

Effective molarity reflects the theoretical reactant concentration at which the reaction rate is equal to the rate for a bimolecular process in the complex, which is largely due to the corresponding decrease in entropy because of the convergence of the reactants and thus the loss of conformational mobility. Compared to a non-catalyzed reaction, the presence of enzymes increases the reaction rate by several orders of magnitude, whereas for supramolecular catalysts this increase rarely exceeds 10 times. This is attributable to the partial entropy conservation upon the polymolecular complex formation due to supramolecular interactions, since during the reaction, the transition state entropy is reduced even further.[911,912] The increase of the reaction rate is determined by a decrease not only in the entropy but also in the whole transition state energy. The latter is possible if the configuration and the electronic state arising from the preliminary binding of reactants in the catalyst (*e.g.*, ligands in a metal complex) are as close as possible to the transition ones. The significant structural differences for the stable supramolecular complex and the transition state can reduce the reaction rate, since non-optimal structure leads to the need for a significant conformational rearrangement of reactants during the transformation and, as a consequence, to an increase in the activation energy. In some cases, *e.g.*, when the reaction is conducted in water, the solvent entropic change upon the substrate binding can play a decisive role.[913,914] Desolvation of the reacting species in a supramolecular complex is also significant.[125]

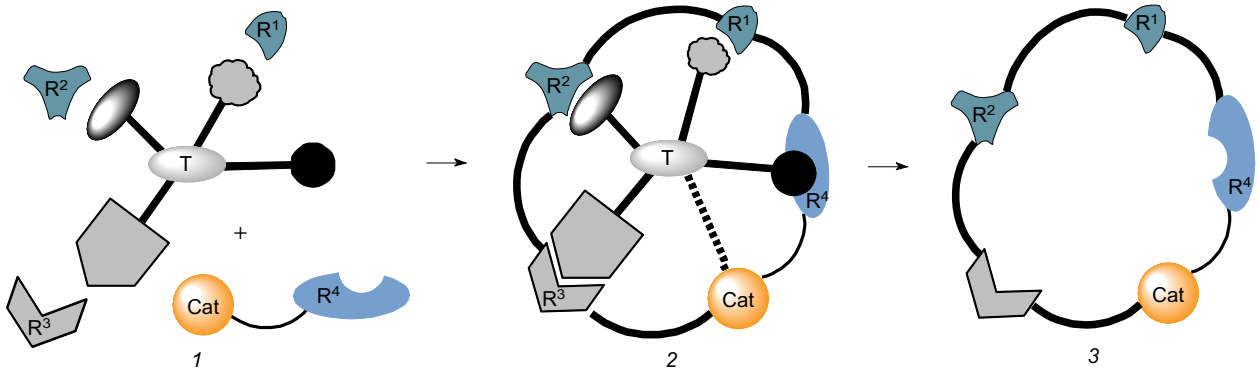


Figure 124. Molecular imprinting steps:[921,922] (*1*) formation of a precursor, (*2*) fixing of the structure, (*3*) removal of the template. In the first step, the moieties of the future catalyst (R^1, R^2, R^3, R^4) being capable of molecular recognition are assembled aroung the complex template molecule (T) having a specified structure. In the second step, these moieties are bound to each other, and the structure is fixed by the template molecule. In the third step, the template is removed, and the resulting catalyst, capable of molecular recognition, selectively interacts only with those substrates whose structure is similar to that of the template.

Depending on the specificity of interactions between the catalyst active site and the substrate, supramolecular catalytic systems can be grouped broadly in the following categories:[72, 915, 916]

— catalysts providing the substrate pre-organization due to the hydrogen bonding, electrostatic, π-ionic or C – H···π-interactions;

— catalysts promoting the formation of host – guest complexes (cyclodextrins, calixarenes, resorcinarenes, verclands, cucurbiturils, *etc*., and assemblies based on glycoluril moieties, molecular capsules with metal ions);

— more complex supramolecular catalysts based on transition metal nanoparticles, dendrimer-containing systems, gels, polymers, *etc*.

Special mention should be made of the formation of catalytic systems during the self-assembly of components driven by the non-covalent interaction with template molecules, which are analogues of the substrate or transition state in the molecular imprinting process.[917 – 920] In this case, the catalyst is synthesized in the presence of such template, while after the structure is immobilized and the template is removed, the resulting material retains its ability to recognize molecules structurally similar to the guest molecule used (Fig. 124).[921, 922]

The molecular imprinting can improve the substate selectivity due to the selective binding of a substrate which is structurally similar to a template (this effect is achieved using the catalysts based on cyclodextrin-containing oligomers in the Wacker oxidation [923]) or increase the reaction rate using a transition state analogue (*e.g*., in the selective amidolysis [924] or hydrolysis [925]).

Examples demonstrating the main features of supramolecular catalytic systems are further considered.

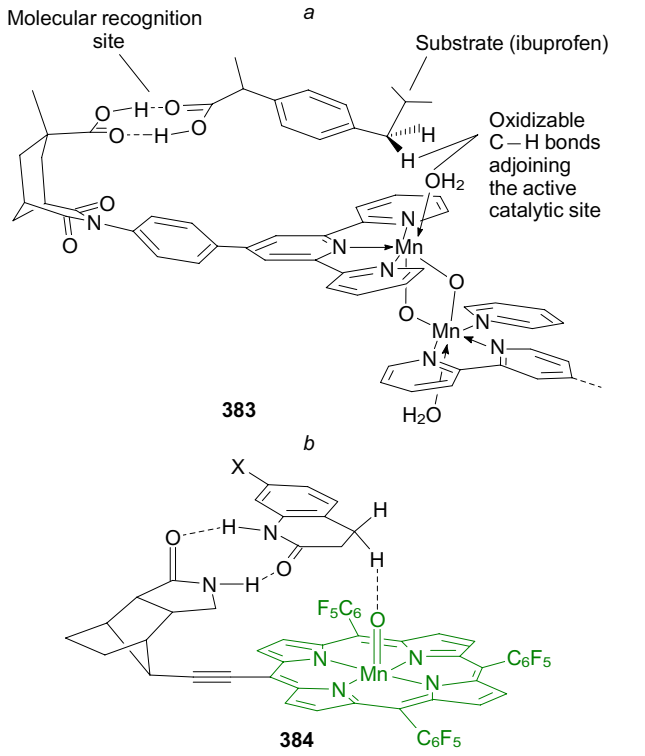


Figure 125. Hydrogen bond formation providing the selective supramolecular catalysis in the oxidation of the C – H bonds using Mn complexes **383** (*a*) and **384** (*b*).[930, 931]

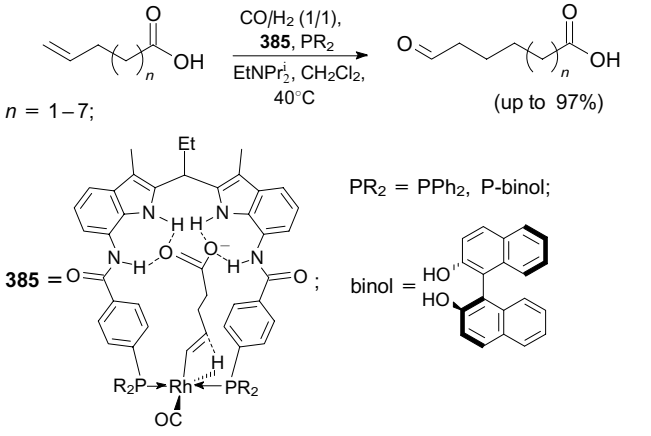
3.5.1. Hydrogen bonding and other non-covalent interactions

Orientation of a substrate relative to the active site due to the hydrogen bonding provides high selectivity of organocatalytic systems and conventional enzymes.[926] This approach has been applied for developing a variety of selective metal complex catalysts.[927] A classic example of such system is a binuclear manganese complex **383**.[928 – 930] The oxidation selectivity for substrates bearing a terminal carboxyl group is governed by the formation of the hydrogen bond with the carboxyl group of the ligand.Thus, the selectivity of ibuprofen oxidation at the α-position of the side chain exceeded 98% (Fig. 125 *a*).

It has recently been shown that this approach is suitable for the pre-orientation of substrates due to hydrogen bonding between the amide moieties of the manganese porphyrin complex **384** and dihydroquinoline substrate.[931] As a result, oxidation of the C – H bonds proceeded not only regio- but also enantioselectively (see Fig. 125 *b*).

The possibility to control the selectivity of metal complex catalysis *via* hydrogen bonding was demonstrated in the hydroformylation of but-3-enoic acid (Scheme 63).[932, 933] The use of Rh^I complex **385** with phosphine ligands containing acylguanidine moieties led to an increase in the reaction rate and selectivity to the linear product with the linear/iso product ratio exceeding 20.[934, 935] The bidentate binol ligand providing the selective binding of the carboxyl group, on the one hand, favorous a high selectivity to the linear product for terminal carboxylic acids and, on the other hand, leads to inversion of the traditional selectivity in the hydroformylation of 2-carboxyvinylarenes giving *iso*-aldehyde as the major product.[932, 933, 936, 937] Similar approach was also applied in the enantioselective hydrogenation in the presence of rhodium complexes.[938 – 940]

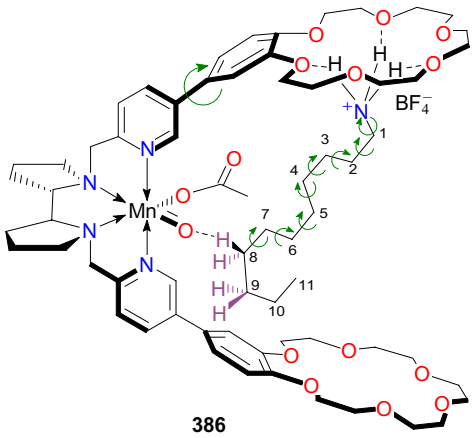
Scheme 63



It should be noted that the hydrogen bonding largely determines the high efficiency of dendrimer-containing polymer-immobilized catalysts based on noble metal nanoparticles. Thus, for the systems based on poly(propylene imine) dendrimers and ruthenium nanoparticles, the hydrogen bonding is a key factor for high catalyst activity in hydrogenation of phenols and levulinic acid.[941 – 945]

Moreover, the reaction selectivity related to the supramolecular complex formation (*e.g*., **386**) can be significantly improved by the use of ligands bearing functional groups being able to bind positively charged species in the sub-

Structure 386



strate. In particular, crown ethers. Thus, the oxidation of $C_{10}-C_{14}$ alkylammonium salts by hydrogen peroxide in the presence of a manganese complex proceeded only at the C(8) and C(9) atoms, whereas for complexes comprising no crown ether moiety, the reaction was unselective.[946]

The C—H···π-interactions govern the stereoselectivity of the ketone hydrogenation catalyzed by ruthenium η^6-complexes with arene [947,948] or styrene polymerization catalyzed by scandium complexes in THF medium.[949] It is noteworthy that such interactions are important for the hydrogenation of aromatic compounds on heterogeneous catalysts.[950,951]

3.5.2. Catalytic systems based on receptor molecules

The use of receptor molecules capable of forming host–guest complexes with a substrate offers various approaches for the development of supramolecular catalysts (Figs 126, 127) ranging from phase transfer catalysts acting as a kind of protective groups for the moiety encapsulated within the host cavity to the design of complex systems providing the selective binding and pre-orientation of the substrate relative to the active site. Application examples for catalysts based on various receptor molecules are considered below.

3.5.2.1. Receptor molecules as phase transfer catalysts

The use of modified host molecules such as cyclodextrines, calixarenes, resorcinarenes and cucurbiturils of different ring size (Fig. 126) as components of two-phase systems, in which the metal complex is located in the aqueous phase and the non-polar substrate is in the organic phase (Fig. 127 *a*) provides high reaction rates and the possibility for the catalyst to be reused in the aqueous phase.[907,908,952–971]

In this case the increase in the reaction rate for non-polar substrates depends on the compatibility between the cavity size of the receptor molecule (3.8 and 5.0 Å for calix[4]- and calix[6]phenolarenes;[459] and 5.7, 7.8 and 9.5 Å for α-, β-, and γ-cyclodextrins, respectively [971]), on the one hand, and the size and properties of the guest substrate, on the other hand. For the Wacker process with calixarenes sulfonated at the lower rim, the increase in the reaction rate was the highest for the pairs of calix[4]arene and hex-1-ene, calix[6]arene and oct-1-ene, while when cyclodextrins were used, styrenes reacted much faster than terminal alkenes.[907,908,957–959] In the oxidation of disubstituted cyclohexanes with persulfate, γ-cyclodextrin provided

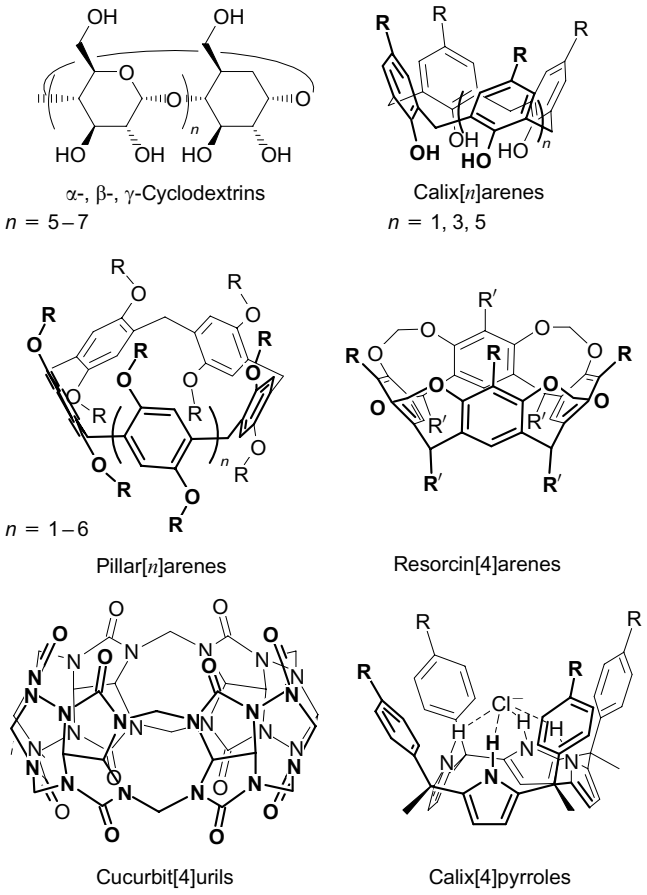


Figure 126. Structures of the host molecules.

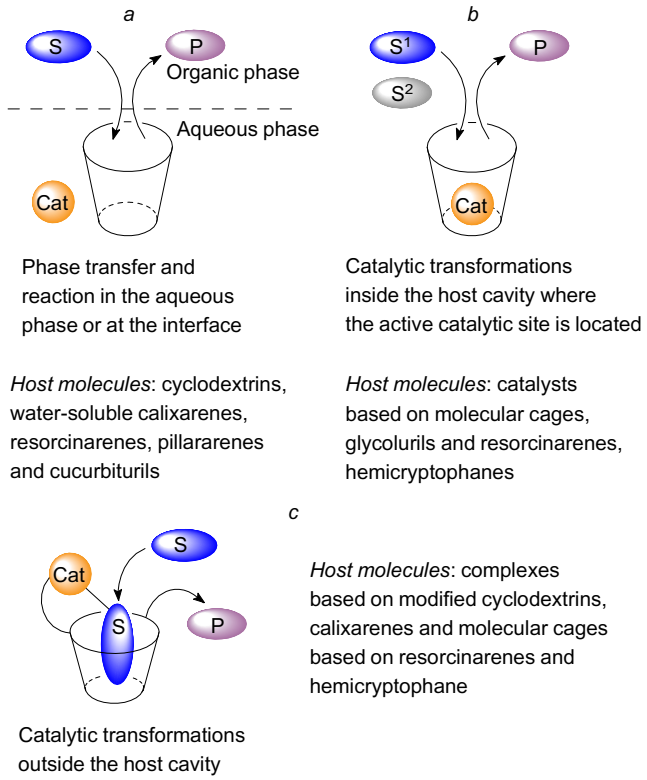


Figure 127. Types of catalytic systems (*a*–*c*) based on various host molecules.

much higher product yields than lower-sized cyclodextrins.[972]

For such systems, a host molecule can serve as a kind of the protective group, since when the catalyst is present in the reaction medium, the groups being arranged inside the cavity do not react, hence substantially increasing the regioselectivity. Thus, the hydroxylation of phenol with hydrogen peroxide in the presence of iron salts using oxyethylated cyclodextrins afforded hydroquinone and benzoquinone as the major products, while in the oxidation of disubstituted alkyl aromatics, only substituents located outside the cavity of β-cyclodextrin participated in the reaction.[908, 953 – 955] In the oxidation of 3,7-dimethyloctyl esters of aromatic acids in the presence of β-cyclodextrin, the yield of alcohol at position 7 was markedly increased.[973]

The use of host molecules in two-phase systems influences the regioselectivity of consecutive processes, for example, the stepwise hydrogenation. If the stability constant for the complex with one of the products is sufficiently high, the complex leaves the reaction medium; as a consequence, an unusual selectivity to intermediate products can be observed. Thus, when introducing modified cyclodextrins into the catalytic system based on rhodium nanoparticles stabilized with polyacrylic acid, hydrogenation of phenol yielded cyclohexanone as the major product; this was accompanied by the formation of cyclohexenones with the double bond conjugated with the carbonyl group.[974]

Rhodium complexes can be used in hydroformylation of vinylarenes in the presence of unmodified cyclodextrins without solvent under mechanochemical activation. In this case the selectivity to the normal aldehyde increases due to the formation of the host – guest complex in which the substrate is deeply immersed into the β-cyclodextrin cavity.[975] Cyclodextrins showed high efficiency in the hydroformylation[960 – 966] and hydroamination of triglycerides,[976 – 978] cross-coupling[979] and oxidative desulfurization reactions.[980]

It is worth noting that in some cases, the formation of the host – guest complexes between cyclodextrin and the substrate molecule is hampered because of the competition from the ligand; therefore, to maintain high selectivity to the substrate, a special design of ligands is required.[981, 982] Thus, the use of cyclodextrins modified with methyl or hydroxypropylene groups significantly improved the activity of catalytic systems in various processes. The sharp increase in the reaction rate in the presence of amphiphilic cyclodextrins should be particularly noted. Thus, being involved in the reaction, β-cyclodextrin modified with methyl ester of succinic and oleic acid dimer increased the rate of aqueous hydroformylation of dodec-1-ene by a factor of 4 as compared to that in the presence of methylated cyclodextrin.[983] The use of β-cyclodextrin dimer provided the mutual orientation of the substrate and the metal complex, where non-polar substrate was bound by one cyclodextrin moiety, while the metal complex containing the specially designed ligand was bound to another moiety. As a consequence, the reaction rate increased more than twofold.[984]

Water-soluble calixarenes and resorcinarenes were employed as phase transfer catalysts in the Suzuki cross coupling and Wacker oxidation processes.[985, 986] The system based on calix[4]arene modified with diethylammonium moieties at the lower rim and polyoxomolybdate showed high selectivity in the oxidation of a variety of aromatic sulfides to sulfoxides with hydrogen peroxide.[987]

Water-soluble pillar[5]arenes modified with carboxylic or oxyethyl groups proved to be very effective in the two-phase hydroformylation of higher alkenes in the presence of rhodium complexes.[988] They also acted as phase transfer catalysts in the heteropolyacid-catalyzed oxidation of aldehydes to the corresponding carboxylic acids.[989]

Cucurbiturils (see Fig. 126), the host molecules of another type, were used in the reduction of unsaturated compounds by formic acid under two-phase conditions in the presence of ruthenium complexes as catalysts.[952] Also cucurbiturils significantly improved the performance of the hydrogenation and Suzuki cross-coupling catalysts based on palladium nanoparticles.[990, 991] In relation to hydrocarbon oxidation by hydrogen peroxide or iodosobenzene catalyzed by the vanadyl complex $[CB[6] \cdot VO]^{2+}$ (CB[6] is cucurbit[6]uril), the existence of substrate selectivity for cucurbiturils was demonstrated: whereas cyclohexane was not oxidized because of steric restrictions arising from the formation of the host – guest complex with cucurbit[6]uril, the oxidation of n-alkanes, on the contrary, proceeded rather rapidly.[992]

3.5.2.2. Catalytic systems based on molecular capsules and cages

A characteristic feature of another type of supramolecular catalytic system, which can be assembled from receptor molecules, is that the process *per se* occurs directly inside the cavity of the receptor molecule, in which the catalyst active site is encapsulated (see Fig. 127 *b*). In this case, the host molecule acts as a molecular nanoreactor, *i.e.* a 'molecular flask' in which the reaction is carried out.[78, 97]

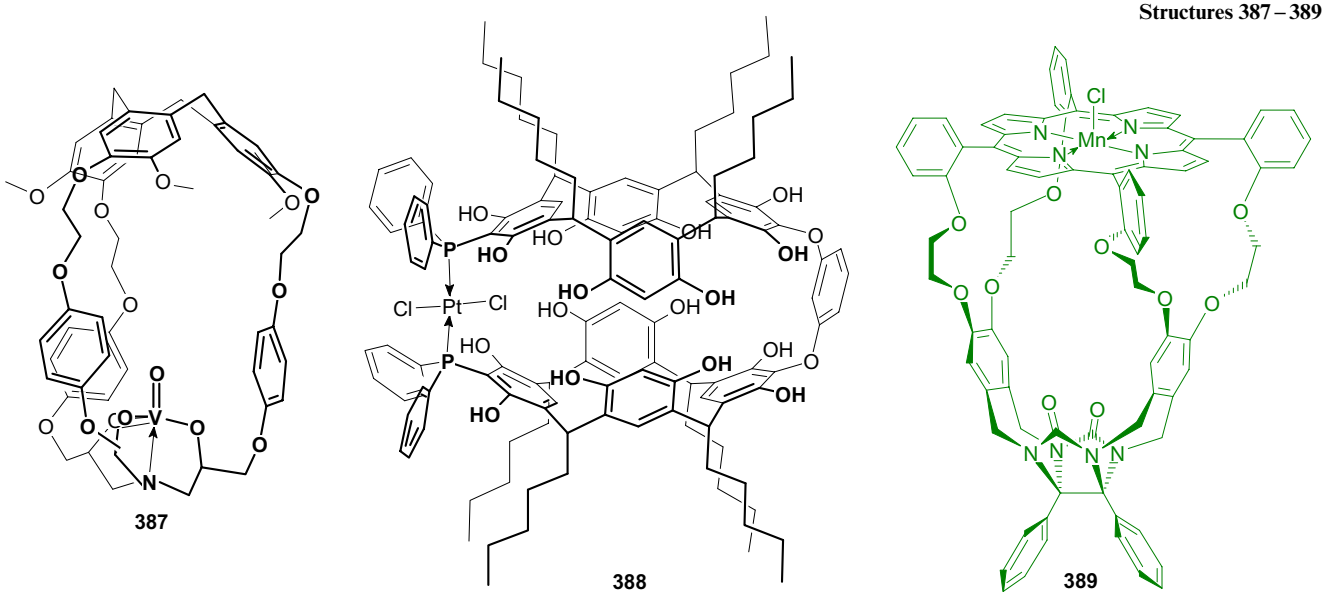
Examples of supramolecular transition metal catalysts based on macrocyclic receptors include vanadyl complex **387** bearing a hemicryptophane moiety,[993, 994] platinum complex **388** of modified resorcinarene[995] and a molecular clip **389** containing a Mn porphyrin complex.[971, 996, 997]

Systems of this type are characterized by the high substrate selectivity due to the specificity of the substrate binding to the receptor molecule. The features of substrate pre-orientation inside the cavity determine which part of the substrate remains accessible for the reaction and, as a consequence, the regioselectivity of the reaction, as well as the possibility for mono- and bimolecular cyclization reactions.[77, 78, 125, 671, 998 – 1002] The most commonly used systems are those based on molecular capsules, molecular cages, *etc.*, for which a straightforward design of catalysts for carrying out the reactions within a confined space is possible.[76, 78, 916, 1001, 1003, 1004]

Among the organic host molecules, resorcinarenes and hemicryptophanes, the cavities in which are formed by one or more rings of the initial macrocycle and a metal complex (see structures **387**, **388**), proved to be most suitable for the construction of such systems.[671] Catalysts based on hemicryptophanes were used for oxidative desulfurization and oxidation of alkanes and alcohols. In particular, owing to the fact that the reaction occurred in the cavity formed by the terphenylene rings, vanadium hemicryptophane complexes **387** were three times more efficient in the oxidation of methyl phenyl sulfide with hydrogen peroxide than the macrocycle-free system.[993, 994]

Likewise, copper complexes with structurally similar ligand displayed higher stability and twice higher efficiency than the typical low-molecular-weight system for cyclohexane oxidation with hydrogen peroxide; moreover, cyclohexane appeared more preferable substrate than adamantane.[1005, 1006] Ruthenium complexes with this ligand

Structures 387 – 389



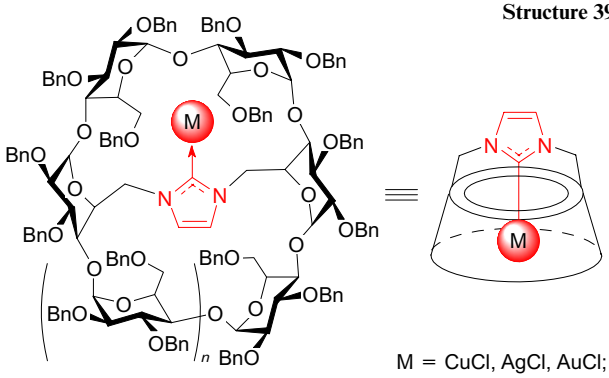
provided higher selectivity to the formation of aldehydes in the oxidation of primary alcohols with oxygen as compared to secondary alcohols.[1007]

The use of resorcin[4]arenes as ligands made it possible to sandwich the active catalytic site, *e.g.*, platinum complex **388**, between two macrocycles forming a molecular capsule. The resulting complex provided a high substrate selectivity in the hydroformylation of styrene.[995] Resorcinarene capsules showed high activity in the hydration of alkynes catalyzed by gold complexes of N-heterocyclic carbenes.[76, 97, 1008 – 1010] In the case of aliphatic alkynes, the highest hydration rate was found for substrates bearing cyclohexyl moieties,[76, 97, 1008] whereas for arylalkynes it sharply decreased with increasing size of substituent in the *para*-position relative to the C≡C bond.[1009] The hydration of 4-phenylbutyne using gold NCH-complex in the presence of resorcinarene capsule resulted in 4-phenylbutanal, 1,2-dihydrotetralin and 4-phenylutan-2-one simultaneously, while in the absence of resorcinarene, 4-phenylbutan-2-one was the major reaction product.[1009, 1010]

A similar effect was also observed in the oxidation of sulfides to sulfoxides by hydrogen peroxide; the substrate was bound here through the formation of capsules consisting of six resorcinarene molecules.[76, 1011] The capsules based on resorcin- and pyrogallolarenes showed high activity and selectivity in the hydrogen transfer imine reduction, terpene cyclization, amide synthesis, intramolecular hydroxyalkylation, Friedel – Crafts alkylation of heterocycles, metathesis of alkenes and carbonyl compounds.[76, 96, 97] At the same time, it was found that under certain conditions, resorcinarene cages can hinder the oxidation of sulfides[76] and alkyne dimerization.[1009]

An example of cyclodextrin-based molecular cages are gold and copper complexes of N-heterocyclic carbene **390**.[1009, 1012] For gold complexes with benzylated cyclodextrin, an effect of substrate cooperative binding in the cage and pre-organization in the cycloisomerization of 1,6-enynes was observed: instead of a five-membered ring typical of a low-molecular-weight analogue, a six-membered ring was formed due to stabilization inside the host cavity.[1013] The use of similar copper complexes of α- and β-cyclodextrins in the hydroboration of substituted phenylacetylenes resulted in a sharp difference in the selectivity as compared to unmodified ligands: the cooperative binding of the substrate inside the cage led to the predominant formation of an iso-product, in which the boron atom was bonded to the α-carbon at the phenyl substituent.[1014]

Structure 390



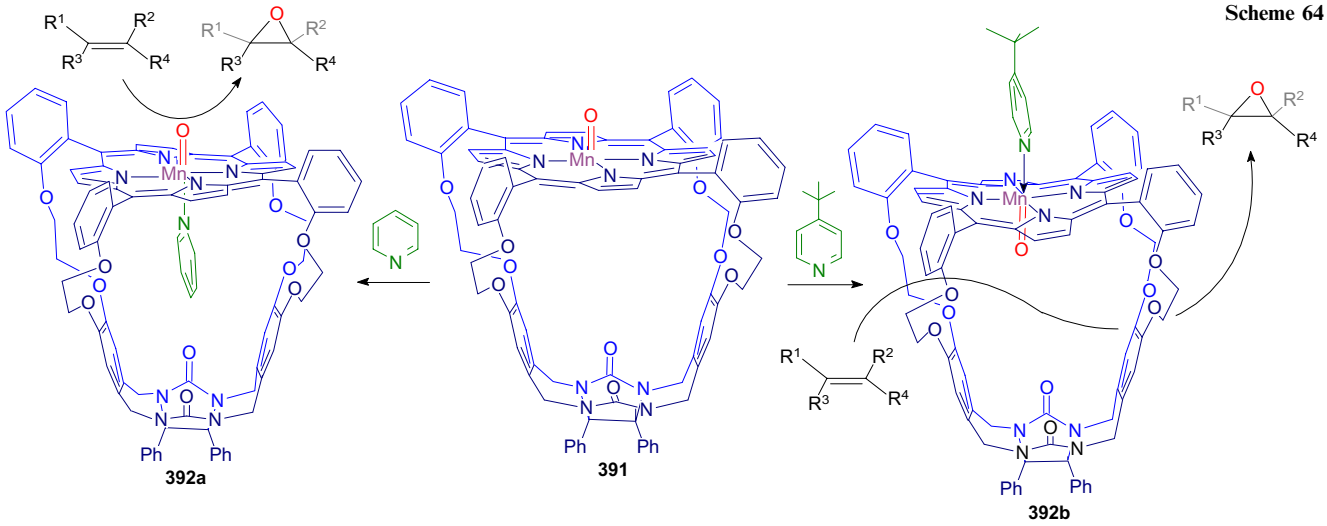
390
[(α-ImCD)M or (β-ImCD)M]

Molecular cages based on glycoluril clips and manganese porphyrin complex (see structure **389**) were proposed in the early 2000s by Nolte and co-workers as catalysts for the C=C double bond epoxidation with sodium hypochlorite[996, 1015] and oxygen combined with benzaldehyde.[1016] The substrate binding inside the cavity occured upon activation of complex **391** with dipyridine or 4-*tert*-butylpyridine, which was coordinated to manganese(III) from the outside of the cavity to form complexes **392a**,**b** (Scheme 64).[997, 1017]

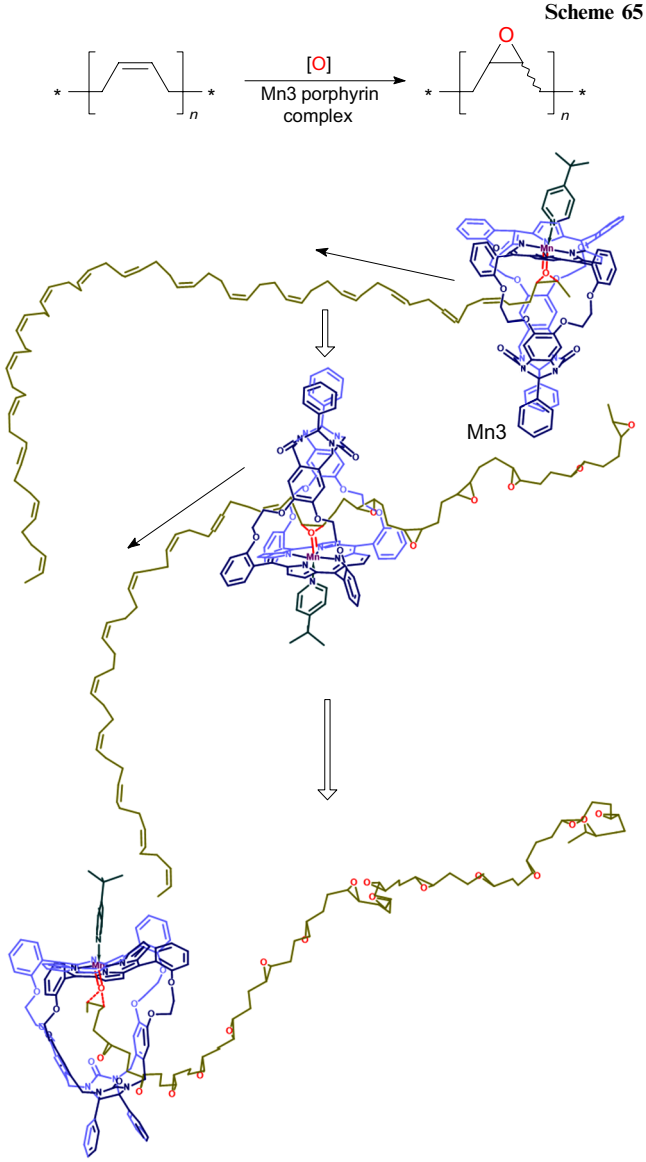
This system provided an access to selective epoxidation of polymers such as polybutadiene, with the catalysts functioning as a kind of a molecular machine, moving along the polymer backbone. The mechanism of action of cages based on clip molecule **392b** is illustrated in Scheme 65 (the arrows indicate the direction of the clip).[997, 1015, 1018]

Over the past decade and a half, considerable attention of researchers has been focused on molecular cages with a regular structure of the $[M^{II}_n L_m]^{k+}$ type, in which metal

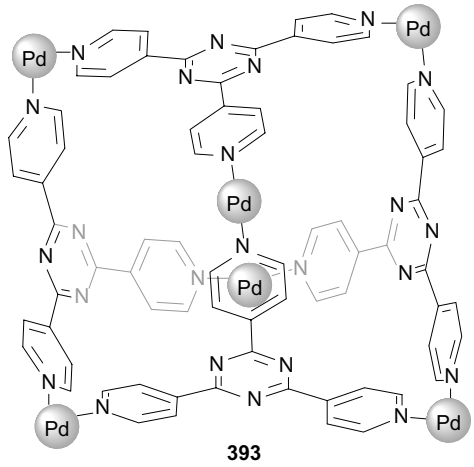
Scheme 64



Scheme 65



Structure 393

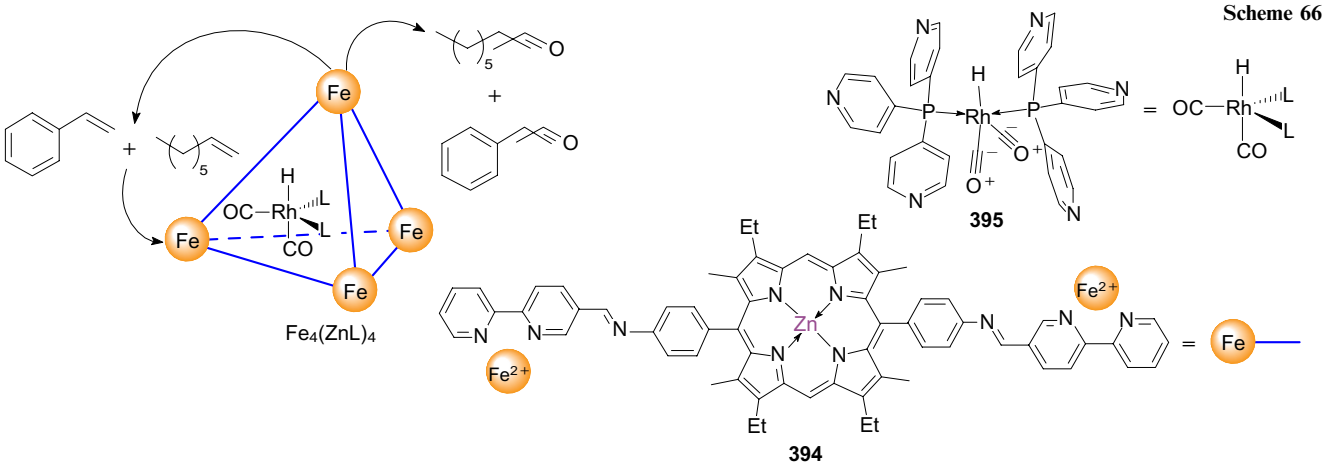


atoms occupy polyhedron vertices.[77, 78, 1000 – 1002] In this case, the metal complex can be fixed both on the wall and inside the cage, the shape and size of which determine the regio- and stereoselectivity of the process. Thus, the high efficiency of octahedral complexes $[Pd_6L_4]^{12+}$ [*e.g.*, 2,4,6-tris(4-pyridyl)-1,3,5-triazine complex **393**] as catalysts for the Wacker oxidation[78, 1019, 1020] and epoxidation of hydrophobic substrates was demonstrated in the early 2000s.[1021] Excellent performance and regioselectivity of such systems were achieved due to high stability constants with hydrophobic substrates: binding inside the cage made the substrate inaccessible for a subsequent reaction. In particular, epoxidation and the Wacker oxidation of alkenes selectively proceeded at the terminal double bond, which was located outside the cage.[1020, 1021]

The use of a tetrahedral molecular cage $Fe_4(ZnL)_4$ with zinc porphyrin complex **394** in the edge allowed the immobilization of rhodium tris(4-pyridyl)phosphine complex **395** inside the cage due to coordination to the zinc atoms in porphyrin moieties (Scheme 66).[1022, 1023]

The tetrahedral geometry of the complex led to the equatorial arrangement of phosphine ligands at the rhodium atom, thus facilitating the predominant formation of n-aldehydes in the hydroformylation of terminal alkenes of the normal structure. The reaction occurring within the cage was substrate-selective: alkenes with an even number of carbon atoms underwent hydroformylation much faster than alkenes with an odd number of carbon atoms or

Scheme 66



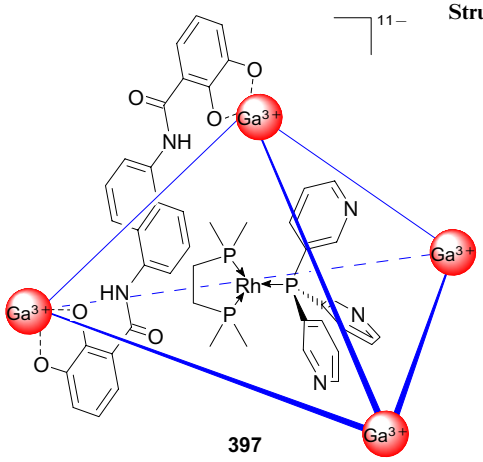
styrenes, which was attributed to peculiarities of complex formation within the molecular cage.[1022, 1023] Thus, hydroformylation of an equimolar mixture of styrene and oct-1-ene gave a mixture of alkyl- and arylalkylaldehydes in a ratio of 6.6 : 1.

Encapsulation of rhodium complex with an optically active monodentate ligand based on binol phosphite within a $Pd_8(ZnL)_2$ cage (where ZnL is a porphyrin-containing moiety), owing to coordination of pyridine units to the zinc atoms, resulted in catalyst **396**, providing styrene hydroformylation with the enantioselectivity of up to 74% *ee*.[1024]

Epoxidation of styrenes in a two-phase system using iodobenzene as an oxidant was catalyzed by Mn porphyrin complex encapsulated in a cavity of $Fe_8(ZnL)_6$ cubic cavity. For sterically hindered substrates a 2- to 3-fold decrease in the reaction rate was observed, while for unsubstituted styrene, the rate, on the contrary, drastically increased.[1025] Tetrahedral copper-containing cages proved to be active in the allylic oxidation of a series of substrates such as tetralin, dihydroindole, ethylbenzene, isopropylbenzene and diphenyl by *tert*-butyl hydroperoxide; the substrate activity increased at the nitrate anion encapsulation into the cavity.[1026]

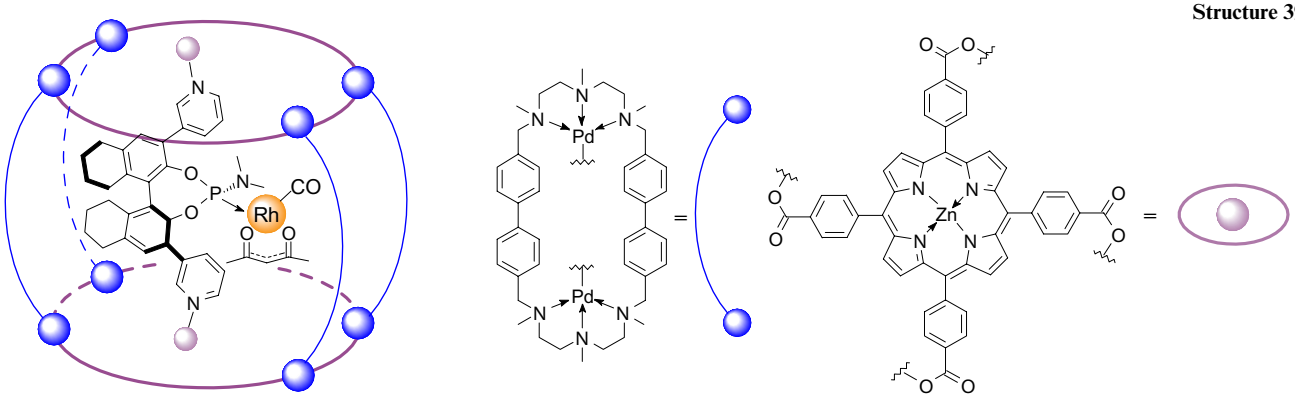
An interesting example of substrate selectivity is a system in which a positively charged rhodium complex was immobilized within a negatively charged tetrahedral cage assembled from gallium complex. Catalyst **397** (whether it comprised rhodium or ruthenium) facilitates a successful isomerization of allyl alcohol to n-propanal, with only unsubstituted alcohols undergoing the reaction.[1027, 1028]

Structure 397

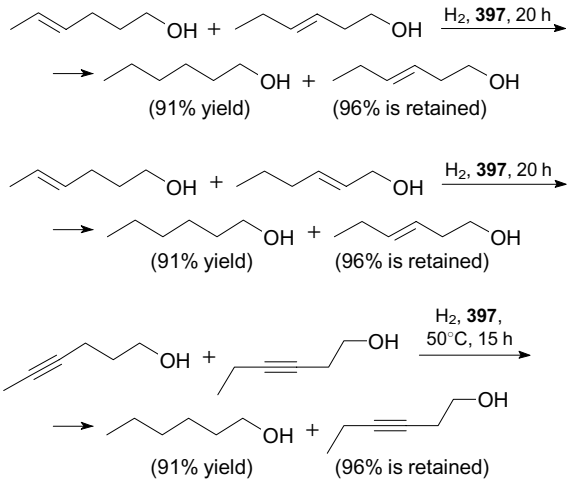


An equally interesting effect was observed when hydrogenation of unsaturated alcohols was carried out in the presence of such catalyst (Scheme 67). With substrates containing double ot triple bonds in the β-position to the terminal methyl group, the reaction proceeded smoothly to give the corresponding saturated alcohols. If a multiple bond was more distant from the terminal carbon atom, the reaction was very slow and the yields of the saturated products did not exceed 5%. The observed substrate selectivity was attributed to steric hindrances, interfering with the formation of the π-complex between the ruthenium

Structure 396



Scheme 67



atom and the ethyl-substituted double or triple bond.[1029] Encapsulation of the gold complex of trimethylphosphine into such cage helped to avoid the hydratation during the cyclization of propargyl ethers.[1030]

3.5.2.3. Supramolecular catalytic systems displaying the cooperative binding effect

The design of systems in which different parts of the receptor molecule simultaneously bind both the substrate and the metal centre, thereby providing their interaction (see Fig. 127 *c*) is one of the most successful trends in the supramolecular catalysis.[93, 908, 971, 986, 1031 – 1034] As a classic example of such systems, one may mention the Breslow enzyme, a manganese porphyrin complex modified with cyclodextrins, which provide the desirable pre-orientation of the substrate towards the active site.[1035 – 1040] As a result, oxidation occurs strictly selectively on the C—H bond at position 6 of the steroid substrate (Fig. 128).

Catalysts based on nanoparticles and transition metal complexes with modified cyclodextrins were applied in the Wacker oxidation,[908, 954, 955, 957, 962] hydroxylation of phenols,[953 – 955] hydrogenation,[965, 1041 – 1043] and hydroformylation.[960, 962, 964, 966, 1023, 1041, 1043] High performance and selectivity of such systems were attained *via* the cooperative binding effect: the receptor molecule provided the desirable pre-orientation of the substrate, which immediately underwent a transformation on a proximate metal centre.

Thus, when reducing acetophenone with isopropyl alcohol in the presence of palladium complex **398** with β-cyclodextrin modified by *N*-(2-pyridyl)-1,3-diaminopropane, a twofold increase in the reaction rate was observed as compared to the system consisting of a low-molecular-weight palladium complex and unmodified β-cyclodextrin; in the absence of cyclodextrin, changes in the reaction rate were negligible.[1044] A significant rate enhancement as compared to the low-molecular-weight analogues took place in the presence of palladium complexes with modified cyclodextrins in the cross-coupling reactions[1045 – 1049] and for ruthenium complexes in the metathesis polymerization of diols.[1050]

Simultaneous substrate binding with both rhodium atom and cavity of the host molecule, namely, β-cyclodextrin modified with sulfonated diphenylphosphine moiety (catalyst **399**), resulted not only in a sharp increase in the reaction rate but also in a change in the selectivity of hydroformylation. The normal to iso product ratio reached 2.6 *vs* 1.7 for the system with unbound sulfonated triphenylphosphine.[1051] Furthermore, the presence of the sulfonyl moiety hindered the formation of the inclusion complex between the phenyl group of the phosphine ligand and the cyclodextrin cavity, thus preventing 'self-poisoning' of the catalyst. In addition, a conceptual possibility of developing the polymeric hydroformylation catalysts containing both cyclodextrin moieties and sulfonated phosphine ligands was been demonstrated; in this case, the aldehyde yield increased up to 60% (*vs* 1% in the presence of a low-molecular-weight catalyst based on sulfonated phosphine solely); however, the normal to iso product ratio was only 1.9 (*vs* 2.7 for the low-molecular-weight catalyst).[1052] Rhodium complex **400**, containing optically active sites in the cyclodextrin moiety, displayed high enantioselectivity in the hydroformylation of styrene (the proportion of *R*-isomer reached 93 – 95%).[1053]

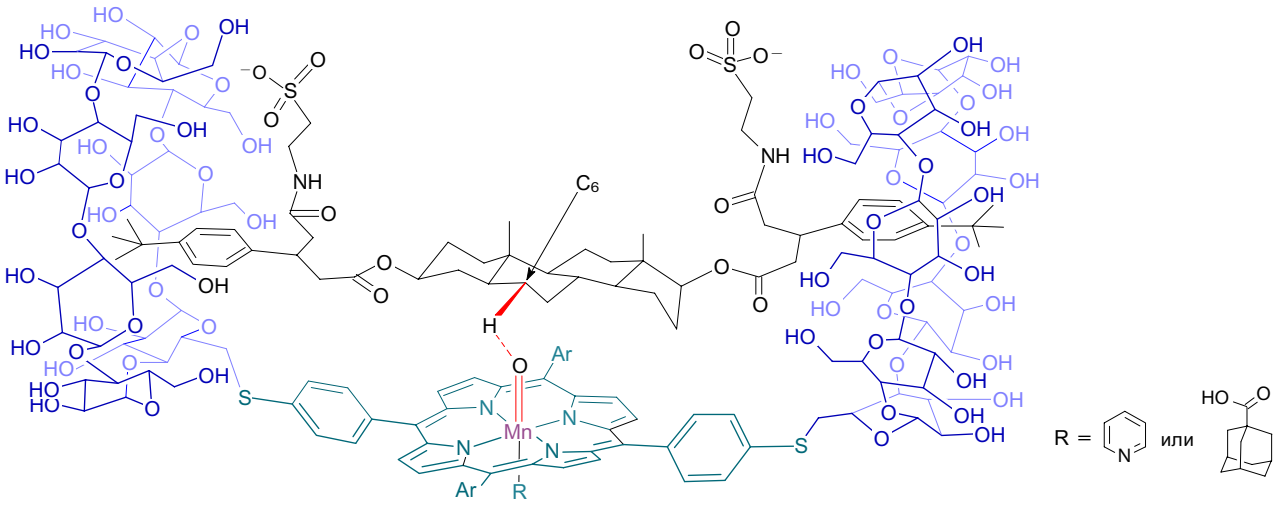
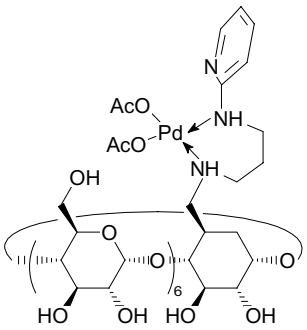
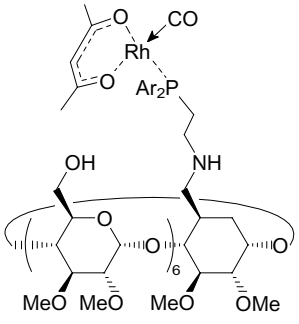


Figure 128. Supramolecular oxidation system based on manganese complex with porphyrin modified with cyclodextrins, proposed by Breslow.[1039, 1040]

Structures 398 – 400

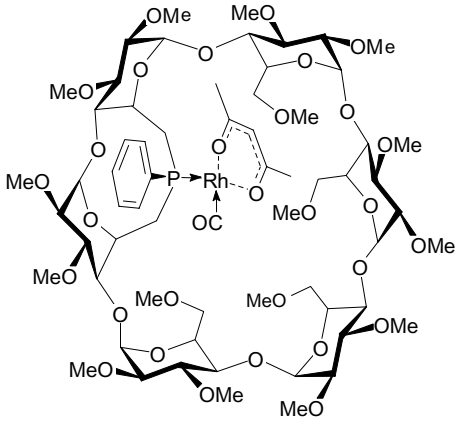


398 (Ref. 1044)



399 (Ref. 1051)

Ar = 3-NaOSO$_2$C$_6$H$_4$



400 (Ref. 1053)

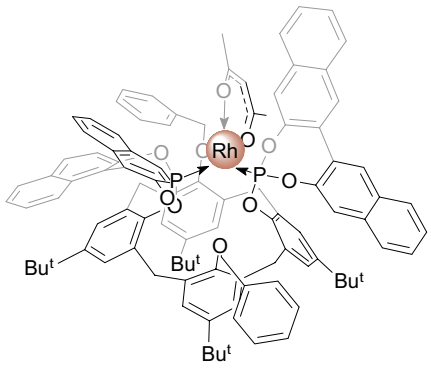
A plethora of studies is devoted to the application of resorcinarenes, calixarenes and calixpyrroles as platforms for preparing catalysts capable of cooperative binding (see Fig. 126). Thus, based on calix[4]pyrroles, there were developed catalysts for epoxidation of alkenes [1054] and for hydrogenation of levulinic acid [1055] and nitrobenzene.[1056]

Modification of calix[4]- and calix[6]arenes with phosphine ligands opens access to high-performance catalysts for hydrogenation and hydroformylation.[967, 1057] Varying the size of calixarene, the nature and number of phosphine moieties as well as their position at the upper or lower rim of calixarene, the selectivity of the catalyst can be tuned (see structure **401**) in such a way as to obtain an aldehyde of strictly normal or iso structure.[1057]

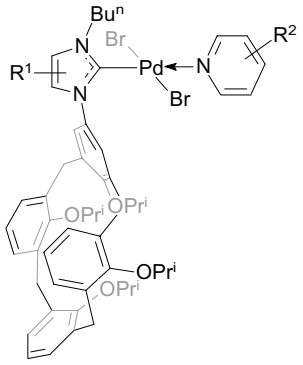
Modified calixarenes were used to prepare catalysts for polymerization of ethylene [1058, 1059] and cyclic esters,[1060] epoxidation [1061] and cross coupling.[1062] Palladium complexes with nitrile-substituted calixarenes performed well in the Wacker oxidation.[986]

The calixarene conformation has a significant effect on the possibility of cooperative binding of the substrate and, consequently, on the reaction rate and selectivity. Thus, the conformation of complex **402** did not allow the cooperative binding of the substrate, resulting in the absence of supramolecular effects in the Suzuki cross-coupling reaction.[1063] At the same time, the reaction rate significantly increased when palladium NCH-complex with amphiphilic calix[4]arenes **403** in the *1,3-alternate* conformation was used for the reaction the carried out in water. Apparently, in the aqueous medium there arises a configuration favourable for the cooperative binding.[525] For nickel N-heterocyclic carbene complexes with modified calix[6]arenes, it was demon-

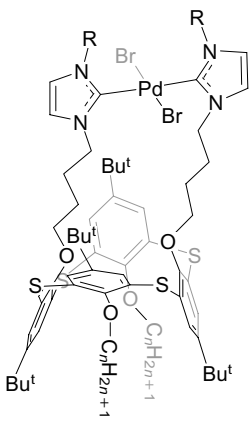
Structures 401 – 405



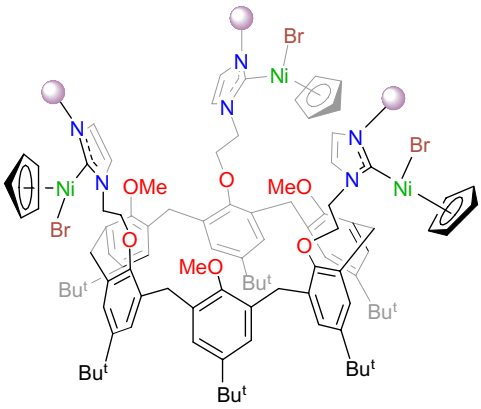
401 (Ref. 1057)



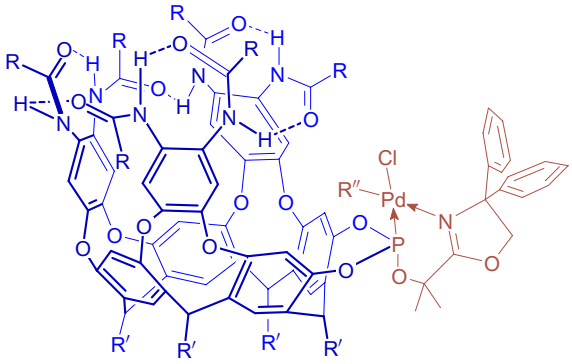
402 (Ref. 1063)



403 (Ref. 525)



404 (Ref. 1064) = Mes (2,4,6-Me$_3$C$_6$H$_2$)



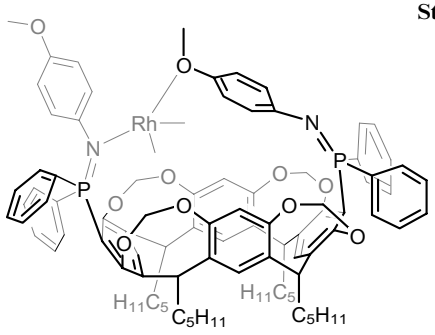
405 (Ref. 1066)

R = n-C$_7$H$_{15}$,
R′ = n-C$_{11}$H$_{23}$,
R″ = C$_3$H$_5$

strated that a reasonable reaction rates and product yields can be achieved only at an optimal distance between the nickel centre and calixarene cavity providing an effective binding (see structure **404**).[1064]

Similarly to calixarenes, resorcinarenes can also find application in the design of catalytic systems capable of cooperative substrate binding *via* the formation of a host–guest complex and its simultaneous coordination to the metal centre, fixed on the larger rim of the macrocyclic cone and located above the cavity of the receptor molecule.[1065] Depending on the nature of substituents or functional groups used to modify resorcinarene and the location of the metal centre in the receptor molecule, one can attain high selectivity to different substrates. Thus, the allylic alkylation in the presence of palladium complex **405** demonstrated a much higher reaction rate for the substrated bearing cyclohexyl substituents as compared to the reaction with their analogues with iso-structure of the carbon-containing moiety.[1066] For rhodium complex **406**, an unusual substrate selectivity was observed in the hydrogenation of hex-1-ene, which reacted almost 40 times faster than branched 3-ethylpent-1-ene; this can be explained by the lack of interaction of the latter with the macrocycle cavity upon coordination to the rhodium atom.[1067]

Structures 406



406 (Ref. 1061)

Similarly, gold complexes of resorcinarenes provided a considerable growth of the reaction rate and selectivity in the dimerization of substituted acetylenes due to the additional supramolecular interaction of the substrate with the receptor cavity.[1068–1070]

The results obtained over the past 25 years since the appearance of the first supramolecular systems provide the basis for the design of more complex, not only homogeneous, but also heterogeneous, catalysts.[1071] For each of the above-mentioned types of homogeneous catalysts based on macrocyclic receptors, the corresponding analogues among heterogeneous systems can be found. Thus, for molecular cages, this will be metal-organic frameworks, the crystalline structures with metal atoms the nodes linked by rigid organic linkers.[1072] For cyclodextrins, one may mention different types of polymers, including those stabilizing metal nanoparticles or forming gel-like systems.[1073–1076] For calixarenes and other aromatic host molecules the most suitable analogues for designing heterogeneous catalysts are regular porous systems based on resols, ordered phenol formaldehyde resins,[1077–1081] or polyaromatic frameworks.[1082–1087] The above-mentioned trends are of special interest for the development of supramolecular catalysis.

3.6. Co-self-assembly of macrocyclic compounds: new prospects for the design of supramolecular systems

Various classes of macrocycles such as cyclodextrins,[1088] (thia)calix[*n*]arenes,[454] cucurbit[*n*]urils[1089] and pillar[*n*]-arenes[1090] are important building blocks (Fig. 129) for supramolecular assemblies on the nanoscale.

Analysis of the literature data[454, 1088–1090] shows that there are two main strategies for the supramolecular assembly of macrocyclic compounds for the design of various types of materials with a controlled dimensionality of the internal architecture:

— fabrication of supramolecular assemblies based on host–guest complexes,

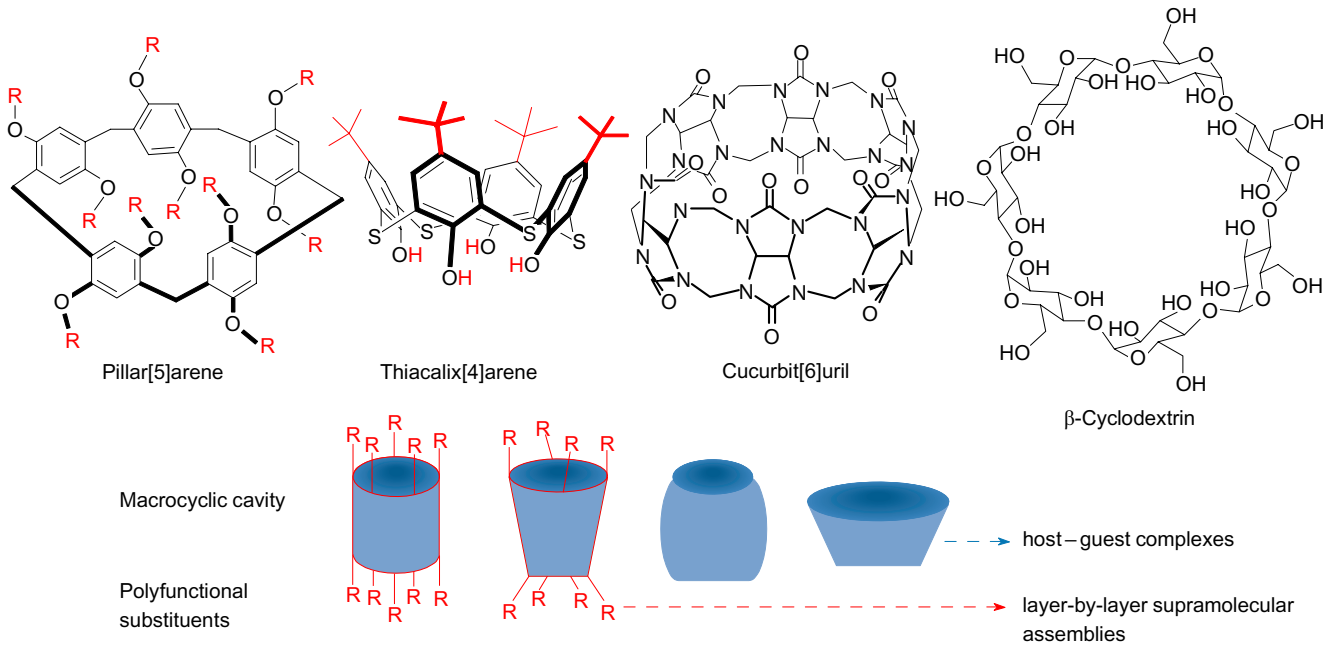


Figure 129. Examples of macrocyclic structures, components of supramolecular assemblies.

— layer-by-layer assembly of supramolecular assemblies due to ion–ion interactions.

The first approach is based on the fact that macrocyclic compounds are able to encapsulate guest molecules or their fragments into their cavities (see Fig. 129), thus forming host–guest complexes. This unique ability of macrocycles to molecular recognition is used for their supramolecular assembly *via* incorporation of parts of connecting blocks into the molecular cavity. The second strategy involves functionalization of macrocyclic compounds with charged groups, which allows the formation of layer-by-layer supramolecular assemblies due to ion–ion interactions.

The formation of continuous porous structures through self-assembly of macrocyclic compounds can not only provide cooperative binding of guest molecules, but also introduce new properties that would differ from simple host–guest type complexation. For example, one-dimensional (1D) channels constructed by linking macrocyclic systems can be used as transmembrane channels for water, ions or neutral small molecules. Additional voids can be formed in two-dimensional (2D) and three-dimensional (3D) structures of assemblies, which also provide new binding sites for more complex molecules such as proteins, DNA and RNA. Most supramolecular assemblies are obtained through non-covalent interactions such as hydrogen bonds, metal coordination bonds, host–guest interactions and π–π stacking based on a single macrocyclic platform. Recently, combination of multiple macrocyclic platforms to increase the diversity of supramolecular nanoparticles has become a relevant trend.[1091–1095] Extension and systematization of studies of the systems obtained by the co-self-assembly of two macrocyclic platforms contribute to understanding of self-assembly patterns and allow deliberate selection of components guided by the acquired knowledge. Combining several macrocycles often leads to better results than using each of them separately. From the point of view of synthesis and applications of new polyfunctional particles, these solutions significantly expand the possibilities of using macrocycles.

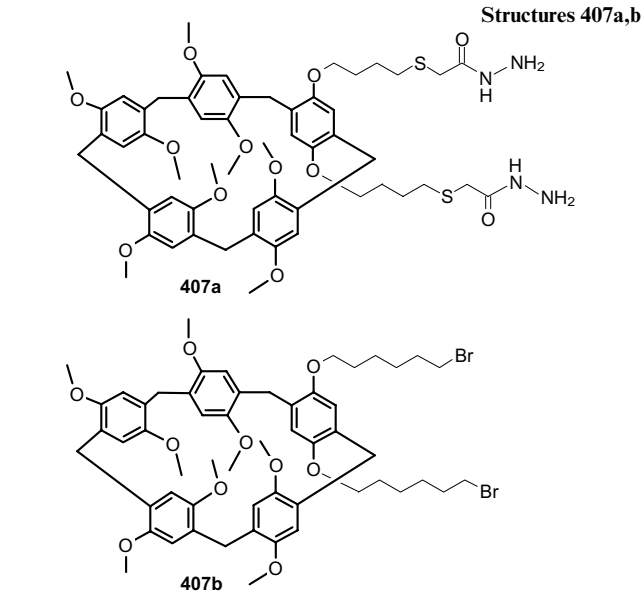
This part of the review addresses two trends of co-self-assembly of macrocyclic compounds:

— formation of new materials with desired properties due to the ability of macrocycles to encapsulate guest molecules in their cavity,

— layer-by-layer assembly of macrocycles through electrostatic interactions with the formation of supramolecular assemblies for creation of biomimetic systems.

3.6.1. Supramolecular assemblies based on host–guest complexes

Using the ability of pillar[5]arenes to bind linear aliphatic guest molecules, Lin *et al.*[1096] constructed a two-dimensional supramolecular framework formed through the host–guest interaction (Fig. 130). For this purpose, two pillar[5]arenes were chosen, one of which was functionalized with two thioacetylhydrazine moieties (**407a**) and the other with two 5-bromohexyl groups in the *para*-position of the aromatic ring (**407b**), with fragments of the latter acting as guests for the second host. Compared to the dense structures constructed by lateral π–π stacking of pillar[5]arenes in which macrocycles as polyhedra are closely arranged to one another with their faces and interact non-covalently by overlapping with neighbouring π-orbitals of the aromatic system, this assembly appears less dense and, as a consequence, more porous.[1096] The free bis(thioacetylhydrazine) moieties not involved in complexation demonstrated a high



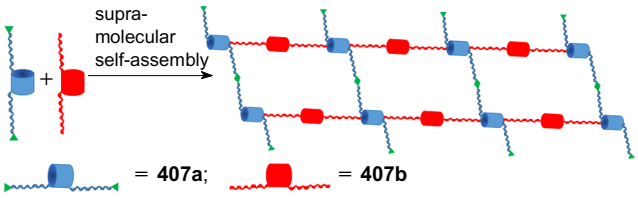


Figure 130. Schematic representation of the two-dimensional supramolecular framework formed by the host–guest interaction involving derivatives of pillar[5]arene **407a**,**b**.[1096]

ability to bind Hg^{2+}, Cr^{3+}, Cu^{2+} and Fe^{3+} cations as well as to detect F^-, Br^- and L-cysteine anions through their sensitive fluorescence response.

These planar 2D structures can easily be constructed from identical pillar[5]- or pillar[6]arenes. Most of such supramolecular assemblies are similar due to the use of the same building blocks; as a consequence, the diversity and functionality of such structures is very limited.[454, 1092–1098] To expand their range, so-called self-sorting materials based on two different macrocyclic platforms, crown ether **408** and pillar[5]arene **407c** were synthesised [1099] (Fig. 131). In this case, the ability of pillar[*n*]arenes to form complexes

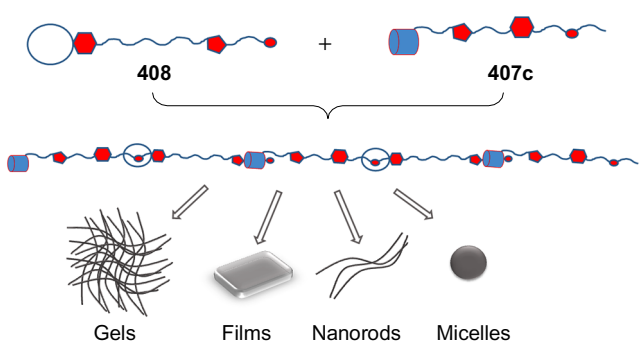
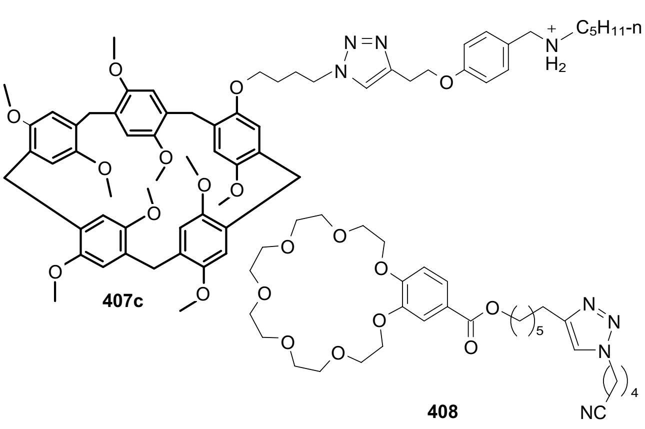


Figure 131. Self-sorting materials based on two macrocyclic platforms, crown ether **408** and pillar[5]arene **407c**.

Structures 407c, 408



with positively charged and neutral molecules combined with the propensity of crown ethers to bind ammonium groups was exploited. This strategy involves the integration of these two types of non-covalent interactions to produce supramolecular alternating polymers capable of forming zero- to three-dimensional hierarchical materials, by varying only solvent evaporation rate.

More complex self-sorting systems were obtained by Manganaro *et al.*[1100] Self-sorting was based on the ability of different molecules to selectively recognize their mutual counterparts even in the presence of competing molecules.

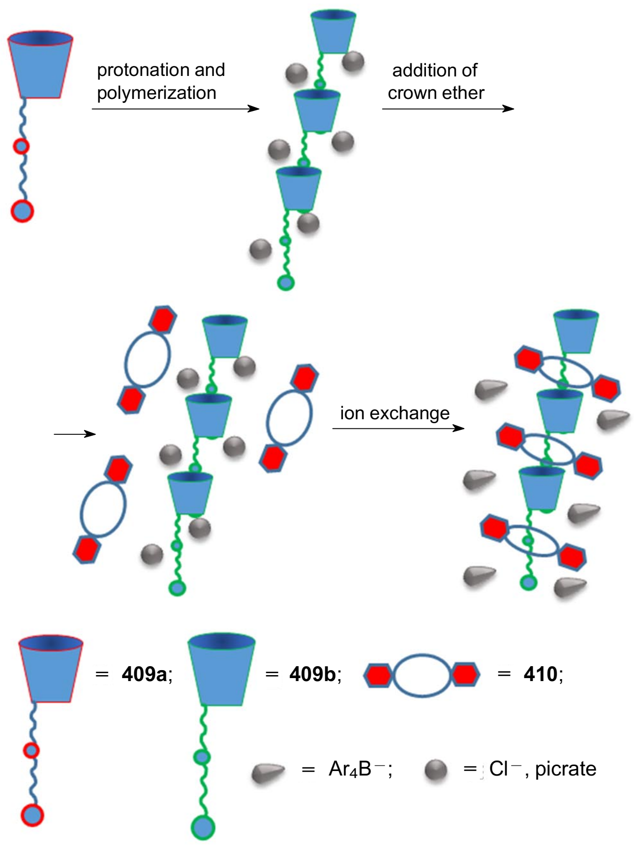
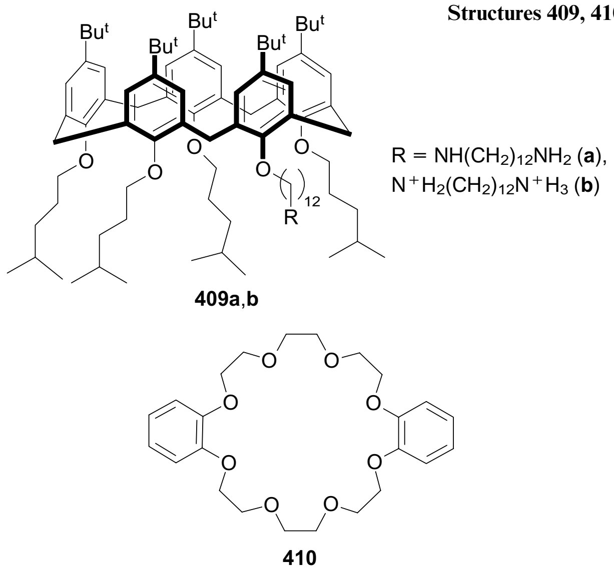


Figure 132. Self-sorting system based on two macrocyclic platforms, calix[5]arene **409a** and crown ether **410**, in the presence of the Ar_4B^- organic anion [Ar = 3,5-$(F_3C)_2C_6H_3$].[1100]

A multicomponent supramolecular system consisting of two different hosts (calix[5]arene **409a** and dibenzo-24-crown-8-ether **410**) and two different guests (alkyl- and dialkylammonium cations) is able to self-assemble into a strictly defined supramolecular architecture. This is due to the self-sorting of the host – guest pairs, calix[5]arene with a primary alkylammonium ion (NH_3^+) and dibenzo-24-crown-8-ether with a secondary dialkylammonium ion (NH_2^+), controlled by the action of counter ions (Fig. 132). In light of recent applications[1101 – 1103] of polypseudorotaxanes in nanomedicine and materials science, Manganaro *et al.*[1100] demonstrated a new approach to produce highly organized supramolecular materials.

Structures 409, 410



The combination of self-assembly and the self-sorting principle in a multicomponent system comprising two hosts (crown ethers) and three guests was used[1101] to assemble two new tris[2]pseudorotaxanes (Fig. 133). The multicomponent assembly was controlled by the implementation of two types of non-covalent interactions (metal – ligand and host – guest interactions), while self-sorting was controlled by the size of the guest molecules and steric effects.

Heteropseudorotaxanes were obtained involving cucurbit[8]urils and cyclodextrins[1102, 1103] by mixing two complexes, cucurbit[8]uril complex with adamantanyl viologen and β-cyclodextrin complex with 2-hydroxynaphthalene. During the formation of this system, exchange of guest molecules was observed, so that the adamantyl moiety was located in the cyclodextrin cavity, while naphthalene was located in the cavity of cucurbituril. Cyclodextrin played a key role in the assembly of this system. In the absence of CD, cucurbituril mainly bound the adamantyl moiety of the guest molecule, so its cavity could not participate in the formation of a stable charge transfer complex of adamantanyl viologen with hydroxynaphthalene.

The application of cooperative assembly of cucurbituril and cyclodextrin can also be extended to the construction of more complex supramolecular architectures, two-dimensional pseudopolyrotaxanes. For instance, a pseudorotaxane was synthesized from monosubstituted β-cyclodextrin and cucurbit[6]uril.[1104] The subsequent addition of a linear polymer to this pseudorotaxane led to the formation of pseudopolyrotaxanes simultaneously in the main and side

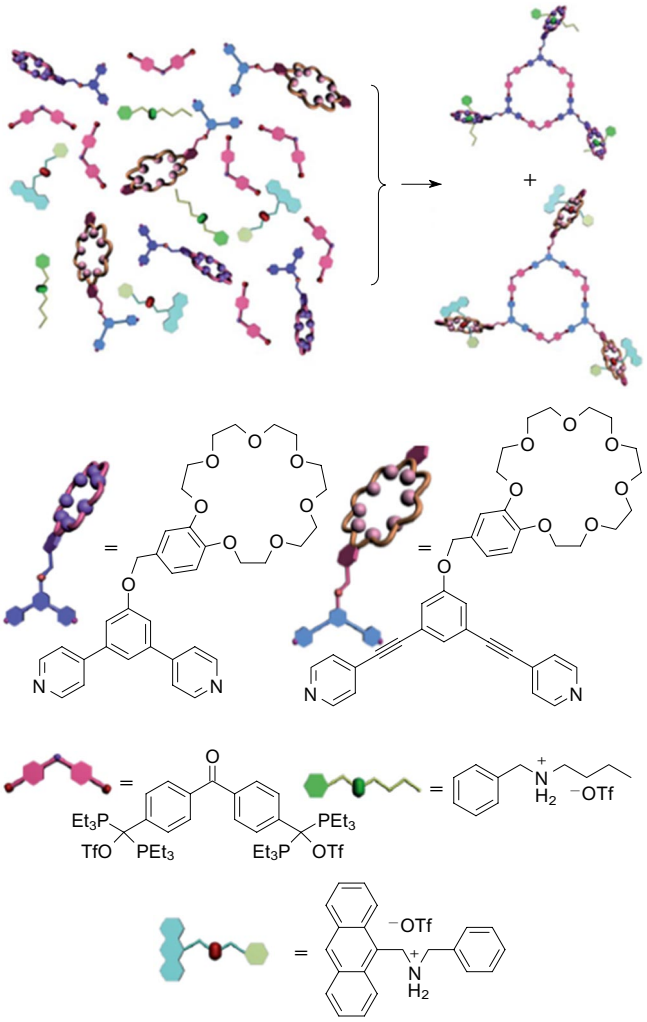


Figure 133. Schematic representation of the synthesis of tris[2]-pseudorotaxane based on self-assembly and the principle of self-sorting.[1101]

chains. Notably, the 2D-pseudopolyrotaxane in the main chain transformed into 1D pseudopolyrotaxane in the presence of a base. Subsequent addition of α-cyclodextrins can lead to a reverse switching to 2D-pseudopolyrotaxane. The topological structures and reversible interconversions of pseudopolyrotaxanes are not only applicable for the development of novel supramolecular polyrotaxanes and multicatenanes, but also provide an opportunity to design and develop molecular switches and machines based on pseudopolyrotaxane.

Hetero[4]rotaxanes were synthesized on the basis of cucurbit[6]uryl and pillar[6]arene.[1105] In these structures, a pillar[6]arene molecule located between two cucurbit[6]uril moleculess is conformationally mobile in solution and assumes energetically advantageous conformation with C_{3V} local symmetry in solid state. This study demonstrated the importance of hydrogen bonds for accelerating alkyne – azide 1,3-dipolar cycloaddition reactions in which cucurbit[6]uryl acts as a template.

Mixing of five- and six-membered macrocycles can lead to warping of the surface to give spherical assemblies similar to fullerene C_{60} molecule. Indeed, three-dimensional vesicular assemblies were obtained[1106] by co-assembly of the pentagonal pillar[5]arene and the hexagonal pillar[6]arene

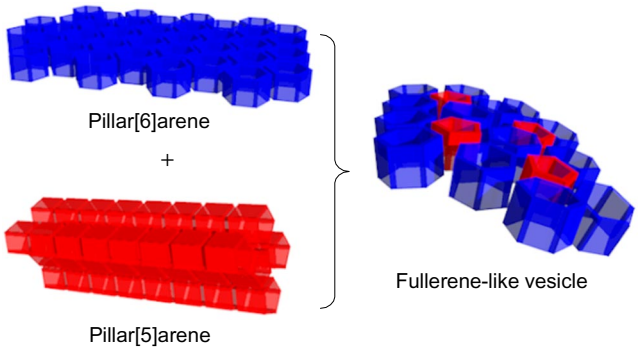


Figure 134. Schematic representation of three-dimensional vesicular assemblies formed by the co-assembly of pentagonal a pillar[5]-arene and a hexagonal pillar[6]arene.[1106] Published with permission from the American Chemical Society.

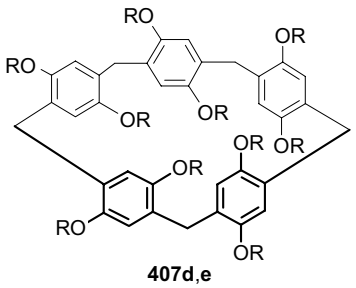
(Fig. 134). As shown above, the highly symmetric pillar[6]-arene easily forms 2D layers. The addition of a low-symmetry pillar[5]arene leads to surface bending and transition from a layered (2D) structure to a three-dimensional (3D) structure. When the ratio of five- and six-membered macrocycles is 12 : 20, the co-assembled structure becomes similar to the structure of fullerene C_{60} molecules, also composed of penta- and hexagons. The five-membered rings in fullerene provide the curvature required to form its spherical structure. Thus, pillar[5]arene provided the curvature for the formation of the vesicular structure.

Consequently, using the ability of macrocyclic compounds to encapsulate guest molecules into their cavity, not only host – guest type complexes can be obtained, but also new materials of various dimensionality (1D, 2D, 3D) can be formed upon combination of either similar or different macrocycles.

3.6.2. Layer-by-layer assembly of supramolecular assemblies through ion – ion interactions

The pillar-like shape of pillar[*n*]arenes is ideal for surface modification and formation of one-dimensional (1D) channels.[1107] The regular polygonal prism shape of pillar[*n*]arenes facilitates the construction of highly ordered structures, such as two-dimensional (2D) layers and three-dimensional (3D) spheres. The multilayer films obtained by layer-by-layer alternation of pillar[5]arene **407d** containing ten positively charged terminal moieties and pillar[5]arene **407e** with ten anionic groups selectively bind the guest molecules, dinitrobenzene derivatives, according to their geometrical size (Fig. 135). For instance, the cavity size of pillar[5]arene is ~4.7 Å, which is larger than that of the *p*-dinitrobenzene molecule (~4.3 Å), but smaller than that

Structures 407d,e



407d,e

R = $(CH_2)_3NH_2^+$ (**d**), $CH_2CO_2^-$ (**e**)

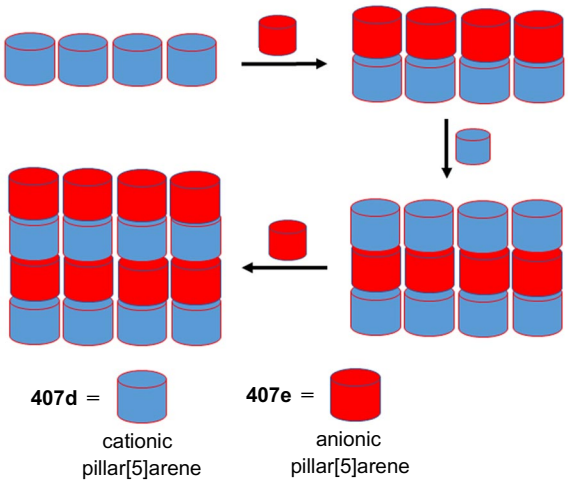


Figure 135. Multilayer films obtained by layer-by-layer alternation of pillar[5]arenes **407d**,**e**.[1108] Published with permission from the American Chemical Society.

of the *o*-dinitrobenzene (~5.9 Å) or *m*-dinitrobenzene (~5.9 Å) molecules. Therefore, this multilayer film selectively binds only *p*-dinitrobenzene.[1108]

The volume of such pores can be controlled by varying the number of deposited layers, which is a new method for constructing controlled microporous thin films that can potentially find application in molecular separation and storage of substrates.

Layer-by-layer structures of this kind were obtained using another macrocyclic platform, thiacalix[4]arene. Yakimova *et al.*[1109] carried out self-assembly of supramolecular building blocks, cationic and anionic derivatives of thiacalix[4]arene, and thus obtained polyionic mixed nanoparticles of various sizes with different stability and morphology. Quaternary ammonium salts **411a**,**b** based on thiacalix[4]arene in the *cone* and *1,3-alternate* configurations were used as cationic macrocycles. The second building block was an oppositely charged macrocycle, thiacalix[4]arene **411c** in the *cone* configuration, functionalized at the lower rim with four alkylsulfonate fragments (Fig. 136). The authors have shown that by changing the configuration of the macrocycle included in the associate, it is possible to change its affinity to biopolymers.

The self-assembly of water-soluble pyridinium-substituted porphyrins with functionalized calixarenes containing carboxylate moieties at one rim and sulfonate moieties at the other rim leads to the formation of associates with well-defined stoichiometry, which is regulated by pH.[1110] At pH 2 and 6 and various porphyrin : calixarene ratios, two types of architectures are formed. Both complexes are stabilized by the synergism of non-covalent interactions such as

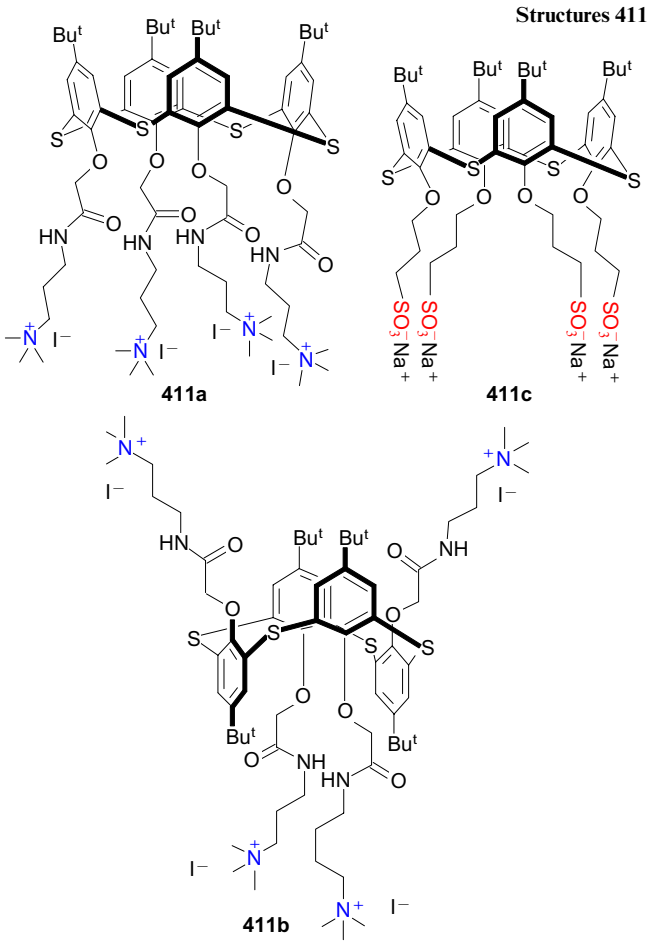
— electrostatic interactions between the positively charged groups on the porphyrin rings and the anionic sulfonate groups,

— π – π stacking between the porphyrin rings,

— CH···π interactions between the N^+ – Me group and the calixarene molecule.

The same stoichiometry of the complexes is maintained both in solution and in the solid state.

By combining water-soluble bis(*p*-sulfonatocalix[5]arenes) **412a**,**b** and cationic porphyrins **413a**,**b**, Guo



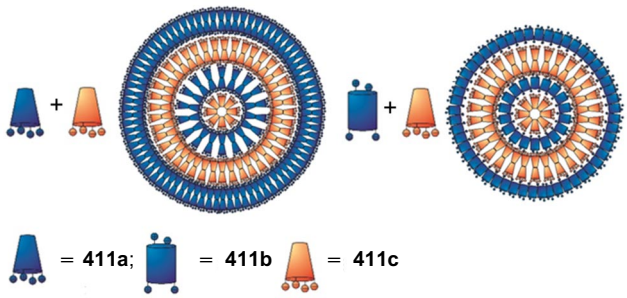
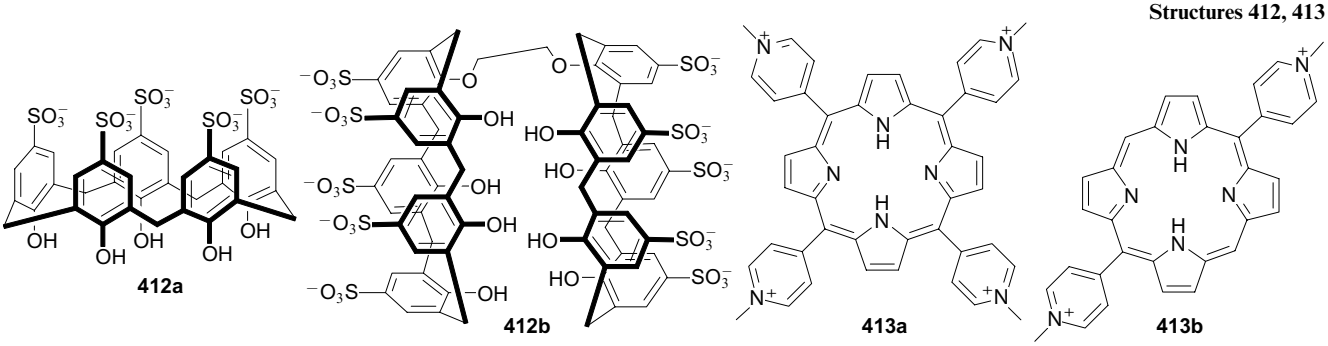


Figure 136. Layer-by-layer structures based on the cationic and anionic derivatives of thiacalix[4]arene **411a – c** in the *cone* and *1,3-alternate* configurations.[1109] Figure adapted from Ref. 1109 and published with permission from Springer Nature.

et al.[1111] obtained two types of supramolecular nanoarchitectures with 2D network and one-dimensional linear topological structures (Fig. 137). When forming these architectures, charged moieties of the porphyrin macrocycle act as guests, and self-assembly itself is driven by electrostatic interactions. The combination of two types of intermolecular interactions makes it easy to synthesise high-purity supramolecular aggregates by simple stoichiometric mixing. The result is well-ordered nanostructures with well-defined size, shape and spatial distribution that can be controlled by the design of host and guest binding sites. Moreover, in these supramolecular systems, calixarenes and porphyrins act not only as interacting tectons, but also as efficient

Structures 412, 413



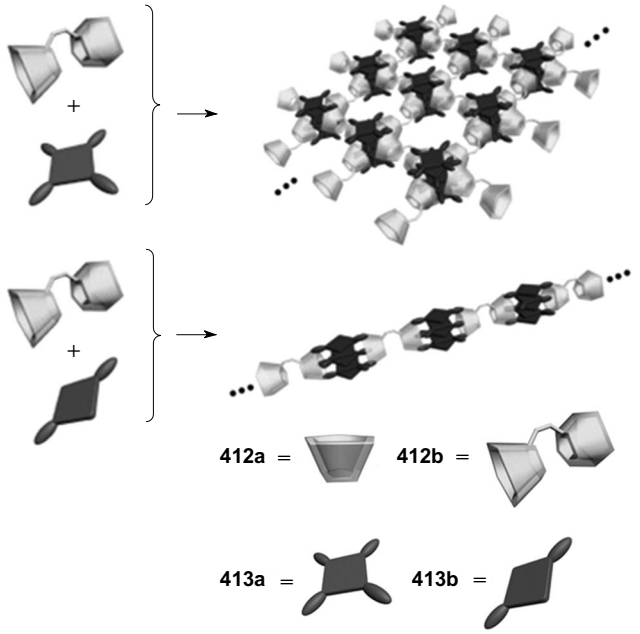


Figure 137. Supramolecular nanoarchitectures with two-dimensional network and one-dimensional linear topological structures based on water-soluble *p*-sulfonatocalix[5]arenes **412a**,**b** and cationic porphyrins **413a**,**b**.[1111] Published with permission from Wiley.

donor-acceptor electronic systems. As a consequence, the constructed supramolecular aggregates exhibit photoelectric properties with electron transfer between building blocks in the nanoscale region. These results are important for potential applications in artificial photosynthesis, as well as in engineering molecular electronics and optoelectronics.

Xu *et al.*[1112] made use of the heterovalence principle widespread in Nature to combine two different macrocyclic receptors (amphiphilic calixarene **414** and cyclodextrin **415**) into one assembly intended for heteromultivalent molecular recognition of model peptides (Fig. 138). These receptors were used to study interactions with proteins, in particular, inhibition of fibrillation and dissolution of amyloid β-peptides through interactions with the 42-membered amyloid β-peptide (Aβ 42). This approach is currently very relevant, since the implementation of the principle of heteromultivalence *via* covalent cross-linking of various macrocycles into one framework is still a challenge, as labourious procedures are often required to fabricate complex covalent structures.

Thus, the relative ease of functionalization of some macrocycles, such as (thia)calix[*n*]arenes and pillar[*n*]arenes, allows the development of new approaches to the synthesis of polyfunctional species for medical puposes, providing high regularity of their structure, hydrophilic – hydrophobic balance and compatibility with biological receptors, high affinity towards substrates with different structure, hydrophilicity and molecular weight, as well as the possibility to control the above properties by varying the nature of the host substituents in the polyelectrolyte associates.

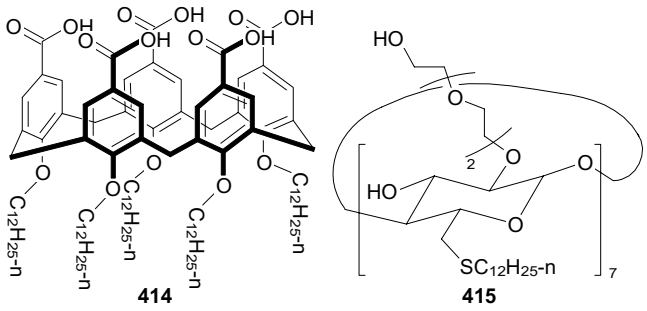
To summarize the material in this Section, we can conclude that the co-assembly of macrocyclic compounds of different classes opens up the possibility of obtaining 1D, 2D and 3D supramolecular assemblies using two basic approaches:

— polyelectrolyte assembly of polyions (layer-by-layer),

— application of host – guest complexes (with inclusion complexes as a special case) characteristic of macrocycles.

The simultaneous implementation of the above approaches is often possible for a limited range of macrocyclic derivatives, such as (thia)calix[*n*]arenes and pillar[*n*]arenes. However, in the case of most synthetically difficult to access polyfunctional macrocycles (cucurbiturils, cyclodextrins, crown ethers), self-assembly is usually based

Structures 414, 415



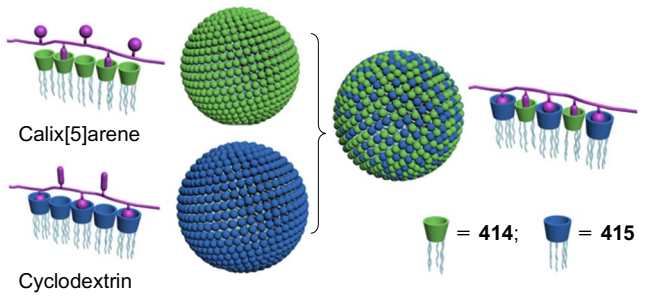


Figure 138. Supramolecular assemblies based on amphiphilic calix[5]arene **414** and cyclodextrin **415**.[1112]

on their ability to form inclusion complexes. The co-self-assembly of several macrocycles allows the creation of intricately organized biomimetic systems according to the heterovalence principle, which can become a fundamental basis for the construction of artificial biological systems.

3.7. Self-organization and self-assembly of nanostructures based on short-chain oligopeptides

3.7.1. Oligopeptides and nanostructures based on them

Oligopeptides are natural or synthetic substances the molecules of which are composed of amino-acid residues linked by amide bonds. The number of amino acid residues in oligopeptides is not clearly defined and can vary from 2 to 10.[1113–1115] In the solid state and in solution, oligopeptides exist mostly in zwitterionic form, and in the gas phase, they exist in the molecular form.[1116, 1117] Depending on the nature of the side chains in the α-amino acid residues occurring in oligopeptides, their molecules can display hydrophobic, hydrophilic, basic and acidic properties,[1118] and also possess various capacities for self-assembly and self-organization.[1119–1121]

An important feature of oligopeptides is their ability to form porous or plate-like crystals[1119, 1122] and various nanostructures including particles,[1123] fibres,[1124] rods,[1125] tubes,[1126] spheres,[1127] dendritic structures,[1128] *etc.*[1120] (Fig. 139). These nanostructures can exhibit piezoelectric,[1129] nonlinear optical,[1130] semiconducting[1131] or luminiscent[1132] properties and demonstrate electrochemical activity[1130] and unique stiffness, which exceeds that of steel.[1133] Due to their low toxicity, biocompatibility and environmental friendliness, oligopeptide nanostructures are often considered as good alternatives to inorganic nanomaterials.[1119, 1122, 1134]

The scope of application of materials based on oligopeptides (Fig. 140) is constantly expanding.[1135, 1136] They are employed in biosensing systems for selective detection of neurotoxins,[1137] for producing hybrid organic-inorganic [1138] and composite nanomaterials, including energy storage devices[1139] and microfluidic reactor systems,[1140] for producing stable supramolecular hydro-[1141] and organogels,[1124] self-cleaning superhydrophobic surfaces,[1142] high-performance catalysts,[1143] piezoelectric materials for biomedicine,[1144] biodegradable hybrid materials for electronics,[1145] triboelectric energy generators,[1146] optical waveguides,[1147] and materials for optoelectronic devices.[1148] Porous crystals of oligopeptides can be used for gas separation,[1149] desalination of seawater through reverse osmosis,[1150] and encapsulation of volatile anaesthetics.[1151]

To be effectively used in various fields and technologies, oligopeptide-based structures should meet the specific requirements for supramolecular architecture. For example, biomedical applications relating to tissue engineering or drug delivery systems require biocompatible fibrillar structures tending to form gels,[1152] or cell-penetrating vesicles.[1153] High-sensitivity sensor systems or energy storage devices require highly stable nanotubes.[1135] When developing superhydrophobic or self-cleaning surfaces, nanorods are preferably used.[1154] Porous crystals of oligopeptides proved to be suitable for the effective separation of gas mixtures and binding of single gases.[1149, 1155]

3.7.2. Methods for producing nanostructures based on oligopeptides

Organic nanostructures and crystals of oligopeptides can be produced *via* self-assembly from solutions in various solvents,[1117, 1156] by treatment of amorphous oligopeptide films with vapours of compounds at elevated temperatures,[1154] by vapour deposition from powders,[1157] by plasma-enhanced chemical vapour deposition[1158] and enzy-

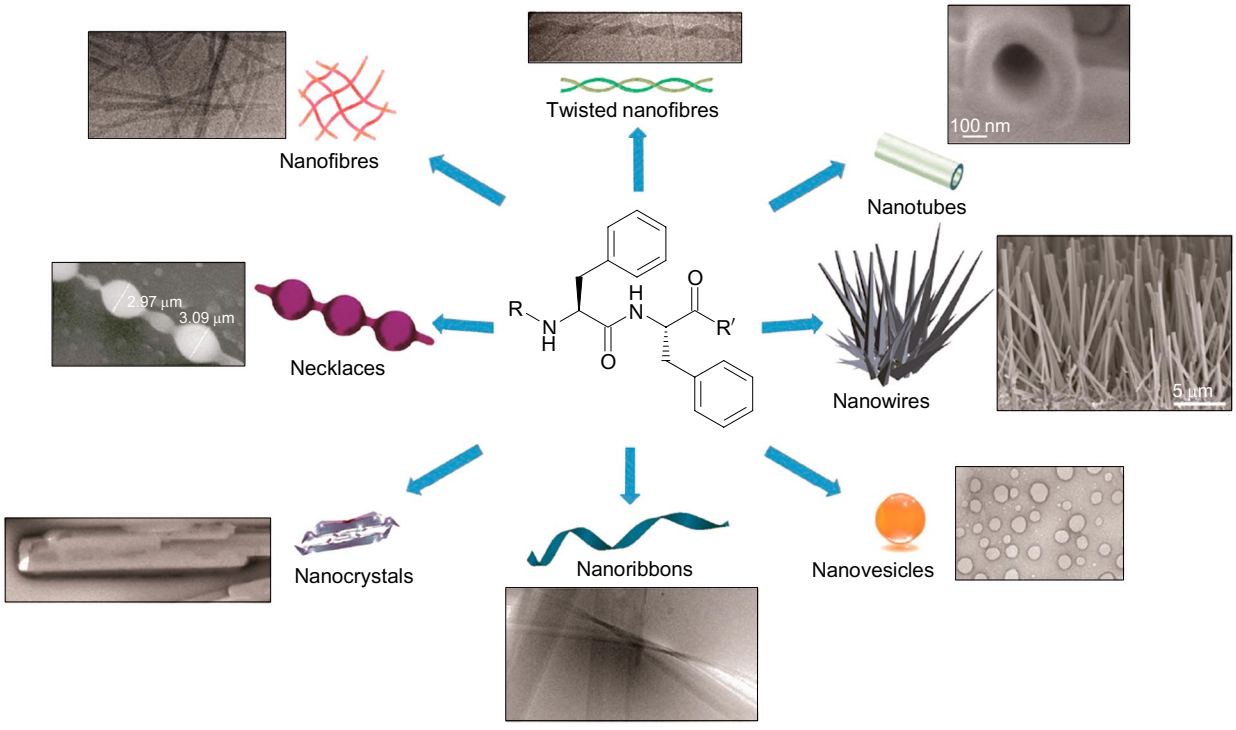


Figure 139. Nanostructures based on diphenylalanine (Phe-Phe) derivatives.[1120]

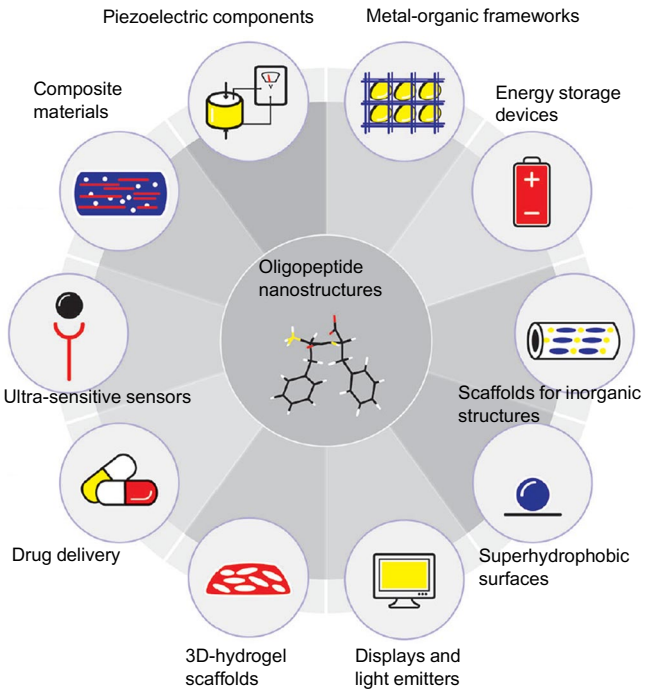


Figure 140. Application of nanostructures based on diphenylalanine.[1135] Reproduced with permission from the Royal Society of Chemistry.

matic catalysis.[1159] Below, thermodynamic features of the formation of oligopeptide-based nanostructures are considered.

3.7.2.1. Molecular self-organization and molecular self-assembly

As mention above, self-association of oligopeptide molecules to form well-ordered structures occurs as a result of self-assembly or self-organization, which can be defined as processes of ordering of molecular units into supramolecular structures due to intermolecular non-covalent interactions.[1160–1162] From a thermodynamical point of view, self-assembly and self-organization are different processes.[1163] Self-assembly occurs as a spontaneous ordering of molecules into supramolecular architectures due to specific and/or non-specific interactions. Self-assembly decreases the free energy of the system, and the system reaches thermodynamic equilibrium. Self-organization, on the contrary, occurs away from thermodynamic equilibrium in open systems with an external energy source. Self-organizing systems are involved in interaction with the environment; therefore, the outcome of self-organization depends both on the structure of interacting species and on the environmental conditions.[1163]

The driving forces of self-assembly and self-organization of oligopeptides, and forces stabilizing the resulting structures, include specific and non-specific intermolecular interactions such as hydrogen bonding, $\pi-\pi$ stacking, electrostatic, hydrophobic and van der Waals forces and also surface tension.[1153, 1164–1166] Depending on the structure of oligopeptides, the contribution of each type of interaction to the self-association processes can vary, thus providing nanostructures of different structures and properties.

3.7.2.2. Kinetic and thermodynamic control of oligopeptide self-association

The thermodynamic stability of the formed nanostructures is defined by a combination of the above-mentioned non-covalent interactions occurring in the system. At the same time, due to the relatively low energy of these interactions, self-association can be usually controlled by varying thermodynamic and kinetic parameters including the concentration of oligopeptide, temperature, pH value, type and ratio of the solvents, *etc.*[1167] Under the controlled change of kinetic parameters, the resulting nanostructures can be fixed in the metastable states such as fibrils (gel), ribbons and nanospheres (NS) (Fig. 141). Further, if the kinetic parameters stop changing, the generated metastable structures transform into thermodynamically more favourable states, *e.g.*, crystals, nanotubes (NT), and nanowires (NW) (see Fig. 141).[1167]

However, it should be noted that significant progress in the field of producing oligopeptide structures with a given molecular organization or methods for predicting the type of structure formed under specific conditions still has to be achieved. The main challenge is that self-assembly and self-organization processes proved to be very sensitive to the influence of various factors.

3.7.3. Factors affecting the self-association of oligopeptides

The outcome of self-assembly and self-organization of oligopeptides depends on the type,[1119] sequence[1168] and number[1121, 1169] of amino acid residues in the molecules, presence of protecting groups,[1170] concentration of oligopeptide in solution and pH of the medium in which the structures are formed,[1171] physicochemical properties and the ratio of solvents,[1168, 1172, 1173] exposure to low or high temperatures,[1171, 1174] UV irradiation,[1175] acoustic,[1166] magnetic[1176] and electric[1177] fields, the type of substrate on which the structures are assembled,[1128, 1178] the presence of traces of the second solvent,[1179] relative humidity of the system,[1180, 1181] the type of vapour used to saturate the oligopeptide film,[1182–1184] *etc.* On one hand, the above factors offer important opportunities for control of the self-association of oligopeptides to prepare various micro- and nanostructures with specific properties. On the other hand, they make it much more challenging or even impos-

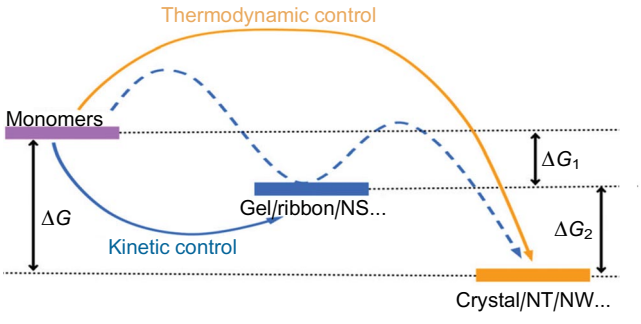


Figure 141. Self-association of oligopeptides under thermodynamic and kinetic control.[1167] Under thermodynamic control (orange solid line), the final structures occur in the minimum free energy states. By varying parameters that affect the self-assembly kinetics (pH, temperature), one can 'freeze' metastable states (blue solid line), which can further transform into thermodynamically more preferable states (blue dashed line). Reproduced with permission from the Royal Society of Chemistry.

sible to predict the type of structures that can be formed in the systems. Therefore, the search for correlations between each of the above-mentioned factors or group of factors and the result of self-association of oligopeptides is a trend of critical importance for the production of functional materials based on these systems with specified structure and properties.

3.7.3.1. Effect of the type and sequence of amino acid residues in the oligopeptide molecule

Depending on the type of amino acids making up oligopeptides, their self-assembly can lead to porous crystals containing hydrophilic or hydrophobic helical channels or plate-like crystals with two- or three-dimensional hydrogen-bond network (Fig. 142).[1119, 1122]

The effect of the sequence of amino acid residues on the self-assembly outcome is clear from the example of Leu-Ile and Ile-Leu dipeptides (see Fig. 142). The crystals of Leu-Ile contain hydrophobic columns, the inner space of which is inaccessible to the solvent molecules, whereas Ile-Leu forms porous crystals with hydrophilic channels, the diameter of which allows them to retain water molecules.[1119] The oligopeptides Ala-Val and Val-Ala crystallize to form porous crystals comprising hydrophobic channels of similar size,[1119] but the interaction of the films of these dipeptides with vapours of organic compounds considerably changes the morphology of the Val-Ala film, unlike that of Ala-Val.[1182]

A change in the sequence of amino acid residues in tetrapeptides also influences the outcome of their self-assembly. Under similar conditions, the tetrapeptide Phe-Phe-Pro-Pro forms nanorings, Pro-Pro-Phe-Phe generates fibrils, and Pro-Phe-Phe-Pro produces globules (Fig. 143).[1185] The chirality of amino acid residues constituting oligopeptides is yet another factor strongly affecting their supramolecular behaviour and self-assembly outcome even at a similar sequence of amino acid residues.[1186 – 1188]

There are currently no approaches to elucidate the effect of the oligopeptide structure on the type of nanostructures assembled from them. Self-assembly processes are studied by simply varying combinations of various amino acids, focusing on those systems and oligopeptides that provide any ordered structures. An original approach proposed by Ziganshin *et al.*[1189] may facilitate the process of such screening. The authors demonstrated the possibility to predict the results of changes in morphologies of crystals and amorphous films of oligopeptides under the action of organic vapours. For this purpose, the $S \times MR_D$ product was used, where S is the adsorption capacity of oligopeptide

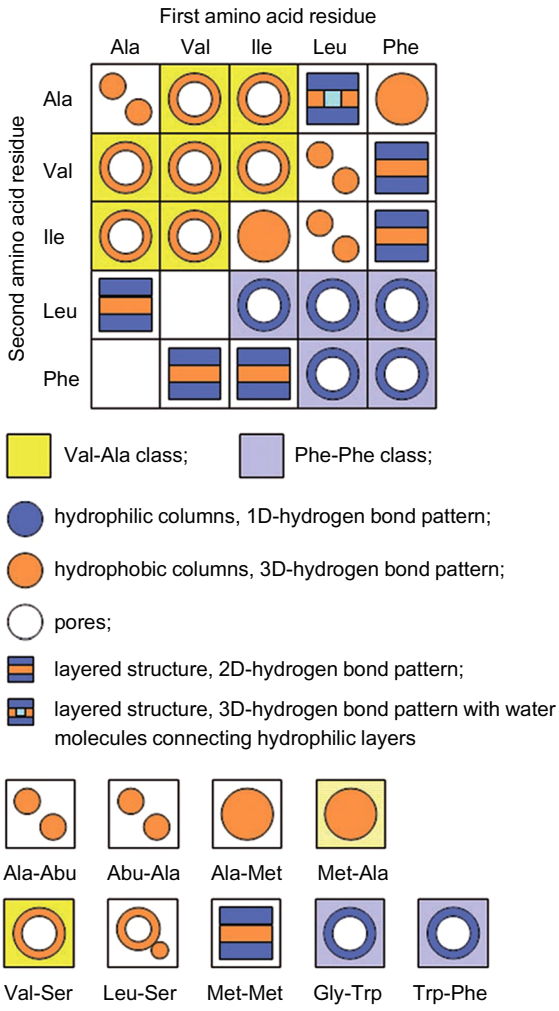


Figure 142. Types of crystals based on dipeptides.[1119] Reproduced with permission from Wiley.

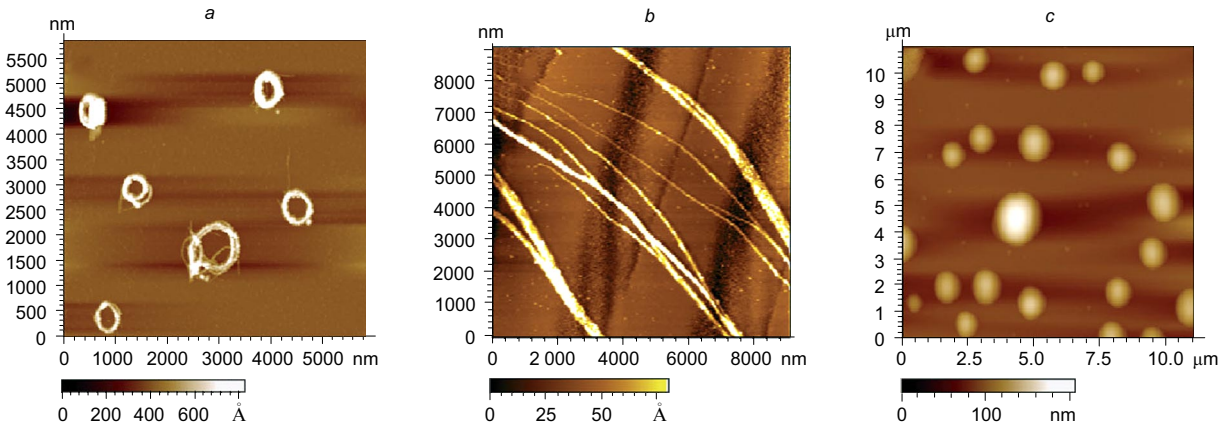


Figure 143. AFM images of structures based on peptides Phe-Phe-Pro-Pro (*a*), Pro-Pro-Phe-Phe (*b*) and Pro-Phe-Phe-Pro (*c*).[1185] Reproduced with permission from Wiley.

towards an organic guest (moles of guest per mole of host) and MR_D is the molar refraction of the guest representing the size parameter of the molecule. The S value was measured experimentally using quartz crystal microbalance sensor,[1190] the oscillators of which were coated with the oligopeptide layer. Organic guests with maximum $S \times MR_D$ values, according to the data of the sensor study, can initiate the self-assembly of the studied oligopeptide to give various structures.[1183]

3.7.3.2. Effect of the number of amino acid residues in the oligopeptide molecule

By varying the number of amino acid residues in molecules of homo-oligopeptides, one can dramatically change the results of their self-assembly under similar conditions.[1191] When going from diphenylalanine (Phe-Phe) to triphenylalanine (Phe-Phe-Phe) and further to tetraphenylalanine (Phe-Phe-Phe-Phe), the type of evolving structures changes from well-ordered nanotubes to plate-like structures composed of β-sheets (Fig. 144),[1114] and back to nanotubes, showing, however, a lot of structural imperfections compared to those based on Phe-Phe.[1192]

Another feature of tripeptides is their tendency to crystallize [1169, 1189] under conditions where dipeptides form amorphous films [1178, 1182, 1183] (Fig. 145).

3.7.3.3. Effect of temperature on self-organization of oligopeptides

Temperature is a significant kinetic factor that determines the pattern of self-organization of oligopeptides [1193, 1194] and induces transformation of some structures into other ones.[1195, 1196] A typical example of the temperature effect is the formation of various nanostructures of ferrocene-modified diphenylalanine at different temperatures. For this dipeptide, the plate-like crystal packing is thermodynamically stable. Variations of the temperature provide control over its self-organization in solution (Fig. 146).[1193] At temperatures >37 °C, path *1* is implemented, resulting in the formation of helical nanostructures (kinetic control). At $T < 30$ °C, due to low self-organization rate, thermodynamically stable flat crystals are formed (path *2*, thermodynamic control). In the range of $30 < T < 37$ °C, the originally formed metastable helical nanostructures are converted within 1–3 days to thermodynamically stable structures representing large crystals (path *3*).

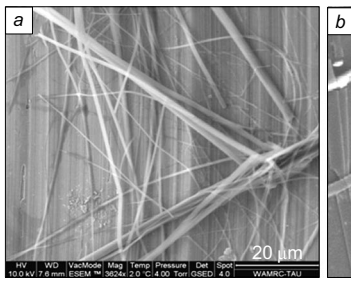


Figure 144. SEM images of nanotubes based on diphenylalanine (*a*) and plate structures based on triphenylalanine (*b*).[1114] Reproduced with permission from Elsevier.

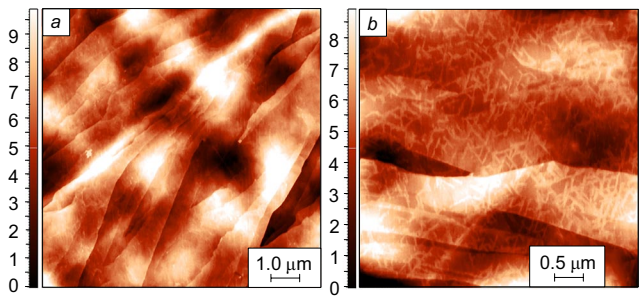


Figure 145. AFM images of the surface of an amorphous film of dipeptide Gly-Gly (*a*) and crystals of tripeptide Gly-Gly-Gly (*b*) formed on the surface of highly oriented pyrolytic graphite (HOPG) from a methanol solution.[1169]

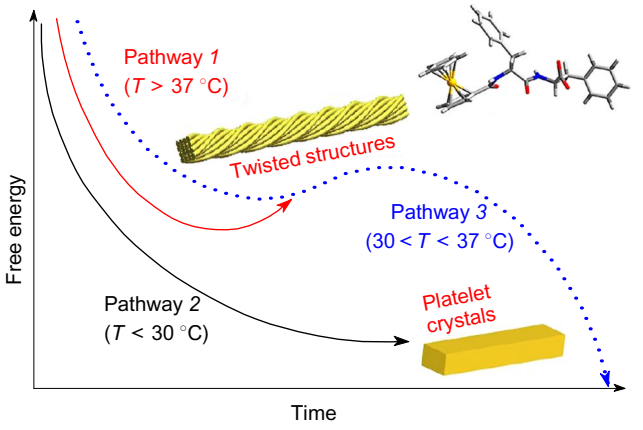


Figure 146. Scheme for the kinetically controlled self-organization of ferrocene-modified diphenylalanine. Adapted from Ref. 1193 and published with permission from the American Chemical Society.

Heating oligopeptide-based nanostructures above a certain temperature enables their transformation into other structures possessing different properties. For example, nanotubes derived from Leu-Leu and Phe-Phe and nanospheres obtained from Phe-Phe-Phe transform into fibrils at >180 °C (Fig. 147).[1121, 1195] As a result of this transformation, nanostructures lose their piezoelectric and nonlinear optical properties, but become able to generate visible (green and blue) photoluminiscence emission. The reasons for the observed transformation of nanostructures at elevated temperatures will be discussed below.

3.7.3.4. Thermally induced chemical reactions of oligopeptides in the solid state

The main challenge in the thermal treatment of oligopeptides to produce nanostructures is in the uncertainty of the final state of the system. Heating can promote chemical reactions in the solid state of oligopeptides similar to those which are well known for their solutions, namely, cyclization reactions to afford 2,5-diketopiperazine derivatives.[1196, 1197] Chemical transformations might be responsible for the formation of various nanostructures (nanowires and nanotubes) on the surface of an amorphous diphenylalanine film upon heating to 150 °C under aniline vapour or by incubation with water vapour at 25 °C.[1198] The same reason can also account for the loss of piezoelectric properties by a diphenylalanine nanotube upon heating to 140–150 °C and for the observed transition of hexagonal packing of oligopeptide to the centrosymmetric orthorhombic crystal system.[1199]

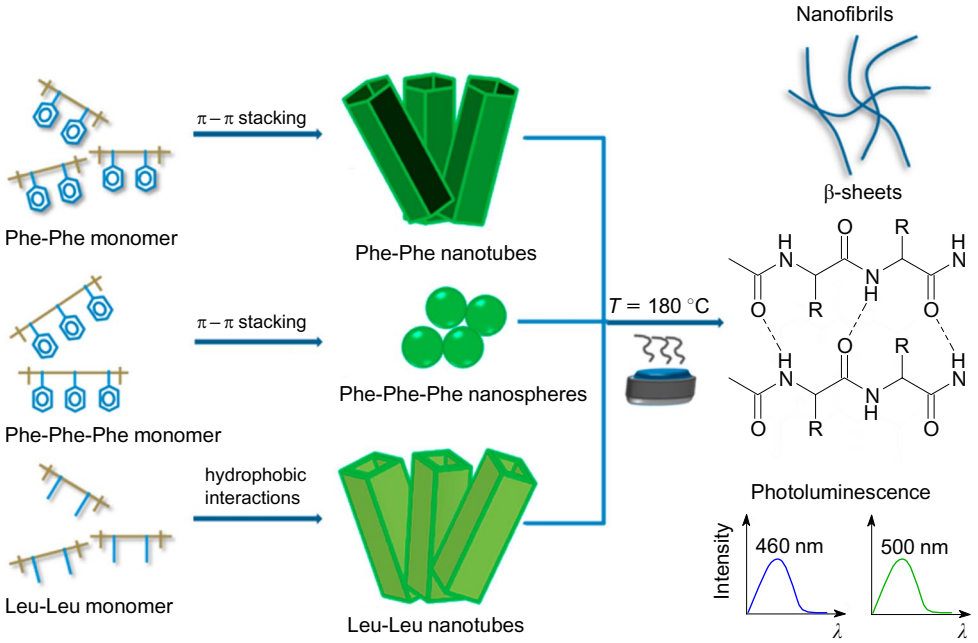


Figure 147. Scheme for the formation of nanostructures from oligopeptides and their transitions at elevated temperatures.[1121] Reproduced with permission from the American Chemical Society.

Meanwhile, thermally induced cyclizations of oligopeptides in the solid state remain underinvestigated. Glycylglycine is known to form a cyclic product in a yield of >60% when heated above 219–230 °C.[1169, 1200] The formation of 2,5-diketopiperazine derivatives in the quantitative (close to 100%) yield was found for diphenylalanine and isoleucylalanine, which began to react at 147–150 °C (Refs 1201, 1202) and 206 °C,[1203] respectively. Heating of Leu-Leu above 177 °C leads to the formation of its cyclic product, which undergoes self-assembly to afford plate structures.[1204] Therefore, for the results of thermal treatment of oligopeptides to be properly interpreted, it is necessary to know the critical temperature above which self-organization of the products of chemical reactions occurs rather than self-organization of the initial molecules. At the same time, the development of methods for the preparation of 2,5-diketopiperazine derivatives in high yields is a practically relevant task, since these compounds are of great interest for biomedicine, food industry and various production processes.[1205, 1206]

Analysis of the onset point of solid-state cyclization as a function of oligopeptide structure revealed that an increase in the size of substituents in amino acids that make up the dipeptides generally decreases the reaction temperature (Fig. 148).[1203] The detected correlation can be used to estimate the temperature range in which a linear dipeptide would form ordered structures without undergoing a chemical transformation.

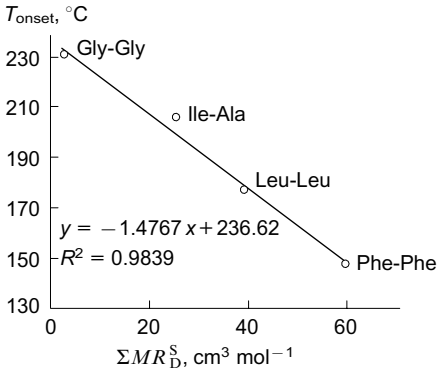


Figure 148. Correlation between the onset point (T_{onset}) of dipeptide cyclization and the values of molar refraction of substituents in their molecules (ΣMR^S_D).[1203] R^2 is the correlation coefficient. Reproduced with permission from Wiley.

3.7.3.5. Effect of the solvent on the self-assembly of oligopeptides

The physicochemical properties of solvents can significantly affect the self-assembly of oligopeptides and the type of the resulting structures,[1168, 1172, 1173, 1183, 1203] thereby allowing for the fabrication of various materials using only one oligopeptide. For example, the self-assembly of Val-Ala oligopeptide from methanol generates tubular structure and that from acetonitrile, isopropyl alcohol and chloroform leads to irregular fibre structures; in the case of pyridine, close-packed rectangular crystals are formed, while in the case of toluene and n-hexane, layered structures are obtained (Fig. 149).[1168]

One of the main properties of solvents affecting the oligopeptide self-assembly is their ability to form hydrogen bonds.[1124, 1168, 1178, 1183] Therefore, the presence of even small (trace) amounts of H-donor or H-acceptor solvents in aprotic media can drastically change the outcome of self-assembly of an oligopeptide. Thus, the addition of water to a solution of Phe-Phe in ethanol leads to self-assembly of the oligopeptide into nanotubes rather than nanorods.[1147] From the solution of Phe-Phe in dichloromethane, flat crystalls are formed, while the addition of small amounts of a second solvent such as ethanol, *N*,*N*-dimethylformamide or acetone gives rise to fibre structures in which the hydrogen bonding of the oligopeptide with the second solvent plays a crucial role (Fig. 150).[1179]

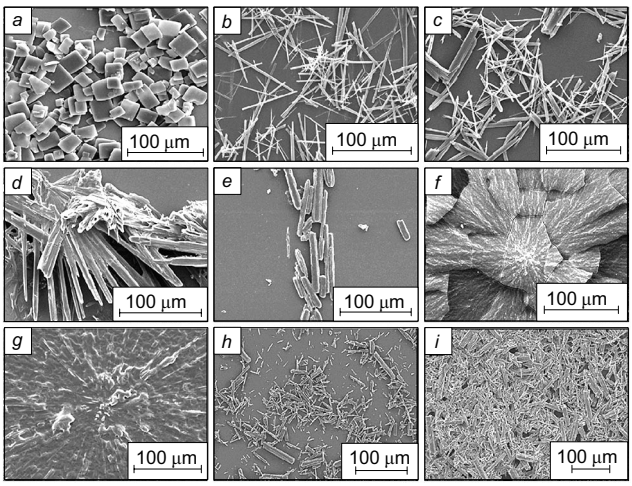


Figure 149. SEM images of Val-Ala structures obtained from various solvents: pyridine (*a*), propan-2-ol (*b*), ethanol (*c*), methanol (*d*), acetone (*e*), toluene (*f*), n-hexane (*g*), acetonitrile (*h*) and chloroform (*i*).[1168] Reproduced with permission from the American Chemical Society.

A trace amount of water present in benzene is sufficient for generating a supramolecular organogel from cyclo(leucyl-leucyl).[1124] A study of the mechanism of water influence on the self-assembly processes suggested that water induces aggregation and nucleation involving oligopeptide molecules [1207] and stabilizes the intermediate structures, which are further transfomed into final stable products.[1208, 1209]

Various nanostructures can be produced by treating amorphous oligopeptide films deposited onto solid substrates with vapours of various solvents at room temperature.[1182, 1183, 1210] Saturation of an amorphous Leu-Leu film obtained from a methanol solution on the surface of highly oriented pyrolytic graphite (HOPG) (Fig. 151 *a*) with chloroform vapour produces helical crystals (see Fig. 151 *b*). Under similar conditions, dichloromethane vapour induces self-assembly of the oligopeptide into fibrillar structures (see Fig. 151 *c*).[1183] The observed dependence of the morphology of oligopeptide nanostructures on the molecular structure of the solvents used in this way is an example of molecular recognition.[1211]

To predict the possibilities of preparing nano- and microstructures on the surface of amorphous oligopeptide film by treatment with certain organic vapours, the Hansen solubility parameters are sometimes used.[1178]

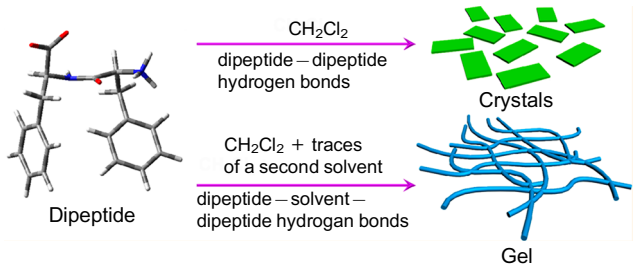


Figure 150. Scheme for the formation of various nanostructures from a solution of the dipeptide in pure dichloromethane and in dichloromethane containing traces of a second solvent (ethanol, DMF, acetone).[1179] Reproduced with permission from the American Chemical Society.

3.7.3.6. Effect of air humidity on the self-assembly of oligopeptides

The self-assembly of oligopeptides is critically affected not only by water contained in the solvents but also by water present in the air. Water vapour with thermodynamic activity † < 0.5 (air humidity $< 50\%$) does not affect the morphology of the amorphous film of diphenylalanine (Fig. 152). In the 0.5 – 0.9 range of thermodynamic activity, water triggers self-assembly of oligopeptide into small spherical aggregates, whereas at the activity of water above 0.9, diphenylalanine forms nanorods (see Fig. 152).[1125]

Air humidity also affects the self-assembly of oligopeptides on the solid substrates. The deposition of a methanol solution of Val-Val onto the surface of HOPG followed by evaporation of the solvent at 50% air humidity leads to the formation of a film non-uniformly coated with pyramidal microcrystals (Fig. 153 *a*).[1184] An increase in the air humidity up to 60% promotes the formation of two groups of pyramidal objects differing in size. The height of the first group is 24 – 50 nm (see Fig. 153 *b*), while the height of the second one is 50 – 95 nm. Further increase in the air humidity (up to 80%) alters the outcome of the Val-Val self-assembly: complex objects shaped as truncated cones appear on the film surface (see Fig. 153 *c*).

3.7.3.7. Effect of the substrate on the self-assembly of oligopeptides

When obtaining nanostructures based on oligopeptides through their self-assembly from solutions or amorphous films on solid surfaces, it is necessary to take into account the properties of the substrate, since they can have a significant effect on the configuration of the first adsorbed

† This dimentionless value is calculated as the ratio of the water vapour pressure over a salt solution to the vapour pressure over pure water.

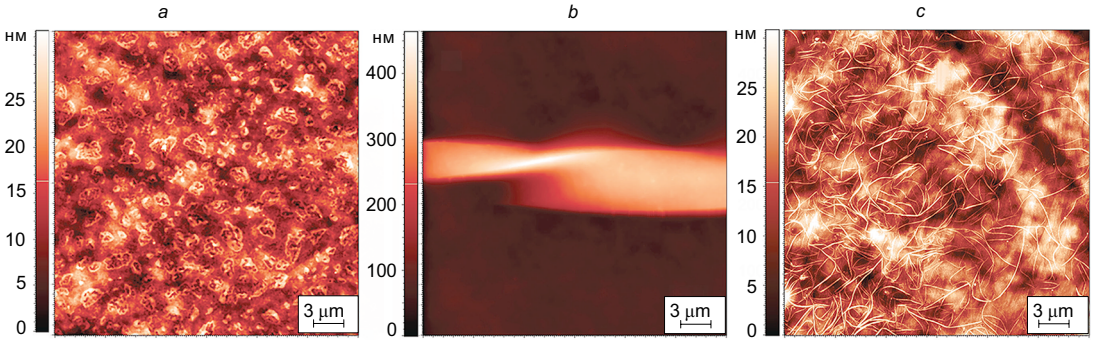


Figure 151. AFM images of the surface of an amorphous Leu-Leu film obtained on HOPG from methanol solution (*a*) and saturated with chloroform (*b*) or dichloromethane (*c*) vapour.[1183]

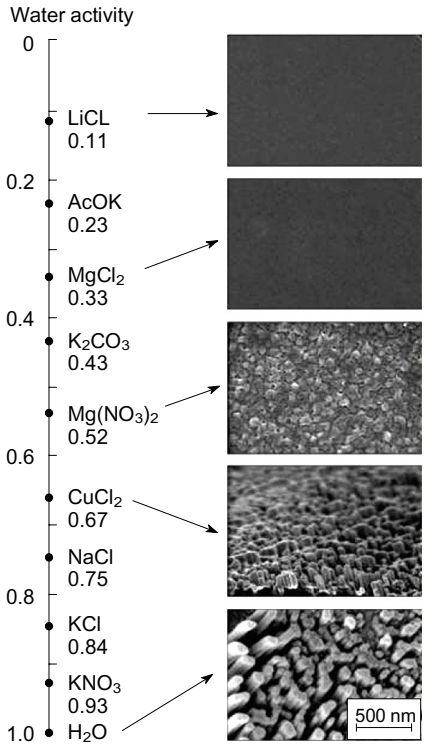


Figure 152. Effect of water activity on the morphology of nanostructures formed on the surface of the amorphous film of diphenylalanine (Phe-Phe).[1125] Reproduced with permission from the American Chemical Society.

layer and eventually on the type of formed micro- and nanostructures.[1212, 1213]

The absence of strong interactions between the HOPG surface and Gly-Gly facilitates the formation of an amorphous film of the dipeptide upon drying of its solution (Fig. 154 *a*).[1178] The amorphous Gly-Gly film is also formed on the surface of mica (see Fig. 154 *b*). However, in this case, the causes for amorphization include good wettability of the substrate, resulting in the formation of a virtually two-dimensional droplet of the oligopeptide solution, and the presence of a negative charge on the mica surface, which prevents the diffusion of oligopeptide molecules necessary for crystal growth. On a silicon wafer, Gly-Gly dipeptide deposited from an aqueous methanol solution forms elongated objects with tapered ends (see Fig. 154 *c*) due to the limited wettability of the substrate and the presence of carbonyl and hydroxyl groups orienting the oligopeptide molecules in the first adsorption layer.

3.7.3.8. Effect of the oligopeptide concentration in solution on the self-assembly

A change in the concentration (C) of the cationic oligopeptide H-Phe-Phe-$NH_2 \cdot HCl$ in solution makes it possible to initiate its self-assembly into vesicular structures (upon dilution) or into nanotubes (upon concentrating) (Fig. 155).[1214] The study carried out by the molecular dynamics method[1215] revealed that at low concentrations of the oligopeptide, the aggregation of its molecules to form small vesicles is preferable. At the same time, at high concentrations, self-assembly first produces bilayers, which are then bent into nanotubes. Interestingly, according to the performed calculations, the formation of various nanostructures results from a subtle balance between oligopeptide – oligopeptide and oligopeptide – water interactions. This conclusion once again highlights the need for taking into account the water content (even in trace amounts) in organic solvents used to obtain nanostructures. Consideration should also be given to the fact that self-assembly will lead to a decrease in the concentration of the oligopeptide in the solution. Consequently, crystallization from solutions

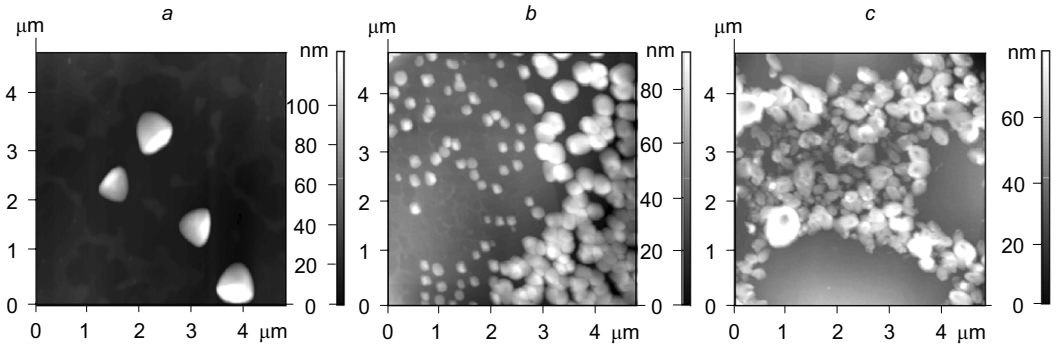


Figure 153. AFM images of the surface of dipeptide Val-Val film deposited onto HOPG at an air humidity of 50 (*a*), 60 (*b*), and 80% (*c*).[1184] Reproduced with permission from Springer Nature.

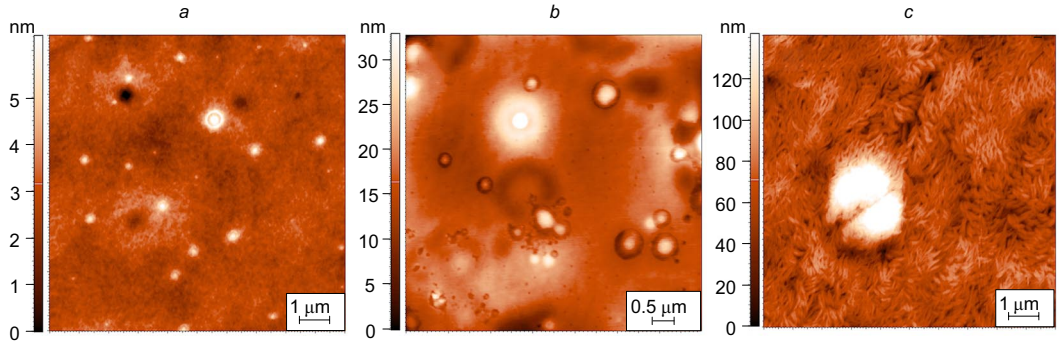


Figure 154. AFM images of Gly-Gly films deposited from an aqueous methanol solution onto HOPG (*a*), mica (*b*) and silicon wafer (*c*).[1178] Reproduced with permission from Taylor and Francis.

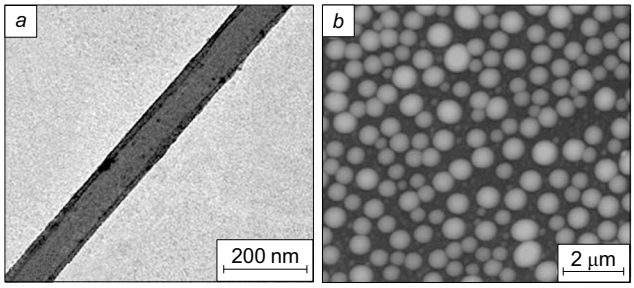


Figure 155. TEM image of a nanotube (C = 10 mg mL^{-1}) (*a*) and AFM image of vesicles (C = 1 mg mL^{-1}) of the cationic dipeptide H-Phe-Phe-$NH_2 \cdot HCl$ (*b*).[1214] Reproduced with permission from Wiley.

should provide structures that are stable at low concentrations.

3.7.3.9. Effect of pH of the medium on self-organization

The existence of the zwitterionic form of unsubstituted oligopeptides and the presence of the carboxyl group in protected oligopeptides provide for the control over their self-assembly and the properties of materials by changing pH of the medium.[1216, 1217] For example, using the indicated method, various nanostructures were obtained from substituted oligopeptide Fmoc-Phe-Phe (Fmoc is 9- fluorenylmethoxycarbonyl). At pH 9.5 – 10.2, nanofibrils are formed that reassemble into nanoribbons when pH is decreased to 5.2 – 6.2 with the subsequent aggregation and precipitating (Fig. 156).[1216]

The mechanism of this transformation is associated with a change in the secondary structure formed by the oligopeptide at different pH values. In an aqueous solution, the molecules of Fmoc-Phe-Phe are neutral and during the self-assembly, they form β-sheets that assemble into flat fibrils. An increase in the pH of the medium leads to deprotonation of the oligopeptide to generate negatively charged species, for which self-organization into helical fibrils consisting of α-spirals is preferable.[1218]

To conclude, it should be noted that in the last decade, biocompatible micro- and nanostructures based on oligopeptides have become objects of intensive research, due to the possibility of their practical applications as functional materials in various technologies and in medicine. The methods for producing nanoobjects in a diversity of shapes have been elaborated, and the basic conditions for their formation have been found. Meanwhile, the factors affecting the self-assembly and self-organization of oligopeptides are not limited only to those listed in this Section. Their diversity, as well as possible solid-state chemical reactions, provide almost infinite opportunities for obtaining materials with different structures and properties based on oligopeptides. A complex mechanism of the dependence of the self-assembly and self-organization processes of oligopeptides on external factors makes it relevant to elucidate the relationships between molecular structure, self-association conditions and nanostructure type to create new functional bionanomaterials.

4. Biomimetics

4.1. Dye – DNA complexes: interaction principles, biological and medical applications

Deoxyribonucleic acid is a macromolecule that is able to store genetic information, transmit it from generation to generation and execute the genetic programme for the development and functioning of living organisms.[1219, 1220] It is a polymer composed of nucleotides as monomeric units.[1221] A nucleotide consists of three main components: a carbohydrate moiety (deoxyribose), heterocyclic residue (adenosine, guanosine, thymine or cytosine) and phosphate. The structures of 2′-deoxyadenosine-, 2′-deoxyguanosine-, 2′-deoxycytidine- and 2′-deoxytymidine 5′-monophosphates (**416** – **419**, respectively) are shown.

The DNA molecule consists of two antiparallel strands of nucleotides. The antiparallelism lies in the opposite direction of the two strands of the DNA double helix; one strand has a direction from 5′ to 3′, the other from 3′ to 5′ [the numbers 5′ and 3′ indicate the number of the carbon atom in the sugar residue that starts or ends the chain (Fig. 157)]. The nitrogenous bases of the two strands are linked by hydrogen bonds, which stabilize the structure, together with the interactions that occur between the parallel planes of the nucleobases. In addition, nucleotide chains twist in space around each other and a common axis, forming a double helix.

DNA molecules exhibit polymorphism and exist in several conformations.[1222] The main conformations, A-DNA, B-DNA and Z-DNA, differ in the degree of twist, the orientation of the nucleobase planes relative to the helix axis and biological functions. The B-form, which includes a minor and a major groove, differing in width and depth [1223] (Fig. 158), is the predominant one.

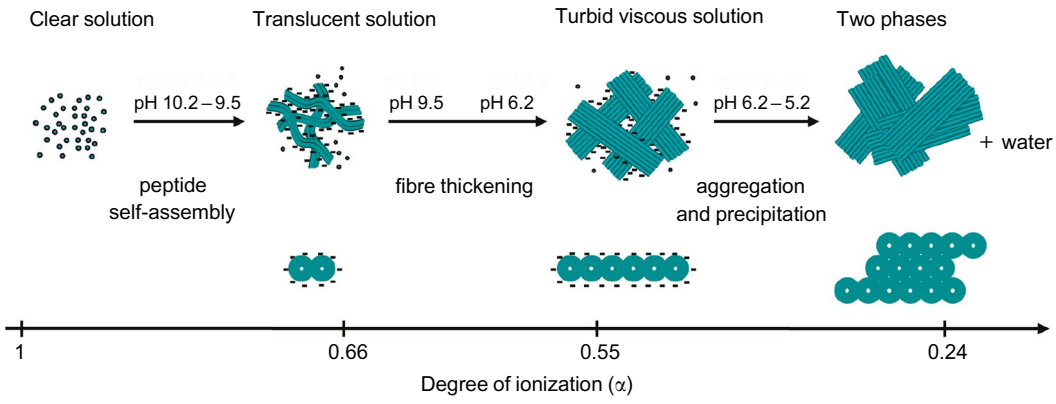
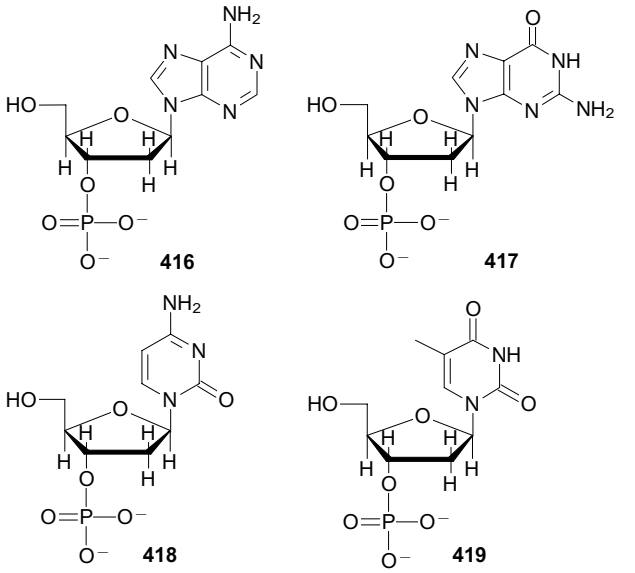


Figure 156. Effect of pH on self-organization of the substituted oligopeptide Fmoc-Phe-Phe.[1216] Reproduced with permission from the American Chemical Society.

Stuctures 416 – 419



The DNA molecule is able to bind to various species such as metal ions and drug and dye molecules. The formation of complexes with low-molecular-weight ligands can lead to changes in the DNA structure, disrupt the transmission of genetic information (replication, transcription and translation), cause single- and double-strand breaks in DNA, as well as block protein synthesis and cause genetic abnormalities. Ligand binding to the DNA of pathogens leads to inhibition of their reproduction and, in the case of cancer, can inhibit unregulated division of cancer cells.[1223] The interaction of dyes with DNA molecules provides fluorescent labelling of biopolymers. The development of highly specific fluorescent markers has given rise to a new field of biomedical imaging, fluorescence molecular imaging, the scope of research of which ranges from the subcellular level to the whole organism level.[1224]

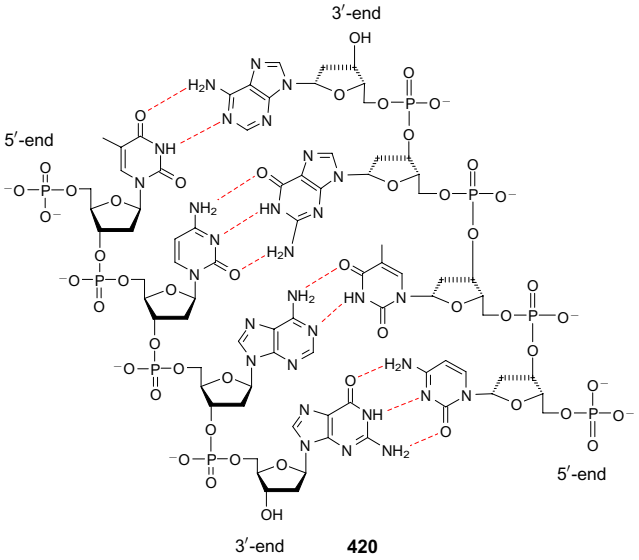


Figure 157. Fragment of a DNA molecule. The red dashed lines show hydrogen bonds.

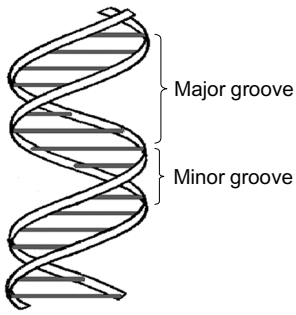


Figure 158. Minor and major grooves in the B-form of DNA.

There are three types of interactions between low-molecular-weight molecules and double-stranded DNA (Fig. 159).[1225, 1226] Among these interactions, hydrogen bonds, electrostatic, hydrophobic and π – π stacking interactions and van der Waals forces are important.

1. The external binding mechanism is based on electrostatic interactions between positively charged atoms in the binding molecule and negatively charged DNA phosphate groups, which link nucleosides.

2. Intercalation is the second mode of ligand binding to DNA. The main interactions are reduced to the insertion of an intercalator molecule between DNA base pairs. The intercalator molecule must be flat, sufficiently hydrophobic and capable of π – π stacking interactions with nucleobases.

3. Ligand binding in the DNA groove is the third type of binding of molecules to DNA. The positioning into DNA minor or major groove differs in terms of steric effects and hydrogen bonding energy. The minor groove tends to accommodate longer molecules because it is longer and deeper. Therefore, the minor groove is a more attractive target for complexation of low-molecular-weight substances with DNA. Proteins or other biomolecules are usually embedded into the major groove.[1220, 1225, 1226]

Compounds acting as intercalators or binding to the DNA minor groove are usually potentially suitable for the development of drugs based on them. However, external electrostatic ligand – DNA interactions also play an important role, as the association of positively charged counterions with the DNA polyanion has a strong influence on the conformation and stability of the nucleic acid molecule and on its ability to bind to RNA or other biomolecules.[1226, 1227]

Most intercalating agents are used as antibacterial, antiparasitic and antitumour drugs, since their intercalation

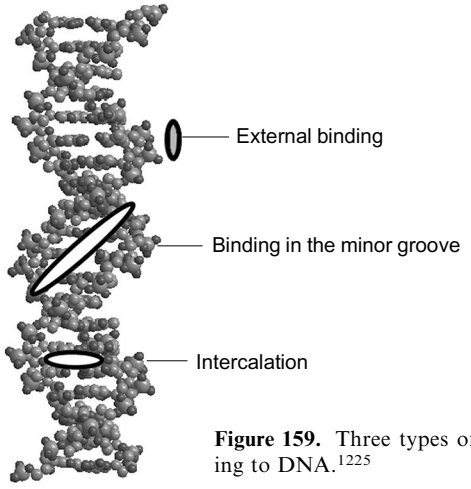


Figure 159. Three types of ligand binding to DNA.[1225]

inhibits DNA replication and transcription, thereby suppressing cell division and growth.[1228–1230]

Molecules that bind to the DNA minor groove often show high potential as therapeutic agents.[1231] Sequence-specific ligands can be used in chromosomal analysis. In addition, such compounds exhibit various biological activities: antitumour, antiprotozoal, antiviral and antibacterial. Most of the studies on compounds binding to the DNA minor groove are devoted to the development of anticancer drugs.

To date, a large number of organic molecules demonstrating affinity for DNA have been identified.[1232–1234] In this section, complexes of DNA with styryl dyes, which are often used for the determination of nucleic acids, are considered. Styrene derivatives have a high DNA binding affinity and show intense fluorescence when fom complexes with nucleic acids. A pronounce increase in the quantum yield of fluorescence upon immobilization of styryl dyes in a biopolymer molecule is associated with the suppression of nonradiative relaxation as a result of hindrance of intramolecular rotation of the chromophore groups. As a result, radiative relaxation (fluorescence), which is an analytical signal, becomes the main relaxation channel of molecules in an excited state. In addition, styrene derivatives are able to penetrate into the cell, which is used for visualization of intracellular DNA.[1235]

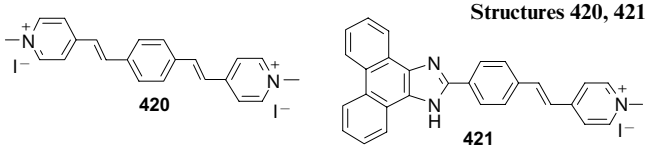
However, DNA imaging is not the only application of styryl dyes in biology. For example, bis-styryl derivatives have been used to determine amyloids and inhibit the formation of amyloid aggregates and fibrils. Amyloids β (Aβ) and their fibrillar deposits in tissues result from protein misfolding and are a sign of serious diseases such as Alzheimer's and Parkinson's diseases, type II diabetes, *etc*.

Mono-, bis- and tris-styryl dyes have the ability to bind to DNA, with bis-styryl derivatives being the best ligands. For this reason, a large number of studies are devoted to complexation of bis-styryl derivatives with DNA, while information on the interaction of mono-styryl and tris-styryl derivatives with DNA is scarce.

Dye **420** can be regarded as an example of a styrene derivative demonstrating external binding of a dye to DNA.[1236] Compound **421** was also used for a comparative analysis of the association with DNA. These compounds have low fluorescence intensity in aqueous solutions, but when double-stranded DNA is added, a ponounced fluorescence enhancement is observed, confirming the dye binding to DNA. The calculated stability constants (K_b) of the formed complexes with DNA are 3.06×10^5 and 1.08×10^6 L mol^{-1} for compounds **421** and **420**, respectively.

However, when salts (NaCl or KCl) are addded to a solution of the DNA–**420** complex, fluorescence is quenched, which is associated with the destruction of this complex. Indeed, inorganic cations are coordinated to the outer phosphate groups of DNA, thus displacing the dye molecules. This effect is not observed for compound **421**, for which the authors assumed that DNA binding occurs through an intercalation mechanism. Studies of the action of dyes **420** and **421** on HeLa cells (MMT assay) showed that the compounds have low toxicity and can be used for two-photon detection of DNA in living cells.

Structures 420, 421

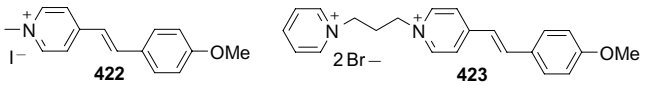


Ustimova *et al.*[1237] investigated the effect of the N-substituent in the 4-styrylpyridine dye on the mode of interaction with the calf thymus DNA (Fig. 160, Table 8). For this purpose, two compounds were taken, dyes **422** and **423**.

The data presented in Table 8 indicate that the interaction of dyes **422** and **423** with DNA leads to a change in the optical characteristics of the compounds, which was used to calculate the stability constants of complexes with DNA and to evaluate the binding site.

N-Methyl-substituted dye **422** has a lower binding constant and a moderate interaction area with DNA (n = 3.74),

Structures 422, 423



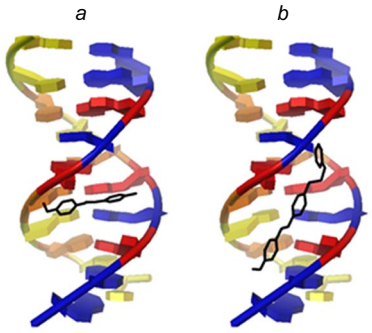


Figure 160. Image of DNA complexes with dyes **422** (*a*) and **423** (*b*).[1237] Published with permission from Elsevier.

Table 8. Characteristics of free and DNA- or polynucleotide-bound dyes **422** and **423**.[1237]

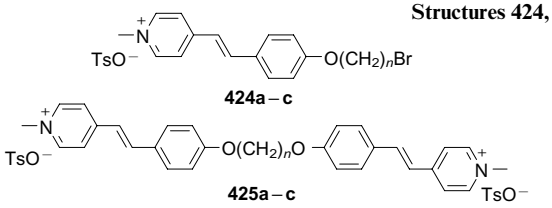
Ligand	λ_{abs}, nm		λ_{fl}, nm		I_{max}/I_0	$\varphi_{ligand}^{free}/\varphi_{ligand}^{bound}$	K_b, L mol^{-1}	n
	see [a]	see [b]	see [a]	see [b]				
				ctDNA				
422	373	395	501	501	2.1	1.20/2.33	2.4×10^3 (see [c])	3.74
423	382	404	511	506	2.3	3.36/6.49	2.5×10^4 (see [c])	7.46
				Poly(dG-dC)$_2$				
423	382	396	515	512	0.47	3.36/1.0	1.3×10^4 (see [d])	–
				Poly(dA-dT)$_2$				
423	382	393	515	514	4.9	3.36/14.4	1.3×10^4 (see [d])	–

Note. λ_{abs} and λ_{fl} are wavelengths of the absorption and emission maxima, respectively; I_{max}/I_0 and $\varphi_{ligand}^{free}/\varphi_{ligand}^{bound}$-bound are relative changes in the fluorescence intensity and quantum yields upon binding of a dye to DNA; n is the number of heterocyclic base pairs included in complexes with dyes in an aqueous buffer: ctDNA is calf thymus DNA, poly(dG-dC)$_2$ and poly(dA-dT)$_2$ are polynucleotides. [a] For free ligand; [b] for bound ligand; [c] calculated using McGhee–von Hippel method; [d] calculated using SpecFit/32 program.

indicating intercalation of the dye between DNA base pairs. The *N*-(3-pyridiniopropyl) substituent provides a stronger binding to DNA and has a larger binding site. Considering additional data on the interaction obtained by circular dichroism, the authors concluded that dye **423** is able to reside in the DNA minor groove. As a rule, compounds that fit into the groove show specific binding to the A – T pairs of DNA. For compound **423**, this fact was also established by comparing the interaction with poly(dG-dC)$_2$ and poly(dA-dT)$_2$ polynucleotide chains.

Further studies of 4-styrylpyridine dyes as DNA ligands involved the modification of the alkyl substituent in the phenyl core of the dye (**424a – c**) as well as the synthesis and study of bis-styryl dyes **425a – c** containing two 4-styrylpyridine moieties.[1238]

Structures 424, 425

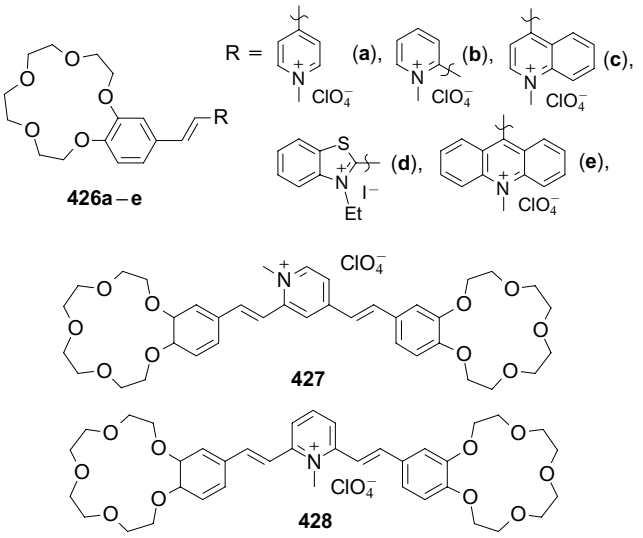


n = 3 (**a**), 6 (**b**), 10 (**c**); Ts is *p*-toluenesulfonyl (tosyl)

It was found that variation of the length of the alkyl substituent in the benzene ring of the monostyryl dye has a crucial effect on the mode of interaction with calf thymus DNA. Thus, compound **424a** ($n = 3$) intercalates with DNA, compound **424b** ($n = 6$) fits into the minor groove of DNA, and compound **424c** ($n = 9$) fits into the major groove. In the case of bis-styryl dyes **425**, no intercalation was detected upon interaction with DNA, compounds **425a**,**b** are inserted into the DNA minor groove, and compound **425c** is bound in the major groove. Note that the fact of location of relatively simple molecules in the major groove, established in this study, is quite unique, since it was previously believed that this is possible only for large biomolecules.

Apart from substituents, the nature of the heterocyclic moiety plays an important role in the association of the monostyryl dye with DNA. For instance, Berdnikova *et al.*[1239] varied the nature and structure of the heterocycle in the monostyryl moiety and also compared the results for bis-styryl analogues. It was shown that increase in the heterocyclic moiety from pyridine to acridine leads to increasing strength of the associates with DNA. Moreover, in the case of compounds **426a – c** the interaction with DNA occurs *via* intercalation, whereas for acridine derivative **426d** a mixed interaction mode is observed: along with intercalation, binding of molecules in the minor groove also takes place. Comparison of the binding of compounds

Structures 426 – 428



426a,**b** and dimers **427** and **428** showed that the *para*-arrangement of the styryl moiety relative to the pyridine nitrogen atom produces a structure more suitable for binding to DNA, which provides for higher complexation constants.

The presence of a crown ether moiety has no specific effect on the coordination to DNA. Berdnilova *et al.*[1239] analyzed the complexation with DNA in the presence and in the absence of metal salts capable of being located in the 15-crown-5 ether cavity and found no differences. This fact was also noted in the analysis of complexation with DNA of bis-styryl dyes connected through a 18-crown-6 ether moiety.[1240]

The interaction of styryl derivatives containing various heterocyclic residues with DNA has been studied.[1241, 1242] The studies confirmed the fact that cationic styryl dyes are appopriate ligands for DNA, their binding constants are in the range of $10^5 – 10^6$ L mol^{-1}.

Akbay *et al.*[1243] addressed the interaction of a series of mono- and bis-styryl dyes **429a**,**b** and **430a**,**b** with double-stranded DNA. The results they obtained led to a number of important conclusions. Thus, monostyryl compounds intercalate between DNA base pairs, and bis-styryl dyes are located in a minor groove. The latter was confirmed by the fact that bis-styryl dyes have a large binding site ($n = 14.5$, Table 9) and preferential coordination to A–T pairs. The introduction of an N-alkylammonium substituent (compound **429b**) into the molecule leads to an increase in the binding constant by a factor of 3 in comparison with the analogous parameter of dye **429a** (see Table 9). For bis-styryl dye **430a** with a positively charged linker, the binding constant to DNA increases by a factor of 5 compared to the

Structures 429, 430

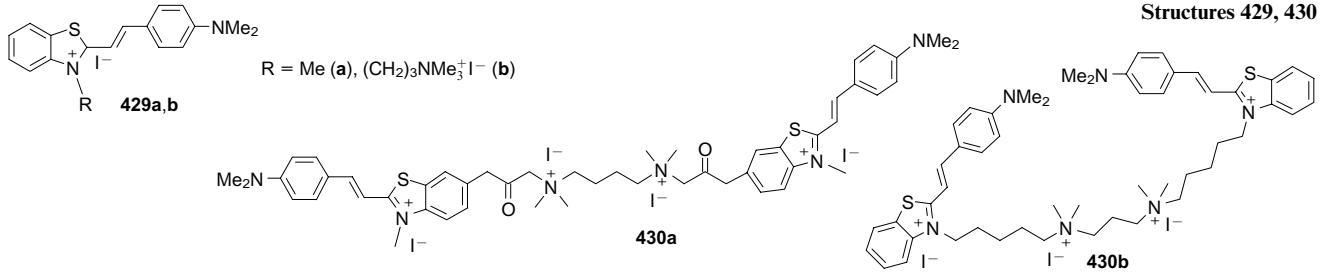


Table 9. Stability constants of dye – DNA complexes and numbers of heterocyclic base pairs included in the complexes with dyes **429** and **430** in an aqueous buffer.[1243]

Dye	$K_b \cdot 10^{-4}$, L mol^{-1}	n
429a	1.8 ± 0.3	3.4 ± 0.8
429b	6.2 ± 0.9	2.3 ± 0.5
430a	10.0 ± 1.4	4.9 ± 2.2
430b	2.7 ± 0.8	14.5 ± 3.2

initial monomer **429a**. However, the DNA binding constant of another bis-styryl dye (**430b**) is close to that of compound **429a** (see Table 9). Thus, the position of the binding linker and its structure significantly affect the DNA affinity.

As noted above, the most intensive research is carried out in the field of the synthesis of ligands for DNA based on bis-styryl dyes. Some of these ligands are considered below.[1244 – 1247] In general, dyes **431** – **435** give a significant fluorescence response when bound to nucleic acids: the fluorescence intensity of these dyes increases 2.9 – 134-fold in the presence of DNA, 4 – 25-fold in the presence of RNA, and 1.2 – 55-fold in the presence of BSA. Hence, compounds **431** – **435** are promising fluorescent markers for biological assays.

Intensive studies of bis-styryl dyes as ligands for DNA have not only established the fundamental laws of the complexation mechanism, but also identified practical applications for this knowledge. For example, recently, the interest of researchers in the two-photon fluorescence microscopy has increased. An advantage of this method over confocal microscopy is high localization of excitation and a significant depth of imaging (up to 1 mm), which allows studying various processes in tissues and organs. In addition, the use of lower energy photons for excitation protects the samples from photodegradation. The combination of nonlinear optical properties and DNA affinity of the styryl chromophore gives rise to ligands with necessary properties for use in two-photon fluorescence microscopy of biological objects. Mono-, bis- and tris-styryl pyridinium derivatives **436a** – **c** were obtained on the basis of the triphenylamine moiety. These products have a large photon absorption cross-section, and compounds **436b**,**c** also showed high affinity for DNA duplexes.[1248] One- and two-photon confocal cell imaging using these compounds showed that dyes **436b**,**c** performed red staining (λ_{fl} = 660 – 680 nm) of nuclear DNA with excellent contrast.

The successful use of styrene compounds as markers for biological tissue imaging requires a solution to the problem of selective binding to a particular cell component. Testing libraries of styryl derivatives allowed Feng *et al.*[1249] to find a bis-styryl dye **437**, which can selectively bind double-stranded DNA (ds-DNA) in cell culture samples.

This compound fluoresces in the green spectral range (λ_{fl} = 540 nm) and allows visualization of the nuclei of A549 and HeLa cell lines both *in vitro* and *in vivo* (Fig. 161). The binding capacity of dye **437** to ds-DNA was found to be 10 times greater than that to RNA, far exceeding that of the commercially available SYTO dye and comparable to that of Hoechst and DAPI dyes used in biochemical assays.[1250 – 1252] Besides imaging, dye **437** was successfully used to quantify cellular DNA content by flow cytometry.

Taking into account the structure of known inhibitors of the formation of Aβ fibrils, a number of bis(styryl)pyridine and bis(styryl)benzene derivatives with Aβ inhibitory activity were obtained.[1253] An advantage of most of these compounds over known analogues is their higher inhibitory activity combined with low cytotoxicity.

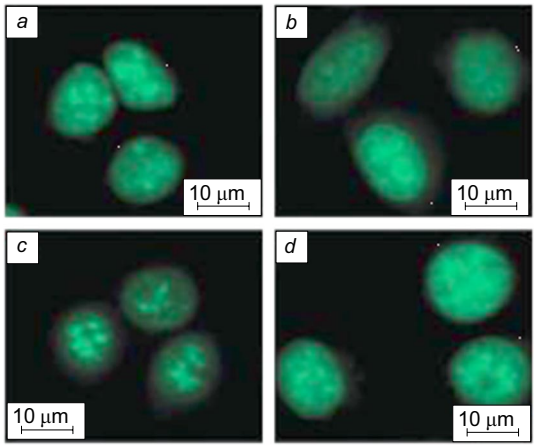
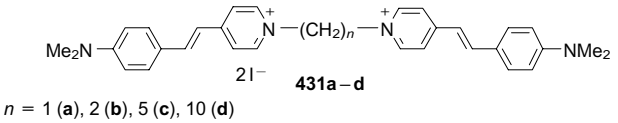
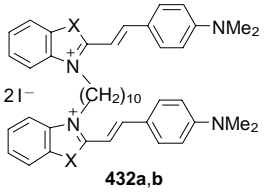
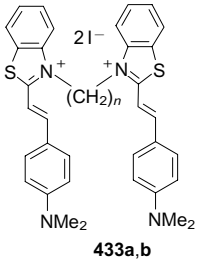


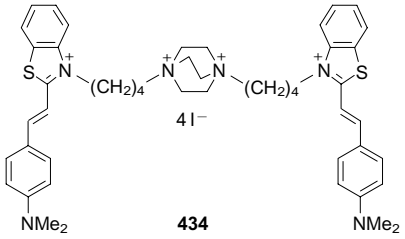
Figure 161. Imaging of live (*a*, *b*) and fixed (*c*, *d*) A549 and HeLa cells, respectively, using dye **437** under flow cytometry conditions.[1249] Published with permission frrom the Royal Society of Chemistry.

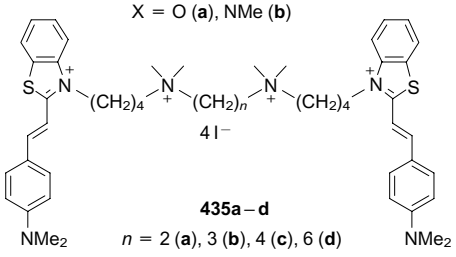
Structures 431 – 435



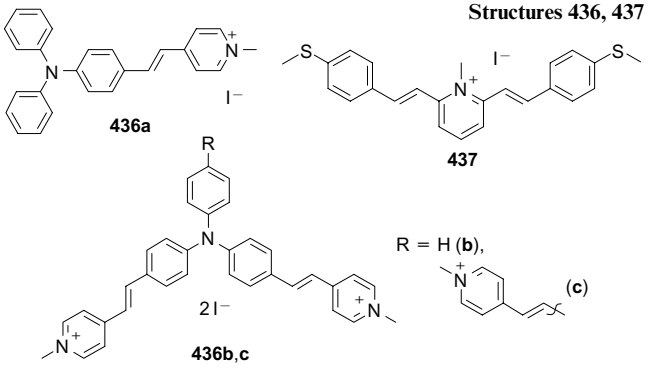








Structures 436, 437

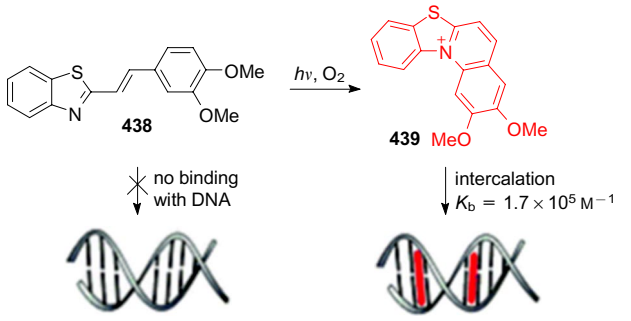


Another area of application of styryl dyes in biology is the determination of the histochemical localization of the activity of peroxidase enzymes using fluorescence microscopy. In this case, the mechanism of action of the styryl label is the covalent binding of the fluorescent marker to the enzyme. Krieg's research team[1254] obtained several bis-styryl dyes based on pyridine, quinoline, benzothiazole and indole that could act as fluorescent labels for the visualization of mast cells, nucleic acids, keratin and cartilage tissues. The efficiency of interaction of a molecular probe with the listed objects increases with increasing number and donor capacity of functional groups in the dye molecule. In addition, it was shown that the selectivity of binding of a fluorescent label to a particular cell structure can be controlled by changing the length of the bridging group between monomer units.

A photocontrolled ligand for binding to DNA was proposed on the basis of 2-styrylbenzothiazole (Scheme 68).[1255] The discovered phenomenon is based on the fact that uncharged (*E*)-2-(3,4-dimethoxystyryl)benzo[*d*]thiazole (**438**) is unable to be coordinated to DNA. Upon irradiation with light at 300 nm, the compound is converted to a positively charged polycyclic derivative *via* photochemical electrocyclization. The aromatic cation **439** does react with DNA. It was shown that the transformation of styrene **438** into heterocyclic cation **439** proceeds in the presence of DNA without affecting the latter. In a later study, the products of photochemical electrocyclization and other styrylazines demonstrated a high DNA affinity.[1256]

This reaction formed the basis for the construction of a complex system that simulates the delivery of a substituted 2-styrylpyridine molecule **440** to DNA as a part of a complex with (2-hydroxypropyl)-β-cyclodextrin (HP-β-CD), photocyclization of styryl into heterocyclic cation **441**, its release from the cyclodextrin cavity and

Scheme 68



Published with permission of the Royal Society of Chemistry.[1255]

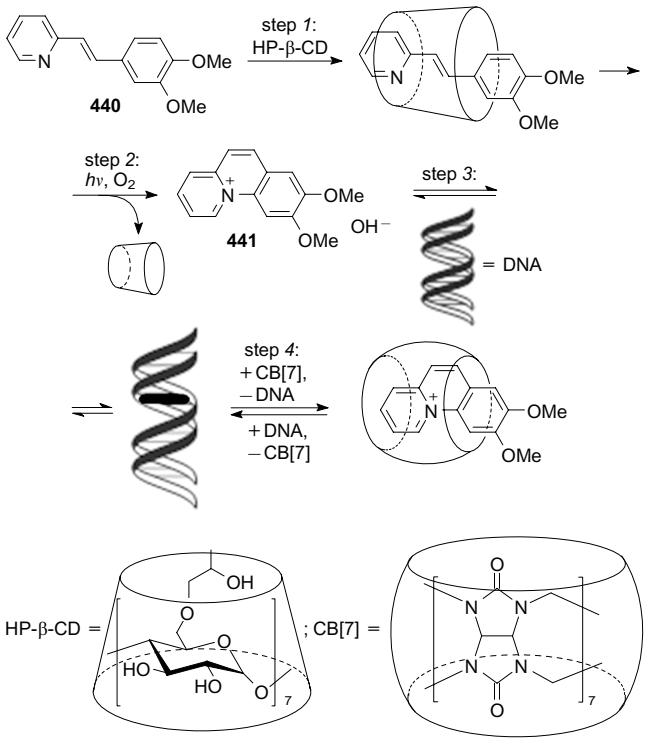
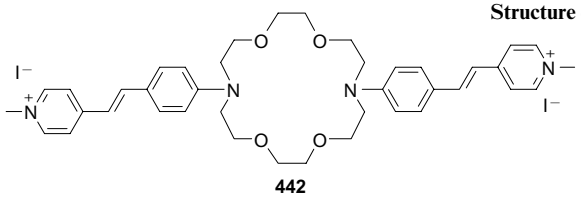


Figure 162. Scheme of DNA binding to dye **440**.[1257] Published with permission from the Royal Society of Chemistry.

intercalation between the DNA base pairs (Fig. 162).[1257] The release of the heterocyclic cation **441** from DNA was performed using cucurbit[7]uril (CB [7]). It is known that this container molecule is capable of binding positively charged species.

Another example of a supramolecular complex with the inclusion of a styryl dye molecule, DNA and cucurbit[7]uril was considered by Chernikova *et al.*[1258] Compound **442**, in which two 4-styrylpyridinium moieties are connected to each other through a diaza-18-crown-6-ether spacer, was used as a dye component.

Structure 442



A three-component assembly was obtained when one of the styryl moieties of bis-styryl **442** occupied the DNA minor groove with the simultaneous penetration of another styryl moiety into the cucurbit[7]uril cavity (Fig. 163).[1258] The structure of the formed assembly was proved by a combination of methods of optical spectroscopy, NMR spectroscopy and circular dichroism, in combination with quantum chemical calculations. This study demonstrates an example of the construction of mixed organo-biological assemblies of molecules using a set of non-covalent interactions.

Thus, styryl dyes are promising ligands for DNA. Their ability to bind to DNA can be varied by introducing

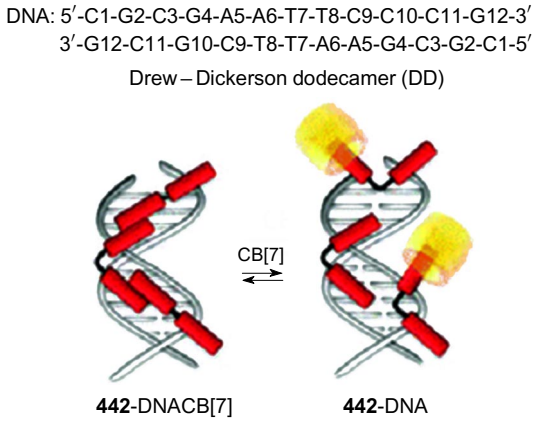


Figure 163. Scheme of DNA binding (Drew – Dickerson dodecamer) to dye **442**.[1258] Red rectangles are moieties of bis-styryl dye **442**, yellow cylinder is CB[7] molecule. Published with permission fom the Royal Society of Chemistry.

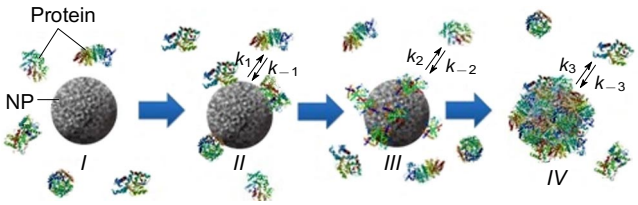


Figure 164. General scheme of formation of supramolecular biochemical systems *via* interaction of proteins with nanoparticles: (*I*) initial time point before interaction of the protein with nanoparticles; (*II*) proteins with low affinity for nanoparticles form caps of single protein molecules; (*III*) soft corona with a large number of defects on the NP surface; (*IV*) hard corona with a high coverage of the NP surface with the protein. k_i and k_{-i} are the dissociation and association constants in the protein – nanoparticle system, respectively.[1277 – 1282]

suitable substituents and switching from monomeric to dimeric structures. These compounds are photostable, unlike the currently widely used cyanine dyes. In addition, styryl dyes demonstrate both high biological activity and properties of markers for biomolecules.

4.2. Supramolecular biochemical systems based on proteins and nanoparticles for bionanotechnology and fundamental medicine

This part of the review addresses the fabrication methods (various techniques and approaches, including rational design), the structure – property relationships and applications of supramolecular biochemical systems (SBS) based on proteins and various sorts of nanoparticles (NPs). Proteins of the following types are considered:

— albumins as the most representative human and animal globular serum proteins,[1259 – 1261]

— various lipases: water-soluble enzymes with a hydrophobic pocket in the active site,[1262 – 1264]

— rhodopsins as relatively simple membrane proteins with photoreceptor and transport functions.[1265 – 1268]

Understanding of molecular mechanisms of interaction between these proteins and the most widely used nanoparticles such as gold,[1269 – 1271] silver,[1272 – 1274] some other metal and metal oxide [1275, 1276] NPs is a necessary condition for the development of bionanohybrid materials. When considering the rational design of various types of SBS, researchers focus on the formation of the protein adsorption layer on the nanoparticle surface (a sort of corona), which is described in a number of studies.[1277 – 1282] It is known that the interaction of nanoparticles with proteins is a dynamic process, with the exchange between the surface-bound and bulk proteins occurring on different time scales (Fig. 164).[1277 – 1282]

Indeed, proteins with low affinity for nanoparticles rapidly interact with the NP surface (see Fig. 164, system *I*) and are replaced over short time periods (seconds or minutes). Initially, caps of single protein molecules are formed (see Fig. 164, system *II*) *via* adsorption – desorption processes (k_1 and k_{-1}, respectively), which is followed by the formation of so-called 'soft corona' (k_2 and k_{-2}) with a low surface coverage by the protein (see Fig. 164, system *III*).[1277, 1282] Proteins with high affinity for the NP surface slowly exchange in adsorption – desorption processes (k_3 and k_{-3}) and form a 'hard corona' with a high surface coverage (see Fig. 164, system *IV*). In this case, the structure of tightly bound protein molecules of the inner adsorption layer is retained for rather long periods of time (hours or even days).[1277, 1282] Modern data [1277, 1282 – 1284] indicate that particularly the protein corona on the nanoparticle surface [1282 – 1284] (rather than the NPs themselves) determines the biological identity of SBS (in particular, immunogenicity [1279 – 1283]) under physiological conditions. The protein corona acts as the boundary layer between NP and the cell, intercellular space and so on.[1284 – 1286] Below we consider in detail the processes and parameters that influence the formation and composition of the corona such as particle size [1287] and shape,[1288] surface properties,[1277] protein concentration in the medium, the rate of protein – NP association and dissociation [1283] and the properties and composition of the biological fluid.[1279 – 1282] The formation mechanism and composition of the corona are very important for the toxicity,[1278 – 1282] internalization [1285] and other biomedical aspects of SBS application.[1278 – 1282, 1286 – 1288] To our knowledge, most of studies were carried out for SBS with long-lived and fairly stable hard corona; furthermore, these SBS can be quantitatively isolated (separated from the incubation medium, *etc.*) by centrifugation and washing.[1286] In this Section, we consider, first of all, gold and silver nanoparticles, because they are most popular scaffolds for the fabrication of nanostructured materials meant for biological systems.

4.2.1. Systems based on albumins and nanoparticles

4.2.1.1. Albumin and its analogues

Albumin and its analogues are of considerable interest for physicochemical biology and medicine, because they are most abundant proteins of blood plasma (serum), milk and human and animal tissues.[1259 – 1261] These are globular proteins readily soluble in water, stable over a broad pH range (from 4 to 9) and resistant to some organic solvents (*e.g.*, alcohols). In addition, albumins have fairly good biocompatibility and high storage stability when used in *in vitro* models, which is especially important for bio- and nanotechnological applications. Albumins have quite a few important biochemical functions: regulation of blood pH and osmotic pressure; binding and transport of both necessary ions or metabolites (calcium, fatty acids of various types, degradation products of haemoglobin, *etc.*) and hazardous substances (heavy metals, undesirable biologi-

cally active compounds, reactive oxygen species, *etc.*), thus controlling the blood levels of these compounds.[1259 – 1261] Albumin and its analogues can be derived from various sources such as bovine blood serum (BSA), human blood serum (HSA), milk (lactoalbumin), egg (ovalbumin), blood sera of small laboratory animals (mice and rats) and gramineous plants (soy and other).[1259 – 1261, 1277 – 1281, 1289] It is important that BSA, HSA and ovalbumin are commercially available and inexpensive; therefore, they are more often used as standards in biophysical and biochemical research than other albumins and other proteins. The key characteristics of ovalbumin, BSA and HSA are shown below:[1259 – 1261, 1289]

Parameter	Ovalbumin	BSA	HSA
Molecular weight (MW), kDa	43	66	66
Isoelectric point	4.8	4.7	4.7
Number of S – S bridges	1	17	17
Number of free SH groups	4	1	1
Number of amino acids	385	583	585

Ovalbumin, BSA and HSA have very similar molecular structures: all three proteins are globules formed from a single polypeptide chain consisting mainly of α-helices (60 to 70%); they contain hydrophilic and hydrophobic areas and exhibit acidic properties. The structures of these proteins differ insignificantly. Below we consider only BSA, which is most important for biomedical and bionanotechnological applications. This protein consists of three homologous domains, which are products of two subdomains and differ in the specificity (affinity) in metabolite binding and formation of ligand – protein complexes. The slight intrinsic fluorescence of BSA is mainly caused by the presence of two tryptophan residues (Trp-134 in the first domain and Trp-212 in the second domain) and other aromatic amino acid residues, which is helpful for BSA detection and use as a drug delivery agent.[1259 – 1261, 1289]

4.2.1.2. Fabrication strategies of supramolecular biochemical systems from albumin and nanoparticles

Characteristics of the structural domains of albumin allow its binding to biologically active compounds and various metal nanoparticles. In the general case, SBS structures composed of NPs on the protein surface can be obtained [1289 – 1297] (Fig. 165), or albumin can serve as a nanocage, with NPs or other compounds being encapsulated within the cage (especially if NPs are smaller than large protein globule).[1277 – 1282, 1289 – 1292]

The formation of such systems can be attained in several ways.

1. Passive adsorption (see Fig. 165 *a*)[1277, 1289 – 1292] is a process in which proteins can interact with NP surface *via* numerous charged groups or dipoles. Nanoparticles can be attached by either covalent bonds (between the SH groups of cysteine residues and metal ions on the NP surface) or non-covalent interactions (simple adsorption of NPs upon incubation in a protein solution). The process is implemented without the use of additional reagents or drastic conditions, and the ease of implementation is combined with economic feasibility.[1277, 1289 – 1292] This can be considered as a preparation method of SBS of the first level of complexity.

2. Active adsorption (see Fig. 165 *b*) [1277, 1289 – 1292] is an integrated process involving protein modification (*e.g.*, by carboxylation or thiolation of albumin, which changes the overall charge of the protein). This process can include the stage of preliminary adsorption of polymers [for example, polyethylene glycol (PEG) or polyvinylpyrrolidone (PVP)] on the NP before incubation with BSA, which markedly increases the number and strength of bonds between molecules — components of SBS of the second level of complexity.

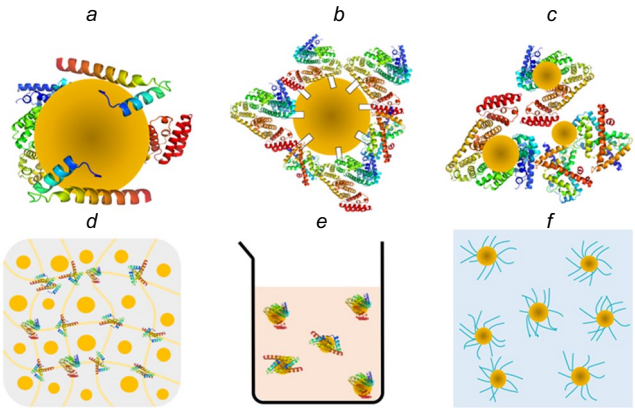


Figure 165. Types of interaction of BSA with nanoparticles: passive interaction of BSA with the gold NP surface (*a*); active interaction of BSA modified by functional groups for improving binding to the NP surface (*b*); growing (co-synthesis) of NPs in a BSA solution giving NPs encapsulated into BSA (*c*); coacervation allowing cross-linking of the whole protein globule with encapsulated NPs by chemical agents (*d*); emulsification, that is, formation of an emulsion of BSA with NPs, promising for the encapsulation of lipophilic drugs (*e*); gelation due to a change in the structure of the protein upon change in temperature (*f*). [1282 – 1297]

3. In the co-synthesis (see Fig. 165 *c*),[1289, 1292 – 1294] albumin is used as either a reducing agent or a building block for the NP@BSA type SBS. When BSA is added during one-pot synthesis, NPs are efficiently coated by the protein,[1292 – 1294] which formally corresponds to SBS of the first level of complexity. In order to synthesize SBS of the second level of complexity, foaming, stabilizing and other agents are used.[1292 – 1294] In addition, encapsulation of NPs into the protein globule is possible, which allows loading of poorly soluble agents and protect compounds from decomposition.[1277, 1292 – 1294]

4. Coacervation (see Fig. 165 *d*) [1289, 1295] is a process involving cross-linking of not only the surface, but also the interior of the protein globule with encapsulated NPs by chemical agents (*e.g.*, glutaraldehyde). Most often, NPs are added to a protein solution as seeds for the formation of capsules, and then an organic solvent (methanol, ethanol or acetone) is gradually added until albumin aggregates are formed and cross-linked,[1277, 1295] which corresponds to SBS of the third level of complexity.

5. Colloidal chemical method (see Fig. 165 *e*) [1289, 1294 – 1296] consists in mixing of an albumin solution with an oil phase to obtain an emulsion (owing to hydrophobic or functionalized parts of the molecule), which forms the shell around the core for the interaction with NPs. The solvent can be removed by evaporation, in particular at a reduced pressure.[1289] This strategy is promising for encapsulation of lipophilic compounds to increase their biocompatibility and solubility in aqueous medium.[1289, 1294 – 1296]

6. Physicochemical method (see Fig. 165*f*)[1289, 1297] is based on the change in the protein structure (*e.g.*, by gelation) upon temperature increase (or, in some cases, decrease). In the simplest case of thermal gelation, an aqueous solution of albumin is heated to induce unfolding of the protein molecule, which results in linking of both NPs and protein molecules *via* hydrophobic, electrostatic, disulfide or hydrogen bonding.[1297] This NP and protein self-assembly is a simple and efficient method for the fabrication of first level SBS, but preparation of systems with a specified structure and functional properties is questionable.

4.2.1.3. Surface adsorption of albumin on gold nanoparticles

It is known that modification of the surface of gold nanoparticles with albumins[1286–1290] is among the most vivid examples of fabrication of both standard and functional SBS. In addition, it considerably improves the parameters of dispersion of gold NPs in water, increases their colloidal stability and biocompatibility, modifies cellular uptake and intracellular transport processes and also improves characteristics of blood circulation of these NPs (in comparison with the initial nanoparticles).[1270, 1297] Functionalization of AuNPs with single BSA molecules or their complexes with biologically active compounds and polymers (*e.g.*, PEG, PVP) reduces the interaction of these SBS with plasma proteins, decreases the nanoparticle phagocytosis and accumulation in liver and spleen, increases their half-life in the bloodstream and allows selective NP delivery to tumour cells.[1298] The coating of AuNPs with albumin can be accomplished both *via* electrostatic or hydrophobic interactions between NPs and albumin and *via* chemisorption of thiol groups preliminarily grafted to the gold surface.[1299] Procedures involving direct incubation of AuNPs in a protein solution with controlled parameters such as concentration, ionic strength and pH of the medium have recently appeared. Control of pH is needed to adjust the degree of ionization of the AuNP@BSA system with allowance for the albumin isoelectric point and ζ-potential of NPs in order to enhance the electrostatic interaction between the components. A remarkable result concerning AuNP@BSA encapsulated systems was reported by Murawala *et al.*[1300] The indicated SBS were used to load a large amount of methotrexate for the delivery of this drug to breast cancer cells.

The active and passive transport of NP@BSA systems is now studied with the goal to develop systems for drug delivery to a tumour. The former implies the interaction of the nanosystem with the overexpressed or specific receptors of the tumour, which leads to drug uptake and further internalization at the tumour site or within cancer cells. For example, albumin can interact with a number of specific receptors, in particular with glycoproteins (Gp18, Gp30 and Gp60) and SPARC protein (secreted protein acidic and cysteine rich), which is responsible for its uptake and transcytosis.[1301] Owing to the biocompatibility and the possibility of active transport, SBS of this type were proposed for overcoming the drawbacks of unmodified drugs. It is important that several albumin-based drugs have already been approved and are now actively used for the treatment of some diseases.[1300–1302]

Thus, BSA- and NP-based SBS are among the few types of nanotransporters that demonstrate a broad range of benefits for the drug therapy[1301] over single components — albumin or NPs.[1298–1302]

Both the size of initial nanoparticles (which often determines the size of SBS, since the size of BSA is virtually constant) and the nature of interaction between NPs and albumin are important factors for biomedical applications. Small gold nanoparticles interact with albumin more efficiently than larger ones; nanoparticle shape also considerably influences the protein adsorption, which was repeatedly described in relation to AuNPs.[1303–1305] In the case of BSA adsorption on branched-shaped nanoparticles (BNPs), the hydrodynamic radius of the resulting SBS increases.[1305] This is facilitated by higher surface area to volume ratio of BNPs. It was shown that among BNP types, the predominant type are nanorods (NRs),[1303–1305] which induce certain changes in the stability and structure of human albumin. These changes depend on both NP geometry and the nature and thickness of the adsorption layer. For example, a CTAB layer coated on the NP surface resulted in a higher aggregation level of the system, which was attributed to the positive charge of the cation, whereas pegylated (PEG-coated) NPs have a nearly zero charge.[1306]

A comparison of the BSA interaction with AuNPs of various geometries[1307, 1308] showed that

— AuNRs have higher permanent adsorption values,

— geometric shapes with large flat surfaces (nanoprisms and nanocubes[1303–1305]) lead to lower adsorption of BSA (*i.e.*, flat surfaces reduce the accessibility and the level of interaction with the protein).

To summarize the discussed results, it can be concluded that the deformation of albumin decreases in the following order, depending on the NP geometry and the nature of the adsorption layer:[1307, 1308]

$$\text{CTAB}-\text{AuNR@BSA} > \text{CTAB}-\text{AuBNP@BSA} > \\ > \text{Au@BSA}-\text{CTAB} > \text{AuNR@BSA}-\text{PEG} > \\ > \text{AuBNP@BSA}-\text{PEG} > \text{AuNS@BSA}-\text{PEG}.$$

Thus, the stability and structure of adsorbed albumins depend on both the NP geometry and the nature and thickness of the adsorbed surfactant or polymer layer on the NP surface.

4.2.1.4. Bovine serum albumin on the surface of silver nanoparticles

Bovine serum albumin is one of the first proteins to be successfully adsorbed on the silver nanoparticle surface.[1278] Since BSA is a relatively simple and adequate model system, it is widely used to study the interactions with AgNPs.[1278–1284] For example, Treuel *et al.*[1284] carried out a detailed comparative study of BSA adsorption on th following silver nanoparticles:

— citrate-coated NPs 20 nm in diameter (with a surface area of 3×10^{14} nm^2 mL^{-1});

— citrate-coated NPs 40 nm in diameter (3×10^{15} nm^2 mL^{-1});

— PVP-coated NPs 70 nm in diameter.

The unfolding of the polypeptide chain upon adsorption of the protein on silver NPs was evaluated by determining the content of α-helices in a BSA globule using circular dichroism spectroscopy.[1284] The CD signal (*i.e.*, the intensity ratio at 208 and 220 nm wavelengths) decreased with increasing surface area of citrate-coated AgNPs present in the mixture, which corresponded to a decrease in the content of α-helices in the BSA globule. The total amount of the protein (removed from the solution) and the surface area of all citrate-stabilized AgNPs determined by Treuel *et al.*[1284] were in good agreement with the calculated

amount of the protein that can be adsorbed as a monolayer on a particular type of nanoparticles.[1284] Conversely, the adsorption of BSA on the PVP-stabilized silver nanoparticles resulted in a considerable decrease in the intensity of the band at 208 nm in comparison with the relative minimum at 220 nm, which emphasizes a more intricate pattern of BSA interaction with Ag-PVP nanoparticles than with citrate-coated silver NPs (Ag-Cit).[1284]

Treuel *et al.*[1309] confirmed the substantial influence of polymer coatings on the interaction of albumin (and some other analogous hydrophilic proteins) with metal nanoparticles using surface enhanced Raman scattering. The strong interaction between the sulfur-containing groups of the protein and the metal surface in the Ag-Cit@BSA system was reduced in the presence of a polymer coating (for the Ag-PVP@BSA system).[1309] A subsequent study of Podila *et al.*[1310] allowed the authors to estimate not only the physicochemical, but also physiological parameters for the interaction of BSA (as a simple protein corona) with silver nanoparticles stabilized by either PVP or citrate. According to transmission electron microscopy and dynamic light scattering data, uncoated silver nanoparticles (obtained by laser ablation and designated by LA-Ag) were spherical and had a unimodal diameter distribution (24 nm), and they bound more protein at 37 °C in 1 h than citrate- or PVP-coated AgNPs with a similar average diameter ($\sim$20 nm). Furthermore, citrate- and PVP-coated AgNPs were aggregated when interacted with the protein, which indicates insufficient electrostatic stabilization of their surfaces, unlike that of LA-Ag nanoparticles. It is known that the I_{1630}/I_{1650} ratio, determined by FTIR spectroscopy, is a quantitative measure of the change in the protein entropy upon transition from disordered structures to elements of the secondary structure such as α-helices. For native BSA, this ratio is always <1, which attests to prevalence of ordered forms in the protein (*i.e.*, implies a large fraction of α-helices). After the interaction of BSA with nanoparticles, this value was $\sim$1.5, $\sim$2.5 and $\sim$9.5 for Ag-Cit, Ag-PVP and LA-Ag nanoparticles, respectively, which attests to increase in entropy and conformational mobility of the protein and decrease in the content of α-helices in this series.

This conclusion is in line with the results of Shannahan *et al.*,[1311] who found that 20 nm AgNPs bind to hydrophobic proteins more strongly than the same NPs of larger size (110 nm). The differences in the formation of protein corona for AgNPs of different sizes are probably related to both the curvature of the NP surface and the energy of protein adsorption and agglomeration processes.[1311] These results are important for interpreting the data on NP interaction with albumin and other blood plasma proteins.[1260, 1277 – 1280, 1285 – 1290] The details of electrostatic and hydrophobic interactions involved in the formation of the protein corona around the nanoparticles also affect the biological and toxicological properties of SBS.[1277 – 1280, 1285 – 1290] Bovine serum albumin was also used as an emulsifier and/or stabilizer in the synthesis of NPs of various metals (Pt, Cu, Se, Ni, *etc.*) and Ag – Au or Ag – Pt bimetallic compounds, but there are no systematic biomedical data for such SBS in the literature as yet.

4.2.1.5. Interaction of albumin with metal oxide or sulfide nanoparticles

Recently, a lot of attention has been paid to fabrication of SBS and materials based on metal oxide nanoparticles and proteins.[1312 – 1317] We will consider only the most advanced systems meant for biomedical and veterinary applications. Nosrati *et al.*[1312] demonstrated loading of NPs with curcumin (CUR) — a natural biologically active polyphenol of plant origin. This gives structures Fe@BSA@CUR of 56 ± 11 nm size and with a negative ζ-potential (-10.1 mV); the magnetic properties of these structures are slightly worse than those of iron. However, all cytotoxic properties of curcumin are retained upon loading into NPs at a level of 6.88% and upon quantitative release from Fe@BSA@CUR at 37 °C in buffer solutions. Nosrati *et al.*[1312] carried out thorough cytotoxicity assays using HFF-2 cell culture and Fe_3O_4, Fe@BSA and Fe@BSA@CUR nanoparticles in concentrations from 15 to 950 μmol L^{-1}. After incubation for 72 h, no significant differences from the control (without addition of NP) were found, except for Fe_3O_4 NPs. The latter represented nanoparticles without an additional adsorption layer, the cytotoxicity of which markedly increased at higher concentrations. More encouraging results were obtained using Fe@BSA@CUR and their analogues against the MCF-7 cell line (invasive human breast adenocarcinoma).[1312] It was found that the cytotoxicity of Fe@BSA@CUR and free curcumin increased with increase in their concentrations and, especially, in the incubation time (from 72 to 96 h), unlike that of Fe@BSA or the control. The LD_{50} values for MCF-7 were 275 and 915 μmol L^{-1} upon incubation with Fe@BSA@CUR and 300 and 730 μmol L^{-1} upon incubation with free curcumin for 96 and 72 h, respectively. Thus, the cytotoxicity of Fe@BSA@CUR increased 3.2-fold as the incubation time increased from 72 to 96 h, which makes this system promising for the treatment of cancer.

Interesting data were obtained in the synthesis of so-called non-degradable nanoparticles and SBS derivatives meant for the theranostics of cancer.[1313] The authors developed a simple method of biomineralization using BSA to obtain SBS based on polymer gallic acid (GA) and Fe^{III} NPs, the combination of which was proposed by Todd *et al.*[1314] These complex systems designated as Fe-GA@BSA (*i.e.*, BSA-coated GA and Fe nanoparticles) were ultrasmall (3.5 nm) and showed pronounced absorption in the visible near-IR range.[1313] They had low hemolysis ($<0.33\%$), good biocompatibility and low cytotoxicity ($\sim$80% at concentrations of $\sim$200 μmol L^{-1}) against HEK293T cells and human macrophages (using the CCK-8 assay) and against red blood cells obtained from healthy BALB/c mice. The longitudinal (r_1) and transverse (r_2) relaxivity values of water protons for the Fe-GA@BSA system were 0.89 and 0.95 mmol s^{-1} for the times T_1 and T_2, respectively. These results were comparable with the data for other contrast agents used in magnetic resonance imaging (MRI). Since the $r_2:r_1$ ratio found for Fe-GA@BSA was 1.06, which is below 3 (found previously for other MRI agents), Mu *et al.*[1313] first suggested and then experimentally proved that this SBS provided a good T_1-weighted contrast and was superior in this characteristic to other MRI agents.

Žukiene *et al.*[1315] studied SBS based on albumin and ZnO NPs with an average size of $\sim$20 nm, which were coated with BSA at temperatures of 4 – 20 °C by means of covalent and non-covalent interactions. The interaction of ZnO NPs with BSA was studied by UV and visible spectroscopy, conventional and synchronous fluorescence and various modifications of Raman spectroscopy. The Raman

spectra of BSA in the presence of ZnO NPs confirmed for the first time a decrease in the content of α-helices and increase in the content of disordered BSA structures. The synchronous fluorescence spectra showed that the hydrophobicity of the tyrosine residue of the protein was decreased, and that of the tryptophan residue was increased. This observation was confirmed by Ledesma *et al.*[1316] by Raman and FTIR spectroscopy. It was shown that when the BSA concentration was >30 μmol L^{-1}, the protein signal overlapped with emission of ZnO nanoparticles due to self-oligomerization. The authors[1316] predicted that the most probable binding site of BSA is located near domains IB and IIA, and ionic interactions are the main cause of binding to ZnO NPs.[1316] For the first time, these changes in the BSA structure were found to be related to ZnO NP cytotoxicity, which was evaluated considering the viability of CHO cells and formation of reactive oxygen species (ROS) *in vitro*.[1315] Both covalent and non-covalent binding to BSA reduced the cytotoxicity of ZnO NPs (which also depended on the conformational changes in the protein) and suppressed the formation of ROS.[1315] Interestingly, the denaturation temperature of BSA increased from 57 to 65 °C in the presence of ZnO NPs, and their esterase-like activity improved.[1316]

Naskar *et al.*[1317] synthesized the ZnO@ZnO-rGO (ZG) composites from ZnO nanoparticles (obtained using polyvinyl alcohol foam precursor), which were combined with reduced graphene oxide (rGO) in the presence of hydrazine. The parameters of ZG nanocomposite (crystallinity, shape, size, polydispersity, *etc.*) were determined by X-ray diffraction analysis, field emission scanning electron microscopy, transmission electron microscopy, FTIR spectroscopy and Raman spectroscopy. The results confirmed the complex formation between the rGO functional groups and ZnO/Zn^{2+} to give ZG nanocomposite.[1317] The interaction of BSA with ZG nanocomposite, which was proved by UV-Vis and photoluminescence spectroscopy,[1317] resulted in 'biofunctionalization' of metal oxide nanoparticles, which may be used in pharmacology, drug delivery and oncology.

Huang *et al.*[1318] investigated SBS based on albumin and copper sulfide NPs (CuS@BSA) using directly copper salts and thioacetamide. The CuS@BSA nanocomposites were nearly spherical, had diameters ranging from 10 to 35 nm and good dispersibility, depending on the BSA concentration. The nanocomposites formed by BSA and sulfur-containing NPs were comprehensively studied by a set of physicochemical methods and showed good prospects for application in biomedical engineering and microelectronics.

In conclusion, mention should be made of a small study[1319] which demonstrated the formation of a BSA corona on synthetic Co, Cr and Mo oxide nanoparticles and not only on pure (standard) oxide materials incubated with BSA. The important achievements of this study are, first of all, fundamental results establishing the highest BSA affinity for MoO NPs in comparison with other metal oxide NPs, in particular, in the presence of blood serum proteins. In practice, systems of this type serve as the models for studying wear of hip implants in the presence of serum albumin. Apparently, the NP composites with various blood serum proteins would form the most promising SBS for various technological and biomedical applications.

4.2.2. Systems based on lipase and nanoparticles

Supramolecular biochemical systems based on enzymes are employed in virtually all fields of human activity: various branches of industry, medicine, agriculture and science, *e.g.*, theoretical biochemistry and physicochemical biology.[1262 – 1264, 1320] Both the fundamental research and applied studies are complicated by problems related to high cost of many enzymes (especially highly purified products), their low stability on storage and under thermal or electrophysical impacts, difficulty of repeated use and isolation of enzymes from reaction mixtures.[1321 – 1323] These problems obstruct the use of enzyme-based SBS.

Immobilization is known to be the most facile way for the fabrication of SBS based on enzymes with a set of desired characteristics such as stability, possibility of reuse, easy purification, higher yield of products of hydrolysis in comparison with native enzymes, *etc.* For example, immobilization of lipase is promising for addressing problems of disposal of waste oil products, removal of complex fat contaminants, water treatment and environmental protection.[1321 – 1323] Metal and metal oxide nanoparticles are actively studied and already practically used as enzyme carriers; these carriers are subject to high requirements concerning technological and cost issues. The following Sections describe the immobilization of lipases of various origins on metal and metal oxide nanoparticles.[1322 – 1327]

4.2.2.1. Gold nanoparticles for lipase immobilization

Gold nanoparticles are often used in the laboratory enzymology[1322 – 1324] of lipases, but they are rather expensive for the application in industrial biotechnology.[1320] Lv *et al.*[1324] described immobilization of porcine pancreatic lipase on gold NPs and also proposed bioreactors using reversible immobilization of the enzyme on a special porous support. This support contained thiol groups to be further functionalized with AuNPs. The support was obtained by thermal polymerization of glycidyl methacrylate and ethylene dimethacrylate in the presence of cyclohexanol and 1-dodecanol as porogens.[1324] For repeated use of this support, the following operations were conducted: inactive enzyme was stripped from the NP surface by treatment with 2-mercaptoethanol, and a fresh portion of lipase was deposited on the cleaned nanoparticles (Fig. 166).[1324]

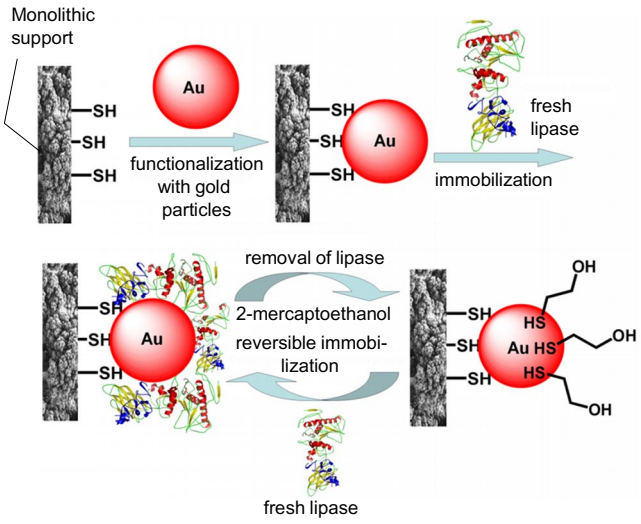


Figure 166. Scheme of formation of composite SBS: fabrication of the AuNP-functionalized support and enzyme immobilization followed by regeneration.[1324] Published with permission from Wiley.

Tributyrin (glyceryl tributyrate) served as the substrate for the model reaction on this SBS, and the continuous cycle in the reactor allowed control over time (4 h) and temperature (37–40 °C) for process optimization.[1324] This system proved to be highly active, and the maximum reaction rate (5.0 mmol $L^{-1} min^{-1}$) was 1000 times as high as that for non-immobilized lipases.[1324] The benefits of the proposed immobilization procedure include both the strong adsorption of lipase on AuNPs [1320] and the possibility of lipase regeneration.

Brennan *et al.*[1325] reported an efficient process for enzyme immobilization on nanoparticles, which was developed rather recently owing to the appearance of click chemistry approaches. Azide-functionalized gold nanoparticles were covalently bound to lipase from *Thermomyces lanuginosus* and incubated for 3 days at room temperature (the reaction was catalyzed by copper salts). The resulting aqueous dispersions of AuNPs@lipase were stable for ~90 days (at 4 °C in the dark) and had initial activity of 1.82×10^{-3} U mL^{-1} (at 37 °C). According to calculations, this corresponds to immobilization of ~7 lipase molecules per AuNP. Unfortunately, the incubation of AuNPs for ⩾ 72 h considerably decreased the lipase activity. For further discussion of these important results, it is appropriate to cite Brennan *et al.*,[1325] who stated that immobilization of lipase on gold nanoparticles stabilizes lipase, increases its thermal stability and makes it more resistant to denaturing factors. In our opinion, this statement is not entirely true for the case of long-term incubation of lipase with NPs at a temperature ⩾ 18 °C.

4.2.2.2. Silver nanoparticles for lipase immobilization

The fabrication of SBS based on silver nanoparticles and lipase is an exceptionally important line of research, because immobilization of proteins on nano-sized silver is used rather widely.[1324–1326] Dumri and Anh [1326] studied the interaction of AgNPs (10–20 nm size) with polydopamine and effect of this system on the pancreatic lipase activity. It was found that this SBS has antibacterial properties. A drawback of this study is that good results on lipase activation (by 10–20%) and lipase stabilization (6 h at temperatures of 50–55 °C) after the fabrication of AgNP@lipase SBS were attained in the presence of Tween 80. The latter is a fairly exotic substrate for lipases,[1326] even when their activity is determined by spectrophotometry (in this case, at 232 nm). This approach requires special attention to the length of the molecular spacer [1320] between AgNP and lipase, since too short spacers or no spacer may considerably inhibit the enzyme catalytic activity.[1320–1322]

4.2.2.3. Metal oxide nanoparticles for lipase immobilization

Among enzyme carriers, mention should be made of a large group of metal oxide NPs. In view of the restricted size of this part of the review, we will consider only magnetite (Fe_3O_4) and its analogues,[1322, 1327–1329] which have a set of unique properties and are widely used in various fields of science and technology.[1321] Surface functionalization of NPs of magnetite and its derivatives with various biomolecules, polymers and medicinal agents, which endow them with the desired properties such as therapeutic activity, higher stability, lower toxicity and the capability for specific interactions with target molecules [1322, 1329] (*e.g.*, cell receptors), is becoming a global trend in science. A promising method is the fabrication of a carbon-based layer with various functional groups on the magnetite surface for binding to lipases.[1322, 1327, 1328]

Qi *et al.*[1327] immobilized lipase isolated from porcine pancreas on Fe_3O_4 NPs (Fig. 167) that were cross-linked with glutaraldehyde to poly(carboxybetaine methacrylate) (PCMA) to form the PCMA–Fe_3O_4@lipase SBS. This system efficiently hydrolyzed 4-nitrophenyl palmitate as a substrate.

The PCMA–Fe_3O_4@lipase system was relatively stable up to a temperature of ~75 °C; in addition, the optimal temperature for functioning of this SBS was ~45 °C, which was higher than that for the initial lipase. Moreover, this system perfectly withstood changes in the pH, while the initial lipase loses a considerable part of its activity in this case. After seven operation cycles, the PCMA–Fe_3O_4@lipase system retained ⩾ 60% of its initial activity, and its catalytic efficiency (K_{cat}/K_m ratio, where K_{cat} is the catalytic constant, K_m is the Michaelis constant) was higher than that for the initial lipase by 50%. It is noteworthy that PCMA–Fe_3O_4 particles did not exhibit cytotoxicity.[1327]

Wang *et al.*[1328] described an SBS based on lipase from *Candida rugosa* adsorbed on the hydrophobic surface of magnetite NPs, which were coated by trimethoxysilane derivatives containing various alkyl substituents (propyl, octyl and octadecyl). The sizes of such systems were 13.5 to

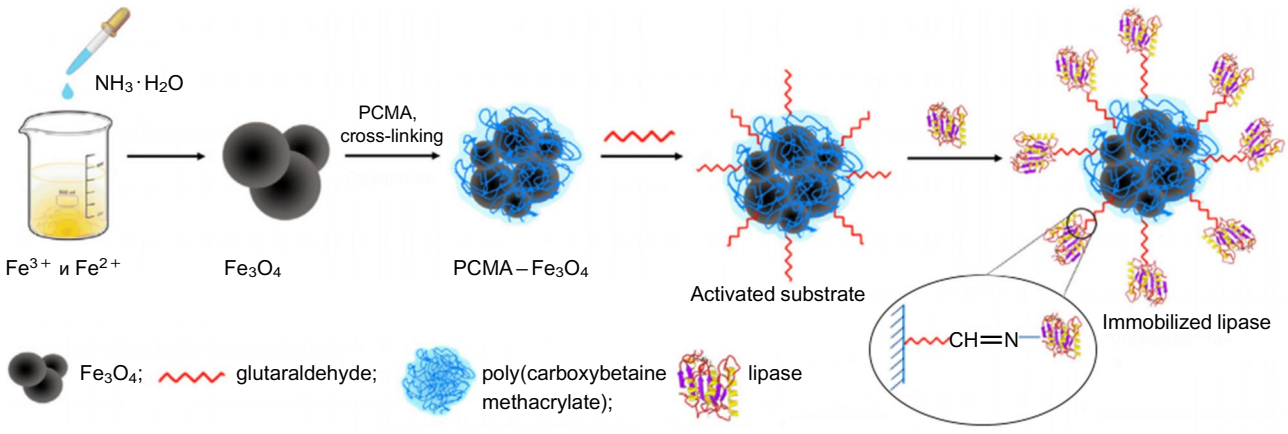


Figure 167. Scheme of SBS preparation by immobilization of lipase on magnetic PCMA–Fe_3O_4 composites.[1327] Published with permission from Elsevier.

14.0 nm depending on the chain length in the alkylsilane. The specific activity of the Fe_3O_4@lipase SBS ($\sim 2.1 \times 10^{-6}$ mol min^{-1} mg^{-1} towards *p*-nitrophenyl acetate) was also directly correlated with this parameter.[1328] It is important that the activity of lipase-containing SBS was $\geqslant 2$ times higher than the activity of native lipase (0.76×10^{-6} mol min^{-1} mg^{-1}) or lipase adsorbed on naked magnetite particles (1.07×10^{-6} mol min^{-1} mg^{-1}). This is attributable to an increase in the SBS hydrophobicity and increase in the distance between lipase and the surface of magnetite NP [in the case of trimethoxy(octadecyl)silane]. In addition, the authors noted the possibility of enzyme regeneration: after seven operation cycles of immobilized lipase, the SBS activity amounted to 65% of the initial activity. Relying on the obtained results,[1322, 1327–1329] one can state that magnetite NPs are promising materials for the design of biocatalytic SBS with good biocompatibility.

Analysis of the published data [1322–1329] demonstrated that lipase immobilization on inorganic NPs has a beneficial effect on many operating parameters of SBS such as activity–stability, pH–temperature, reusability–affordability and other relationships, which is an undoubted advantage for their practical application. Among all NP@lipase systems described above, in our opinion, structures containing Fe_3O_4 NPs modified by polymers for decreasing their toxicity for interaction with biological objects are most multifunctional and cost-efficient for enzyme engineering.

4.2.3. Systems based on bacteriorhodopsin and nanoparticles

4.2.3.1. General characteristics of bacteriorhodopsin

Rhodopsins are membrane proteins with a polypeptide chain that forms seven transmembrane α-helices (A, B, C, D, E, F and G), permeating the lipid bilayer of plasma membranes of the photoreceptor cells of animals and halophilic bacteria.[1265–1268] Bacteriorhodopsin (BR) occurring in the purple membrane (PM) of bacteria has a polypeptide chain consisting of 248 amino acids (MW ~26.5 kDa) with retinal linked to residue Lys216; the structure and conformational changes of retinal were studied by a set of physicochemical methods.[1265–1268] The results of X-ray diffraction, SEM and other studies [1265–1268] indicate that the key structural unit of PM is a 2D hexagonal lattice with a 'unit cell' composed of three BR molecules and 12–14 lipid molecules;[1320] moreover, only this structure (so-called functional unit [1265]) is efficient for proton transfer.[1265–1268] The processes is triggered by the action of light (at 500–600 nm) on BR(PM), which results in converion of the *all-trans* configuration of the chromophore (retinal) to 13-*cis* configuration,[1265–1268] *i.e.*, exposure to light induces the transition of the initial state bR_{568} (with $\lambda_{max} = 568$ nm) to form M_{412} (with $\lambda_{max} = 412$ nm).[1330] The back relaxation of BR takes place when H^+ is transported across the PM into the medium (Fig. 168).[1330]

The following features of BR(PM) are especially valuable for bionanotechnological applications: fast transition from bR_{568} to M_{412} and back giving rise to a photopotential (photocurrent) and to the difference ΔpH; and multiple repetitions and complementarity [1330] of these events without significant influence on other characteristics.[1265–1268, 1330–1333] Generally, both BR(PM) and other photosensitive systems are unique objects that convert light energy to other types of energy [1330] necessary for the body to provide movement of cells and bacterial flagella and synthesis of high-energy bonds of adenosine and guanosine triphosphates (ATP and GTP) and other similar molecules.[1265–1268, 1330–1333] This makes BR(PM)-based SBS unique structural and functional components of promising bionanotechnological materials.[1330]

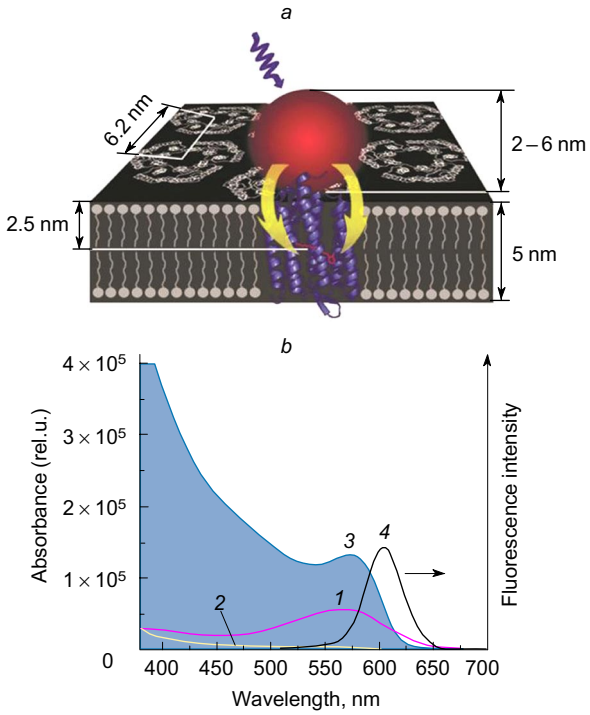


Figure 168. Fabrication of SBS based on purple membranes and quantum dots (*a*) and optical properties of this SBS (*b*).[1330] (*a*) BR molecule (violet figure) contains a chromophore that absorbs in the visible range, and the energy transfer (yellow arrows) from QD (orange sphere) to the BR chromophore occurs by the FRET process; (*b*) absorption spectra of PM (*1*), membranes without a chromophore (*2*) and one of the QD types that absorb in the whole blue-hatched area (*3*); fluorescence spectrum of these QDs (*4*). Published with permission from Springer.

4.2.3.2. Bionanohybrid materials based on bacteriorhodopsin and quantum dots

For bacteriorhodopsin, most appropriate is fabrication of its associates or conjugates (*i.e.*, immobilization by various methods [1265–1268, 1330]) with quantum dots (QDs).[1333–1336] Unique features of QDs include [1333–1336] an exceptionally wide absorption band (with QD emission taking place in a very narrow spectrum range), a quantum yield exceeding 70%, and photostability and absorption cross-section hundreds of times higher than those of the best organic fluorophores.[1330] Since the fluorescence parameters of QDs directly depend on their size, it is relatively easy to obtain QDs that would emit in the absorption region of BR.[1333–1336] A combination of these properties makes it possible to design conceptually new materials based on BR(PM)–QD hybrid nanostructures.

It is known that visual and bacterial rhodopsins use only $\leqslant 1\%$ of energy of light between ~390 and ~760 nm that falls on the photoreceptor membrane.[1333–1336] The formation of BR complex with QDs (see Fig. 168 *a*) [1330] allows the resulting system to use the whole range of light (from far

UV to visible light) and provides efficient transfer of quantum energy from QD to BR by the FRET mechanism for consumption of this energy for the functions of this SBS. An additional benefit is that the BR chromophore is located approximately in the middle of the purple membrane.[1333 – 1336] This distance (even with allowance for the QD radius) is smaller than the average Förster radius (~5 nm), which is highly efficient for this mechanism of energy transfer. The authors showed that it is possible to synthesize QDs with an emission maximum corresponding to the BR absorption range (see Fig. 168 *b*),[1330] with the QD absorption intensity being several-fold higher than that for BR in the 450 – 600 nm range.[1331 – 1336] An important condition for the design of an efficient SBS is the adsorption of QD on PM particularly in the areas where BR domains are located.[1330] This condition can be met by modifying the QD surface with cysteine or thioglycolic acid.[1330] An SBS structure of this type was visualized by AFM.[1334] It was shown that BR trimers (with a height of 0.4 – 0.5 nm and a diameter of ~6.2 nm) considerably change upon conjugation of QD with the PM surface (QD : BR = 1 : 2),[1330] in particular, the height of associates increases by 1.3 – 1.5 nm and the distance between BR trimers decreases by 0.1 nm.[1334] Exactly at this ratio of QD and BR in the SBS, BR domains are observed and QD binding to BR(PM) takes place.[1330, 1334] This specific interaction between QDs and BR(PM) in the SBS results in complete quenching of the quantum dot fluorescence [1334] when the QD to BR(PM) ratio is from 1 : 2 (for the dots with λ_{fl} = 590 nm) or 1 : 1.2 (for the dots with λ_{fl} = 650 nm) to 1 : 1. A series of publications [1334 – 1336] describe detailed studies of the specificity of interaction of QDs with BR(PM) as a function of both the QD size and charge and the thickness of organic coatings on the QDs.[1330] Thus, SBS consisting of the QD@BR functional units and operating by the FRET mechanism can be used in some fields of molecular electronics and for sensing and photovoltaic devices, which attracts attention of numerous researchers.[1330, 1333 – 1341]

For comparing the efficiency of various SBS, consider the data on the formation of composite materials composed of BR or BSA and QDs.[1334 – 1336] In the CdTe(537)@BSA system (1 : 9), fluorescence of the initial QDs does not change (since BSA does not contain a chromophore absorbing in the visible range), while in the CdTe(537)@BR(PM) system (1 : 9), QD fluorescence markedly decreases (by 95% of the initial value for single QDs), *i.e.*, effective energy transfer from QD to BR takes place.[1332] An important achievement of Nabiev *et al.*[1335] was the development of a QD- and BR-based SBS capable of generating direct current and reversible photoelectric changes upon light activation (λ = 410 nm) with a power of 7 mW cm^{-2}. These photocurrents differ in the magnitude and in the form from those generated in the same SBS on exposure to light with a power of 6.5 mW cm^{-2} (λ = 570 nm) or in the control BR(PM) system with the M_{410} form[1336] The authors proposed a model explaining the FRET and generation of stationary photocurrents in the QD@BR system, which could not be done before.[1330 – 1333] In another series of experiments,[1337] simultaneous double-beam illumination (λ = 570 ± 10 and 410 ± 10 nm) of CdTe@BR(PM) SBS was carried out. The authors claimed that protons are not released to the extracellular space, but oscillate inside the membrane, which accounts for the generation of a stationary photocurrent under these conditions.[1336, 1337] Similar double beam illumination models in various combinations were considered by other specialists,[1338, 1339] which generated prospects for the use of hybrid QD@BR SBS as a new type of multifunctional materials.

Griep *et al.*[1340 – 1342] proposed an original method for the fabrication of the layered QD@BR(PM) system with a 23% increase in the photovoltaic output in comparison with the control. In addition, fluorescence quenching [1341] of 54.0 and 43.8% relative to the control was detected for CdSe/ZnS@BR(PM) (*I*) and CdSe/ZnS + streptavidin@-biotin + BR(PM) (*II*) systems, respectively. It is surprising that a minor change (from ⩽1.5 nm to 6 – 8 nm [1341]) in the distance between BR(PM) and CdSe/ZnS for systems *I* and *II* is accompanied by the above-indicated decrease in the fluorescence intensity. The photopotentials of system *II* are 306 and −200 mV for light switching on and off, respectively, while these potentials for the control system are 249 and −158 mV.[1341] Hence, the CdSe/ZnS + streptavidin@ biotin + BR(PM) system is more efficient in the photovoltaic parameters due to the FRET effect.[1340 – 1342] Regarding the possible practical application, active patenting [1343] of the SBS based on BR and QD layers and the results of their test functioning is an encouraging factor. Griep *et al.*[1340 – 1343] traced a regular increase in the characteristics of these systems, which is promising for their subsequent use in both optical and molecular electronics [1332] and other bionanotechnological fields.

4.2.3.3. Interaction of bacteriorhodopsin with gold and silver nanoparticles

Studies of the plasmon effects of gold and silver NPs [1330 – 1334] in relation to the photoinduced changes in BR(PM)-based systems [1265 – 1268, 1330] represent a relevant trend in the field of development of SBS for bionanotechnology. For example, the plasmon effects of AgNPs [1330 – 1334] in these SBS are manifested as a change in the kinetic and spectral characteristics of BR(PM) following variation of the size and shape of nanoparticles, especially when these systems are irradiated with blue light (Fig. 169 *a*).[1330]

Experiments showed that the combined action of blue light and short-pulse laser excitation (λ = 532 nm) on BR in the presence of AgNPs markedly accelerates both regeneration of the ground state (bR_{568}) from the M-form (M_{410}) and the rate of proton pumping across the membrane as a result of direct conversion of form M to the ground state *via* a bypass, which takes ~200 ns (instead of 15 ms) (see Fig. 169 *a*).[1330] It is surprising that the rates of transformation of M_{410} in the presence of AgNPs with sizes of 40 and 8 nm differ 400-fold![1344] The authors attributed this result to both enhancement of the plasmonic field and more efficient overlap of the M_{410} absorption bands with the bands of 40 nm AgNPs compared with that for smaller nanoparticles.[1345]

This difference (400-fold) is close to the calculated value of 375. This value is the product of the change in the plasmonic field strength with increasing AgNP size (~125-fold) and acceleration of the energy transfer in this SBS due to enhancement of the spectral overlap (~3-fold). It was suggested [1342 – 1346] that acceleration of the $bR_{568} \rightarrow M_{410}$ 'reversible transition' may make an additional contribution to this effect. Furthermore, Chu *et al.*[1346] developed the following original engineering approaches for optimization of all processes in a complex SBS:

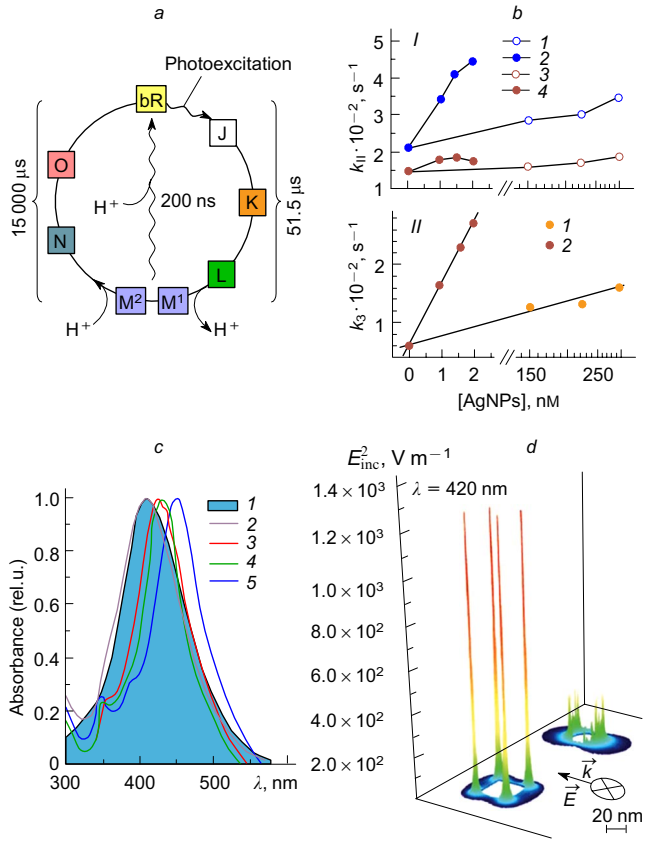


Figure 169. Electromagnetic field effect in the SBS based on BR(PM) and AgNPs.[1330] (*a*) Photoinduced transitions from bR_{568} to M_{410} (M^1 and M^2 forms) *via* intermediate forms J, K, L and back transition *via* intermediate forms O, N; (*b*) plots for rate constants in the normal (k_{II}, plot *I*) and shortened (k_3, plot *II*) BR photocycles in the SBS containing AgNPs of 8 (*1*, *3*) and 40 nm (*2*, *4*) size in the absence (*1*, *2*) and under the action of blue light irradiation (*3*, *4*) of BR(PM); (*c*) areas of spectral overlap of the spheres (*1*, *2*), cuboids A (*3*) and B (*4*) and cubes (*5*) of 40 nm AgNPs with form M_{410} (blue hatched area); (*d*) electromagnetic field strength (E^2_{inc}) near AgNPs as a function of NP shape: for spheres with a diameter of 40 nm (on the right) and cubes with a 40 nm edge (on the left). Published with permission from Springer.

— increase in the efficiency of charge carrier separation by photoactivation of the system in the proton-selective Nafion membrane;

— retention of the maximum plasmonic field effect by using polyvinylpyrrolidone as a polymer coating of nanoparticles;

— use of specially synthesized nanoparticles of a specified shape (spheres, cubes and cuboids with high curvature surface sites), which increases the efficiency of electromagnetic field enhancement (see Fig. 169 *d*).[1330]

Yen *et al.*[1344] published unique results on measurement of the photocurrent (~210 nA cm^{-2}) in SBS based on BR(PM) and AgNPs of specified size and shape. Electrochemical cells with LB films comprising a large number of alternating BR(PM) and polyelectrolyte layers characterized by photocurrents of ~100–420 nA cm^{-2} were also obtained.[1347–1349] In the Langmuir–Schaefer PM films, the photocurrents were ~50–200 nA cm^{-2},[1350] while those in the bilayer lipid membranes with PM varied from 100 to 150 nA cm^{-2}.[1351] The indicated values[1347–1352] are comparable with those presented above (see Ref. 1347) or are even higher.[1350] Efficient nanobiohybrid SBS based on BR with various types of NPs are not commercially manufactured so far; however, it is beyond doubt that that they will be in-demand as technological materials in the future.

Thus, albumins, lipases and rhodopsins are promising biologically active compounds for the interaction with NPs and for the development of SBS with a set of specified properties. This can be used to design new and to improve existing bionanomaterials. The proposed methods for fabrication of SBS provide increase in their stability, decrease in the interaction with blood plasma proteins, biocompatibility and other important properties. Albumin-based systems demonstrate a considerable practical potential regarding the space- and time-controlled release, in addition to their theranostic applications. Systems composed of BSA and metal NPs are among the few types of nanotransporters *in vivo* that exhibit a dual capability (passive and active targeting of a tumour) and a wide range of drug therapy possibilities compared with the single components. Lipases tend to interact with metal oxide NPs to give SBS with high catalytic properties and stability for practical applications *in vitro*.

The SBS based on rhodopsins and QD type nanoparticles, possessing a set of unique photodynamic properties, are most promising for biomedical diagnosis. However, the QD carriers are fairly toxic when used without an additional polymer coating, which imposes certain restrictions on the selection of SBS for biomedical purposes.

Thus, the demonstrated approaches to the fabrication of SBS based on structurally and functionally different proteins and nanoparticles make it possible to create modern bionanomaterials with a set of properties required to solve particular biomedical problems.

4.3. Development of multifunctional nanoparticles for biomedical applications on the basis of silica nanoplatforms

The development of modern diagnostic techniques for various pathologies, such as magnetic resonance imaging, computed tomography, positron emission tomography (PET) and fluorescence imaging, requires the development of new effective and safe contrast agents.[1353–1356] When different techniques are used simultaneously, artifacts are reduced, facilitating more accurate disease diagnosis.[1356] In addition, the creation of bimodal materials that have a magnetothermal, photothermal, or photodynamic effect on cancer cells is considered today as a promising basis for the development of new types of theranostics that simultaneously perform therapeutic and diagnostic functions.[1357–1360]

In the last decades, the design of new methods for the synthesis of multifunctional nanosized polymer particles performing a dual function has become a priority area of nanomedicine and biology.[1357–1360] A silica matrix could be a promising basis for multifunctional polymeric NPs of various sizes and porosities.The main advantages of silica NPs are the simplicity of synthesis, which does not require high temperatures, the absence of swelling of NPs in solution with a change in pH, transparency and low toxicity.[1361] Doping of various compounds into silica NPs is widely used to fabicate functional materials. The inclusion of dopants into the silica matrix eliminates or reduces the problem of their toxicity and increases their stability, while the simplicity of methods for modifying the silica surface by introducing anchor groups necessary for binding

biological objects [1271, 1362–1364] can serve to vary the morphology and functional properties of nanoparticles.[1365, 1366]

Silica NPs are synthesized most often using the Stöber method,[1367–1379] reverse water-in-oil microemulsion method [1363–1367, 1380–1397] and direct oil-in-water microemulsion method.[1398–1404] These methods are based on alkaline hydrolytic polycondensation of tetraethoxysilane to form spherical three-dimensional structures.[1364] The choice of one or another synthesis technique is often determined by the nature of the dopant introduced into the silica matrix. This Section focuses on the theoretical and applied aspects of the development of multifunctional NPs based on silica matrices.

4.3.1. Methods for producing silica nanoparticles

4.3.1.1. Stöber method

Historically, the Stöber method,[1367] based on alkaline hydrolysis of orthosilicic acid esters and the subsequent polycondensation in aqueous alcohol, was the first method for preparing silica NPs. This procedure gives spherical particles of controlled size (10 nm and above) with variable polydispersity by varying the nature of reagents (alcohols and bases), their concentrations and ratio.[1367–1379] The method is relatively simple, does not require purification from surfactants and can afford particles with inclusion of both water-soluble and water-insoluble inorganic and organic compounds.

There are several approaches to the synthesis of silica NPs using the Stöber method, each having advantages and disadvantages.

The first approach is based on doping of the polymer matrix with one (or more) water- or alcohol-soluble components that act as seeds (nuclei) for the formation of spherical silica NPs (Fig. 170 *a*). Electrostatic interactions between the dopant and the silica matrix usually promote incorporation of positively charged components and prevent inclusion of negatively charged ones.[1369–1372] The most common examples are the introduction of fluorophores such as fluorescein and its derivatives,[1368] rhodamine B [1368] and positively charged ruthenium(II) complexes.[1369–1372] The non-covalent adsorption of positively charged dopant on a negatively charged silica surface followed by additional silica coating produces particles with dopants introduced into different layers of the polymer matrix.[1369–1371]

The second approach involves preliminary covalent binding of the dopant to a silicon derivative and its subsequent introduction as a precursor into silica synthesis (see Figure 170 *b*).[1368, 1374–1377] Covalent binding leads to dopant attachment and prevents its leaching from the silica matrix.[1376] Disadvantages of this method are poor solubility of the resulting silicon derivative in a water–ethanol mixture, complexity of synthesis and low doping efficiency.[1376, 1377]

The third approach is based on the pre-synthesis of nuclei containing a dopant followed by the addition of new portions of tetraethoxysilane (TEOS) during the reaction (see Fig. 170 *c*).[1372, 1373] This method is based on the use of amino acids as catalysts for alkaline hydrolysis of TEOS and can be implemented at lower pH (~9–10). Its advantages are the formation of particles of a specified size and controlled monodispersity.[1372, 1373] The method can be used to incorporate both positively charged [1372] and neutral dyes, such as rhodamine B and fluorescein, into a silica particle without peliminary covalent binding to 3-aminopropyltriethoxysilane (APTES).[1373]

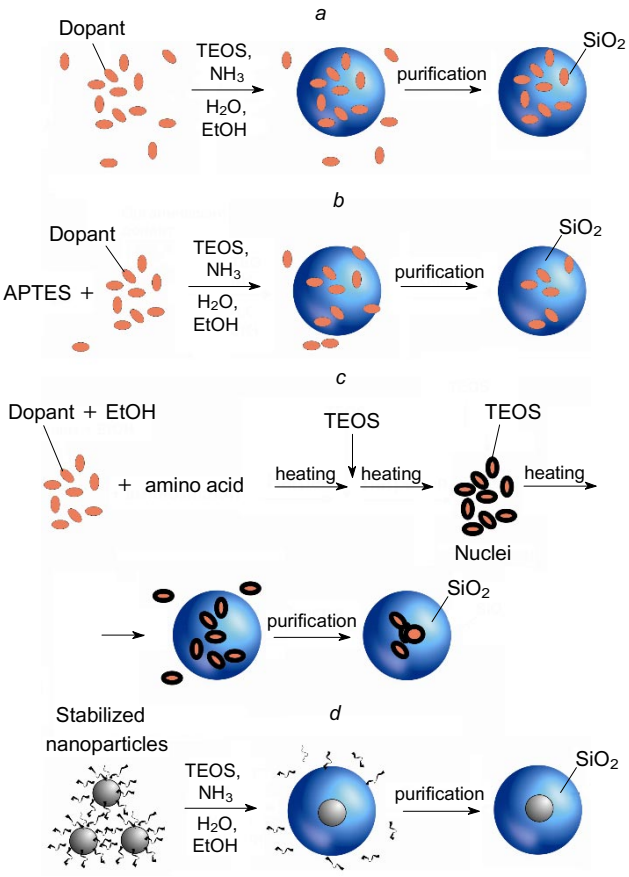


Figure 170. Approaches to the synthesis of silica nanoparticles containing a dopant by the Stöber method (*a*–*d*, see text). The figure was created by the authors using data of Refs 1367–1379.

The fourth approach consists in the introduction of preliminarily obtained stabilized NPs [iron oxide, silver(0), gold(0) NPs and quantum dots] as precursors for the subsequent growth of the silica layer on their surface (see Fig. 170 *d*).[1376–1379] The crucial factor affecting the monodispersity of the obtained silica NPs is the colloidal stability of the initial nanoparticles in a water–ethanol medium. Double superparamagnetic highly luminescent silica particles [with a diameter (*d*) of 97 nm] based on Fe_3O_4 (d = 18 nm) and CdSe@CdS@ZnS quantum dots (QDs) (d = 4.5 nm) were obtained by the modified St@ber method.[1378] The presence of thiol groups provided for efficient adsorption of oleate-stabilized quantum dots on the silica surface of iron oxide nanoparticles through ligand exchange. To increase the colloidal stability and reduce the toxicity of QDs, the authors used an additional thin silica coating, thus obtaining the Fe_3O_4@SiO_2@QD NPs system. These magnetic-luminescent nanoparticles can be used for multimodal cell separation.[1378]

4.3.1.2. Microemulsion methods

More recently developed methods for producing monodisperse silica NPs are microemulsion methods, which are based on the formation of thermodynamically stable water-in-oil [1363, 1365, 1366, 1380–1397] or oil-in-water [1398–1404] type microemulsions.

Reverse water-in-oil microemulsion method. A reverse water-in-oil microemulsion typically consists of four components: oil (most commonly cyclohexane), water, surfac-

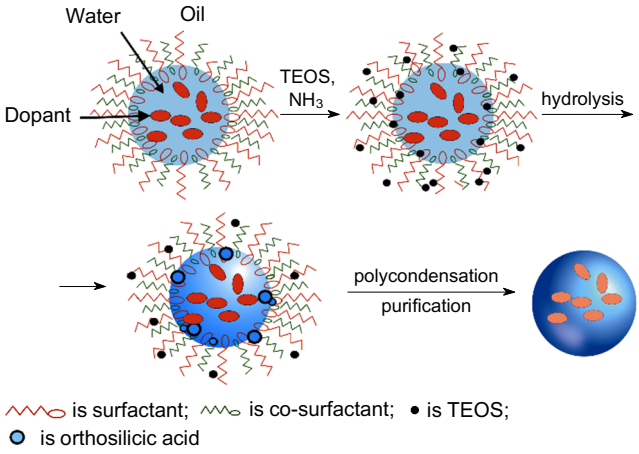


Figure 171. Synthesis of dopant-containing silica nanoparticles by the reverse microemulsion method. The figure was created by the authors using data of Ref. 1377.

tant (Triton X100, Bridge 30, Igepal or AOT) and co-surfactant (heptanol or octanol). Nanosized water droplets in oil stabilized by surfactant and co-surfactant molecules serve as nanoreactors for hydrolysis of orthosilicic acid esters and the subsequent polycondensation to form spherical monodispersed silica particles (Fig. 171). The size of particles obtained by reverse microemulsion method can be varied in a controlled manner from 15 to 200 nm by varying conditions such as water to surfactant ratio, nature of organic solvent and surfactant, ammonia concentration, amount of added TEOS and the nature of dopant.[1363, 1365, 1366, 1377, 1380–1397]

A key advantage of the microemulsion synthesis over the Stöber method is the production of silica nanoparticles with a narrow size distribution. In addition, this technique yields smaller particles of more complex morphology.[1380] It should be noted that for purification of the obtained silica nanoparticles from surfactants and unreacted substances in the reverse microemulsion method, a sequence of washing, ultrasonic treatment and centrifugation is usually repeated many times. However, it was shown [1364, 1377, 1397] that complete removal of surfactant traces from the silica surface is vitually impossible; this can affect the properties and applications of the dispersions.

Water-soluble compounds such as tris(dipyridine)-ruthenium(II),[30, 31] lanthanide(III) complexes [1363, 1365, 1366, 1383–1385] or metal clusters [1386–1388] are commonly used as dopants in the reverse microemulsion method. Unlike the Stöber method, in the microemulsion technique, the dopants can be either electrically neutral or negatively or positively charged.[1380]

The hydrophilicity of the doping dye and its aggregation behaviour during the growth of silica NPs have a significant effect on the distribution of the dopant in the silica matrix and the photophysical characteristics of the obtained fluorescent silica nanoparticles (Fig. 172).[1364, 1389, 1390] Indocarbocyanine dyes differing in the number of sulfonate groups and, hence, in the hydrophilicity, were used to demonstrate the possibility to control the distribution of the fluorophore in the silica matrix (in the core or near the silica/water interface) by varying the hydrophilicity of the dopant (see Fig. 172).

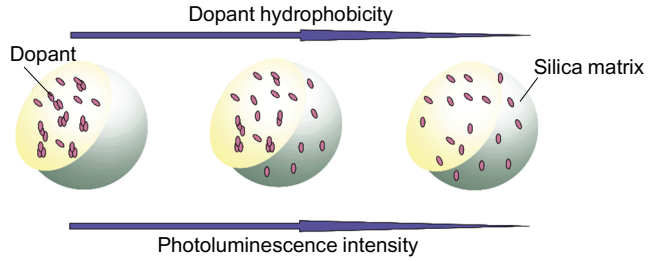


Figure 172. Schematic view of the dependence of the dopant distribution in a silica matrix on the dopant hydrophobicity. The figure was created by the authors using data of Ref. 1389.

Fluorophores with low hydrophilicity are distributed throughout the entire volume of the silica matrix, which leads to the absence of concentration quenching of their photoluminescence in the NPs.[1389] High hydrophilicity and water solubility of fluorophores, on the contrary, lead to their aggregation in nanoparticles, which deteriorates the photophysical characteristics in comparison with those of less hydrophilic fluorophores (see Fig. 172).

The influence of aggregative behaviour of lanthanide complexes in silica nanoparticles on their photophysical properties was studied with the participation of the authors of this Section. For this purpose, double silica nanoparticles characterized by intense luminescence in the green and near-infrared (NIR) spectral regions were obtained on the basis of isostructural lanthanide(III) complexes (Fig. 173).[1383]

The photophysical characteristics of the obtained double silica NPs were found to significantly depend on the method of addition (as a solution or a dispersion) and the aggregation state of isostructural lanthanides(III) complexes. The energy exchange between lanthanide blocks was shown to occur in relation to isostructural *p*-sulfonatothiacalix[4]arene complexes of terbium(III) and ytterbium(III) in the silica matrix (see Fig. 173). It was found that Tb–Yb silica nanoparticles are characterized by low leaching of the complexes from the silica matrix and insignificant toxicity. They were able to efficiently and quickly penetrate into cells while maintaining a luminescent response, which is a prerequisite for their use as cell markers.[1383]

Shahabi's research team group reported [1391] the preparation of silica NPs with double luminescence by adding organic fluorophores. It was shown that, depending on the structure of fluorophores, the optimal introduction method can be either the pre-synthesis of luminescent silica nuclei by covalent binding of dyes to APTES or their non-covalent doping into the silica layer. Such particles are characterized by double high-intensity luminescence in the green (blue) and red regions of the spectrum; they have low toxicity and have a great potential for various biological studies *in vivo*.[1391]

A number of studies address the incorporation of various metal clusters into the silica matrix to produce structures characterized by the distribution of cluster units (or their aggregates) throughout the volume of the silica matrix.[1386–1388] For example, Aubert *et al.*[1387] doped rhenium-based metal clusters, $K_4[Re_6S_8(OH)_6]$, $K_4[Re_6Se_8(OH)_6]$ and $Cs_{1.68}K_{2.32}[Re_6S_8(CN)_4(OH)_2]$, into the silica matrix. The obtained particles exhibit luminescence in the red spectral range and may find application in biotechnology.

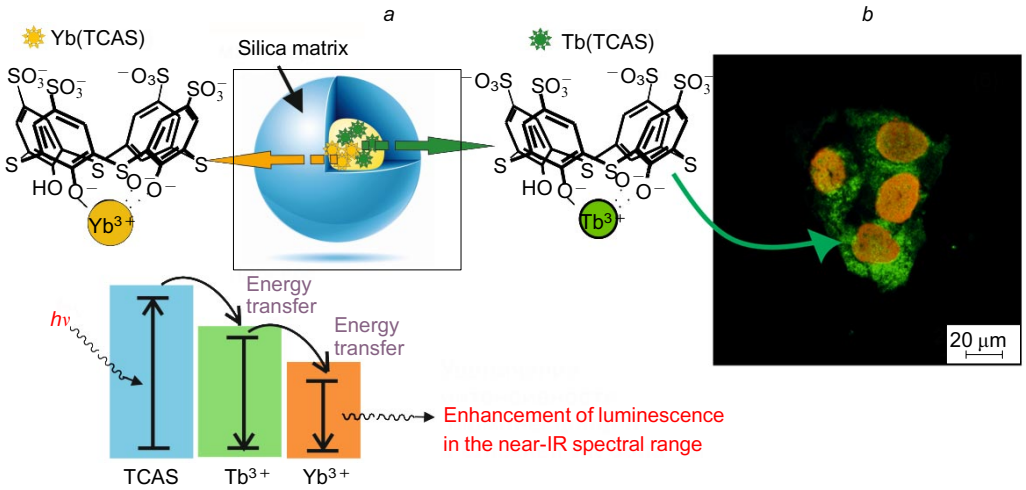


Figure 173. Schematic view of silica nanoparticles based on Tb^{III} and Yb^{III} complexes with *p*-sulfonatothiacalix[4]-arene (TCAS) and energy transfer mechanism (*a*); confocal laser microscopy micrographs of normal cells incubated with amino-modified silica nanoparticles based on Tb^{III} and Yb^{III} complexes with TCAS (*b*).[1383]

There are examples of incorporation of water-insoluble hydrophilic nanoparticles [in particular, NPs of gold(0), silver(0), and $ZnFe_2O_4$ stabilized by hydrophilic ligands] into a polymer silica matrix. The NPs act as nuclei that are subsequently coated with a silica shell.[1380, 1392, 1393]

More recent papers describe examples of hydrophobic water-insoluble nanoparticles [NPs of iron oxide or lanthanide oxides and salts and gold(0) and quantum dots] doped into the silica matrix.[1379, 1380, 1383 – 1385, 1394 – 1396] The reason for the successful incorporation of hydrophobic NPs into the silica matrix using the reverse microemulsion method is ligand exchange with the replacement of hydrophobic ligand (oleylamine or sodium oleate) on the surface of the original nanoparticle with surfactant or TEOS (or orthosilicic acid), which facilitates the formation of monodisperse colloidal stable silica particles.[1380, 1394]

Direct oil-in-water microemulsion method. Direct oil-in-water microemulsions are used for the synthesis of ultrasmall and highly dispersed silica NPs. The method is mainly used to obtain organically modified silica nanoparticles (ORMOSIL).[1359] A direct oil-in-water microemulsion is based on alkaline hydrolysis of a silicon derivative of vinyltriethoxysilane (VTES) and APTES followed by polycondensation in oil (1-butanol) nanodroplets stabilized by surfactants (AOT or Tween-80) and DMF (or DMSO) in water. The addition of APTES in the direct microemulsion method generates a weakly alkaline medium and thus stops further growth of nanoparticles.[1399] The size of NPs obtained by the direct microemulsion method can vary from 5 to 100 nm.[1377] Many examples of ORMOSIL particles doped with various water-insoluble dyes (Nile red, indocyanine green),[1399, 1400] agents for photodynamic therapy,[1401] antitumour agents (doxorubicin, curcumin)[1400, 1402, 1403] and water-insoluble hydrophobic NPs (iron oxide, quantum dots) can be found in the literature.[1399, 1404] Since the surface of silica nanoparticles obtained by the direct microemulsion method is more porous, preliminary covalent binding of dopants to silicon derivatives is preferable, in order to reduce leaching of the dopant from the silica matrix.[1359] However, the presence of pores may give rise to NPs for which a slow release of the dopant from the polymer matrix is a necessary stage fo biomedical application. For example, Prasad's research team[1401] obtained a number of luminescent ORMOSIL particles containing doxorubicin. It was found that these NPs can release 70% of the drug within two weeks; they are able to enter the pancreatic cancer cells and have a cytotoxic effect. Doxorubicin-containing ORMOSIL nanoparticles can be used for further incoporation of photosensitizers functioning as agents for photodynamic therapy.

A new type of bimodal ORMOSIL particles was developed on the basis of doxorubicin and the indocyanine green dye, which exhibits luminescence in the red and near-IR spectral regions.[1400] To obtain bimodal ORMOSIL particles, the authors used two strategies: non-covalent doping of indocyanine green by physical adsorption and non-covalent (or covalent) doping of doxorubicin. Bimodal ORMOSIL particles with a covalently bound drug had pronounced colloidal properties and showed low cytotoxicity against cancer cells. Upon IR irradiation of cells incubated with the obtained products, the temperature inside the cell increased and doxorubicin was released from the polymer matrix to induce the destruction of cancer cells. These bimodal particles can be used in chemotherapy, hyperthermia and fluorescence imaging of cells.[1400]

4.3.2. Effect of the dopant on the size and polydispersity of silica nanoparticles

At present, there is virtually no systematic information in the literature on the effect of the dopant nature and intrroduction method on the size, shape, and polydispersity of silica nanoparticles obtained by the reverse microemulsion method. However, according to our data, nanosized and molecular dopants are important components of reverse microemulsions that can have a significant, not always expected and unambiguous, effect on the size and shape of the formed silica NPs.[1365, 1381, 1383 – 1385]

4.3.3. Mutual influence of components in composite silica nanoparticles considered for nanoparticles of iron oxide, silver(0) and metal complexes

Magnetic resonance imaging is widely used as a direct and non-invasive method of medical diagnosis of various pathologies.[1405, 1406] The development of new effective and low-toxic contrast agents (CAs) meant to increase the image contrast in the MRI method is a priority area of medicinal chemistry.[1407, 1408] A promising way to increase the efficiency and reduce the toxicity of contrast agents is to include them in polymer NPs.[1409 – 1411] In addition, doping of contrast agents into the same polymer matrix produces so-called bimodal T_1- and T_2-contrast agents, the combined use of which eliminates image artifacts, thus providing for

more accurate imaging.[1407, 1408] Gadolinium(III) chelates are used most widely as T_1-contrast agents in clinical diagnosis, while superparamagnetic iron oxide particles (SPION) are known for their high T_2-contrast efficiency.[1412–1414] There are many synthetic approaches for combining Gd^{III} chelates (T_1-CA) and superparamagnetic iron oxide nanoparticles (T_2-CA) in the same polymer matrix.[1405, 1407, 1408, 1415–1417] A crucial factor determining the dual contrast efficiency is the thickness of separation layer between the T_1- and T_2-components. The optimum spacing at which there is usually no adverse effect of the local SPION magnetic field on the spin–lattice relaxation of Gd^{III} chelates, is >20 nm.[1407] In addition, the ratio of transverse to longitudinal relaxivity values ($r_2 : r_1$) should be <2.[1418, 1419]

Silica matrix is a convenient platform for the development of bimodal T_1- and T_2-contrast agents with optimal spacing between the two components. Like the Stöber method, the reverse microemulsion method allows the synthesis of NPs of various morphologies with the incorporation of dopants into different layers of the polymer matrix, thus producing nanoparticles with specified sizes and properties.[1365, 1366, 1382, 1384, 1385] For instance, Fedorenko *et al.*[1365] showed that preferential localization of gadolinium(III) complexes with *p*-sulfonatothiacalix[4]arene [Gd(TCAS)] in the surface layer of silica nanoparticles leads to a ponounced enhancement of their relaxation characteristics and an almost tenfold incease in r_1 as compared with those for similar species when the complexes are localized in the core (Fig. 174). High relaxivity and low cytotoxicity of the obtained NPs are due to doping of gadolinium complexes into the surface layer of silica nanoparticles (55 nm in size); this prevents the complexes from leaching from the silica matrix, but provides their effective hydration.[1365]

The developed technique [1365] was used to obtain efficient silica NP-based bimodal T_1- and T_2-contrast agents with a core–shell structure, SPION inclusion ($d = 6$ nm) in the core and preferential localization of Gd(TCAS) in the outer silica layer (Fig. 175).[1384] The poducts had high longitudinal and transverse relaxation values ($r_1 = 34.7$ mmol^{-1} s^{-1} and $r_2 = 64.7$ mmol^{-1} s^{-1}) and low $r_2 : r_1$ ratio at 0.47 T. The shorter distance between SPION and the Gd(TCAS) complexes ($\sim$12 nm) resulted in a minor effect of suppression of iron oxide NP spin–lattice relaxation (see Fig. 175).[1365, 1384] The NP aggregation in the presence of protein in buffer solutions led to a decrease in the longitudinal and increase in the transverse relaxation. The bimodal silica NPs provided efficient T_1- and T_2-contrast on a 1.5 T MRI scanner and had low cytotoxicity and high colloidal stability in aqueous solutions.[1384]

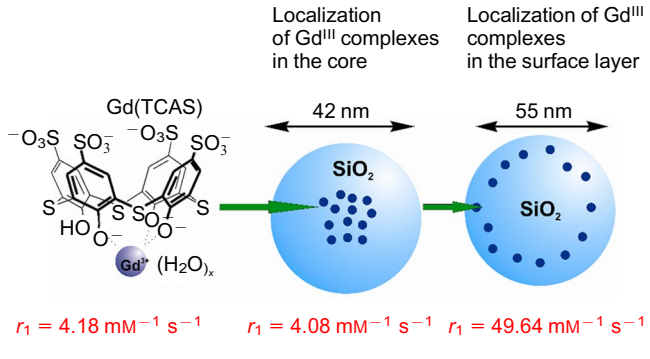


Figure 174. Schematic view of silica nanoparticles with different positions of the Gd(TCAS) complex in the silica matrix and r_1 values for aqueous solution of Gd(TCAS) and aqueous dispersions of silica nanoparticles.[1365] Published with permission from Elsevier.

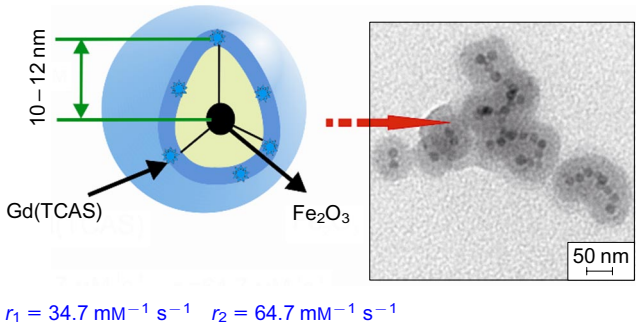


Figure 175. Schematic view of a bimodal T_1- and T_2-contrast agent based on silica nanoparticles doped with Gd(TCAS) complexes and Fe_2O_3 NPs and TEM image of the resulting sample.[1384] Published with permission from Elsevier.

Neramboug *et al.*[1388] also found a mutual influence of dopants in silica NPs, which must be taken into account in the design of multifunctional nanomaterials. In particular, the authors intended to obtain magnetic-luminescent silica NPs based on Fe_2O_3, metal clusters $[Mo_6Br_{14}]^{2-}$ and plasmon Au^0 NPs. The synthesis included simultaneous introduction of hydrophilic magnetic Fe_2O_3 cores and metal clusters into a reverse water-in-oil microemulsion. These bimodal nanoparticles had superparamagnetic properties and intense red luminescence. The signal intensity significantly decreased with increasing size of the doped iron oxide cores, which is due to their ability to absorb light at 400–450 nm, which is used to induce the photoluminescence of the clusters. Coating of the bimodal nanoparticles with gold(0) clusters was carried out by adsorption of Au^{3+} on the negatively charged silica surface at pH 12 followed by reduction in exposure to UV radiation. The obtained bimodal magnetic-luminescent silica nanoparticles $[Cs_2Mo_6Br_{14}-Fe_2O_3]@SiO_2-Au^0$ can be used for biomedical purposes and for theranostics. However, the question of how alkaline hydrolysis of clusters, which is inevitable under such alkaline conditions, affects the composition and content of clusters within and on the surface of silica NPs remained unanswered.

The permeability of the silica matrix to OH^- and H^+ ions accounts for the degradation of the complexes both within and on the surface of silica nanoparticles. This was also noted in a number of studies in which silicaNPs contained terbium(III) complexes as dopants.[1420] For example, hydrogen peroxide treatment of Tb(TCAS)-containing composite silica nanoparticles coated with silver(0) nanoparticles was used to reduce the Ag^0 particle size tenfold (from 30 to 3 nm) and promoted their uniform distribution over the silica surface. However, the hydroxide ions generated under these conditions led to a decrease in the terbium content in the composite sample and to a decrease in the intensity of Tb-centered luminescence due to partial destruction and washing out of complexes from the NPs.[1420]

4.3.4. Covalent and non-covalent surface modification of silica nanoparticles

Modification of the silica surface with target proteins or other target ligands is a necessary stage in the production of multifunctional silica NPs with a specific effect on the targets.[1421]

Covalent binding and physical adsorption are the main ways to modify the surface of silica NPs. Physical adsorption of biomolecules or polymers [PEG, polyethyleneimine (PEI)] is simple to implement, ergonomic and gives rise to a crown on the silica surface. Coating the silica surface with PEG affects the efficiency of particle uptake by cells, reduces the particle cytotoxicity and increases their *in vivo* stability. Also, it ensables the covalent binding of proteins, enzymes, *etc.*[1364, 1422] Layer-by-layer adsorption of various polymers (in particular, PEIs) can lead to recharging of the surface of NPs, which can significantly affect their cellular uptake.[1422] However, protein desorption, which occurs when other biomolecules with higher NP affinity are present in the system, significantly complicates the use of this method. It is known that protein adsorption on the NP surface can lead to undesirable changes in its structure and functional activity. In addition, changes in pH or ionic strength of the solution can also cause desorption of proteins from the silica surface. Therefore, the conjugation of biomolecules *via* covalent binding to nanoobjects is preferable.[1364]

The high chemical reactivity of the Si—OH groups pomotes surface decoration of silica nanoparticles. The covalent binding of target ligands requires the presence of certain functional anchor groups on the silica surface; most commonly, amino, carboxy, thiol and epoxy groups serve for this purpose.[1364, 1423, 1424] Bioconjugation can be performed by applying cross-linking reagents, which are chosen depending on the anchor groups present on the NP surface. Both small molecules (*e.g.*, folic acid) and macromolecules (*e.g.*, oligosaccharides, peptides, proteins, antibodies and aptamers) can be used as the target ligands.[1421, 1425 – 1430]

The conjugation processes of biomolecules to micro- and nanoparticles and the choice of cross-linking agents are discussed most comprehensively in the publication of Hermanson.[1430] The main cross-linking agent for the conjugation of carboxy-modified NPs to biological objects containing amine or amino acid residues is 1-(3-dimethylaminopropyl)-3-ethylcarbodiimide.[1425 – 1430] The use of *N*-hydroxysulfosuccinimide reduces the pobability of undesirable hydrolysis of *O*-acylisourea, an active intermediate produced during the reaction.[1430]

Glutaraldehyde is widely used as a cross-linking agent (cross-linker) for bioconjugation of amino-modified silica NPs.[1430] The reaction of covalent binding of biomolecules proceeds through the formation of a Schiff base.[1430] However, the presence of a large number of amine residues in biological objects and nanoparticles precludes selective binding of biomolecules to certain groups and promotes the formation of cross-linked particles, which can finally lead to their irreversible aggregation.[1363, 1364, 1430] Moreover, the choice of the bioconjugation strategy and cross-linking agents has a significant impact on the production of NPs with specified characteristics and properties.[1363]

Significant aggregation of amino-modified silica NPs and formation of cross-linked nanoparticles when glutaraldehyde [SNs(COH)] is used as the cross-linking agent prevent efficient decoration of particles with a target protein, α-bungarotoxin (α-BGT), and affect the sensing

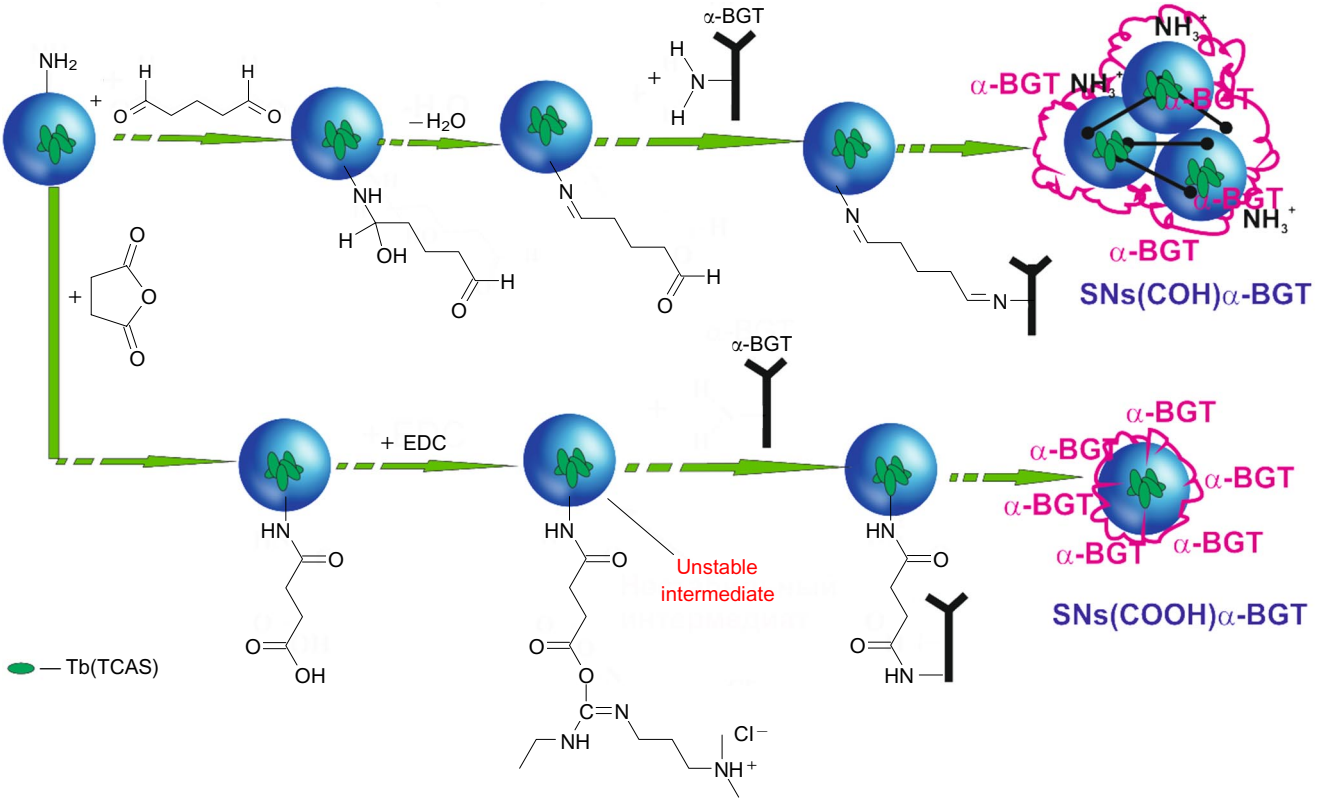


Figure 176. Routes of α-bungarotoxin modification of silica nanoparticles doped with Tb(TCAS) complexes. The figure was created by the authors using data of Ref. 1363.

capacity of modified particles (Fig. 176).[1363] Conversely, the successful bioconjugation of carboxy-modified silica NPs (SNs(COOH)) with the α-BGT target protein through interaction with EDC made it possible to localize nanoparticles in the synaptic cleft, as was established in *ex vivo* experiments on frog muscle tissues.[1363]

The obtained α-BGT-modified silica nanoparticles doped with Tb(TCAS) complexes were shown to be applicable as pH sensors for the enzymatic hydrolysis of acetylcholine. In *ex vivo* experiments, fluorescence microscopy demonstrated effective quenching of the terbium luminescence of nanoparticles due to the release of acetic acid into the synaptic cleft induced by the enzymatic hydrolysis of acetylcholine upon electrical stimulation of muscle tissues.[1363]

A relatively new trend in bioconjugation is the use of click chemistry, that is, reactions proceeding with high regioselectivity and high product yield under various conditions, including physiological conditions.[1364, 1430] However, the discussion of this issue is beyond the scope of this Section.

Adsorption of inorganic nanoparticles (Ag^0, Au^0, $Cu_{2-x}S$) [1368, 1420, 1431] or other compounds (dyes, clusters) [1432, 1433] on silica surface *via* electrostatic or coordination interactions is a widely known method for the fabication of multifunctional silica NPs. Composite materials based on silica particles coated with a shell of small particles of noble metals (Ag^0, Au^0) are of great interest because of their possible application in medicine, biosensorics and catalysis.[1420, 1430, 1431] The immobilization of metal nanoparticles on a silica surface suppresses uncontrolled aggregation of NPs in solution and represents a promising alternative to their colloidal stabilization by coating with a polymer matrix to form a core–shell structure.[1392, 1420] For example, coating of highly luminescent silica NPs based on Tb(TCAS) complexes with ultrafine silver(0) nanoparticles made it possible to obtain composite NPs, which were effective cellular contrast agents capable of inducing cancer cell death (Fig. 177).[1420]

Effective internalization of composite nanoparticles into Hep-2 (human laryngeal adenocarcinoma) cells was demonstrated using confocal laser and transmission electron microscopy of ultrathin sections of cancer cells. Comparative analysis of the cytotoxicity of normal (DK-4) and cancer (Hep-2) cells incubated with composite nanoparticles at different concentrations showed a significant cytotoxic effect on cancer cells (see Fig. 177 *b*). These results indicate that the obtained composite nanoparticles are promising for use in the diagnosis and treatment of cancer.[1420]

Irreversible or quasi-irreversible adsorption of aggregates of luminescent complexes (including clusters) on a silica surface is an effective method for obtaining multifunctional silica nanoparticles. This approach provides for attachment of a large number of luminescent complexes to a silica surface without noticeable washing out for several months. Irreversible adsorption is the result of cooperative effect of electrostatic and coordination interactions of metal complexes with silanol and amino groups on the NP surface. Elistratova *et al.*[1433] described successful modification of the surface of amino-modified silica NPs by adsorption of luminescent hexamolybdenum clusters, known for their ability to generate singlet oxygen, which can find application in photodynamic therapy.[1433]

4.3.5. Correlation between cellular internalization and surface properties of of silica nanoparticles

Monitoring and understanding of the mechanisms of cellular uptake of nanoobjects, their residence time in various organs and tissues and cytotoxicity is a step forward from the development and fabrication of nanoparticles to their practical application in biomedicine. The rate and mechanism of internalization of nanoobjects into cells and the cytotoxicity significantly depend on the size and shape of these nanoobjects.[1422, 1434–1438] Endocytosis is the main mechanism of cellular uptake of silica particles < 50 nm in sized.[1435–1438] The optimal size of nanoparticles to allow effective endocytosis depends on many factors, including the surface properties of the particles and type of cell culture used.[1438] The negatively charged surface of unmodified silica nanoparticles prevents their effective internalization into cells.[1438–1441] The formation of a protein corona upon physical adsorption of proteins on the surface of nanoparticles when they are released into biological fluids hides the particles, changes their colloidal stability and affects their cellular uptake, the degree of accumulation in organs and the rate of excretion from the body.[1285, 1442]

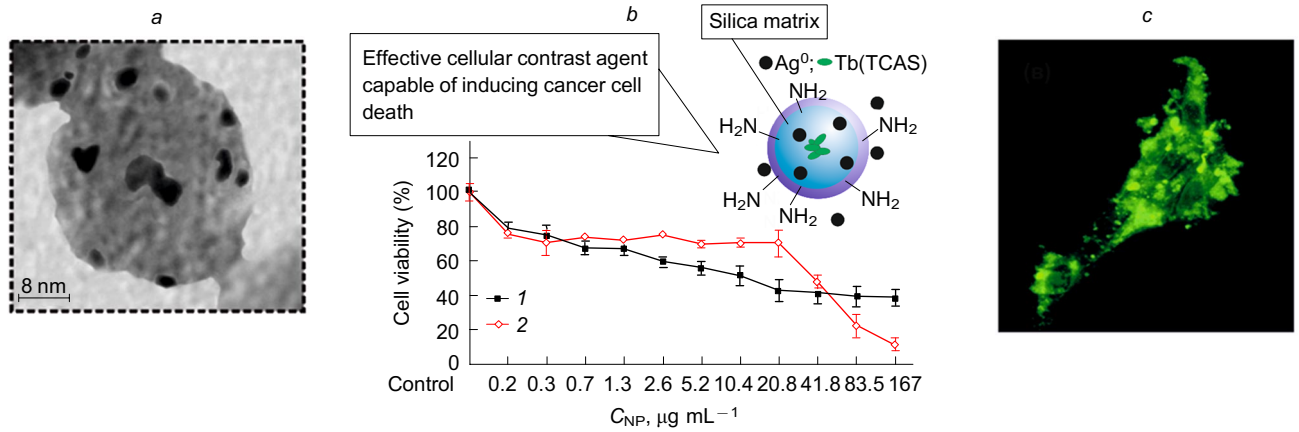


Figure 177. TEM image of composite Tb(TCAS)-doped aminomodified silica nanoparticles coated with ultrafine Ag^0 nanoparticles (*a*); dependence of the viability of cancer (Hep-4, curve *1*) and normal (DK-4, *2*) cells on the concentration of incubated composite nanoparticles (shown schematically) (*b*) and confocal laser microscopy image of cancer cells incubated with composite nanoparticles (*c*).[1420] Published with permission from Elsevier.

There are many published examples of modification of a silica surface with various target ligands or functional groups that facilitate the penetration of particles through the cell membrane.[1364, 1421, 1425 – 1430] This procedure can also be used to improve the colloidal stability of silica NPs in biological systems and reduce toxicity.[1422, 1434] The introduction of amino groups on a silica surface is the simplest and most effective way to change the surface charge of silica NPs.[1439 – 1441, 1443] The protonation of NH_2 groups at physiological pH leads to silica surface recharge, thus facilitating the cellular uptake of amino-modified NPs.[1439 – 1441, 1443]

It is worth noting that the aggregation of amino-modified silica NPs does not significantly suppress their penetration into the cells.[1439 – 1441, 1443] Moreover, it was shown [1381] that the presence of NH_2 groups on the silica surface favours their uptake by motor neurons, providing a greater penetration rate, in contrast to similar smaller unmodified silica NPs (Fig. 178).

Location of double magnetic-luminescent aminomodified silica NPs in the cytoplasm of motor neurons and their movement under the action of a constant magnetic field lead to increasing neuronal activity of motor neurons due to the increase in calcium flux through mechanosensitive N-type calcium channels (see Fig. 178).[1381]

Thus, the variety of ways to create multifunctional NPs opens up wide new opportunities for obtaining various nanomaterials for theranostics. The number of publications in this area has increased significantly over the past decade. A silica matrix is a versatile substrate that may povide particles of different morphologies with specific sizes, shapes and desired properties. The introduction of dopants into the silica matrix reduces the toxicity of the dopants and increases their colloidal stability. Non-covalent binding of dopants to the silica matrix is more preferable, since it allows a significant increase in the number of introduced dopants, while increasing their kinetic and photo stability with retention (or improvement) of the photophysical and/or relaxation characteristics due to inclusion into the nanoscale platform. In this case, the surface of the silica matrix remains free, which facilitates its modification with targeting molecules necessary for a targeted action.

4.4. Calixarenes and pillararenes containing amino acid moieties: from supramolecular self-assembly to biomimetics

Oligo- and polyamino acids are of interest from the point of view of their application not only in molecular biology and in the design of targeted delivery systems, but also in technologies that are in demand for the development of organic nanomaterials.[93, 1444] Combination of peptide and amino acid moieties on various synthetic platforms (ranging from aromatic compounds to inorganic nanoparticles) are used in the development of biomimetic systems.[1444] In the last decade, interesting results have been obtained in the study of the properties of amino acid and peptide derivatives of the most accessible and popular macrocyclic platforms, namely, calix[*n*]arenes (including thiacalix[4]arenes, resorcin[4]arenes) and pillar[*n*]arenes (Fig. 179).

The use of lateral macrocyclic structures as peptidomimetics is relevant due to their optical activity and a wide variety of functional groups to which amino acid residues can be attached. It has been shown that these macrocycles are able to bind, with high selectivity, a wide range of substrates, such as metal cations, anions, small optically active organic molecules, proteins, nucleic acids.[93, 1444] The unique properties of supramolecular systems based on amino acid and peptide derivatives of macrocycles open up prospects for solving various research tasks in the molecular recognition chemistry and in the creation of biomimetic structures.

4.4.1. Amino acid derivatives of calix[*n*]arenes and their applications

Currently, calix[*n*]arenes are among the most studied classes of cage host molecules [451] and belong to metacyclophanes: their aromatic moieties are linked together by bridging methylene groups located in *meta*-positions relative to each other. Efficient and selective receptors for a variety of ions and molecules have been designed on the basis of calix[*n*]arenes. The relatively low toxicity of these macro-

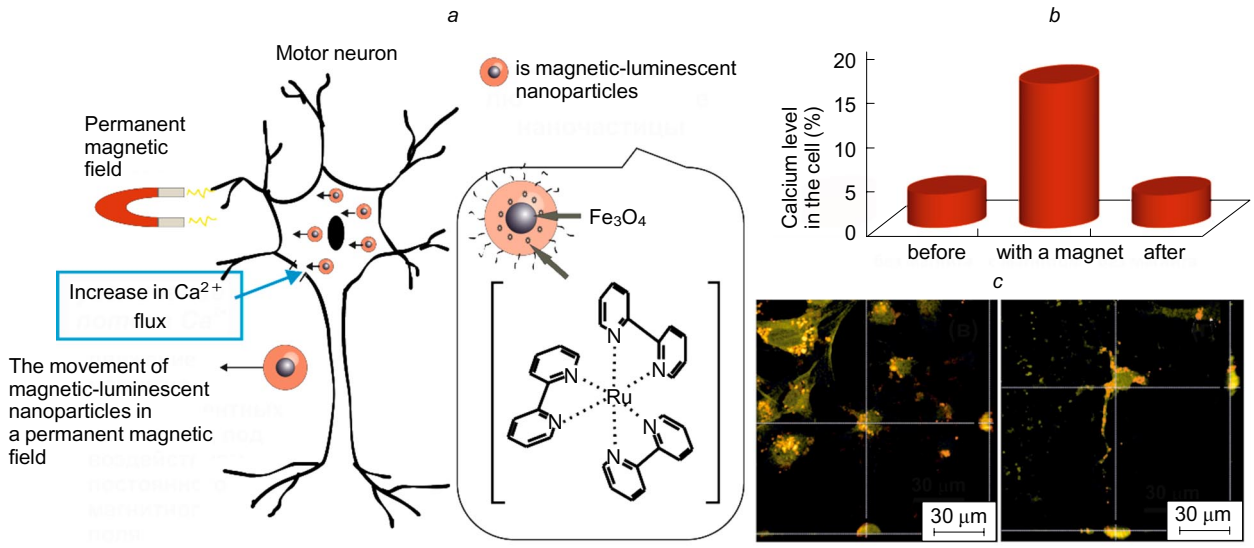


Figure 178. Schematic view of bimodal magnetic-luminescent silica nanoparticles based on Fe_3O_4 and $Ru(bipy)_3^{2+}$ used to increase the level of Ca^{2+} in motor neurons (*a*); average Ca^{2+} level in motor neurons before, during and after the application of the magnetic field (*b*); orthogonal projections (*xy*, *xz* and *yz*) of the cells after 24 h of incubation with magnetic luminescent nanoparticles, obtained by confocal laser microscopy (*c*). The figure was created by the authors using data of Ref. 1381.

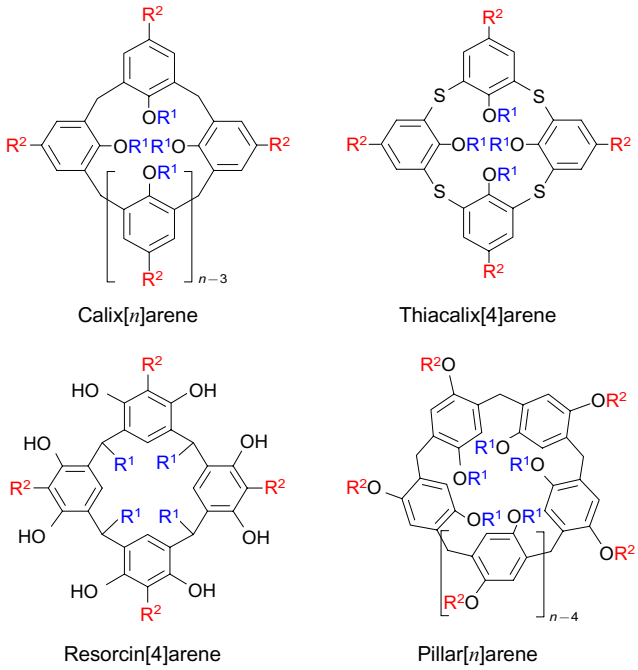
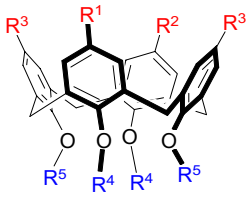


Figure 179. Structures of synthetic macrocyclic platforms designed for amino acid modification.

cycles suggests that they are suitable for biomedical applications, especially in the study of the molecular basis for the regulation of biological processes and in the development of new therapeutic agents.[93] The introduction of amino acid moieties into calix[*n*]arene molecules leads to macrocyclic structures capable of recognizing cations, anions, amino acids, carbohydrates, proteins and nucleic acids.[1444]

Initially, the attention of researchers was focused on the recognition of low-molecular-weight guests such as cations, anions, amino acids. It has been shown that the presence of amide groups in amino acid derivatives of calix[*n*]arenes promotes their effective and selective interaction with metal cations.[1444] Moreover, the introduction of a tryptophan residue into calix[4]arene molecule allows for studying of the complexing properties of the obtained compounds by fluorescence spectroscopy.[1445, 1446] Calix[4]arene **443** with two tryptophan residues at the lower rim is an effective receptor for Li^+, Na^+, K^+, Rb^+, Cs^+, Eu^{3+} and NH_4^+, H_3O^+ cations.[1445] Calix[4]arene **444**, modified with four tryptophan moieties, is capable of forming the [Na – **444** – F] ternary complex.[1446] In this case, the sodium cation is coordinated at the oxygen atoms of the oxymethylene and amide groups, while the fluoride anion interacts with the NH group of the indole moiety. The structures of other currently known amino acid derivatives of calix[*n*]arenes **445** – **484** are given in Table 10.

Structures 443 – 484



443 – 484

Research teams led by Professors Ungaro and Casnati[1447] have extensively investigated approaches to the preparation of calix[4]arene derivatives containing residues of amino acids (glycine, alanine, isoleucine, arginine, lysine) and peptides at the upper and/or lower rim and demonstrated their use as selective receptors and targeted delivery systems.

For instance, it was shown[1447] that calix[4]arene **445** tetrasubstituted with alanine moieties forms inclusion complexes with α-amino acids (tryptophan, tyrosine, phenylalanine, leucine, valine, alanine, glycine) and ammonium salts (tetramethylammonium, trimethylphenylammonium, benzyltrimethylammonium chlorides). Compound **445** was found to interact most efficiently with the guest molecules containing aromatic moieties, which is attributable to the formation of host – guest complexes due to the inclusion of aromatic moieties into the cavity of the macrocycle.

A number of *p-tert*-butylcalix[4]arene derivatives substituted at the lower rim **446** – **451** containing simultaneously urea moieties and glycine, L-alanine and L-isoleucine residues were obtained.[1447] Using NMR spectroscopy and electrospray ionization mass spectrometry (ESIMS), it was shown that the ability of such compounds to bind the anions of *N*-acetyl-D,L-alanine and *N*-acetyl-D,L-phenylalanine decreases with an increase in the size of the amino acid side chain. In this case, compound **450** has the ability to effectively bind the *N*-acetyl-D-phenylalaninate anion with high enantioselectivity (the ratio of binding constants $K^D/K^L = 4.14$). The authors attributed this enantiomeric discrimination to a special type of three-point substrate binding.

Enantioselective sensors for the recognition of chiral carboxylic acids and amino alcohols have been developed on the basis of tryptophan derivatives calix[4]arenes 1,3-disubstituted at the lower rim (**452** – **454**).[1448] Receptor **452** exhibits excellent enantioselective fluorescence recognition of the N-Boc-protected alanine anion, and compound **453** exhibits good enantioselective ability in recognizing the enantiomers of mandelic acid anion (2-hydroxy-2-phenylacetate).[1461]

Under the guidance of Prof. Yilmaz,[1450 – 1453] a series of calix[4]arenes **457** – **463** functionalized with proline residues were synthesized. These compounds can be used as organocatalysts for enantioselective aldol condensation. It was also shown that their low-molecular-weight non-macrocyclic analogue containing one proline moiety is catalytically inactive. The authors explained the high enantioselectivity (up to 95% *ee*) of substituted calix[4]arenes by the presence of a hydrophobic macrocyclic cavity.

Functionalization of the upper rim of calix[4]arene with one or two proline moieties gave rise to organocatalysts **464** – **469**, which were used for enantioselective aldol reactions involving cyclic ketones and aromatic aldehydes in the presence of water.[1454] It should be noted that these compounds were superior to their 1,3-di- and tetrasubstituted analogues in the enantioselectivity (up to 99% *ee*) and diastereoselectivity (the ratio of diastereomers reached 99 : 1) of the above reactions.

The use of amino acid derivatives of calix[*n*]arenes as receptors is not limited to the recognition of only low-molecular-weight substrates. The literature contains examples[1455 – 1460, 1462, 1463] of chiral recognition by such macrocycles of carbohydrates, heparin, proteins and nucleic acids, which may be in demand for the design of sensors for biomacromolecules and systems for their targeted delivery.

Table 10. Amino acid derivatives of calix[*n*]arenes.

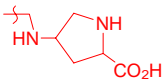
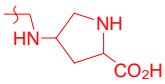
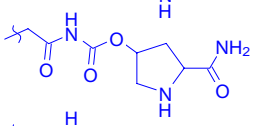
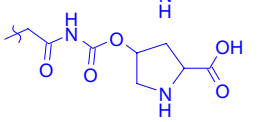
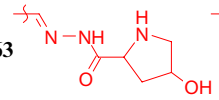
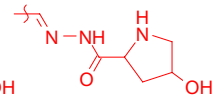
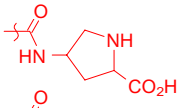
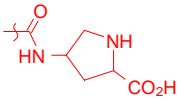
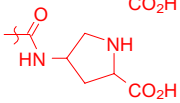
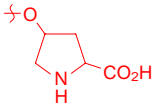
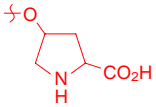
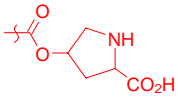
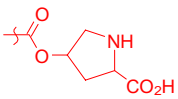
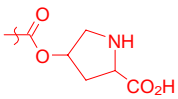
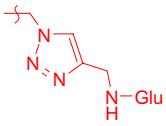
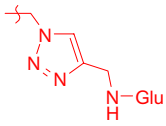
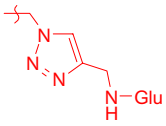
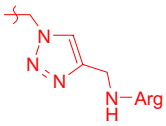
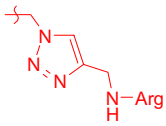
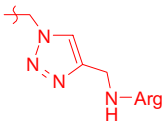
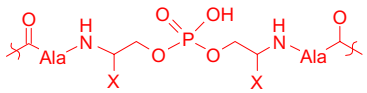
Compound	R^1	R^2	R^3	R^4	R^5	Yeild (%)	Ref.
443	Bu^t	Bu^t	Bu^t	Me	$CH_2C(O)$-Trp-OMe	55	1446
444	Bu^t	Bu^t	Bu^t	$CH_2C(O)$-Trp-OMe	$CH_2C(O)$-Trp-OMe	64	1446
445	$CH_2C(O)$-Ala-OH	$CH_2C(O)$-Ala-OH	$CH_2C(O)$-Ala-OH	Pr^n	Pr^n	99	1447
446	Bu^t	Bu^t	Bu^t	H	$(CH_2)_3NHC(O)$-Gly-OMe	70	1447
447	Bu^t	Bu^t	Bu^t	H	$(CH_2)_3NHC(O)$-Ala-OMe	88	1447
448	Bu^t	Bu^t	Bu^t	H	$(CH_2)_3NHC(O)$-Ile-OMe	90	1447
449	Bu^t	Bu^t	Bu^t	Pr^n	$(CH_2)_3NHC(O)$-Gly-OMe	88	1447
450	Bu^t	Bu^t	Bu^t	Pr^n	$(CH_2)_3NHC(O)$-Ala-OMe	83	1447
451	Bu^t	Bu^t	Bu^t	Pr^n	$(CH_2)_3NHC(O)$-Ile-OMe	89	1447
452	Bu^t	Bu^t	Bu^t	H	$CH_2C(O)$-Trp-OMe	38	1448
453	Bu^t	Bu^t	Bu^t	H	$CH_2C(O)NHNH$-Trp-Boc	23	1448
454	Bu^t	Bu^t	Bu^t	H	$CH_2C(O)NH(CH_2)_2NH$-Trp-Boc	28	1448
455	Bu^t	Bu^t	Bu^t	$(CH_2)_4NH$-Ala-Ts	H	58	1449
456	Bu^t	Bu^t	Bu^t	$(CH_2)_4NH$-Val-Ts	H	60	1449
457	Bu^t	Bu^t	Bu^t	H	$(CH_2)_3NH$-Pro	70	1450
458			Bu^t	H	H	99	1451
459	Bu^t	Bu^t	Bu^t	H	$CH_2C(O)NH(CH_2)_2NH$-Pro	71	1450
460	Bu^t	Bu^t	Bu^t	H		83	1452
461	Bu^t	Bu^t	Bu^t	H		44	1452
462	Bu^t	Bu^t	Bu^t	H		82	1452
463			Bu^t	H	CH_2CO_2Me	80	1453
464	H		H	Pr^n	Pr^n	90	1454
465			H	Pr^n	Pr^n	71	1454
466	H		H	Pr^n	Pr^n	81	1454
467	OH		H	Pr^n	Pr^n	64	1454
468	H		H	Pr^n	Pr^n	68	1454
469			H	Pr^n	Pr^n	65	1454

Table 10 (continued).

Compound	R^1	R^2	R^3	R^4	R^5	Yeild (%)	Ref.
470	See [a] (X = Bn)	See [a] (X = Bn)	H	CH_2CO_2Et	CH_2CO_2Et	73	1447
471	See [a] (X = CH_2Ind)	See [a] (X = CH_2Ind)	H	CH_2CO_2Et	CH_2CO_2Et	35	1447
472 [b]	CH_2NH-Lys	CH_2NH-Lys	CH_2NH-Lys	Pr^n	Pr^n	80	1455
473	$CH_2C(O)$-Ala-OMe	$CH_2C(O)$-Ala-OMe	H	Pr^n	Pr^n	76	451
474	$CH_2C(O)$-Ala-NHC(O)CH_2OPh	$CH_2C(O)$-Ala-NHC(O)CH_2OPh	H	Pr^n	Pr^n	67	451
475	CH_2-Pro-OH	CH_2-Pro-OH	CH_2-Pro-OH	H	H	77	1456
476				Pr^n	Pr^n	77	1457
477	NH-Lys	NH-Lys	NH-Lys	n-C_6H_{13}	n-C_6H_{13}	75	1458
478	NH-Arg	NH-Arg	NH-Arg	n-C_6H_{13}	n-C_6H_{13}	99	1458
479	H	H	H	$(CH_2)_3$NH-Arg	$(CH_2)_3$NH-Arg	65	1458
480				n-C_6H_{13}	n-C_6H_{13}	67	1459
481	Bu^t	Bu^t	Bu^t	$CH_2C(O)$-Pro-OH	$CH_2C(O)$-Pro-OH	85	1460
482	H	H	H	$CH_2C(O)$-Pro-OH	$CH_2C(O)$-Pro-OH	80	1460
483	Bu^t	Bu^t	Bu^t	H	$CH_2C(O)$-Pro-OH	85	1460
484	H	H	H	H	$CH_2C(O)$-Pro-OH	80	1460

[a] R^1-R^2 =  ; [b] n = 8; in other cases n = 4; Ind is 3-indolyl.

By introducing a cyclic moiety with an alanine residue into the upper rim of the calix[4]arene, the macrobicyclic receptors **470** and **471** were obtained.[1447] Compound **470** is an effective and selective receptor for simple carbohydrate derivatives, which was confirmed by ^{1}H NMR spectroscopy. The authors attributed this selectivity to the synergistic effect of the introduction of the phosphate group and the amino acid residues.

It was shown that positively charged calix[8]arene **472** with lysine residues can interact with heparin and neutralize it both in physiological saline and in blood.[1462] The authors compared the recognition of heparin molecules by derivative **472** with the action of two other heparin antagonists, protamine and polylysine. It was found that the arrangement of several functional groups on the flexible macrocyclic core of calix[8]arene, compared to the conformationally rigid protamine and low-ordered polylysine, allows for mutual adaptability between the polycationic calixarene and heparin, which significantly improved the recognition characteristics. Subsequently, a new polymeric material for the fabrication of filters or membranes that can remove heparin from the blood was developed on the basis of macrocycle **472**. Calix[8]arene **472** can also recognize the surface of the trypase (serine protease) enzyme.[1455] Inhibitors of this enzyme have been proposed to be used as therapeutic agents in the treatment of some diseases.

To create new systems for targeted drug delivery, it is initially necessay to establish the possibility of supramolecular self-assembly of the macrocyclic compounds. Peptide moieties promote self-assembly due to the tendency to form multiple intermolecular hydrogen bonds. Calix[4]arenes **473** and **474**, 1,3-disubstituted at the upper rim with alanine moieties, were synthesized and found to form self-organized nanotubes in the solid state due to intermolecular hydrogen bonds between the peptide groups of substituents of neighbouring macrocycles.[451]

Calix[4]arene **475**, functionalized with proline residues along the upper rim, is capable of forming hydrogels.[1456] A study of the macrocycle structure in solution and in the solid state showed that the formation of a hydrogel occurs when a proline moiety is embedded in the adjacent cavity of the macrocycle, resulting in the formation of extended helical structures.

Enantiomers of compound **475** containing L- and D-proline residues were investigated as promising agents against human papillomavirus (HPV).[1463] For this purpose, the interaction of compound **475** with the capsid protein L1 of HPV 16 was studied using ^{1}H NMR spectroscopy, MALDI‡ mass spectrometry and quantum chemical calculations. It was found that calix[4]arene **475**, being bound to the protein, prevents the formation of its pentamer. The authors believe that this opens up the possibility of developing enantioselective and inexpensive inhibitors of L1 capsid protein pentamer formation based on compound **475** to be used as a new type of agent against HPV and other viruses.

The amphiphilic calix[4]arene derivative **476** contains propyl groups at the lower rim and glutamic acid moieties at the upper rim.[1457] The shape of micelles obtained by self-assembly of macrocycle **476** in water changes with pH variation from spherical in acid media to cylindrical in

‡ MALDI is matrix assisted laser desorption/ionization.

neutral media and again to spherical in alkaline media. The authors explained their results by the fact that in the pH range of 6 to 12, the compound is in the zwitter-ionic form, while at pH <6 and pH >12 it is positively and negatively charged, respectively.

It is known that peptides with a large number of positively charged lysine and arginine residues are capable of efficient penetration into the cell and can be used as carriers of various molecules inside the cell.[504] Calix[4]arenes **477** – **479**, tetrasubstituted at the upper or lower rim with arginine and lysine moieties, were capable of efficient delivery and transfection of DNA into various cell lines.[1458] The authors noted that compound **478** with arginine residues interacts more efficiently with DNA than compound **477** with lysine residues. This can be explained by the high affinity of guanidinium moieties for DNA phosphate residues.

The use of peptide nucleic acids (PNA, *i.e.*, DNA without carbohydrate and phosphate moieties) for gene therapy is limited by their low cellular uptake. One of the most promising approaches to overcoming this drawback is the covalent modification of the PNA structure with polyarginine moieties; in this case, each PNA molecule must be modified, which is very expensive and difficult to implement. On the basis of argininocalixarene **480**, tetrasubstituted at the upper rim, systems for the cellular delivery of PNA were devised, the efficiency of which was comparable to that of PNA covalently modified with eight arginine residues.[1459] These results are of interest for the development of new systems for targeted delivery of unmodified PNA into cells, which can simplify and accelerate their study and use in gene and antisense therapy of cancer.

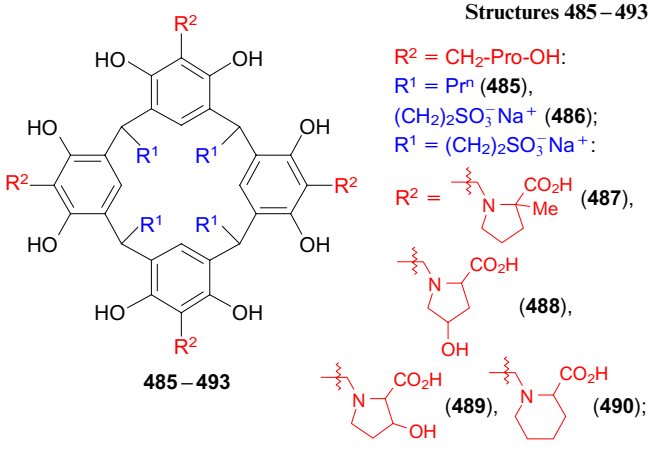
New 1,3-di(proline)- and tetra(proline)-substituted calix[4]arenes have been investigated as potential antitumour agents.[1460] The cytotoxicity of these compounds was evaluated *in vitro* on human tumour cells (HEPG2, PC-3, A-549 and DLD-1 lines) and on healthy human epithelial cells (PNT1A). Compounds **475**, **481** – **484** have cytotoxic effects on human colorectal carcinoma cells (DLD-1) with half-maximal inhibitory concentration (IC_{50}) values of 29 – 65 μmol L^{-1}. Macrocycle **481** leads to apoptotic cell death, especially in the early stage of apoptosis. The authors suggest that such macrocycles could be considered as potential drugs for the treatment of lung and colon cancer.

Resorcinarenes, 1,3-hydroxybenzene tetramers, represent a rather attractive class of macrocycles with a hydrophobic cavity capable of encapsulating small molecules. The functionalization of resorcinarenes usually consists in the modification of hydroxy groups and aromatic moieties, as well as in the variation of the structure of the aldehyde used in the synthesis of the macrocycle. To date, only resorcinarenes modified with amino acid residues along the upper rim have been synthesized, while the hydroxy groups remain unsubstituted.

The complexing properties of resorcinarenes **485** and **486**, containing proline residues in the upper rim, towards a series of ammonium and imidazolium derivatives were studied by polarometry.[1464] Due to electrostatic Coulomb and π – π interactions and desolvation effects of such reagents, 1 : 1 and 1 : 2 host – guest type complexes are formed.

Wenzel[1465] found that chiral resorcinarene derivatives containing amino acid residues (L-proline, hydroxy-L-proline, α-methyl-L-proline, L-pipecolic acid) can be used as reagents for enantiomer differentiation in NMR spectroscopy. The upper-rim tetrasubstituted resorcin[4]arene derivatives **486** – **490** are efficient chiral NMR solvating agents for water-soluble compounds with phenyl, pyridyl, bicyclic aromatic or indole moeties. These aromatic compounds form host – guest complexes with resorcin[4]arenes **486** – **490** in water. It was suggested that the complexation of substrates with the macrocycle is facilitated by the hydrophobic effect, with association constants with more hydrophobic bicyclic substrates being greater than those with similar phenyl-containing compounds.

Structures 485 – 493



Resorcinarenes **491** – **493** containing glycine, alanine and valine residues have been synthesized.[1466 – 1468] The resorcin[4]arene **491** – sodium dodecyl sulfate (SDS) supramolecular system can encapsulate the hydrophobic drug 2,2′-bibenzimidazole depending on the pH. In acidic medium, protonation of the nitrogen atom of the macrocycle promotes a more efficient interaction between resorcin[4]arene molecules **491** and SDS, which reduces the solubilizing properties. In alkaline medium, the upper rim of resorcin[4]arene **491** acquires a negative charge due to dissociation of carboxyl groups. The electrostatic repulsion of these groups from each other and from the SDS molecules gives rise to a space for 2,2′-bibenzimidazole in the hydrophobic part of the SDS micelles.

Thiacalix[4]arenes are heterocyclic analogues of the classical calix[4]arenes in which the methylene bridges are replaced by sulfur atoms.[1469] Because of this, the thiacalix[4]arene platform is more mobile and more prone to form different geometric isomers (*cone*, *partial cone* and *1,3-alternate* conformations), unlike calix[4]arenes, the modification of which usually results in the *cone* conformation. Due to high flexibility of molecular structure and ability to bind metals (presence of S bridges) thiacalixarenes are more frequently used to developm supramolecular structures than conventional calixarenes.

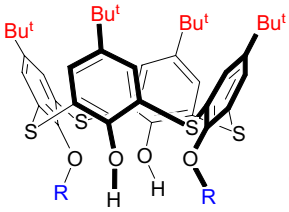
To compare the properties of the amino acid derivatives of calix[4]arene and its thia analogue, derivatives **455, 456** and **494, 495** containing two alanine and valine molecules were synthesized.[1449] The products were able to recognize *N*-tosylate derivatives of L- and D-amino acids in chloroform. The thiacalix[4]arene derivatives were found to recognize the enantiomers of amino acids more efficiently than their carbon analogues. In particular, thiacalix[4]arene **494** showed the highest efficiency in recognizing tosylated leucine, while receptor **495** was most efficient in recognizing tosylated phenylalanine. The authors attributed this differ-

ence to different patterns of hydrogen bonding between the guest and host molecules.

The synthesis of 1,3-di(lysine)- (**496**) and tetra(lysine)-substituted (**497**) thiacalix[4]arenes has been described.[1470] The authors noted that the tetrasubstituted compound **497** is in the *1,3-alternate* conformation. On the basis of these thia analogues, dendrimeric structures were derived, which can be further used as molecular receptors or targeted drug delivery systems.

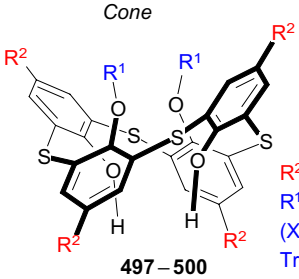
The difficulty of using tetrasubstituted (thia)calix[4]arene derivatives is their low solubility in water. One of the solutions to this problem is to introduce an additional polar group, for example, an ammonium group, into the molecule. A number of thiacalix[4]arene-based ammonium salts **498** – **500** containing amino acid residues (glycine, alanine, tryptophan) in the *cone* and *1,3-alternate* conformations were synthesized by the research team of Prof. Stoikov.[1471 – 1473] It was shown that thiacalix[4]arene derivative **498** with glycine residues interacts with salmon milt DNA to form nanoparticles of 99 – 192 nm size; this was confirmed by means of TEM and dynamic light scattering techniques. Macrocyclic ammonium salt **500**, containing tryptophan residues, is capable of forming chiral fluorescent nanoparticles in water with a hydrodynamic diameter of 86 – 134 nm.[489] It was shown by NMR spectroscopy that the mutual repulsion of charged ammonium groups makes the peptide bond with the tryptophan residue sterically accessible to enzymes.[1474] Subsequently, using kinetic methods, it was shown that compound **500** in the *cone* conformation is able to competitively inhibit the enzyme chymotrypsin.[1475] The mechanism of inhibitory action was established to consist in the binding of tryptophan residues of the macrocycle to the active site of the enzyme, thus blocking the active site.

Structures 494 – 500



494 – 496
Cone

R = $(CH_2)_4$NH-Ala-Ts (**494**),
$(CH_2)_4$NH-Val-Ts (**495**),
$CH_2C_6H_4C(O)NH(CH_2)_2$NHLys-4 (**496**)



497 – 500
1,3-Alternate

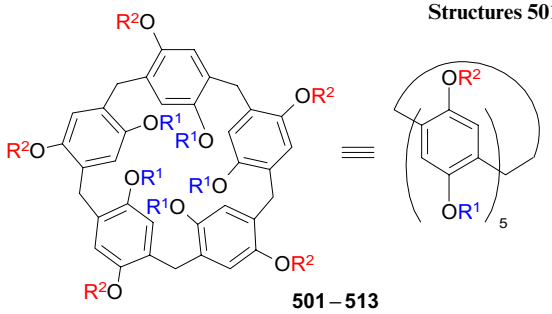
R^2 = Bu^t,
R^1 = $CH_2C(O)NH(CH_2)_3NMe_2^+CH_2C(O)X$
(X = Gly-OEt (**497**), Ala-OEt (**498**),
Trp-OEt (**499**));
R^1 = $CH_2C_6H_4C(O)NH(CH_2)_2$NHLys-4,
R^2 = H (**500**)

Thus, using the example of calix[*n*]arene derivatives, it was shown that the introduction of amino acid residues is a promising trend of the design of supramolecular biomimetic systems. These systems have a wide range of applications ranging from binding of cations, anions and amino acids to the recognition of proteins, carbohydrates and nucleic acids. They can also be used to create selective catalysts for organic reactions, potential systems for targeted drug delivery and drugs for cancer therapy.

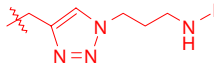
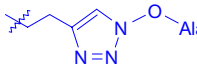
4.4.2. Amino acid derivatives of pillar[*n*]arenes and their applications

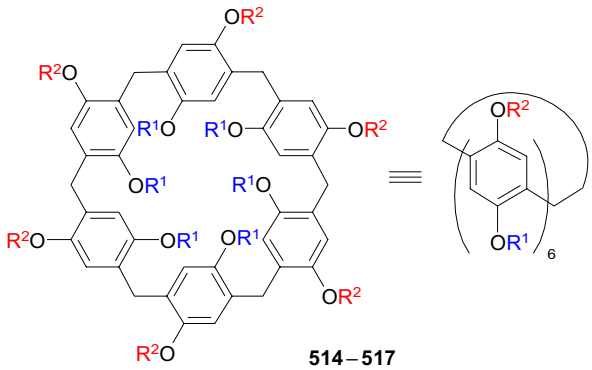
Pillar[*n*]arenes, representing *para*-cyclophanes of a new class (see Fig. 179), were obtained for the first time In 2008 and described in detail by Ogoshi *et al.*[1476] Currently, the pillar[*n*]arene platform is one of the most promising due to their easy synthesis, unique shape of the macrocycle, interesting host – guest complexing properties and peculiar supramolecular assembly characteristics.[1477] Amino acid derivatives of pillar[5]- and pillar[6]arenes are represented by structures **501** – **513** and **514** – **517**, respectively.

Structures 501 – 517



501 – 513

R^1 = R^2 = $CH_2C(O)$-Gly-OH (**501**), $CH_2C(O)$-Gly-$NHNH_2$ (**502**);
R^1 = R^2 = $CH_2C(O)$-Gly-Gly-OH (**503**), $CH_2C(O)$-Gly-Gly (**504**);
R^1 = n-C_5H_{11}, R^2 =  (**505**);
R^1 = R^2 = $(CH_2)_3NHC(O)$-Trp-OH (**506**),  (**507**),
$(CH_2)_3SCH_2CH(CO_2H)NHAc$ (**508**), $CH_2C(O)X$
(X = Phe-Phe-Phe-OH (**509**), Phe-Phe-Phe-OEt (**510**),
Phe-Phe-Arg-OEt (**511**), Phe-Arg-Phe-OEt (**512**),
Arg-Phe-Phe-OEt (**513**))



514 – 517

R^1 = R^2 = $CH_2C(O)X$ (X = Phe-OH (**514**), Phe-Phe-OH (**515**),
Phe-Phe-Phe-OH (**516**), $(CH_2)_2$NH-Ala (**517**))

The Prof. Stoikov's reseach team synthesized pillar[5]-arene derivatives **501** – **504** with glycine residues.[1478 – 1481] Macrocycles **501** and **503** were shown to efficiently interact with the Bismarck brown Y dye and with alkali metal cations (Li^+, Na^+, K^+, Cs^+). Pillar[5]arenes **502** and **504**, containing hydrazide groups along with glycine residues, actively encapsulate the anticancer drugs 5-fluorouracil and floxuridine (5-fluoro-2′-deoxyuridine). These drugs are used to treat colorectal, liver and gastric cancer, but their

high toxicity causes numerous side effects. The addition of pillar[5]arenes **502** and **504** results in reduced toxicity.

Like in the case of calyx[*n*]arene derivatives, self-assembled supramolecular structures based on pillar[*n*]arenes were fabricated; they can be used as promising systems for targeted drug delivery. Amphiphilic macrocycle **505** containing both positively charged lysine moieties and pentyl groups was shown to self-assemble in water into a bimolecular micelle, in which alkyl tails face each other and the hydrophobic parts are completely covered by long hydrophilic groups.[1482]

Water-soluble decasubstituted pillar[5]arene **506** with tryptophan moieties forms a host–guest complex capable of self-assembling into vesicles.[1483] These vesicles efficiently encapsulate the anticancer drug doxorubicin (DOX). The DOX-loaded vesicles demonstrate sensitivity to pH: in acidic medium, rapid release of the drug occurs, and the entry of the drug into the body can be conbtolled in this way. The supramolecular system showed higher cytotoxicity against cancer cells compared to free DOX.

It is worth noting that, unlike metacyclophanes, pillar[*n*]arene molecules have inherent planar chirality, which, in combination with chiral amino acid moieties, gives rise to unique properties. Modification of the gold electrode surface by pillar[5]arene **507** containing alanine residues produced an electrochemical sensor suitable for quantitative determination of calf thymus DNA with a detection limit of 0.159 ± 0.001 μg mL^{-1}.[1484] The authors suggest that these results can be used to design chiral biodevices that will combine the advantages of chiral surfaces and functional materials.

Due to the unique hollow-column-like shape of pillar[5]-arene molecules, they represent the molecular analogues of carbon nanotubes.[1485] For this reason, pillar[5]arenes can be embedded in membranes and used to create artificial molecular and ion channels. Due to the fact that in the molecules of pillar[5]arene amino acid derivatives, the amide and carbonyl groups form multiple intramolecular hydrogen bonds, the use of these derivatives to create channels is quite promising.

Hou and co-wokers [1486] obtained peptide derivatives of pillar[*n*]arenes ($n = 5$, 6) **509**–**512** containing D- and/or L-phenylalanine residues. Using ^{1}H NMR and IR spectroscopy, the authors found that molecules of these compounds form a tubular architecture in solution and in the lipid bilayer membrane. Kinetic measurements using fluorescent labelling with lipid vesicles showed that the obtained molecules can efficiently transport amino acids (glycine, alanine, serine, threonine, valine, leucine, phenylalanine) across lipid membranes.

In the subsequent work,[1487] this research team synthesized pillar[5]arene derivatives **509**, **511**–**513**, containing tripeptide moieties with phenylalanine and arginine residues, with the goal to fabricate a transmembrane channel. It was shown by fluorescence spectroscopy and patch clamp experiments that by varying the potential, it is possible to force the macrocycle molecules to be inserted into and released from the lipid bilayer and thus to switch on and off the transport of K^+ ions. Macrocycle **512** was also found to exhibit antimicrobial activity against *Bacillus subtilis*. The half-maximal inhibitory concentration was 10 mmol L^{-1}, which is close to this parameter for the natural potential-controlled channel-forming peptide alamethicin ($IC_{50} = 2$ mmol L^{-1}).

Macrocycle **509** was used to develop highly permeable artificial water channels.[1488] It was shown that incorporation of pillar[5]arene molecules **509** into a polymeric membrane results in a system with a water conductivity of $3.5 \pm 1.0 \times 10^8$ mol. $H_2O\,s^{-1}$, which is close to the values for natural water channel proteins, aquaporins [$(3.4–40.3) \times 10^8$ mol. $H_2O\,s^{-1}$] and carbon nanotubes (9.0×10^8 mol. $H_2O\,s^{-1}$). In addition, channels based on pillararene **509** can self-assemble into two-dimensional arrays in lipid bilayers. The authors claim that the obtained water channels have an advantage over the known natural and synthetic channels due to their relatively easy synthesis, chemical stability and tendency to form arrays.

The next step in improving the efficiency of water channels was to study the effect of chirality of the pillar[5]-arene platform.[1489] It was found that channels based on *pR*-pillar[5]arene (*pR*)-**509** compete with aquaporins in terms of water permeability and are far superior to those based on diastereomers (*pS*)-**509**. Using the molecular dynamics computations, the authors showed that the reduced water permeability in the case of *pS*-diastereomers is explained by the arrangement of phenyl moieties of phenylalanine perpendicular to the membrane, impeding water movement.

Professor Li's research team [1490] investigated the possibility of developing new molecular and ionic channels by modifying the existing synthetic nanochannels with pillar[*n*]arene derivatives. It was found that dodecasubstituted pillar[6]arene **517** with L-alanine residues forms a host–guest complex with a guest fixed on the surface of a polyethylene terephthalate membrane. By controlling the transmembrane ionic current, it was shown that a channel made of a membrane modified in this way can be switched off by D-glucose and swithed on by L-glucose. The authors showed that the host–guest complex selectively interacts with D-glucose (10 times more efficiently than with L-glucose) due to the formation of multiple hydrogen bonds. The adsorption of D-glucose molecules on the channel surface leads to a decrease in the transmembrane ionic current and its switching off.

In a later publication of this research team,[1491] a molecular channel capable of protein transport was obtained. To fabricate this channel, the authors performed self-assembly of pillar[5]arene **508** molecules with acetylcysteine moieties on the surface of a synthetic channel modified with hexane-1,6-diamine. The resulting molecular channel had good selectivity for the histone protein. The authors showed that this protein channel could be controlled by varying the pH of the solution. In acid medium, the free carboxyl groups of macrocycle **508** are protonated; this results in its precipitation and destruction of the host–guest complex. Thus, the protein channel is switched off. Repeated addition of this macrocycle causes the channel to switch on.

Thus, selective receptors for metal cations and biologically important dyes have been developed on the basis of amino acid derivatives of pillar[*n*]arenes. A special field of application of polypeptide derivatives of pillar[5]arenes is the design of supramolecular biomimetic systems, molecular and ion channels, which can be used to fabricate cell membrane models and new porous materials.

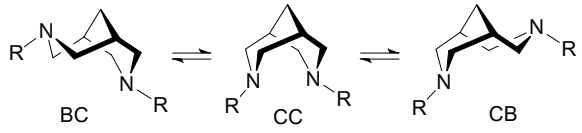
In conclusion of this Section, we would like to note that development of supramolecular systems using amino acid and peptide derivatives of macrocycles is a promising area, which would give rise to new systems for the targeted

delivery of drugs and functional materials. It is particularly worth noting that the design and study of the properties of biomimetics as models of biological systems of living organisms allows a better understanding of the molecular mechanisms of biological processes.

4.5. Supramolecular recognition in the chemistry of 3,7-diazabicyclo[3.3.1]nonanes: design of biologically active molecules, functional materials and catalysts

This Section addresses features of the structure and applications of 3,7-diazabicyclo[3.3.1]nonanes — saturated bicyclic carbon backbones containing two nitrogen atoms (Scheme 69).

Scheme 69



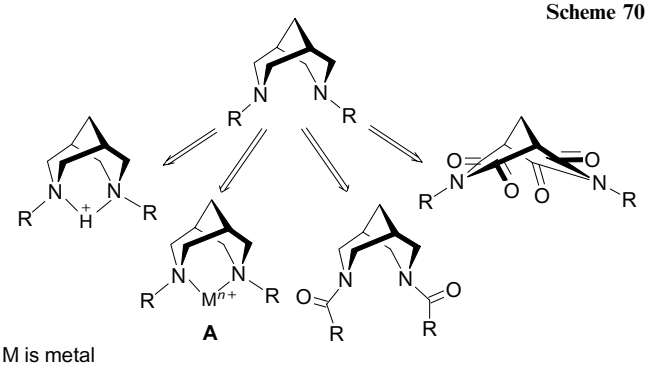
The introduction of two nitrogen atoms into any carbocyclic structure, on the one hand, reduces the possibility for its functionalization compared to the carbon analogue (three instead of four substituents), but on the other hand, the presence of lone pairs dictates a set of conformations different from carbocycles, determined by stereoelectronic interactions, and provides a donation of electron density to Lewis acid sites such as protons or metal ions. Moreover, the high polarity of the nitrogen – carbon bond allows for cost-efficient unique synthetic procedures, facilitating the synthesis of target azaalkanes from readily available precursors. The presence of two nitrogen atoms gives way to the chelation of such compounds in specific conformations, which contributes to the production of coordination supramolecular assemblies with higher thermodynamic stability.

3,7-Diazabicyclo[3.3.1]nonane (or bispidine), abundant in living nature, is a functional building block (scaffold). This compound is being intensively studied by specialists in the field of organic and supramolecular chemistry and catalysis.[1492] It combines the complexing properties of nitrogen atoms, preorganized into a chelating configuration in the chair – chair conformation, and the rigid geometry of the bicyclic cage. In this case, lone pairs of heteroatoms are directed towards approximately the same region of space.[1493] This results in selectivity in the complexation with metal ions and neutral molecules the size of which fits into the free space of the receptor.[1494] Broad opportunities for modification, choice of substituents in the backbone and control of the conformational equilibrium of six-membered rings allow fine tuning of bispidine for solving specific problems.

For half a century, bispidines have been a preferred object of conformational analysis.[1492] The main conformational equilibrium of this bicycle is the boat – chair (BC) — chair – chair (CC) — chair – boat (CB) equilibrium (see Scheme 69).

Control over the conformational equilibrium is a key problem in the design of bispidine derivatives for specific applied purposes such as complexation, catalysis, synthesis of biologically active compounds. In most cases, it is necessary to lock the double chair conformation, which can be accomplished in several ways, namely, by protonation, complexation with metals, acylation and conversion into tetraone derivatives (Scheme 70). Of particular note is the occurrence of a stable configuration of 2-metalla-1,3-diazaadamantane **A** upon the formation of bispidine chelates.

Scheme 70



In principle, the stability of the double chair conformation can be due to the same factors as stability of the chair conformation of piperidine derivatives. However, in the 3,7-diazabicyclic structure, additional repulsive interactions between the lone pairs of the nitrogen atoms directed towards the same region of space may occur (the 'hockey sticks' effect).[1495, 1496] Nevertheless, we have demonstrated the existence of an attractive interaction between the nitrogen atoms, which stabilizes the double chair conformation.[1497] All of the considered transitions have energies around 3 – 4 kcal mol^{-1}, which allows the researcher to control the conformation over a wide range by introducing additional substituents to the nitrogen atoms.

Another way to reach a stable double chair conformation is the protonation of one or two nitrogen atoms. For example, Cui *et al.*[1498] found that *N*,*N*′-unsubstituted bispidine reacts with dichloromethane to give a number of products, from which mono- and dihydrochloride were isolated, and studied by X-ray diffraction analysis. In these structures, mono- and diprotonated bispidines are assembled into one-dimensional supramolecular polymers by intermolecular hydrogen bonds with the participations of chloride anions.

In our study,[1499] protonated 1,5-dimethylbispidinone was shown to crystallize with an acetate counter-ion to afford supramolecular polymers, in which bispidine moieties are bridged by acetate anions. Also, the simple hydrate of the same bispidinone forms a one-dimensional supramolecular polymer with an original conformation of the N – H units in the crystal: they are directed inside the cavity and form hydrogen bonds with the oxygen atom of water. The key role of intermolecular hydrogen bonding in the formation of bispidine-containing supramolecular polymers in the crystal and gel phases has been recently established by Vatsadze and co-workers.[1500]

While characterizing the general properties of bispidines, one has to mention that some researchers classify these compounds as 'proton sponges'.[1501]

4.5.1. Coordination compounds of bispidines: general issues

The first bispidine coordination compounds were synthesized in 1957.[1502] Potentially tetradentate glycine derivative of bispidinone was first described by Stetter and Dieminger,[1503] who have prepared its complex salts with Co^{II}, Ni^{II}, and Cu^{II}. The authors measured the stability constants of these salts but reported no structural data. Only in 2006,

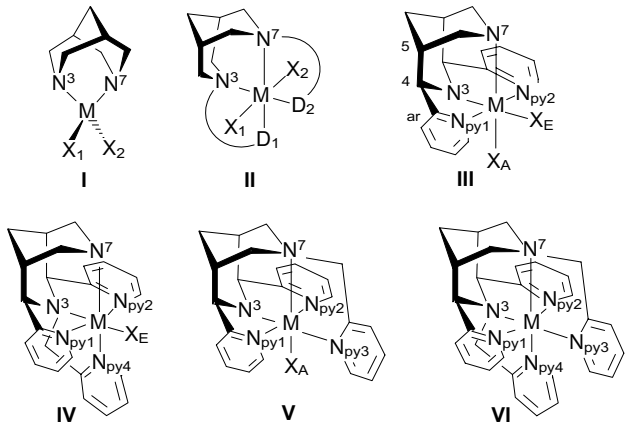


Figure 180. Structural types of bispidine complexes.[1505] M is metal; X_1, X_2 are counter-ions or co-ligands of different nature; X_E and X_A are in-plane equatorial (*trans* to N^3) and axial (*trans* to N^7) co-ligands. D_1 and D_2 are intramolecular moieties for complexation. Reproduced with permission from Wiley.

Vatsadze *et al.*[1504] synthesized and structurally characterized a series of N_2O_2 type tetradentate ligands and their Cu^{II} complexes. High geometric complementarity of the arrangement of four donor atoms of the ligand and divalent copper ion is reflected in the redox stability of the resulting chelates.

The intensive development of the coordination chemistry of bispidines began around the end of the 1990s; the studies published from that time until 2007 are summarized in a fairly voluminous and professionally written review of Comba *et al.*[1505] This Section highlights the most notable achievements on this topic over the past 14 years, with most of the information being given in Section 4.5.3 devoted to catalysis, since this is the main field of application of bispidine complexes.

According to Comba s classification, structurally characterized complexes of bispidines can be divided into 6 types (Fig. 180).

The hallmark of all known bispidine complexes with metals is a rather narrow distribution of the N···N bond lengths, averaging 2.9 Å. Such a restriction is due to the relative conformational rigidity of the bicyclic backbone supplemented by the presence of a metal atom in position 2 of the 'metalladiazaadamantane'. This property has far-reaching implications in the case when the stability and the possibility of the formation of a complex with one or another metal are considered. Indeed, bispidines display high supramolecular selectivity towards relatively small ions such as Cu^{II}, Ni^{II}, Pd^{II} and Zn^{II}. It is this fact that determines the prevalence of certain transformations with the participation of bispidine complexes as catalysts; this also places certain limitations on the possible types of such reactions, which depend primarily on the nature of the complexing metal.

In conclusion of this brief look at the general issues of bispidine complexes, it should be noted that compounds containing substituents in positions 1 and 5 with metal coordinating groups have not yet been reported. It is also important to point out that, according to the available data, bispidines were not used as ligands or components for the production of coordination polymers, metal-organic frameworks or similar supramolecular architectures.

4.5.2. Application of bispidine complexes as bioimaging materials

High stability constants, good solubility in water, and redox stability of bispidine complexes with metals, particularly with copper(II), have enabled the development of several types of compounds that can serve as components of bioimaging materials. The main use of such complexes presented in the literature is positron emission tomography (PET).

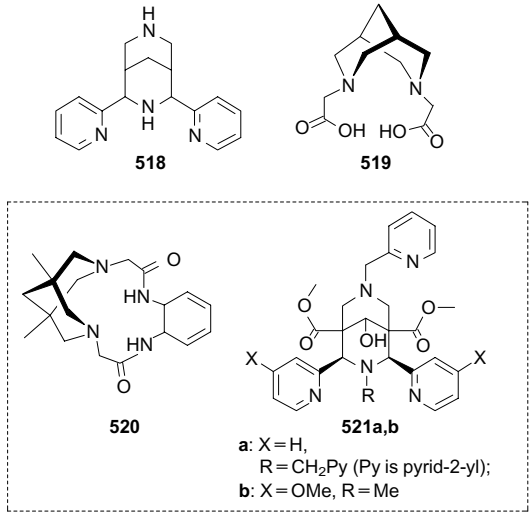
Positron emission tomography refers to non-invasive bioimaging methods that track the behaviour of various molecules in the human body.[1506 – 1509] For this purpose, a biologically active molecule is labelled with a radionuclide undergoing β-plus decay. The emitted positrons are annihilated with the electrons of the surrounding molecules giving rise to two γ quanta, which are recorded by a tomograph. The applicability of PET is largely determined by the pool of available biologically active labelled compounds, the so-called radiopharmaceuticals, which are preliminarily introduced into the human body.[1510] The radiolabels used for PET include biologically relevant short-lived (^{18}F, Ref. 1511) and ultra-short-lived (^{11}C, ^{13}N, ^{15}O) positron-emitting radionuclides.[1512, 1513] It is important to mention that in recent years, alternative positron emitters have begun to be used, including those with longer half-lives, which makes it possible to diagnose processes with slow pharmacokinetics. Among such radionuclides, ^{68}Ga and ^{64}Cu are already used, while ^{89}Zr and ^{86}Y have good prospects.[1514 – 1516]

When designing metal-containing radiopharmaceuticals, the following requirements should be addressed: the complex must be formed quickly, be soluble in water and biological fluids, stable for a sufficiently long time under these conditions, highly resistant to redox transitions into other valence states (important for copper), and exhibit low toxicity.

To be successfully used in PET, ligands are required with a large number of donor atoms, usually containing one or two macroheterocycles. It is clear that bispidine derivatives ideally suit this role. In the design of such ligands for the copper variant of PET, three approaches could be distinguished:

— introduction of additional donor groups into positions 2 and 4 of the backbone (compound **518**),[1517]

Structures 518 – 521



— introduction of donor groups into the substituents at the nitrogen atoms (compound **519**),[1518] and

— combining these two approaches (compounds **520** and **521**).[1519, 1520]

When pursuing any approach, it is necessary to envisage the possibility of attachment of 'vector' moieties for the selective delivery of a positron-emitting radionuclide to the target organ.[1521]

To conclude this subsection, mention should be made of successful attempts to use coordination compounds of lanthanides (Sm^{III}, Eu^{III}, Tb^{III}, Dy^{III}, Ho^{III}) with bispidine ligands for producing bioluminescent labels.[1522]

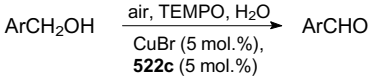
4.5.3. The use of bispidine derivatives in catalytic transformations

Combination of the ability of bispidines and their derivatives to coordinate metal atoms and the possibility of fine tuning of the electronic properties and steric hindrance of the approach of reactants during the functionalization of bispidines makes them promising ligands for metal complex catalysis. The publications focused on the catalytic properties of bispidines that appeared before 2010 are detailed in reviews.[1523, 1524] Here only new advances in this important field of chemistry are considered.

Biomimetic pentadentate $Fe^{III/IV}$ complexes with ligand **522a** have a high $Fe^{III/IV}$-redox potential and are highly efficient catalysts for the oxidation of alkenes (Scheme 71).[1525] To enhance the performance of the catalytic complex by increasing the rigidity of its backbone, Comba *et al.*[1526] introduced an additional phenyl moiety into the only conformationally flexible pyridinemethylene substituent in ligand **522a**. The use of $Fe^{III/IV}$ complex with the optimized ligand **522b** in styrene oxidation with PhIO indeed increased both the catalytic activity and (what is particularly important!) the reaction selectivity: whereas the complex with ligand **522a** provided the ratio of styrene epoxide and benzaldehyde of 3.4 : 1, in the case of ligand **522b**, this ratio exceeded 50 : 1. Ligand **522b** has an asymmetric centre and was obtained in optically pure form; however, because of the remoteness of the chiral C-atom (marked with an asterisk) from the catalytic centre, asymmetric induction was virtually absent when this ligand was used.[1526] Complex of ligand **523** with Mn^{IV}=O, prepared by the treatment of Mn^{II}-containing precursor with cerium(IV) ammonium nitrate, proved to be effective in oxidation of thioanisole to the corresponding sulfoxide using water as a source of oxygen.[1527]

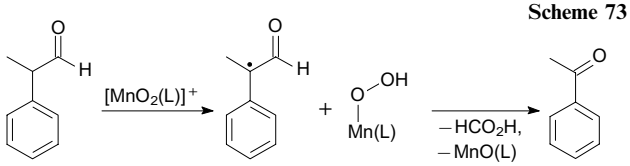
Fluorine-containing bispidinone **522c**, being a ligand of the same structural type, was successfully employed in (2,2,6,6-tetramethylpiperidine-1-yl)oxyl (TEMPO)-promoted aerobic oxidation of benzyl alcohols to give the corresponding aldehydes in an aqueous medium (Scheme 72).[1528] The presence of a fluorinated aliphatic substituent in the ligand gives it the surfactant properties and accelerates the reaction compared to those with non-fluorinated analogues devoid of long-chain aliphatic substituents. The replacement of copper atoms with iron atoms in various oxidation states proved to be ineffective. It is noteworthy that oxidation under these conditions proceeded also in the absence of ligands, though in lower yield.

Scheme 72



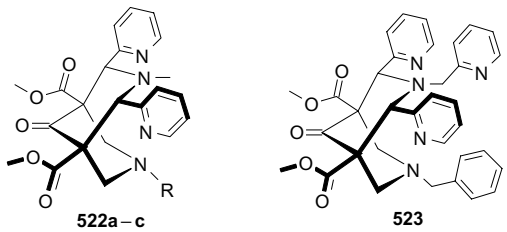
The manganese peroxo complex with ligand **523** was used to carry out the deformylation of 2-phenylpropanal to acetophenone (Scheme 73).[1529] Studies of the kinetic features of this reaction resulted in the assumption that the reaction preferably proceeds *via* the hydrogen transfer rather than *via* nucleophilic addition to the aldehyde carbon atom.

Scheme 73



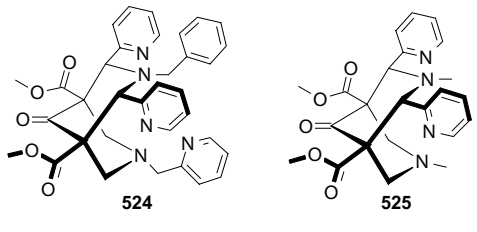
Going to ligand **524**, in which the pyridinemethylene and benzyl substituents at nitrogen atoms changed places as compared to compound **522**, led to an increase in the rate of the deformylation reaction by a factor of 5.[1530] The similar reaction mechanism involving hydrogen transfer was also proposed for copper-containing complex $[Cu^{II}$-**525**-$(OOBu^t)]^+$.[1531]

Structures 522, 523

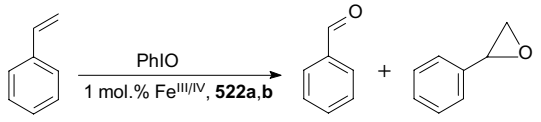


R = CH_2Py-2 (**a**), C*H(Ph)Py-2 (**b**), $(CH_2)_2C_8F_{17}$-n (**c**)

Structures 524, 525



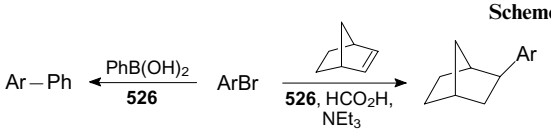
Scheme 71



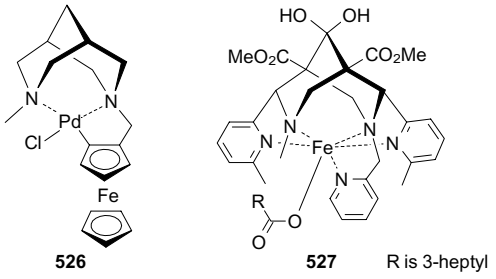
Bispidine ferrocene palladium complex **526** proved to be an effective catalyst for cross-coupling reactions including the Suzuki and Heck reactions (Scheme 74).[1532] The process provides high yields, in some instances quantitative ones. The use of complex **526** has proved to be more effective than its ferrocene bipyridine analogue.

The replacement of cobalt-based siccatives for alkyd resins, which are widely used in paints and inks, is an

Scheme 74



Structures 526, 527

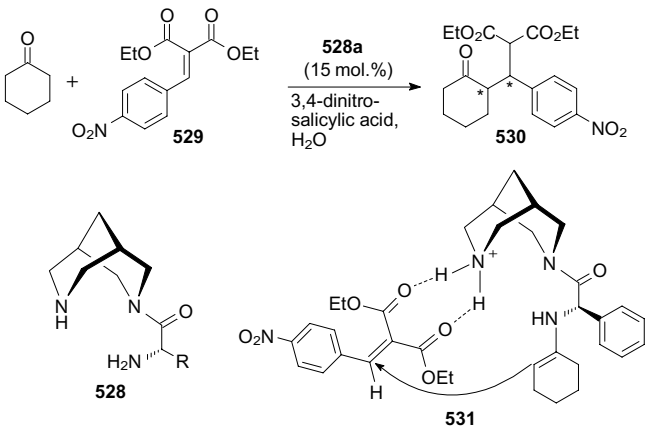


important issue concerning the possible carcinogenicity of Co complexes.[1533] Iron-based complex **527** was shown to efficiently catalyze curing of alkyd resins.[1534] It must be pointed out that parameters of the curing kinetics in the presence of compound **527** differ significantly from those of commercial cobalt-containing siccatives, which suggests further research.

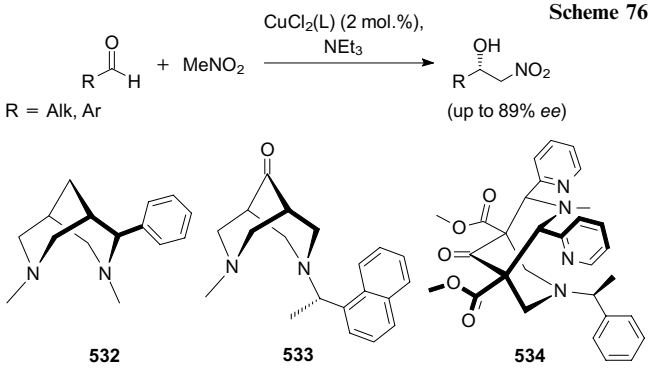
The conformationally rigid structure of bispidines makes them a promising basis for the design of ligands or organocatalysts for asymmetric transformations. Examples of the use of monosubstituted α-amino acid-derived bispidines **528** (Scheme 75) as organocatalysts for aldol reaction and the Michael reaction, which were published before 2010, are considered in detail in the review.[1535] Thus, the use of compound **528a** (R = Ph) as a co-catalyst in the reaction of cyclohexanone with 4-nitrobenzylidenemalonate **529** gave rise to the corresponding Michael adducts **530** in quantitative yields and high dia- and enantioselectivities (see Scheme 75).[1536] 3,5-Dinitrosalicylic acid served as the second, achiral component of the organocatalyst, while water proved to be an optimal solvent. The authors assumed that the high stereoselectivity of the reaction is due to the ability of bispidine **528** to activate simultaneously both components affording supramolecular complex **531** with a specified site of attack.

The complex of ligand **532** with $CuCl_2$ proved to be an effective catalyst for the asymmetric Henry reaction

Scheme 75



Scheme 76



between aromatic or aliphatic aldehydes and nitromethane.[1537] The yields of the desired products were 77–95% with an enantiomeric excess (*ee*) ranging from 73 to 89% (Scheme 76).

The use of complexes of bispidinone-based ligands **533** and **534** for the asymmetric catalysis of this reaction with $Cu(OAc)_2$ (0.1 mol.%) was significantly less efficient (see Scheme 76).[1538] Despite good yields (up to 93%), enantiomeric excess values were moderate: in the case of ligand **533**, they ranged from 10 to 74%, depending on the substituent in the aromatic ring of the aldehyde. Under catalysis of copper-based complexes with ligand **534**, the enantiomeric excess did not exceed 20%. Both ligands led to racemic products of the Henry reaction when aliphatic aldehydes were used as substrates. It may be assumed that high conformational mobility of ligands **533** and **534** hampers effective asymmetric induction.[1538, 1539]

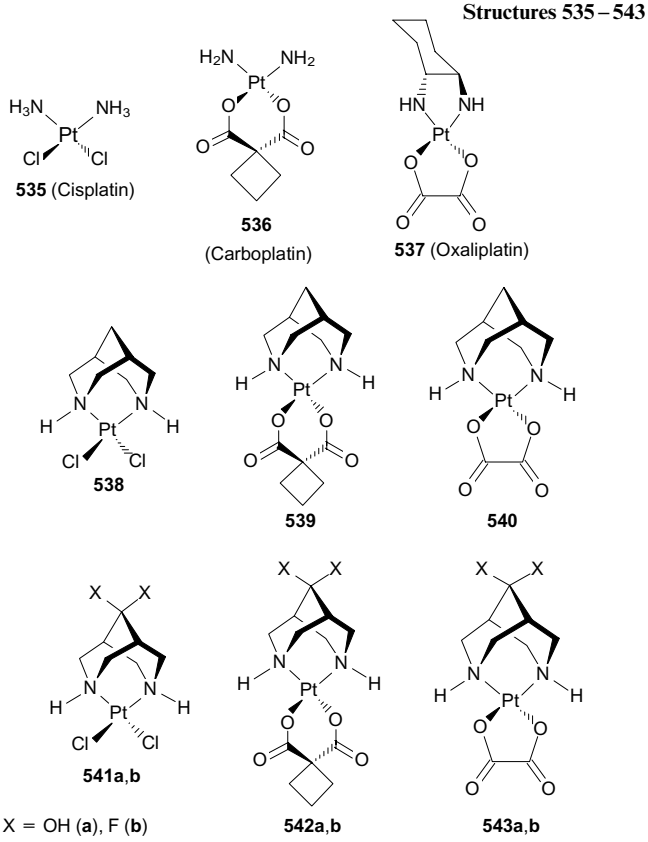
To sum up, owing to wide opportunities for varying substituents and conformational mobility, bispidines are attractive scaffolds for the design of catalytic systems. The use of metal complexes not only makes it possible to carry out redox reactions but also further increases the rigidity of the structure, therefore, most examples of the successful implementation of bispidine compounds specifically relate to metal complex catalysis.

4.5.4. The use of bispidine derivatives and their complexes with metals to interact with biological targets

The combination of a bulky rigid backbone and conformationally flexible six-membered rings makes bispidines attractive compounds for the targeted design of ligands interacting with various biological targets. Thus, based on the results of chemoinformatic analysis, bispidine was recommended as one of the highly promising biomimetic scaffolds for the design of new drugs.[1540] In a recent review,[1541] biological properties of many bispidine derivatives are described in detail, their antimicrobial activity is especially highlighted. This Section addresses only those publications in which complexes of bispidines with metals were used or the features of intermolecular interactions of bispidine ligands with biological targets were discussed.

In the last decade, significant attention has been paid to the design of novel analogues of cisplatin using Pt complexes of bispidines. Platinum-containing compounds are rather highly demanded as anticancer drugs; however, they have various side effects, and tumours are capable of developing resistance to them.[1542] Therefore, the search for novel types of ligands to produce biologically active Pt complexes remains an ongoing challenge. Bispidine-based complexes **538**–**540**, analogues of cisplatin (**535**), carbopla-

Structures 535 – 543



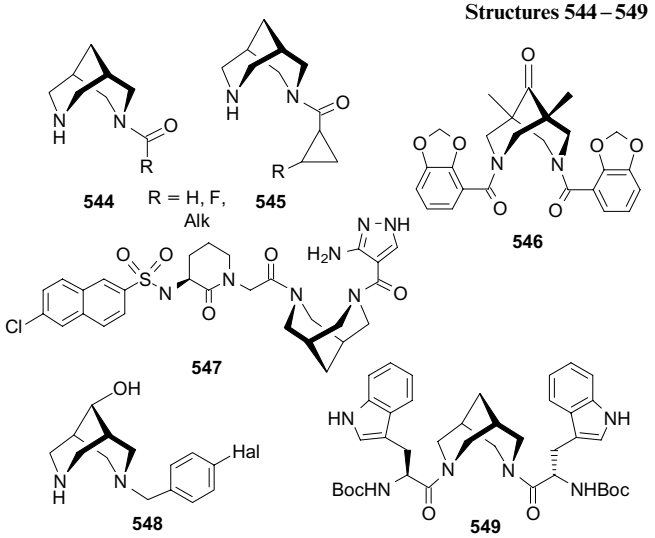
tin (**536**) and oxaliplatin (**537**), respectively, showed lower cytotoxicity against tumour cell lines compared to original drugs, particularly in the case of oxaliplatin.[1543] At the same time, the study of the anticancer activity against the cisplatin-resistant cell line showed that when using compound **538**, no such a sharp decrease in activity occurs compared with the cisplatin-sensitive cell line, as was observed for cisplatin. As a result, complex **538** exhibited even a slightly higher activity against the cisplatin-resistant cells than cisplatin. At the same time, the activity of complex **540** against the resistant tumour cells was comparable to that of oxaliplatin. To improve the hydrophilicity of bispidine-based complexes and affect their configuration, 9,9-dihydroxy analogues of complexes **538** – **540**, namely, compounds **541a**, **542a**, **543a** were synthesized.[1544] In organic solvents (DMF, DMSO), these compounds were in equilibrium with their keto analogues, resulting from dehydration. Complexes **541a**, **542a** and **543a** were less potent against A2780 ovarian cancer cell line than cisplatin, carboplatin and oxaliplatin, respectively, but in contrast to these drugs, they were almost non-toxic against conditionally normal HEK293 cell line. Dihydroxy derivatives **541a**, **542a** and **543a** also proved to be less active than their bispidine analogues **538** – **540**. Replacing hydroxyl groups with fluorine atoms in bispidine ligands (compounds **541b**, **542b**, **543b**) led to a further decrease in antitumour activity.[1545] The authors assumed that this effect can be associated with the possible reduction in the membrane permeability of fluorine-containing complexes.

A large pool of bispidine amides **544** and **545** was synthesized and tested for their ability to bind to nicotinic acetylcholine receptors.[1546] Nicotinic acetylcholine receptor agonists (nAChR) are considered to be promising drugs for improving memory and symptomatic treatment of Alzheimer's disease.[1547] Compound **545** turned out to be the most active ligands for nACh receptors, with the absolute configuration of carbon atoms in the cyclopropane substituent being of critical importance. The most active compound (1*S*,2*R*)-**545a** (R = Me) showed high affinity to α4β2-subtype of nACh-receptor in the nanomolar concentration range. At the same time, it exhibited low selectivity, interacting also with other nAChR subtypes (α3β4, α7) in the nanomolar concentration range. This compound was shown to act as an agonist of the α3β4-, but not α4β2R-receptor. Based on molecular modelling, it was assumed that novel inhibitors form hydrogen bonds with Trp149 and Tyr197 residues of the receptor α3β4 subtype, which involved the basic nitrogen atom and the oxygen atom of the amide moiety of substituted bispidine, respectively.[1548]

A novel structural type of positive allosteric modulators of ionic AMPA receptors (AMPA is α-aminomethylisoxazolepropionic acid) was developed based on dimethylbispidinone.[1549] Such modulators could be useful in the therapy of various neurological disorders including depression, schizophrenia, Alzheimer's and Parkinson's diseases, *etc*. Diamide derivative **546** increased the AMPA receptor currents *in vitro* and also reduced the duration of amnesia induced by scopolamine and maximal electroshock in the *in vivo* studies. Based on the molecular modelling data, it was suggested that two molecules of bispidinone **546** can bind to the positive allosteric site of the AMPA receptor to provide the observed pronounced biological effect.

With the use of bispidine scaffold, a novel high-selective serine protease factor Xa inhibitor was developed, promising for use as an antithrombotic agent.[1550] Ligand **547** was proposed based on analysis of the X-ray diffraction data for the complex of its analogue with protease factor Xa. The authors suggest that it was precisely due to the introduction of a bispidine moiety containing a hydrophilic substituent that it was possible to significantly increase the activity of inhibitors of this class. Another type of compound exhibiting anthrombotic activity was developed based on bispidinol.[1550] Compounds **548**, containing a halogen atom in the benzyl substituent, moderately inhibited thrombin in *in vitro* studies to form, as was suggested based on molecular modelling studies, hydrogen and halogen-π-bonds with the Tyr-228 residue.[1551, 1552] Figure 181 illustrates examples of possible intermolecular interactions of bispidine deriva-

Structures 544 – 549



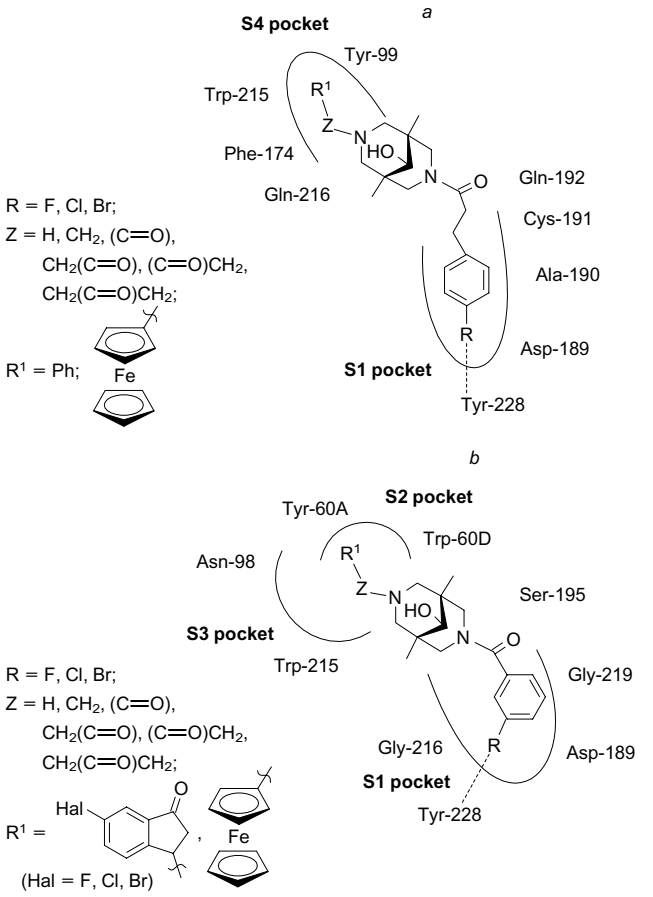


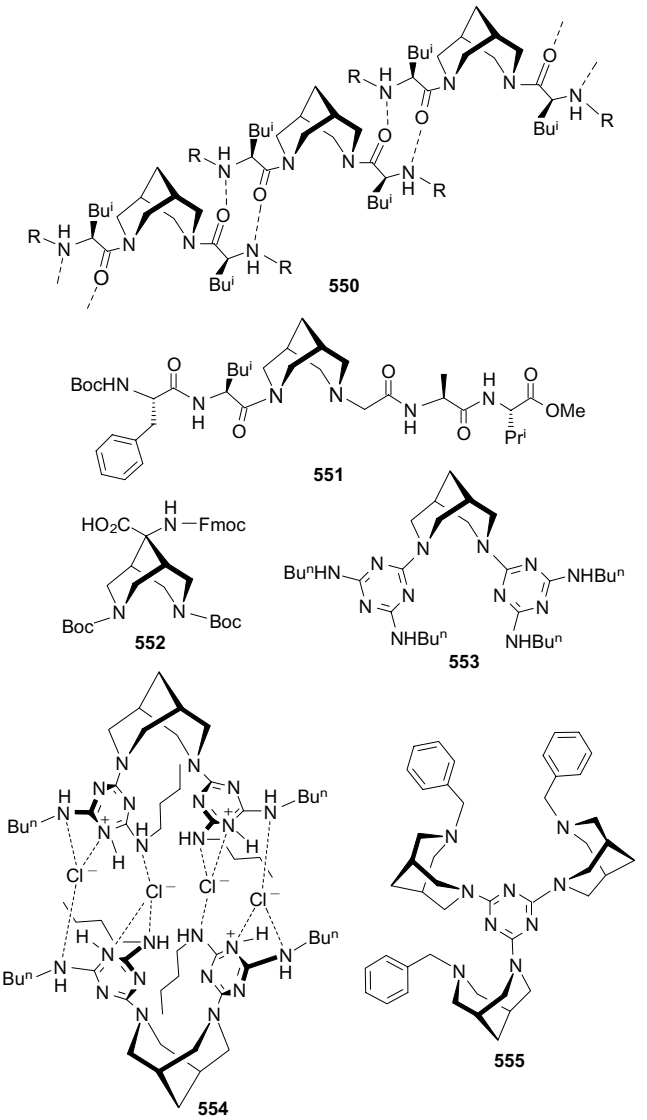
Figure 181. Possible intermolecular interactions of bispidine derivatives with amino acids, which form active sites of thrombin (*a*) and factor Xa (*b*). The figure was created by the authors using data of Refs 1551 and 1552.

tives with amino acids producing active sites of thrombin (S4 pocket) and factor Xa (S3 pocket).[1552]

The di(Boc)-protected conjugate of bispidine **549** bearing two tryptophan moieties exhibited high antiviral activity against mosquito-borne Japanese encephalitis.[1553] Interestingly, Boc-deprotection led to the complete disappearance of the antiviral effect. The authors suggest that the importance of the presence of the bispidine moiety is associated with its ability to mimic the secondary structure of proteins. Inhibition of virus replication was shown to occur at the step of replication of viral RNA, and as potential targets, RNA polymerase NS5 or RNA helicase NS3 can be considered.

Due to the sufficiently rigid three-dimensional cage of bispidine and the possibility to tune its conformations *via* changing the pH of the medium,[1554] bispidine conjugates with amino acids, for example, complex **550**, can mimic the protein secondary structure.[1555] It is important that even short bispidine – peptide conjugates, including compound **551**, can adopt a right-handed helical conformation.[1556] Protected amino acid **552**, in which the amine and acid functionalities are located at the bridging carbon atom leaving the bispidine nitrogen atoms available for further modification, provides additional opportunities for the use of substituted bispidines in the design of synthetic peptide analogues.[1557]

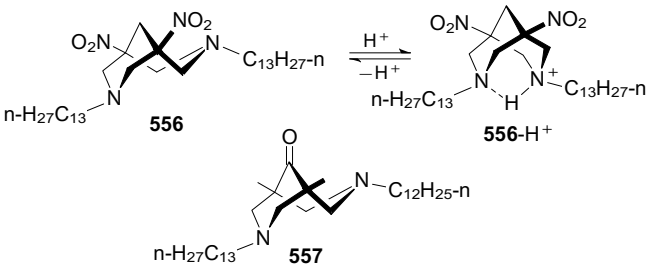
Structures 550 – 555



A unique ability to perform efficient transmembrane transport of H^+ and Cl^- ions was demonstrated for bispidine derivative **553**, which contains two melamine moieties substituted with n-butyl groups.[1558] According to X-ray diffraction data, such bispidines form intricate supramolecular complexes with protons and Cl^- ions (see structure **554**), capable of transporting ions through model membranes. As a result, two molecules of compound **553** can deliver up to four ions at a time across membranes. An alternative approach to the design of the Cl^- ion transporter based on melamine involved the attachment of three substituted pyridine residues to melamine. Compound **555** in the presence of HCl formed a cavity shaped by three bispidine molecules and allowing an efficient transport of chloride ions across the membrane.[1559]

pH-Mediated conformational changes in bispidine **556** (Scheme 77) bearing long-chain aliphatic arms opened access to liposomes with acid-driven membrane permeability.[1560] With the use of bispidinone **557** it was possible to control the permeability of liposomal membranes by adding aqueous solutions of divalent copper salts.[1561] pH-Dependent changes of a liposomal membrane charge were observed

Scheme 77



also for analogues of compound **557** containing long aliphatic amide substituents.[1562]

To conclude, unique architecture of a bicyclic bridged backbone and the possibility of its relatively simple functionalization make bispidine an attractive base unit for the design of various biological targets and also molecular machines for the controlled change of membrane permeability, which can be used for targeted drug delivery, for example, to tumour cells.

4.6. Suprampolecular systems based on macrocyclic meroterpenoids: biological activity and membranotropic properties

At the current stage of development of medicinal chemistry, scientists pay increasing attention to natural compounds and their analogues.[1563] This is due, first of all, to ready availability and diversity of natural organic compounds exhibiting a broad spectrum of biological activity.[1563, 1564] Among the variety of natural structures, several classes of compounds of mixed biogenetic origin deserve particular attention. These products of conjugate biosynthesis contain isoprene units and some other natural metabolite groups (flavonoid, alkaloid, *etc*.) synthesized by routes other than isoprenoid pathway.[1565, 1566] Compounds of this type that contain an isoprene residue (most often, hemiterpene or monoterpene one) as a functional group are designated by the prefix 'mero' (*e.g*., meroterpenoids).[1564, 1566]

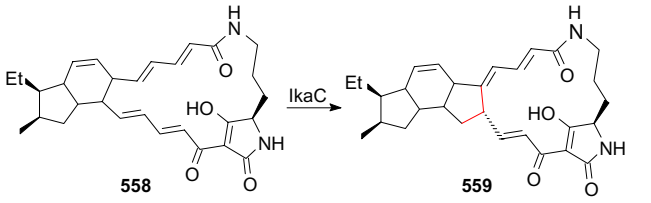
The chemistry of meroterpenoids has been actively developed in the last decade,[1567, 1568] which is due to their unique properties. The role of plant feedstock as a source of meroterpenoids gradually decreases, being replaced by synthetic methods for the production of these compounds.[1569] This is caused by the necessity to prepare relatively large amounts of products meant for wide practical application. Therefore, it is important to develop new synthetic approaches for functionalization of compounds of various classes with terpenoid pharmacophore moieties with the goal to increase their biological activity and to decrease their toxicity.[1570]

The combination of structures of different types in one molecule for fabricating synthetic receptors can be attained by combining fragments of several organic molecules into one hybrid macrocyclic platform. Such macrocyclic meroterpenoids would exhibit properties of the moieties that make up the molecule. Terpenoid moieties are attractive pharmacophore groups, the presence of which in the macrocyclic platform may reduce the toxicity and increase the cell membrane affinity and susceptibility to self-association and aggregation.

Macrocyclic meroterpenoids can be divided into two main classes. The first class includes natural macrocycles prepared by conjugate biosynthesis, with macrocyclization occurring *via* enzyme-mediated cascade reactions.[1571] The second class comprises synthetic macrocycles in which the core is assembled by either macrocyclization of separate terpene moieties or introduction of terpene residues into the macrocyclic platform *via* various transformations.[1566, 1569]

Among natural macrocyclic meroterpenoids, prenylated flavonoids and phenols,[1568, 1572] isoprenoid lipids,[1573] prenylated amino acids [1574] and alkaloids and isoprenylpolyketides [1567] have been studied most comprehensively. All these macrocyclic meroterpenoids are isolated directly from natural sources. The formation of macrocyclic secondary metabolites during biosynthesis is a thermodynamically favourable process, because one metabolite can be converted to a series of final biochemical products *via* transannular cyclization of the macrocyclic structure.[1575] Zhang *et al.*[1576] showed that alcohol dehydrogenase (IkaC) catalyzes an unusual reductive cyclization of compound **558** to ikarugamycin (**559**) with the formation of internal five-membered ring (Scheme 78). Usually, ikarugamycin is isolated from the bacterial strains *Streptomyes*. Apart from exhibiting strong antiprotozoal, antiulcer, antibacterial, antiviral, cytotoxic and apoptosis-inducing activities, compound **559** inhibits penetration of oxidized low-density lipoproteins into macrophage cells, thus preventing the formation of atherosclerosis plaques, and also inhibits clathrin-dependent endocytosis, which opens up the possibility of using this compound as a therapeutic agent.

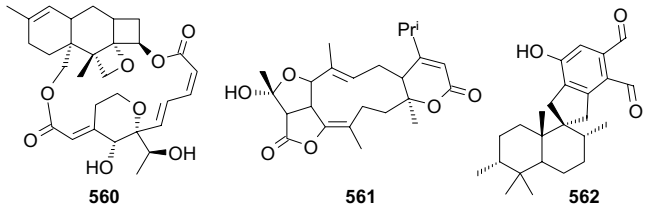
Scheme 78



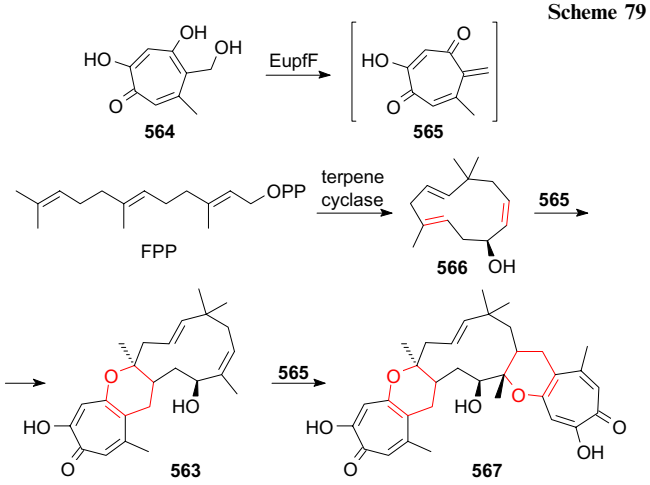
Studying the formation of secondary metabolites in the fungi *Stachybotrys*, namely, the mycelial culture DSMZ 12880 (chemotype *S*), resulted in the detection of three novel meroterpenoids **560** – **562**.[1572] These compounds contain a chromene ring moiety with an attached isoprenoid side chain. Considering the biosynthetic pathway, it can be assumed that stachybotrychromene C (**562**) is the final product, while stachybotrychromene A (**560**) and stachybotrychromene B (**561**) are intermediates. Compounds **560** and **561** showed a moderate cytotoxic action on HepG2 cells after a 24-h exposure, whereas meroterpenoid **562** did not show cytotoxicity in the tested concentration range (0.1 – 100 μmol L^{-1}).[1572]

The Diels – Alder reaction is one of the most popular synthetic transformations that can give rise to complex natural products and their analogues.[1577] However, there

Structures 560 – 562



Scheme 79



are only several examples of application of this reaction for enzyme-mediated cascade reactions in the biosynthesis of macrocyclic meroterpenoids.[1578, 1579] Hu and co-workers[1580] reported the use of intermolecular hetero Diels–Alder reaction in the biosynthesis of macrocyclic sesquiterpenes. It is noteworthy that neosetophomone B (**563**), isolated as an optically pure isomer from various fungi, can be prepared by one or two tandem hetero Diels–Alder reactions (Scheme 79). This compound contains three annulated rings — 11-membered macrocycle and dihydropyran and tropolone rings — and has a high antitumour activity (in the nanomolar concentration range). It was shown that hydroxymethyl-containing tropolone **564** is dehydrated under the action of the EupfF enzyme to give reactive *o*-quinone tropolone **565**, which provides additional stereoselective control of the subsequent intermolecular hetero Diels–Alder reaction with (1*E*,4*E*,8*Z*)-humulenol (**566**), which is obtained from farnesyl pyrophosphate (FPP) under the action of the terpene cyclase enzyme. This gives enantiomerically pure neosetophomone B (**563**), which is treated with an excess of tropolone **565** to give eupenifeldin (**567**) — a neosetophomone containing two dihydropyran rings.

It is noteworthy that although most of natural meroterpenoids obtained in the enzyme-mediated cascade reactions of conjugate biosynthesis are macrocyclic compounds, they do not exhibit classical supramolecular properties. They are important secondary metabolites formed in various biochemical processes. Many of these compounds show relatively high biological activities, which makes them potential drug candidates.[1563] However, compounds that behave as supramolecular systems still can be found among natural macrocyclic meroterpenoids. This refers to prenylated bacterial non-ribosomal lipopeptides,[1581] which represent the smallest group of isoprenoids obtained by conjugate biosynthesis, but which have been actively studied in the last decades. Studying prenylated macrocyclic peptides as allosteric activators of chambered bacterial proteases showed that they can be considered to be potential antibiotics. The first representatives of these compounds are acyldepsipeptides **568**–**570**.[1574, 1581, 1582]

Since the structure and composition of non-ribosomal lipopeptides are not limited or not determined by the genetic code, they may contain non-proteinogenic (ornithine, homoserine, β-amino acids) and modified (hydroxylated, chlorinated, *N*-methylated or glycosylated) amino acids in L- or D-configurations. The fatty acid moiety contains, most often, linear, cyclic or branched terpene tail of variable length (usually, C_6-C_{18}) and functional groups (*e.g.*, hydroxy or amino group). The macrocycle of prenylated non-ribosomal lipopeptides is formed between the C-end of the peptide and the hydroxy, phenolic or amino group that belongs to either amino acid side chain or the terpene moiety. The macrolacones or -lactams thus formed differ in the ring size and contain 4 to 16 amino acids.[1574]

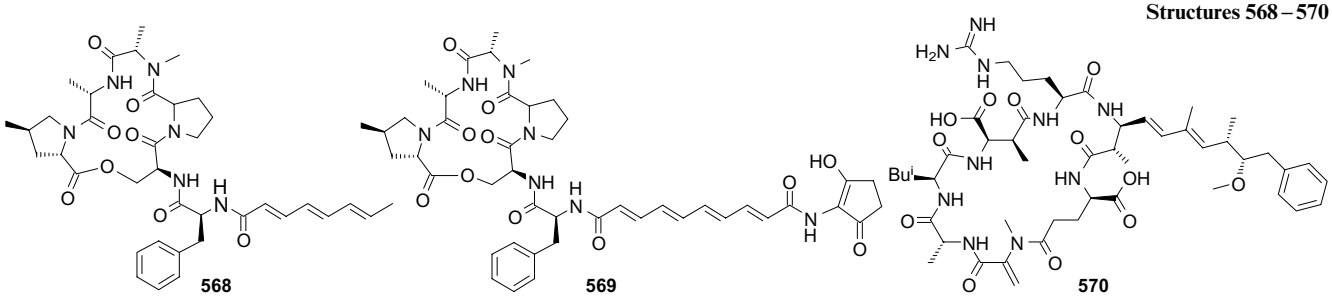
Many prenylated non-ribosomal lipopeptides possess amphiphilic properties, which allow them to be used as efficient biosurfactants.[1583] They affect the biofilm formation or degradation by changing the surface tension of the surrounding medium. Prenylated non-ribosomal lipopeptides also have membranotropic properties. In addition, they are capable of forming supramolecular associates containing water-insoluble nutrients, which provides cellular uptake of even poorly water-soluble nutrients.[1584]

Synthetic macrocyclic meroterpenoids are prepared by combining classical macrocyclic platforms such as cyclodextrins or meta- and paracyclophanes with various terpenoid moieties or by macrocyclization of several terpene derivatives.[1566]

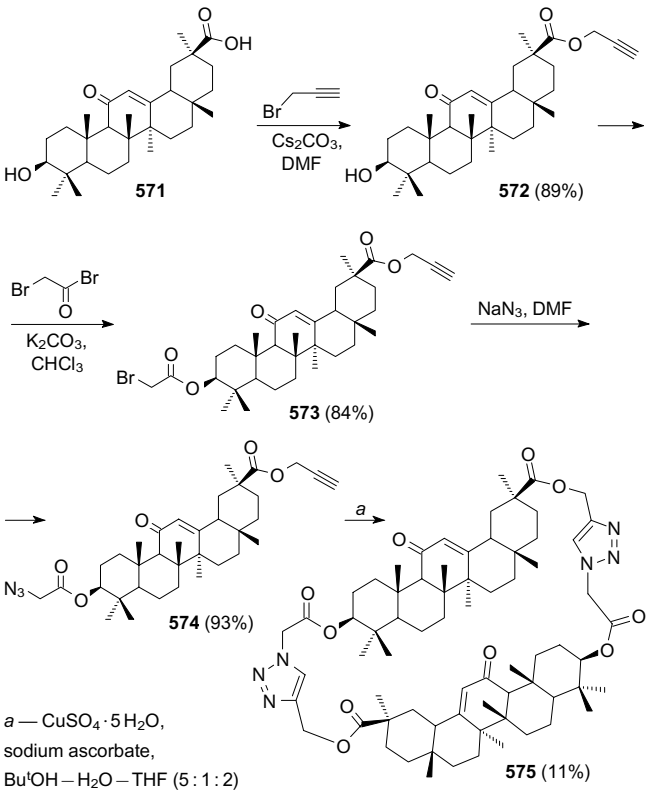
Hu *et al.*[1585] synthesized a new macrocycle from 18b-glycyrrhetinic acid (**571**) using click chemistry methods (Scheme 80). This acid was allowed to react with propargyl bromide in the presence of caesium carbonate, which gave derivative **572** in 89% yield. The subsequent acylation of **572** afforded bromo derivative **573** in a good yield. To accomplish the final cyclization, precursor **573** was converted to azide **574**, which was subjected to the Huisgen reaction. The target macrocycle **575**, which was isolated in 11% yield, showed a remarkable selectivity in the recognition of fluoride ions *via* $C-H\cdots F^-$ hydrogen bonding. It was also highly selective in the recognition of Hg^{2+} *via* the 1,2,3-triazole moiety and the carbonyl group as the binding sites.

Carreira s research team[1586] obtained novel calix[4]arene derivatives **576** and **577**, containing four meroterpenoid amphotericin B moieties. The synthesized macromolecules take a cone conformation, which mimics the structure of the

Structures 568–570



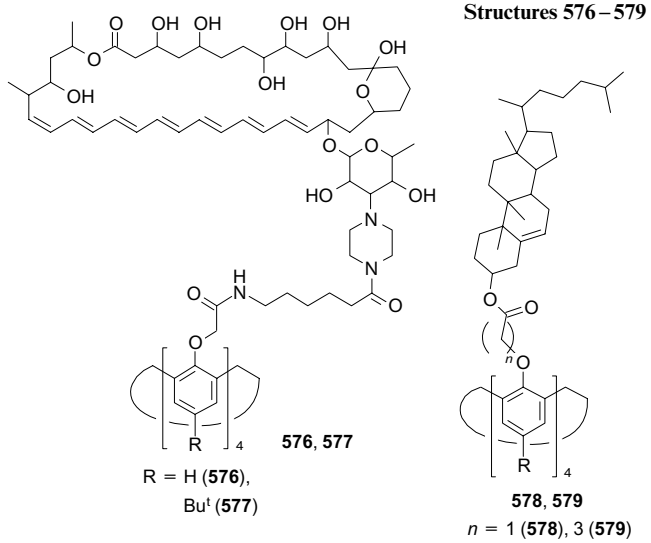
Scheme 80



transmembrane pore. The antifungal activity of **576** and **577** proved to be similar to that of the starting amphotericin B: the minimal inhibitory concentrations (MIC) were 0.10 and 0.25 mol L^{-1}, respectively. Also, the new derivatives were much less hemotoxic (by a factor of at least 10) than monomeric amphotericin B. Finally, the ability to form ion channels in the lipid bilayer was demonstrated for **576** and **577**.[1586]

Lai's research team[1587] synthesized the first liquid crystals from calix[4]arene-cholesterol derivatives **578** and **579** (50–80% yields). Their liquid crystal behaviour was studied by polarized light microscopy, differential scanning calorimetry and X-ray diffraction. Compounds **578** and **579** showed mesomorphic properties.

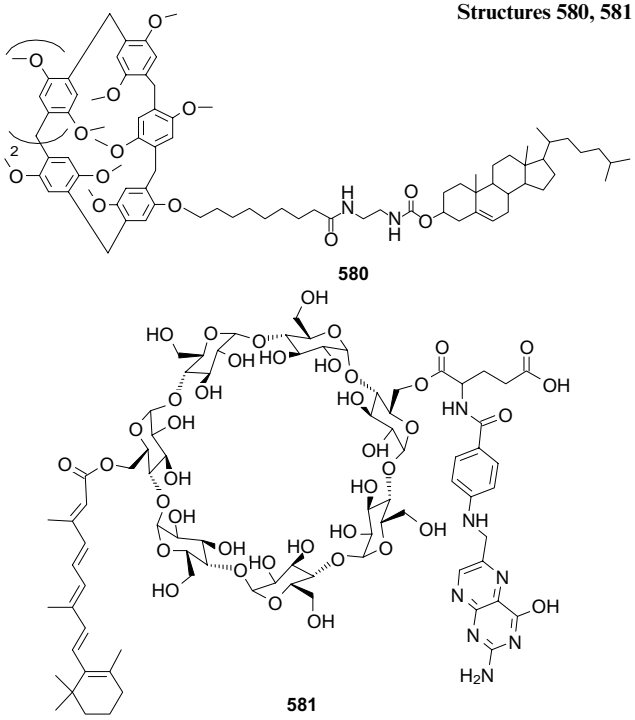
Structures 576–579



Wang and co-workers[1588] used pillar[6]arene **580** functionalized by a cholesterol derivative as a low-molecular-weight gelator. In a cyclohexane–n-hexanol mixture (10:1 v/v) at 10 °C, this compound forms an organogel, which reversibly responds to temperature changes and forms host–guest complexes.

Varshosaz *et al.*[1589] successfully synthesized meroterpenoid **581** based on β-cyclodextrin and folic and retinoic acids. In water, macrocycle **581** formed stable submicrometre self-associates. The stability of the colloidal system thus formed was additionally confirmed by ζ-potential measurement. It was shown that macrocycle **581** can efficiently encapsulate the antitumour drug doxorubicin.[1589]

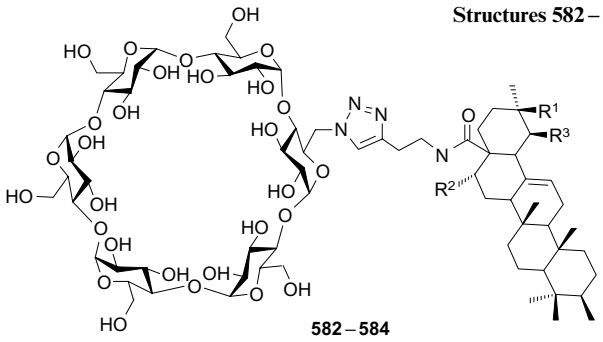
Structures 580, 581



Xiao *et al.*[1590] reported a series of water-soluble meroterpenoids **582**–**584**, which were prepared in good yields from α-cyclodextrin and pentacyclic titerpenoids **585**–**588**. Inhibition of the entry of hepatitis C virus (HCV) into the cell is a key problem for the therapy of chronic hepatitis C. The activity of HCV entry inhibition was determined by analyzing the entry of virus pseudo particles (HCVpp/VSVGpp). The best results were observed for compounds **582** and **583**, which showed the most promising inhibitory activity against HCV entry with average IC_{50} values of 1.18 and 0.25 mmol L^{-1}, respectively. The *in vitro* cytotoxic activity of these two compounds against model mammalian epithelial cells (MDCK) was not observed at a concentration of 100 mmol L^{-1}. To determine the mechanism of their action, five stages of binding were identified. Compounds **582** and **583** were found to show an inhibitory activity after binding to glycoproteins in the HCV envelope and to prevent the virus entry into the cell.[1590]

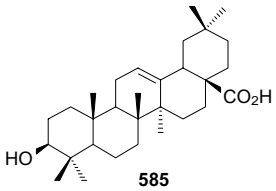
These results are in line with the results obtained for β-cyclodextrins.[1591] Previously, it was found that oleanolic (**585**) and echinocystic (**586**) acids isolated from *Dipsacus asperoides* inhibit the HCV entry into the cell. The main

Structures 582 – 588

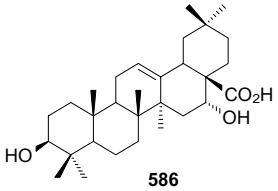


582 – 584

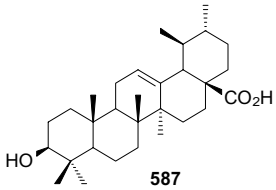
R^1 = Me, R^3 = H: R^2 = H (**582**), OH (**583**);
R^1 = R^2 = H, R^3 = Me (**582**)



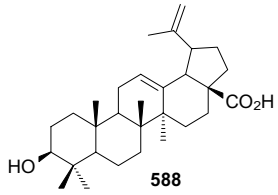
585
(Oleanolic acid)



586
(Echinocystic acid)



587
(Ursolic acid)

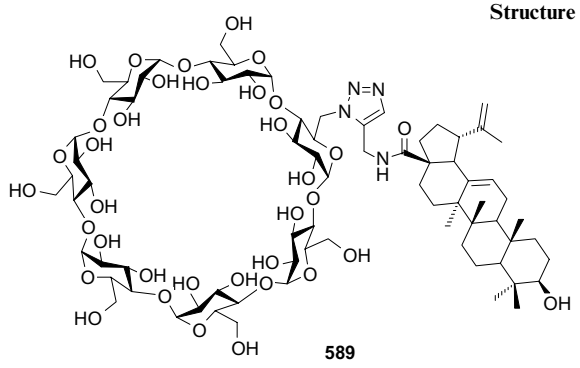


588
(Betulinic acid)

problem faced when using this type of tritepenes is their low solubility in water. The introduction of hopanoid moieties **585 – 588** into α- and β-cyclodextrins increases the water solubility of terpenes. In the case of meroterpenoid **589** based on β-cyclodextrin, moderate inhibition of the HCV entry was found. None of the meroterpenoids showed cytotoxicity according to the alamar Blue assay carried out for HeLa, HepG2 (human hepatocellular carcinoma cell line), MDCK and 293T cells. It is also noteworthy that combining terpene and β-cyclodextrin moieties in one molecule resulted in disappearance of the hemolytic activity of triterpenes. A facile synthetic approach to the preparation of meroterpenoids exhibiting the properties of both β-cyclodextrin and pentacyclic triterpenoids is based on the use of click chemistry concept and gives rise to a new class of inhibitors of HCV entry into the cell.[1590, 1591]

Thus, the above data provide the conclusion that development of the supramolecular chemistry of macrocyclic meroterpenoids can be used to design highly efficacious drugs and to develop new-generation non-toxic materials. Large resources of renewable natural raw materials stimulate continuation of studies directed towards the synthesis of new representatives of this class of natural compounds and determination of structure – activity relationships for the products.

Structure 589



589

5. Molecular machines and devices

5.1. Development of photoactive supramolecular machines and devices

Currently, it has become clear that the mainstream of the development of global technosphere is related to miniaturization of devices and machines. There are two key strategies for the design of nano-scale architectures, bottom-up and top-down ones. According to the latter strategy, nanoparticles and nano-scale systems are obtained by disintegration of larger objects. The bottom-up strategy can be implemented, first of all, by organic synthesis and supramolecular self-assembly.[1592]

At the present time, a new trend has formed in the bottom-up nanotechnology, that is, supramolecular engineering of supramolecular devices and machines for various purposes.[1593 – 1596] Supramolecular devices are structurally organized and functionally integrated chemical systems. The devices in which the implementation of some function is associated with physical motion of components relative to each other are classified as supramolecular machines.[1, 4] Both the former and the latter can be used to design mechanisms for generation, conversion and transfer of energy, for motion at the nanolevel and to develop tools for the monitoring and diagnosis of nano-quantities of materials and substances.[13, 1597 – 1602]

Supramolecular devices and machines can be controlled in different ways by means of various external stimuli:

— photoswitching (under the action of *hν*),
— electrochemical switching (e^-),
— chemical switching (H^+ or M^{n+}),
— thermal switching (Δ).

Light, which can be easily controlled as regards both the wavelength and the intensity, is the most convenient type of stimulus.[1603, 1604]

In the living nature, photoactive supramolecular systems provide for photosynthesis and phototropism in plants, visual perception of animals and phototaxis in bacteria: by absorbing a photon, chlorophyll and retinal molecules undergo rearrangements, resulting in changes in their reactivity.[1605, 1606] In these systems, light acts as the trigger, which initiates a number of vital processes. The major photochemical processes that take place in this case include fluorescence, energy transfer, electron transfer and light-induced structural changes.

Thus, molecules that compose photoactive supramolecular systems must have an antenna to absorb a photon with subsequent change in the molecular structure and a moiety (functional block) that can change its reactivity as a result of photoinduced structural rearrangement (Fig. 182).

For a long time, attempts have been made to fabricate artificial photoactive supramolecular systems of different degree of complexity, which would, on the one hand, possess the most valuable properties inherent in natural objects and, on the other hand, provide the possibility of new applications.

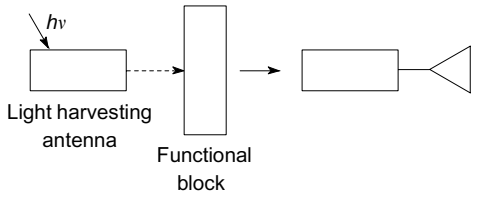
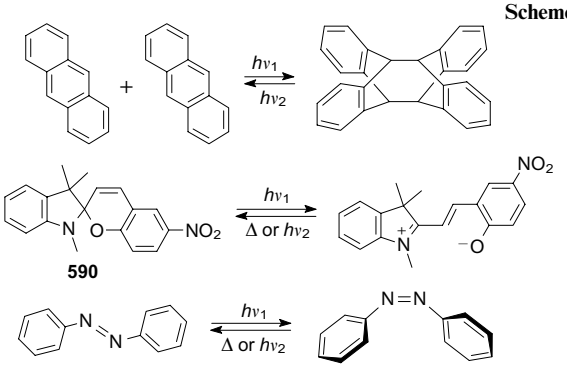


Figure 182. Basic diagram of changes in the photoactive supramolecular system upon absorption of a photon.

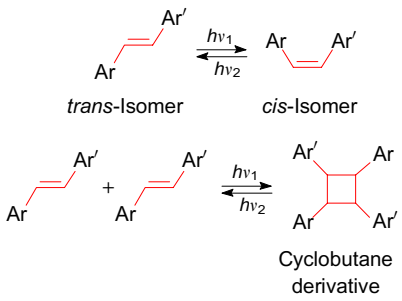
Photochromic derivatives of anthracene and spiro compounds (*e.g.*, compound **590**) were studied as light harvesting antennae for supramolecular devices and machines.[1607] However, most often, azobenzene derivatives containing N=N bond were used for this purpose (Scheme 81).[1608, 1609] A key drawback of azobenzenes is that they are able to undergo only *trans*–*cis* and *cis*–*trans* photoisomerization reactions.[1610]

Scheme 81



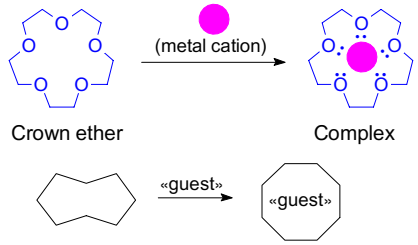
In this regard, compounds containing a carbon–carbon double bond (unsaturated compounds) have a number of advantages. The major one is the ability to undergo not only photoisomerization,[1611] but also other reversible photoreactions resulting in considerable structural changes, *e.g.*, [2 + 2]-photocycloaddition reactions, giving rise to cyclobutane derivatives (Scheme 82).[1612, 1613]

Scheme 82



The most popular functional blocks, *i.e.*, molecular moieties highly responsive to a change in the molecular structure upon photoswitching, are crown compounds. These are macrocyclic compounds containing heteroatoms with lone pairs of electrons, capable of forming coordination bonds with metal ions. A fundamental feature of these molecules is the capability (highly dependent on the chemical and spatial structure) of self-assembly in solutions,

Scheme 83



together with ions or other molecules (guests), to give systems of higher complexity (Scheme 83).[1614]

If a crown ether and a photoactive compound are linked by covalent bonds in such a way that one or two heteroatoms of the macrocycle are in conjugation with the chromophore, the additivity of the specific properties of such crown-containing photoactive compounds would be disrupted. Transformations of the photoactive moiety under the action of light would change the efficiency of binding of metal cations to the crown ether moiety, while self-assembly, in turn, would change the spectral and photochemical characteristics of the photoactive moiety. Conjugate reactions of this type take place in the supramolecular structures formed upon self-assembly involving molecules of the crown-containing photoactive compounds and metal ions, which is used to develop and fabricate photoswitchable supramolecular devices.

Thus, photoswitchable supramolecular devices based on unsaturated compounds and crown ethers can be sketched in the following way (Fig. 183): these are hybrid molecules that contain an unsaturated moiety as the antenna and one or two crown ether moieties capable of binding a metal ion.[1235, 1615–1617] In this case, self-assembly to give supramolecular structures would change the spectral and photochemical characteristics of the unsaturated moiety, with the self-assembly of these crown-containing molecules being, in turn, controlled by light.



Figure 183. Sketch of photoswitchable supramolecular devices based on crown-containing unsaturated compounds (CUC).

As the prototypes of photoswitchable supramolecular machines in which the components can physically move relative to each other (Fig. 184), one can consider the shuttle-like pseudorotaxane complexes involving unsaturated compounds (axis) and macrocyclic cucurbiturils or

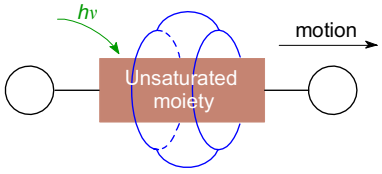


Figure 184. Sketch of light-controlled supramolecular machines based on unsaturated compounds and cucurbiturils or cyclodextrins.

cyclodextrins (rotor). For this purpose, the components must not be connected by strong chemical bonds.

Cucurbiturils (see Fig. 129), which are used as rotors in the pseudorotaxane complexes, are macrocyclic compounds $(C_6H_6N_4O_2)_n$, with their shape resembling a pumpkin (cucurbita in Latin) or a barrel. Their inner cavity can accommodate organic molecules as guests to form complexes. Oxygen atoms of highly polarized carbonyl groups are located at the barrel top and bottom.[1089, 1618] This facilitates the formation of inclusion complexes, especially with positively charged guest molecules, which refers to most of photoactive unsaturated compounds.[1619]

Cyclodextrins (see Fig. 129) are cyclic oligosaccharides consisting of α-D-glucopyranose residues connected by 1,4-glycosidic bonds. The shape of the cyclodextrin molecule resembles a hollow truncated cone. The cavity of the cone is hydrophobic, since all OH groups in cyclodextrins are located on the outer surface. These structural features give cyclodextrins the ability to form inclusion complexes with hydrophobic molecules, in particular with the molecules of photoactive organic compounds, in aqueous solutions.[1620]

In the living nature, the enormous diversity of supramolecular architectures is based on limited sets of components. An example of such molecular meccano is the set of nucleotides,[1621] which are used by nature to construct nucleic acids of different degrees of hierarchy.

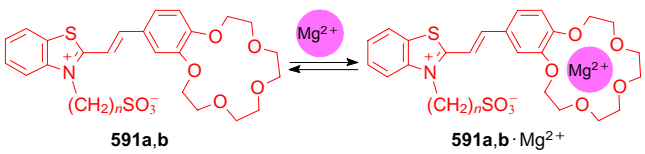
The molecular meccano strategy could become a versatile technique for the bottom-up construction of photoactive supramolecular devices and machines with a specified architecture and diverse properties. However, no such approaches have yet been developed in nanotechnology.

Crown-containing unsaturated compounds (CUC) with the C=C bond as the light harvesting antenna and an aryl and hetaryl substituent at this bond were synthesized.[1622] This allowed photoswitching of the molecule to be accomplished by visible light. Simultaneously, methods have been proposed for the synthesis of a number of compounds undescribed previously, but highly promising for the design of various types of photoactive supramolecular devices, namely, crown ether derivatives, including hard-to-prepare ones, *e.g.*, derivatives containing various combinations of N, O and S atoms in the macrocycle. This might suggest that the self-assembly of the CUC molecules and metal cations would give rise to intricate supramolecular complexes, also capable of photoswitching.

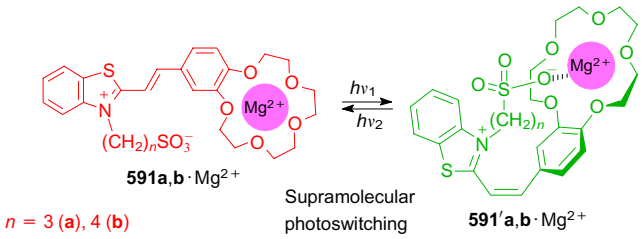
It was found that crown-containing styryl dyes **591a**,**b**, which have the SO_3^- terminal anionic group capable of coordination, are most promising among CUC for the design of photoswitchable supramolecular devices. These dyes and metal cations were self-assembled to give supramolecular complexes (Scheme 84).

Depending on the actinic light wavelength, these complexes may 'put on' and 'take off' their anionic cap (SO_3^- group), *i.e.*, they are capable of supramolecular photoswitching from structure **591** to structure **591′** (Scheme 85).[1623, 1624]

Scheme 84



Scheme 85



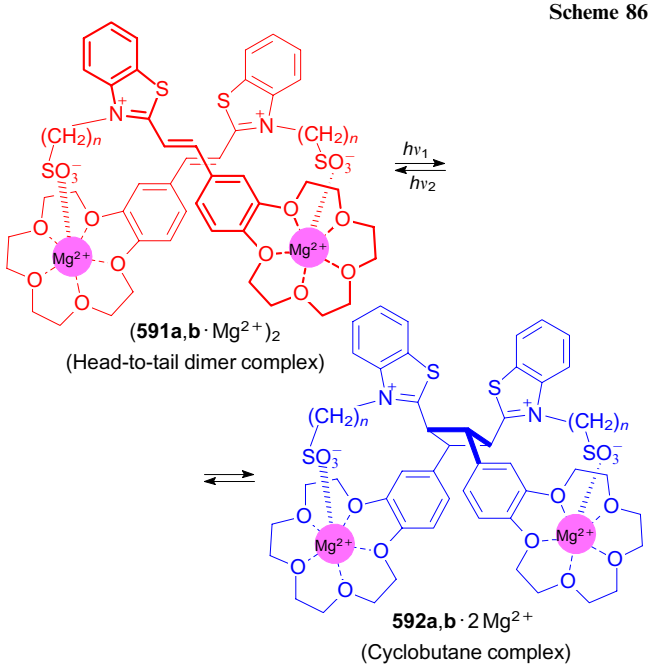
It was also shown that the *cis*-isomers of the above styryl dyes form much more stable complexes than the *trans*-isomers (the ratio of the stability constants reaches 500). This means that using light, it is possible to change the affinity of these CUC for the metal cation, *i.e.*, to control the complex formation. These supermolecules are commonly referred to as photoswitchable supramolecular devices. Thus, photoswitchable supramolecular devices were obtained for the first time on the basis of crown-containing styryl dyes.

Supramolecular complexes based on CUC also offer opportunities for the design of more intricate photoswitchable supramolecular devices.

According to the results of photochemical studies, in the presence of metal cations, the crown-containing styryl dye molecules are self-assembled to give photoactive sandwich structures (head-to-tail dimers), in which the C=C bonds are arranged one above the other. If solutions of these supramolecular dimeric complexes are exposed to light at a definite wavelength, highly efficient photocycloaddition reaction takes place to give cyclobutane derivatives **592a**,**b** (Scheme 86).[1625]

If the cation is removed, cyclobutane **592** can be converted to the starting styryl dye **591** by irradiation at a shorter wavelength, and then the formation of the dimeric complex can be repeated. In addition, it turned out that

Scheme 86



these cyclobutane derivatives bind metal cations much more efficiently than the initial dyes. Hence, in this case, too, the complex formation can be controlled by light and the dimeric complexes are also photoswitchable supramolecular devices.[1615]

It is noteworthy that the supramolecular photocycloaddition gives only one out of the 11 theoretically possible cyclobutane isomers; in other words, this reaction is stereospecific.[1626] This allows for targeted design of photoswitchable supramolecular devices of a strictly definite structure.

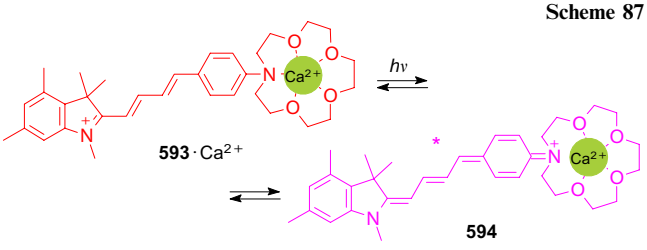
According to the currently available data, it can be stated that metal cations in the CUC dimeric complexes do not have a direct effect on the photocycloaddition reaction; they act as a 'molecular glue', bringing the molecules closer together to a distance at which the reaction is already possible and simultaneously ensuring relative orientation of the C=C bonds that is favourable for this reaction.[1627]

Unlike anion-capped complexes, photocycloaddition products, that is, crown-containing cyclobutanes without metal ions, represent a new type of photoswitchable host molecules, possessing two cation binding sites. Considering the arrangement of crown ether moieties in these molecules, one can expect their simultaneous participation in the formation of a sandwich type complex with a large metal cation such as Ba^{2+} or Cs^{+} or a small organic cation.

Thus, photoswitchable supramolecular devices with specified characteristics can be obtained from two CUC molecules and two metal cations *via* self-assembly of supramolecular dimeric complexes in solutions followed by photoconversion to crown-containing cyclobutanes, which differ in the complexing properties. If necessary, it is possible to disassemble cyclobutanes into the initial compounds by irradiation with light at a shorter wavelength.[1615]

It was of interest to find out how the presence of an additional C=C bond in crown-containing butadienyl dyes affects their complexing and photochemical properties. Among butadienyl dyes, an example of simple photoswitchable supramolecular device with a switching time of 20 ps was found (Scheme 87). In complex **593**·Ca^{2+}, the metal cation forms coordination bonds with all heteroatoms of the crown ether moiety; however, upon photoexcitation of the complex, the calcium–nitrogen bond is cleaved (see structure **594**) and is formed once again after deactivation of the excited state. Thus, in this photoswitchable supramolecular device, the calcium–nitrogen bond formation is the controllable function.[1628]

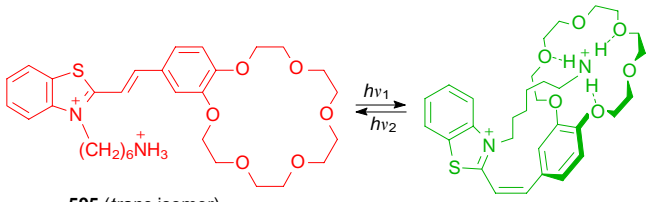
Scheme 87



Photoinduced recoordination reaction

A supramolecular device characterized by photoswitchable intramolecular complex formation involving hydrogen bonds in the absence of metal cations was obtained by introducing the long *N*-ammonioalkyl substituent into the heterocyclic moiety of the styryl dye (compound **595**, Scheme 88).[1629]

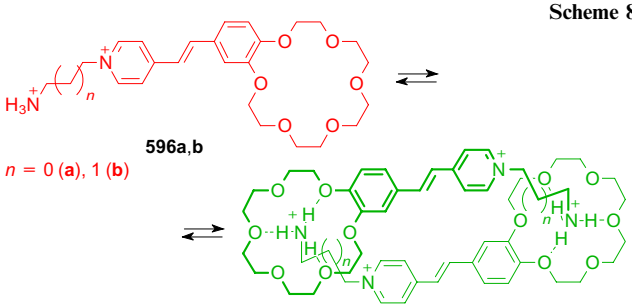
Scheme 88



595 (*trans*-isomer)

595′ (intramolecular complex of the *cis*-isomer)

Scheme 89



596a,b

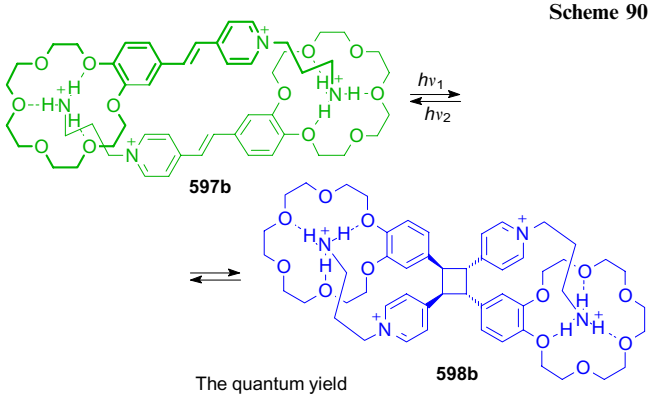
597a,b

Styryl dyes **596a,b**, which have shorter ammonioalkyl substituents at the heterocyclic nitrogen atom, can form dimeric complexes **597** in solution *via* spontaneous supramolecular self-assembly involving hydrogen bonding (Scheme 89).

It was shown that the chromophore moieties of two molecules in complexes **597a,b** are located at a short distance and are nearly parallel to each other, with the mutual orientation of the central C=C bonds being favourable for [2+2]-photocycloaddition to give, for example, cyclobutane **598b** (Scheme 90).[1630] It is not surprising that in this case, stereospecific [2+2]-photocycloaddition reactions were conducted in solution with exceptionally high quantum yields. The discovered feature gives hope that these new photoswitchable supramolecular devices would be used in the optical data recording and storage technology.

An important line of research is self-assembly of photocontrolled supramolecular machines based on photoactive unsaturated compounds and cucurbiturils.[1625, 1626] It was found that cucurbiturils form relatively stable host–guest inclusion complexes with positively charged unsaturated compounds.

Scheme 90



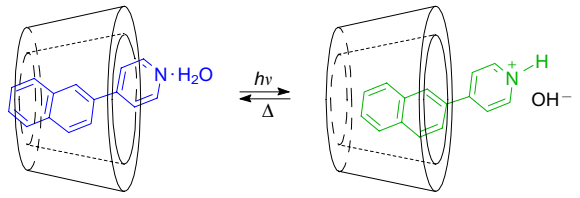
597b

598b

The quantum yield of photocycloaddition is 0.38

It was of interest to study the possibility of photocontrol over physical motion in supramolecular machines. The simplest supramolecular machine of this type was developed using the inclusion complex of 4-(2-naphthyl)pyridine (**599**) with β-cyclodextrin. In this case, photoirradiation leads to reversible protonation and, as a consequence, to the physical displacement of the guest molecule in the macrocycle cavity (Scheme 91).[1631]

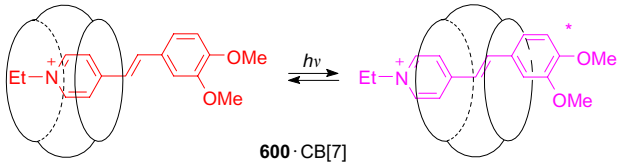
Scheme 91



599·H_2O@HP-β-CD **599**-H^+OH^-@HP-β-CD

A simple fast photocontrolled supramolecular machine is based on the inclusion complex of styryl dye **600** and cucurbit[7]uril (CB[7]). It was found that considerable increase in the fluorescence lifetime of dye **600** is associated with the physical movement of the electronically excited dye cation inside the cavity of the host molecule in the first several picoseconds (Scheme 92).[1632]

Scheme 92



600·CB[7]

A more complex photocontrolled supramolecular machine is based on the pseudorotaxane complex of cucurbit[8]uril (CB[8]) with bis(quinolyl)ethylene derivative **601**. In this case, irradiation with light causes reversible *trans*–*cis*-photoisomerization of the unsaturated guest molecule (Fig. 185).[1633] The spatial structure of this supramolecular machine after light irradiation determined by X-ray diffraction (see the lower part of Fig. 185) indicates that the intricate physical movement of the guest molecule **601** in the cavity of the host macrocycle, which resembles coiling, is easy to implement.

It was found that the cucurbit[8]uril cavity can accommodate two molecules of (*E*)-3-[4-(3,4-dimethoxystyryl)-pyridinium-1-yl]propanesulfonate betaine (**602**). Figure 186 presents the structure of the corresponding supramolecular pseudorotaxane inclusion complex **603**.[1634] The relative positions of the unsaturated moieties of two molecules of dye **602** in this complex proved to be favourable for the photocycloaddition to occur. It was shown that the cyclobutane thus formed is bound to cucurbituril less strongly than the starting components, *i.e.*, not only the physical motion of photoactive molecules inside the macrocycle, but also the strength of binding of the components can be controlled by light.

These properties were exploited to develop a cucurbit[8]uril-based light controlled supramolecular assembler.[1634]

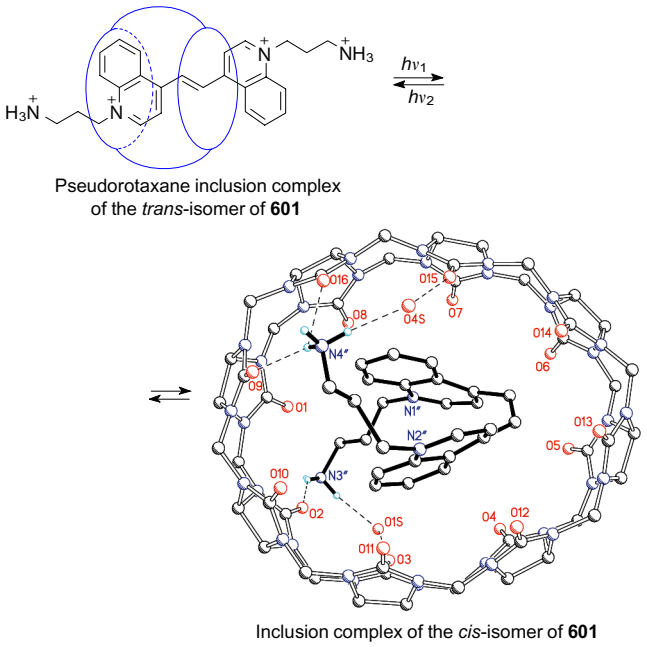


Figure 185. Light controlled supramolecular machine based on pseudorotaxane inclusion complex of bis(quinolyl)ethylene derivative **601** with cucurbit[8]uril.[1633] Published with permission from the Royal Society of Chemistry.

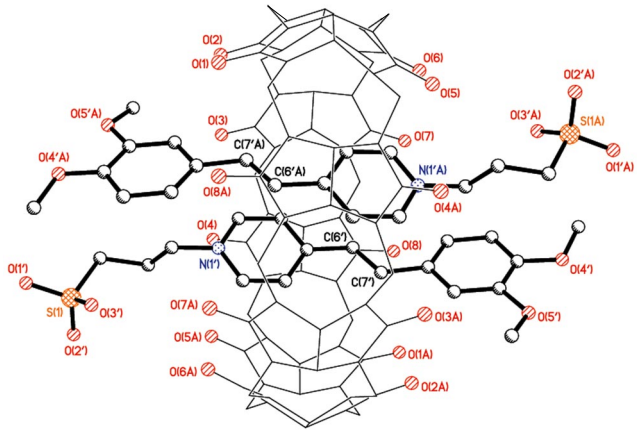
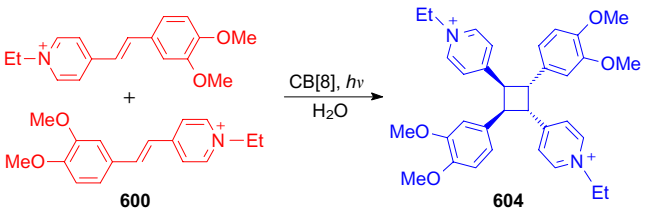


Figure 186. Residence of two molecules of styryl dye **602** in the cucurbit[8]uril molecule in the pseudorotaxane inclusion complex **603**.[1634] Published with permission from Wiley-VCH.

The term assembler is referred to supramolecular machines capable of directing chemical reactions by changing the positions of molecules (*i.e.*, guest molecules are the moving parts of the machine in this case). In the living nature, ribosome represents an example of assembler meant for the synthesis of cellular proteins from amino acids. In our case, the presence of only 5 mol.% cucurbit[8]uril provides for complete stereospecific conversion of the starting styryl dye **600** to cyclobutane derivative **604** on exposure to light (Scheme 93; functioning of the light-controlled supramolecular assembler is shown in Fig. 187).

Thus, using cucurbituril, it is possible to assemble trimolecular pseudorotaxane complexes, perform photo-

Scheme 93



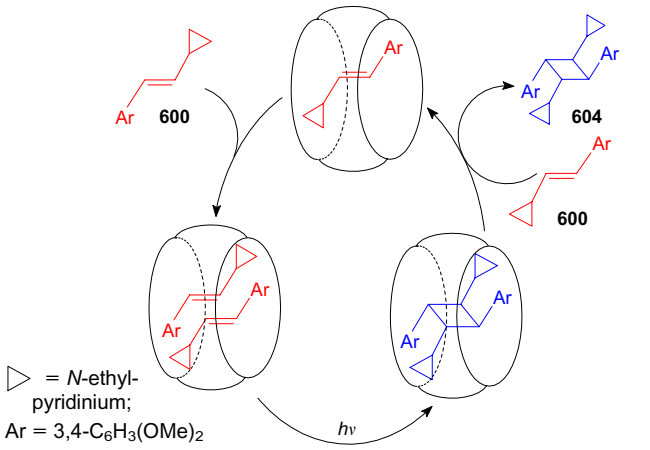


Figure 187. Photocontrolled supramolecular assembler based on cucurbit[8]uril for the assembly of cyclobutane derivatives from styryl dyes.[1634] Published with permission from Wiley-VCH.

cycloaddition reaction in these complexes and repeat this cycle as many times as needed.

In the supramolecular systems considered in this Section, all the main types of photoprocesses are implemented.[1615, 1623, 1626, 1635]

The results imply that unsaturated and macrocyclic compounds form the basis of a molecular meccano of photoactive supramolecular systems, possessing a unique set of required characteristics:[1615]

— availability from the standpoint of organic synthesis,

— tendency to self-organization into diverse supramolecular architectures,

— ability to undergo various types of photochemical reactions depending on the structure,

— capacity for highly efficient molecular photoswitching.

The above characteristics provide the possibility to assemble photoswitchable supramolecular devices, light-controlled supramolecular machines and photoactive supramolecular systems with a specified architecture and diverse properties in solutions, at interfaces and in the solid state.

It is necessary to pay attention to the applied potential of these studies, as they offer a new methodology for the fabrication of materials for supramolecular and nano photonics, which was demonstrated, first of all, by the design of photoswitchable supramolecular devices, light-controlled supramolecular machines, supramolecular switches, optical chemosensor materials and systems for optical data recording and storage.[1623–1626, 1636]

5.2. Dendrimer porphyrin-based supramolecular devices: synthesis and practical applications

Much effort has been made in recent years to develop dendrimer porphyrin-based supramolecular devices that mimic the naturally occurring molecular recognition and directional energy transfer processes.[1637–1647] Analysis of the literature suggests that the dendrimer architecture can serve as a useful tool for tuning the optical properties and reactivity of the dendrimer tetrapyrrole core.[1600, 1648–1651] The use of different dendrons and spacers offers opportunities to vary considerably the diffusion rate of certain types of guest molecules in the bulk of dendrimer shell. Consequently, the accessibility of the core to both the solvent and the guest molecules can vary within several orders of magnitude. This phenomenon can be considered both in terms of both useful shielding and adverse effect that slows down the recognition processes.

It is known that deactivation pathways of excitation energy in tetrapyrrole compounds depend on the nature and state of the coordination centre: whether the ligand contains a metal cation or is in molecular, protonated, or deprotonated forms. The electronic nature of the substituents, steric hindrances and conformational flexibility of the dendrimer branches and tetrapyrrole macrocycle, local changes in the viscosity and polarity of the medium and the accessibility of the coordination centre for molecular oxygen significantly affect the photophysical and spectral characteristics of the porphyrin dendrimer.[1600, 1648–1651]

The unique properties and practical applications of porphyrin dendrimers are determined by the synergistic combination of the 'local chemistry' of the dendrimer periphery and limited accessibility of its tetrapyrrole core. Owing to this structure, these systems are widely used as building blocks for the design of nanoscale systems for selective delivery and prolonged release of broad-spectrum drugs.[14, 1652–1656] The application of the general concept of active core isolation in polyfunctional systems is extremely relevant for the fields at the boundary between chemistry, biology and materials science such as the design of light-harvesting antennas and the development of advanced optoelectronic devices.[1657–1662] This Section addresses methods of controlling the shape, size and optoelectronic properties of porphyrin dendrimers, characteristic features of their self-assembly processes and promising applications, thus illustrating the main trends in the development of the chemistry of these compounds and supramolecular devices based on them.

Scheme 94

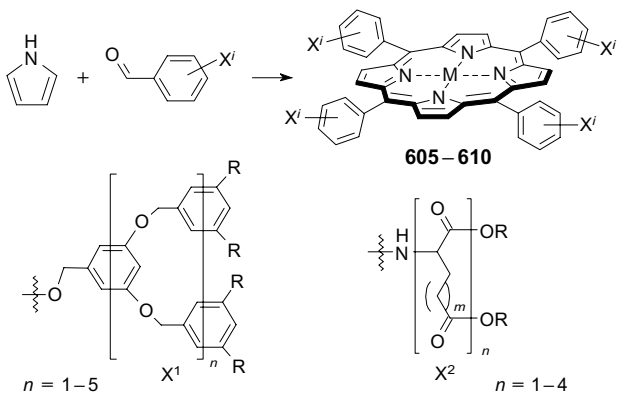


Table 11. Synthesis of homogeneous dendrimers based on tetraarylporphyrins by the convergent method (see Scheme 94).

Compound	X^i	R	M	Ref.
605	4-X^1	OBu^n	2 H	1663
606	3,5-X^1_2	OMe	Zn	1648
607	3,5-X^1_2	CO_2^-	Zn	1648
608	3,5-X^1_2	$C(O)NH(CH_2)_2N^+Me_3$	Zn	1648
609	4-X^2	Me ($m = 0$)	2 H	1650
610	4-X^2	H ($m = 1$)	2 H	1650

5.2.1. Types of porphyrin dendrimers and methods for their synthesis

The first works on porphyrin dendrimers began to appear in the 1990s. At present, the chemistry of porphyrin dendrimers has developed into a separate independent branch of research.[1600, 1648 – 1651] In most cases, the tetrapyrrole macrocycle in such systems acts as the core. However, compounds in which porphyrin molecules are fragments of dendrimer branches have no less interesting properties.[1659, 1661]

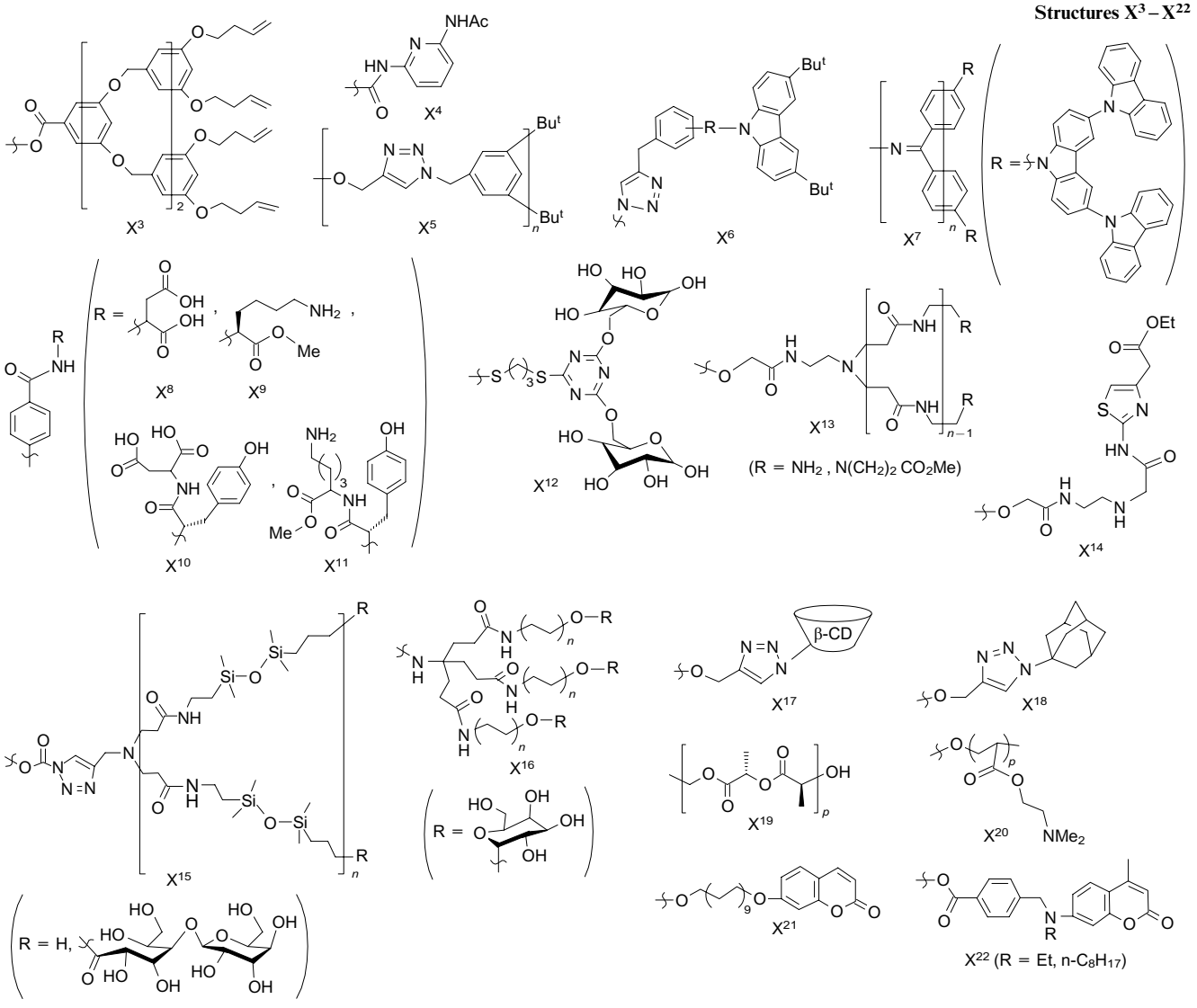
Currently, there are two main strategies for dendrimer synthesis: divergent and convergent approaches. Both approaches consist of iterative sequences of reaction steps, each resulting in the synthesis of one generation layer (*i.e.*, a dendrimer or dendrons of generation G are converted to generation G + 1 macromolecule). In the divergent method, the synthesis is carried out from the centre of the dendrimer towards the outer layer, while in the convergent method, the synthesis proceeds from the periphery towards the centre.

Usually, in the convergent approach, the dendrimer branches of various generations are constructed separately, and the tetrapyrrole core itself is formed in the last step of the synthesis, which is cyclocondensation of pyrrole and an aldehyde containing the dendrimer moieties (Scheme 94, Table 11).§ This method facilitates the purification of compounds due to the pronounced differencen between chromatographic mobilities of key intermediates and target compounds, but loses out in product yields because it strongly depends on the flexibility of the molecular fragments involved in the cyclocondensation forming the dendrimer.[1664]

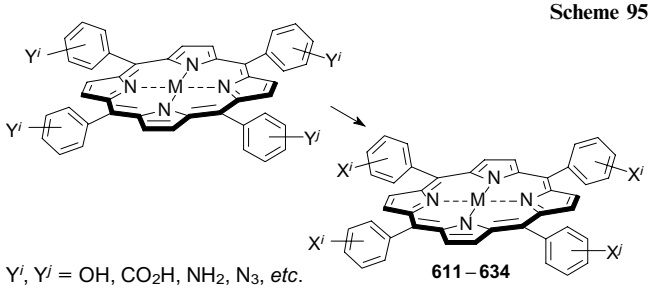
The divergent approach (Scheme 95) implies grafting of dendrimeric branches onto an already formed tetrapyrrole core. The most common reaction centres of porphyrin macrocycles are readily modifiable carboxy, hydroxy, amine, azide or fluoride reaction centres.[1663 – 1677] Por-

§ In this Section, square brackets with a lower index *n* are used in some cases to denote the generation of dendrimers.

Structures $X^3 – X^{22}$



Scheme 95



phyrin macrocycles **611**–**634** with dendrons containing benzyl ether (X^3),[1671] triazole, triazolecarbazole and carbazole (X^5–X^7),[1650, 1666–1668] polyamidoamine (PAMAM) (X^{13}, X^{14}),[1669, 1670] amino acid (peptide) (X^8–X^{11}),[1672] glycol (X^{12}, X^{15}, X^{16}),[1650, 1673–1676] macrocyclic (X^{17}, X^{18}),[1678, 1679] polymeric (X^{19}, X^{20}),[1680, 1681] coumarin (X^{21}, X^{22})[1682, 1683] and other moieties have been synthesized by this method. The divergent method allows consecutive generation of dendrimer branches,[1669] thus creating homogeneous (**611**–**632**: $X^i = X^j$; Table 12) or heterogeneous dendrimers. The latter contain substituents of different nature and can be represented by structures **633** [M = Zn: $X^i = X^1$ (R = OMe, n = 1), $X^j = X^4$][1668] and **634** [M = Zn: $X^i = X^1$ (R = O(CH$_2$CH$_2$O)$_2$Me, n = 1, $X^j = X^2$].[1677]

Supramolecular dendrimers formed by non-covalent interactions were described by Maurer *et al.*[1684] and Concellón *et al.*[1685] In the case of system **635**, dendrimers

Structures 635, 636

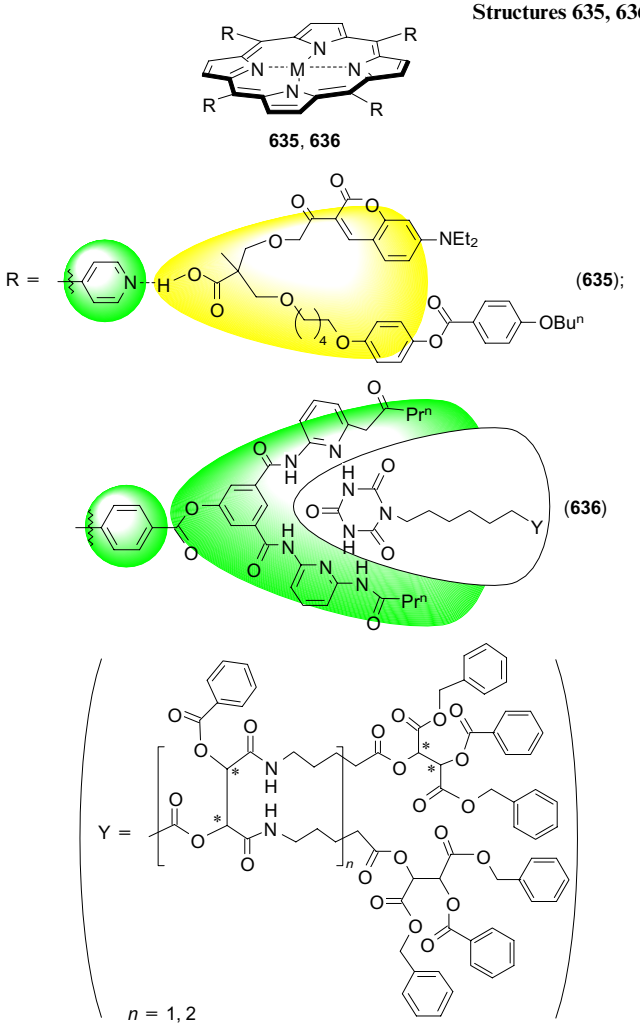


Table 12. Synthesis of homogeneous dendrimers based on tetraarylporphyrins by the divergent method (see Scheme 95).

Compound	(n or the position of R)	M	Ref.
611	4-X^3	Zn	1671
612	3,5-X_2^5 (n = 2)	Zn	1666
613	4-X^6 (4-R, 3,5-R_2)	Zn	1667
614	3,5-X_2^6 (4-R); 2,4,6-Me_3	Zn	1667
615	3,5-X_2^6 (3,5-R_2); 2,4,6-Me_3	Zn	1667
616	4-X^7 (n = 1)	Zn	1668
617	4-X^7 (n = 2)	Zn	1668
618	4-X^8	Zn	1672
619	4-X^9	2 H	1672
620	4-X^{10}	2 H	1672
621	4-X^{11}	Zn	1672
622	4-X^{12}; 2,3,5,6-F_4	Zn	1676
623	4-X^{13} (n = 1, 2)	2 H	1669
624	4-X^{14}	2 H	1670
625	4-X^{15} (n = 1–3)	2 H	1673, 1674
626	4-X^{16} (n = 1, 2)	2 H	1650
627	3,5-X_2^{17}	Zn	1678
628	3,5-X_2^{18}	2 H	1679
629	4-X^{19}	2 H	1680
630	4-X^{20}	Zn	1681
631	3,4,5-X_3^{21}	2 H, Zn, Cu	1682
632	3,5-X_2^{22}	2 H	1683

were obtained due to electrostatic interactions between the peripheral cationic pyridyl groups of *meso*-tetrakis(4-pyridyl)porphyrin (or its Zn complex) with the anionic carboxylate groups of coumarin dendrons.[1680]

In another case, the formation of supramolecular dendrimers involves binding of dendrons to already existing dendritic chains of the tetrapyrrole macrocycle. For example, Maurer *et al.*[1684] synthesized chiral supramolecular dendrimers **636** (M = 2 H) with depsipeptide dendrons containing cyanuric acid moieties as binding sites. Supramolecular porphyrin dendrimers also include tetrapyrrole macrocycles containing dendritic ligands of the same or different nature at the axial positions of the macrocycle coordination centre.[1637] Optimized versions of the considered approaches make it possible to obtain porphyrin dendrimers with various numbers, natures and relative positions of complex dendrimer branches.

5.2.2. Possible practical applications of supramolecular devices based on porphyrin dendrimers

The practical application of porphyrin dendrimers in many cases involves the use of their inner space, *e.g.*, for the encapsulation of a target compound or as a nanoreactor. Consequently, they can act as carriers in the targeted delivery (active or passive) of various biologically active molecules. Porphyrin dendrimers can be used to modify the bioavailability, stability and rate of release of the drugs they carry, thus reducing systemic toxicity and providing the desired therapeutic effect at lower drug doses.[1686–1688]

Another relevant application of porphyrin dendrimers is the design of light-harvesting antennae, which can be useful in artificial photosynthesis systems. In the design of light-harvesting systems, it is necessary to introduce a large number of chromophores into the molecule to form a high effective absorption cross-section. In addition, these chromophores must be spatially organized to facilitate cooperative directed energy transfer.[1689–1692] These requirements

are met by dendrimer structures in which large numbers of porphyrin chromophores are placed at the periphery of dendritic macromolecules and/or in their branches. In this Subsection, the receptor properties of such dendrimers and examples of practical applications of porphyrin dendrimer-based supramolecular devices in biomedicine and design of synthetic light-harvesting antennae are discussed.

5.2.1.1. Recognition and selective binding of substrates of various nature

Porphyrins and their metal complexes are interesting objects of supramolecular chemistry, since they can effectively bind substrates of various nature and form supramolecular assemblies of a high degree of complexity. Chemical modification of the tetrapyrrole macrocycle by dendrimer branches of various generations gives rise to systems with specific properties not observed in small molecules. In such systems, the effects of spatial constraints, encapsulation, and multicentre interactions become decisive. Spatial effects are especially important in cases where communicating cavities or channels are deeply embedded in the dendrimeric environment of the tetrapyrrole macrocycle. Dendrimers can contain a large number of retention cavities, which can actively participate in substrate – receptor interactions.

The receptor capacity of porphyrin-based dendrimers towards various small substrates (guest molecules) is largely determined by the nature and number of generations of dendritic chains, which affect the size and shape of intramolecular cavities above and below the porphyrin core. An increase in generation of the dendrimer, especially in the case of flexible-chain dendrons, leads to the formation of fully or partially closed intramolecular cavities (Fig. 188). An increase in the number of branches at the periphery of the dendrimer makes both the binding of guest molecules and their release through the shell more dfficult. In small dendrimers of the first or second generation, the presence of rigid dendritic chains provides the formation of open intramolecular cavities of a unique shape.

The receptor functions of dendrimers **605**, **606**, the Zn tetraphenylporphyrin core of which contains dendritic branches of several generations based on benzoic acid ester in *meso*-positions of the macrocycle, for 3- and 4-substituted pyridine derivatives caused by substrate coordination on zinc cation were reported by Shinoda *et al.*[1665] The complexing cavity above the coordination centre of the porphyrin cores in these dendrimers (even in the case of fourth-generation dendrimers) is relatively open; nevertheless, the conformational mobility of the dendritic chains in solution has a significant inhibitory effect on the binding of the guest molecule.

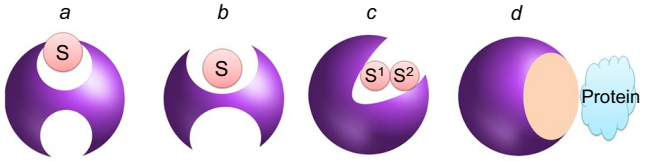
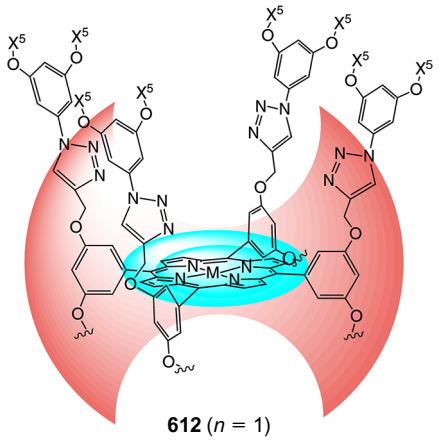


Figure 188. Schematic view of dendrimers (marked in purple) based on Zn porphyrins with closed (*a*) and open (*b*) intramolecular cavities, which can contain substrate molecules (S, S^1, S^2), pocket dendrimers (*c*) and proteo-dendrimers representing hydrophobic dendrimers with a partially hydrophilic surface (shown in beige) (*d*). The figure was created by the authors using data from Refs 1664 – 1679, 1683 – 1698.

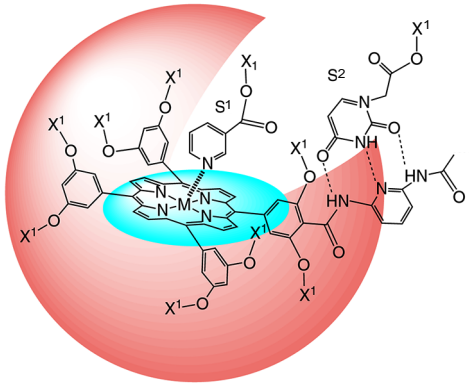
The so-called pocket dendrimers (see Fig. 188 *c*), compounds with asymmetrical arrangement of dendritic branches, possess high selectivity towards small organic molecules. Shinoda and Tsukube[1677] described dendrimer receptors **634**, in which the Zn tetraphenylporphyrin core contained a polybenzyl ether shell of several generations in positions 5, 10 and 15 of the macrocycle. Since one of the *meso*-positions of the tetrapyrrole macrocycle is not substituted, such dendrimers form pockets capable of selective binding of substrates of a particular type, like pyridine and its derivatives. The introduction of the diamidopyridyl moiety into position 20 of the macrocycle enables the dendrimer to accomplish simultaneous selective binding of two guest molecules of different nature, pyridine (S1) and thymine (S2) molecules containing benzoic acid moieties. It was shown that when the pyridine derivative is coordinated to the zinc cation of the reaction centre of tetrapyrrole macrocycle, the corresponding thymine derivative binds to the *meso*-diamidopyridyl moiety through oxygen atoms *via* hydrogen bonding to form complex [**634**(S^1)(S^2)] (see the depicted structure; blue colour highlights the porphyrin core, the dendritic shell is pink).

Kimura *et al.*[1666] synthesized a series of dendrimers **612**, in which the polybenzyl ether shell was linked to the Zn tetraarylporphyrin core through 1,2,3-triazole spacers. In the study of the absorption and fluorescence spectra of dendrimers, the possibility of intramolecular coordination of triazole moieties of the dendron environment by zinc cations was established, with the position of triazole moi-

Structures 612, [634(S^1)(S^2)]



612 (n = 1)

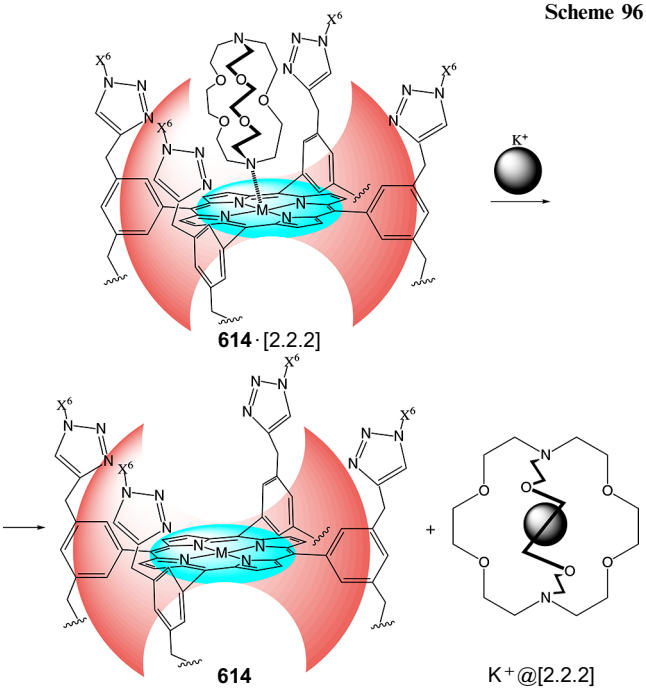


[**634**(S^1)(S^2)]

eties having a strong effect on the stability of intradendrimeric axial complexes. In the case where the porphyrin core is linked to aryl ether dendrons through triazole spacers, a significant increase in the rate of photoinduced electron transfer is observed as compared to that for a similar porphyrin dendrimer, in which there are no triazole moieties. Consequently, the coordination of the triazole moiety provides the transfer of an electron between the Zn porphyrin cores and the peripheral electron acceptors of the dendron environment. Such complexes are good models of natural biosystems involved in photosynthesis, oxygen transport and catalysis.

Dendrimers with triazolecarbazole dendrons **613**–**615** do not exhibit similar intramolecular binding of triazole moiety by the zinc cation of the macrocycle. However, owing to the four rigid-chain carbazole branches, dendrimers **614** and **615** have intramolecular cavities, which provide efficient binding of amine, imidazole and cryptand derivatives, *e.g.*, [2.2.2]cryptand ([2.2.2]).[1693–1695] In the case of cryptands, reversible substrate binding processes are cation-controlled for Li^+, Na^+, K^+ (Scheme 96).[1694, 1695]

Scheme 96



Porphyrin dendrimer **617** containing carbazole moieties shows recognition ability for fullerenes C_{60}, C_{70} and C_{84}.[1668, 1696] In this case, the receptor properties of the dendrimer can be controlled by additional axial coordination of small organic ligands by the metal cation of the reaction centre on the opposite side of the tetrapyrrole macrocycle.

Examples of nanoscale protein receptors include porphyrin dendrimers **618**–**622**, **625**, **626** and **633**, which contain amino acid, peptide or glycol molecules in their dendritic chains.[1663, 1665, 1674–1677] Dendrimer **633** has several key features:[1665, 1677]

— asymmetric distribution of polyanionic heptaglutamine moieties responsible for interactions with the polycationic region on the surface of cytochrome *c*;

— zinc porphyrin core, which functions as a fluorescent signalling device;

— hydrophilic polyether surface to enhance solubility in water;

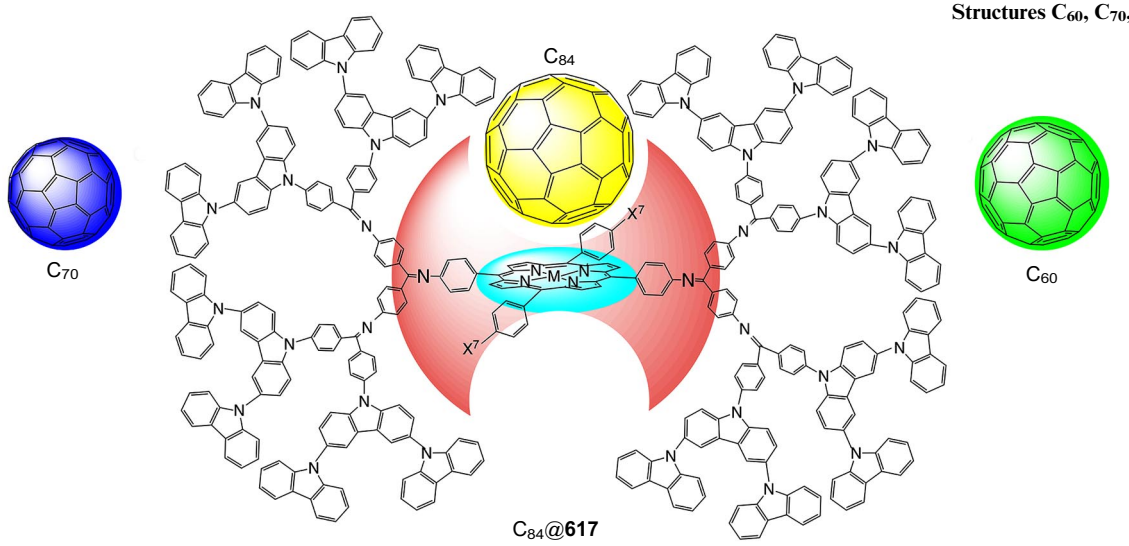
— non-peptide dendritic components providing a peripheral hydrophobic structure.

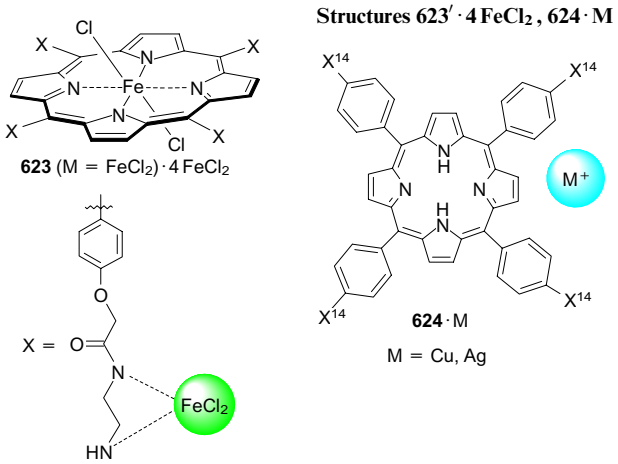
Owing to its structure, dendrimer **633** is able to bind to cytochrome *c* proteins in aqueous medium, and this process is easily detected by quenching of fluorescence of the metal porphyrin core. The aryl ether moieties of the dendrimer do not imply specific interactions with proteins, but they favourably influence the protein–dendrimer interactions.

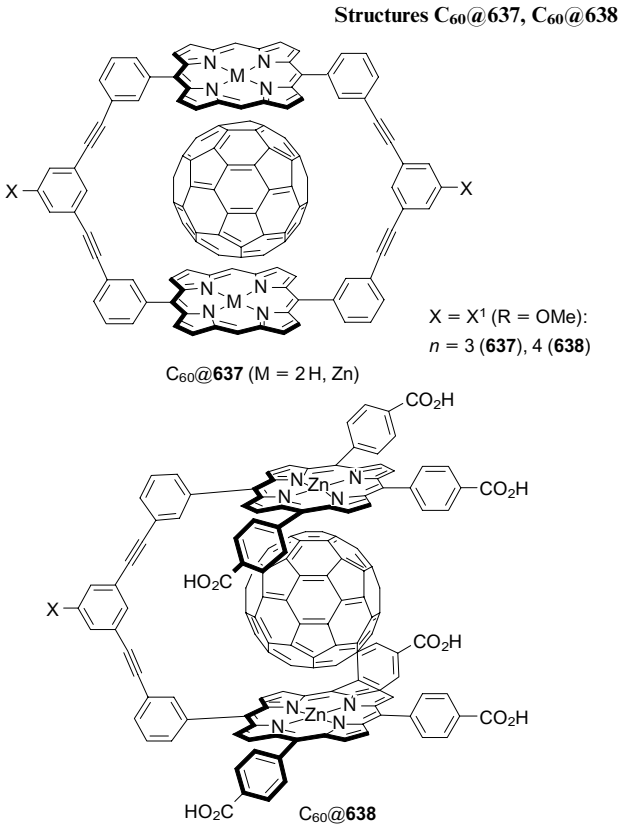
High selectivity towards cytochrome *c* and ferredoxin was shown for dendrimers **618**–**621** containing amino acid and peptide moieties in the dendritic branches.[1677] For example, dendrimers with asparagine and tyrosine units in their dendrons have the highest affinity for cytochrome *c*, whereas ferredoxin binds efficiently to dendrimers with alternating lysine and tyrosine residues in their dendrons. The amino acid moieties provide electrostatic interactions with the complementary protein surface, while the tyrosine moieties are crucial for stimulating protein–protein interactions.

The glycosylated porphyrin dendrimers **622** synthesized by Wang *et al.*[1675] demonstrated the ability to recognize

Structures C_{60}, C_{70}, C_{84}@617







lectin, efficiency of singlet oxygen generation and high thermal sensitivity and selectivity to tumours as photosensitizers for photodynamic therapy (PDT) of cancer.

Ramirez *et al.*[1669, 1670] addressed the receptor properties of porphyrin dendrimers towards metal cations of various nature. It was shown that porphyrin-PAMAM dendrimers of various generations (**623**, **624**) bind Pb^{II}, Cr^{II} and Fe^{II} cations with the retention factor of 99% and bind more than 50% of Co^{II}, Cu^{II}, Cd^{II} and Ag^{I}. It should be noted that in the latter case, the ions are rediced to give metal particles.

The processes of supramolecular self-assembly of porphyrin dendrimers **627**, **628** containing eight cyclodextrin or adamantane moieties (four moieties on each side of the tetrapyrrole macrocycle) to give nanorods were described by Fathalla *et al.*[1678, 1679] The nanorods were formed either from dendrimer **627** due to double-sided binding to fulerene C_{60} molecules or from dendrimers **627** and **628** by complexation of cyclodextrin cavities of one dendrimer and adamantane moieties of the other (Fig. 189).

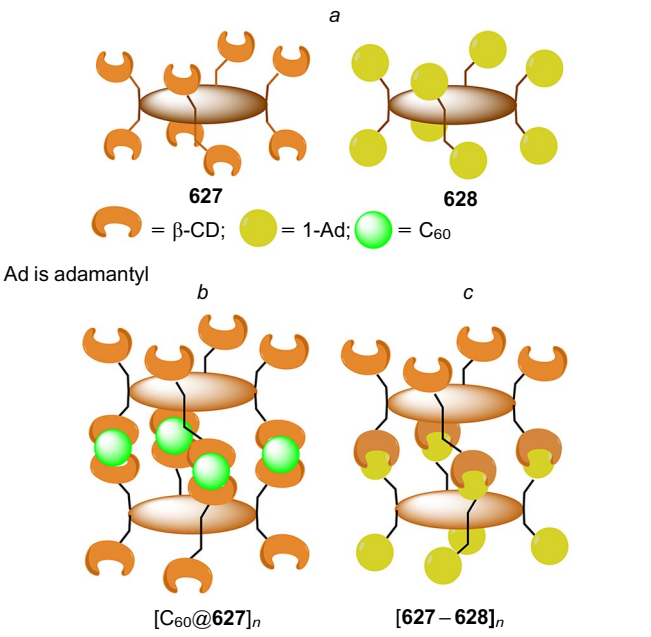


Figure 189. Schematic view of dendrimers **627**, **628** (*a*) and examples of their self-assembly into nanorods with fullerene C_{60} (*b*) and with one another (*c*). The figure was created by the authors using data from Refs 1678, 1679.

Tashiro and Aida[1697] synthesized dendrimer **637**, in which the core of cyclophane dimeric porphyrin is surrounded by a shell based on benzoic acid ester. The incorporation of fullerenes into the interporphyrin cavity in such systems occurs not only due to van der Waals interactions, but also due to π-electron charge transfer from metal porphyrin moieties of the host molecule to the guest fullerene molecules. The receptor ability of the dendrimer towards fullerenes can be tuned by changing the nature of metal cations in the coordination centre of the tetrapyrrole macrocycle.

Tashiro and Aida[1697] also synthesized another type of host dendrimer containing an acyclic zinc porphyrin dimer in the core. It was found that in the presence of fullerenes C_{60} and C_{70}, dendrimer **638** self-organizes into a low-dimensional nanostructure (supramolecular peapod), in which the included fullerene molecules line up along the dendrimer-coated cavity of supramolecular porphyrin nanotube (Fig. 190 *a*). Self-organization of the dendrimer occurs through the formation of hydrogen bonds between the terminal carboxy groups (see Fig. 190 *b*). The nanotube is several micrometres long and 15 nm in diameter.

With the goal of developing photoactive composite materials, Ozawa *et al.*[1698] synthesized dendron-protected porphyrin wires and one-dimensional assemblies (**639**) of gold nanoparticles chemically bound to the wires (Fig. 191).

For this purpose, gold nanoparticles containing 2-(4-pyridyl)ethylsulfanyl and (2-methylundec-2-yl)sulfanyl groups on their surface were deposited using the Langmuir – Blodgett films, which were obtained from π-conjugated Zn porphyrin polymer wrapped into dendron wedges based on benzoic acid ester. It was shown by circular

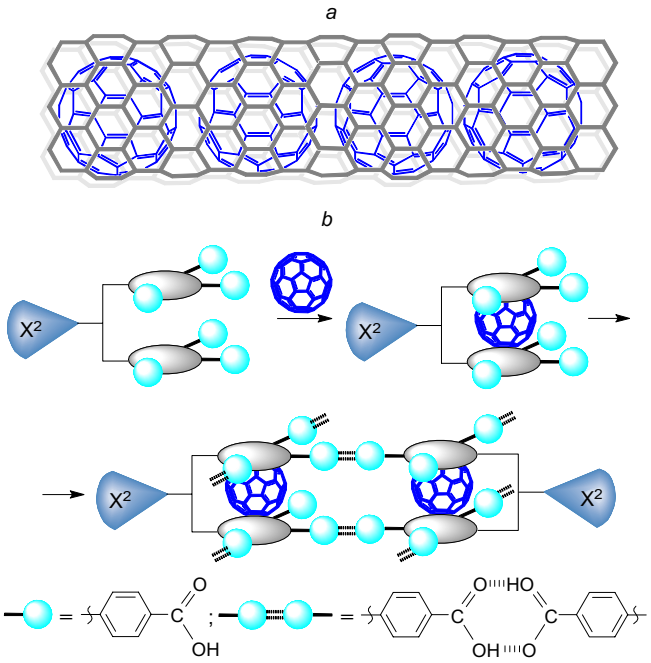


Figure 190. Schematic view of a carbon nanotube containing coordinated fullerene C_{60} molecules (shown in blue) (*a*) and its self-assembly mechanism (*b*). The figure was created by the authors using data from Ref. 1697.

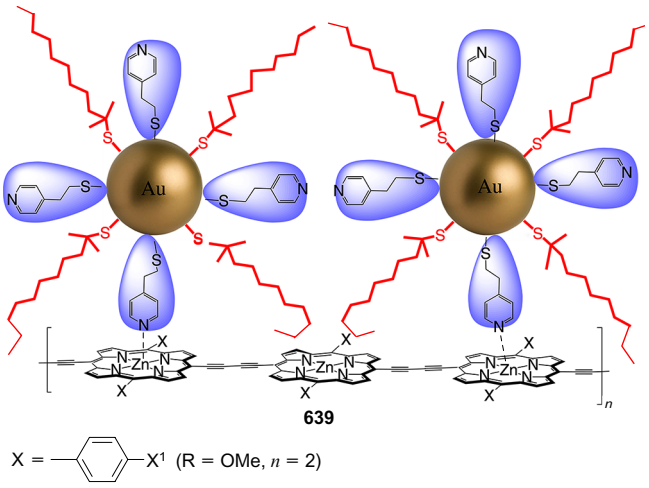


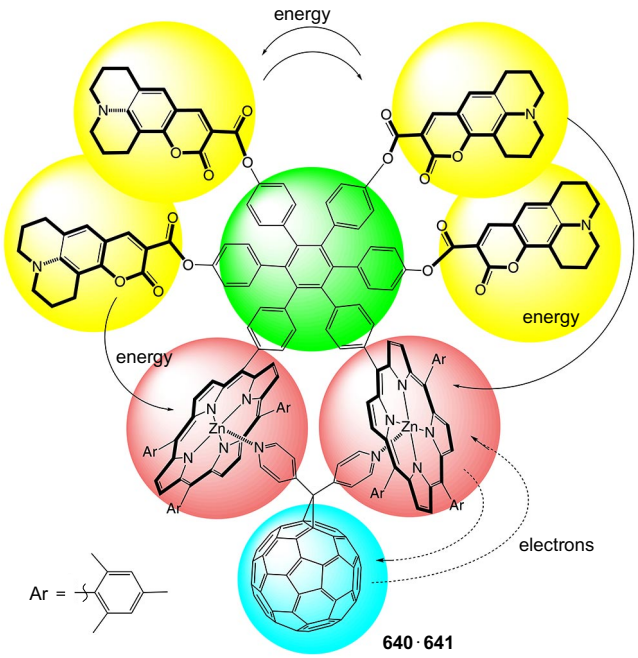
Figure 191. One-dimensional assemblies **639** of gold nanoparticles chemically bonded to dendron-protected porphyrin wires. The figure was created by the authors using data from Ref. 1698.

dichroism that porphyrin dendrimers having 12, 24 and 36 macrocyclic units of the zinc porphyrin complex are capable of recognizing chiral dipyridine.

5.2.2.2. Design of light-harvesting antennae

In the photosynthesis, sunlight is mainly absorbed by antenna chromophores, which transmit singlet excitation energy to reaction centres to convert it into useful electrochemical energy. In fact, for implementation of so-called antenna effect, which is important for biological systems, many chromophore-containing dendrimers have now been developed. Among them, porphyrin dendrimers attract

Structure 640 · 641



particular attention, since natural systems use porphyrin derivatives as light-sensitive pigments.

For the design of porphyrin-containing light-harvesting antennae, Gar *et al.*[1660] obtained molecular hexamer **640**, containing two porphyrin moieties and four coumarin chromophores, located as *para*-substituents in the hexaphenylbenzene backbone. Light absorbed by any of the coumarin moieties of the hexamer is transferred to the porphyrin macrocycle over a period of 1 to 10 ps, depending on the site of initial excitation. The quantum yield of the singlet–singlet energy transfer is 1.0. The rate constants of energy transfer are consistent with the Förster dipole–dipole mechanism. Hexamer **640** containing zinc porphyrin complex moieties is capable of coordinating pyridyl-substituted fullerene **641** with the formation of the **640 · 641** heptamer. It was found that the charge separated state $Por^{\bullet+}-C_{60}^{\bullet-}$ (Por is the corresponding porphyrin) is formed as a result of photoinduced electron transfer with a total quantum yield of 1.0 and decays in a 1,2-difluorobenzene solution with a time constant of 230 ps.

Guo *et al.*[167] synthesized porphyrin dendrimers **632** [R = Et (**a**), n-C_8H_{17} (**b**)] containing eight coumarin moieties, promising for the design of light-harvesting antennae, on the basis of *meso*-tetrakis(3,5-dihydroxyphenyl)porphyrin. Study of the photophysical properties of these dendrimers in dichloromethane solution and in thin films revealed intramolecular energy transfer from coumarin units to the porphyrin core. Comparison of the optical properties of dendrimers showed that the energy transfer efficiency is higher for compound **632b** both in the solid film and in solution. This can probably be explained by the presence of a longer octyl side chain in this dendrimer, which improves the solubility of the dendrimer and, as a consequence, prevents the self-quenching of the coumarin moieties. Dendrimers **632a**,**b** emit red light with higher fluorescence quantum yields compared to that of the parent porphyrin.

Fujumoto *et al.*[1661] devised supramolecular light-harvesting devices that mimic the chromophores of plant

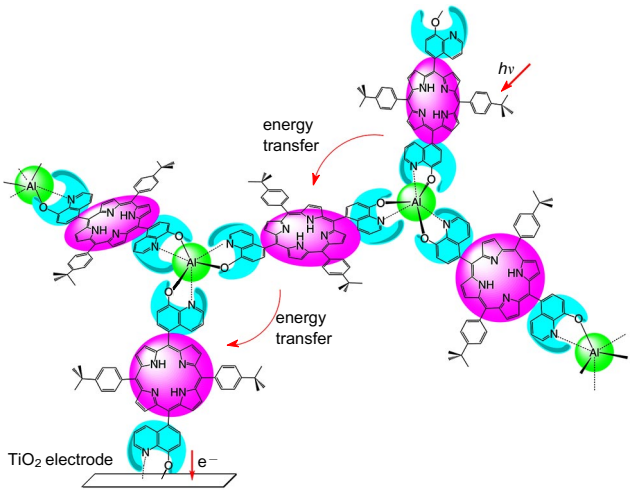
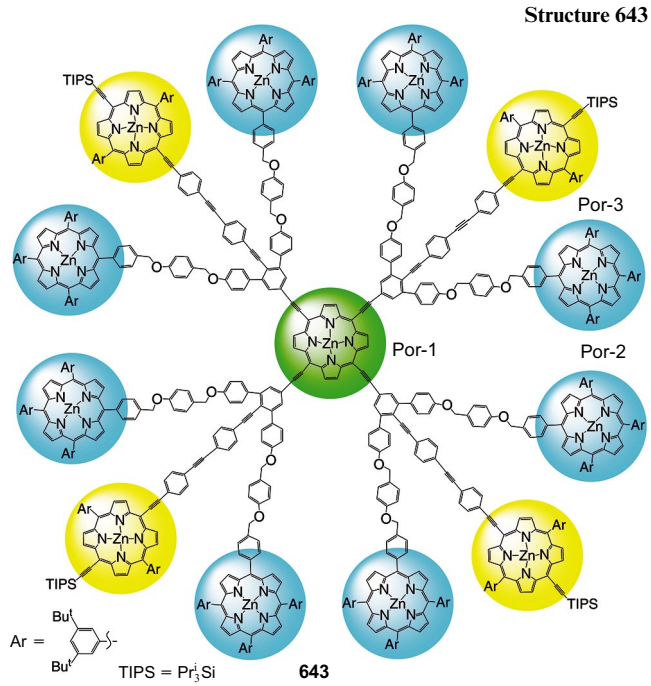


Figure 192. Schematic view of the structure of supramolecular light-harvesting antennae based on metal-coordinated bis(8-hydroxyquinoline)-substituted porphyrin dendrimers **642**.[1661]

antennae on the basis of metal-coordinated bis(8-hydroxyquinoline)- substituted porphyrin dendrimers **642** (Fig. 192). It was found that the generated photocurrents in the obtained supramolecular light-harvesting antennae can be optimized according to two methods of self-assembly of porphyrins owing to the antenna effect — a change in the number of collected porphyrin monolayers and the number of generations of metal-coordinated porphyrin dendrimers. In the former self-assembly method, one side of the 8-hydroxyquinoline moiety of porphyrin is adsorbed on the TiO_2 electrode, and the other one is used to form metal-coordinated porphyrin networks (type *I*). The latter method involves preliminary preparation of metal-coordinated porphyrin dendrimers and their subsequent adsorption on a TiO_2 electrode (type *II*). Type *I* is adsorbed on TiO_2 by the central porphyrin block, while type *II* is adsorbed by the terminal porphyrin moieties. Quantum chemical calculations established that the effect of the light-harvesting antenna is most significant when the distance between the porphyrin centres of the dendrimer is 16 Å. It was shown that intermolecular interactions of porphyrin moieties in the seventh generation dendrimer lead to a significant decrease in the photocurrent.

Light-harvesting antenna **643**, containing three sorts of porphyrins with different numbers of ethynyl groups in the *meso*-positions of macrocycles (Por-1, Por-2 and Por-3, highlighted in green, blue and yellow, respectively) was synthesized by Uetomo *et al.*[1699] Antenna **643** exhibits intense absorption across the entire visible spectrum (up to 700 nm). It was found that energy transfer from the singlet excited state occurs from the peripheral porphyrin moieties (Por-2 and Por-3) to the central moiety (Por-1) with an efficiency of >90% and rate constants of the order of 10^{10} s^{-1}. Considering the fact that benzyl groups in antenna **643** can be easily replaced by other dendritic structures, this approach may be promising in terms of the design of light-harvesting snowflake-like antennas with a large number of chromophores of various natures.

The method of electrostatic self-assembly can be effectively used to form pH-sensitive aggregates of porphyrin dendrimers in water on the basis of cationic porphyrin, tetrakis(4-tetramethylammoniophenyl)porphyrin (TAPP),



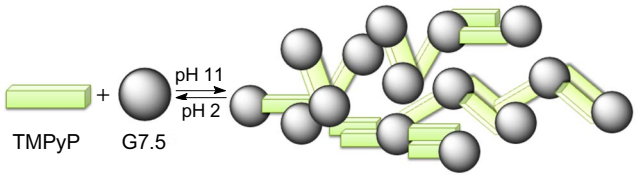


Figure 193. Schematic view of the formation of [TAPP-G7.5] aggregate formation. The figure was created by the authors using data from Ref. 1700.

and anionic dendrimer, poly(amidoamine) with ethylenediamine core (G7.5) (Fig. 193).[1700]

It was found that, depending on the pH of the environment, the resulting dendrimers form J- or H-aggregates,

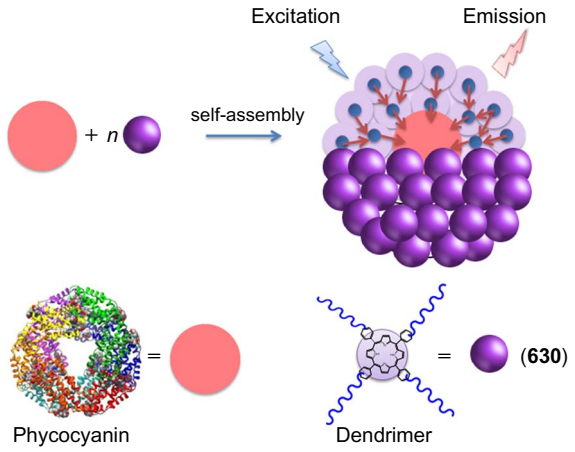


Figure 194. Schematic view of the electrostatic self-assembly of the phycocyanin scaffold protein and the star-shaped dendrimeric porphyrin **630** into a garnet-like light-harvesting nanosystem. The figure was created by the authors using data from Ref. 1681.

which are characterized by a high fluorescence quantum yield and exhibit the ability to generate singlet oxygen under visible light irradiation. Using the model photocatalytic oxidation of an anionic dye, methyl orange, it was shown that J-aggregates of the porphyrin dendrimer [TAPP-G7.5] exhibit a 1.5-fold higher ability to generate singlet oxygen than H-aggregates and can be used as light-harvesting systems for the conversion of solar energy.

Liu *et al.*[1681] performed electrostatic self-assembly of star-shaped dendrimer porphyrin **630** with poly[2-(dimethylamino)ethyl methacrylate] moieties and phycocyanin, directed by this scaffold protein to obtain a micelle-like hybrid core – shell light-harvesting nanosystem. It consists of a centrally located acceptor (phycocyanin) and multiple donors (porphyrins) in the shell (Fig. 194). The specific garnet-like structure of the nanosystem ensures efficient transfer of excitation energy (~80.1%) from 179 porphyrin donors to a single phycocyanin acceptor. This regular multidonor and single-acceptor structure is similar to the natural light-harvesting system of plants and could be useful for creating a biomimetic high-efficiency light-harvesting antenna with a high donor-to-acceptor ratio.

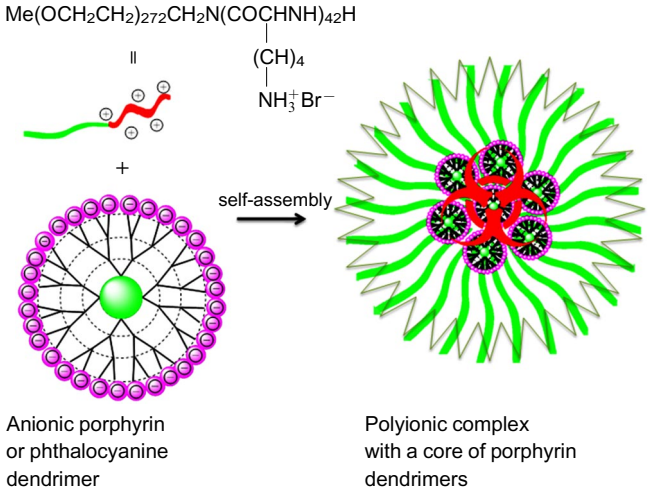


Figure 195. Scheme of the formation of supramolecular micelles, polyionic complexes of porphyrin and phthalocyanine dendrimers.The figure was created by the authors using data from Refs 1706 and 1707.

5.2.2.3. Biomedical applications

Due to their unique photophysical properties (fluorescence emission, large absorption cross section, photosensitizing ability, *etc.*), porphyrins are widely used as photofunctional nanodevices.[14, 1652 – 1656, 1673, 1680, 1701 – 1714] When excited by light they can fluoresce or transfer their excitation energy or electron to an appropriate acceptor molecule. This unique property makes porphyrins useful for the study of microenvironments and for the use as photosensitizers in PDT. However, since porphyrins are hydrophobic and capable of strong π-conjugation, they often form aggregates. Aggregated porphyrins lose their photofunctional properties with time.[1675] Meanwhile, the dendrimeric forms of these molecules are soluble in an aqueous medium due to the large number of anionic functional groups on the shell surface. In addition, large dendritic wedges efficiently prevent aggregation. The high solubility of porphyrin dendrimers allows their use in PDT for the treatment of cancer. This method consists in the systemic administration of photosensitizers followed by irradiation of the target tissue with laser light. Irradiation excites photosensitizers, which transfer their excitation energy or electrons to oxygen molecules in the target tissue to generate highly toxic reactive oxygen species, which ultimately destroy tumour cells.

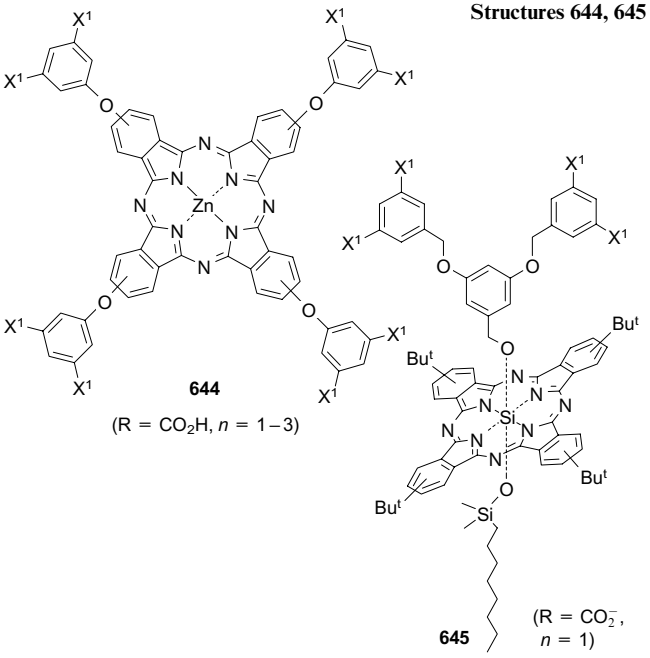
The ionic surfaces of porphyrin dendrimers are effectively used to form micelles of polyionic complexes *via* electrostatic interactions. Experiments *in vitro* and *in vivo* have shown that micelles of polyionic complexes can be successfully used for PDT. The inclusion of dendrimer molecules into spherical polyionic micelles increases their ability to selectively accumulate in tumour tissue due to the effect of increased permeability and retention. Immobilization of the dendrimer into a micelle almost completely eliminates aggregation, which leads to an increase in the generation of singlet oxygen.

It was shown[1706, 1707] that zinc porphyrin dendrimers with ionic surfaces can be successfully used as a new class of photosensitizers for PDT. Experiments using Lewis lung carcinoma (LLC) cells demonstrated that porphyrin dendrimers **607** and **608** can be absorbed by LLC cells and ultimately localize in organelles separated by a membrane. Upon photoirradiation, positively charged dendrimer **608** exhibits a higher photosensitizing ability (by several orders of magnitude) compared to protoporphyrin IX, which is commonly used for PDT. The effect of negatively charged dendrimer **607** is much less pronounced than that of compound **608**, probably due to electrostatic repulsion between the CO_2^- groups of porphyrin and negatively charged cell membranes. Dendrimer **607** exhibits a lower propensity for cell association than dendrimer **608**. Both porphyrin dendrimers have much lower dark toxicity to cells than protoporphyrin IX. It was also found that the inclusion of dendrimer **607** in the micelle of the polyionic complex (PIC) (Fig. 195) obtained by mixing this porphyrin with a positively charged block copolymer (for example, poly(ethylene glycol) – poly(L-Lys)) increases its cellular uptake 6 – 8-fold. PIC micelles are very stable even at high salt concentrations, but they are sensitive to changes in pH (they can be easily destroyed in the weakly acidic environment of tumour tissues). Approximately 38 molecules of dendrimer **607** are clustered within the micelle, but they do not cause fluorescence quenching even after the PIC micelles are absorbed by the cells. This unique photochemical property is provided by the insulating effect of the large dendrimer shell.

Conventional porphyrin derivatives absorb light at wavelengths between 400 and 600 nm, and *in vivo* excitation of porphyrin derivatives is hindered by skin tissues. For this reason, zinc phthalocyanine dendrimer **644**, which absorbs light at a longer wavelength than its porphyrin analogues, was used as a potential photosensitizer for PDT.[1704 – 1707]

This dendrimer can also be applied as a sensitizer in photochemical technologies that use light to facilitate the delivery of DNA, drugs and other biologically active species directly inside cells.[1648] In this case, plasmid DNA packed with cationic peptides (Fig. 196) is surrounded by anionic phthalocyanine dendrimers. The endocytic uptake of such ternary complexes by polarized cells results in their predominant localization in endosomes and lysosomes. Upon photoirradiation, dendrimer **644** generates $^1O_2$ which disrupts endosomal-lysosomal membranes and releases a ternary complex suitable for DNA transport.

Structures 644, 645



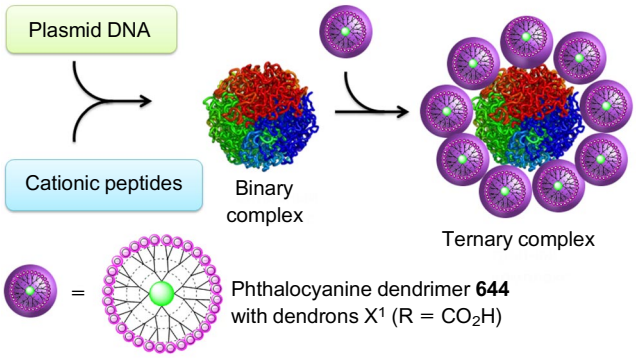


Figure 196. Scheme of the formation of a ternary complex by electrostatic self-assembly of plasmid DNA, cationic peptides and anionic phthalocyanine dendrimer **644**. The figure was created by the authors using data from Ref. 1648.

Herlambang *et al.*[1708] obtained a spherical micelle based on self-organizing Si phthalocyanine **645** having a hydrophobic part and containing a bulky hydrophilic polyaryl ether dendritic moiety with terminal carboxy groups as one of the axial ligands. It was shown by gel permeation chromatography and electron microscopy that a micelle is formed in highly dilute solutions, and, depending on the pH of the medium, it can move between the aqueous and organic phases, capturing the hydrophobic molecules present in the solution. Thus, when acetic acid is added to an aqueous solution containing a micelle, the micelle is destroyed and dendrimer **645** is extracted into the organic phase (Fig. 197). When an excess of KOH solution is added to the resulting two-phase system, the dendrimer returns back to the aqueous phase with the formation of the initial micelle. The latter can be used as a molecular capsule for pH-dependent binding, transfer across the interface and release of substances. The presence in the considered micelle of phthalocyanine moieties exhibiting photo and redox activity makes it promising for PDT of cancer.

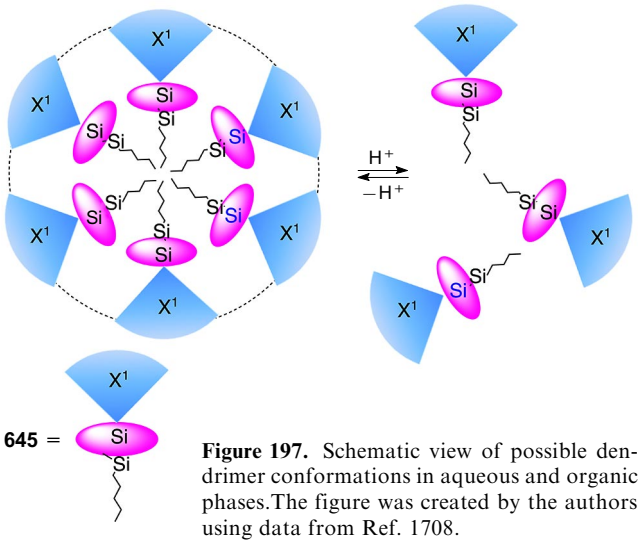
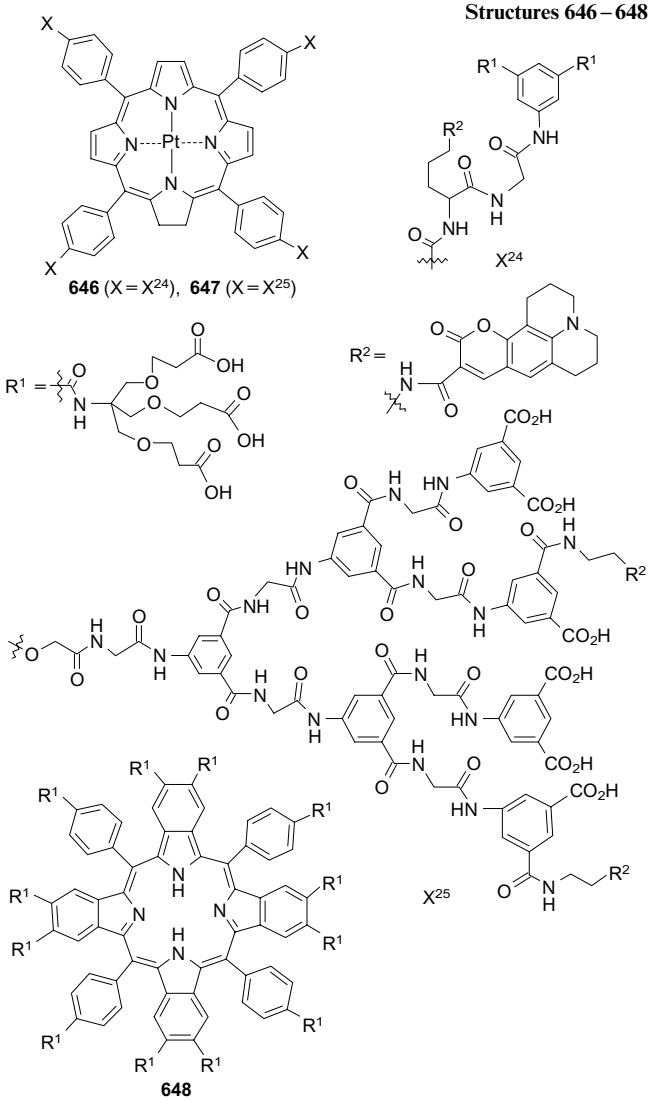


Figure 197. Schematic view of possible dendrimer conformations in aqueous and organic phases.The figure was created by the authors using data from Ref. 1708.

It is known [1680, 1709] that Pd^{II} and Pt^{II} porphyrin complexes exhibit phosphorescence in an inert atmosphere. Phosphorescent dyes based on Pt and Pd porphyrins, traditionally used as phosphors in biological oxygen measure-

Structures 646 – 648



ments, exhibit extremely low two-photon absorption cross sections. Brias *et al.*[1680] developed a nanosensor for the detection of molecular oxygen. The central component of the design of this sensor is polyfunctional Pt porphyrin (compound **646**) with strong emission in the triplet state at ambient temperature, which occurs in the near infrared region. Chromophores (in particular, coumarin) are chosen in such a way that their absorption is maximum in the near-IR region and their fluorescence bands overlap with the absorption bands of meta porphyrin, which is necessary to ensure effective antenna–core resonance. The metal porphyrin antenna structure is embedded into a protective dendritic shell, which isolates the core from interaction with biological macromolecules, controls oxygen diffusion and makes the entire sensor water-soluble. A pair of coumarin-343 and a Pt complex of *meso*-tetrakis(4-alkoxyphenyl)porphyrin (**647**) was used to create a probe in which the antenna moieties were linked to the core by polyarylglycine dendrons.[1710] Dendrons, forming an insulating layer between porphyrin and the antenna, simultaneously control the rate of fluorescence quenching by oxygen (Stern–Volmer quenching constant). Modification of the dendrimer periphery with oligoethylene glycol residues makes the probe signal insensitive to the presence of proteins and other macromolecular solutes.

The dependence of fluorescence of porphyrin ligands on the protonation or deprotonation of nitrogen atoms of the macrocycle coordination centre was used to develop polyesteramide (**610**, M = 2 H, n = 4) and polyglutamate dendrimers (**648**) for pH detection in biological systems.[1711]

The polyesteramide (**610**, M = 2 H, n = 4) and polyglutamate (**648**) dendrimers form an effective indicator pair for proton gradient determination.[1711] Peripheral groups with charges on the dendrimers ensure complete membrane impermeability of the synthesized indicators. This was demonstrated by placing porphyrin dendrimers with two spectroscopically different cores inside and outside the phospholipid vesicles and independently determining the pH of the medium in both moieties using bulk spectroscopic measurements (Fig. 198). In the selective arrangement of dendrimers **610** and **648** inside and outside the phospholipid vesicles, respectively, only the fluorescence spectra of the outside dendrimers **648** respond to changes in pH of the medium caused by the addition of acid or base to the solution. In the presence of the channel-forming peptide

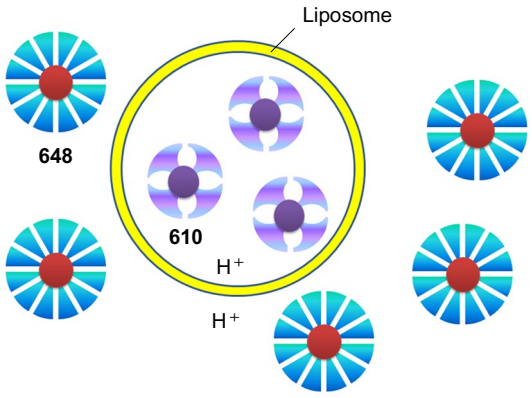


Figure 198. Phospholipid liposome (yellow rim) with trapped dendrimers **610** inside and dendrimers **648** left outside. The figure was created by the authors using data from Ref. 1711.

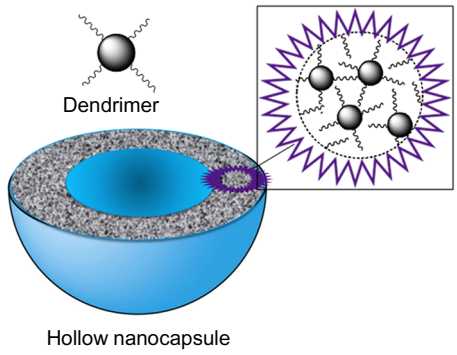


Figure 199. Schematic view of nanocapsules with a thickness of 19 nm and a cavity radius of 35 nm formed by dendrimers **629**. The figure was created by the authors using data from Ref. 1712.

gramicidin, however, both dendrimers respond to changes in pH, which is reflected in their absorption and fluorescence spectra.

Hsu *et al.*[1712] described the synthesis and structure of hollow nanocapsules (vesicles) formed by self-assembly of dendrimeric four-arm porphyrins **629**, in which the role of arms is played by polylactic acid (PLLA) moieties. These nanocapsules (Fig. 199) can be used as a new stable platform for ultrasound imaging and selective drug delivery to the sites of their functioning. In particular, nanocapsules filled with doxorubicin showed high efficiency in chemotherapy and photodynamic therapy of cancer.[1713]

Multifunctional nanocapsules were obtained by layer-by-layer self-assembly of anionic porphyrin dendrimer **607** in the presence of polyallylamine hydrochloride on negatively charged polystyrene nanoparticles followed by removal of the polystyrene matrix (Fig. 200).[1714] They showed high efficiency as a means of delivery of anticancer drugs in combination therapy of cancer.

The surveyed examples demonstrate that due to their unique receptor and photofunctional properties, porphyrin dendrimers can be successfully used as supramolecular devices for targeted drug delivery and prolonged drug release, effective photosensitizers for PDT and artificial

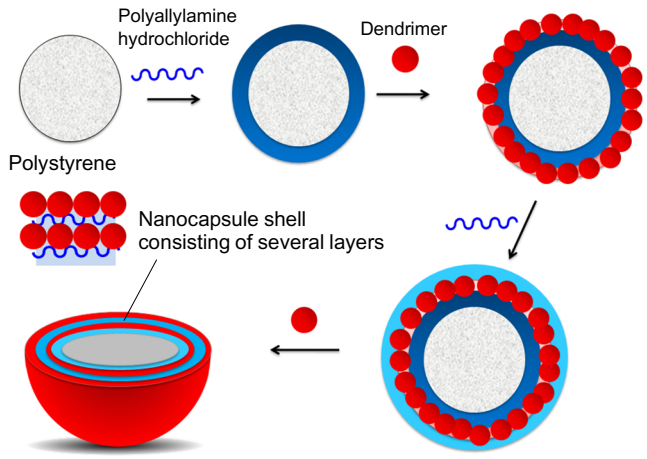


Figure 200. Scheme of layer-by-layer self-assembly of anionic porphyrin dendrimer **607** (M = Zn, n = 2) in the presence of polyallylamine on negatively charged polystyrene nanoparticles. The figure was created by the authors using data from Ref. 1714.

light-harvesting antennas with a spatial organization of porphyrin chromophores enabling joint directed energy transfer. Further development of this field of research will certainly provide new opportunities for the design of efficient polyfunctional nanomaterials for optoelectronics and biomedicine.

6. Conclusion

In conclusion, we would like to note that the prospects of application of functional supramolecular materials based on various molecular platforms would certainly be expanded in the near future. This line of research will affect more and more fields of modern technology, medicine and materials science. Ordering and self-assembly of molecular building blocks result in the spontaneous formation of supramolecular structures by means of weak non-covalent interactions between them. The diversity of these structures is restricted only by chemist's imagination and ability to synthesize the conceived molecules with atomic precision.

Targeted control over intermolecular interactions enables supramolecular engineering of molecular assemblies, crystals, polymers, *etc*.; this promotes the development of supramolecular materials science. These dynamic assemblies often behave as living polymers, which are able to grow and shorten, restructure their motifs, exchange components, undergo annealing, self-heal and adapt. Even now, the use of principles of supramolecular engineering makes it possible to propose elegant approaches and elements of technologies of control over nanoobjects and nanoparticles. The implementation of these techniques is expected to induce revolutionary changes in almost all branches of industry and in everyday life of people, for example, in quantum electronics and photonics; in the fabrication of nanoporous electrodes in supercapacitors, storage batteries and solar cells; and in the development of nanosensors and smart coatings, which change their properties depending on the external conditions.

The diversity of functional supramolecular systems and their properties depicted in this review demonstrates fantastic opportunities for using these systems in the bottom-up design of self-assembled materials and devices that function according to molecular recognition and multipoint binding principles.

Section 2.1 of the review (written by Yu.G.Gorbunova, A.G.Martynov, P.A.Stuzhin, A.Yu.Tsivadze) was prepared with the financial support of the Russian Science Foundation (RSF) (Project Nos 19-13-00410, 20-13-00285); Section 2.2 (written by A.S.Ovsyannikov, S.E.Solov'eva, I.S.Antipin) was supported by RSF (Project No. 19-73-20035) and by the Russian Foundation for Basic Research (RFBR) (Project No. 19-03-00519); Section 2.3 (written by A.S.Potapov, V.P.Fedin) was supported by RSF (Project No. 19-73-20087); Section 2.4 (written by Ya.Z.Voloshin, S.V.Dudkin) was supported by RSF (Project No. 16-13-10475) and by RFBR (Project Nos 18-03-00675, 19-03-00357); Section 2.5 (written by V.S.Korenev, M.N.Sokolov) was supported by RFBR (Project No. 19-43-543037); Section 2.6 (written by S.N.Shtykov) was supported by RSF (Project No. 21-13-00267); Section 3.1 (written by V.A.Burilov, S.E.Solov'eva, I.S.Antipin) was supported by RSF (Projects No. 18-73-10033, No. 19-13-00095); Section 3.2 (written by V.V.Arslanov, M.A.Kalinina, S.L.Selektor) was prepared with the support of the Ministry of Education and Science of the RF (Grant for large research projects in the priority areas of the science and engineering development, agreement No. 075-15-2020-782), RSF (Projects No. 17-73-20268, No. 20-13-00279) and RFBR (Project No. 18-29-04026-mk); Section 3.3 (written by M.A.Shcherbina, S.N.Chvalun) was supported by RSF (Project No. 19-73-20236); Section 3.4 (written by R.R.Kashapov, L.Ya.Zakharova) was supported by RSF (Project No. 19-73-30012); Section 3.6 (written by L.S.Yakimova, I.I.Stoikov) was supported by RFBR (Project Nos 18-03-00315, 20-03-00816) and by RF President Grant (NSh-2499.2020.3); Section 3.7 (written by M.A.Ziganshin, V.V.Gorbachuk) was prepared using the subsidy granted to the Kazan Federal University to perform the state assignment in the field of scientific activity (Project No. 0671-2020-0061); Section 4.1 (written by Yu.V.Fedorov, O.A.Fedorova) was supported by RFBR (Project Nos 19-03-00535, 19-03-00625); Section 4.2 (written by S.Yu.Zaitsev) was supported by an RSF grant (Project No. 20-16-00032, subsections 4.2.1 and 4.2.2) and an RFBR grant (Project No. 19-03-00717, subsection 4.2.3); Section 4.3 (written by A.R.Mustafina, S.V.Fedorenko) was prepared using the subsidy granted to the Federal Research Center 'Kazan Scientific Center of the Russian Academy of Sciences' to perform the state assignment in the field of scientific activity (reg. No. AAAA-A18-118041760011-2); Section 4.4 (written by P.L.Padnya, I.I.Stoikov) was supported by RFBR (Project Nos 18-03-00315, 18-33-20148) and by RF President Grants (MK-12.2020.3 and NSh-2499.2020.3); Section 4.5 (written by E.V.Suslov, K.P.Volcho, S.Z.Vatsadze) was supported by RSF (Project No. 19-73-20090); Section 4.6 (written by D.N.Shurpik, I.I.Stoikov) was supported by RFBR (Project Nos 18-03-00315, 18-33-20148) and by RF President Grant (NSh-2499.2020.3); Section 5.1 (written by M.V.Alfimov, S.P.Gromov, E.N.Ushakov) was supported by RSF (Project No. 19-13-00020); Section 5.2 (written by G.M.Mamardashvili, N.Zh.Mamardashvili, O.I.Koifman) was supported by RSF (Project No. 19-73-20079) and performed within the state assignment (subject No. FZZW-2020-0008).

7. List of acronyms and abbreviations

234-BSA-Na* — sodium 2,3,4-tris(11-methacryloylundecyloxy)benzenesulfonate,
Abu — (*S*)-2-aminobutyric acid,
ADMET — absorption, distribution, metabolism, excretion and toxicity,
ADP — adenosine diphosphate,
AFM — atomic force microscopy,
Ala — alanine,
AMPA — α-amino-3-hydroxy-5-methylisoxazole-4-propionic acid,
APTES — (3-aminopropyl)triethoxysilane,
Asc — ascorbate,
ATP — adenosine triphosphate,
BCLC — bent-core liquid crystals,
BD — butadienyl dye,
α-BGT — α-bungarotoxin,
BLG — β-lactoglobulin,
BNP — branched-shaped nanoparticle,
Boc — *tert*-butoxycarbonyl,
bpa — 1,4-bis(4-pyridyl)acetylene,
bpp — 1,3-bis(4-pyridyl)propane,
bpy — 4,4′-bipyridine,

BR — bacteriorhodopsin,
BSA — bovine serum albumin,
15C5 – 15-crown-5 ether,
9C3 – 9-crown-3 ether,
C12 – 1,8-diaminoanthraquinone modified with two [(acetylamino)methyl]diethoxyphosphoryl groups and two dodecyloxy groups,
CA — contrast agent,
CAC — critical aggregation concentration,
CB[7] — cucurbit[7]uril,
CB[8] — cucurbit[8]uril,
CD — circular dichroism (Section 2.4),
CD — cyclodextrin (Sections 3.4 – 3.6, 4.1, 4.2)
CMC — critical micelle concentration,
Cp — cyclopentadienyl,
CTB — charge transfer band,
CTAB — cetyltrimethylammonium bromide,
CuAAC — copper catalyzed azide – alkyne cycloaddition,
CUC — crown-containing unsaturated compounds,
CUR — curcumin,
DABCO — 1,4-diazabicyclo[2.2.2]octane,
DCC — dicyclohexylcarbodiimide,
DEDC — 1-(3-dimethylaminopropyl)-3-ethylcarbodiimide,
DEF — diethylformamide,
DiO — 3,3′-dioctadecyloxacarbocyanine perchlorate,
DLS — dynamic light scattering,
DMT-MM — 4-(4,6-dimethoxy-1,3,5-triazin-2-yl)-4-methylmorpholinium chloride,
DNAP —DNA polymerase,
DODA — dimethyldioctadecylammonium,
DOX — doxorubicin,
dpni — *N*,*N*′-di(4-pyridyl)naphthalene-1,4,5,8-tetracarboxydiimide,
DPPC — dipalmitoylphosphatidylcholine,
EDC — 1-(3-dimethylaminopropyl)-3-ethylcarbodiimide,
EDD — electron density distribution,
Fmoc — 9-fluorenylmethyloxycarbonyl,
FRET — Förster resonance energy transfer,
FT-IR — Fourier transform infrared spectroscopy,
GA — polymeric gallic acids,
Gly — glycine,
GO — graphene oxide,
H_2ataia — 5-[(4,6-diamino-1,3,5-triazin-2-yl)amino]-isophthalic acid,
H_2bdc — benzene-1,4-dicarboxylic acid,
H_3tdc — benzene-1,3,5-tricarboxylic acid,
H_2dobdc — 2,5-dihydroxybenzene-1,4-dicarboxylic acid,
H_2DPP — dodecaphenylporphyrin,
H_2gly — 1,2-diols,
H_2ip — isophthalic acid,
H_2mpba — 4-(1*H*-3,5-dimethylpyrazol-4-yl)benzoic acid,
H_2ndc — naphthalene-2,6-dicarboxylic acid,
H_2obb — 4,4′-oxybis(benzoic) acid,
HOBT — 1-hydroxybenzotriazole,
HP-β-CD — hydroxypropyl-β-cyclodextrin,
H_2PzC — 1*H*-pyrazole-4-carboxylate,
H_3tatb — 4,4′,4″-*s*-triazine-2,4,6-triylbenzoic acid,
H_2TCPP — *meso*-tetrakis(4-carboxyphenyl)porphyrin,
H_2tdc — thiophene-2,5-dicarboxylic acid,
H_2TSPP — *meso*-tetrakis(4-sulfophenyl)porphyrin,
Heim — 2-ethylimidazole,
hBN — hexagonal boron nitride,
Hep-2 — human laryngeal adenocarcinoma cell line,
HCV — hepatitis C virus,
HCVpp / VSVGpp — hepatitis C virus pseudo particles,
HepG2 — human hepatocellular carcinoma cell line,
HfPc — hafnium(IV) phthalocyanine complex,
HKUST — Hong Kong University of Science and Technology,
Hmim — 2-methylimidazole,
Hmpba — 4-(3,5-dimethyl-1*H*-pyrazol-4-yl)benzoic acid,
HOF — hydrogen-bonded organic framework,
HOPG — highly oriented pyrolytic graphite,
Hpypz — 4-(1*H*-pyrazol-4-yl)pyridine,
HPV — human papillomavirus,
HSA — human serum albumin,
IAST — ideal adsorbed solution theory,
IC_{50} — half-maximal inhibitory concentration,
ICD — induced circular dichroism,
ILC — ionic liquid crystals,
K-4 — human embryo skin cells,
Ile — isoleucine,
ITO — indium tin oxide,
LB — Langmuir – Blodgett,
LBF — Lanmuir – Blodgett film,
LbL — layer-by-layer (assembly),
LC — liquid crystal,
LCWdV — liquid crystals formed through van der Waals forces,
LD_{50} — half-lethal dose,
Leu — leucine,
MCF-7 — human invasive breast adenocarcinoma cell line,
MEKC — micellar electrokinetic chromatography,
MEEKC — microemulsion electrokinetic chromatography,
MDCK — model mammalian epithelial cells,
Met — methionine,
MLC — micellar liquid chromatography,
MOC — metal-organic cages,
MOF — metal-organic frameworks,
MOP — metal-organic polyhedra,
MRI — magnetic resonance imaging,
MW — molecular weight,
Nc — naphthalocyanine,
NBS — *N*-bromosuccinimide,
NHS — *N*-hydroxysuccinimide,
Nic — nicotinate anion,
NIR — near infrared spectral region,
Ni-Ra — Raney nickel,
NP — nanoparticle,
Oc — oxanthrenocyanine,
ORMOSIL — organically modified silica nanoparticles,
OTS — octadecyltrichlorosilane,
ONu — oligonucleotide,
PAH — polyallylamine hydrochloride,
PAMAM — polyamidoamine,
pbda — [(2-(*tert*-butyl)-1,4-phenylene)bis(oxy)]-4,4′-dibenzoic acid,
Pc — phthalocyanine,
PCMA — poly(carboxybetaine methacrylate),

PDT — photodynamic therapy,
PEG — polyethylene glycol,
PEO — polyethylene oxide,
PET — positron emission tomography,
PETP — poly(ethylene terephthalate),
Phe — phenylalanine,
Pht — phthalimido,
PM — purple membrane,
Pro — proline,
PNA — peptide nucleic acid,
PSS — poly(sodium 4-styrenesulfonate),
PTCD-C10 — bis(*p*-decylimido)perylene,
PVDF-HFP — polyvinylidene fluoride and hexafluoropropylene copolymer,
PVP — polyvinylpyrrolidone,
Pyz — pyrazine,
QCM — quartz crystal microbalance,
QD — quantum dot,
rGO — reduced graphene oxide,
RNA — ribonucleic acid,
RNA polymerase NS5 — nonstructural protein 5 representing RNA polymerase,
RNA helicase NS3 — nonstructural protein 3 representing RNA helicase,
ROS — reactive oxygen species,
rt — room temperature,
RTP — room-temperature phosphorescence,
S — sublayer,
SA — stearic acid,
SAM — self-assembled monolayers,
SBS — supramolecular biochemical systems,
SC[4]A — sulfonate calix[4]arene,
SC[4]R — sulfonate calix[4]resorcinarene,
SDS — sodium dodecyl sulfate,
SEM — scanning electron microscopy,
Ser — serine,
SMM — single-molecule magnet,
SPIONP — superparamagnetic iron oxide nanoparticle,
SPR — surface plasmon resonance,
s-RTP — sensitized room-temperature phosphorescence,
SURMOF — surface-mounted metal-organic framework,
TAP — trigonal antiprismatic,
TCAS — *p*-sulfonatothiacalix[4]arene,
TCD — thiolated cyclodextrin,
TCNQ-TCNQ — 1,2-bis[4-(dicyanomethylene)cyclohexa-2,5-dien-1-yl]ethane-1,1,2,2- tetracarbonitrile,
TEM — transmission electron microscopy,
TEMPO — (2,2,6,6-tetramethylpiperidin-1-yl)oxyl,
TEOS — tetraethylorthosilane,
TMA — trimethylammonium,
TON — turnover number,
TP — trigonal prismatic,
TPP — triphenylphosphonium,
triazoleH — 4(5)-carboxy-1,2,3-triazole-1-acetic acid,
Trp — tryptophan,
Tr — triphenylmethyl (trityl),
Ts — *p*-toluenesulfonyl (tosyl),
TPM – two-photon fluorescence microscopy,
T-T — triplet – triplet energy transfer,
TPE-BDC — 4′,4‴-(1,2-diphenylethane-1,2-diyl)(*E*)-bis([1,1′-biphenyl]-4-carboxylate),
Tyr — tyrosine,
Val — valine,
VTES — vinyltriethoxysilane,
r_1 and r_2 — longitudinal and transverse relaxivity,
T_1 and T_2 — longitudinal and transverse relaxation times of water protons,
$\Delta\chi$ — anisotropy of the magnetic susceptibility tensor.

8. About authors

I.S.Antipin. Corresponding Member of the RAS, Doctor of Chemical Sciences, Professor, Head of the Department of Organic Chemistry, Kazan Federal University (KFU).
E-mail: iantipin54@yandex.ru
Current research interests: supramolecular chemistry, macrocyclic compounds, synthesis, calixarenes, host – guest complexes, nanoparticles
M.V.Alfimov. Academician, Doctor of Physical and Mathematical Sciences, Scientific Head of the Photochemistry Center, RAS, FSRC 'Crystallography and Photonics', RAS.
E-mail: alfimov@photonics.ru
Current research interests: photochemistry, supramolecular chemistry.
V.V.Arslanov. Doctor of Chemical Sciences, Professor, Chief Researcher at the Institute of Physical Chemistry and Electrochemistry (IPCE RAS).
E-mail: vladimir.arslanov@gmail.com
Current research interests: colloidal and surface chemistry, supramolecular chemistry, nanotechnology, fundamental effects in low-dimensional systems, miniaturization of information devices.
V.A.Burilov. Candidate of Chemical Sciences, Associate Professor at the Department of Organic Chemistry, KFU.
E-mail: ultrav@bk.ru
Current research interests: calixarenes, supramolecular amphiphiles, catalysis, molecular recognition.
S.N.Chvalun. Corresponding Member of the RAS, Doctor of Chemical Sciences, Professor, Head of the Laboratory of Functional Polymer Structures, Institute of Synthetic Polymer Materials (ISPM RAS).
E-mail: s-chvalun@yandex.ru, serge@ispm.ru
Current research interests: polymer structure and properties, X-ray diffraction analysis, partially ordered mesophases of decreased symmetry, biodegradable materials.
S.V.Dudkin. Candidate of Chemical Sciences, Senior Researcher at the Laboratory for Aliphatic Organoboron Compounds, Institute of Organoelement Compounds (INEOS RAS).
E-mail: sdudkin@ineos.ac.ru, semdudkin@gmail.com
Current research interests: functional dyes, hybrid systems based on cage metal complexes and tetrapyrrolic macroheterocyclic compounds, macrocyclic compounds, tetraazachlorins, clathrochelates.
V.P.Fedin. Corresponding Member of the RAS, Doctor of Chemical Sciences, Professor, Head of the Laboratory for Metal-Organic Coordination Polymers, Nikolaev Institute of Inorganic Chemistry (NIIC SB RAS).
E-mail: cluster@niic.nsc.ru
Current research interests: synthesis and functional properties of metal-organic coordination polymers, supramolecular chemistry.
S.V.Fedorenko. PhD in Chemistry, Senior Researcher at Institute of Organic and Physical Chemistry (IOPC), FRC Kazan Scientifc Center, RAS.
E-mail: svetlana.fedorenko@yahoo.com

Current research interests: physical and colloidal chemistry, materials chemistry, nanotechnology, supramolecular chemistry, inorganic chemistry, multifunctional silica nanoparticles for biochemistry, rare earth-based silica nanoparticles, development of T_1 and T_2 contrast agent based on silica nanoparticles for MRI, luminescent nanomaterials, luminescence sensors.

O.A.Fedorova. Doctor of Chemical Sciences, Professor, Deputy Director of INOEC RAS.
E-mail: fedorova@ineos.ac.ru
Current research interests: supramolecular chemistry, organic photochemistry, dye chemistry.

Y.V.Fedorov. Doctor of Chemical Sciences, Leading Researcher at INEOC RAS.
E-mail: fedorov@ineos.ac.ru
Current research interests: supramolecular chemistry, photochemistry, complex formation.

V.V.Gorbatchuk. Doctor of Chemical Sciences, Professor of the Department of Physical Chemistry, KFU.
E-mail: Valery.Gorbatchuk@kpfu.ru
Current research interests: supramolecular chemistry, chemical thermodynamics, molecular recognition, smart materials, calixarenes, cyclodextrins polymorphism.

Y.G.Gorbunova. Corresponding Member of the RAS, Professor, Chief Researcher at the Institute of General and Inorganic Chemistry (IGIC RAS), Chief Researcher at IPCE RAS.
E-mail: yulia@igic.ras.ru, yulia.gorbunova@gmail.com
Current research interests: coordination and supramolecular chemistry of tetrapyrrolic macrocycles and crown-ethers, lanthanides, functional materials.

S.P.Gromov. Corresponding Member of the RAS, Doctor of Chemical Sciences, Professor, Head of the Photochemistry Center of the RAS, FSRC 'Crystallography and Photonics', RAS.
E-mail: spgromov@mail.ru
Current research interests: supramolecular chemistry; organic photochemistry; organic chemistry.

M.A.Kalinina. Doctor of Chemical Sciences, Professor of the RAS, Chief Researcher at IPCE RAS.
E-mail: kalinina@phyche.ac.ru
Current research interests: self-assembly in colloid systems, biomimetic systems, supramolecular composites and hybrid materials.

E.A.Karakhanov. Doctor of Chemical Sciences, Professor, Head of Division of Petroleum Chemistry and Organic Catalysis, Faculty of Chemistry, Moscow State University (MSU).
E-mail: kar@petrol.chem.msu.ru
Current research interests: petroleum chemistry, catalysis, organic chemistry, supramolecular chemistry, new materials.

R.R.Kashapov. PhD (Chemistry), Senior Researcher at the Laboratory of Highly Organized Media, IOPC, FRC Kazan Scientifc Center, RAS.
E-mail: kashapov@iopc.ru
Current research interests: self-assembly, amphiphiles, cyclophanes, polymers, nanocontainers, drug delivery systems, sensors.

O.I.Koifman. Corresponding Member of the RAS, Doctor of Chemical Sciences, Professor, Chief Researcher of the Laboratory for New Materials Based on Macrocyclic Compounds, Institute of Solution Chemistry (ISC RAS), President and Head of the Department of Chemistry and Technology of Macromolecular Compounds, Ivanovo State University of Chemical Technology (ISUCT).
E-mail: oik@isuct.ru
Current research interests: synthesis, chemical structure and reactivity of macroheterocyclic compounds and supramolecular systems based on them.

V.S.Korenev. Candidate of Chemical Sciences, Senior Researcher of NIIC SB RAS.
E-mail: wkorenev@niic.nsc.ru
Current research interests: chemistry of cluster compounds, supramolecular chemistry.

A.L.Maksimov. Corresponding Member of the RAS, Doctor of Chemical Sciences, Director of Topchiev Institute of Petrochemical Synthesis (TIPS RAS).
E-mail: max@ips.ac.ru
Current research interests: petrochemistry, oil refining, renewable feedstock refining, homogeneous and heterogeneous catalysis, green chemistry, immobilized catalysts.

N.Z.Mamardashvili. Doctor of Chemical Sciences, Professor, Deputy Director for Research of ISC RAS, Head of the Laboratory of the Coordination Chemistry of Macrocyclic Compounds.
E-mail: ngm@isc-ras.ru
Current research interests: synthesis and design of chemical substances and materials based on macrocyclic compounds with a specified molecular architecture and functional properties.

G.M.Mamardashvili. Doctor of Chemical Sciences, Leading Researcher at the Laboratory for New Materials Based on Macrocyclic Compounds, ISC RAS.
E-mail: gmm@isc-ras.ru
Current research interests: supramolecular and colloidal chemistry of tetrapyrrolic macrocycles.

A.G.Martynov. Doctor of Chemical Sciences, Leading Researcher at IPCE RAS.
E-mail: martynov@phyche.ac.ru, martynov.alexandre@gmail.com
Current research interests: coordination and supramolecular chemistry of tetrapyrrolic macrocycles and crown ethers, spectroscopy and theoretical modelling, single-molecule magnets, non-linear optics.

A.R.Mustafina. Doctor of Chemical Sciences, Associate Professor, Chief Researcher at IOPC, FRC Kazan Scientifc Center, RAS.
E-mail: asiyamust@mail.ru
Current research interests: physical and colloidal chemistry, chemistry of materials, nanotechnology, supramolecular chemistry, inorganic chemistry, multifunctional silica nanoparticles in biochemistry, rare earth-based silica nanoparticles, development of T_1 and T_2 contrast agent based on silica nanoparticles for MRI, luminescent nanomaterials, luminescence sensors.

R.I.Nugmanov. PhD, Senior Researcher of KFU.
E-mail: RaINugmanov@kpfu.ru
Current research interests: supramolecular chemistry, chemoinformatics, molecular modelling, data mining.

A.S.Ovsyannikov. Candidate of chemical sciences, Senior Researcher at IOPC, FRC Kazan Scientifc Center, RAS.
E-mail: osaalex2007@rambler.ru
Current research interests: design of supramolecular architectures in the crystalline phase using pre-organized molecular building blocks. Creation of crystalline functional materials with specified magnetic, luminescent and adsorption properties.

P.L.Padnya. Candidate of Chemical Sciences, Senior Researcher at KFU.
E-mail: padnya.ksu@gmail.com
Current research interests: development of supramolecular systems and nanomaterials based on synthetic macrocycles, including (thia)calixarenes and pillararenes, for biomedical applications.
A.S.Potapov. Doctor of Chemical Sciences, Associate Professor, Leading Researcher at NIIC SB RAS.
E-mail: potapov@niic.nsc.ru
Current research interests: synthesis of heterocyclic nitrogen ligands, coordination polymers.
S.L.Selektor. Doctor of Chemical Sciences, Associate Professor, Chief Researcher, Head of Laboratory of IPCE RAS.
E-mail: sofs@list.ru
Current research interests: Langmuir monolayers, Langmuir – Blodgett films, cyclic voltammetry, electrochemical impedance, spectroelectrochemistry, fluorescence, redox isomerism, energy transfer.
S.N.Shtykov. Doctor of Chemical Sciences, Professor at the Department of Analytical Chemistry and Chemical Ecology, Institute of Chemistry, Saratov State University.
E-mail: shtykovsn@mail.ru
Current research interests: analytical chemistry, nanoanalytics, molecular spectrometry, thermodynamics of solutions, supramolecular chemistry.
D.N.Shurpik. Candidate of Chemical Sciences, Senior Lecturer at KFU.
E-mail: dnshurpik@mail.ru
Current research interests: synthesis and supramolecular self-assembly of functionalized pillar[*n*]arenes, calixarenes and various classes of macrocyclic meroterpenoids.
M.A.Shcherbina. Candidate of Physical and Mathematical Sciences, Leading Researcher at the Laboratory of Functional Polymer Structures and Deputy Director for Innovations, ISPM RAS.
E-mail: max-shcherbina@yandex.ru, shcherbina@ispm.ru
Current research interests: polymer structure and properties, X-ray diffraction analysis, partially ordered mesophases of decreased symmetry, biodegradable materials.
M.N.Sokolov. Doctor of Chemical Sciences, Professor of the RAS, Head of the Laboratory for the Synthesis of Complex Compounds, NIIC SB RAS.
E-mail: caesar@niic.nsc.ru
Current research interests: chemistry of cluster compounds, supramolecular chemistry.
S.E.Solovieva. Doctor of Chemical Sciences, Associate Professor, Leading Researcher at IOPC, FRC Kazan Scientifc Center, RAS.
E-mail: evgersol@yandex.ru
Current research interests: synthesis, structure and reactivity of organic compounds, supramolecular chemistry, cyclophanes, complexes, colloidal systems.
I.I.Stoikov. Doctor of Chemical Sciences, Professor, Director of A.M. Butlerov Institute of Chemistry, KFU.
E-mail: Ivan.Stoikov@mail.ru
Current research interests: development of supramolecular assemblies and hybrid materials, their application for the recognition of biologically active organic species and biopolymers.
P.A.Stuzhin. Doctor of Chemical Sciences, Professor, Head of the Department of Organic Chemistry, ISUCT.
E-mail: stuzhin@isuct.ru
Current research interests: pyrrole-containing macrocycles, porphyrins, phthalocyanines and their heterocyclic analogues.
E.V.Suslov. PhD, Head of Laboratory of Directed Transformations of Natural Compounds, Novosobirsk Institute of Organic Chemistry (NIOCH SB RAS).
E-mail: suslov@nioch.nsc.ru
Current research interests: medicinal chemistry, chemistry of natural products, asymmetric synthesis.
A.Y.Tsivadze. Academician, Doctor of Chemical Sciences, Professor, Head of Laboratory and Scientific Supervisor of IPCE RAS, Head of Laboratory at IGIC RAS.
E-mail: tsiv@phyche.ac.ru, atsi43@mail.ru
Current research interests: coordination and supramolecular chemistry of tetrapyrrolic macrocycles and crown ethers, isotope separation, extraction.
E.N.Ushakov. Doctor of Chemical Sciences, Leading Researcher at the Institute of Problems of Chemical Physics (IPCP RAS).
E-mail: en-ushakov@mail.ru; eushakov@icp.ac.ru
Current research interests: organic photochemistry, supramolecular chemistry, computational chemistry.
S.Z.Vatsadze. Doctor of Chemical Sciences, Professor of the RAS, Professor of the Division of Organic Chemistry, Faculty of Chemistry, MSU.
E-mail: szv@org.chem.msu.ru
Current research interests: supramolecular chemistry, macrocyclic receptors, asymmetric synthesis.
Y.Z.Voloshin. Doctor of Chemical Sciences, Professor, Head of the Laboratory of Nanobiomaterials and Bioeffectors for the Theranostics of Socially Significant Diseases, IGIC RAS.
E-mail: voloshin@igic.ras.ru
Current research interests: coordination chemistry, clathrochelates, macrocyclic compounds, topological drugs, electrocatalytic hydrogen production, molecular probes.
K.P.Volcho. Doctor of Chemical Sciences, Professor of the RAS, Chief Researcher at NIOCH SB RAS.
E-mail: volcho@nioch.nsc.ru
Current research interests: medicinal chemistry, chemistry of natural products, asymmetric synthesis.
L.S.Yakimova. Candidate of Chemical Sciences, Associate Professor at the Department of Organic Chemistry, A.M.Butlerov Institute of Chemistry, KFU.
E-mail: mila.yakimova@mail.ru
Current research interests: supramolecular self-assembly and synthesis of nanostructured hybrid systems based on polyfunctional (thia)calixarenes, pillar[5]arenes, and chemically modified silica by covalent or non-covalent self-assembly.
S.Y.Zaitsev. Doctor of Chemical Sciences, Doctor of Biological Sciences, Professor, Head of the Group of Analytical Biochemistry of the Department of the Physiology and Biochemistry of Agricultural Animals, Federal Research Center for Animal Husbandry named after Academy Member L.K.Ernst.
E-mail: s.y.zaitsev@mail.ru
Current research interests: supramolecular systems, biochemistry of animals, bionanotechnological materials, diagnostic methods, polymers, colloids and biomembranes.
L.Y.Zakharova. Doctor of Chemical Sciences, Professor, Chief Researcher at the Laboratory of Highly Organized Media, IOPC, FRC Kazan Scientifc Center, RAS.
E-mail: lucia@iopc.ru
Current research interests: self-assembly, amphiphiles,

cyclophanes, polymers, reactivity, supramolecular catalysis, immobilized nanoreactors, nanocontainers, polyelectrolyte capsules, drug delivery systems.

M.A.Ziganshin. Doctor of Chemical Sciences, Professor of the Department of Physical Chemistry, KFU.
E-mail: Marat.Ziganshin@kpfu.ru
Current research interests: supramolecular chemistry, chemical thermodynamics, molecular recognition, smart materials, polymorphism, oligopeptides.
A.V.Zolotukhina. Candidate of Chemical Sciences, Researcher at TIPS RAS.
E-mail: anisole@yandex.ru
Current research interests: homogeneous and heterogeneous catalysis, chemistry of new organic and hybrid materials, nanocatalysis.

References

1. J.-M.Lehn. *Supramolecular Chemistry*: *Concepts and Perspectives*. (1st Edn). (Weinheim: VCH, 1995)
2. J.W.Steed, D.R.Turner, K.Wallace. *Core Concepts in Supramolecular Chemistry and Nanochemistry*. (Chichester: Wiley, 2007)
3. V.A.Smirnov, N.N.Denisov, M.V.Alfimov. *Nanotechnol. Russ.,* **8** (1-2), 1 (2013)
4. J.W.Steed, J.L.Atwood. *Supramolecular Chemistry*. (Chichester: Wiley, 2009)
5. A.I.Konovalov. *Russ. Chem. Bull., Int. Ed.*, **60**, 1 (2011)
6. A.Y.Tsivadze, G.V.Ionova, V.K.Mikhalko, Y.N.Kostrubov. *Russ. Chem. Rev.*, **76**, 213 (2007)
7. M.Bengisu, M.Ferrara. *Materials That Move: Smart Materials, Intelligent Design*. (Springer International Publishing, 2018)
8. J.Mohd Jani, M.Leary, A.Subic, M.A.Gibson. *Mater. Des.*, **56**, 1078 (2014)
9. H.Janocha. *Adaptronics and Smart Structures: Basics, Materials, Design, and Applications*. (2nd Edn). (Berlin, Heidelberg: Springer-Verlag, 2007)
10. J.F.Stoddart. *Angew. Chem., Int. Ed.*, **56**, 11094 (2017)
11. J.-P.Sauvage. *Angew. Chem., Int. Ed.*, **56**, 11080 (2017)
12. B.L.Feringa. *Angew. Chem., Int. Ed.*, **56**, 11060 (2017)
13. A.G.Martynov, E.A.Safonova, A.Y.Tsivadze, Y.G.Gorbunova. *Coord. Chem. Rev.*, **387**, 325 (2019)
14. M.A.Rajora, J.W.H.Lou, G.Zheng. *Chem. Soc. Rev.*, **46**, 6433 (2017)
15. I.P.Beletskaya, V.S.Tyurin, A.Y.Tsivadze, R.Guilard, C.Stern. *Chem. Rev.*, **109**, 1659 (2009)
16. C.M.Drain, A.Varotto, I.Radivojevic. *Chem. Rev.*, **109**, 1630 (2009)
17. U.Chilakamarthi, L.Giribabu. *Chem. Rec.*, **17**, 775 (2017)
18. F.Dumoulin, M.Durmuş, V.Ahsen, T.Nyokong. *Coord. Chem. Rev.*, **254**, 2792 (2010)
19. X.Li, D.Lee, J.-D.Huang, J.Yoon. *Angew. Chem., Int. Ed.*, **57**, 9885 (2018)
20. X.Li, E.-Y.Park, Y.Kang, N.Kwon, M.Yang, S.Lee, W.J.Kim, C.Kim, J.Yoon. *Angew. Chem., Int. Ed.*, **59**, 8630 (2020)
21. C.J.Medforth, Z.Wang, K.E.Martin, Y.Song, J.L.Jacobsen, J.A.Shelnutt. *Chem. Commun.*, **7345**, 7261 (2009)
22. Y.Tian, C.M.Beavers, T.Busani, K.E.Martin, J.L.Jacobsen, B.Q.Mercado, B.S.Swartzentruber, F.van Swol, C.J.Medforth, J.A.Shelnutt, D.K.E.Martin, F.Van Swol, A.John. *Nanoscale*, **4**, 1695 (2012)
23. V.B.Sheinin, E.V.Bobritskaya, S.Shabunin, O.I.Koifman. *Macroheterocycles*, **7**, 209 (2014)
24. V.B.Sheinin, O.M.Kulikova, O.I.Koifman. *J. Mol. Liq.*, **277**, 397 (2019)
25. S.M.Vlaming, R.Augulis, M.C.A.Stuart, J.Knoester, P.H.M.Van Loosdrecht. *J. Phys. Chem. B*, **113**, 2273 (2009)
26. D.Jariwala, V.K.Sangwan, L.J.Lauhon, T.J.Marks, M.C.Hersam. *Chem. Soc. Rev.*, **42**, 2824 (2013)
27. A.G.Martynov, I.V.Nefedova, N.N.Efimov, E.A.Ugolkova, V.V.Minin, Y.G.Gorbunova, A.Y.Tsivadze. *Macroheterocycles*, **11**, 390 (2018)
28. I.V.Nefedova, A.G.Martynov, A.A.Averin, G.A.Kirakosyan, A.Y.Tsivadze, Y.G.Gorbunova. *Isr. J. Chem.*, **56**, 181 (2016)
29. H.Yi, G.Zeng, C.Lai, D.Huang, L.Tang, J.Gong, M.Chen, P.Xu, H.Wang, M.Cheng, C.Zhang, W.Xiong. *Chem. Eng. J.*, **330**, 134 (2017)
30. C.García-Simón, M.Garcia-Borràs, L.Gómez, T.Parella, S.Osuna, J.Juanhuix, I.Imaz, D.Maspoch, M.Costas, X.Ribas. *Nat. Commun.*, **5**, 2 (2014)
31. V.Novakova, L.Lochman, I.Zajícová, K.Kopecky, M.Miletin, K.Lang, K.Kirakci, P.Zimcik. *Chem. – Eur. J.*, **19**, 5025 (2013)
32. L.Lochman, J.Svec, J.Roh, K.Kirakci, K.Lang, P.Zimcik, V.Novakova. *Chem. – Eur. J.*, **22**, 2417 (2016)
33. O.Yavuz, Y.Alcay, K.Kaya, M.Sezen, S.Kirlangic Atasen, M.S.Yildirim, Y.Ozkilic, N.Ş.Tuzun, I.Yilmaz. *Inorg. Chem.*, **58**, 909 (2019)
34. Y.G.Gorbunova, A.G.Martynov, A.Y.Tsivadze. In *Handbook of Porphyrin Science*. (Eds K.M.Kadish, K.M.Smith, R.Guilard). (World Scientific Publishing, 2012). P. 271
35. E.A.Safonova, M.A.Polovkova, A.G.Martynov, Y.G.Gorbunova, A.Y.Tsivadze. *Dalton Trans.*, **47**, 15226 (2018)
36. E.A.Safonova, A.G.Martynov, V.I.Zolotarevskii, S.E.Nefedov, Y.G.Gorbunova, A.Y.Tsivadze. *Dalton Trans.*, **44**, 1366 (2015)
37. E.A.Safonova, A.G.Martynov, S.E.Nefedov, G.A.Kirakosyan, Y.G.Gorbunova, A.Y.Tsivadze. *Inorg. Chem.*, **55**, 2450 (2016)
38. L.A.Lapkina, V.E.Larchenko, G.A.Kirakosyan, A.Y.Tsivadze, S.I.Troyanov, Y.G.Gorbunova. *Inorg. Chem.*, **57**, 82 (2018)
39. F.D'Souza, E.Maligaspe, K.Ohkubo, M.E.Zandler, N.K.Subbaiyan, S.Fukuzumi. *J. Am. Chem. Soc.*, **131**, 8787 (2009)
40. L.A.Lapkina, Y.G.Gorbunova, D.O.Gil, V.K.Ivanov, N.Y.Konstantinov, A.Y.Tsivadze. *J. Porphyrins Phthalocyanines*, **17**, 564 (2013)
41. J.Mack, S.Mkhize, E.A.Safonova, A.G.Martynov, Y.G.Gorbunova, A.Y.Tsivadze, T.Nyokong. *J. Porphyrins Phthalocyanines*, **20**, 505 (2016)
42. Q.Liu, J.Wang, D.Liu, R.Li, T.Peng. *J. Power Sources*, **396**, 57 (2018)
43. Y.Horii, S.Kishiue, M.Damjanović, K.Katoh, B.K.Breedlove, M.Enders, M.Yamashita. *Chem. – Eur. J.*, **24**, 4320 (2018)
44. A.G.Martynov, M.A.Polovkova, G.S.Berezhnoy, A.A.Sinelshchikova, F.M.Dolgushin, K.P.Birin, G.A.Kirakosyan, Y.G.Gorbunova, A.Y.Tsivadze. *Inorg. Chem.*, **59**, 9424 (2020)

45. Y.G.Gorbunova, A.D.Grishina, A.G.Martynov, T.V.Krivenko, A.A.Isakova, V.V.Savel'ev, S.E.Nefedov, E.V.Abkhalimov, A.V.Vannikov, A.Y.Tsivadze. *J. Mater. Chem. C*, **3**, 6692 (2015)
46. M.Z.Papiz, S.M.Prince, T.Howard, R.J.Cogdell, N.W.Isaacs. *J. Mol. Biol.*, **326**, 1523 (2003)
47. M.J.Llansola-Portoles, F.Li, P.Xu, S.Streckaite, C.Ilioaia, C.Yang, A.Gall, A.A.Pascal, R.Croce, B.Robert. *Biochim. Biophys. Acta — Bioenerg.*, **1861**, 148078 (2020)
48. F.Liao, H.Yuan, K.J.Du, Y.You, S.Q.Gao, G.B.Wen, Y.W.Lin, X.Tan. *Mol. Biosyst.*, **12**, 3139 (2016)
49. J.Zeng, Y.Zhao, W.Li, X.Tan, G.B.Wen, Y.W.Lin. *J. Mol. Catal. B*, **111**, 108 (2015)
50. W.Suzuki, H.Kotani, T.Ishizuka, M.Kawano, H.Sakai, T.Hasobe, K.Ohkubo, S.Fukuzumi, T.Kojima. *J. Phys. Chem. C*, **123**, 11529 (2019)
51. T.Ishizuka, M.Sankar, Y.Yamada, S.Fukuzumi, T.Kojima. *Chem. Commun.*, **48**, 6481 (2012)
52. X.-T.He, Y.-H.Luo, Z.-Y.Zheng, C.Wang, J.-Y.Wang, D.-L.Hong, L.-H.Zhai, L.-H.Guo, B.-W.Sun. *ACS Appl. Nano Mater.*, **2**, 7719 (2019)
53. X.Rui, Q.Z.Zha, T.T.Wei, Y.S.Xie. *Inorg. Chem. Commun.*, **48**, 111 (2014)
54. J.Lu, L.Zhou, Q.Meng, H.Sui, Y.Li, X.Tai. *Dyes Pigm.*, **113**, 138 (2015)
55. W.Yang, B.Li, H.Wang, O.Alduhaish, K.Alfooty, M.A.Zayed, P.Li, H.D.Arman, B.Chen. *Cryst. Growth Des.*, **15**, 2000 (2015)
56. J.Janczak. *ACS Omega*, **4**, 3673 (2019)
57. P.A.Tarakanov, M.P.Donzello, O.I.Koifman, P.A.Stuzhin. *Macroheterocycles*, **4**, 177 (2011)
58. P.A.Tarakanov, E.N.Tarakanova, P.V.Dorovatovskii, Y.V.Zubavichus, V.N.Khrustalev, S.A.Trashin, K.De Wael, M.E.Neganova, D.V.Mischenko, J.L.Sessler, P.A.Stuzhin, V.E.Pushkarev, L.G.Tomilova. *Dalton Trans.*, **47**, 14169 (2018)
59. P.A.Stuzhin, P.Tarakanov, S.Shiryaeva, A.Zimenkova, O.I.Koifman, E.Viola, M.P.Donzello, C.Ercolani. *J. Porphyrins Phthalocyanines*, **16**, 968 (2012)
60. Y.Jiang, C.Liu, X.Wang, T.Wang, J.Jiang. *Langmuir*, **33**, 7239 (2017)
61. Y.Yamada, M.Okamoto, K.Furukawa, T.Kato, K.Tanaka. *Angew. Chem., Int. Ed.*, **51**, 709 (2012)
62. N.Mihara, Y.Yamada, H.Takaya, Y.Kitagawa, S.Aoyama, K.Igawa, K.Tomooka, K.Tanaka. *Chem. – Eur. J.*, **23**, 7508 (2017)
63. Y.Yamada, N.Mihara, S.Shibano, K.Sugimoto, K.Tanaka. *J. Am. Chem. Soc.*, **135**, 11505 (2013)
64. Y.Yamada, K.Tanaka. *J. Incl. Phenom. Macrocycl. Chem.*, **96**, 197 (2020)
65. N.Mihara, Y.Yamada, H.Takaya, Y.Kitagawa, K.Igawa, K.Tomooka, H.Fujii, K.Tanaka. *Chem. – Eur. J.*, **25**, 3369 (2018)
66. P.Afanasiev, A.B.Sorokin. *Acc. Chem. Res.*, **49**, 583 (2016)
67. S.Pullen, G.H.Clever. *Acc. Chem. Res.*, **51**, 3052 (2018)
68. L.Chen, Q.Chen, M.Wu, F.Jiang, M.Hong. *Acc. Chem. Res.*, **48**, 201 (2015)
69. A.M.Castilla, W.J.Ramsay, J.R.Nitschke. *Acc. Chem. Res.*, **47**, 2063 (2014)
70. A.Schmidt, A.Casini, F.E.Kühn. *Coord. Chem. Rev.*, **275**, 19 (2014)
71. W.M.Bloch, G.H.Clever. *Chem. Commun.*, **53**, 8506 (2017)
72. C.Deraedt, D.Astruc. *Coord. Chem. Rev.*, **324**, 106 (2016)
73. Z.Wu, K.Zhou, A.V.Ivanov, M.Yusobov, F.Verpoort. *Coord. Chem. Rev.*, **353**, 180 (2017)
74. C.M.A.Gangemi, A.Pappalardo, G.Trusso Sfrazzetto. *RSC Adv.*, **5**, 51919 (2015)
75. M.D.Ward, C.A.Hunter, N.H.Williams. *Acc. Chem. Res.*, **51**, 2073 (2018)
76. A.Pappalardo, R.Puglisi, G.Trusso Sfrazzetto. *Catalysts*, **9**, 630 (2019)
77. Y.Fang, J.A.Powell, E.Li, Q.Wang, Z.Perry, A.Kirchon, X.Yang, Z.Xiao, C.Zhu, L.Zhang, F.Huang, H.-C.Zhou. *Chem. Soc. Rev.*, **48**, 4707 (2019)
78. R.J.Severinsen, G.J.Rowlands, P.G.Plieger. *J. Incl. Phenom. Macrocycl. Chem.*, **96**, 29 (2020)
79. C.J.Brown, F.D.Toste, R.G.Bergman, K.N.Raymond. *Chem. Rev.*, **115**, 3012 (2015)
80. F.J.Rizzuto, L.K.S.von Krbek, J.R.Nitschke. *Nat. Rev. Chem.*, **3**, 204 (2019)
81. M.Yoshizawa, M.Yamashina. *Chem. Lett.*, **46**, 163 (2017)
82. R.Custelcean. *Chem. Soc. Rev.*, **43**, 1813 (2014)
83. T.Hasell, A.I.Cooper. *Nat. Rev. Mater.*, **1**, 16053 (2016)
84. M.D.Ward, C.A.Hunter, N.H.Williams. *Chem. Lett.*, **46**, 2 (2017)
85. A.Casini, B.Woods, M.Wenzel. *Inorg. Chem.*, **56**, 14715 (2017)
86. W.Zhu, J.Guo, Y.Ju, R.E.Serda, J.G.Croissant, J.Shang, E.Coker, J.O.Agola, Q.Zhong, Y.Ping, F.Caruso, C.J.Brinker. *Adv. Mater.*, **31**, 1806774 (2019)
87. A.Pöthig, A.Casini. *Theranostics*, **9**, 3150 (2019)
88. A.Ahmedova. *Front. Chem.*, **6**, 620 (2018)
89. H.Vardhan, M.Yusubov, F.Verpoort. *Coord. Chem. Rev.*, **306**, 171 (2016)
90. H.Li, Z.-J.Yao, D.Liu, G.-X.Jin. *Coord. Chem. Rev.*, **293 – 294**, 139 (2015)
91. E.-S.M.El-Sayed, D.Yuan. *Chem. Lett.*, **49**, 28 (2020)
92. Y.-Y.Zhang, W.-X.Gao, L.Lin, G.-X.Jin. *Coord. Chem. Rev.*, **344**, 323 (2017)
93. *Comprehensive Supramolecular Chemistry II*. (Eds J.L.Atwood, G.W.Gokel, L.Barbour). (Amsterdam: Elsevier, 2017)
94. M.Yamanaka, K.Kobayashi. *Asian J. Org.Chem.*, **2**, 276 (2013)
95. K.Kobayashi, M.Yamanaka. *Chem. Soc. Rev.*, **44**, 449 (2015)
96. Q.Zhang, L.Catti, K.Tiefenbacher. *Acc. Chem. Res.*, **51**, 2107 (2018)
97. C.Gaeta, C.Talotta, M.De Rosa, P.La Manna, A.Soriente, P.Neri. *Chem. – Eur. J.*, **25**, 4899 (2019)
98. P.P.Cholewa, S.J.Dalgarno. *CrystEngComm*, **16**, 3655 (2014)
99. A.S.Rathnayake, H.W.L.Fraser, E.K.Brechin, S.J.Dalgarno, J.E.Baumeister, J.White, P.Rungthanaphatsophon, J.R.Walensky, C.L.Barnes, S.J.Teat, J.L.Atwood. *Nat. Commun.*, **9**, 2119 (2018)
100. A.Ovsyannikov, S.Solovieva, I.Antipin, S.Ferlay. *Coord. Chem. Rev.*, **352**, 151 (2017)
101. E.F.Chernova, A.S.Ovsyannikov, S.Ferlay, S.E.Solovieva, I.S.Antipin, A.I.Konovalov, N.Kyritsakas, M.W.Hosseini. *Tetrahedron Lett.*, **59**, 1377 (2018)
102. A.S.Ovsyannikov, S.Ferlay, E.F.Chernova, S.E.Solovieva, I.S.Antipin, M.W.Hosseini. *Macroheterocycles*, **10**, 410 (2017)

103. E.F.Chernova, A.S.Ovsyannikov, S.E.Solovieva, I.S.Antipin, N.Kyritsakas, M.W.Hosseini, S.Ferlay. *Inorg. Chem. Commun.*, **106**, 197 (2019)
104. A.S.Ovsyannikov, I.V.Khariushin, S.E.Solovieva, I.S.Antipin, H.Komiya, N.Marets, H.Tanaka, H.Ohmagari, M.Hasegawa, J.J.Zakrzewski, S.Chorazy, N.Kyritsakas, M.W.Hosseini, S.Ferlay. *RSC Adv.*, **10**, 11755 (2020)
105. M.N.Kozlova, S.Ferlay, N.Kyritsakas, M.W.Hosseini, S.E.Solovieva, I.S.Antipin, A.I.Konovalov. *Chem. Commun.*, 2514 (2009)
106. H.Takezawa, T.Murase, G.Resnati, P.Metrangolo, M.Fujita. *Angew. Chem., Int. Ed.*, **54**, 8411 (2015)
107. R.Plessius, N.Orth, I.Ivanoviå-Burmazović, M.A.Siegler, J.N.H.Reek, J.I.van der Vlugt. *Chem. Commun.*, **55**, 12619 (2019)
108. P.Bonakdarzadeh, F.Topiå, E.Kalenius, S.Bhowmik, S.Sato, M.Groessl, R.Knochenmuss, K.Rissanen. *Inorg. Chem.*, **54**, 6055 (2015)
109. T.Sawada, M.Yoshizawa, S.Sato, M.Fujita. *Nat. Chem.*, **1**, 53 (2009)
110. B.M.Schmidt, T.Osuga, T.Sawada, M.Hoshino, M.Fujita. *Angew. Chem., Int. Ed.*, **55**, 1561 (2016)
111. D.Samanta, J.Gemen, Z.Chu, Y.Diskin-Posner, L.J.W.Shimon, R.Klajn. *Proc. Natl. Acad. Sci. USA*, **115**, 9379 (2018)
112. D.Samanta, D.Galaktionova, J.Gemen, L.J.W.Shimon, Y.Diskin-Posner, L.Avram, P.Král, R.Klajn. *Nat. Commun.*, **9**, 641 (2018)
113. B.Kilbas, S.Mirtschin, R.Scopelliti, K.Severin. *Chem. Sci.*, **3**, 701 (2012)
114. M.Han, R.Michel, B.He, Y.-S.Chen, D.Stalke, M.John, G.H.Clever. *Angew. Chem., Int. Ed.*, **52**, 1319 (2013)
115. R.Li, M.Han, J.Tessarolo, J.J.Holstein, J.Lübben, B.Dittrich, C.Volkmann, M.Finze, C.Jenne, G.H.Clever. *ChemPhotoChem*, **3**, 378 (2019)
116. Z.Li, N.Kishi, K.Yoza, M.Akita, M.Yoshizawa. *Chem. – Eur. J.*, **18**, 8358 (2012)
117. T.Tsutsui, S.Kusaba, M.Yamashina, M.Akita, M.Yoshizawa. *Chem. – Eur. J.*, **25**, 4320 (2019)
118. S.Matsuno, M.Yamashina, Y.Sei, M.Akita, A.Kuzume, K.Yamamoto, M.Yoshizawa. *Nat. Commun.*, **8**, 749 (2017)
119. S.Ganta, D.K.Chand. *Inorg. Chem.*, **57**, 3634 (2018)
120. T.Y.Kim, L.Digal, M.G.Gardiner, N.T.Lucas, J.D.Crowley. *Chem. – Eur. J.*, **23**, 15089 (2017)
121. K.Sarkar, M.Paul, P.Dastidar. *Chem. Commun.*, **52**, 13124 (2016)
122. J.Wang, C.He, P.Wu, J.Wang, C.Duan. *J. Am. Chem. Soc.*, **133**, 12402 (2011)
123. M.Pan, K.Wu, J.-H.Zhang, C.-Y.Su. *Coord. Chem. Rev.*, **378**, 333 (2019)
124. A.J.Metherell, M.D.Ward. *Dalton Trans.*, **45**, 16096 (2016)
125. G.Norjmaa, J.-D.Maréchal, G.Ujaque. *J. Am. Chem. Soc.*, **141**, 13114 (2019)
126. M.D.Levin, D.M.Kaphan, C.M.Hong, R.G.Bergman, K.N.Raymond, F.D.Toste. *J. Am. Chem. Soc.*, **138**, 9682 (2016)
127. C.Brückner, R.E.Powers, K.N.Raymond. *Angew. Chem., Int. Ed.*, **37**, 1837 (1998)
128. W.Cullen, A.J.Metherell, A.B.Wragg, C.G.P.Taylor, N.H.Williams, M.D.Ward. *J. Am. Chem. Soc.*, **140**, 2821 (2018)
129. J.S.Wright, A.J.Metherell, W.M.Cullen, J.R.Piper, R.Dawson, M.D.Ward. *Chem. Commun.*, **53**, 4398 (2017)
130. C.G.P.Taylor, J.R.Piper, M.D.Ward. *Chem. Commun.*, **52**, 6225 (2016)
131. S.Turega, M.Whitehead, B.R.Hall, A.J.H.M.Meijer, C.A.Hunter, M.D.Ward. *Inorg. Chem.*, **52**, 1122 (2013)
132. J.R.Piper, L.Cletheroe, C.G.P.Taylor, A.J.Metherell, J.A.Weinstein, I.V.Sazanovich, M.D.Ward. *Chem. Commun.*, **53**, 408 (2017)
133. P.Bonakdarzadeh, F.Pan, E.Kalenius, O.Jurček, K.Rissanen. *Angew. Chem., Int. Ed.*, **54**, 14890 (2015)
134. H.S.Scott, R.W.Staniland, P.E.Kruger. *Coord. Chem. Rev.*, **362**, 24 (2018)
135. N.Mihara, T.K.Ronson, J.R.Nitschke. *Angew. Chem., Int. Ed.*, **58**, 12497 (2019)
136. J.Jiao, Z.Li, Z.Qiao, X.Li, Y.Liu, J.Dong, J.Jiang, Y.Cui. *Nat. Commun.*, **9**, 4423 (2018)
137. F.J.Rizzuto, J.R.Nitschke. *Nat. Chem.*, **9**, 903 (2017)
138. W.Meng, B.Breiner, K.Rissanen, J.D.Thoburn, J.K.Clegg, J.R.Nitschke. *Angew. Chem., Int. Ed.*, **50**, 3479 (2011)
139. G.Liu, Z.Ju, D.Yuan, M.Hong. *Inorg. Chem.*, **52**, 13815 (2013)
140. M.Sun, Q.-Q.Wang, C.Qin, C.-Y.Sun, X.-L.Wang, Z.-M.Su. *Chem. – Eur. J.*, **25**, 2824 (2019)
141. D.Nam, J.Huh, J.Lee, J.H.Kwak, H.Y.Jeong, K.Choi, W.Choe. *Chem. Sci.*, **8**, 7765 (2017)
142. J.Liu, W.Duan, J.Song, X.Guo, Z.Wang, X.Shi, J.Liang, J.Wang, P.Cheng, Y.Chen, M.J.Zaworotko, Z.Zhang. *J. Am. Chem. Soc.*, **141**, 12064 (2019)
143. W.-H.Xing, H.-Y.Li, X.-Y.Dong, S.-Q.Zang. *J. Mater. Chem. A*, **6**, 7724 (2018)
144. H.S.Lee, S.Jee, R.Kim, H.-T.Bui, B.Kim, J.-K.Kim, K.S.Park, W.Choi, W.Kim, K.M.Choi. *Energy Environ. Sci.*, **13**, 519 (2020)
145. J.-R.Li, A.A.Yakovenko, W.Lu, D.J.Timmons, W.Zhuang, D.Yuan, H.-C.Zhou. *J. Am. Chem. Soc.*, **132**, 17599 (2010)
146. G.A.Craig, P.Larpent, S.Kusaka, R.Matsuda, S.Kitagawa, S.Furukawa. *Chem. Sci.*, **9**, 6463 (2018)
147. C.A.Rowland, G.R.Lorzing, E.J.Gosselin, B.A.Trump, G.P.A.Yap, C.M.Brown, E.D.Bloch. *J. Am. Chem. Soc.*, **140**, 11153 (2018)
148. G.R.Lorzing, E.J.Gosselin, B.A.Trump, A.H.P.York, A.Sturluson, C.A.Rowland, G.P.A.Yap, C.M.Brown, C.M.Simon, E.D.Bloch. *J. Am. Chem. Soc.*, **141**, 12128 (2019)
149. P.-C.Shi, X.Lin, J.Liang, X.-X.Li, Y.-B.Huang, R.Cao. *Inorg. Chem. Commun.*, **78**, 28 (2017)
150. J.M.Teo, C.J.Coghlan, J.D.Evans, E.Tsivion, M.Head-Gordon, C.J.Sumby, C.J.Doonan. *Chem. Commun.*, **52**, 276 (2016)
151. E.Amayuelas, A.Fidalgo-Marijuán, B.Bazán, M.-K.Urtiaga, G.Barandika, M.-I.Arriortua. *CrystEngComm*, **18**, 1709 (2016)
152. A.Carné-Sánchez, G.A.Craig, P.Larpent, T.Hirose, M.Higuchi, S.Kitagawa, K.Matsuda, K.Urayama, S.Furukawa. *Nat. Commun.*, **9**, 2506 (2018)
153. A.Carné-Sánchez, G.A.Craig, P.Larpent, V.Guillerm, K.Urayama, D.Maspoch, S.Furukawa. *Angew. Chem., Int. Ed.*, **58**, 6347 (2019)
154. M.A.Andrés, A.Carné-Sánchez, J.Sánchez-Laínez, O.Roubeau, J.Coronas, D.Maspoch, I.Gascón. *Chem. – Eur. J.*, **26**, 143 (2020)

155. T.Grancha, A.Carné-Sánchez, L.Hernández-López, J.Albalad, I.Imaz, J.Juanhuix, D.Maspoch. *J. Am. Chem. Soc.*, **141**, 18349 (2019)
156. R.Kumar, C.N.R.Rao. *Dalton Trans.*, **46**, 7998 (2017)
157. X.-Y.Xie, F.Wu, X.Liu, W.-Q.Tao, Y.Jiang, X.-Q.Liu, L.-B.Sun. *Chem. Commun.*, **55**, 6177 (2019)
158. X.-Y.Xie, F.Wu, X.-Q.Liu, L.-B.Sun. *Dalton Trans.*, **48**, 17153 (2019)
159. Y.Qin, Q.Zhang, Y.Li, X.Liu, Z.Lu, L.Zheng, S.Liu, Q.Cao, Z.Ding. *J. Mater. Chem. B*, **5**, 9365 (2017)
160. J.Park, L.-B.Sun, Y.-P.Chen, Z.Perry, H.-C.Zhou. *Angew. Chem., Int. Ed.*, **53**, 5842 (2014)
161. Y.Jiang, J.Park, P.Tan, L.Feng, X.-Q.Liu, L.-B.Sun, H.-C.Zhou.Elsevier, *J. Am. Chem. Soc.*, **141**, 8221 (2019)
162. Y.Bi, S.Du, W.Liao. *Coord. Chem. Rev.*, **276**, 61 (2014)
163. C.Tan, J.Jiao, Z.Li, Y.Liu, X.Han, Y.Cui. *Angew. Chem., Int. Ed.*, **57**, 2085 (2018)
164. F.-R.Dai, Y.Qiao, Z.Wang. *Inorg. Chem. Front.*, **3**, 243 (2016)
165. M.V.Kniazeva, A.S.Ovsyannikov, D.R.Islamov, A.I.Samigullina, A.T.Gubaidullin, S.E.Solovieva, I.S.Antipin, S.Ferlay. *Crystals*, **10**, 364 (2020)
166. W.-Y.Pei, J.Yang, H.Wu, W.Zhou, Y.-W.Yang, J.-F.Ma. *Chem. Commun.*, **56**, 2491 (2020)
167. T.-T.Guo, D.-M.Cheng, J.Yang, X.Xu, J.-F.Ma. *Chem. Commun.*, **55**, 6277 (2019)
168. R.A.S.Vasdev, D.Preston, J.D.Crowley. *Chem. – Asian J.*, **12**, 2513 (2017)
169. N.Hosono, S.Kitagawa. *Acc. Chem. Res.*, **51**, 2437 (2018)
170. V.V.Butova, M.A.Soldatov, A.A.Guda, K.A.Lomachenko, C.Lamberti. *Russ. Chem. Rev.*, **85**, 280 (2016)
171. H.Furukawa, K.E.Cordova, M.O'Keeffe, O.M.Yaghi. *Science*, **341**, 1230444 (2013)
172. M.O.Barsukova, S.A.Sapchenko, D.N.Dybtsev, V.P.Fedin. *Russ. Chem. Rev.*, **87**, 1139 (2018)
173. S.B.Peh, A.Karmakar, D.Zhao. *Trends Chem.*, **2**, 199 (2020)
174. A.Y.Tsivadze, O.E.Aksyutin, A.G.Ishkov, M.K.Knyazeva, O.V.Solovtsova, I.E.Men'shchikov, A.A.Fomkin, A.V.Shkolin, E.V.Khozina, V.A.Grachev. *Russ. Chem. Rev.*, **88**, 925 (2019)
175. Y.Lin, C.Kong, Q.Zhang, L.Chen. *Adv. Energy Mater.*, **7**, 1601296 (2017)
176. R.-B.Lin, S.Xiang, W.Zhou, B.Chen. *Chem.*, **6**, 337 (2020)
177. B.R.Barnett, M.I.Gonzalez, J.R.Long. *Trends Chem.*, **1**, 159 (2019)
178. P.Iacomi, F.Formalik, J.Marreiros, J.Shang, J.Rogacka, A.Mohmeyer, P.Behrens, R.Ameloot, B.Kuchta, P.L.Llewellyn. *Chem. Mater.*, **31**, 8413 (2019)
179. Z.Bao, G.Chang, H.Xing, R.Krishna, Q.Ren, B.Chen. *Energy Environ. Sci.*, **9**, 3612 (2016)
180. S.Mukherjee, A.V.Desai, S.K.Ghosh. *Coord. Chem. Rev.*, **367**, 82 (2018)
181. J.Pei, K.Shao, L.Zhang, H.-M.Wen, B.Li, G.Qian. *Top. Curr. Chem.*, **377**, 33 (2019)
182. J.Li, H.Wang, X.Yuan, J.Zhang, J.W.Chew. *Coord. Chem. Rev.*, **404**, 213116 (2020)
183. J.R.Li, J.Sculley, H.C.Zhou. *Chem. Rev.*, **112**, 869 (2012)
184. S.Mukherjee, B.Joarder, B.Manna, A.V.Desai, A.K.Chaudhari, S.K.Ghosh. *Sci. Rep.*, **4**, 5761 (2014)
185. D.S.Sholl, R.P.Lively. *Nature (London)*, **532**, 435 (2016)
186. Y.H.Kim. *Energy*, **100**, 58 (2016)
187. H.A.Mohameed, B.A.Jdayil, K.Takrouri. *Chem. Eng. Process. Process Intensif.*, **46**, 25 (2007)
188. M.Rasouli, N.Yaghobi, S.Chitsazan, M.H.Sayyar. *Microporous Mesoporous Mater.*, **152**, 141 (2012)
189. M.Rasouli, N.Yaghobi, F.Allahgholipour, H.Atashi. *Chem. Eng. Res. Des.*, **92**, 1192 (2014)
190. A.A.Alomair, Y.Alqaheem. *ACS Omega*, **4**, 19005 (2019)
191. E.Farsouni Eydi, A.Shariati, M.R.Khosravi-Nikou. *J. Dispers. Sci. Technol.*, **40**, 453 (2019)
192. C.Wang, L.Zhang, X.Huang, Y.Zhu, G.Li, Q.Gu, J.Chen, L.Ma, X.Li, Q.He, J.Xu, Q.Sun, C.Song, M.Peng, J.Sun, D.Ma. *Nat. Commun.*, **10**, 1 (2019)
193. C.H.Seo, Y.H.Kim. *Sep. Purif. Technol.*, **209**, 1 (2019)
194. M.Minceva, A.E.Rodrigues. *AIChE J.*, **53**, 138 (2007)
195. M.A.Moreira, A.F.P.Ferreira, J.C.Santos, J.M.Loureiro, A.E.Rodrigues. *Chem. Eng. Technol.*, **37**, 1483 (2014)
196. R.N.Devi, M.Edgar, J.Gonzalez, A.M.Z.Slawin, D.P.Tunstall, P.Grewal, P.A.Cox, P.A.Wright. *J. Phys. Chem. B*, **108**, 535 (2004)
197. Q.K.Liu, J.P.Ma, Y.B.Dong. *Chem. – Eur. J.*, **15**, 10364 (2009)
198. L.Alaerts, C.E.A.Kirschhock, M.Maes, M.A.Van Der Veen, V.Finsy, A.Depla, J.A.Martens, G.V.Baron, P.A.Jacobs, J.F.M.Denayer, D.E.De Vos. *Angew. Chem., Int. Ed.*, **46**, 4293 (2007)
199. V.Finsy, H.Verelst, L.Alaerts, D.De Vos, P.A.Jacobs, G.V.Baron, J.F.M.Denayer. *J. Am. Chem. Soc.*, **130**, 7110 (2008)
200. L.Alaerts, M.Maes, P.A.Jacobs, J.F.M.Denayer, D.E.De Vos. *Phys. Chem. Chem. Phys.*, **10**, 2979 (2008)
201. Z.Y.Gu, X.P.Yan. *Angew. Chem., Int. Ed.*, **49**, 1477 (2010)
202. P.Trens, H.Belarbi, C.Shepherd, P.Gonzalez, N.A.Ramsahye, U.H.Lee, Y.K.Seo, J.S.Chang. *Microporous Mesoporous Mater.*, **183**, 17 (2014)
203. C.X.Yang, X.P.Yan. *Anal. Chem.*, **83**, 7144 (2011)
204. W.Huang, J.Jiang, D.Wu, J.Xu, B.Xue, A.M.Kirillov. *Inorg. Chem.*, **54**, 10524 (2015)
205. R.Lyndon, J.Bacsa, M.L.Jue, R.P.Lively. *Cryst. Growth Des.*, **18**, 2890 (2018)
206. A.Torres-Knoop, R.Krishna, D.Dubbeldam. *Angew. Chem., Int. Ed.*, **53**, 7774 (2014)
207. S.-I.Kim, S.Lee, Y.G.Chung, Y.-S.Bae. *ACS Appl. Mater. Interfaces*, **11**, 31227 (2019)
208. X.Yang, H.-L.Zhou, C.-T.He, Z.-W.Mo, J.-W.Ye, X.-M.Chen, J.-P.Zhang. *Research*, Art. ID 9463719 (2019)
209. K.Nath, K.Biradha. *Cryst. Growth Des.*, **16**, 5606 (2016)
210. M.P.M.Nicolau, P.S.Bárcia, J.M.Gallegos, J.A.C.Silva, A.E.Rodrigues, B.Chen. *J. Phys. Chem. C*, **113**, 13173 (2009)
211. S.-Q.Wang, S.Mukherjee, E.Patyk-Kaźmierczak, S.Darwish, A.Bajpai, Q.-Y.Yang, M.J.Zaworotko. *Angew. Chem., Int. Ed.*, **58**, 6630 (2019)
212. Z.He, Y.Yang, P.Bai, X.Guo. *J. Ind. Eng. Chem.*, **77**, 262 (2019)
213. M.I.Gonzalez, M.T.Kapelewski, E.D.Bloch, P.J.Milner, D.A.Reed, M.R.Hudson, J.A.Mason, G.Barin, C.M.Brown, J.R.Long. *J. Am. Chem. Soc.*, **140**, 3412 (2018)
214. P.Navarro, A.Ovejero-Pérez, M.Ayuso, N.Delgado-Mellado, M.Larriba, J.García, F.Rodríguez. *J. Mol. Liq.*, **289**, 111120 (2019)
215. S.Feng, J.Sun, Z.Ren, Z.Zhou, F.Zhang, W.Liu. *Can. J. Chem. Eng.*, **97**, 3138 (2019)
216. M.Ayuso, A.Cañada-Barcala, M.Larriba, P.Navarro, N.Delgado-Mellado, J.García, F.Rodríguez. *Sep. Purif. Technol.*, **240**, 116583 (2020)

217. J.P.Garcia Villaluenga, A.Tabe-Mohammadi. *J. Membr. Sci.*, **169**, 159 (2000)
218. T.Xi, Y.Lu, X.Ai, L.Tang, L.Yao, W.Hao, P.Cui. *Polymer (Guildf.)*, **185**, 121948 (2019)
219. C.Zhao, N.Wang, L.Wang, S.Sheng, H.Fan, F.Yang, S.Ji, J.-R.Li, J.Yu. *AIChE J.*, **62**, 3706 (2016)
220. A.Banerjee, S.K.Ray. *J. Membr. Sci.*, **597**, 117729 (2020)
221. M.J.Emparan-Legaspi, J.Gonzalez, G.Gonzalez-Carrillo, S.G.Ceballos-Magaña, J.Canales-Vazquez, I.A.Aguayo-Villarreal, R.Muñiz-Valencia. *Microporous Mesoporous Mater.*, **294**, 109942 (2020)
222. G.Wang, B.Dou, Z.Zhang, J.Wang, H.Liu, Z.Hao. *J. Environ. Sci.*, **30**, 65 (2015)
223. W.Yang, K.Samanta, X.Wan, T.U.Thikekar, Y.Chao, S.Li, K.Du, J.Xu, Y.Gao, H.Zuilhof, A.C.-H.Sue. *Angew. Chem., Int. Ed.*, **59**, 3994 (2020)
224. J.Zhou, G.Yu, Q.Li, M.Wang, F.Huang. *J. Am. Chem. Soc.*, **142**, 2228 (2020)
225. S.Shimomura, S.Horike, R.Matsuda, S.Kitagawa. *J. Am. Chem. Soc.*, **129**, 10990 (2007)
226. Y.-X.Tan, Y.-P.He, J.Zhang. *Inorg. Chem.*, **51**, 9649 (2012)
227. A.Karmakar, A.V.Desai, B.Manna, B.Joarder, S.K.Ghosh. *Chem. – Eur. J.*, **21**, 7071 (2015)
228. L.Zhou, S.Wang, Y.Chen, C.Serre. *Microporous Mesoporous Mater.*, **290**, 109674 (2019)
229. C.-T.He, L.Jiang, Z.-M.Ye, R.Krishna, Z.-S.Zhong, P.-Q.Liao, J.Xu, G.Ouyang, J.-P.Zhang, X.-M.Chen. *J. Am. Chem. Soc.*, **137**, 7217 (2015)
230. V.A.Logvinenko, D.N.Dybtsev, V.A.Bolotov, V.P.Fedin. *J. Therm. Anal. Calorim.*, **121**, 491 (2015)
231. A.Liu, X.Peng, Q.Jin, S.K.Jain, J.M.Vicent-Luna, S.Calero, D.Zhao. *ACS Appl. Mater. Interfaces*, **11**, 4686 (2019)
232. S.Mukherjee, B.Manna, A.V.Desai, Y.Yin, R.Krishna, R.Babarao, S.K.Ghosh. *Chem. Commun.*, **52**, 8215 (2016)
233. A.Kondo, T.Suzuki, R.Kotani, K.Maeda. *Dalton Trans.*, **46**, 6762 (2017)
234. A.Santra, M.Francis, S.Parshamoni, S.Konar. *ChemistrySelect*, **2**, 3200 (2017)
235. S.Mukherjee, R.Babarao, A.V.Desai, B.Manna, S.K.Ghosh. *Cryst. Growth Des.*, **17**, 3581 (2017)
236. B.Manna, S.Mukherjee, A.V.Desai, S.Sharma, R.Krishna, S.K.Ghosh. *Chem. Commun.*, **51**, 15386 (2015)
237. A.Karmakar, P.Samanta, A.V.Desai, S.K.Ghosh. *Acc. Chem. Res.*, **50**, 2457 (2017)
238. Y.Huang, Z.Lin, H.Fu, F.Wang, M.Shen, X.Wang, R.Cao. *ChemSusChem*, **7**, 2647 (2014)
239. P.Das, S.K.Mandal. *ACS Appl. Mater. Interfaces*, **10**, 25360 (2018)
240. B.Joarder, S.Mukherjee, A.K.Chaudhari, A.V.Desai, B.Manna, S.K.Ghosh. *Chem. – Eur. J.*, **20**, 15303 (2014)
241. A.A.Lysova, D.G.Samsonenko, P.V.Dorovatovskii, V.A.Lazarenko, V.N.Khrustalev, K.A.Kovalenko, D.N.Dybtsev, V.P.Fedin. *J. Am. Chem. Soc.*, **141**, 17260 (2019)
242. J.-H.Wang, D.Luo, M.Li, D.Li. *Cryst. Growth Des.*, **17**, 3387 (2017)
243. E.Quartapelle-Procopio, F.Linares, C.Montoro, V.Colombo, A.Maspero, E.Barea, J.A.R.Navarro. *Angew. Chem., Int. Ed.*, **49**, 7308 (2010)
244. Y.Hijikata, S.Horike, M.Sugimoto, H.Sato, R.Matsuda, S.Kitagawa. *Chem. – Eur. J.*, **17**, 5138 (2011)
245. C.-T.He, Z.-M.Ye, Y.-T.Xu, Y.Xie, X.-L.Lian, J.-P.Zhang, X.-M.Chen. *Inorg. Chem. Front.*, **5**, 2777 (2018)
246. A.L.Nuzhdin, A.S.Shalygin, E.A.Artiukha, A.M.Chibiryaev, G.A.Bukhtiyarova, O.N.Martyanov. *RSC Adv.*, **6**, 62501 (2016)
247. Y.Voloshin, I.Belaya, R.Krämer. *The Encapsulation Phenomenon: Synthesis, Reactivity and Applications of Caged Ions and Molecules*. (Switzerland: Springer International Publishing, 2016)
248. Y.Voloshin, I.Belaya, R.Krämer. *Cage Metal Complexes: Clathrochelate Revisited*. (Switzerland: Springer International Publishing, 2017)
249. M.D.Wise, K.Severin. *Chimia*, **69**, 191 (2015)
250. S.M.Jansze, K.Severin. *Acc. Chem. Res.*, **51**, 2139 (2018)
251. R.M.Islamova, Y.B.Monakov. *Polym. Sci., Ser. C*, **53**, 27 (2011)
252. R.M.Islamova. *Russ. J. Gen. Chem.*, **86**, 125 (2016)
253. Y.Z.Voloshin, V.N.Novikov, Y.V.Nelyubina. *RSC Adv.*, **5**, 72621 (2015)
254. Y.Z.Voloshin, V.M.Buznik, A.G.Dedov. *Pure Appl. Chem.*, **92**, 1159 (2020)
255. S.M.Jansze, D.Ortiz, F.Fadaei-Tirani, R.Scopelliti, L.Menin, K.Severin. *Chem. Commun.*, **54**, 9529 (2018)
256. G.Cecot, B.Alameddine, S.Prior, R.De Zorzi, S.Geremia, R.Scopelliti, F. F.Fadaei-Tirani, E.Solari, K.Severin. *Chem. Commun.*, **52**, 11243 (2016)
257. G.Cecot, M.Marmier, S.Geremia, R.De Zorzi, A.V.Vologzhanina, P.Pattison, E.Solari, F.Fadaei-Tirani, R.Scopelliti, K.Severin. *J. Am. Chem. Soc.*, **139**, 8371 (2017)
258. G.Cecot, M.T.Doll, O.M.Planes, A.Ramorini, R.Scopelliti, F.Fadaei-Tirani, K.Severin. *Eur. J. Inorg. Chem.*, 2972 (2019)
259. S.M.Jansze, M.D.Wise, A.V.Vologzhanina, R.Scopelliti, K.Severin. *Chem. Sci.*, **8**, 1901 (2017)
260. M.Marmier, G.Cecot, A.V.Vologzhanina, J.L.Bila, I.Zivkovic, H.M.Ronnow, B.Nafradi, E.Solari, P.Pattison, R.Scopelliti, K.Severin. *Dalton Trans.*, **45**, 15507 (2016)
261. J.L.Bila, J.Pijeat, A.Ramorini, F.Fadaei-Tirani, R.Scopelliti, E.Baudat, K.Severin. *Dalton Trans.*, **48**, 4582 (2019)
262. J.L.Bila, M.Marmier, K.O.Zhurov, R.Scopelliti, I.Živković, H.M.Rønnow, N.E.Shaik, A.Sienkiewicz, C.Fink, K.Severin. *Eur. J. Inorg. Chem.*, 3118 (2018)
263. Z.Qin, F.Han, C.Ge, R.Zhang, Y.Zhang, X.Zhang. *Inorg. Chim. Acta*, **479**, 36 (2018)
264. O.M.Planes, P.A.Schouwink, J.L.Bila, F.Fadaei-Tirani, R.Scopelliti, K.Severin. *Cryst. Growth Des.*, **20**, 1394 (2020)
265. S.V.Dudkin, N.R.Erickson, A.V.Vologzhanina, V.V.Novikov, H.M.Rhoda, C.D.Holstrom, Y.V.Zatsikha, M.S.Yusubov, Y.Z.Voloshin, V.N.Nemykin. *Inorg. Chem.*, **55**, 11867 (2016)
266. G.E.Zelinskii, S.V.Dudkin, A.S.Chuprin, A.A.Pavlov, A.V.Vologzhanina, E.G.Lebed, Y.V.Zubavichus, Y.Z.Voloshin. *Inorg. Chim. Acta*, **463**, 29 (2017)
267. S.V.Dudkin, A.S.Belov, Y.V.Nelyubina, A.V.Savchuk, A.A.Pavlov, V.V.Novikov, Y.Z.Voloshin. *New J. Chem.*, **41**, 3251 (2017)
268. S.V.Dudkin, S.A.Savkina, A.S.Belov, Y.Z.Voloshin. *Macroheterocycles*, **11**, 418 (2018)
269. O.V.Gradov, M.A.Gradova, S.V.Dudkin, Y.Z.Voloshin, A.V.Lobanov. *Macroheterocycles*, **10**, 540 (2017)

270. S.A.Belova (Savkina), S.V.Dudkin, A.S.Belov, Y.V.Nelyubina, V.V.Novikov, Y.V.Zubavichus, Y.Z.Voloshin. *Macroheterocycles*, **12**, 193 (2019)
271. G.E.Zelinskii, A.S.Belov, A.V.Vologzhanina, I.P.Limarev, A.A.Pavlov, V.A.Olshevskaya, A.V.Makarenkov, P.V.Dorovatovskii, E.G.Lebed, Y.Z.Voloshin. *ChemistrySelect*, **4**, 11572 (2019)
272. J.Blechinger, O.A.Varzackii, V.Kovalska, G.E.Zelinskii, Y.Z.Voloshin, E.Kinski, A.Mokhir. *Bioorg. Med. Chem. Lett.*, **26**, 626 (2016)
273. O.A.Varzatskii, A.V.Vologzhanina, V.V.Novikov, S.V.Vakarov, R.V.Oblap, Y.Z.Voloshin. *Inorg. Chim. Acta*, **482**, 90 (2018)
274. A.S.Belov, V.V.Novikov, G.E.Zelinskii, A.V.Vologzhanina, O.A.Varzatskii, B.F.Myasoedov, Y.Z.Voloshin. *Inorg. Chem. Commun.*, **72**, 23 (2016)
275. G.E.Zelinskii, A.S.Belov, A.V.Vologzhanina, A.A.Pavlov, V.V.Novikov, O.A.Varzatskii, Y.Z.Voloshin. *Inorg. Chim. Acta*, **448**, 7 (2016)
276. R.A.Selin, N.V.Chornenka, V.Y.Chernii, A.Mokhir, A.V.Vologzhanina, A.S.Belov, A.L.Pomadchik, Y.Z.Voloshin. *Inorg. Chim. Acta*, **496**, 119047 (2019)
277. V.B.Kovalska, S.V.Vakarov, M.V.Kuperman, M.Y.Losytskyy, E.Gumienna-Kontecka, Y.Z.Voloshin, O.A.Varzatskii. *Dalton Trans.*, **47**, 1036 (2018)
278. V.Kovalska, M.Kuperman, M.Losytskyy, S.Vakarov, S.Potocki, S.Yarmoluk, Y.Voloshin, O.Varzatskii, E.Gumienna-Kontecka. *Metallomics*, **11**, 338 (2019)
279. V.Kovalska, S.Vakarov, M.Losytskyy, M.Kuperman, N.Chornenka, Y.Toporivska, E.Gumienna-Kontecka, Y.Voloshin, O.Varzatskii, A.Mokhir. *RSC Adv.*, **9**, 24218 (2019)
280. S.V.Vakarov, M.V.Kuperman, V.B.Koval'skaya, O.A.Varzatskii. *Ukr. Khim. Zh.*, **81**, 116 (2015)
281. S.I.Shylin, M.V.Pavliuk, L.D'Amario, F.Mamedov, J.Sá, G.Berggren, I.O.Fritsky. *Chem. Commun.*, **55**, 3335 (2019)
282. S.I.Shylin, M.V.Pavliuk, L.D'Amario, I.O.Fritsky, G.Berggren. *Faraday Discuss.*, **215**, 162 (2019)
283. Y.Z.Voloshin, V.V.Novikov, Y.V.Nelyubina, A.S.Belov, D.M.Roitershtein, A.Savitsky, A.Mokhir, J.Sutter, M.E.Miehlich, K.Meyer. *Chem. Commun.*, **54**, 3436 (2018)
284. T.M.Ozvat, M.E.Peña, J.M.Zadrozny. *Chem. Sci.*, **10**, 6727 (2019)
285. A.A.Pavlov, S.A.Savkina, A.S.Belov, Y.Z.Voloshin, Y.V.Nelyubina, V.V.Novikov. *ACS Omega*, **3**, 4941 (2018)
286. A.Müller, E.Krickemeyer, H.Bögge, M.Schmidtmann, F.Peters. *Angew. Chem., Int. Ed.*, **37**, 3359 (1998)
287. A.Müller. *Science*, **300**, 749 (2003)
288. A.Müller. *Chem. Commun.*, 803 (2003)
289. A.Müller, S.Sarkar, S.Q.N.Shah, H.Bögge, M.Schmidtmann, S.Sarkar, P.Kögerler, B.Hauptfleisch, A.X.Trautwein, V.Schünemann. *Angew. Chem., Int. Ed.*, **38**, 3238 (1999)
290. A.Müller, M.Luban, C.Schröder, R.Modler, P.Kögerler, M.Axenovich, J.Schnack, P.Canfield, S.Bud'ko, N.Harrison. *ChemPhysChem*, **2**, 517 (2001)
291. T.Liu. *J. Am. Chem. Soc.*, **124**, 10942 (2002)
292. T.Liu. *J. Am. Chem. Soc.*, **125**, 312 (2003)
293. T.Liu, B.Imber, E.Diemann, G.Liu, K.Cokleski, H.Li, Z.Chen, A.Müller. *J. Am. Chem. Soc.*, **128**, 15914 (2006)
294. T.Liu. *J. Clust. Sci.*, **14**, 215 (2003)
295. A.Müller, E.Krickemeyer, S.K.Das, P.Kögerler, S.Sarkar, H.Bögge, M.Schmidtmann, S.Sarkar. *Angew. Chem., Int. Ed.*, **39**, 1612 (2000)
296. A.Müller, S.K.Das, E.Krickemeyer, P.Kögerler, H.Bögge, M.Schmidtmann. *Solid State Sci.*, **2**, 847 (2000)
297. A.M.Todea, J.Szakács, S.Konar, H.Bögge, D.C.Crans, T.Glaser, H.Rousselière, R.Thouvenot, P.Gouzerh, A.Müller. *Chem. – Eur. J.*, **17**, 6635 (2011)
298. A.Müller, A.M.Todea, H.Bögge, J.van Slageren, M.Dressel, A.Stammler, M.Rusu. *Chem. Commun.*, 3066 (2006)
299. A.Müller, S.K.Das, H.Bögge, M.Schmidtmann, A.Botar, A.Patrut. *Chem. Commun.*, 657 (2001)
300. A.Müller, S.K.Das, P.Kögerler, H.Bögge, M.Schmidtmann, A.X.Trautwein, V.Schünemann, E.Krickemeyer, W.Preetz. *Angew. Chem., Int. Ed.*, **39**, 3413 (2000)
301. A.M.Todea, A.J.M.Al-Karawi, T.Glaser, S.Walleck, L.-M.Chamoreau, R.Thouvenot, P.Gouzerh, A.Müller. *Inorg. Chim. Acta*, **389**, 107 (2012)
302. A.Müller, S.K.Das, M.O.Talismanova, H.Bögge, P.Kögerler, M.Schmidtmann, S.S.Talismanov, M.Luban, E.Krickemeyer. *Angew. Chem., Int. Ed.*, **41**, 579 (2002)
303. A.Müller, S.Q.N.Shah, H.Bögge, M.Schmidtmann, P.Kögerler, B.Hauptfleisch, S.Leiding, K.Wittler. *Angew. Chem., Int. Ed.*, **39**, 1614 (2000)
304. A.M.Todea, A.Merca, H.Bögge, J.van Slageren, M.Dressel, L.Engelhardt, M.Luban, T.Glaser, M.Henry, A.Müller. *Angew. Chem., Int. Ed.*, **46**, 6106 (2007)
305. M.L.Kistler, T.Liu, P.Gouzerh, A.M.Todea, A.Müller. *Dalton Trans.*, 5094 (2009)
306. A.Müller, A.M.Todea, J.van Slageren, M.Dressel, H.Bögge, M.Schmidtmann, M.Luban, L.Engelhardt, M.Rusu. *Angew. Chem., Int. Ed.*, **44**, 3857 (2005)
307. B.Botar, P.Kögerler, C.L.Hill. *Chem. Commun.*, 3138 (2005)
308. A.Müller, B.Botar, H.Bögge, P.Kögerler, A.Berkle. *Chem. Commun.*, 2944 (2002)
309. B.Botar, P.Kögerler, A.Müller, R.Garcia-Serres, C.L.Hill. *Chem. Commun.*, 5621 (2005)
310. A.Müller, H.Bögge, F.L.Sousa, M.Schmidtmann, D.G.Kurth, D.Volkmer, J.van Slageren, M.Dressel, M.L.Kistler, T.Liu. *Small*, **3**, 986 (2007)
311. A.M.Todea, A.Merca, H.Bögge, T.Glaser, J.M.Pigga, M.L.K.Langston, T.Liu, R.Prozorov, M.Luban, C.Schröder, W.H.Casey, A.Müller. *Angew. Chem., Int. Ed.*, **49**, 514 (2010)
312. A.M.Todea, A.Merca, H.Bögge, T.Glaser, L.Engelhardt, R.Prozorov, M.Luban, A.Müller. *Chem. Commun.*, 3351 (2009)
313. Y.Li, Y.-G.Li, Z.-M.Zhang, Q.Wu, E.-B.Wang. *Inorg. Chem. Commun.*, **12**, 864 (2009)
314. M.L.Kistler, A.Bhatt, G.Liu, D.Casa, T.Liu. *J. Am. Chem. Soc.*, **129**, 6453 (2007)
315. D.Volkmer, A.Du Chesne, D.G.Kurth, H.Schnablegger, P.Lehmann, M.J.Koop, A.Müller. *J. Am. Chem. Soc.*, **122**, 1995 (2000)
316. D.G.Kurth, P.Lehmann, D.Volkmer, A.Müller, D.Schwahn. *J. Chem. Soc., Dalton Trans.*, 3989 (2000)
317. A.Müller, S.Polarz, S.K.Das, E.Krickemeyer, H.Bögge, M.Schmidtmann, B.Hauptfleisch. *Angew. Chem., Int. Ed.*, **38**, 3241 (1999)
318. A.Müller, V.P.Fedin, C.Kuhlmann, H.Bögge, M.Schmidtmann. *Chem. Commun.*, 927 (1999)

319. C.Schäffer, A.M.Todea, H.Bögge, O.A.Petina, D.Rehder, E.T.K.Haupt, A.Müller. *Chem. – Eur. J.*, **17**, 9634 (2011)
320. C.Schäffer, H.Bögge, A.Merca, I.A.Weinstock, D.Rehder, E.T.K.Haupt, A.Müller. *Angew. Chem., Int. Ed.*, **48**, 8051 (2009)
321. A.Müller, L.Toma, H.Bögge, M.Henry, E.T.K.Haupt, A.Mix, F.L.Sousa. *Chem. Commun.*, 3396 (2006)
322. C.Besson, S.Schmitz, K.M.Capella, S.Kopilevich, I.A.Weinstock, P.Kögerler. *Dalton Trans.*, **41**, 9852 (2012)
323. A.Ziv, A.Grego, S.Kopilevich, L.Zeiri, P.Miro, C.Bo, A.Müller, I.A.Weinstock. *J. Am. Chem. Soc.*, **131**, 6380 (2009)
324. A.Müller, S.K.Das, S.Talismanov, S.Roy, E.Beckmann, H.Bögge, M.Schmidtmann, A.Merca, A.Berkle, L.Allouche, Y.Zhou, L.Zhang. *Angew. Chem., Int. Ed.*, **42**, 5039 (2003)
325. A.Müller, E.Krickemeyer, H.Bögge, M.Schmidtmann, B.Botar, M.O.Talismanova. *Angew. Chem., Int. Ed.*, **42**, 2085 (2003)
326. M.Rubčiá, V.S.Korenev, L.Toma, H.Bögge, V.P.Fedin, A.Müller. *Inorg. Chem. Front.*, **1**, 740 (2014)
327. S.Garai, E.T.K.Haupt, H.Bögge, A.Merca, A.Müller. *Angew. Chem., Int. Ed.*, **51**, 10528 (2012)
328. A.Müller, E.Krickemeyer, H.Bögge, M.Schmidtmann, S.Roy, A.Berkle. *Angew. Chem., Int. Ed.*, **41**, 3604 (2002)
329. F.Bannani, S.Floquet, N.Leclerc-Laronze, M.Haouas, F.Taulelle, J.Marrot, P.Kögerler, E.Cadot. *J. Am. Chem. Soc.*, **134**, 19342 (2012)
330. E.Cadot, B.Salignac, S.Halut, F.Sécheresse. *Angew. Chem., Int. Ed.*, **37**, 611 (1998)
331. V.S.Korenev, A.G.Boulay, M.Haouas, F.Bannani, V.P.Fedin, M.N.Sokolov, E.Terazzi, S.Garai, A.Müller, F.Taulelle, J.Marrot, N.Leclerc, S.Floquet, E.Cadot. *Chem. – Eur. J.*, **20**, 3097 (2014)
332. C.Schäffer, A.Merca, H.Bögge, A.M.Todea, M.L.Kistler, T.Liu, R.Thouvenot, P.Gouzerh, A.Müller. *Angew. Chem., Int. Ed.*, **48**, 149 (2009)
333. V.S.Korenev, P.A.Abramov, C.Vicent, A.A.Zhdanov, A.R.Tsygankova, M.N.Sokolov, V.P.Fedin. *Dalton Trans.*, **44**, 8839 (2015)
334. T.Shibahara, H.Akashi, S.Nagahata, H.Hattori, H.Kuroya. *Inorg. Chem.*, **28**, 362 (1989)
335. C.Schäffer, A.M.Todea, H.Bögge, S.Floquet, E.Cadot, V.S.Korenev, V.P.Fedin, P.Gouzerh, A.Müller. *Dalton Trans.*, **42**, 330 (2013)
336. C.Schäffer, A.M.Todea, H.Bögge, E.Cadot, P.Gouzerh, S.Kopilevich, I.A.Weinstock, A.Müller. *Angew. Chem., Int. Ed.*, **50**, 12326 (2011)
337. S.Kopilevich, A.Gil, M.Garcia-Ratés, J.Bonet-Ávalos, C.Bo, A.Müller, I.A.Weinstock. *J. Am. Chem. Soc.*, **134**, 13082 (2012)
338. N.V.Izarova, O.A.Kholdeeva, M.N.Sokolov, V.P.Fedin. *Russ. Chem. Bull., Int. Ed.*, **58**, 134 (2009)
339. F.Jalilian, B.Yadollahi, M.R.Farsani, S.Tangestaninejad, H.A.Rudbari, R.Habibi. *RSC Adv.*, **5**, 70424 (2015)
340. F.Jalilian, B.Yadollahi, M.R.Farsani, S.Tangestaninejad, H.A.Rudbari, R.Habibi. *Catal. Commun.*, **66**, 107 (2015)
341. E.Nikbakht, B.Yadollahi, M.R.Farsani. *Inorg. Chem. Commun.*, **55**, 135 (2015)
342. H.Taghiyar, B.Yadollahi. *Polyhedron*, **156**, 98 (2018)
343. H.Taghiyar, B.Yadollahi. *Sci. Total Environ.*, **708**, 134860 (2020)
344. A.Rezaeifard, R.Haddad, M.Jafarpour, M.Hakimi. *J. Am. Chem. Soc.*, **135**, 10036 (2013)
345. S.Floquet, E.Terazzi, A.Hijazi, L.Guénée, C.Piguet, E.Cadot. *New J. Chem.*, **36**, 865 (2012)
346. S.Floquet, E.Terazzi, V.S.Korenev, A.Hijazi, L.Guénée, E.Cadot. *Liq. Cryst.*, **41**, 1000 (2014)
347. G.Jin, S.-M.Wang, W.-L.Chen, C.Qin, Z.-M.Su, E.-B.Wang. *J. Mater. Chem. A*, **1**, 6727 (2013)
348. M.Xie, W.Chen, Y.Dong, L.Chen, J.Li, E.Wang. *Dyes Pigm.*, **166**, 174 (2019)
349. V.Fazylova, N.Shevtsev, S.Mikhailov, G.Kim, A.Ostroushko, K.Grzhegorzhevskii. *Chem. – Eur. J.*, **26**, 5685 (2020)
350. A.A.Ostroushko, I.F.Gette, S.Y.Medvedeva, I.G.Danilova, E.A.Mukhlynina, M.O.Tonkushina, M.V.Morozova. *Nanotechnol. Russ.*, **8**, 672 (2013)
351. A.A.Ostroushko, I.F.Gette, I.G.Danilova, E.A.Mukhlynina, M.O.Tonkushina, K.V.Grzhegorzhevskii. *Nanotechnol. Russ.*, **9**, 577 (2014)
352. M.O.Tonkushina, I.D.Gagarin, K.V.Grzhegorzhevskii, A.A.Ostroushko. *Vestn. Ural. Med. Akad. Nauk*, **49**, 62 (2014)
353. A.A.Ostroushko, K.V.Grzhegorzhevskii, G.P.Bystrai, S.A.Okhotnikov. *Russ. J. Phys. Chem.*, **89**, 1638 (2015)
354. I.D.Gagarin, N.A.Kulesh, M.O.Tonkushina, D.A.Vlasov, A.A.Ostroushko. In *Fiziko-Khimicheskie Aspekty Izucheniya Klasterov, Nanostruktur i Nanomaterialov. (Mezhvuz. Sb. Nauch. Tr.). [Physicochemical Aspects of the Study of Clusters, Nanostructures and Nanomaterials (Interuniversity Collection of Scientific Papers)*. (Eds V.M.Samsonov, N.Yu. Sdobnyakova). (Tver': Tver. State Univ, 2017). No. 9, P. 147
355. A.A.Ostroushko, I.D.Gagarin, M.O.Tonkushina, K.V.Grzhegorzhevskii, I.G.Danilova, I.F.Gette, G.A.Kim. *Russ. J. Phys. Chem.*, **91**, 1811 (2017)
356. A.Ostroushko, I.Gagarin, M.Tonkushina, K.Grzhegorzhevskii, O.Russkikh. *J. Clust. Sci.*, **29**, 111 (2017)
357. I.G.Danilova, I.F.Gette, S.Y.Medvedeva, E.A.Mukhlynina, M.O.Tonkushina, A.A.Ostroushko. *Nanotechnol. Russ.*, **10**, 820 (2015)
358. I.G.Danilova, I.F.Gette, S.Y.Medvedeva, A.V.Belousova, M.O.Tonkushina, A.A.Ostroushko. *Nanotechnol. Russ.*, **11**, 653 (2016)
359. I.F.Gette, S.Yu.Medvedeva, A.A.Ostroushko. *Russ. J. Immunol.,* **11** (2), 280 (2017)
360. A.A.Ostroushko, I.G.Danilova, S.A.Brilliant, I.F.Gette. *Nanotechnol. Russ.*, **14**, 159 (2019)
361. A.A.Ostroushko, M.V.Ulitko, M.O.Tonkushina, I.V.Zubarev, S.Y.Medvedeva, I.G.Danilova, O.V.Gubaeva, I.D.Gagarin, I.F.Gette. *Nanotechnol. Russ.*, **13**, 1 (2018)
362. A.A.Ostroushko, I.D.Gagarin, K.V.Grzhegorzhevskii, I.F.Gette, D.A.Vlasov, A.A.Ermoshin, O.N.Antosyuk, S.V.Shikhova, I.G.Danilova. *J. Mol. Liq.*, **301**, 110910 (2020)
363. K.V.Grzhegorzhevskii, M.O.Tonkushina, A.V.Fokin, K.G.Belova, A.A.Ostroushko. *Dalton Trans.*, **48**, 6984 (2019)
364. J.Elistratova, B.Akhmadeev, A.Gubaidullin, V.Korenev, M.Sokolov, I.Nizameev, A.Stepanov, I.Ismaev, M.Kadirov, A.Voloshina, A.Mustafina. *New J. Chem.*, **41**, 5271 (2017)

365. J.Elistratova, B.Akhmadeev, V.Korenev, M.Sokolov, I.Nizameev, A.Gubaidullin, A.Voloshina, A.Mustafina. *Soft Matter*, **14**, 7916 (2018)
366. S.Pizzanelli, R.Zairov, M.Sokolov, M.C.Mascherpa, B.Akhmadeev, A.Mustafina, L.Calucci. *J. Phys. Chem. C*, **123**, 18095 (2019)
367. J.Elistratova, B.Akhmadeev, V.Korenev, M.Sokolov, I.Nizameev, I.Ismaev, M.Kadirov, A.Sapunova, A.Voloshina, R.Amirov, A.Mustafina. *J. Mol. Liq.*, **296**, 111821 (2019)
368. E.V.Anslyn. *J. Org. Chem.*, **72**, 687 (2007)
369. L.You, D.Zha, E.V.Anslyn. *Chem. Rev.*, **115**, 7840 (2015)
370. J.L.Atwood, J.W.Steed. *Encyclopedia of Supramolecular Chemistry*. (Boca Raton, FL: CRC Press, Taylor and Francis, 2004)
371. E.Busseron, Y.Ruff, E.Moulin, N.Giuseppone. *Nanoscale*, **5**, 7098 (2013)
372. A.J.Savyasachi, O.Kotova, S.Shanmugaraju, S.J.Bradberry, G.M.Ó'Máille, T.Gunnlaugsson. *Chem*, **3**, 764 (2017)
373. N.F.Goldshleger, A.S.Lobach, V.E.Baulin, A.Y.Tsivadze. *Russ. Chem. Rev.*, **86**, 269 (2017)
374. D.J.Cram. *J. Incl. Phenom.*, **6**, 397 (1988)
375. A.Ballesteros-Gómez, M.D.Sicilia, S.Rubio. In *Encyclopedia of Analytical Chemistry*. (Ed. R.A.Meyers). (Chichester: Wiley, 2010). P. 1; https://doi.org/10.1002/9780470027318.a9181
376. A.Ballesteros-Gómez, M.D.Sicilia, S.Rubio. *Anal. Chim. Acta*, **677**, 108 (2010)
377. S.Rubio, D.Pérez-Bendito. *TrAC – Trends Anal. Chem.*, **22**, 470 (2003)
378. E.R.Garcia, A.M.B.Gómez. In *Encyclopedia of Analytical Chemistry: Applications, Theory and Instrumentation*. (Chichester: Wiley, 2019). P. 1
379. A.Ballesteros-Gómez, N.Caballero-Casero, S.Garcia-Fonseca, L.Lunar, S.Rubio. *Chemosphere*, **223**, 569 (2019)
380. E.Pramauro, E.Pelizzetti. *Surfactants in Analytical Chemistry*. (Amsterdam: Elsevier, 1996)
381. S.B.Savvin, R.K.Chernova, S.N.Shtykov. *Poverkhnostno-aktivnye Veshestva. (Surfactants)*. (Moscow: Nauka, 1991)
382. S.N.Shtykov. *J. Anal. Chem.*, **55**, 608 (2000)
383. S.N.Shtykov. *J. Anal. Chem.*, **57**, 859 (2002)
384. A.Ballesteros-Gómez, S.Rubio, D.Pérez-Bendito. *J. Chromatogr. A*, **1216**, 530 (2009)
385. S.N.Shtykov. In *Analiticheskaya Khimiya. Instrumental'nye Metody Analiza*. (Analytical chemistry. Instrumental Analysis Methods) Vol. 3. Pt. 2. (Ed.A.A.Ishchenko). (Moscow: Fizmatlit, 2020). P. 96
386. S.N.Shtykov. In. *Nanoob'ekty i Nanotekhnologii v Khimicheskom Analize. (Ser. Problemy Analiticheskoi-Khimii. Nauchnyi Sovet po Analiticheskoi Khimii OKhNM RAN). [Nanoobjects and Nanotechnologies in Chemical Analysis. (Ser. Problems of Analytical Chemistry. Scientific Council for Analytical Chemistry, OKHNM RAS)]*. Vol. 20. (Ed. S.N.Shtykov). (Moscow: Nauka, 2015). P. 11
387. S.N.Shtykov. In *Uspekhi Analiticheskoi Khimii: k 75-letiyu Akademika Yu.A.Zolotova. (Advances in Analytical Chemistry: to the 75th Anniversary of Academician Yu.A.Zolotov)*. (Moscow: Nauka, 2007). P. 301
388. S.N.Shtykov. In *Nanoanalytics*: *Nanoobjects and Nanotechnologies in Analytical Chemistry*. (Ed. S.Shtykov). (Berlin: De Gruyter, 2018). P. 3
389. S.B.Savvin, S.N.Shtykov, A.V.Mikhailova. *Russ. Chem. Rev.*, **75**, 341 (2006)
390. S.N.Shtykov. In *Lyuminestsentnyi Analiz. (Ser. Problemy Analiticheskoi Khimii. Nauchnyi Sovet po Analiticheskoi Khimii OKhNM RAN). [Luminescence Analysis (Ser. Problems of Analytical Chemistry. Scientific Council for Analytical Chemistry, OKHNM RAS)]*. Vol. 19. (Ed. G.I.Romanovskaya). (Moscow: Nauka, 2015). P. 121
391. S.N.Shtykov, I.Yu.Goryacheva *Opt. Spectrosc.*, **83**, 645 (1997)
392. G.K.Ziyatdinova, E.R.Ziganshina, H.C.Budnikov. *J. Anal. Chem.*, **67**, 869 (2012)
393. D.Y.Pharr. *Phys. Sci. Rev.*, **2**, 20170006 (2017)
394. J.J.S.Rodriguez, Z.S.Ferrera, D.V.Moreno, M.E.T.Padrón, C.M.Santana. *Anal. Bioanal. Chem.*, **391**, 725 (2008)
395. A.Ballesteros-Gómez, L.Lunar, M.D.Sicilia, S.Rubio. *Chromatographia*, **82**, 111 (2019)
396. A.Melnyk, L.Wolska, J.Namieśnik. *J. Chromatogr. A*, **1339**, 1 (2014)
397. F.Merino, S.Rubio, D.Pérez-Bendito. *J. Sep. Sci.*, **28**, 1613 (2005)
398. S.Gangula, S.-Y.Suen, E.D.Conte. *Microchem. J.*, **95**, 2 (2010)
399. T.D.Smirnova, S.N.Shtykov, E.A.Zhelobitskaya. *Phys. Sci. Rev.*, **4**, 20189981 (2018)
400. E.G.Sumina, S.N.Shtykov, N.V.Tyurina. *J. Anal. Chem.*, **58**, 720 (2003)
401. E.M.Basova, V.M.Ivanov, O.A.Shpigun. *Russ. Chem. Rev.*, **68**, 983 (1999)
402. N.G.Tolmacheva, M.Zhang, A.V.Pirogov, M.V.Popik, O.A.Shpigun. *J. Anal. Chem.*, **72**, 602 (2017)
403. A.V.Pirogov, O.A.Shpigun. *J. Anal. Chem.*, **75**, 139 (2020)
404. L.A.Kartsova, E.G.Strel'nikova. *J. Anal. Chem.*, **64**, 156 (2009)
405. A.A.Derbina, A.V.Pirogov, I.D.Kargin, O.A.Shpigun. *J. Anal. Chem.*, **70**, 1271 (2015)
406. M.F.Silva, E.S.Cerutti, L.D.Martinez. *Microchim. Acta*, **155**, 349 (2006)
407. N.O.Mchedlov-Petrossyan. *Pure Appl. Chem.*, **80**, 1459 (2008)
408. N.A.Vodolazkaya, Y.A.Gurina, N.V.Salamanova, N.O.Mchedlov-Petrossyan. *J. Mol. Liq.*, **145**, 188 (2009)
409. S.N.Shtykov, E.V.Parshina. *Zh. Anal. Khim.*, **50**, 740 (1995)
410. S.B.Savvin, I.N.Marov, R.K.Chernova, S.N.Shtykov, A.B.Sokolov. *Zh. Anal. Khim.*, **36**, 850 (1981)
411. H.Ishii, H.Watanabe. *Bunseki Kagaku*, **26**, 86 (1977)
412. B.Fröschl, G.Stangl, R.Niessner. *Fresenius J. Anal. Chem.*, **357**, 743 (1997)
413. R.Carabias-Martínez, E.Rodríguez-Gonzalo, B.Moreno-Cordero, J.L.Pérez-Pavón, C.García-Pinto, E.F.Laespada. *J. Chromatogr. A*, **902**, 251 (2000)
414. S.N.Shtykov, E.G.Sumina, M.I.Malova. *J. Anal. Chem.*, **52**, 636 (1997)
415. I.Y.Goryacheva, S.N.Shtykov, A.S.Loginov, I.V.Panteleeva. *Anal. Bioanal. Chem.*, **382**, 1413 (2005)
416. D.W.Armstrong, S.J.Henry. *J. Liq. Chromatogr.*, **3**, 657 (1980)
417. D.W.Armstrong, R.Q.Terrill. *Anal. Chem.*, **51**, 2160 (1979)
418. S.N.Shtykov, E.G.Sumina, E.V.Smushkina, N.V.Tyurina. *J. Planar Chromatogr. — Mod. TLC*, **13**, 182 (2000)

419. S.N.Shtykov, E.G.Sumina, V.Z.Uglanova, O.N.Sorokina. *J. Anal. Chem.*, **72**, 870 (2017)
420. E.G.Sumina, S.N.Shtykov, O.N.Sorokina, V.Z.Uglanova. *J. Anal. Chem.*, **69**, 1009 (2014)
421. L.A.Kartsova, E.G.Strel'nikova. *J. Anal. Chem.*, **62**, 872 (2007)
422. A.Boichenko, I.Makhno, A.Renkevich, L.Loginova. *J. Planar Chromatogr. — Mod. TLC*, **24**, 463 (2011)
423. S.Terabe, K.Otsuka, K.Ichikawa, A.Tsuchiya, T.Ando. *Anal. Chem.*, **56**, 111 (1984)
424. H.Watarai. *Chem. Lett.*, **20**, 391 (1991)
425. *Kapillyarnyi Elektroforez.(Ser. Problemy Analiticheskoi Khimii. Nauchnyi Sovet po Analiticheskoi Khimii OKhNM RAN)*. [Capillary Electrophoresis. (Ser. Problems of Analytical Chemistry. Scientific Council for Analytical Chemistry, OKHNM RAS)]. Vol. 18. (Ed. L.A.Kartsova) (Moscow: Nauka, 2014)
426. R.von Wandruszka. *Crit. Rev. Anal. Chem.*, **23**, 187 (1992)
427. A.V.Antonovich, Yu.V.Egorova, D.I.Skripinets, V.P.Aleksandrova. *Metod. Ob'ekt. Khim. Analiza*, **5**, 180 (2010)
428. L.J.C.Love, M.Skrilec, J.G.Habarta. *Anal. Chem.*, **52**, 754 (1980)
429. L.V.Levshin, S.N.Shtykov, I.Yu.Goryacheva, G.V.Mel'nikov. *J. Appl. Spectrosc.*, **66**, 212 (1999)
430. A.Sanz-Medel, J.I.G.Alonso, E.B.Gonzalez. *Anal. Chem.*, **57**, 1681 (1985)
431. G.V.Mel'nikov, I.Yu.Goryacheva, S.N.Shtykov. *Dokl. Akad. Nauk*, **361**, 72 (1998)
432. I.Yu.Goryacheva, G.V.Mel'nikov, S.N.Shtykov. *J. Anal. Chem.*, **55**, 874 (2000)
433. G.Melnikov, S.Shtykov, I.Goryacheva. *Anal. Chim. Acta*, **439**, 81 (2001)
434. S.Lis, M.Elbanowski, B.Makowska, Z.Hnatejko. *J. Photochem. Photobiol. A*, **150**, 233 (2002)
435. N.Arnaud, J.Georges. *Spectrochim. Acta, Part A*, **59**, 1829 (2003)
436. T.D.Smirnova, S.N.Shtykov, V.I.Kochubei, E.S.Khryachkova. *Opt. Spectrosc.*, **110**, 60 (2011)
437. S.N.Shtykov, T.D.Smirnova, Y.G.Bylinkin. *J. Anal. Chem.*, **59**, 438 (2004)
438. N.Selivanova, K.Vasilieva, Y.Galyametdinov. *Luminescence*, **29**, 202 (2013)
439. S.N.Shtykov, T.D.Smirnova, Y.V.Molchanova. *J. Anal. Chem.*, **56**, 920 (2001)
440. T.D.Smirnova, N.V.Nevryueva, S.N.Shtykov, V.I.Kochubei, D.A.Zhemerichkin. *J. Anal. Chem.*, **64**, 1114 (2009)
441. R.Hein, P.D.Beer, J.J.Davis. *Chem. Rev.*, **120**, 1888 (2020)
442. P.Pallavicini, Y.A.Diaz-Fernandez, L.Pasotti. *Coord. Chem. Rev.*, **253**, 2226 (2009)
443. L.Vogel, P.Wonner, S.M.Huber. *Angew. Chem., Int. Ed.*, **58**, 1880 (2018)
444. Y.-T.Tseng, H.-Y.Chang, S.G.Harroun, C.-W.Wu, S.-C.Wei, Z.Yuan, H.-L.Chou, C.-H.Chen, C.-C.Huang, H.-T.Chang. *Anal. Chem.*, **90**, 7283 (2018)
445. S.Chakravarty, D.Saikia, P.Sharma, N.C.Adhikary, D.Thakur, N.Sen Sarma. *Analyst*, **139**, 6502 (2014)
446. *Biokhimicheskie Metody Analiza (Ser. Problemy Analiticheskii Khimii. Nauchnyi Sovet po Analiticheskoi Khimii OKhNM RAN). [Biochemical Methods of Analysis (Ser. Problems of Analytical Chemistry. Scientific Council for Analytical Chemistry, OKHNM RAS)]*. Vol. 12. (Ed. B.B.Dzantiev). (Moscow: Nauka, 2010)
447. T.Shimizu, M.Masuda, H.Minamikawa. *Chem. Rev.*, **105**, 1401 (2005)
448. S.Fleming, R.V.Ulijn. *Chem. Soc. Rev.*, **43**, 8150 (2014)
449. S.Shinkai, S.Mori, H.Koreishi, T.Tsubaki, O.Manabe. *J. Am. Chem. Soc.*, **108**, 2409 (1986)
450. K.Jie, Y.Zhou, Y.Yao, F.Huang. *Chem. Soc. Rev.*, **44**, 3568 (2015)
451. H.Zhu, L.Shangguan, B.Shi, G.Yu, F.Huang. *Mater. Chem. Front.*, **2**, 2152 (2018)
452. N.Basilio, V.Francisco, L.Garcia-Rio. *Int. J. Mol. Sci.*, **14**, 3140 (2013)
453. J.Wang, X.Ding, X.Guo. *Adv. Colloid Interface Sci.*, **269**, 187 (2019)
454. H.-W.Tian, Y.-C.Liu, D.-S.Guo. *Mater. Chem. Front.*, **4**, 46 (2020)
455. L.García-Rio, N.Basílio. *Curr. Opin. Colloid Interface Sci.*, **44**, 225 (2019)
456. M.A.Markowitz, R.Bielski, S.L.Regen. *Langmuir*, **5**, 276 (1989)
457. P.Shahgaldian, A.W.Coleman, S.S.Kuduva, M.J.Zaworotko. *Chem. Commun.*, 1968 (2005)
458. S.Shinkai, S.Mori, T.Tsubaki, T.Sone, O.Manabe. *Tetrahedron Lett.*, **25**, 5315 (1984)
459. S.Shinkai, K.Araki, O.Manabe. *J. Chem. Soc., Chem. Commun.*, 187 (1988)
460. S.Shinkai, T.Arimura, K.Araki, H.Kawabata, H.Satoh, T.Tsubaki, O.Manabe, J.Sunamoto. *J. Chem. Soc., Perkin Trans. 1*, 2039 (1989)
461. D.Coquière, H.Cadeau, Y.Rondelez, M.Giorgi, O.Reinaud. *J. Org. Chem.*, **71**, 4059 (2006)
462. S.Houmadi, D.Coquière, L.Legrand, M.C.Fauré, M.Goldmann, O.Reinaud, S.Rémita. *Langmuir*, **23**, 4849 (2007)
463. G.Gattuso, A.Notti, A.Pappalardo, S.Pappalardo, M.F.Parisi, F.Puntoriero. *Tetrahedron Lett.*, **54**, 188 (2013)
464. Z.Qin, D.-S.Guo, X.-N.Gao, Y.Liu. *Soft Matter*, **10**, 2253 (2013)
465. Y.-X.Wang, Y.-M.Zhang, Y.-L.Wang, Y.Liu. *Chem. Mater.*, **27**, 2848 (2015)
466. L.S.Yakimova, L.H.Gilmanova, V.G.Evtugyn, Y.N.Osin, I.I.Stoikov. *J. Nanoparticle Res.*, **19**, 173 (2017)
467. L.S.Yakimova, P.L.Padnya, A.F.Kunafina, A.R.Nugmanova, I.I.Stoikov. *Mendeleev Commun.*, **29**, 86 (2019)
468. M.Strobel, K.Kita-Tokarczyk, A.Taubert, C.Vebert, P.A.Heiney, M.Chami, W.Meier. *Adv. Funct. Mater.*, **16**, 252 (2006)
469. D.Elend, U.Pieles, P.Shahgaldian. *Chim. Int. J. Chem.*, **64**, 45 (2010)
470. K.Suwinska, O.Shkurenko, C.Mbemba, A.Leydier, S.Jebors, A.W.Coleman, R.Matar, P.Falson. *New J. Chem.*, **32**, 1988 (2008)
471. I.Alam, S.K.Sharma, C.D.Gutsche. *J. Org. Chem.*, **59**, 3716 (1994)
472. M.Kellermann, W.Bauer, A.Hirsch, B.Schade, K.Ludwig, C.Böttcher. *Angew. Chem., Int. Ed.*, **43**, 2959 (2004)
473. M.S.Becherer, B.Schade, C.Böttcher, A.Hirsch. *Chem. – Eur. J.*, **15**, 1637 (2009)
474. F.Rodler, B.Schade, C.M.Jäger, S.Backes, F.Hampel, C.Böttcher, T.Clark, A.Hirsch. *J. Am. Chem. Soc.*, **137**, 3308 (2015)
475. S.Song, J.Wang, H.-T.Feng, Z.-H.Zhu, Y.-S.Zheng. *RSC Adv.*, **4**, 24909 (2014)

476. M.Almi, A.Arduini, A.Casnati, A.Pochini, R.Ungaro. *Tetrahedron*, **45**, 2177 (1989)
477. P.Shahgaldian, A.W.Coleman, V.I.Kalchenko. *Tetrahedron Lett.*, **42**, 577 (2001)
478. E.Houel, A.Lazar, E.Da Silva, A.W.Coleman, A.Solovyov, S.Cherenok, V.I.Kalchenko. *Langmuir*, **18**, 1374 (2002)
479. A.D.Martin, E.Houlihan, N.Morellini, P.K.Eggers, E.James, K.A.Stubbs, A.R.Harvey, M.Fitzgerald, C.L.Raston, S.A.Dunlop. *ChemPlusChem*, **77**, 308 (2012)
480. E.James, P.K.Eggers, A.R.Harvey, S.A.Dunlop, M.Fitzgerald, K.A.Stubbs, C.L.Raston. *Org. Biomol. Chem.*, **11**, 6108 (2013)
481. J.Mo, P.K.Eggers, X.Chen, M.R.H.Ahamed, T.Becker, L.Y.Lim, C.L.Raston. *Sci. Rep.*, **5**, 10414 (2015)
482. Mei.Li, L.Mao, M.Chen, Min.Li, K.Wang, J.Mo. *Front. Bioeng. Biotechnol.*, **7**, 238 (2019)
483. S.Arimori, T.Nagasaki, S.Shinkai. *J. Chem. Soc., Perkin Trans. 2*, 679 (1995)
484. M.Frank, G.Maas, J.Schatz. *Eur. J. Org. Chem.*, 607 (2004)
485. T.Fahlbusch, M.Frank, J.Schatz, H.Schmaderer. *Eur. J. Org. Chem.*, 1899 (2006)
486. R.V.Rodik, A.S.Klymchenko, N.Jain, S.I.Miroshnichenko, L.Richert, V.I.Kalchenko, Y.Mély. *Chem. – Eur. J.*, **17**, 5526 (2011)
487. Y.-X.Wang, D.-S.Guo, Y.Cao, Y.Liu. *RSC Adv.*, **3**, 8058 (2013)
488. E.A.Andreyko, P.L.Padnya, I.I.Stoikov. *Colloids Surf., A*, **454**, 74 (2014)
489. P.L.Padnya, I.A.Khripunova, O.A.Mostovaya, T.A.Mukhametzyanov, V.G.Evtugyn, V.V.Vorobev, Y.N.Osin, I.I.Stoikov. *Beilstein J. Nanotechnol.*, **8**, 1825 (2017)
490. T.Sun, L.Qi, W.Li, Y.Li, X.Shuai, Z.Cai, H.Chen, X.Qiao, L.Ma. *J. Chromatogr. A*, **1601**, 310 (2019)
491. M.Dudič, A.Colombo, F.Sansone, A.Casnati, G.Donofrio, R.Ungaro. *Tetrahedron*, **60**, 11613 (2004)
492. F.Sansone, M.Dudič, G.Donofrio, C.Rivetti, L.Baldini, A.Casnati, S.Cellai, R.Ungaro. *J. Am. Chem. Soc.*, **128**, 14528 (2006)
493. S.Licen, V.Bagnacani, L.Baldini, A.Casnati, F.Sansone, M.Giannetto, P.Pengo, P.Tecilla. *Supramol. Chem.*, **25**, 631 (2013)
494. L.Baldini, R.Cacciapaglia, A.Casnati, L.Mandolini, R.Salvio, F.Sansone, R.Ungaro. *J. Org. Chem.*, **77**, 3381 (2012)
495. R.Salvio, S.Volpi, T.Folcarelli, A.Casnati, R.Cacciapaglia. *Org. Biomol. Chem.*, **17**, 7482 (2019)
496. Z.Zheng, W.-C.Geng, J.Gao, Y.-Y.Wang, H.Sun, D.-S.Guo. *Chem. Sci.*, **9**, 2087 (2018)
497. H.C.Kolb, M.G.Finn, K.B.Sharpless. *Angew. Chem., Int. Ed.*, **40**, 2004 (2001)
498. C.Wang, D.Ikhlef, S.Kahlal, J.-Y.Saillard, D.Astruc. *Coord. Chem. Rev.*, **316**, 1 (2016)
499. G.C.Feast, T.Lepitre, X.Mulet, C.E.Conn, O.E.Hutt, G.P.Savage, C.J.Drummond. *Beilstein J. Org. Chem.*, **10**, 1578 (2014)
500. O.E.Hutt, X.Mulet, G.P.Savage. *ACS Comb. Sci.*, **14**, 565 (2012)
501. S.P.Bew, R.A.Brimage, N.L'Hermit, S.V.Sharma. *Org. Lett.*, **9**, 3713 (2007)
502. P.-F.Gou, W.-P.Zhu, Z.-Q.Shen. *J. Polym. Sci., Part A: Polym. Chem.*, **48**, 5643 (2010)
503. S.Aleandri, A.Casnati, L.Fantuzzi, G.Mancini, G.Rispoli, F.Sansone. *Org. Biomol. Chem.*, **11**, 4811 (2013)
504. L.Gallego-Yerga, M.Lomazzi, V.Franceschi, F.Sansone, C.Ortiz Mellet, G.Donofrio, A.Casnati, J.M.García Fernández. *Org. Biomol. Chem.*, **13**, 1708 (2015)
505. J.Dauvergne, E.M.Desuzinges, C.Faugier, S.Igonet, M.Soulié, E.Grousson, D.Cornut, F.Bonneté, G.Durand, E.Dejean, A.Jawhari. *ChemistrySelect*, **4**, 5535 (2019)
506. S.Fujii, Y.Sanada, T.Nishimura, I.Akiba, K.Sakurai, N.Yagi, E.Mylonas. *Langmuir*, **28**, 3092 (2012)
507. S.Fujii, K.Sakurai, T.Okobira, N.Ohta, A.Takahara. *Langmuir*, **29**, 13666 (2013)
508. S.Fujii, K.Nishina, S.Yamada, S.Mochizuki, N.Ohta, A.Takahara, K.Sakurai. *Soft Matter*, **10**, 8216 (2014)
509. K.Yoshida, S.Fujii, R.Takahashi, S.Matsumoto, K.Sakurai. *Langmuir*, **33**, 9122 (2017)
510. J.H.Lee, S.Fujii, R.Takahashi, K.Sakurai. *Langmuir*, **34**, 12109 (2018)
511. E.Mylonas, N.Yagi, S.Fujii, K.Ikesue, T.Ueda, H.Moriyama, Y.Sanada, K.Uezu, K.Sakurai, T.Okobira. *Sci. Rep.*, **9**, 1982 (2019)
512. V.A.Burilov, R.I.Nugmanov, R.R.Ibragimova, S.E.Solovieva, I.S.Antipin. *Mendeleev Commun.*, **25**, 177 (2015)
513. V.A.Burilov, D.A.Mironova, R.R.Ibragimova, S.E.Solovieva, B.König, I.S.Antipin. *RSC Adv.*, **5**, 101177 (2015)
514. V.A.Burilov, R.R.Ibragimova, B.H.Gafiatullin, S.E.Solovieva, I.S.Antipin. *Butlerov Commun.*, **47**, 23 (2016)
515. V.A.Burilov, D.A.Mironova, R.R.Ibragimova, S.E.Solovieva, I.S.Antipin. *Bionanoscience*, **6**, 427 (2016)
516. V.A.Burilov, D.A.Mironova, R.R.Ibragimova, R.I.Nugmanov, S.E.Solovieva, I.S.Antipin. *Colloids Surf., A*, **515**, 41 (2017)
517. R.R.Ibragimova, V.A.Burilov, A.R.Aimetdinov, D.A.Mironova, V.G.Evtugyn, Y.N.Osin, S.E.Solovieva, I.S.Antipin. *Macroheterocycles*, **9**, 433 (2016)
518. G.A.Fatykhova, V.A.Burilov, M.N.Dokuchaeva, S.E.Solov'eva, I.S.Antipin. *Dokl. Chem.*, **479**, 64 (2018)
519. V.A.Burilov, G.A.Fatikhova, M.N.Dokuchaeva, R.I.Nugmanov, D.A.Mironova, P.V.Dorovatovskii, V.N.Khrustalev, S.E.Solovieva, I.S.Antipin. *Beilstein J. Org. Chem.*, **14**, 1980 (2018)
520. G.A.Fatykhova, E.G.Makarov, D.A.Mironova, E.D.Sultanova, V.A.Burilov, S.E.Solovieva, I.S.Antipin. *Russ. J. Phys. Chem. B*, **13**, 401 (2019)
521. V.Burilov, A.Valiyakhmetova, D.Mironova, R.Safiullin, M.Kadirov, K.Ivshin, O.Kataeva, S.Solovieva, I.Antipin. *RSC Adv.*, **6**, 44873 (2016)
522. V.Burilov, A.Valiyakhmetova, D.Mironova, E.Sultanova, V.Evtugyn, Y.Osin, S.Katsyuba, T.Burganov, S.Solovieva, I.Antipin. *New J. Chem.*, **42**, 2942 (2018)
523. A.M.Valiyakhmetova, E.D.Sultanova, V.A.Burilov, S.E.Solovieva, I.S.Antipin. *Russ. Chem. Bull., Int. Ed.*, **68**, 1067 (2019)
524. V.A.Burilov, R.R.Ibragimova, B.H.Gafiatullin, R.I.Nugmanov, S.E.Solovieva, I.S.Antipin. *Macroheterocycles*, **10**, 215 (2017)

525. V.A.Burilov, B.K.Gafiatullin, D.A.Mironova, E.D.Sultanova, V.G.Evtugyn, Y.N.Osin, D.R.Islamov, K.S.Usachev, S.E.Solovieva, I.S.Antipin. *Eur. J. Org. Chem.*, 2180 (2020)
526. A.G.Slater (née Phillips), P.H.Beton, N.R.Champness. *Chem. Sci.*, **2**, 1440 (2011)
527. W.C.Bigelow, D.L.Pickett, W.A.Zisman, I.Oleophobic. *J. Colloid Sci.*, **1**, 513 (1946)
528. I.Haller. *J. Am. Chem. Soc.*, **100**, 8050 (1978)
529. J.Sagiv. *J. Am. Chem. Soc.*, **102**, 92 (1980)
530. R.Maoz, L.Netzer, J.Gun, J.Sagiv. *J. Chim. Phys.*, **85**, 1059 (1988)
531. J.J.Gooding, S.Ciampi. *Chem. Soc. Rev.*, **40**, 2704 (2011)
532. J.Huang, X.Liu, X.Qiu, L.Xie, B.Yan, X.Wang, Q.Huang, H.Zeng. *J. Phys. Chem. B*, **121**, 3151 (2017)
533. C.Arisio, C.A.Cassou, M.Lieberman. *Langmuir*, **29**, 5145 (2013)
534. R.M.Parker, D.J.Wales, J.C.Gates, P.G.R.Smith, M.C.Grossel. *J. Mater. Chem. C*, **4**, 1178 (2016)
535. C.Yan, R.Yuan, J.Nishida, M.D.Fayer. *J. Phys. Chem. C*, **119**, 16811 (2015)
536. J.Ou, Y.Wang, J.Wang, S.Liu, Z.Li, S.Yang. *J. Phys. Chem. C*, **115**, 10080 (2011)
537. R.G.Nuzzo, D.L.Allara. *J. Am. Chem. Soc.*, **105**, 4481 (1983)
538. B.D.Ratner, A.S.Hoffman. In *Biomaterials Science: An Introduction to Materials in Medicine*. (Eds B.D.Ratner, A.S.Hoffman, F.J.Schoen, J.E.Lemons). (3rd Edn). (Oxford: Academic Press, 2012). P. 259
539. S.Clair, D.G.de Oteyza. *Chem. Rev.*, **119**, 4717 (2019)
540. C.Meltzer, J.Paul, H.Dietrich, C.M.Jäger, T.Clark, D.Zahn, B.Braunschweig, W.Peukert. *J. Am. Chem. Soc.*, **136**, 10718 (2014)
541. E.Ermakova, O.Raitman, A.Shokurov, M.Kalinina, S.Selector, A.Tsivadze, V.Arslanov, M.Meyer, A.Bessmertnykh-Lemeune, R.Guilard. *Analyst*, **141**, 1912 (2016)
542. L.Zhang, M.Zhou, A.Wang, T.Zhang. *Chem. Rev.*, **120**, 683 (2019)
543. C.A.Schoenbaum, D.K.Schwartz, J.W.Medlin. *Acc. Chem. Res.*, **47**, 1438 (2014)
544. N.A.Yewdall, H.Venugopal, A.Desfosses, V.Abrishami, Y.Yosaatmadja, M.B.Hampton, J.A.Gerrard, D.C.Goldstone, A.K.Mitra, M.Radjainia. *Structure*, **24**, 1120 (2016)
545. L.J.Domigan, H.Ashmead, S.Dimartino, J.Malmstrom, F.G.Pearce, M.Blunt, D.E.Williams, J.A.Gerrard. *Biointerphases*, **12**, 04E405 (2017)
546. I.Langmuir, V.J.Schaefer. *J. Am. Chem. Soc.*, **60**, 1351 (1938)
547. P.Dynarowicz-Łkatka, A.Dhanabalan, O.N.Oliveira. *Adv. Colloid Interface Sci.*, **91**, 221 (2001)
548. S.D.Stuchebryukov, S.L.Selektor, D.A.Silant'eva, A.V.Shokurov. *Protection of Metals and Physical Chemistry of Surfaces* **49**, 189 (2013); https://doi.org/10.1134/S2070205113020044
549. M.A.Shcherbina, S.N.Chvalun, S.A.Ponomarenko, M.V.Kovalchuk. *Russ. Chem. Rev.*, **83**, 1091 (2014)
550. N.R.Faye, F.Moroté, C.G.Heywang, T.C.Bouhacina. *Int. J. Nanotechnol.*, **10**, 390 (2013)
551. C.Grauby-Heywang, F.Moroté, M.Mathelié-Guinlet, I.Gammoudi, N.R.Faye, T.Cohen-Bouhacina. *Chem. Phys. Lipids*, **200**, 74 (2016)
552. A.V.Shokurov, D.N.Novak, M.A.Grin, A.V.Zaitseva, V.V.Arslanov, S.L.Selektor, C.Grauby-Heywang, T.Cohen-Bouhacin. *Protection of Metals and Physical Chemistry of Surfaces*, **54**, 19 (2018); https://doi.org/10.1134/S2070205118010124
553. A.Kausar. *Polym. Plast. Technol. Eng.*, **56**, 932 (2016)
554. K.Choudhary, R.K.Gupta, R.Pratibha, B.K.Sadashiva, V.Manjuladevi. *Liq. Cryst.*, **46**, 1494 (2019)
555. M.Castillo-Vallés, M.Cano, A.Bermejo-Sanz, N.Gimeno, M.B.Ros. *J. Mater. Chem. C*, **8**, 1998 (2020)
556. Y.Kang, K.Liu, X.Zhang. *Langmuir*, **30**, 5989 (2014)
557. Y.Chang, Y.Jiao, H.E.Symons, J.-F.Xu, C.F.J.Faul, X.Zhang. *Chem. Soc. Rev.*, **48**, 989 (2019)
558. E.Y.Chernikova, D.V.Berdnikova, Y.V.Fedorov, O.A.Fedorova. *Macroheterocycles*, **6**, 234 (2013)
559. S.L.Selektor, A.V.Shokurov. *Protection of Metals and Physical Chemistry of Surfaces*, **51**, 171 (2015); https://doi.org/10.1134/S2070205115020161
560. J.J.Ramsden. In *Supramolecular Chemistry: From Molecules to Nanomaterials*. Vol. 2. (Eds J.W.Steed, P.A.Gale). (Chichester: Wiley, 2012). P. 529
561. E.A.Silva, M.L.Braunger, A.Gregori, C.A.Olivati. *SN Appl. Sci.*, **1**, 200 (2019)
562. E.S.Seven, S.K.Sharma, D.Meziane, Y.Zhou, K.J.Mintz, R.R.Pandey, C.C.Chusuei, R.M.Leblanc. *Langmuir*, **35**, 6708 (2019)
563. G.García-Espejo, M.Pérez-Morales, M.Goldmann, M.T.Martín-Romero, J.J.Giner-Casares, L.Camacho. *J. Colloid Interface Sci.*, **508**, 583 (2017)
564. N.Reitzel, D.R.Greve, K.Kjaer, P.B.Howes, M.Jayaraman, S.Savoy, R.D.McCullough, J.T.McDevitt, T.Bjørnholm. *J. Am. Chem. Soc.*, **122**, 5788 (2000)
565. N.Akhtar, R.Y.N.Gengler, T.T.M.Palstra, P.Rudolf. *J. Phys. Chem. C*, **116**, 24130 (2012)
566. S.Selector, O.Fedorova, E.Lukovskaya, A.Anisimov, Y.Fedorov, N.Tarasova, O.Raitman, F.Fages, V.Arslanov. *J. Phys. Chem. B*, **116**, 1482 (2012)
567. J.Pazinato, D.M.Hoffmeister, K.P.Naidek, E.Westphal, H.Gallardo, H.Winnischofer. *Electrochim. Acta*, **153**, 574 (2015)
568. H.Kuhn, D.Möbius, H.Bücher. In *Physical Methods of Chemistry*. Vol. 1. (Eds A.Weissberger, B.Rossiter). (New York: Wiley, 1972). P. 577
569. E.Johnson, R.Aroca. *Can. J. Chem.*, **69**, 1728 (1991)
570. N.K.Ibrayev, A.K.Aimukhanov, E.V.Seliverstova. *High Energy Chem.*, **43**, 577 (2009)
571. S.L.Selector, L.B.Bogdanova, A.V.Shokurov, P.A.Panchenko, O.A.Fedorova, V.V.Arslanov. *Macroheterocycles*, **7**, 311 (2014)
572. I.I.Shepeleva, A.V.Shokurov, N.V.Konovalova, V.V.Arslanov, P.A.Panchenko, S.L.Selektor. *Russ. Chem. Bull., Int. Ed.*, **67**, 2159 (2018)
573. D.L.Dexter. *J. Lumin.*, **18 – 19**, 779 (1979)
574. L.Fang, N.Alderman, L.Danos, T.Markvart. *Mater. Res. Innov.*, **18**, 494 (2014)
575. L.Danos, N.R.Halcovitch, B.Wood, H.Banks, M.P.Coogan, N.Alderman, L.Fang, B.Dzurnak, T.Markvart. *Faraday Discuss.*, **222**, 405 (2020)
576. S.L.Selektor, A.V.Shokurov, O.A.Raitman, L.S.Sheinina, V.V.Arslanov, K.P.Birin, Y.G.Gorbunova, A.Y.Tsivadze. *Colloid J.*, **74**, 334 (2012)
577. S.L.Selektor, A.V.Shokurov, V.V.Arslanov, Y.G.Gorbunova, K.P.Birin, O.A.Raitman, F.Morote, T.Cohen-Bouhacina, C.Grauby-Heywang, A.Y.Tsivadze. *J. Phys. Chem. C*, **118**, 4250 (2014)

578. A.V.Shokurov, D.S.Kutsybala, A.G.Martynov, A.V.Bakirov, M.A.Shcherbina, S.N.Chvalun, Y.G.Gorbunova, A.Y.Tsivadze, A.V.Zaytseva, D.Novikov, V.V.Arslanov, S.L.Selektor. *Langmuir*, **36**, 1423 (2020)
579. S.H.Mir, L.A.Nagahara, T.Thundat, P.Mokarian-Tabari, H.Furukawa, A.Khosla. *J. Electrochem. Soc.*, **165**, B3137 (2018)
580. V.V.Arslanov, M.A.Kalinina, E.V.Ermakova, O.A.Raitman, Y.G.Gorbunova, O.E.Aksyutin, A.G.Ishkov, V.A.Grachev, A.Y.Tsivadze. *Russ. Chem. Rev.*, **88**, 775 (2019)
581. A.B.Descalzo, R.Martinez-Máñez, F.Sancenón, K.Hoffmann, K.Rurack. *Angew. Chem., Int. Ed.*, **45**, 5924 (2006)
582. A.Kumar, K.Banerjee, P.Liljeroth. *Nanotechnology*, **28**, 082001 (2017)
583. S.Das, J.A.Robinson, M.Dubey, H.Terrones, M.Terrones. *Annu. Rev. Mater. Res.*, **45**, 1 (2015)
584. D.D.Kulkarni, I.Choi, S.S.Singamaneni, V.V.Tsukruk. *ACS Nano*, **4**, 4667 (2010)
585. M.M.Velázquez, T.Alejo, D.López-Díaz, B.Martín-García, M.D.Merchán. In *Two-Dimensional Materials. Characterization and Potential Applications*. (Ed. P.K.Nayak). (InTech, 2016). P. 21; https://doi.org/10.5772/63495
586. A.Kouloumpis, E.Thomou, N.Chalmpes, K.Dimos, K.Spyrou, A.B.Bourlinos, I.Koutselas, D.Gournis, P.Rudolf. *ACS Omega*, **2**, 2090 (2017)
587. E.V.Ermakova, A.A.Ezhov, A.E.Baranchikov, Y.G.Gorbunova, M.A.Kalinina, V.V.Arslanov. *J. Colloid Interface Sci.*, **530**, 521 (2018)
588. K.Ou, X.Xu, Y.Shao, W.-J.Wang, W.-B.Zhang, S.-G.Yang. *Chin. J. Polym. Sci.*, **37**, 604 (2019)
589. M.L.Cortez, A.Lorenzo, W.A.Marmisollé, C.von Bilderling, E.Maza, L.Pietrasanta, F.Battaglini, M.Ceol'in, O.Azzaroni. *Soft Matter*, **14**, 1939 (2018)
590. F.Huang, O.A.Scherman. *Chem. Soc. Rev.*, **41**, 5879 (2012)
591. L.Séon, A.Parat, F.Gaudière, J.-C.Voegel, R.Auzély-Velty, P.Lorchat, L.Coche-Guérente, B.Senger, P.Schaaf, L.Jierry, F.Boulmedais. *Langmuir*, **30**, 6479 (2014)
592. Y.Li, X.Wang, J.Sun. *Chem. Soc. Rev.*, **41**, 5998 (2012)
593. J.Zhang, Y.Liu, G.Wu, M.Schönhoff, X.Zhang. *Langmuir*, **27**, 10370 (2011)
594. J.J.Richardson, M.Bjornmalm, F.Caruso. *Science*, **348**, aaa2491 (2015)
595. P.K.Deshmukh, K.P.Ramani, S.S.Singh, A.R.Tekade, V.K.Chatap, G.B.Patil, S.B.Bari. *J. Control. Release*, **166**, 294 (2013)
596. J.F.Quinn, A.P.R.Johnston, G.K.Such, A.N.Zelikin, F.Caruso. *Chem. Soc. Rev.*, **36**, 707 (2007)
597. R.K.Iler. *J. Colloid Interface Sci.*, **21**, 569 (1966)
598. G.Decher. *Science*, **277**, 1232 (1997)
599. R.P.Feynman. *There's Plenty of Room at the Bottom. Engineering and Science*. (Pasadena, CA: California Institute of Technology, 1960)
600. R.Feynman. *J. Microelectromech. Syst.*, **2**, 4 (1993)
601. O.Crespo-Biel, B.Dordi, D.N.Reinhoudt, J.Huskens. *J. Am. Chem. Soc.*, **127**, 7594 (2005)
602. T.Salditt, U.S.Schubert. *Rev. Mol. Biotechnol.*, **90**, 55 (2002)
603. M.M.Naseer, S.Hameed. *CrystEngComm*, **14**, 4247 (2012)
604. F.Caruso. *Chem. – Eur. J.*, **6**, 413 (2000)
605. H.Ejima, J.J.Richardson, K.Liang, J.P.Best, M.P.van Koeverden, G.K.Such, J.Cui, F.Caruso. *Science*, **341**, 154 (2013)
606. Y.Wang, A.S.Angelatos, F.Caruso. *Chem. Mater.*, **20**, 848 (2008)
607. O.S.Sakr, G.Borchard. *Biomacromolecules*, **14**, 2117 (2013)
608. X.Lian, Y.Fang, E.Joseph, Q.Wang, J.Li, S.Banerjee, C.Lollar, X.Wang, H.-C.Zhou. *Chem. Soc. Rev.*, **46**, 3386 (2017)
609. R.Chapman, M.H.Stenzel. *J. Am. Chem. Soc.*, **141**, 2754 (2019)
610. X.Chen, W.Wu, Z.Guo, J.Xin, J.Li. *Biomaterials*, **32**, 1759 (2011)
611. L.I.Kazakova, L.I.Shabarchina, S.Anastasova, A.M.Pavlov, P.Vadgama, A.G.Skirtach, G.B.Sukhorukov. *Anal. Bioanal. Chem.*, **405**, 1559 (2012)
612. M.Delcea, A.Yashchenok, K.Videnova, O.Kreft, H.Möhwald, A.G.Skirtach. *Macromol. Biosci.*, **10**, 465 (2010)
613. M.-L.De Temmerman, J.Demeester, S.C.De Smedt, J.Rejman. *Nanomedicine*, **7**, 771 (2012)
614. K.A.D.Gregersen, Z.B.Hill, J.C.Gadd, B.S.Fujimoto, D.J.Maly, D.T.Chiu. *ACS Nano*, **4**, 7603 (2010)
615. J.Cui, M.P.van Koeverden, M.Müllner, K.Kempe, F.Caruso. *Adv. Colloid Interface Sci.*, **207**, 14 (2014)
616. W.Tong, X.Song, C.Gao. *Chem. Soc. Rev.*, **41**, 6103 (2012)
617. A.Finnemore, P.Cunha, T.Shean, S.Vignolini, S.Guldin, M.Oyen, U.Steiner. *Nat. Commun.*, **3**, 966 (2012)
618. S.De Koker, R.Hoogenboom, B.G.De Geest. *Chem. Soc. Rev.*, **41**, 2867 (2012)
619. G.K.Such, A.P.R.Johnston, F.Caruso. *Chem. Soc. Rev.*, **40**, 19 (2011)
620. Z.Poon, J.B.Lee, S.W.Morton, P.T.Hammond. *Nano Lett.*, **11**, 2096 (2011)
621. G.Paramasivam, V.Sharma, A.Sundaramurthy. *IOP Conf. Ser. Mater. Sci. Eng.*, **225**, 12080 (2017)
622. A.Bétard, R.A.Fischer. *Chem. Rev.*, **112**, 1055 (2012)
623. O.Shekhah, H.Wang, S.Kowarik, F.Schreiber, M.Paulus, M.Tolan, C.Sternemann, F.Evers, D.Zacher, R.A.Fischer, C.Wöll. *J. Am. Chem. Soc.*, **129**, 15118 (2007)
624. L.Heinke, M.Cakici, M.Dommaschk, S.Grosjean, R.Herges, S.Bräse, C.Wöll. *ACS Nano*, **8**, 1463 (2014)
625. S.Ahmad, J.Liu, C.Gong, J.Zhao, L.Sun. *ACS Appl. Energy Mater.*, **1**, 249 (2018)
626. A.K.Reshetnikova, A.I.Zvyagina, Y.Y.Enakieva, V.V.Arslanov, M.A.Kalinina. *Colloid J.*, **80**, 684 (2018)
627. Jin.Liu, W.Zhou, Jian.Liu, Y.Fujimori, T.Higashino, H.Imahori, X.Jiang, J.Zhao, T.Sakurai, Y.Hattori, W.Matsuda, S.Seki, S.K.Garlapati, S.Dasgupta, E.Redel, L.Sun, C.Wöll. *J. Mater. Chem. A*, **4**, 12739 (2016)
628. D.-H.Chen, R.Haldar, B.L.Neumeier, Z.-H.Fu, C.Feldmann, C.Wöll, E.Redel. *Adv. Funct. Mater.*, **29**, 1903086 (2019)
629. I.Stassen, N.Burtch, A.Talin, P.Falcaro, M.Allendorf, R.Ameloot. *Chem. Soc. Rev.*, **46**, 3185 (2017)
630. J.Liu, O.Shekhah, X.Stammer, H.K.Arslan, B.Liu, B.Schüpbach, A.Terfort, C.Wöll. *Materials (Basel)*, **5**, 1581 (2012)
631. H.Gliemann, C.Wöll. *Mater. Today*, **15**, 110 (2012)

632. O.Zybaylo, O.Shekhah, H.Wang, M.Tafipolsky, R.Schmid, D.Johannsmann, C.Wöll. *Phys. Chem. Chem. Phys.*, **12**, 8092 (2010)
633. G.Bolla, A.S.Myerson. *CrystEngComm*, **20**, 2084 (2018)
634. A.Bétard, H.Bux, S.Henke, D.Zacher, J.Caro, R.A.Fischer. *Microporous Mesoporous Mater.*, **150**, 76 (2012)
635. D.Zacher, K.Yusenko, A.Bétard, S.Henke, M.Molon, T.Ladnorg, O.Shekhah, B.Schüpbach, T.De los Arcos, M.Krasnopolski, M.Meilikhov, J.Winter, A.Terfort, C.Wöll, R.A.Fischer. *Chem. – Eur. J.*, **17**, 1448 (2011)
636. M.C.So, S.Jin, H.-J.Son, G.P.Wiederrecht, O.K.Farha, J.T.Hupp. *J. Am. Chem. Soc.*, **135**, 15698 (2013)
637. O.Shekhah, H.Wang, T.Strunskus, P.Cyganik, D.Zacher, R.Fischer, C.Wöll. *Langmuir*, **23**, 7440 (2007)
638. L.Heinke, C.Wöll. *Phys. Chem. Chem. Phys.*, **15**, 9295 (2013)
639. Z.-G.Gu, A.Pfriem, S.Hamsch, H.Breitwieser, J.Wohlgemuth, L.Heinke, H.Gliemann, C.Wöll. *Microporous Mesoporous Mater.*, **211**, 82 (2015)
640. A.I.Zvyagina, E.K.Melnikova, A.A.Averin, A.E.Baranchikov, A.R.Tameev, V.V.Malov, A.A.Ezhov, D.A.Grishanov, J.Gun, E.V.Ermakova, V.V.Arslanov, M.A.Kalinina. *Carbon*, **134**, 62 (2018)
641. A.I.Zvyagina, A.A.Shiryaev, A.E.Baranchikov, V.V.Chernyshev, Y.Y.Enakieva, O.A.Raitman, A.A.Ezhov, I.N.Meshkov, D.A.Grishanov, O.S.Ivanova, Y.G.Gorbunova, V.V.Arslanov, M.A.Kalinina. *New J. Chem.*, **41**, 948 (2017)
642. I.N.Meshkov, A.I.Zvyagina, A.A.Shiryaev, M.S.Nickolsky, A.E.Baranchikov, A.A.Ezhov, A.G.Nugmanova, Y.Y.Enakieva, Y.G.Gorbunova, V.V.Arslanov, M.A.Kalinina. *Langmuir*, **34**, 5184 (2018)
643. S.Laokroekkiat, M.Hara, S.Nagano, Y.Nagao. *Langmuir*, **32**, 6648 (2016)
644. W.Zhou, S.Begum, Z.Wang, P.Krolla, D.Wagner, S.Bräse, C.Wöll, M.Tsotsalas. *ACS Appl. Mater. Interfaces*, **10**, 1528 (2018)
645. Z.Sun, T.Ma, H.Tao, Q.Fan, B.Han. *Chem*, **3**, 560 (2017)
646. X.Yang, X.Lin, Y.S.Zhao, D.Yan. *Chem. – Eur. J.*, **24**, 6484 (2018)
647. O.Shekhah, H.Wang, M.Paradinas, C.Ocal, B.Schüpbach, A.Terfort, D.Zacher, R.A.Fischer, C.Wöll. *Nat. Mater*, **8**, 481 (2009)
648. A.P.Kutenina, A.I.Zvyagina, O.A.Raitman, Y.Y.Enakieva, M.A.Kalinina. *Colloid J.*, **81**, 401 (2019)
649. D.-J.Li, Z.-G.Gu, I.Vohra, Y.Kang, Y.-S.Zhu, J.Zhang. *Small*, **13**, 1604035 (2017)
650. S.Okur, Z.Zhang, M.Sarheed, P.Nick, U.Lemmer, L.Heinke. *Sens. Actuators, B*, **306**, 127502 (2020)
651. A.S.Varela, W.Ju, P.Strasser. *Adv. Energy Mater.*, **8**, 1703614 (2018)
652. R.Haldar, S.Diring, P.K.Samanta, M.Muth, W.Clancy, A.Mazel, S.Schlabach, F.Kirschhöfer, G.Brenner-Weiß, S.K.Pati, F.Odobel, C.Wöll. *Angew. Chem., Int. Ed.*, **57**, 13662 (2018)
653. Y.-Y.Wang, S.-M.Chen, R.Haldar, C.Wöll, Z.-G.Gu, J.Zhang. *Adv. Mater. Interfaces*, **5**, 1800985 (2018)
654. Jin Liu, W.Zhou, Jian Liu, I.Howard, G.Kilibarda, S.Schlabach, D.Coupry, M.Addicoat, S.Yoneda, Y.Tsutsui, T.Sakurai, S.Seki, Z.Wang, P.Lindemann, E.Redel, T.Heine, C.Wöll. *Angew. Chem., Int. Ed.*, **54**, 7441 (2015)
655. M.Adams, M.Kozlowska, N.Baroni, M.Oldenburg, R.Ma, D.Busko, A.Turshatov, G.Emandi, M.O.Senge, R.Haldar, C.Wöll, G.U.Nienhaus, B.S.Richards, I.A.Howard. *ACS Appl. Mater. Interfaces*, **11**, 15688 (2019)
656. R.Haldar, K.Batra, S.M.Marschner, A.B.Kuc, S.Zahn, R.A.Fischer, S.Bräse, T.Heine, C.Wöll. *Chem. – Eur. J.*, **25**, 7847 (2019)
657. X.Liu, M.Kozlowska, T.Okkali, D.Wagner, T.Higashino, G.Brenner-Weiß, S.M.Marschner, Z.Fu, Q.Zhang, H.Imahori, S.Bräse, W.Wenzel, C.Wöll, L.Heinke. *Angew. Chem., Int. Ed.*, **58**, 9590 (2019)
658. J.-M.Lehn. *Science*, **227**, 849 (1985)
659. J.-M.Lehn. *Angew. Chem., Int. Ed.*, **27**, 89 (1988)
660. H.Ringsdorf, B.Schlarb, J.Venzmer. *Angew. Chem., Int. Ed.*, **27**, 113 (1988)
661. *Frontiers in Supramolecular Organic Chemistry and Photochemistry*. (Eds H.J.Schneider, H.Durr). (Weinheim: VCH, 1993)
662. J.-M.Lehn. *Makromol. Chem. Macromol. Symp.*, **69**, 1 (1993)
663. A.Z.Asadabadi, S.J.Hoseini, M.Bahrami, S.M.Nabavizadeh. *New J. Chem.*, **43**, 6513 (2019)
664. P.Ballester, A.Scarso. *Front. Chem.*, **7**, 174 (2019)
665. J.M.Köster, D.Häussinger, K.Tiefenbacher. *Front. Chem.*, **6**, 639 (2019)
666. V.Mouarrawis, R.Plessius, J.I.van der Vlugt, J.N.H.Reek. *Front. Chem.*, **6**, 623 (2018)
667. M.De Rosa, P.La Manna, C.Talotta, A.Soriente, C.Gaeta, P.Neri. *Front. Chem.*, **6**, 84 (2018)
668. C.Pereira, M.Simões, J.Tomé, F.A.Paz. *Molecules*, **21**, 1348 (2016)
669. C.Kim, B.A.Ondrusek, H.Chung. *Org. Lett.*, **20**, 736 (2018)
670. G.Faubert. *J. Electrochem. Soc.*, **145**, 2985 (1998)
671. D.Zhang, A.Martinez, J.-P.Dutasta. *Chem. Rev.*, **117**, 4900 (2017)
672. Z.Matharu, A.J.Bandodkar, V.Gupta, B.D.Malhotra. *Chem. Soc. Rev.*, **41**, 1363 (2012)
673. M.V.Koval'chuk, V.V.Koechkovskaya, L.A.Feigin. *Priroda*, (11), 11 (2003)
674. E.V.Agina, I.A.Usov, O.V.Borshchev, J.Wang, A.Mourran, M.A.Shcherbina, A.V.Bakirov, S.Grigorian, M.Möller, S.N.Chvalun, S.A.Ponomarenko. *Langmuir*, **28**, 16186 (2012)
675. E.V.Agina, A.A.Mannanov, A.S.Sizov, O.Vechter, O.V.Borshchev, A.V.Bakirov, M.A.Shcherbina, S.N.Chvalun, V.G.Konstantinov, V.V.Bruevich, O.V.Kozlov, M.S.Pshenichnikov, D.Y.Paraschuk, S.A.Ponomarenko. *ACS Appl. Mater. Interfaces*, **9**, 18078 (2017)
676. C.Honorato-Rios, A.Kuhnhold, J.R.Bruckner, R.Dannert, T.Schilling, J.P.F.Lagerwall. *Front. Mater.*, **3**, 21 (2016)
677. M.Y.Tolstykh, V.V.Makarova, A.V.Semakov, V.G.Kulichikhin. *Polym. Sci., Ser. A*, **52**, 144 (2010)
678. S.H.Cho, P.Purushotham, C.Fang, C.Maranas, S.M.Diaz-Moreno, V.Bulone, J.Zimmer, M.Kumar, B.T.Nixon. *Plant Physiol.*, **175**, 146 (2017)
679. J.N.Izraelachvili. *Intermolecular and Surface Forces*. (New York: Academic Press, 1992)
680. D.Paprocki, A.Madej, D.Koszelewski, A.Brodzka, R.Ostaszewski. *Front. Chem.*, **6**, 502 (2018)

681. P.Mariani, V.Luzzati, H.Delacroix. *J. Mol. Biol.*, **204**, 165 (1988)
682. H.Haken. *Information and Self-Organization: A Macroscopic Approach to Complex Systems. (Springer Series in Synergetics)*. (3rd Edn). (Springer, 2006)
683. I.Prigogine, G.Nicolis. *Self-Organization in Nonequilibrium Systems: From Dissipative Structures to Order Through Fluctuations*. (New York: Wiley, 1978)
684. P.Bak. *How Nature Works: The Science of Self-Organised Criticality*. criticality. (New York, NY: Copernicus Press, 1996)
685. E.N.Knyazeva, S.P.Kurdyumov. *Osnovaniya Sinergetiki. Rezhimy s Obostreniem, Samoorganizatsiya, Tempomiry. (Foundations of Synergetics. Exacerbation Modes, Self-organization, Tempomirs)*. (Saint Petersburg: Aleteiya, 2002)
686. S.P.Kurdyumov. *Ekology Zhizn*, **5**, 42 (2000)
687. E.N.Knyazeva, S.P.Kurdyumov. *Zakony Evolyutsii i Samoorganizatsii Slozhnykh Sistem. (The Laws of Evolution and Self-organization of Complex Systems)*. (Moscow: Nauka, 1994)
688. M.W.Matsen, F.S.Bates. *Macromolecules*, **29**, 1091 (1996)
689. M.W.Matsen, F.S.Bates. *Macromolecules*, **29**, 7641 (1996)
690. L.Leibler. *Macromolecules*, **13**, 1602 (1980)
691. A.N.Semenov. *Zh. Eksp. Teor. Fiz.*, **61**, 733 (1985)
692. S.M.Gruner. *J. Phys. Chem.*, **93**, 7562 (1989)
693. D.M.Anderson, S.M.Gruner, S.Leibler. *Proc. Natl. Acad. Sci. USA*, **85**, 5364 (1988)
694. D.C.Turner, S.M.Gruner, J.S.Huang. *Biochemistry*, **31**, 1356 (1992)
695. M.A.Shcherbina, S.N.Chvalun. *Russ. J. Phys. Chim*, **92**, 1171 (2018)
696. *Liquid Crystals and Plastic Crystals. (Ellis Horwood Ser. In Physical Chemistry*. Vols 1, 2). (Eds G.W.Gray, P.A.Winsor). (Chichester: Ellis Horwood, 1974)
697. D.Reuter, P.Lunkenheimer, A.Loidl. *J. Chem. Phys.*, **150**, 244507 (2019)
698. J.Even, M.Carignano, C.Katan. *Nanoscale*, **8**, 6222 (2016)
699. P.S.Whitfield, N.Herron, W.E.Guise, K.Page, Y.Q.Cheng, I.Milas, M.K.Crawford. *Sci. Rep.*, **6**, 35685 (2016)
700. A.V.Bakirov, E.A.Tatarinova, S.A.Milenin, M.A.Shcherbina, A.M.Muzafarov, S.N.Chvalun. *Soft Matter*, **14**, 9755 (2018)
701. G.Ungar. *Polymer (Guildf.)*, **34**, 2050 (1993)
702. B.Wünderlich, M.Möller, J.Grebowicz, H.Baur. In *Conformational Motion and Disorder in Low and High Molecular Mass (Ser. Advances in Polymer Science*. Vol. 87). (Berlin, Heidelberg: Springer-Verlag, 1988)
703. *Developments in Crystalline Polymers*. (Ed. D.C.Bassett). (London: Applied Science Publishers, 1982)
704. M.A.Shcherbina, S.N.Chvalun, V.I.Selikhova, V.M.Neverov, V.A.Aulov, A.N.Ozerin, N.F.Bakeev. *Polym. Sci., Ser. A*, **41**, 1121 (1999)
705. .A.Shcherbina, S.N.Chvalun, V.A.Aulov, V.I.Selikhova, N.F.Bakeev. *Polym. Sci., Ser. A*, **43**, 72 (2001)
706. M.A.Shcherbina, A.V.Bakirov, A.N.Yakunin, V.Percec, U.Beginn, M.Möller, S.N.Chvalun. *Crystallography Rep.*, **57**, 151 (2012)
707. M.A.Shcherbina, S.N.Chvalun. *Russ. J. Phys. Chem. A*, **92**, 1161 (2018)
708. M.Mansueto, W.Frey, S.Laschat. *Chem. – Eur. J.*, **19**, 16058 (2013)
709. S.-P.Ji, M.Tang, L.He, G.-H.Tao. *Chem. – Eur. J.*, **19**, 4452 (2013)
710. A.Abate, A.Petrozza, G.Cavallo, G.Lanzani, F.Matteucci, D.W.Bruce, N.Houbenov, P.Metrangolo, G.Resnati. *J. Mater. Chem. A*, **1**, 6572 (2013)
711. R.Rohini, C.-K.Lee, J.-T.Lu, I.J.B.Lin. *J. Chinese Chem. Soc.*, **60**, 745 (2013)
712. R.Rondla, J.C.Y.Lin, C.T.Yang, I.J.B.Lin. *Langmuir*, **29**, 11779 (2013)
713. W.S.Chi, H.Jeon, S.J.Kim, D.J.Kim, J.H.Kim. *Macromol. Res.*, **21**, 315 (2013)
714. E.Westphal, D.H.da Silva, F.Molin, H.Gallardo. *RSC Adv.*, **3**, 6442 (2013)
715. M.Yang, B.Mallick, A.-V.Mudring. *Cryst. Growth Des.*, **13**, 3068 (2013)
716. M.R.Schenkel, R.Shao, L.A.Robertson, B.R.Wiesenauer, N.A.Clark, D.L.Gin. *Liq. Cryst.*, **40**, 1067 (2013)
717. Y.Ji, R.Shi, Y.Wang, G.Saielli. *J. Phys. Chem. B*, **117**, 1104 (2013)
718. Y.Gao, J.M.Slattery, D.W.Bruce. *New J. Chem.*, **35**, 2910 (2011)
719. A.Getsis, A.-V.Mudring. *Eur. J. Inorg. Chem.*, **2011**, 3207 (2011)
720. L.Douce, J.-M.Suisse, D.Guillon, A.Taubert. *Liq. Cryst.*, **38**, 1653 (2011)
721. S.Sauer, S.Saliba, S.Tussetschläger, A.Baro, W.Frey, F.Giesselmann, S.Laschat, W.Kantlehner. *Liq. Cryst.*, **36**, 275 (2009)
722. F.Mathevet, P.Masson, J.-F.Nicoud, A.Skoulios. *J. Am. Chem. Soc.*, **127**, 9053 (2005)
723. M.Butschies, M.Mansueto, J.C.Haenle, C.Schneck, S.Tussetschläger, F.Giesselmann, S.Laschat. *Liq. Cryst.*, **41**, 821 (2014)
724. U.Beginn, L.Yan, S.N.Chvalun, M.A.Shcherbina, A.Bakirov, M.Möller. *Liq. Cryst.*, **35**, 1073 (2008)
725. M.A.Shcherbina, A.V.Bakirov, A.N.Yakunin, U.Beginn, L.Yan, M.Möller, S.N.Chvalun. *Soft Matter*, **10**, 1746 (2014)
726. M.A.Shcherbina, A.V.Bakirov, L.Yan, U.Beginn, X.Zhu, M.Möller, S.N.Chvalun. *Mendeleev Commun.*, **25**, 142 (2015)
727. M.A.Shcherbina, A.V.Bakirov, U.Beginn, L.Yan, X.Zhu, M.Möller, S.N.Chvalun. *Chem. Commun.*, **53**, 10070 (2017)
728. W.S.Fall, M.-H.Yen, X.Zeng, L.Cseh, Y.Liu, G.A.Gehring, G.Ungar. *Soft Matter*, **15**, 22 (2019)
729. M.-H.Yen, J.Chaiprapa, X.Zeng, Y.Liu, L.Cseh, G.H.Mehl, G.Ungar. *J. Am. Chem. Soc.*, **138**, 5757 (2016)
730. X.Cheng, M.Prehm, M.K.Das, J.Kain, U.Baumeister, S.Diele, D.Leine, A.Blume, C.Tschierske. *J. Am. Chem. Soc.*, **125**, 10977 (2003)
731. B.Chen. *Science*, **307**, 96 (2005)
732. X.Zeng, R.Kieffer, B.Glettner, C.Nurnberger, F.Liu, K.Pelz, M.Prehm, U.Baumeister, H.Hahn, H.Lang, G.A.Gehring, C.H.M.Weber, J.K.Hobbs, C.Tschierske, G.Ungar. *Science*, **331**, 1302 (2011)
733. S.George, C.Bentham, X.Zeng, G.Ungar, G.A.Gehring. *Phys. Rev. E*, **95**, 062126 (2017)
734. A.V.Bakirov, A.N.Yakunin, M.A.Shcherbina, S.N.Chvalun, X.Zhu, U.Beginn, M.Möller. *Nanotechnol. Russ.*, **5**, 762 (2010)

735. X.Feng, S.Nejati, M.G.Cowan, M.E.Tousley, B.R.Wiesenauer, R.D.Noble, M.Elimelech, D.L.Gin, C.O.Osuji. *ACS Nano*, **10**, 150 (2015)
736. X.Feng, M.E.Tousley, M.G.Cowan, B.R.Wiesenauer, S.Nejati, Y.Choo, R.D.Noble, M.Elimelech, D.L.Gin, C.O.Osuji. *ACS Nano*, **8**, 11977 (2014)
737. S.N.Chvalun, M.A.Shcherbina, I.V.Bykova, J.Blackwell, V.Percec. *Polym. Sci., Ser. A* , **44**, 2134 (2002)
738. T.Ichikawa, M.Yoshio, A.Hamasaki, J.Kagimoto, H.Ohno, T.Kato. *J. Am. Chem. Soc.*, **133**, 2163 (2011)
739. T.Ikeda. *J. Mater. Chem.*, **13**, 2037 (2003)
740. N.Kawatsuki. *Chem. Lett.*, **40**, 548 (2011)
741. B.Soberats, E.Uchida, M.Yoshio, J.Kagimoto, H.Ohno, T.Kato. *J. Am. Chem. Soc.*, **136**, 9552 (2014)
742. T.Kosa, L.Sukhomlinova, L.Su, B.Taheri, T.J.White, T.J.Bunning. *Nature (London)*, **485**, 347 (2012)
743. Y.Zakrevskyy, J.Stumpe, C.F.J.Faul. *Adv. Mater.*, **18**, 2133 (2006)
744. B.Soberats, M.Yoshio, T.Ichikawa, S.Taguchi, H.Ohno, T.Kato. *J. Am. Chem. Soc.*, **135**, 15286 (2013)
745. B.-H.Tan, M.Yoshio, T.Kato. *Chem. – Asian J.*, **3**, 534 (2008)
746. X.Su, S.Voskian, R.P.Hughes, I.Aprahamian. *Angew. Chem., Int. Ed.*, **52**, 10734 (2013)
747. A.M.Lowe, N.L.Abbott. *Chem. Mater.*, **24**, 746 (2011)
748. Y.Sagara, T.Kato. *Angew. Chem., Int. Ed.*, **50**, 9128 (2011)
749. A.Beneduci, S.Cospito, M.La Deda, L.Veltri, G.Chidichimo. *Nat. Commun.*, **5**, 3105 (2014)
750. T.Kato, M.Yoshio, T.Ichikawa, B.Soberats, H.Ohno, M.Funahashi. *Nat. Rev. Mater.*, **2**, 17001 (2017)
751. K.Tanabe, Y.Suzui, M.Hasegawa, T.Kato. *J. Am. Chem. Soc.*, **134**, 5652 (2012)
752. K.Lava, Y.Evrard, K.Van Hecke, L.Van Meervelt, K.Binnemans. *RSC Adv.*, **2**, 8061 (2012)
753. T.Cardinaels, K.Lava, K.Goossens, S.V.Eliseeva, K.Binnemans. *Langmuir*, **27**, 2036 (2011)
754. J.-T.Lu, C.-K.Lee, I.J.B.Lin. *Soft Matter*, **7**, 3491 (2011)
755. S.Taguchi, T.Ichikawa, T.Kato, H.Ohno. *Chem. Commun.*, **48**, 5271 (2012)
756. T.Ichikawa, M.Yoshio, A.Hamasaki, S.Taguchi, F.Liu, X.Zeng, G.Ungar, H.Ohno, T.Kato. *J. Am. Chem. Soc.*, **134**, 2634 (2012)
757. A.Jankowiak, J.Kanazawa, P.Kaszynski, R.Takita, M.Uchiyama. *J. Organomet. Chem.*, **747**, 195 (2013)
758. J.Pecyna, A.Sivaramamoorthy, A.Jankowiak, P.Kaszynski. *Liq. Cryst.*, **39**, 965 (2012)
759. C.S.P.Tripathi, J.Leys, P.Losada-Pérez, K.Lava, K.Binnemans, C.Glorieux, J.Thoen. *Liq. Cryst.*, **40**, 329 (2013)
760. G.Saielli, G.A.Voth, Y.Wang. *Soft Matter*, **9**, 5716 (2013)
761. P.Dechambenoit, S.Ferlay, B.Donnio, D.Guillon, M.W.Hosseini. *Chem. Commun.*, **47**, 734 (2011)
762. V.Percec, G.Johansson, J.Heck, G.Ungarb, S.V.Battyb. *J. Chem. Soc., Perkin Trans. 1*, 1411 (1993)
763. V.Percec, J.Heck, D.Tomazos, F.Falkenberg, H.Blackwell, G.Ungar. *J. Chem. Soc., Perkin Trans. 1*, 2799 (1993)
764. V.Percec, J.Heck, G.Johansson, D.Tomazos, G.Ungar. *Macromol. Symp.*, **77**, 237 (1994)
765. Y.K.Kwon, C.Danko, S.Chvalun, J.Blackwell, J.A.Heck, V.Percec. *Macromol. Symp.*, **87**, 103 (1994)
766. Y.K.Kwon, S.Chvalun, A.-I.Schneider, J.Blackwell, V.Percec, J.A.Heck. *Macromolecules*, **27**, 6129 (1994)
767. S.N.Chvalun, J.Blackwell, Y.K.Kwon, V.Percec. *Macromol. Symp.*, **118**, 663 (1997)
768. S.N.Chvalun, J.Blackwell, J.D.Cho, Y.K.Kwon, V.Percec, J.A.Heck. *Polymer (Guildf.)*, **39**, 4515 (1998)
769. S.N.Chvalun, M.A.Shcherbina, I.V.Bykova, J.Blackwell, V.Percec, Y.K.Kwon, J.D.Cho. *Polym. Sci. Ser. A*, **43**, 40 (2001)
770. D.A.Wilson, K.A.Andreopoulou, M.Peterca, P.Leowanawat, D.Sahoo, B.E.Partridge, Q.Xiao, N.Huang, P.A.Heiney, V.Percec. *J. Am. Chem. Soc.*, **141**, 6162 (2019)
771. V.Nanda, A.Andrianarijaona, C.Narayanan. *Protein Sci.*, **16**, 1667 (2007)
772. Z.Chen, P.A.Lichtor, A.P.Berliner, J.C.Chen, D.R.Liu. *Nat. Chem.*, **10**, 420 (2018)
773. A.Cecconello, F.C.Simmel. *Small*, **15**, 1805419 (2019)
774. V.Percec, A.E.Dulcey, V.S.K.Balagurusamy, Y.Miura, J.Smidrkal, M.Peterca, S.Nummelin, U.Edlund, S.D.Hudson, P.A.Heiney, H.Duan, S.N.Magonov, S.A.Vinogradov. *Nature (London)*, **430**, 764 (2004)
775. B.M.Rosen, M.Peterca, K.Morimitsu, A.E.Dulcey, P.Leowanawat, A.-M.Resmerita, M.R.Imam, V.Percec. *J. Am. Chem. Soc.*, **133**, 5135 (2011)
776. C.Roche, H.-J.Sun, M.E.Prendergast, P.Leowanawat, B.E.Partridge, P.A.Heiney, F.Araoka, R.Graf, H.W.Spiess, X.Zeng, G.Ungar, V.Percec. *J. Am. Chem. Soc.*, **136**, 7169 (2014)
777. A.J.Markvoort, H.M.M.ten Eikelder, P.A.J.Hilbers, T.F.A.de Greef, E.W.Meijer. *Nat. Commun.*, **2**, 509 (2011)
778. F.Helmich, M.M.J.Smulders, C.C.Lee, A.P.H.J.Schenning, E.W.Meijer. *J. Am. Chem. Soc.*, **133**, 12238 (2011)
779. C.Kulkarni, J.A.Berrocal, M.Lutz, A.R.A.Palmans, E.W.Meijer. *J. Am. Chem. Soc.*, **141**, 6302 (2019)
780. E.Yashima, N.Ousaka, D.Taura, K.Shimomura, T.Ikai, K.Maeda. *Chem. Rev.*, **116**, 13752 (2016)
781. K.V.Rao, D.Miyajima, A.Nihonyanagi, T.Aida. *Nat. Chem*, **9**, 1133 (2017)
782. K.Yano, Y.Itoh, F.Araoka, G.Watanabe, T.Hikima, T.Aida. *Science*, **363**, 161 (2019)
783. E.Krieg, M.M.C.Bastings, P.Besenius, B.Rybtchinski. *Chem. Rev.*, **116**, 2414 (2016)
784. F.Freire, E.Quiñoá, R.Riguera. *Chem. Rev.*, **116**, 1242 (2015)
785. K.Cobos, E.Quiñoá, R.Riguera, F.Freire. *J. Am. Chem. Soc.*, **140**, 12239 (2018)
786. M.A.Shcherbina, X.Zeng, T.Tadjiev, G.Ungar, S.H.Eichhorn, K.E.S.Phillips, T.J.Katz. *Angew. Chem., Int. Ed.*, **48**, 7837 (2009)
787. A.A.Stupnikov, M.A.Shcherbina, S.N.Chvalun. *Russ. Chem. Bull., Int. Ed.*, **67**, 1547 (2018)
788. S.Yadav, A.K.Sharma, P.Kumar. *Front. Bioeng. Biotechnol.*, **8**, 127 (2020)
789. P.C.Griffiths, I.A.Fallis, T.Chuenpratoom, R.Watanesk. *Adv. Colloid Interface Sci.*, **122**, 107 (2006)
790. M.Qi, Y.Zhou. *Mater. Chem. Front.*, **3**, 1994 (2019)
791. S.Chen, S.Hanning, J.Falconer, M.Locke, J.Wen. *Eur. J. Pharm. Biopharm.*, **144**, 18 (2019)
792. X.Ge, M.Wei, S.He, W.-E.Yuan. *Pharmaceutics*, **11**, 55 (2019)
793. C.Zhou, Y.Wang. *Curr. Opin. Colloid Interface Sci.*, **45**, 28 (2020)
794. J.Y.Wang, J.Q.Li, Y.M.Xiao, B.Fu, Z.H.Qin. *ChemMedChem*, **15**, 404 (2020)
795. S.Chowdhury, A.Rakshit, A.Acharjee, B.Saha. *ChemistrySelect*, **4**, 6978 (2019)

796. L.Y.Zakharova, R.R.Kashapov, T.N.Pashirova, A.B.Mirgorodskaya, O.G.Sinyashin. *Mendeleev Commun.*, **26**, 457 (2016)
797. L.Y.Zakharova, T.N.Pashirova, S.Doktorovova, A.R.Fernandes, E.Sanchez-Lopez, A.M.Silva, S.B.Souto, E.B.Souto. *Int. J. Mol. Sci.*, **20**, 5534 (2019)
798. A.Tehrani-Bagha, K.Holmberg. *Curr. Opin. Colloid Interface Sci.*, **12**, 81 (2007)
799. A.B.Mirgorodskaya, R.A.Kushnazarova, S.S.Lukashenko, A.D.Voloshina, O.A.Lenina, L.Y.Zakharova, O.G.Sinyashin. *J. Mol. Liq.*, **269**, 203 (2018)
800. A.B.Mirgorodskaya, R.A.Kushnazarova, S.S.Lukashenko, L.Y.Zakharova. *J. Mol. Liq.*, **292**, 111407 (2019)
801. A.B.Mirgorodskaya, S.S.Lukashenko, R.A.Kushnazarova, R.R.Kashapov, L.Y.Zakharova, O.G.Sinyashin. *Russ. J. Org. Chem.*, **54**, 987 (2018)
802. A.B.Mirgorodskaya, R.A.Kushnazarova, S.S.Lukashenko, E.N.Nikitin, K.O.Sinyashin, L.M.Nesterova, L.Y.Zakharova. *Colloids Surf., A*, **586**, 124252 (2020)
803. R.Sharma, R.K.Mahajan. *RSC Adv.*, **4**, 748 (2014)
804. D.A.Samarkina, D.R.Gabdrakhmanov, S.S.Lukashenko, A.R.Khamatgalimov, V.I.Kovalenko, L.Y.Zakharova. *Colloids Surf., A*, **529**, 990 (2017)
805. D.A.Samarkina, D.R.Gabdrakhmanov, S.S.Lukashenko, I.R.Nizameev, M.K.Kadirov, L.Y.Zakharova. *J. Mol. Liq.*, **275**, 232 (2019)
806. M.Damen, A.J.J.Groenen, S.F.M.van Dongen, R.J.M.Nolte, B.J.Scholte, M.C.Feiters. *Med. Chem. Commun.*, **9**, 1404 (2018)
807. R.Modi, L.Khamari, A.Nandy, S.Mukherjee. *Spectrochim. Acta, Part A*, **216**, 52 (2019)
808. D.A.Kuznetsova, D.R.Gabdrakhmanov, L.R.Ahtamyanova, S.S.Lukashenko, A.M.Kusova, Y.F.Zuev, A.D.Voloshina, A.S.Sapunova, N.V.Kulik, D.M.Kuznetsov, I.R.Nizameev, M.K.Kadirov, L.Y.Zakharova. *J. Mol. Liq.*, **298**, 111961 (2020)
809. D.A.Kuznetsova, D.R.Gabdrakhmanov, S.S.Lukashenko, D.A.Faizullin, Y.F.Zuev, I.R.Nizameev, M.K.Kadirov, D.M.Kuznetsov, L.Y.Zakharova. *J. Mol. Liq.*, **307**, 113001 (2020)
810. D.A.Kuznetsova, D.R.Gabdrakhmanov, S.S.Lukashenko, A.D.Voloshina, A.S.Sapunova, R.R.Kashapov, L.Y.Zakharova. *Chem. Phys. Lipids*, **223**, 104791 (2019)
811. D.A.Kuznetsova, D.R.Gabdrakhmanov, S.S.Lukashenko, A.D.Voloshina, A.S.Sapunova, N.V.Kulik, I.R.Nizameev, M.K.Kadirov, R.R.Kashapov, L.Y.Zakharova. *J. Mol. Liq.*, **289**, 111058 (2019)
812. D.A.Kuznetsova, D.R.Gabdrakhmanov, S.S.Lukashenko, L.Y.Zakharova. *Russ. J. Phys. Chem.*, **93**, 1584 (2019)
813. F.M.Menger, J.S.Keiper. *Angew. Chem., Int. Ed.*, **39**, 1906 (2000)
814. R.Zana. *J. Colloid Interface Sci.*, **248**, 203 (2002)
815. V.Sharma, M.Borse, V.K.Aswal, N.K.Pokhriyal, J.V.Joshi, P.S.Goyal, S.Devi. *J. Colloid Interface Sci.*, **277**, 450 (2004)
816. L.Y.Zakharova, D.R.Gabdrakhmanov, A.R.Ibragimova, E.A.Vasilieva, I.R.Nizameev, M.K.Kadirov, E.A.Ermakova, N.E.Gogoleva, D.A.Faizullin, A.G.Pokrovsky, V.A.Korobeynikov, S.V.Cheresiz, Y.F.Zuev. *Colloids Surf., B*, **140**, 269 (2016)
817. D.R.Gabdrakhmanov, E.A.Vasilieva, M.A.Voronin, D.A.Kuznetsova, F.G.Valeeva, A.B.Mirgorodskaya, S.S.Lukashenko, V.M.Zakharov, A.R.Mukhitov, D.A.Faizullin, V.V.Salnikov, V.V.Syakaev, S.K.Latypov, Y.F.Zuev, L.Y.Zakharova. *J. Phys. Chem. C*, **124**, 2178 (2020)
818. A.B.Mirgorodskaya, F.G.Valeeva, S.S.Lukashenko, R.A.Kushnazarova, T.M.Prokop'eva, T.M.Zubareva, V.A.Mikhailov, L.Y.Zakharova. *J. Mol. Liq.*, **250**, 229 (2018)
819. E.P.Zhil'tsova, M.R.Ibatullina, S.S.Lukashenko, M.P.Kutyreva, M.M.Anuar, V.I.Kovalenko, L.Y.Zakharova. *Russ. J. Gen. Chem.*, **87**, 2620 (2017)
820. M.R.Ibatullina, E.P.Zhil'tsova, S.S.Lukashenko, A.D.Voloshina, A.S.Sapunova, O.A.Lenina, I.R.Nizameev, M.P.Kutyreva, L.Y.Zakharova. *Russ. J. Gen. Chem.*, **88**, 2359 (2018)
821. E.P.Zhiltsova, M.R.Ibatullina, S.S.Lukashenko, F.G.Valeeva, T.N.Pashirova, M.P.Kutyreva, L.Y.Zakharova. *Colloid J.*, **79**, 621 (2017)
822. E.P.Zhiltsova, T.N.Pashirova, M.R.Ibatullina, S.S.Lukashenko, A.T.Gubaidullin, D.R.Islamov, O.N.Kataeva, M.P.Kutyreva, L.Y.Zakharova. *Phys. Chem. Chem. Phys.*, **20**, 12688 (2018)
823. E.P.Zhil'tsova, M.R.Ibatullina, S.S.Lukashenko, M.P.Kutyreva, L.Y.Zakharova. *Russ. J. Org. Chem.*, **54**, 431 (2018)
824. M.R.Ibatullina, E.P.Zhil'tsova, S.S.Lukashenko, L.Y.Zakharova. *Colloid J.*, **82**, 8 (2020)
825. G.A.Gainanova, G.I.Vagapova, V.V.Syakaev, A.R.Ibragimova, F.G.Valeeva, E.V.Tudriy, I.V.Galkina, O.N.Kataeva, L.Y.Zakharova, S.K.Latypov, A.I.Konovalov. *J. Colloid Interface Sci.*, **367**, 327 (2012)
826. G.A.Gaynanova, G.I.Vagapova, F.G.Valeeva, E.A.Vasilieva, I.V.Galkina, L.Y.Zakharova, O.G.Sinyashin. *Colloids Surf., A*, **489**, 95 (2016)
827. L.Y.Zakharova, G.I.Kaupova, D.R.Gabdrakhmanov, G.A.Gaynanova, E.A.Ermakova, A.R.Mukhitov, I.V.Galkina, S.V.Cheresiz, A.G.Pokrovsky, P.V.Skvortsova, Y.V.Gogolev, Y.F.Zuev. *Phys. Chem. Chem. Phys.*, **21**, 16706 (2019)
828. E.Yuba. *J. Mater. Chem. B*, **8**, 1093 (2020)
829. D.A.Kuznetsova, D.R.Gabdrakhmanov, S.S.Lukashenko, L.R.Ahtamyanova, I.R.Nizameev, M.K.Kadirov, L.Y.Zakharova. *Colloids Surf., B*, **178**, 352 (2019)
830. D.A.Kuznetsova, G.A.Gaynanova, L.A.Vasileva, G.V.Sibgatullina, D.V.Samigullin, A.S.Sapunova, A.D.Voloshina, I.V.Galkina, K.A.Petrov, L.Y.Zakharova. *J. Mater. Chem. B*, **7**, 7351 (2019)
831. D.Lombardo, M.A.Kiselev, S.Magazù, P.Calandra. *Adv. Condens. Matter Phys.*, 1 (2015)
832. Y.Razuvayeva, R.Kashapov, L.Zakharova. *Supramol. Chem.*, **32**, 178 (2020)
833. Z.Li, C.Hu, Y.Cheng, H.Xu, X.Cao, X.Song, H.Zhang, Y.Liu. *Sci. China Chem.*, **55**, 2063 (2012)
834. Y.-C.Liu, Y.-Y.Wang, H.-W.Tian, Y.Liu, D.-S.Guo. *Org. Chem. Front.*, **3**, 53 (2016)

835. R.R.Kashapov, Y.S.Razuvayeva, A.Y.Ziganshina, R.K.Mukhitova, L.Y.Zakharova. *Colloids Surf., A*, **583**, 124033 (2019)
836. C.Costa, V.Francisco, S.G.Silva, M.L.C.do Vale, L.García-Río, E.F.Marques. *Colloids Surf., A*, **480**, 71 (2015)
837. R.R.Kashapov, Y.S.Razuvayeva, A.Y.Ziganshina, R.K.Mukhitova, A.S.Sapunova, A.D.Voloshina, L.Y.Zakharova. *Colloids Surf., B*, **175**, 351 (2019)
838. R.R.Kashapov, Y.S.Razuvayeva, A.Y.Ziganshina, R.K.Mukhitova, A.S.Sapunova, A.D.Voloshina, L.Y.Zakharova. *Macroheterocycles*, **12**, 346 (2019)
839. R.R.Kashapov, S.V.Kharlamov, Y.S.Razuvayeva, A.Y.Ziganshina, I.R.Nizameev, M.K.Kadirov, S.K.Latypov, L.Y.Zakharova. *J. Mol. Liq.*, **261**, 218 (2018)
840. S.K.Mehta, N.Jindal, G.Kaur. *Colloids Surf., B*, **87**, 173 (2011)
841. S.Akhter, S.Kushwaha, M.H.Warsi, M.Anwar, M.Z.Ahmad, I.Ahmad, S.Talegaonkar, Z.I.Khan, R.K.Khar, F.J.Ahmad. *Drug Dev. Ind. Pharm.*, **38**, 84 (2011)
842. M.Bragagni, N.Mennini, C.Ghelardini, P.Mura. *J. Pharm. Pharm. Sci.*, **15**, 184 (2012)
843. L.Di Marzio, C.Marianecci, F.Rinaldi, S.Esposito, M.Carafa. *Lett. Drug Des. Discov.*, **9**, 494 (2012)
844. C.Marianecci, F.Rinaldi, M.Mastriota, S.Pieretti, E.Trapasso, D.Paolino, M.Carafa. *J. Control. Release*, **164**, 17 (2012)
845. R.Ganguly, A.Kunwar, B.Dutta, S.Kumar, K.C.Barick, A.Ballal, V.K.Aswal, P.A.Hassan. *Colloids Surf., B*, **152**, 176 (2017)
846. G.P.Kumar, P.Rajeshwarrao. *Acta Pharm. Sinica B*, **1**, 208 (2011)
847. R.K.Sahoo, N.Biswas, A.Guha, N.Sahoo, K.Kuotsu. *Biomed. Res. Int.*, Art. ID 263604 (2014)
848. T.T.Pham, C.Jaafar-Maalej, C.Charcosset, H.Fessi. *Colloids Surf., B*, **94**, 15 (2012)
849. F.Rinaldi, P.N.Hanieh, A.Imbriano, D.Passeri, E.Del Favero, M.Rossi, C.Marianecci, S.De Panfilis, M.Carafa. *J. Drug Deliv. Sci. Technol.*, **55**, 101339 (2020)
850. H.Abdelkader, S.Ismail, A.Kamal, R.G.Alany. *J. Pharm. Sci.*, **100**, 1833 (2011)
851. P.M.E.Gaafar, O.Y.Abdallah, R.M.Farid, H.Abdelkader. *J. Liposome Res.*, **24**, 204 (2014)
852. A.Abdelbary, H.F.Salem, R.A.Khallaf, A.M.A.Ali. *Pharm. Dev. Technol.*, **22**, 409 (2016)
853. G.A.Abdelbary, M.H.Aburahma. *J. Liposome Res.*, **25**, 107 (2014)
854. L.Di Marzio, S.Esposito, F.Rinaldi, C.Marianecci, M.Carafa. *Colloids Surf., B*, **104**, 200 (2013)
855. R.S.Abdel-Rashid, D.A.Helal, M.M.Omar, A.M.El Sisi. *Int. J. Nanomed.*, **14**, 2973 (2019)
856. H.M.Aboud, A.A.Ali, S.F.El-Menshawe, A.A.Elbary. *Drug Deliv.*, **23**, 2471 (2016)
857. S.Ghanbarzadeh, S.Arami. *J. Drug Deliv. Sci. Technol.*, **23**, 587 (2013)
858. H.F.Salem, R.M.Kharshoum, H.A.Abou-Taleb, D.M.Naguib. *AAPS PharmSciTech*, **20**, 181 (2019)
859. Y.Singh, J.G.Meher, K.Raval, F.A.Khan, M.Chaurasia, N.K.Jain, M.K.Chourasia. *J. Control. Release*, **252**, 28 (2017)
860. L.Jones, L.E.Downie, D.Korb, J.M.Benitez-del-Castillo, R.Dana, S.X.Deng, P.N.Dong, G.Geerling, R.Y.Hida, Y.Liu, K.Y.Seo, J.Tauber, T.H.Wakamatsu, J.Xu, J.S.Wolffsohn, J.P.Craig. *Ocul. Surf.*, **15**, 575 (2017)
861. F.Lallemand, M.Schmitt, J.-L.Bourges, R.Gurny, S.Benita, J.-S.Garrigue. *Eur. J. Pharm. Biopharm.*, **117**, 14 (2017)
862. L.Gan, J.Wang, M.Jiang, H.Bartlett, D.Ouyang, F.Eperjesi, J.Liu, Y.Gan. *Drug Discov. Today*, **18**, 290 (2013)
863. R.L.Walenga, A.H.Babiskin, X.Zhang, M.Absar, L.Zhao, R.A.Lionberger. *J. Pharm. Sci.*, **108**, 620 (2019)
864. L.Lalu, V.Tambe, D.Pradhan, K.Nayak, S.Bagchi, R.Maheshwari, K.Kalia, R.K.Tekade. *J. Control. Release*, **268**, 19 (2017)
865. P.Daull, F.Lallemand, J.-S.Garrigue. *J. Pharm. Pharmacol.*, **66**, 531 (2013)
866. F.Lallemand, P.Daull, S.Benita, R.Buggage, J.-S.Garrigue. *J. Drug Deliv.*, Art. ID 604204 (2012)
867. B.J.Dukovski, M.Juretić, D.Bračko, D.Randjelović, S.Savić, M.C.Moral, Y.Diebold, J.Filipović-Grčić, I.Pepić, J.Lovrić. *Int. J. Pharm.*, **576**, 118979 (2020)
868. D.J.Brayden, J.Gleeson, E.G.Walsh. *Eur. J. Pharm. Biopharm.*, **88**, 830 (2014)
869. D.-H.Oh, K.-H.Chun, S.-O.Jeon, J.-W.Kang, S.Lee. *Eur. J. Pharm. Biopharm.*, **79**, 357 (2011)
870. V.V.Prasanth, A.Puratchikody, S.T.Mathew, K.B.Ashok. *Res. Pharm. Sci.*, **9**, 259 (2014)
871. H.A.S.Favacho, R.O.do Couto, M.P.F.Duarte, M.P.G.Peixoto, R.F.V.Lopez, V.Pedrazzi, C.M.de Gaitani, O.de Freitas. *Mater. Sci. Eng. C*, **108**, 110373 (2020)
872. A.Me'ndez-Ardoy, N.Guilloteau, C.Di Giorgio, P.Vierling, F.Santoyo-González, C.O.Mellet, J.M.G.Fernández. *J. Org. Chem.*, **76**, 5882 (2011)
873. V.V.Khutoryanskiy. *Macromol. Biosci.*, **11**, 748 (2010)
874. K.Kamiński, M.Kujdowicz, M.Kajta, M.Nowakowska, K.Szczubiałka. *Eur. J. Pharm. Biopharm.*, **91**, 111 (2015)
875. I.Popiołek, A.Niziołek, K.Kamiński, U.Kwolek, M.Nowakowska, K.Szczubiałka. *Bioorg. Med. Chem.*, **27**, 1414 (2019)
876. Y.Zhang, Y.-L.Cui, L.-N.Gao, H.-L.Jiang. *Int. J. Biol. Macromol.*, **59**, 363 (2013)
877. C.Godugu, A.R.Patel, R.Doddapaneni, J.Somagoni, M.Singh. *PLoS One*, **9**, e89919 (2014)
878. Y.Zhang, F.-C.Meng, Y.-L.Cui, Y.-F.Song. *J. Agric. Food Chem.*, **59**, 10919 (2011)
879. J.Barthelmes, G.Perera, J.Hombach, S.Dünnhaupt, A.Bernkop-Schnürch. *Int. J. Pharm.*, **416**, 339 (2011)
880. A.Moghadam, M.Ijaz, M.H.Asim, A.Mahmood, M.Jelkmann, B.Matuszczak, A.Bernkop-Schnürch. *Int. J. Nanomed.*, **13**, 4003 (2018)
881. M.H.Asim, A.Jalil, I.Shahzadi, M.Khan, B.Matuszczak, A.Bernkop-Schnürch. *Future Microbiol.*, **14**, 411 (2019)
882. M.Ijaz, M.Ahmad, N.Akhtar, F.Laffleur, A.Bernkop-Schnürch. Polymer (Guildf.)*J. Pharm. Sci.*, **105**, 2848 (2016)
883. M.Ijaz, A.Bernkop-Schnürch. *Expert Opin. Drug Deliv.*, **12**, 1269 (2015)
884. M.Ijaz, M.Prantl, N.Lupo, F.Laffleur, M.H.Asim, B.Matuszczak, A.Bernkop-Schnürch. *Int. J. Pharm.*, **534**, 339 (2017)
885. M.H.Asim, A.Moghadam, M.Ijaz, A.Mahmood, R.X.Götz, B.Matuszczak, A.Bernkop-Schnürch. *J. Colloid Interface Sci.*, **531**, 261 (2018)

886. M.Ijaz, B.Matuszczak, D.Rahmat, A.Mahmood, S.Bonengel, S.Hussain, C.W.Huck, A.Bernkop-Schnürch. *Carbohydr. Polym.*, **132**, 187 (2015)
887. M.Ijaz, J.A.Griessinger, A.Mahmood, F.Laffleur, A.Bernkop-Schnürch. *J. Pharm. Sci.*, **105**, 1714 (2016)
888. V.Laquintana, M.H.Asim, A.Lopedota, A.Cutrignelli, A.Lopalco, M.Franco, A.Bernkop-Schnürch, N.Denora. *Int. J. Pharm.*, **572**, 118820 (2019)
889. C.Mendes, G.C.Meirelles, C.G.Barp, J.Assreuy, M.A.S.Silva, G.Ponchel. *Carbohydr. Polym.*, **195**, 586 (2018)
890. C.Mendes, A.Buttchevitz, A.Barison, F.M.M.Ocampos, L.S.Bernardi, P.R.Oliveira, M.A.S.Silva. *Expert Rev. Anti-Infect. Ther.*, **13**, 131 (2014)
891. P.W.J.Morrison, C.J.Connon, V.V.Khutoryanskiy. *Mol. Pharm.*, **10**, 756 (2013)
892. A.E.-G.H.A.El-Gawad, O.A.Soliman, M.S.El-Dahan, S.A.S.Al-Zuhairy. *AAPS PharmSciTech*, **18**, 1795 (2016)
893. P.W.J.Morrison, N.N.Porfiryeva, S.Chahal, I.A.Salakhov, C.Lacourt, I.I.Semina, R.I.Moustafine, V.V.Khutoryanskiy. *Mol. Pharm.*, **14**, 3528 (2017)
894. M.A.H.Mohamed, A.A.Mahmoud. *Curr. Eye Res.*, **36**, 208 (2011)
895. G.Jóhannesson, M.D.Moya-Ortega, G.M.Ásgrimsdóttir, S.H.Lund, M.Thorsteinsdóttir, T.Loftsson, E.Stefánsson. *Acta Ophthalmol.*, **92**, 550 (2013)
896. E.A.Mun, P.W.J.Morrison, A.C.Williams, V.V.Khutoryanskiy. *Mol. Pharm.*, **11**, 3556 (2014)
897. J.B.Baruah. *Principles and Advances in Supramolecular Catalysis*. (Boca Raton, FL: CRC Press, 2019)
898. *Supramolecular Catalysis*. (Ed. P.W.N.M.van Leeuwen). (Wiley, 2008)
899. R.Breslow. *Acc. Chem. Res.*, **28**, 146 (1995)
900. Z.Dong, Q.Luo, J.Liu. *Chem. Soc. Rev.*, **41**, 7890 (2012)
901. M.Raynal, P.Ballester, A.Vidal-Ferran, P.W.N.M.van Leeuwen. *Chem. Soc. Rev.*, **43**, 1734 (2014)
902. M.Raynal, P.Ballester, A.Vidal-Ferran, P.W.N.M.van Leeuwen. *Chem. Soc. Rev.*, **43**, 1660 (2014)
903. J.Meeuwissen, J.N.H.Reek. *Nat. Chem*, **2**, 615 (2010)
904. P.Ballester, A.Vidal-Ferran, P.W.N.M.van Leeuwen. In *Advances in Catalysis*. Elsevier, Amsterdam, 2011. P. 63
905. M.W.Hosseini, J.-M.Lehn. *J. Chem. Soc., Chem. Commun.*, 451 (1991)
906. J.M.Lehn. *Appl. Catal. A: Gen.*, **113**, 105 (1994)
907. E.A.Karakhanov, A.L.Maksimov, E.A.Runova, Y.S.Kardasheva, M.V.Terenina, S.V.Kardashev, V.A.Skorkin, L.M.Karapetyan, M.Y.Talanova. *Russ. Chem. Bull., Int. Ed.*, **57**, 780 (2008)
908. A.L.Maksimov, D.A.Sakharov, T.Y.Filippova, A.Y.Zhuchkova, E.A.Karakhanov. *Ind. Eng. Chem. Res.*, **44**, 8644 (2005)
909. E.M.Hobert, A.E.Doerner, A.S.Walker, A.Schepartz. *Isr. J. Chem.*, **53**, 567 (2013)
910. S.Di Stefano, R.Cacciapaglia, L.Mandolini. *Eur. J. Org. Chem.*, 7304 (2014)
911. M.I.Page, W.P.Jencks. *Proc. Natl. Acad. Sci. USA*, **68**, 1678 (1971)
912. J.Åqvist, M.Kazemi, G.V.Isaksen, B.O.Brandsdal. *Acc. Chem. Res.*, **50**, 199 (2017)
913. F.Biedermann, W.M.Nau, H.-J.Schneider. *Angew. Chem., Int. Ed.*, **53**, 11158 (2014)
914. P.W.N.M.van Leeuwen, M.Raynal. In *Supramolecular Chemistry in Water*. (Ed. S.Kubik). (Wiley-VCH, 2019). P. 525
915. O.Bistri, O.Reinaud. *Org. Biomol. Chem.*, **13**, 2849 (2015)
916. S.Sadjadi. *Organic Nanoreactors. From Molecular to Supramolecular Organic Compounds*. (Elsevier, 2016)
917. A.Poma, A.P.F.Turner, S.A.Piletsky. *Trends Biotechnol.*, **28**, 629 (2010)
918. *Advanced Molecularly Imprinting Materials*. (Eds A.Tiwari, L.Uzun). (Hoboken, NJ: Wiley, 2016)
919. M.Komiyama, T.Mori, K.Ariga. *Bull. Chem. Soc. Jpn.*, **91**, 1075 (2018)
920. H.Zhang. *Adv. Mater.*, **32**, 1806328 (2019)
921. S.Muratsugu, S.Shirai, M.Tada. *Tetrahedron Lett.*, **61**, 151603 (2020)
922. D.Mathew, B.Thomas, K.S.Devaky. *Artif. Cells Nanomed. Biotechnol.*, **47**, 1149 (2019)
923. E.A.Karakhanov, A.L.Maximov. *Curr. Org. Chem.*, **14**, 1284 (2010)
924. D.Mathew, B.Thomas, K.S.Devaky. *J. Mol. Catal. A: Chem.*, **415**, 65 (2016)
925. S.Li, Y.Ge, A.P.F.Turner. *Adv. Funct. Mater.*, **21**, 1194 (2011)
926. H.J.Davis, R.J.Phipps. *Chem. Sci.*, **8**, 864 (2017)
927. N.R.Mote, S.H.Chikkali. *Chem. – Asian J.*, **13**, 3623 (2018)
928. S.Das. *Science*, **312**, 1941 (2006)
929. S.Das, G.W.Brudvig, R.H.Crabtree. *J. Am. Chem. Soc.*, **130**, 1628 (2008)
930. D.Balcells, P.Moles, J.D.Blakemore, C.Raynaud, G.W.Brudvig, R.H.Crabtree, O.Eisenstein. *Dalton Trans.*, 5989 (2009)
931. F.Burg, M.Gicquel, S.Breitenlechner, A.Pöthig, T.Bach. *Angew. Chem., Int. Ed.*, **57**, 2953 (2018)
932. P.Dydio, R.J.Detz, J.N.H.Reek. *J. Am. Chem. Soc.*, **135**, 10817 (2013)
933. S.-T.Bai, V.Sinha, A.M.Kluwer, P.R.Linnebank, Z.Abiri, B.Bruin, J.N.H.Reek. *ChemCatChem*, **11**, 5322 (2019)
934. T.Šmejkal, B.Breit. *Angew. Chem., Int. Ed.*, **47**, 311 (2008)
935. T.Šmejkal, D.Gribkov, J.Geier, M.Keller, B.Breit. *Chem. – Eur. J.*, **16**, 2470 (2010)
936. P.Dydio, W.I.Dzik, M.Lutz, B.De Bruin, J.N.H.Reek. *Angew. Chem., Int. Ed.*, **50**, 396 (2011)
937. P.Dydio, J.N.H.Reek. *Angew. Chem., Int. Ed.*, **52**, 3878 (2013)
938. J.Daubignard, R.J.Detz, A.C.H.Jans, B.De Bruin, J.N.H.Reek. *Angew. Chem., Int. Ed.*, **56**, 13056 (2017)
939. V.S.Koshti, A.Sen, D.Shinde, S.H.Chikkali. *Dalton Trans.*, **46**, 13966 (2017)
940. X.Li, C.You, Y.Yang, Y.Yang, P.Li, G.Gu, L.W.Chung, H.Lv, X.Zhang. *Chem. Sci.*, **9**, 1919 (2018)
941. E.M.Zakharyan, G.Ma, A.L.Maksimov, E.A.Karakhanov, Z.D.Voronina. *Pet. Chem.*, **54**, 412 (2014)
942. A.Maximov, A.Zolotukhina, V.Murzin, E.Karakhanov, E.Rosenberg. *ChemCatChem*, **7**, 1197 (2015)
943. E.Karakhanov, Y.Kardasheva, L.Kulikov, A.Maximov, A.Zolotukhina, M.Vinnikova, A.Ivanov. *Catalysts*, **6**, 122 (2016)
944. E.Karakhanov, A.Maximov, A.Zolotukhina, A.Mamadli, A.Vutolkina, A.Ivanov. *Catalysts*, **7**, 86 (2017)

945. A.L.Maximov, A.V.Zolotukhina, A.A.Mamedli, L.A.Kulikov, E.A.Karakhanov. *ChemCatChem*, **10**, 222 (2018); https://chemistry-europe.onlinelibrary.wiley.com/doi/10.1002/cctc.201700691
946. G.Olivo, G.Capocasa, O.Lanzalunga, S.Di Stefano, M.Costas. *Chem. Commun.*, **55**, 917 (2019)
947. A.J.Neel, M.J.Hilton, M.S.Sigman, F.D.Toste. *Nature (London)*, **543**, 637 (2017)
948. M.Yamakawa, I.Yamada, R.Noyori. *Angew. Chem., Int. Ed.*, **40**, 2818 (2001)
949. Y.Zhao, G.Luo, X.Kang, F.Guo, X.Zhu, R.Zheng, Z.Hou, Y.Luo. *Chem. Commun.*, **55**, 6689 (2019)
950. C.R.Forbes, S.K.Sinha, H.K.Ganguly, S.Bai, G.P.A.Yap, S.Patel, N.J.Zondlo. *J. Am. Chem. Soc.*, **139**, 1842 (2017)
951. T.Yang, J.Feng, X.Liu, Y.Wang, H.Ge, D.Cao, H.Li, Q.Peng, M.Ramos, X.-D.Wen, B.Shen. *J. Mater. Res.*, **33**, 3589 (2018)
952. E.A.Karakhanov, L.M.Karapetyan, Y.S.Kardasheva, A.L.Maksimov, E.A.Runova, M.V.Terenina, T.Y.Filippova. *Macromol. Symp.*, **270**, 106 (2008)
953. E.A.Karakhanov, T.Y.Filippova, S.A.Martynova, A.L.Maximov, V.V.Predeina, I.N.Topchieva. *Catal. Today*, **44**, 189 (1998)
954. E.Karakhanov, Y.Kardasheva, A.Kirillov, A.Maximov, V.Predeina, E.Runova. *Macromol. Symp.*, **156**, 137 (2000)
955. E.A.Karakhanov, Y.S.Kardasheva, A.L.Maximov, E.A.Runova, T.A.Buchneva, M.A.Gaevskiy, A.Y.Zhuchkova, T.Y.Filippova. *Polym. Adv. Technol.*, **12**, 161 (2001)
956. E.A.Karakhanov, Y.S.Kardasheva, E.A.Runova, V.A.Semernina. *J. Mol. Catal. A: Chem.*, **142**, 339 (1999)
957. E.Karakhanov, A.Maximov, A.Kirillov. *J. Mol. Catal. A: Chem.*, **157**, 25 (2000)
958. E.Karakhanov, T.Buchneva, A.Maximov, M.Zavertyaeva. *J. Mol. Catal. A: Chem.*, **184**, 11 (2002)
959. A.L.Maksimov, T.S.Buchneva, E.A.Karakhanov. *J. Mol. Catal. A: Chem.*, **217**, 59 (2004)
960. F.Hapiot, L.Leclercq, N.Azaroual, S.Fourmentin, S.Tilloy, E.Monflier. *Curr. Org. Synth.*, **5**, 162 (2008)
961. H.Bricout, F.Hapiot, A.Ponchel, S.Tilloy, E.Monflier. *Curr. Org. Chem.*, **14**, 1296 (2010)
962. S.Tilloy, F.Bertoux, A.Mortreux, E.Monflier. *Catal. Today*, **48**, 245 (1999)
963. H.Bricout, L.Caron, D.Bormann, E.Monflier. *Catal. Today*, **66**, 355 (2001)
964. J.Potier, S.Menuel, D.Fournier, S.Fourmentin, P.Woisel, E.Monflier, F.Hapiot. *ACS Catal.*, **2**, 1417 (2012)
965. S.Noël, B.Léger, A.Ponchel, K.Philippot, A.Denicourt-Nowicki, A.Roucoux, E.Monflier. *Catal. Today*, **235**, 20 (2014)
966. M.Elard, J.Denis, M.Ferreira, H.Bricout, D.Landy, S.Tilloy, E.Monflier. *Catal. Today*, **247**, 47 (2015)
967. M.Durmaz, E.Halay, S.Bozkurt. *Beilstein J. Org. Chem.*, **14**, 1389 (2018)
968. L.Catti, Q.Zhang, K.Tiefenbacher. *Chem. – Eur. J.*, **22**, 9060 (2016)
969. Q.-Q.Wang. In *Handbook of Macrocyclic Supramolecular Assembly*. (Singapore: Springer, 2019). P. 1
970. L.Guo, J.Du, Y.Wang, K.Shi, E.Ma. *J. Incl. Phenom. Macrocycl. Chem.*, **97**, 1 (2020)
971. E.A.Karakhanov, A.L.Maksimov, E.A.Runova. *Russ. Chem. Rev.*, **74**, 97 (2005)
972. B.Yang, J.-F.Cui, M.K.Wong. *RSC Adv.*, **7**, 30886 (2017)
973. Y.-S.Fung, S.-C.Yan, M.-K.Wong. *Org. Biomol. Chem.*, **10**, 3122 (2012)
974. S.Kuklin, A.Maximov, A.Zolotukhina, E.Karakhanov. *Catal. Commun.*, **73**, 63 (2016)
975. K.Cousin, S.Menuel, E.Monflier, F.Hapiot. *Angew. Chem., Int. Ed.*, **56**, 10564 (2017)
976. T.Vanbésien, E.Monflier, F.Hapiot. *ACS Catal.*, **5**, 4288 (2015)
977. T.Vanbésien, J.Le Nôtre, E.Monflier, F.Hapiot. *Eur. J. Lipid Sci. Technol.*, **120**, 1700190 (2017)
978. K.Cousin, T.Vanbésien, E.Monflier, F.Hapiot. *Catal. Commun.*, **125**, 37 (2019)
979. Y.Liu, R.L.Hartman. *React. Chem. Eng.*, **4**, 1341 (2019)
980. M.A.Rezvani, S.Khandan, N.Sabahi, H.Saeidian. *Chin. J. Chem. Eng.*, **27**, 2418 (2019)
981. N.Six, A.Guerriero, D.Landy, M.Peruzzini, L.Gonsalvi, F.Hapiot, E.Monflier. *Catal. Sci. Technol.*, **1**, 1347 (2011)
982. M.Qi, P.Z.Tan, F.Xue, H.S.Malhi, Z.-X.Zhang, D.J.Young, T.S.A.Hor. *RSC Adv.*, **5**, 3590 (2015)
983. A.Cocq, H.Bricout, F.Djedaïni-Pilard, S.Tilloy, E.Monflier. *Catalysts*, **10**, 56 (2020)
984. C.Blaszkiewicz, H.Bricout, E.Léonard, C.Len, D.Landy, C.Cézard, F.Djedaïni-Pilard, E.Monflier, S.Tilloy. *Chem. Commun.*, **49**, 6989 (2013)
985. F.Hapiot, J.Lyskawa, H.Bricout, S.Tilloy, E.Monflier. *Adv. Synth. Catal.*, **346**, 83 (2004)
986. D.M.Homden, C.Redshaw. *Chem. Rev.*, **108**, 5086 (2008)
987. S.Meninno, A.Parrella, G.Brancatelli, S.Geremia, C.Gaeta, C.Talotta, P.Neri, A.Lattanzi. *Org. Lett.*, **17**, 5100 (2015)
988. M.Benatmane, K.Cousin, N.Laggoune, S.Menuel, E.Monflier, P.Woisel, F.Hapiot, J.Potier. *ChemCatChem*, **10**, 5306 (2018)
989. M.Zeng, K.Chen, J.Tan, J.Zhang, Y.Wei. *Front. Chem.*, **6**, 457 (2018)
990. S.Nandi, P.Patel, A.Jakhar, N.H.Khan, A.V.Biradar, R.I.Kureshy, H.C.Bajaj. *ChemistrySelect*, **2**, 9911 (2017)
991. K.Karami, N.H.Naeini. *Appl. Organomet. Chem.*, **29**, 33 (2014)
992. S.M.de Lima, J.A.Gómez, V.P.Barros, G.de S.Vertuan, M.das Dores Assis, C.F.de Oliveira Graeff, G.J.-F.Demets. *Polyhedron*, **29**, 3008 (2010)
993. A.Martinez, J.-P.Dutasta. *J. Catal.*, **267**, 188 (2009)
994. D.Zhang, K.Jamieson, L.Guy, G.Gao, J.-P.Dutasta, A.Martinez. *Chem. Sci.*, **8**, 789 (2017)
995. T.Chavagnan, D.Sémeril, D.Matt, L.Toupet. *Eur. J. Org. Chem.*, 313 (2016)
996. J.A.A.W.Elemans, R.J.M.Nolte. *Chem. Commun.*, **55**, 9590 (2019)
997. S.F.M.van Dongen, J.A.A.W.Elemans, A.E.Rowan, R.J.M.Nolte. *Angew. Chem., Int. Ed.*, **53**, 11420 (2014)
998. L.Zhao, X.Jing, X.Li, X.Guo, L.Zeng, C.He, C.Duan. *Coord. Chem. Rev.*, **378**, 151 (2019)
999. W.-X.Gao, H.-N.Zhang, G.-X.Jin. *Coord. Chem. Rev.*, **386**, 69 (2019)
1000. C.Tan, D.Chu, X.Tang, Y.Liu, W.Xuan, Y.Cui. *Chem. – Eur. J.*, **25**, 662 (2018)
1001. L.J.Jongkind, X.Caumes, A.P.T.Hartendorp, J.N.H.Reek. *Acc. Chem. Res.*, **51**, 2115 (2018)
1002. C.M.Hong, R.G.Bergman, K.N.Raymond, F.D.Toste. *Acc. Chem. Res.*, **51**, 2447 (2018)
1003. *Effects of Nanoconfinement on Catalysis*. (Ed. R.Poli). (Springer International Publishing, 2017)
1004. M.Yoshizawa, J.K.Klosterman, M.Fujita. *Angew. Chem., Int. Ed.*, **48**, 3418 (2009)

1005. O.Perraud, A.B.Sorokin, J.-P.Dutasta, A.Martinez. *Chem. Commun.*, **49**, 1288 (2013)
1006. A.Schmitt, S.Collin, C.Bucher, V.Maurel, J.-P.Dutasta, A.Martinez. *Org. Biomol. Chem.*, **13**, 2157 (2015)
1007. Y.Makita, T.Fujita, T.Danno, M.Inoue, M.Ueshima, S.Fujiwara, A.Ogawa. *Supramol. Catal.*, **1**, 9 (2012)
1008. A.Cavarzan, J.N.H.Reek, F.Trentin, A.Scarso, G.Strukul. *Catal. Sci. Technol.*, **3**, 2898 (2013)
1009. A.C.H.Jans, X.Caumes, J.N.H.Reek. *ChemCatChem*, **11**, 287 (2018)
1010. A.Cavarzan, A.Scarso, P.Sgarbossa, G.Strukul, J.N.H.Reek. *J. Am. Chem. Soc.*, **133**, 2848 (2011)
1011. G.La Sorella, L.Sperni, G.Strukul, A.Scarso. *Adv. Synth. Catal.*, **358**, 3443 (2016)
1012. S.Roland, J.M.Suarez, M.Sollogoub. *Chem. – Eur. J.*, **24**, 12464 (2018)
1013. M.Guitet, P.Zhang, F.Marcelo, C.Tugny, J.Jiménez-Barbero, O.Buriez, C.Amatore, V.Mouriès-Mansuy, J.-P.Goddard, L.Fensterbank, Y.Zhang, S.Roland, M.Ménand, M.Sollogoub. *Angew. Chem., Int. Ed.*, **52**, 7213 (2013)
1014. P.Zhang, J.Meijide Suárez, T.Driant, E.Derat, Y.Zhang, M.Ménand, S.Roland, M.Sollogoub. *Angew. Chem., Int. Ed.*, **56**, 10821 (2017)
1015. P.Thordarson, E.J.A.Bijsterveld, A.E.Rowan, R.J.M.Nolte. *Nature (London)*, **424**, 915 (2003)
1016. I.Bernar, F.Rutjes, J.Elemans, R.Nolte. *Catalysts*, **9**, 195 (2019)
1017. J.A.A.W.Elemans, E.J.A.Bijsterveld, A.E.Rowan, R.J.M.Nolte. *Eur. J. Org. Chem.*, 751 (2007)
1018. P.J.Thomassen, S.Varghese, E.J.A.Bijsterveld, P.Thordarson, J.A.A.W.Elemans, A.E.Rowan, R.J.M.Nolte. *Eur. J. Org. Chem.*, 5246 (2015)
1019. H.Ito, T.Kusukawa, M.Fujita. *Chem. Lett.*, **29**, 598 (2000)
1020. M.Yoshizawa, N.Sato, M.Fujita. *Chem. Lett.*, **34**, 1392 (2005)
1021. H.Takezawa, T.Kanda, H.Nanjo, M.Fujita. *J. Am. Chem. Soc.*, **141**, 5112 (2019)
1022. S.S.Nurttila, W.Brenner, J.Mosquera, K.M.van Vliet, J.R.Nitschke, J.N.H.Reek. *Chem. – Eur. J.*, **25**, 609 (2018)
1023. S.S.Nurttila, P.R.Linnebank, T.Krachko, J.N.H.Reek. *ACS Catal.*, **8**, 3469 (2018)
1024. C.Garćia-Simón, R.Gramage-Doria, S.Raoufmoghaddam, T.Parella, M.Costas, X.Ribas, J.N.H.Reek. *J. Am. Chem. Soc.*, **137**, 2680 (2015)
1025. P.F.Kuijpers, M.Otte, M.Dürr, I.Ivanoviå-Burmazović, J.N.H.Reek, B.de Bruin. *ACS Catal.*, **6**, 3106 (2016)
1026. Q.-T.He, X.-P.Li, L.-F.Chen, L.Zhang, W.Wang, C.-Y.Su. *ACS Catal.*, **3**, 1 (2012)
1027. D.H.Leung, R.G.Bergman, K.N.Raymond. *J. Am. Chem. Soc.*, **129**, 2746 (2007)
1028. C.J.Brown, G.M.Miller, M.W.Johnson, R.G.Bergman, K.N.Raymond. *J. Am. Chem. Soc.*, **133**, 11964 (2011)
1029. T.A.Bender, R.G.Bergman, K.N.Raymond, F.D.Toste. *J. Am. Chem. Soc.*, **141**, 11806 (2019)
1030. W.M.Hart-Cooper, K.N.Clary, F.D.Toste, R.G.Bergman, K.N.Raymond. *J. Am. Chem. Soc.*, **134**, 17873 (2012)
1031. L.Leclercq, G.Douyère, V.Nardello-Rataj. *Catalysts*, **9**, 163 (2019)
1032. M.Jouffroy, D.Armspach, D.Matt. *Dalton Trans.*, **44**, 12942 (2015)
1033. T.Neva, C.O.Mellet, J.M.G.Fernández, J.M.Benito. *J. Carbohydr. Chem.*, **38**, 470 (2019)
1034. S.Tilloy, H.Bricout, S.Menuel, F.Hapiot, E.Monflier. *Curr. Organocatal.*, **3**, 24 (2015)
1035. R.Breslow, Y.Huang, X.Zhang, J.Yang. *Proc. Natl. Acad. Sci. USA*, **94**, 11156 (1997)
1036. R.Breslow, Z.Fang. *Tetrahedron Lett.*, **43**, 5197 (2002)
1037. R.Breslow, X.Zhang, Y.Huang. *J. Am. Chem. Soc.*, **119**, 4535 (1997)
1038. R.Breslow, B.Gabriele, J.Yang. *Tetrahedron Lett.*, **39**, 2887 (1998)
1039. R.Breslow, X.Zhang, R.Xu, M.Maletic, R.Merger. *J. Am. Chem. Soc.*, **118**, 11678 (1996)
1040. D.Vidal, G.Olivo, M.Costas. *Chem. – Eur. J.*, **24**, 5042 (2018)
1041. F.-X.Legrand, N.Six, C.Slomianny, H.Bricout, S.Tilloy, E.Monflier. *Adv. Synth. Catal.*, **353**, 1325 (2011)
1042. S.Tilloy, C.Binkowski-Machut, S.Menuel, H.Bricout, E.Monflier. *Molecules*, **17**, 13062 (2012)
1043. F.Hapiot, E.Monflier. *Catalysts*, **7**, 173 (2017)
1044. R.I.Khan, K.Pitchumani. *ACS Sustain. Chem. Eng.*, **6**, 16130 (2018)
1045. S.D.Dindulkar, D.Jeong, H.Kim, S.Jung. *Carbohydr. Res.*, **430**, 85 (2016)
1046. R.I.Khan, K.Pitchumani. *Green Chem.*, **18**, 5518 (2016)
1047. U.S.Kanchana, E.J.Diana, T.V.Mathew, G.Anilkumar. *Carbohydr. Res.*, **489**, 107954 (2020)
1048. V.Shinde, D.Jeong, S.Jung. *Catalysts*, **9**, 111 (2019)
1049. Y.Guo, J.Li, X.Shi, Y.Liu, K.Xie, Y.Liu, Y.Jiang, B.Yang, R.Yang. *Appl. Organometal. Chem.*, **31**, e3592 (2016)
1050. Y.Takashima, K.Uramatsu, D.Jomori, A.Harima, M.Otsubo, H.Yamaguchi, A.Harada. *ACS Macro Lett.*, **2**, 384 (2013)
1051. J.Leblond, J.Potier, S.Menuel, H.Bricout, C.Machut-Binkowski, D.Landy, S.Tilloy, E.Monflier, F.Hapiot. *Catal. Sci. Technol.*, **7**, 3823 (2017)
1052. J.Potier, S.Menuel, D.Mathiron, V.Bonnet, F.Hapiot, E.Monflier. *Beilstein J. Org. Chem.*, **10**, 2642 (2014)
1053. M.Jouffroy, R.Gramage-Doria, D.Armspach, D.Sémeril, W.Oberhauser, D.Matt, L.Toupet. *Angew. Chem., Int. Ed.*, **53**, 3937 (2014)
1054. P.Buranaprasertsuk, Y.Tangsakol, W.Chavasiri. *Catal. Commun.*, **8**, 310 (2007)
1055. K.Anjali, M.S.Aswini, P.Aswin, V.Ganesh, A.Sakthivel. *Eur. J. Inorg. Chem.*, 4087 (2019)
1056. K.Anjali, M.Ahmed, J.Christopher, A.Sakthivel. *Dalton Trans.*, **47**, 12353 (2018)
1057. C.Bauder, D.Sémeril. *Eur. J. Inorg. Chem.*, 4951 (2019)
1058. J.Espinas, U.Darbost, J.Pelletier, E.Jeanneau, C.Duchamp, F.Bayard, O.Boyron, J.-P.Broyer, J.Thivolle-Cazat, J.-M.Basset, M.Taoufik, I.Bonnamour. *Eur. J. Inorg. Chem.*, 1349 (2010)
1059. C.Redshaw, L.Clowes, D.L.Hughes, M.R.J.Elsegood, T.Yamato. *Organometallics*, **30**, 5620 (2011)
1060. Z.Sun, Y.Zhao, O.Santoro, M.R.J.Elsegood, E.V.Bedwell, K.Zahra, A.Walton, C.Redshaw. *Catal. Sci. Technol.*, **10**, 1619 (2020)
1061. C.Bonaccorso, G.Brancatelli, F.P.Ballistreri, S.Geremia, A.Pappalardo, G.A.Tomaselli, R.M.Toscano, D.Sciotto. *Dalton Trans.*, **43**, 2183 (2014)
1062. K.Hirasawa, S.Tanaka, T.Horiuchi, T.Kobayashi, T.Sato, N.Morohashi, T.Hattori. *Organometallics*, **35**, 420 (2016)
1063. H.Ren, Y.Xu, E.Jeanneau, I.Bonnamour, T.Tu, U.Darbost. *Tetrahedron*, **70**, 2829 (2014)

1064. L.Aloui, R.Abidi, M.J.Chetcuti. *Inorg. Chim. Acta*, **505**, 119494 (2020)
1065. N.Şahin, D.Sémeril, E.Brenner, D.Matt, İ.Özdemir, C.Kaya, L.Toupet. *ChemCatChem*, **5**, 1116 (2013)
1066. C.Gibson, J.Rebek. *Org. Lett.*, **4**, 1887 (2002)
1067. T.Chavagnan, C.Bauder, D.Sémeril, D.Matt, L.Toupet. *Eur. J. Org. Chem.*, 70 (2017)
1068. N.Endo, M.Kanaura, M.P.Schramm, T.Iwasawa. *Eur. J. Org. Chem.*, 2514 (2016)
1069. N.Endo, M.Kanaura, M.P.Schramm, T.Iwasawa. *Tetrahedron Lett.*, **57**, 4754 (2016)
1070. N.Natarajan, E.Brenner, D.Sémeril, D.Matt, J.Harrowfield. *Eur. J. Org. Chem.*, 6100 (2017)
1071. V.I.Parvulescu, H.Garcia. *Catal. Sci. Technol.*, **8**, 4834 (2018)
1072. D.Yang, B.C.Gates. *ACS Catal.*, **9**, 1779 (2019)
1073. W.Fang, Y.Zhang, J.Wu, C.Liu, H.Zhu, T.Tu. *Chem. – Asian J.*, **13**, 712 (2018)
1074. J.Potier, S.Menuel, M.-H.Chambrier, L.Burylo, J.-F.Blach, P.Woisel, E.Monflier, F.Hapiot. *ACS Catal.*, **3**, 1618 (2013)
1075. F.Hapiot, S.Menuel, M.Ferreira, B.Léger, H.Bricout, S.Tilloy, E.Monflier. *ACS Sustain. Chem. Eng.*, **5**, 3598 (2017)
1076. M.Chevry, S.Menuel, B.Léger, S.Noël, E.Monflier, F.Hapiot. *New J. Chem.*, **43**, 9865 (2019)
1077. E.Karakhanov, A.Maximov, M.Boronoev, L.Kulikov, M.Terenina. *Pure Appl. Chem.*, **89**, 1157 (2017)
1078. F.Liu, Q.Wu, C.Liu, C.Qi, K.Huang, A.Zheng, S.Dai. *ChemSusChem*, **9**, 2496 (2016)
1079. I.Muylaert, A.Verberckmoes, J.De Decker, P.Van Der Voort. *Adv. Colloid Interface Sci.*, **175**, 39 (2012)
1080. E.A.Karakhanov, A.L.Maksimov, I.A.Aksenov, V.S.Kuznetsov, T.Y.Filippova, S.V.Kardashev, D.S.Volkov. *Russ. Chem. Bull., Int. Ed.*, **63**, 1710 (2014)
1081. M.P.Boronoev, M.Gotszyun, M.Y.Talanova, E.A.Karakhanov. *Pet. Chem.*, **58**, 412 (2018)
1082. Y.Yuan, G.Zhu. *ACS Cent. Sci.*, **5**, 409 (2019)
1083. Y.Tian, G.Zhu. *Chem. Rev.*, **120**, 8934 (2020)
1084. K.Dong, Q.Sun, X.Meng, F.-S.Xiao. *Catal. Sci.Technol.*, **7**, 1028 (2017)
1085. H.Liang, B.Zhou, D.Wu, J.Li, B.Li. *Adv. Colloid Interface Sci.*, **272**, 1020
1086. L.A.Kulikov, A.V.Akopyan, P.D.Polikarpova, A.V.Zolotukhina, A.L.Maximov, A.V.Anisimov, E.A.Karakhanov. *Ind. Eng. Chem. Res.*, **58**, 20562 (2019)
1087. R.A.Batryshin, D.A.Makeeva, L.A.Kulikov, Y.S.Kardasheva, A.L.Maksimov, E.A.Karakhanov. *Pet. Chem.*, **59**, 575 (2019)
1088. G.Crini. *Chem. Rev.*, **114**, 10940 (2014)
1089. J.Lagona, P.Mukhopadhyay, S.Chakrabarti, L.Isaacs. *Angew. Chem., Int. Ed.*, **44**, 4844 (2005)
1090. T.Ogoshi, T.Yamagishi, Y.Nakamoto. *Chem. Rev.*, **116**, 7937 (2016)
1091. X.-Y.Hu, T.Xiao, C.Lin, F.Huang, L.Wang. *Acc. Chem. Res.*, **47**, 2041 (2014)
1092. Y.Liu, Z.Wang, X.Zhang. *Chem. Soc. Rev.*, **41**, 5922 (2012)
1093. Z.He, W.Jiang, C.A.Schalley. *Chem. Soc. Rev.*, **44**, 779 (2015)
1094. Z.Zhang, Y.Luo, J.Chen, S.Dong, Y.Yu, Z.Ma, F.Huang. *Angew. Chem., Int. Ed.*, **50**, 1397 (2011)
1095. J.Fox, J.J.Wie, B.W.Greenland, S.Burattini, W.Hayes, H.M.Colquhoun, M.E.Mackay, S.J.Rowan. *J. Am. Chem. Soc.*, **134**, 5362 (2012)
1096. Q.Lin, Y.-Q.Fan, P.-P.Mao, L.Liu, J.Liu, Y.-M.Zhang, H.Yao, T.-B.Wei. *Chem. – Eur. J.*, **24**, 777 (2018)
1097. X.Ma, H.Tian. *Acc. Chem. Res.*, **47**, 1971 (2014)
1098. X.Ma, Y.Zhao. *Chem. Rev.*, **115**, 7794 (2014)
1099. H.Li, X.Fan, M.Qi, Z.Yang, H.Zhang, W.Tian. *Chem. – Eur. J.*, **22**, 101 (2015)
1100. N.Manganaro, I.Pisagatti, A.Notti, M.F.Parisi, G.Gattuso. *New J. Chem.*, **43**, 7936 (2019)
1101. W.Wang, Y.Zhang, B.Sun, L.-J.Chen, X.-D.Xu, M.Wang, X.Li, Y.Yu, W.Jiang, H.-B.Yang. *Chem. Sci.*, **5**, 4554 (2014)
1102. Y.Chen, Y.-M.Zhang, Y.Liu. *Isr. J. Chem.*, **51**, 515 (2011)
1103. Z.-J.Ding, H.-Y.Zhang, L.-H.Wang, F.Ding, Y.Liu. *Org. Lett.*, **13**, 856 (2011)
1104. Y.Liu, C.-F.Ke, H.-Y.Zhang, W.-J.Wu, J.Shi. *J. Org. Chem.*, **72**, 280 (2007)
1105. X.Hou, C.Ke, C.Cheng, N.Song, A.K.Blackburn, A.A.Sarjeant, Y.Y.Botros, Y.-W.Yang, J.F.Stoddart. *Chem. Commun.*, **50**, 6196 (2014)
1106. T.Ogoshi, R.Sueto, K.Yoshikoshi, K.Yasuhara, T.Yamagishi. *J. Am. Chem. Soc.*, **138**, 8064 (2016)
1107. S.Fa, T.Kakuta, T.Yamagishi, T.Ogoshi. *CCS Chemistry*, **1**, 50 (2019)
1108. T.Ogoshi, S.Takashima, T.Yamagishi. *J. Am. Chem. Soc.*, **137**, 10962 (2015)
1109. L.Yakimova, P.Padnya, D.Tereshina, A.Kunafina, A.Nugmanova, Y.Osin, V.Evtugyn, I.Stoikov. *J. Mol. Liq.*, **279**, 9 (2019)
1110. L.Di Costanzo, S.Geremia, L.Randaccio, R.Purrello, R.Lauceri, D.Sciotto, F.G.Gulino, V.Pavone. *Angew. Chem., Int. Ed.*, **40**, 4245 (2001)
1111. D.-S.Guo, K.Chen, H.-Q.Zhang, Y.Liu. *Chem. – Asian J.*, **4**, 436 (2009)
1112. Z.Xu, S.Jia, W.Wang, Z.Yuan, B.J.Ravoo, D.-S.Guo. *Nat. Chem.*, **11**, 86 (2018)
1113. *IUPAC Compendium of Chemical Terminology*. (Eds M.Nič, J.Jirát, B.Košata, A.Jenkins, A.McNaught). (Research Triangle Park, NC: IUPAC, 2009)
1114. P.Tamamis, L.Adler-Abramovich, M.Reches, K.Marshall, P.Sikorski, L.Serpell, E.Gazit, G.Archontis. *Biophys. J.*, **96**, 5020 (2009)
1115. M.A.Ziganshin, A.V.Gerasimov, V.V.Gorbatchuk, A.T.Gubaidullin. *J. Therm. Anal. Calorim.*, **119**, 1811 (2014)
1116. J.-Y.Kim, G.-Y.Won, S.Lee. *Bull. Korean Chem. Soc.*, **35**, 798 (2014)
1117. C.H.Görbitz. *Chem. – Eur. J.*, **7**, 5153 (2001)
1118. M.B.Avinash, T.Govindaraju. *Nanoscale*, **6**, 13348 (2014)
1119. C.H.Görbitz. *Chem. – Eur. J.*, **13**, 1022 (2007)
1120. S.Marchesan, A.Vargiu, K.Styan. *Molecules*, **20**, 19775 (2015)
1121. A.Handelman, N.Kuritz, A.Natan, G.Rosenman. *Langmuir*, **32**, 2847 (2016)
1122. R.Afonso, A.Mendes, L.Gales. *J. Mater. Chem.*, **22**, 1709 (2012)
1123. L.Sun, Z.Fan, Y.Wang, Y.Huang, M.Schmidt, M.Zhang. *Soft Matter*, **11**, 3822 (2015)
1124. A.S.Safiullina, S.A.Ziganshina, N.M.Lyadov, A.E.Klimovitskii, M.A.Ziganshin, V.V.Gorbatchuk. *Soft Matter*, **15**, 3595 (2019)
1125. J.Ryu, C.B.Park. *Chem. Mater.*, **20**, 4284 (2008)
1126. I.W.Hamley. *Angew. Chem., Int. Ed.*, **53**, 6866 (2014)
1127. M.Sakurai, P.Koley, M.Aono. *Chem. Commun.*, **50**, 12556 (2014)

1128. V.V.Korolkov, S.Allen, C.J.Roberts, S.J.B.Tendler. *Faraday Discuss.*, **166**, 257 (2013)
1129. S.Vasilev, P.Zelenovskiy, D.Vasileva, A.Nuraeva, V.Y.Shur, A.L.Kholkin. *J. Phys. Chem. Solids*, **93**, 68 (2016)
1130. G.Rosenman, P.Beker, I.Koren, M.Yevnin, B.Bank-Srour, E.Mishina, S.Semin. *J. Pept. Sci.*, **17**, 75 (2010)
1131. J.S.Lee, I.Yoon, J.Kim, H.Ihee, B.Kim, C.B.Park. *Angew. Chem., Int. Ed.*, **50**, 1164 (2010)
1132. S.Semin, A.van Etteger, L.Cattaneo, N.Amdursky, L.Kulyuk, S.Lavrov, A.Sigov, E.Mishina, G.Rosenman, T.Rasing. *Small*, **11**, 1156 (2014)
1133. L.Adler-Abramovich, N.Kol, I.Yanai, D.Barlam, R.Z.Shneck, E.Gazit, I.Rousso. *Angew. Chem., Int. Ed.*, **49**, 9939 (2010)
1134. Q.Zou, M.Abbas, L.Zhao, S.Li, G.Shen, X.Yan. *J. Am. Chem. Soc.*, **139**, 1921 (2017)
1135. L.Adler-Abramovich, E.Gazit. *Chem. Soc. Rev.*, **43**, 6881 (2014)
1136. S.Kim, J.H.Kim, J.S.Lee, C.B.Park. *Small*, **11**, 3623 (2015)
1137. J.H.Kim, J.Ryu, C.B.Park. *Small*, **7**, 718 (2011)
1138. J.Ryu, S.-W.Kim, K.Kang, C.B.Park. *Adv. Mater.*, **22**, 5537 (2010)
1139. J.Ryu, S.-W.Kim, K.Kang, C.B.Park. *ACS Nano*, **4**, 159 (2009)
1140. H.-I.Ryoo, J.S.Lee, C.B.Park, D.-P.Kim. *Lab Chip*, **11**, 378 (2011)
1141. G.Fichman, E.Gazit. *Acta Biomater.*, **10**, 1671 (2014)
1142. K.Liu, L.Jiang. *Annu. Rev. Mater. Res.*, **42**, 231 (2012)
1143. K.S.Lee, J.R.Parquette. *Chem. Commun.*, **51**, 15653 (2015)
1144. K.Ryan, J.Beirne, G.Redmond, J.I.Kilpatrick, J.Guyonnet, N.-V.Buchete, A.L.Kholkin, B.J.Rodriguez. *ACS Appl. Mater. Interfaces*, **7**, 12702 (2015)
1145. S.Khanra, T.Cipriano, T.Lam, T.A.White, E.E.Fileti, W.A.Alves, S.Guha. *Adv. Mater. Interfaces*, **2**, 1500265 (2015)
1146. I.W.Park, J.Choi, K.Y.Kim, J.Jeong, D.Gwak, Y.Lee, Y.H.Ahn, Y.J.Choi, Y.J.Hong, W.-J.Chung, M.Lee, K.Heo. *Nano Energy*, **57**, 737 (2019)
1147. Q.Li, H.Ma, A.Wang, Y.Jia, L.Dai, J.Li. *Adv. Opt. Mater.*, **3**, 194 (2014)
1148. Y.Li, L.Yan, K.Liu, J.Wang, A.Wang, S.Bai, X.Yan. *Small*, **12**, 2575 (2016)
1149. R.V.Afonso, J.Durão, A.Mendes, A.M.Damas, L.Gales. *Angew. Chem., Int. Ed.*, **49**, 3034 (2010)
1150. Z.Zhao, K.M.Gupta, Z.He, J.Jiang. *J. Phys. Chem. C*, **122**, 6026 (2018)
1151. S.Bracco, D.Asnaghi, M.Negroni, P.Sozzani, A.Comotti. *Chem. Commun.*, **54**, 148 (2018)
1152. S.Mondal, S.Das, A.K.Nandi. *Soft Matter*, **16**, 1404 (2020)
1153. X.Yan, P.Zhu, J.Li. *Chem. Soc. Rev.*, **39**, 1877 (2010)
1154. J.S.Lee, J.Ryu, C.B.Park. *Soft Matter*, **5**, 2717 (2009)
1155. D.V.Soldatov, I.L.Moudrakovski, E.V.Grachev, J.A.Ripmeester. *J. Am. Chem. Soc.*, **128**, 6737 (2006)
1156. A.N.Rissanou, E.Georgilis, E.Kasotakis, A.Mitraki, V.Harmandaris. *J. Phys. Chem. B*, **117**, 3962 (2013)
1157. L.Adler-Abramovich, D.Aronov, P.Beker, M.Yevnin, S.Stempler, L.Buzhansky, G.Rosenman, E.Gazit. *Nat. Nanotechnol.*, **4**, 849 (2009)
1158. M.C.Vasudev, H.Koerner, K.M.Singh, B.P.Partlow, D.L.Kaplan, E.Gazit, T.J.Bunning, R.R.Naik. *Biomacromolecules*, **15**, 533 (2014)
1159. J.Li, Y.Gao, Y.Kuang, J.Shi, X.Du, J.Zhou, H.Wang, Z.Yang, B.Xu. *J. Am. Chem. Soc.*, **135**, 9907 (2013)
1160. R.G.Jones, C.K.Ober, P.Hodge, P.Kratochv'il, G.Moad, M.Vert. *Pure Appl. Chem.*, **85**, 463 (2012)
1161. G.M.Whitesides. *Science*, **295**, 2418 (2002)
1162. J.-M.Lehn. *Eur. Rev.*, **17**, 263 (2009)
1163. J.D.Halley, D.A.Winkler. *Complexity*, **14**, 10 (2008)
1164. S.M.M.Reddy, G.Shanmugam. *ChemPhysChem*, **17**, 2897 (2016)
1165. C.Yuan, S.Li, Q.Zou, Y.Ren, X.Yan. *Phys. Chem. Chem. Phys.*, **19**, 23614 (2017)
1166. C.Yuan, W.Ji, R.Xing, J.Li, E.Gazit, X.Yan. *Nat. Rev. Chem.*, **3**, 567 (2019)
1167. J.Wang, K.Liu, R.Xing, X.Yan. *Chem. Soc. Rev.*, **45**, 5589 (2016)
1168. H.Erdogan, E.Babur, M.Yilmaz, E.Candas, M.Gordesel, Y.Dede, E.E.Oren, G.B.Demirel, M.K.Ozturk, M.S.Yavuz, G.Demirel. *Langmuir*, **31**, 7337 (2015)
1169. M.Ziganshin, S.Ziganshina, N.Gubina, A.Gerasimov, V.Gorbatchuk, A.Bukharaev. *Orient. J. Chem*, **31**, 1977 (2015)
1170. E.Mayans, G.Ballano, J.Casanovas, L.J.del Valle, M.M.Pérez-Madrigal, F.Estrany, A.I.Jiménez, J.Puiggalí, C.Cativiela, C.Alemán. *Soft Matter*, **12**, 5475 (2016)
1171. X.Wang, Y.C.Chen, B.Li. *RSC Adv.*, **5**, 8022 (2015)
1172. T.O.Mason, D.Y.Chirgadze, A.Levin, L.Adler-Abramovich, E.Gazit, T.P.J.Knowles, A.K.Buell. *ACS Nano*, **8**, 1243 (2014)
1173. R.Huang, W.Qi, R.Su, J.Zhao, Z.He. *Soft Matter*, **7**, 6418 (2011)
1174. R.Huang, Y.Wang, W.Qi, R.Su, Z.He. *Nanoscale Res. Lett.*, **9**, 653 (2014)
1175. R.Wei, C.-C.Jin, J.Quan, H.Nie, L.-M.Zhu. *Biopolymers*, **101**, 272 (2013)
1176. R.J.A.Hill, V.L.Sedman, S.Allen, P.Williams, M.Paoli, L.Adler-Abramovich, E.Gazit, L.Eaves, S.J.B.Tendler. *Adv. Mater.*, **19**, 4474 (2007)
1177. G.Pandey, J.Saikia, S.Sasidharan, D.C.Joshi, S.Thota, H.B.Nemade, N.Chaudhary, V.Ramakrishnan. *Sci. Rep.*, **7**, 2726 (2017)
1178. M.A.Ziganshin, A.S.Morozova, S.A.Ziganshina, V.V.Vorobev, K.Suwińska, A.A.Bukharaev, V.V.Gorbatchuk. *Mol. Cryst. Liq. Cryst.*, **690**, 67 (2019)
1179. J.Wang, K.Liu, L.Yan, A.Wang, S.Bai, X.Yan. *ACS Nano*, **10**, 2138 (2016)
1180. M.A.Ziganshin, A.A.Bikmukhametova, A.V.Gerasimov, V.V.Gorbatchuk, S.A.Ziganshina, A.A.Bukharaev. *Prot. Met. Phys. Chem. Surf.*, **50**, 49 (2014)
1181. M.Wang, L.Du, X.Wu, S.Xiong, P.K.Chu. *ACS Nano*, **5**, 4448 (2011)
1182. M.A.Ziganshin, N.S.Gubina, A.V.Gerasimov, V.V.Gorbatchuk, S.A.Ziganshina, A.P.Chuklanov, A.A.Bukharaev. *Phys. Chem. Chem. Phys.*, **17**, 20168 (2015)
1183. M.A.Ziganshin, A.S.Safiullina, S.A.Ziganshina, A.V.Gerasimov, V.V.Gorbatchuk. *Phys. Chem. Chem. Phys.*, **19**, 13788 (2017)
1184. M.A.Ziganshin, N.S.Gubina, V.V.Gorbatchuk, S.A.Ziganshina, A.P.Chuklanov, D.A.Bizyaev, A.A.Bukharaev. *J. Surf. Investig.*, **10**, 210 (2016)
1185. K.B.Joshi, S.Verma. *J. Pept. Sci.*, **14**, 118 (2008)
1186. S.Lin, J.Qin, Y.Li, B.Li, Y.Yang. *Langmuir*, **33**, 8246 (2017)
1187. S.Marchesan, C.D.Easton, K.E.Styan, L.J.Waddington, F.Kushkaki, L.Goodall, K.M.McLean, J.S.Forsythe, P.G.Hartley. *Nanoscale*, **6**, 5172 (2014)

1188. P.S.Zelenovskiy, A.S.Nuraeva, S.Kopyl, S.G.Arkhipov, S.G.Vasilev, V.S.Bystrov, D.A.Gruzdev, M.Waliczek, V.Svitlyk, V.Y.Shur, L.Mafra, A.L.Kholkin. *Cryst. Growth Des.*, **19**, 6414 (2019)
1189. M.A.Ziganshin, I.G.Efimova, V.V.Gorbatchuk, S.A.Ziganshina, A.P.Chuklanov, A.A.Bukharaev, D.V.Soldatov. *J. Pept. Sci.*, **18**, 209 (2012)
1190. L.S.Yakimova, M.A.Ziganshin, V.A.Sidorov, V.V.Kovalev, E.A.Shokova, V.A.Tafeenko, V.V.Gorbatchuk. *J. Phys. Chem. B*, **112**, 15569 (2008)
1191. C.Guo, Y.Luo, R.Zhou, G.Wei. *Nanoscale*, **6**, 2800 (2014)
1192. E.Mayans, G.Ballano, J.Casanovas, A.Díaz, M.M.Pérez-Madrigal, F.Estrany, J.Puiggalí, C.Cativiela, C.Alemán. *Chem. – Eur. J.*, **21**, 16895 (2015)
1193. Y.Wang, W.Qi, R.Huang, X.Yang, M.Wang, R.Su, Z.He. *J. Am. Chem. Soc.*, **137**, 7869 (2015)
1194. Z.Arnon, L.Adler-Abramovich, A.Levin, E.Gazit. *Isr. J. Chem.*, **55**, 756 (2015)
1195. A.Handelman, A.Natan, G.Rosenman. *J. Pept. Sci.*, **20**, 487 (2014)
1196. M.Kurbasic, S.Semeraro, A.M.Garcia, S.Kralj, E.Parisi, C.Deganutti, R.De Zorzi, S.Marchesan. *Synthesis*, **51**, 2829 (2019)
1197. A.D.Borthwick. *Chem. Rev.*, **112**, 3641 (2012)
1198. J.Ryu, C.B.Park. *Biotechnol. Bioeng.*, **105**, 221 (2010)
1199. A.Heredia, I.Bdikin, S.Kopyl, E.Mishina, S.Semin, A.Sigov, K.German, V.Bystrov, J.Gracio, A.L.Kholkin. *J. Phys. D: Appl. Phys.*, **43**, 462001 (2010)
1200. A.J.Smith, F.I.Ali, D.V.Soldatov. *CrystEngComm*, **16**, 7196 (2014)
1201. M.A.Ziganshin, A.V.Gerasimov, S.A.Ziganshina, N.S.Gubina, G.R.Abdullina, A.E.Klimovitskii, V.V.Gorbatchuk, A.A.Bukharaev. *J. Therm. Anal. Calorim.*, **125**, 905 (2016)
1202. P.S.Zelenovskiy, A.O.Davydov, A.S.Krylov, A.L.Kholkin. *J. Raman Spectrosc.*, **48**, 1401 (2017)
1203. M.A.Ziganshin, R.A.Larionov, A.V.Gerasimov, S.A.Ziganshina, A.E.Klimovitskii, K.R.Khayarov, T.A.Mukhametzyanov, V.V.Gorbatchuk. *J. Pept. Sci.*, **25**, e3177 (2019)
1204. M.A.Ziganshin, A.S.Safiullina, A.V.Gerasimov, S.A.Ziganshina, A.E.Klimovitskii, K.R.Khayarov, V.V.Gorbatchuk. *J. Phys. Chem. B*, **121**, 8603 (2017)
1205. A.D.Borthwick, N.C.Da Costa. *Crit. Rev. Food Sci. Nutr.*, **57**, 718 (2015)
1206. S.Manchineella, T.Govindaraju. *ChemPlusChem*, **82**, 88 (2016)
1207. J.Wang, C.Yuan, Y.Han, Y.Wang, X.Liu, S.Zhang, X.Yan. *Small*, **13**, 1702175 (2017)
1208. T.D.Do, M.T.Bowers. *Anal. Chem.*, **87**, 4245 (2015)
1209. C.B.Silva, J.G.da Silva Filho, G.S.Pinheiro, A.M.R.Teixeira, F.F.de Sousa, P.T.C.Freire. *Spectrochim. Acta, Part A*, **229**, 117899 (2020)
1210. I.G.Efimova, M.A.Ziganshin, V.V.Gorbatchuk, D.V.Soldatov, S.A.Ziganshina, A.P.Chuklanov, A.A.Bukharaev. *Prot. Met. Phys. Chem. Surf.*, **45**, 525 (2009)
1211. A.K.Gatiatulin, M.A.Ziganshin, V.V.Gorbatchuk. *Front. Chem.*, **7**, 933 (2020)
1212. Y.Yu, J.Hou, L.Yu, Y.Yang, C.Wang. *Surf. Sci.*, **649**, 34 (2016)
1213. M.A.Ziganshin, I.G.Efimova, A.A.Bikmukhametova, V.V.Gorbachuk, S.A.Ziganshina, A.P.Chuklanov, A.A.Bukharaev. *Prot. Met. Phys. Chem. Surf.*, **49**, 274 (2013)
1214. X.Yan, Y.Cui, Q.He, K.Wang, J.Li, W.Mu, B.Wang, Z.Ou-yang. *Chem. – Eur. J.*, **14**, 5974 (2008)
1215. C.Guo, Y.Luo, R.Zhou, G.Wei. *ACS Nano*, **6**, 3907 (2012)
1216. C.Tang, A.M.Smith, R.F.Collins, R.V.Ulijn, A.Saiani. *Langmuir*, **25**, 9447 (2009)
1217. J.D.Tang, C.Mura, K.J.Lampe. *J. Am. Chem. Soc.*, **141**, 4886 (2019)
1218. R.Xing, C.Yuan, S.Li, J.Song, J.Li, X.Yan. *Angew. Chem., Int. Ed.*, **57**, 1537 (2018)
1219. W.Saenger. *Nucleic Acid Structure*. Springer-Verlag, New York, 1984
1220. *Nucleic Acids in Chemistry and Biology*. (Eds G.M.Blackburn, M.J.Gait, D.Loakes, D.M.Williams). (Cambridge; Royal Society of Chemistry, 2007)
1221. W.Saenger. *Principles of Nucleic Acid Structure*. (New York: Springer-Verlag, 1984)
1222. J.Kypr, I.Kejnovska, D.Renciuk, M.Vorlickova. *Nucleic Acids Res.*, **37**, 1713 (2009)
1223. Yu.P.Blagoi. *Soros Educat. J.,* **4** (10), 18 (1998)
1224. N.de Jonge. *Advances in Imaging and Electron Physics*. (Amsterdam: Elsevier, 2015). P. 1
1225. S.M.Yarmoluk, V.B.Kovalska, K.D.Volkova. In *Advanced Fluorescence Reporters in Chemistry and Biology III. Applications in Sensing and Imaging*. (*Springer Series on Fluorescence*. Vol. 113). (Ed. A.P.Demchemko). (Berlin, Heidelberg: Springer, 2011) P. 161
1226. H.Ihmels, D.Otto. In *Supermolecular Dye Chemistry*. (Ed. F.Würthner). (*Ser. Topics in Current Chemistry*. Vol. 258). (Berlin, Heidelberg: Springer, 2005). P. 161
1227. P.H.von Hippel, J.D.McGhee. *Annu. Rev. Biochem.*, **41**, 231 (1972)
1228. L.P.G.Wakelin. *Med. Res. Rev.*, **6**, 275 (1986)
1229. A.Mukherjee, W.D.Sasikala. In *Dynamics of Proteins and Nucleic Acids*. (Amsterdam: Elsevier, 2013). P. 1
1230. W.A.Denny. *Curr. Med. Chem.*, **9**, 1655 (2002)
1231. G.Lenglet, M.-H.David-Cordonnier. *J. Nucleic Acids*, 1 (2010)
1232. *DNA Binders and Related Subjects*. (Eds M.J.Waring, J.B.Chaires). (*Ser. Topics in Current Chemistry*. Vol. 253). (Berlin, Heidelberg: Springer, 2005)
1233. *The Molecular Probes Handbook. A Guide to Fluorescent Probes and Labeling Technologies*. (11th Edn.). (Thermo Fisher Scientific, 2010)
1234. R.V.Sabnis. *Handbook of Fluorescence Dyes and Probes*. (Hoboken: Wiley, 2015)
1235. T.Deligeorgiev, A.Vasilev, S.Kaloyanova, J.J.Vaquero. *Color. Technol.*, **126**, 55 (2010)
1236. C.Gao, S.Liu, X.Zhang, Y.Liu, C.Qiao, Z.Liu. *Spectrochim. Acta, Part A*, **156**, 1 (2016)
1237. M.A.Ustimova, P.A.Chernikova, N.E.Shepel, Y.V.Fedorov, O.A.Fedorova. *Mendeleev Commun.*, **30**, 217 (2020)
1238. D.V.Berdnikova, N.I.Sosnin, O.A.Fedorova, H.Ihmels. *Org. Biomol. Chem.*, **16**, 545 (2018)
1239. D.V.Berdnikova, O.A.Fedorova, E.V.Tulyakova, H.Li, S.Kölsch, H.Ihmels. *Photochem. Photobiol.*, **91**, 723 (2015)
1240. A.Y.Lebedeva, O.A.Fedorova, V.B.Tsvetkov, V.Y.Grinberg, N.V.Grinberg, T.V.Burova, A.S.Dubovik, K.K.Babievsky, Y.V.Fedorov. *Dyes Pigm.*, **157**, 80 (2018)
1241. Z.Seferoğlu, M.M.A.Mahmoud, H.Ihmels. *Dyes Pigm.*, **125**, 241 (2016)
1242. M.Hranjec, M.Kralj, I.Piantanida, M.Sedić, L.Šuman, K.Pavelić, G.Karminski-Zamola. *J. Med. Chem.*, **50**, 5696 (2007)

1243. N.Akbay, M.Y.Losytskyy, V.B.Kovalska, A.O.Balanda, S.M.Yarmoluk. *J. Fluoresc.*, **18**, 139 (2007)
1244. V.B.Kovalska, D.V,Kryvorotenko, A.Balanda, M.Y.Losytskyy, V.Tokar, S.M.Yarmoluk. *Dyes Pigm.*, **67**, 47 (2005)
1245. V.B.Kovalska, I.O.Kocheshev, D.V,Kryvorotenko, A.Balanda, S.M.Yarmoluk. *J. Fluoresc.*, **15**, 215 (2005)
1246. V.P.Tokar, M.Y.Losytskyy, V.B.Kovalska, D.V.Kryvorotenko, A.O.Balanda, V.M.Prokopets, M.P.Galak, I.M.Dmytruk, V.M.Yashchuk, S.M.Yarmoluk. *J. Fluoresc.*, **16**, 783 (2006)
1247. V.M.Yashchuk, V.V.Gusak, I.M.Dmytruk, V.M.Prokopets, V.Y.Kudrya, M.Y.Losytskyy, V.P.Tokar, Y.O.Gumenyuk, S.M.Yarmoluk, V.B.Kovalska, A.O.Balanda, D.V.Kryvorotenko. *Mol. Cryst. Liq. Cryst.*, **467**, 325 (2007)
1248. C.Allain, F.Schmidt, R.Lartia, G.Bordeau, C.Fiorini-Debuisschert, F.Charra, P.Tauc, M.-P.Teulade-Fichou. *ChemBioChem*, **8**, 424 (2007)
1249. S.Feng, Y.K.Kim, S.Yang, Y.-T.Chang. *Chem. Commun.*, **46**, 436 (2010)
1250. P.E.Pjura, K.Grzeskowiak, R.E.Dickerson. *J. Mol. Biol.*, **197**, 257 (1987)
1251. J.Portugal, M.J.Waring. *Biochim. Biophys. Acta, Gene Struct. Expression*, **949**, 158 (1988)
1252. J.Kapuscinski. *Biotech. Histochem.*, **70**, 220 (1995)
1253. S.R.Byeon, J.H.Lee, J.-H.Sohn, D.C.Kim, K.J.Shin, K.H.Yoo, I.Mook-Jung, W.K.Lee, D.J.Kim. *Bioorg. Med. Chem. Lett.*, **17**, 1466 (2007)
1254. R.Krieg, A.Eitner, K.-J.Halbhuber. *Acta Histochem.*, **113**, 682 (2011)
1255. D.Berdnikova, O.Fedorova, E.Gulakova, H.Ihmels. *Chem. Commun.*, **48**, 4603 (2012)
1256. T.M.Aliyeu, D.V.Berdnikova, O.A.Fedorova, E.N.Gulakova, C.Stremmel, H.Ihmels. *J. Org. Chem.*, **81**, 9075 (2016)
1257. D.V.Berdnikova, T.M.Aliyeu, T.Paululat, Y.V.Fedorov, O.A.Fedorova, H.Ihmels. *Chem. Commun.*, **51**, 4906 (2015)
1258. E.Y.Chernikova, A.Y.Ruleva, V.B.Tsvetkov, Y.V.Fedorov, V.V.Novikov, T.M.Aliyeu, A.A.Pavlov, N.E.Shepel, O.A.Fedorova. *Org. Biomol. Chem.*, **18**, 755 (2020)
1259. T.Peters Jr. *All About Albumin: Biochemistry, Genetics, and Medical Applications*. (San Diego, CA: Academic Press, 2012)
1260. F.-F.An, X.-H.Zhang. *Theranostics*, **7**, 3667 (2017)
1261. S.Zaitsev. *Adv. Colloid Interface Sci.*, **235**, 201 (2016)
1262. S.Javed, F.Azeem, S.Hussain, I.Rasul, M.H.Siddique, M.Riaz, M.Afzal, A.Kouser, H.Nadeem. *Prog. Biophys. Mol. Biol.*, **132**, 23 (2018)
1263. N.L.Eremeev, S.Y.Zaitsev. *Mini-Rev. Org. Chem.*, **13**, 78 (2016)
1264. S.Y.Zaitsev, A.A.Savina, I.S.Zaitsev. *Adv. Colloid Interface Sci.*, **272**, 102016 (2019)
1265. M.A.Ostrovsky, T.B.Feldman. *Russ. Chem. Rev.*, **81**, 1071 (2012)
1266. Y.Jin, T.Honig, I.Ron, N.Friedman, M.Sheves, D.Cahen. *Chem. Soc. Rev.*, **37**, 2422 (2008)
1267. K.J.Wise, N.B.Gillespie, J.A.Stuart, M.P.Krebs, R.R.Birge. *Trends Biotechnol.*, **20**, 387 (2002)
1268. S.Y.Zaitsev, D.O.Solovyeva, I.R.Nabiev. *Russ. Chem. Rev.*, **83**, 38 (2014)
1269. L.A.Dykman, N.G.Khlebtsov. *Russ. Chem. Rev.*, **88**, 229 (2019)
1270. X.Yang, M.Yang, B.Pang, M.Vara, Y.Xia. *Chem. Rev.*, **115**, 10410 (2015)
1271. K.E.Sapsford, W.R.Algar, L.Berti, K.B.Gemmill, B.J.Casey, E.Oh, M.H.Stewart, I.L.Medintz. *Chem. Rev.*, **113**, 1904 (2013)
1272. Y.A.Krutyakov, A.A.Kudrinskiy, A.Y.Olenin, G.V.Lisichkin. *Russ. Chem. Rev.*, **77**, 233 (2008)
1273. E.A.Terenteva, V.V.Apyari, E.V.Kochuk, S.G.Dmitrienko, Y.A.Zolotov. *J. Anal. Chem.*, **72**, 1138 (2017)
1274. B.Baruah, M.Kiambuthi. *RSC Adv.*, **4**, 64860 (2014)
1275. R.N.Amirkhanov, V.F.Zarytova, M.A.Zenkova. *Russ. Chem. Rev.*, **86**, 113 (2017)
1276. N.S.Kozhevnikova, A.S.Vorokh, A.A.Uritskaya. *Russ. Chem. Rev.*, **84**, 225 (2015)
1277. J.Mariam, S.Sivakami, P.M.Dongre. *Drug Deliv.*, **23**, 2668 (2016)
1278. N.Durán, C.P.Silveira, M.Durán, D.S.T.Martinez. *J. Nanobiotechnol.*, **13**, 55 (2015)
1279. V.Pareek, A.Bhargava, V.Bhanot, R.Gupta, N.Jain, J.Panwar. *J. Nanosci. Nanotechnol.*, **18**, 6653 (2018)
1280. V.H.Nguyen, B.-J.Lee. *Int. J. Nanomed.*, **12**, 3137 (2017)
1281. C.Corbo, R.Molinaro, A.Parodi, N.E.T.Furman, F.Salvatore, E.Tasciotti. *Nanomedicine*, **11**, 81 (2016)
1282. D.Khang, Y.K.Lee, E.-J.Choi, T.J.Webster, S.-H.Kim. *Int. J. Nanomed.*, 97 (2014)
1283. T.Micluaucs, V.E.Bochenkov, R.Ogaki, K.A.Howard, D.S.Sutherland. *Nano Lett.*, **14**, 2086 (2014)
1284. L.Treuel, M.Malissek, J.S.Gebauer, R.Zellner. *ChemPhysChem.*, **11**, 3093 (2010)
1285. A.Lesniak, F.Fenaroli, M.P.Monopoli, C.Åberg, K.A.Dawson, A.Salvati. *ACS Nano*, **6**, 5845 (2012)
1286. M.Mahmoudi, I.Lynch, M.R.Ejtehadi, M.P.Monopoli, F.B.Bombelli, S.Laurent. *Chem. Rev.*, **111**, 5610 (2011)
1287. C.Röcker, M.Pötzl, F.Zhang, W.J.Parak, G.U.Nienhaus. *Nat. Nanotechnol.*, **4**, 577 (2009)
1288. Z.J.Deng, G.Mortimer, T.Schiller, A.Musumeci, D.Martin, R.F.Minchin. *Nanotechnology*, **20**, 455101 (2009)
1289. K.Bolaños, M.J.Kogan, E.Araya. *Int. J. Nanomed.*, **14**, 6387 (2019)
1290. Z.Ma, H.Xia, Y.Liu, B.Liu, W.Chen, Y.Zhao. *Chin. Sci. Bull.*, **58**, 2530 (2013)
1291. M.Tarhini, H.Greige-Gerges, A.Elaissari. *Int. J. Pharm.*, **522**, 172 (2017)
1292. E.Blanco, H.Shen, M.Ferrari. *Nat. Biotechnol.*, **33**, 941 (2015)
1293. Q.Chen, Z.Liu. *Adv. Mater.*, **28**, 10557 (2016)
1294. B.Bhushan, V.Khanadeev, B.Khlebtsov, N.Khlebtsov, P.Gopinath. *Adv. Colloid Interface Sci.*, **246**, 13 (2017)
1295. H.Nosrati, M.Salehiabar, H.K.Manjili, H.Danafar, S.Davaran. *Int. J. Biol. Macromol.*, **108**, 909 (2018)
1296. R.R.Kudarha, K.K.Sawant. *Mater. Sci. Eng. C*, **81**, 607 (2017)
1297. A.Loureiro, N.G.Azoia, A.C.Gomes, A.Cavaco-Paulo. *Curr. Pharm. Des.*, **22**, 1371 (2016)
1298. D.Pissuwan, C.H.Cortie, S.M.Valenzuela, M.B.Cortie. *Gold Bull.*, **40**, 121 (2007)
1299. L.Mocan, C.Matea, F.A.Tabaran, O.Mosteanu, T.Pop, C.Puia, L.Agoston-Coldea, G.Zaharie, T.Mocan, A.D.Buzoianu, C.Iancu. *Biomaterials*, **119**, 33 (2017)
1300. P.Murawala, A.Tirmale, A.Shiras, B.L.V.Prasad. *Mater. Sci. Eng.*, **34**, 158 (2014)

1301. R.A.Brekken, E.H.Sage. *Matrix Biol.*, **19**, 815 (2001)
1302. M.Bhamidipati, L.Fabris. *Bioconjug. Chem.*, **28**, 449 (2017)
1303. S.Pramanik, P.Banerjee, A.Sarkar, S.C.Bhattacharya. *J. Lumin.*, **128**, 1969 (2008)
1304. R.Garcia-Álvarez, M.Hadjidemetriou, A.Sánchez-Iglesias, L.M.Liz-Marzán, K.Kostarelos. *Nanoscale*, **10**, 1256 (2018)
1305. H.Moustaoui, J.Saber, I.Djeddi, Q.Liu, D.Movia, A.Prina-Mello, J.Spadavecchia, M.L.de la Chapelle, N.Djaker. *Nanoscale*, **11**, 3665 (2019)
1306. S.A.Alex, D.Chakraborty, N.Chandrasekaran, A.Mukherjee. *RSC Adv.*, **6**, 52683 (2016)
1307. C.Carnovale, G.Bryant, R.Shukla, V.Bansal. *Phys. Chem. Chem. Phys.*, **20**, 29558 (2018)
1308. M.S.Maleki, O.Moradi, S.Tahmasebi. *Arab. J. Chem.*, **10**, S491 (2017)
1309. L.Treuel, M.Malissek, S.Grass, J.Diendorf, D.Mahl, W.Meyer-Zaika, M.Epple. *J. Nanoparticle Res.*, **14**, 1102 (2012)
1310. R.Podila, R.Chen, P.C.Ke, J.M.Brown, A.M.Rao. *Appl. Phys. Lett.*, **101**, 263701 (2012)
1311. J.H.Shannahan, X.Lai, P.C.Ke, R.Podila, J.M.Brown, F.A.Witzmann. *PLoS One*, **8**, e74001 (2013)
1312. H.Nosrati, N.Sefidi, A.Sharafi, H.Danafar, H.K.Manjili. *Bioorg. Chem.*, **76**, 501 (2018)
1313. X.Mu, C.Yan, Q.Tian, J.Lin, S.Yang. *Int. J. Nanomed.*, **12**, 7207 (2017)
1314. T.J.Todd, Z.Zhen, J.Xie. *Nanomedicine*, **8**, 1555 (2013)
1315. R.Žukiene, V.Snitka. *Colloids Surf., B*, **135**, 316 (2015)
1316. A.E.Ledesma, D.M.Chemes, M.de los Angeles Fr'ias, M.del Pilar Guauque Torres. *Appl. Surf. Sci.*, **412**, 177 (2017)
1317. A.Naskar, H.Khan, S.Bera, S.Jana. *J. Mol. Liq.*, **237**, 113 (2017)
1318. P.Huang, Z.Li, H.Hu, D.Cui. *J. Nanomater.*, **2010**, 1 (2010)
1319. T.A.Simoes, A.P.Brown, S.J.Milne, R.M.D.Brydson. *J. Phys. Conf. Ser.*, **644**, 12039 (2015)
1320. S.Y.Zaitsev. *Biologicheskaya Khimiya: ot Biologicheski Aktivnykh Veshchestv do Organov i Tkanei Zhivotnykh. (Biological Chemistry: from Biologically Active Substances to Animal Organs and Tissues)*. (Moscow: ZAO 'Kapital Print', 2017)
1321. S.Y.Zaitsev, A.A.Savina, L.S.Garnashevich, M.S.Tsarkova, I.S.Zaitsev. *Bionanoscience*, **9**, 773 (2019)
1322. S.Yu.Zaitsev, M.P.Gil'fanova, A.A.Savina, M.A.Barvinskii, I.S.Zaitsev. *Nauch. Vestn. Andizhan. Gos. Univ.*, **42**, 77 (2019)
1323. A.A.Mendes, P.C.Oliveira, H.F.de Castro. *J. Mol. Catal. B*, **78**, 119 (2012)
1324. Y.Lv, Z.Lin, T.Tan, F.Svec. *Biotechnol. Bioeng.*, **111**, 50 (2014)
1325. J.L.Brennan, N.S.Hatzakis, T.R.Tshikhudo, V.Razumas, S.Patkar, J.Vind, A.Svendsen, R.J.M.Nolte, A.E.Rowan, M.Brust. *Bioconjug. Chem.*, **17**, 1373 (2006)
1326. K.Dumri, D.H.Anh. *Enzyme Res.*, **2014**, 1 (2014)
1327. H.Qi, Y.Du, G.Hu, L.Zhang. *Int. J. Biol. Macromol.*, **107**, 2660 (2018)
1328. J.Wang, G.Meng, K.Tao, M.Feng, X.Zhao, Z.Li, H.Xu, D.Xia, J.R.Lu. *PLoS One*, **7**, e43478 (2012)
1329. A.A.Savina, L.S.Garnashevich, I.S.Zaitsev, M.S.Tsarkova, S.Y.Zaitsev. *Moscow Univ. Chem. Bull.*, **74**, 306 (2019)
1330. V.A.Oleinikov, D.O.Solovyeva, S.Y.Zaitsev. *Biochemistry (Moscow)*, **85**, 196 (2020)
1331. S.Y.Zaitsev, D.O.Solovyeva, I.Nabiev. *Adv. Colloid Interface Sci.*, **183 – 184**, 14 (2012)
1332. S.Y.Zaitsev. *Nanotechnol. Russ.*, **4**, 379 (2009)
1333. V.A.Oleinikov, E.P.Lukashev, S.Y.Zaitsev, A.A.Chistyakov, D.O.Solovyeva, K.E.Mochalov, I.Nabiev. *Opt. Spectrosc.*, **122**, 30 (2017)
1334. A.Rakovich, A.Sukhanova, N.Bouchonville, E.Lukashev, V.Oleinikov, M.Artemyev, V.Lesnyak, N.Gaponik, M.Molinari, M.Troyon, Y.P.Rakovich, J.F.Donegan, I.Nabiev. *Nano Lett.*, **10**, 2640 (2010)
1335. I.Nabiev, A.Rakovich, A.Sukhanova, E.Lukashev, V.Zagidullin, V.Pachenko, Y.P.Rakovich, J.F.Donegan, A.B.Rubin, A.O.Govorov. *Angew. Chem., Int. Ed.*, **49**, 7217 (2010)
1336. R.Li, C.M.Li, H.Bao, Q.Bao, V.S.Lee. *Appl. Phys. Lett.*, **91**, 223901 (2007)
1337. A.V.Patil, T.Premaruban, O.Berthoumieu, A.Watts, J.J.Davis. I.S.Zaitsev*J. Phys. Chem. B*, **116**, 683 (2012)
1338. M.A.Green, K.Emery, Y.Hishikawa, W.Warta. *Prog. Photovolt. Res. Appl.*, **18**, 346 (2010)
1339. J.A.Stuart, D.L.Marcy, K.J.Wise, R.R.Birge. *Synth. Met.*, **127**, 3 (2002)
1340. M.Griep, E.Winder, D.Lueking, C.Friedrich, G.Mallick, S.Karna. *J. Nanosci. Nanotechnol.*, **10**, 6029 (2010)
1341. M.H.Griep, K.A.Walczak, E.M.Winder, D.R.Lueking, C.R.Friedrich. *Biosens. Bioelectron.*, **25**, 1493 (2010)
1342. M.H.Griep, E.M.Winder, D.R.Lueking, G.A.Garrett, S.P.Karna, C.R.Friedrich. *Mol. Biol. Int.*, 1 (2012)
1343. Patent US 20090142852A1 (2009)
1344. C.-W.Yen, S.C.Hayden, E.C.Dreaden, P.Szymanski, M.A.El-Sayed. *Nano Lett.*, **11**, 3821 (2011)
1345. V.Renugopalakrishnan, B.Barbiellini, C.King, M.Molinari, K.Mochalov, A.Sukhanova, I.Nabiev, P.Fojan, H.L.Tuller, M.Chin, P.Somasundaran, E.Padrós, S.Ramakrishna. *J. Phys. Chem. C*, **118**, 16710 (2014)
1346. L.-K.Chu, C.-W.Yen, M.A.El-Sayed. *J. Phys. Chem. C*, **114**, 15358 (2010)
1347. J.Chu, X.Li, J.Zhang, J.Tang. *Biochem. Biophys. Res. Commun.*, **305**, 116 (2003)
1348. J.-A.He, L.Samuelson, L.Li, J.Kumar, S.K.Tripathy. *J. Phys. Chem. B*, **102**, 7067 (1998)
1349. J.He, L.Samuelson, L.Li, J.Kumar, S.K.Tripathy. *Langmuir*, **7463**, 1674 (1998)
1350. R.Li, X.Cui, W.Hu, Z.Lu, C.M.Li. *J. Colloid Interface Sci.*, **344**, 150 (2010)
1351. T.Miyasaka, K.Koyama. *Thin Solid Films*, **210 – 211**, 146 (1992)
1352. S.Yu.Zaitsev. *Supramolekulyarnye Nanorazmernye Sistemy na Granitse Razdela Faz. Kontseptsii i Perspektivy dlya Bionanotekhnologii. (Supramolecular Nanoscale Systems at the Phase Section Boundary. Concepts and Perspectives for Bionanotechnology)* (Moscow: LENAND, 2010)
1353. A.A.Kuchmiy, G.A.Efimov, S.A.Nedospasov. *Biochemistry (Moscow)*, **77**, 1339 (2012)
1354. H.Kobayashi, M.Ogawa, R.Alford, P.L.Choyke, Y.Urano. *Chem. Rev.*, **110**, 2620 (2010)
1355. M.Nedyalkova, B.Donkova, J.Romanova, G.Tzvetkov, S.Madurga, V.Simeonov. *Adv. Colloid Interface Sci.*, **249**, 192 (2017)
1356. M.A.Busquets, J.Estelrich, M.J.Sánchez-Martín. *Int. J. Nanomed.*, 1727 (2015)
1357. Y.Wang, S.Song, S.Zhang, H.Zhang. *Nano Today*, **25**, 38 (2019)
1358. F.Chen, G.Hableel, E.R.Zhao, J.V.Jokerst. *J. Colloid Interface Sci.*, **521**, 261 (2018)
1359. E.Rampazzo, D.Genovese, F.Palomba, L.Prodi, N.Zaccheroni. *Methods Appl. Fluoresc.*, **6**, 22002 (2018)

1360. Z.Xu, X.Ma, Y.-E.Gao, M.Hou, P.Xue, C.M.Li, Y.Kang. *Mater. Chem. Front.*, **1**, 1257 (2017)
1361. L.Wang, K.Wang, S.Santra, X.Zhao, L.R.Hilliard, J.E.Smith, Y.Wu, W.Tan. *Anal. Chem.*, **78**, 646 (2006)
1362. G.De Crozals, R.Bonnet, C.Farre, C.Chaix. *Nano Today*, **11**, 435 (2016)
1363. A.R.Mukhametshina, S.V.Fedorenko, A.M.Petrov, G.F.Zakyrjanova, K.A.Petrov, L.F.Nurullin, I.R.Nizameev, A.R.Mustafina, O.G.Sinyashin. *ACS Appl. Mater. Interfaces*, **10**, 14948 (2018)
1364. V.Gubala, G.Giovannini, F.Kunc, M.P.Monopoli, C.J.Moore. *Cancer Nanotechnol.*, **11**, 1 (2020)
1365. S.V.Fedorenko, S.L.Grechkina, A.R.Mustafina, K.V.Kholin, A.S.Stepanov, I.R.Nizameev, I.E.Ismaev, M.K.Kadirov, R.R.Zairov, A.N.Fattakhova, R.R.Amirov, S.E.Soloveva. *Colloids Surf., B*, **149**, 243 (2017)
1366. A.R.Mukhametshina, A.R.Mustafina, N.A.Davydov, S.V.Fedorenko, I.R.Nizameev, M.K.Kadirov, V.V.Gorbatchuk, A.I.Konovalov. *Langmuir*, **31**, 611 (2014)
1367. W.Stöber, A.Fink, E.Bohn. *J. Colloid Interface Sci.*, **26**, 62 (1968)
1368. E.Alsolmy, W.M.Abdelwahab, G.Patonay. *J. Fluoresc.*, **28**, 1049 (2018)
1369. S.Santoro, V.Sebastian, A.J.Moro, C.A.M.Portugal, J.C.Lima, I.M.Coelhoso, J.G.Crespo, R.Mallada. *J. Colloid Interface Sci.*, **486**, 144 (2017)
1370. M.Mirenda, V.Levi, M.L.Bossi, L.Bruno, A.V.Bordoni, A.E.Regazzoni, A.Wolosiuk. *J. Colloid Interface Sci.*, **392**, 96 (2013)
1371. D.Zhang, Z.Wu, J.Xu, J.Liang, J.Li, W.Yang. *Langmuir*, **26**, 6657 (2010)
1372. Y.Wang, W.Fan, S.R.Nugen. *Mater. Lett.*, **92**, 17 (2013)
1373. S.Shahabi, L.Treccani, K.Rezwan. *J. Nanoparticle Res.*, **18**, 28 (2016)
1374. S.Rajkumar, M.Prabaharan. *Colloids Surf., B*, **186**, 110701 (2020)
1375. F.Meder, S.S.Thomas, L.W.Fitzpatrick, A.Alahmari, S.Wang, J.G.Beirne, G.Vaz, G.Redmond, K.A.Dawson. *ACS Nano*, **10**, 4660 (2016)
1376. S.Yang, Y.Li. *WIRES Nanomed. Nanobi.*, **12**, e1603 (2020)
1377. M.Montalti, L.Prodi, E.Rampazzo, N.Zaccheroni. *Chem. Soc. Rev.*, **43**, 4243 (2014)
1378. S.Kyeong, C.Jeong, H.Y.Kim, D.W.Hwang, H.Kang, J.-K.Yang, D.S.Lee, B.-H.Jun, Y.-S.Lee. *RSC Adv.*, **5**, 32072 (2015)
1379. P.D.Nallathamby, J.Hopf, L.E.Irimata, T.L.McGinnity, R.K.Roeder. *J. Mater. Chem. B*, **4**, 5418 (2016)
1380. J.Wang, Z.H.Shah, S.Zhang, R.Lu. *Nanoscale*, **6**, 4418 (2014)
1381. S.Fedorenko, A.Stepanov, G.Sibgatullina, D.Samigullin, A.Mukhitov, K.Petrov, R.Mendes, M.Rümmeli, L.Giebeler, B.Weise, T.Gemming, I.Nizameev, K.Kholin, A.Mustafina. *Nanoscale*, **11**, 16103 (2019)
1382. S.R.Kandibanda, N.Gundeboina, S.Das, V.M.Sunkara. *J. Photochem. Photobiol. B*, **178**, 270 (2018)
1383. S.Fedorenko, D.Gilmanova, A.Mukhametshina, I.Nizameev, K.Kholin, B.Akhmadeev, A.Voloshina, A.Sapunova, S.Kuznetsova, A.Daminova, S.Katsyuba, R.Zairov, A.Mustafina. *J. Mater. Sci.*, **54**, 9140 (2019)
1384. S.Fedorenko, A.Stepanov, R.Zairov, O.Kaman, R.Amirov, I.Nizameev, K.Kholin, I.Ismaev, A.Voloshina, A.Sapunova, M.Kadirov, A.Mustafina. *Colloids Surf., A*, **559**, 60 (2018)
1385. A.Stepanov, S.Fedorenko, R.Amirov, I.Nizameev, K.Kholin, A.Voloshina, A.Sapunova, R.Mendes, M.Rümmeli, T.Gemming, A.Mustafina, B.Odintsov. *J. Chem. Sci.*, **130**, 125 (2018)
1386. F.Cabello-Hurtado, M.D.Lozano-Baena, C.Neaime, A.Burel, S.Jeanne, P.Pellen-Mussi, S.Cordier, F.Grasset. *J. Nanoparticle Res.*, **18**, 69 (2016)
1387. T.Aubert, A.Y.Ledneva, F.Grasset, K.Kimoto, N.G.Naumov, Y.Molard, N.Saito, H.Haneda, S.Cordier. *Langmuir*, **26**, 18512 (2010)
1388. N.Nerambourg, T.Aubert, C.Neaime, S.Cordier, M.Mortier, G.Patriarche, F.Grasset. *J. Colloid Interface Sci.*, **424**, 132 (2014)
1389. G.Alberto, G.Caputo, G.Viscardi, S.Coluccia, G.Martra. *Chem. Mater.*, **24**, 2792 (2012)
1390. V.Kabanov, D.J.Press, R.P.S.Huynh, G.K.H.Shimizu, B.Heyne. *Chem. Commun.*, **54**, 6320 (2018)
1391. S.Shahabi, L.Treccani, R.Dringen, K.Rezwan. *Acta Biomater.*, **14**, 208 (2015)
1392. Z.Bai, R.Chen, P.Si, Y.Huang, H.Sun, D.-H.Kim. *ACS Appl. Mater. Interfaces*, **5**, 5856 (2013)
1393. Y.Ren, Y.Zhao, Y.Zhang, W.Tang, X.Xin, J.Shen, L.Wang. *Colloids Surf., A*, **486**, 14 (2015)
1394. V.V.Goftman, T.Aubert, D.Vande Ginste, R.Van Deun, N.V.Beloglazova, Z.Hens, S.De Saeger, I.Y.Goryacheva. *Biosens. Bioelectron.*, **79**, 476 (2016)
1395. H.L.Ding, Y.X.Zhang, S.Wang, J.M.Xu, S.C.Xu, G.H.Li. *Chem. Mater.*, **24**, 4572 (2012)
1396. C.Chen, N.Kang, T.Xu, D.Wang, L.Ren, X.Guo. *Nanoscale*, **7**, 5249 (2015)
1397. D.Genovese, E.Rampazzo, S.Bonacchi, M.Montalti, N.Zaccheroni, L.Prodi. *Nanoscale*, **6**, 3022 (2014)
1398. C.Wu, Y.Wu, Y.Jin, P.Zhu, W.Shi, J.Li, Q.Wu, Q.Zhang, Y.Han, X.Zhao. *RSC Adv.*, **9**, 13855 (2019)
1399. P.Kumar, A.Anuradha, I.Roy. *RSC Adv.*, **4**, 16181 (2014)
1400. A.Nagesetti, A.J.McGoron. *Colloids Surf., B*, **147**, 492 (2016)
1401. S.Kim, T.Y.Ohulchanskyy, H.E.Pudavar, R.K.Pandey, P.N.Prasad. *J. Am. Chem. Soc.*, **129**, 2669 (2007)
1402. A.K.Dinda, C.K.Prashant, S.Naqvi, J.Unnithan, M.Samim, A.Maitra. *Int. J. Nanotechnol.*, **9**, 862 (2012)
1403. I.Roy, P.Kumar, R.Kumar, T.Y.Ohulchanskyy, K.-T.Yong, P.N.Prasad. *RSC Adv.*, **4**, 53498 (2014)
1404. W.-C.Law, K.-T.Yong, I.Roy, G.Xu, H.Ding, E.J.Bergey, H.Zeng, P.N.Prasad. *J. Phys. Chem. C*, **112**, 7972 (2008)
1405. A.Szpak, S.Fiejdasz, W.Prendota, T.Strączek, C.Kapusta, J.Szmyd, M.Nowakowska, S.Zapotoczny. *J. Nanoparticle Res.*, **16**, 2678 (2014)
1406. H.Bin Na, T.Hyeon. *J. Mater. Chem.*, **19**, 6267 (2009)
1407. J.Choi, J.-H.Lee, T.-H.Shin, H.-T.Song, E.Y.Kim, J.Cheon. *J. Am. Chem. Soc.*, **132**, 11015 (2010)
1408. T.-H.Shin, J.Choi, S.Yun, I.-S.Kim, H.-T.Song, Y.Kim, K.I.Park, J.Cheon. *ACS Nano*, **8**, 3393 (2014)
1409. P.Caravan, C.T.Farrar, L.Frullano, R.Uppal. *Contrast Media Mol. Imag.*, **4**, 89 (2009)
1410. M.Perrier, S.Kenouche, J.Long, K.Thangavel, J.Larionova, C.Goze-Bac, A.Lascialfari, M.Mariani, N.Baril, C.Guérin, B.Donnadieu, A.Trifonov, Y.Guari. *Inorg. Chem.*, **52**, 13402 (2013)
1411. G.A.Pereira, J.A.Peters, F.A.A.Paz, J.Rocha, C.F.G.C.Geraldes. *Inorg. Chem.*, **49**, 2969 (2010)
1412. F.Carniato, L.Tei, M.Cossi, L.Marchese, M.Botta. *Chem. – Eur. J.*, **16**, 10727 (2010)

1413. W.Xiao, H.Gu, D.Li, D.Chen, X.Deng, Z.Jiao, J.Lin. *J. Magn. Magn. Mater.*, **324**, 488 (2012)
1414. M.Corti, A.Lascialfari, M.Marinone, A.Masotti, E.Micotti, F.Orsini, G.Ortaggi, G.Poletti, C.Innocenti, C.Sangregorio. *J. Magn. Magn. Mater.*, **320**, e316 (2008)
1415. M.Yang, L.Gao, K.Liu, C.Luo, Y.Wang, L.Yu, H.Peng, W.Zhang. *Talanta*, **131**, 661 (2015)
1416. H.Yang, Y.Zhuang, Y.Sun, A.Dai, X.Shi, D.Wu, F.Li, H.Hu, S.Yang. *Biomaterials*, **32**, 4584 (2011)
1417. N.Xiao, W.Gu, H.Wang, Y.Deng, X.Shi, L.Ye. *J. Colloid Interface Sci.*, **417**, 159 (2014)
1418. A.Jedlovszky-Hajdú, E.Tombácz, I.Bányai, M.Babos, A.Palkó. *J. Magn. Magn. Mater.*, **324**, 3173 (2012)
1419. A.S.Lübbe, C.Alexiou, C.Bergemann. *J. Surg. Res.*, **95**, 200 (2001)
1420. S.V.Fedorenko, S.L.Grechkina, A.R.Mukhametshina, A.O.Solovieva, T.N.Pozmogova, S.M.Miroshnichenko, A.Y.Alekseev, M.A.Shestopalov, K.V.Kholin, I.R.Nizameev, A.R.Mustafina. *J. Inorg. Biochem.*, **182**, 170 (2018)
1421. M.C.Gomes, Â.Cunha, T.Trindade, J.P.C.Tomé. *J. Innov. Opt. Heal. Sci.*, **09**, 1630005 (2016)
1422. S.Salatin, S.M.Dizaj, A.Y.Khosroushahi. *Cell Biol. Int.*, **39**, 881 (2015)
1423. D.Knopp, D.Tang, R.Niessner. *Anal. Chim. Acta*, **647**, 14 (2009)
1424. S.Bharathiraja, M.S.Moorthy, P.Manivasagan, H.Seo, K.D.Lee, J.Oh. *Photodiagn. Photodyn. Ther.*, **19**, 212 (2017)
1425. X.Wang, O.Ramström, M.Yan. *Chem. Commun.*, **47**, 4261 (2011)
1426. X.Li, L.Liu, Y.Fu, H.Chen, M.M.A.Abualrejal, H.Zhang, Z.Wang, H.Zhang. *Acta Biomater.*, **104**, 167 (2020)
1427. C.Mi, J.Zhang, H.Gao, X.Wu, M.Wang, Y.Wu, Y.Di, Z.Xu, C.Mao, S.Xu. *Nanoscale*, **2**, 1141 (2010)
1428. F.Chen, X.Zhang, K.Ma, B.Madajewski, M.Benezra, L.Zhang, E.Phillips, M.Z.Turker, F.Gallazzi, O.Penate-Medina, M.Overholtzer, M.Pauliah, M.Gonen, P.Zanzonico, U.Wiesner, M.S.Bradbury, T.P.Quinn. *ACS Appl. Mater.*, **10**, 4379 (2018)
1429. J.Tan, N.Yang, Z.Hu, J.Su, J.Zhong, Y.Yang, Y.Yu, J.Zhu, D.Xue, Y.Huang, Z.Lai, Y.Huang, X.Lu, Y.Zhao. *Nanoscale Res. Lett.*, **11**, 298 (2016)
1430. G.T.Hermanson. In *Bioconjugate Techniques*. (3rd Edn.). (London: Elsevier, 2013). P. 549
1431. M.Xu, G.Yang, H.Bi, J.Xu, S.Dong, T.Jia, Z.Wang, R.Zhao, Q.Sun, S.Gai, F.He, D.Yang, P.Yang. *Chem. Eng. J.*, **382**, 122822 (2020)
1432. S.A.Jadhav, H.B.Garud, A.H.Patil, G.D.Patil, C.R.Patil, T.D.Dongale, P.S.Patil. *Colloid Interface Sci. Commun.*, **30**, 100181 (2019)
1433. J.Elistratova, A.Mukhametshina, K.Kholin, I.Nizameev, M.Mikhailov, M.Sokolov, R.Khairullin, R.Miftakhova, G.Shammas, M.Kadirov, K.Petrov, A.Rizvanov, A.Mustafina. Elsevier,*J. Colloid Interface Sci.*, **538**, 387 (2019)
1434. C.M.Beddoes, C.P.Case, W.H.Briscoe. *Adv. Colloid Interface Sci.*, **218**, 48 (2015)
1435. J.Zhu, L.Liao, L.Zhu, P.Zhang, K.Guo, J.Kong, C.Ji, B.Liu. *Talanta*, **107**, 408 (2013)
1436. I.-L.H.Annika Mareike Gramatke. *J. Nanomed. Nanotechnol.*, **05**, 1000248 (2014)
1437. E.Barron, I.Passagne, A.Auger, A.Travo, E.Rascol, B.L'Azou, I.Forfar. *Anal. Methods*, **8**, 2233 (2016)
1438. L.Shang, K.Nienhaus, G.Nienhaus. *J. Nanobiotechnol.*, **12**, 5 (2014)
1439. K.Saha, S.T.Kim, B.Yan, O.R.Miranda, F.S.Alfonso, D.Shlosman, V.M.Rotello. *Small*, **9**, 300 (2012)
1440. S.Shahabi, L.Treccani, R.Dringen, K.Rezwan. *ACS Appl. Mater. Interfaces*, **7**, 13821 (2015)
1441. C.Graf, Q.Gao, I.Schütz, C.N.Noufele, W.Ruan, U.Posselt, E.Korotianskiy, D.Nordmeyer, F.Rancan, S.Hadam, A.Vogt, J.Lademann, V.Haucke, E.Rühl. *Langmuir*, **28**, 7598 (2012)
1442. V.Francia, K.Yang, S.Deville, C.Reker-Smit, I.Nelissen, A.Salvati. *ACS Nano*, **13**, 11107 (2019)
1443. S.V.Fedorenko, A.R.Mustafina, A.R.Mukhametshina, M.E.Jilkin, T.A.Mukhametzyanov, A.O.Solovieva, T.N.Pozmogova, L.V.Shestopalova, M.A.Shestopalov, K.V.Kholin, Y.N.Osin, O.G.Sinyashin. *Mater. Sci. Eng. C*, **76**, 551 (2017)
1444. R.Brewster, K.Caran, J.Sasine, S.Shuker. *Curr. Org. Chem.*, **8**, 867 (2004)
1445. J.Požar, G.Horvat, M.Čalogović, N.Galić, L.Frkanec, V.Tomišić. *Croat. Chem. Acta*, **85**, 541 (2012)
1446. N.Bregović, N.Cindro, L.Frkanec, V.Tomišić. *Supramol. Chem.*, **28**, 608 (2016)
1447. F.Sansone, L.Baldini, A.Casnati, R.Ungaro. *New J. Chem.*, **34**, 2715 (2010)
1448. G.-Y.Qing, F.Wang, Y.-B.He, C.-G.Hu, X.Yang. *Supramol. Chem.*, **20**, 635 (2008)
1449. J.Bois, I.Bonnamour, C.Duchamp, H.Parrot-Lopez, U.Darbost, C.Felix. *New J. Chem.*, **33**, 2128 (2009)
1450. S.Eymur, E.Akceylan, O.Sahin, A.Uyanik, M.Yilmaz. *Tetrahedron*, **70**, 4471 (2014)
1451. A.Uyanik, M.Bayrakci, S.Eymur, M.Yilmaz. *Tetrahedron*, **70**, 9307 (2014)
1452. M.Aktas, A.Uyanik, S.Eymur, M.Yilmaz. *Supramol. Chem.*, **28**, 351 (2015)
1453. O.Sahin, S.Eymur, A.Uyanik, E.Akceylan, M.Yilmaz. *Polycycl. Arom. Compd.*, **38**, 168 (2016)
1454. Z.-Y.Li, Y.Chen, C.-Q.Zheng, Y.Yin, L.Wang, X.-Q.Sun. *Tetrahedron*, **73**, 78 (2017)
1455. T.Mecca, G.M.L.Consoli, C.Geraci, F.Cunsolo. *Bioorg. Med. Chem.*, **12**, 5057 (2004)
1456. C.Y.Goh, T.Becker, D.H.Brown, B.W.Skelton, F.Jones, M.Mocerino, M.I.Ogden. *Chem. Commun.*, **47**, 6057 (2011)
1457. S.Fujii, R.Takahashi, K.Sakurai. *Langmuir*, **33**, 4019 (2017)
1458. V.Bagnacani, V.Franceschi, M.Bassi, M.Lomazzi, G.Donofrio, F.Sansone, A.Casnati, R.Ungaro. *Nat. Commun.*, **4**, 1721 (2013)
1459. J.Gasparello, A.Manicardi, A.Casnati, R.Corradini, R.Gambari, A.Finotti, F.Sansone. *Sci. Rep.*, **9**, 3036 (2019)
1460. M.Oguz, A.Gul, S.Karakurt, M.Yilmaz. *Bioorg. Chem.*, **94**, 103207 (2020)
1461. G.Qing, Y.He, F.Wang, H.Qin, C.Hu, X.Yang. *Eur. J. Org. Chem.*, 1768 (2007)
1462. T.Mecca, F.Cunsolo. *Polym. Adv. Technol.*, **21**, 752 (2009)
1463. D.-Y.Fu, T.Lu, Y.-X.Liu, F.Li, M.I.Ogden, Y.Wang, Y.Wu, M.Mocerino. *ChemistrySelect*, **1**, 6243 (2016)
1464. M.Russo, P.Lo Meo. *Beilstein J. Org. Chem.*, **13**, 2698 (2017)
1465. T.J.Wenzel. *J. Incl. Phenom. Macrocycl. Chem.*, **78**, 1 (2013)
1466. R.R.Kashapov, L.Y.Zakharova, M.N.Saifutdinova, E.L.Gavrilova, O.G.Sinyashin. *Tetrahedron Lett.*, **56**, 2508 (2015)
1467. L.Y.Zakharova, A.A.Serdyuk, A.B.Mirgorodskaya, I.V.Kapitanov, G.A.Gainanova, Y.Karpichev, E.L.Gavrilova, O.G.Sinyashin. *J. Surfact. Deterg.*, **19**, 493 (2016)

1468. A.M.Bekmukhametova, R.R.Kashapov, M.N.Saifutdinova, E.L.Gavrilova, V.A.Mamedov, N.A.Zhukova, L.Y.Zakharova, O.G.Sinyashin. *Macroheterocycles*, **10**, 164 (2017)
1469. S.E.Solovieva, V.A.Burilov, I.S.Antipin. *Macroheterocycles*, **10**, 134 (2017)
1470. D.Appelhans, M.Smet, G.Khimich, H.Komber, D.Voigt, P.Lhoták, D.Kuckling, B.Voit. *New J. Chem.*, **29**, 1386 (2005)
1471. P.L.Padnya, E.A.Andreyko, O.A.Mostovaya, I.K.Rizvanov, I.I.Stoikov. *Org. Biomol. Chem.*, **13**, 5894 (2015)
1472. P.L.Padnya, E.E.Bayarashov, I.V.Zueva, S.V.Lushchekina, O.A.Lenina, V.G.Evtugyn, Y.N.Osin, K.A.Petrov, I.I.Stoikov. *Bioorg. Chem.*, **94**, 103455 (2020)
1473. O.A.Mostovaya, P.L.Padnya, D.N.Shurpik, A.A.Vavilova, V.G.Evtugyn, Y.N.Osin, I.I.Stoikov. *Macroheterocycles*, **10**, 154 (2017)
1474. P.L.Padnya, O.S.Potrekeeva, E.E.Bayarashov, I.I.Stoikov. *Russ. J. Gen. Chem.*, **88**, 2328 (2018)
1475. O.A.Mostovaya, Y.A.Valiullina, C.T.Chan, O.S.Potrekeeva, P.L.Padnya, Y.F.Zuev, I.I.Stoikov. *Mendeleev Commun.*, **29**, 520 (2019)
1476. T.Ogoshi, T.Kakuta, T.Yamagishi. *Angew. Chem., Int. Ed.*, **58**, 2197 (2019)
1477. P.J.Cragg. *Isr. J. Chem.*, **58**, 1194 (2018)
1478. D.N.Shurpik, P.L.Padnya, L.T.Basimova, V.G.Evtugin, V.V.Plemenkov, I.I.Stoikov. *Mendeleev Commun.*, **25**, 432 (2015)
1479. L.S.Yakimova, D.N.Shurpik, A.R.Makhmutova, I.I.Stoikov. *Macroheterocycles*, **10**, 226 (2017)
1480. D.N.Shurpik, D.A.Sevastyanov, P.V.Zelenikhin, E.V.Subakaeva, V.G.Evtugyn, Y.N.Osin, P.J.Cragg, I.I.Stoikov. *Tetrahedron Lett.*, **59**, 4410 (2018)
1481. D.N.Shurpik, Y.I.Aleksandrova, I.I.Stoikov. *Russ. J. Gen. Chem.*, **88**, 2518 (2018)
1482. T.Nishimura, Y.Sanada, T.Matsuo, T.Okobira, E.Mylonas, N.Yagi, K.Sakurai. *Chem. Commun.*, **49**, 3052 (2013)
1483. K.Yang, Y.Chang, J.Wen, Y.Lu, Y.Pei, S.Cao, F.Wang, Z.Pei. *Chem. Mater.*, **28**, 1990 (2016)
1484. J.Zhang, Z.Wang, S.Lv, X.Zeng, Y.Sun, H.Li, R.Zhang. *Chem. Commun.*, **55**, 778 (2019)
1485. W.-X.Feng, Z.Sun, M.Barboiu. *Isr. J. Chem.*, **58**, 1209 (2018)
1486. L.Chen, W.Si, L.Zhang, G.Tang, Z.-T.Li, J.-L.Hou. *J. Am. Chem. Soc.*, **135**, 2152 (2013)
1487. W.Si, Z.-T.Li, J.-L.Hou. *Angew. Chem., Int. Ed.*, **53**, 4578 (2014)
1488. Y.Shen, W.Si, M.Erbakan, K.Decker, R.De Zorzi, P.O.Saboe, Y.J.Kang, S.Majd, P.J.Butler, T.Walz, A.Aksimentiev, J.Hou, M.Kumar. *Proc. Natl. Acad. Sci. USA*, **112**, 9810 (2015)
1489. Q.Li, X.Li, L.Ning, C.-H.Tan, Y.Mu, R.Wang. *Small*, **15**, 1804678 (2019)
1490. Y.Sun, F.Zhang, J.Quan, F.Zhu, W.Hong, J.Ma, H.Pang, Y.Sun, D.Tian, H.Li. *Nat. Commun.*, **9**, 2617 (2018)
1491. F.Zhang, J.Ma, Y.Sun, Y.Mei, X.Chen, W.Wang, H.Li. *Anal. Chem.*, **90**, 8270 (2018)
1492. N.S.Zefirov, V.A.Palyulin. In *Topics in Stereochemistry*. Vol. 20. (Eds E.L.Iliel, S.H.Wilen). (New York: Wiley-Interscience, 1991). P. 171
1493. P.Comba, W.Schiek. *Coord. Chem. Rev.*, **238 – 239**, 21 (2003)
1494. K.-J.Haack, R.Goddard, K.-R.Pörschke. *J. Am. Chem. Soc.*, **119**, 7992 (1997)
1495. I.S.Bushmarinov, I.V.Fedyanin, K.A.Lyssenko, V.L.Lapteva, S.A.Pisarev, V.A.Palyulin, N.S.Zefirov, M.Y.Antipin. *J. Phys. Chem. A*, **115**, 12738 (2011)
1496. S.A.Pisarev, D.A.Shulga, V.A.Palyulin, N.S.Zefirov. *Struct. Chem.*, **30**, 509 (2019)
1497. S.Z.Vatsadze, A.V.Medved'ko, A.A.Bodunov, K.A.Lyssenko. *Mendeleev Commun.*, **30**, 344 (2020)
1498. H.Cui, R.Goddard, K.R.Pörschke. *J. Phys. Org. Chem.*, **25**, 814 (2012)
1499. S.Z.Vatsadze, V.S.Semashko, M.A.Manaenkova, D.P.Krut'ko, V.N.Nuriev, R.D.Rakhimov, D.I.Davlyatshin, A.V.Churakov, J.A.K.Howard, A.L.Maksimov, W.Li, H.Yu. *Russ. Chem. Bull., Int. Ed.*, **63**, 895 (2014)
1500. A.Medved'ko, A.Dalinger, V.Nuriev, V.Semashko, A.Filatov, A.Ezhov, A.Churakov, J.Howard, A.Shiryaev, A.Baranchikov, V.Ivanov, S.Vatsadze. *Nanomaterials*, **9**, 89 (2019)
1501. L.Toom, A.Kütt, I.Kaljurand, I.Leito, H.Ottosson, H.Grennberg, A.Gogoll. *J. Org. Chem.*, **71**, 7155 (2006)
1502. H.Stetter, R.Merten. *Chem. Ber.*, **90**, 868 (1957)
1503. H.Stetter, K.Dieminger. *Chem. Ber.*, **92**, 2658 (1959)
1504. S.Z.Vatsadze, V.S.Tyurin, N.V.Zyk, A.V.Churakov, L.G.Kuz'mina, E.V.Avtomonov, R.D.Rakhimov, K.P.Butin. *Russ. Chem. Bull., Int. Ed.*, **54**, 1825 (2005)
1505. P.Comba, M.Kerscher, W.Schiek. In *Progress in Inorganic Chemistry*. Vol. 55. (Ed. K.D.Karlin). (New York: Wiley, 2007). P. 613
1506. *Radiopharmaceuticals.Chemistry and Pharmacology*. (Ed. A.D.Nunn). (New York: Marcel Dekker, 1992)
1507. L.E.Williams. *Radiopharmaceuticals. Introduction to Drug Evaluation and Dose Estimation*. (Boca Raton, FL: CRC Press, 2010)
1508. *Positron Emission Tomography*. (Eds A.Granov, L.Tiutin, T.Schwarz). (Berlin, Heidelberg: Springer-Verlag, 2013)
1509. S.Z.Vatsadze, O.E.Eremina, I.A.Veselova, S.N.Kalmykov, V.G.Nenajdenko. *Russ. Chem. Rev.*, **87**, 350 (2018)
1510. I.A.Veselova, E.A.Sergeeva, M.I.Makedonskaya, O.E.Eremina, S.N.Kalmykov, T.N.Shekhovtsova. *J. Anal. Chem.*, **71**, 1155 (2016)
1511. *Fluorine in Pharmaceutical and Medicinal Chemistry. From Biophysical Aspects to Clinical Applications*. (Eds V.Gouverneur, K.Müller). (London: Imperial College Press, 2012)
1512. F.M.Lu, Z.Yuan. *Quant. Imaging Med. Surg.*, **5**, 433 (2015)
1513. K.Oukoloff, M.Cieslikiewicz-Bouet, S.Chao, E.Costa Branquinho, C.Bouteiller, L.Jean, P.-Y.Renard. *Curr. Med. Chem.*, **22**, 3278 (2015)
1514. B.M.Zeglis, J.S.Lewis. *Dalton Trans.*, **40**, 6168 (2011)
1515. A.T.Soderlund, J.Chaal, G.Tjio, J.J.Totman, M.Conti, D.W.Townsend. *J. Nucl. Med.*, **56**, 1285 (2015)
1516. R.N.Krasikova, R.A.Aliev, S.N.Kalmykov. *Mendeleev Commun.*, **26**, 85 (2016)
1517. P.Comba, M.Kerscher, K.Rück, M.Starke. *Dalton Trans.*, **47**, 9202 (2018)
1518. A.V.Medved'ko, B.V.Egorova, A.A.Komarova, R.D.Rakhimov, D.P.Krut'ko, S.N.Kalmykov, S.Z.Vatsadze. *ACS Omega*, **1**, 854 (2016)
1519. R.Gillet, A.Roux, J.Brandel, S.Huclier-Markai, F.Camerel, O.Jeannin, A.M.Nonat, L.J.Charbonnière. *Inorg. Chem.*, **56**, 11738 (2017)

1520. P.Comba, U.Jermilova, C.Orvig, B.O.Patrick, C.F.Ramogida, K.Rück, C.Schneider, M.Starke. *Chem. – Eur. J.*, **23**, 15945 (2017)
1521. H.Stephan, M.Walther, S.Fahnemann, P.Ceroni, J.K.Molloy, G.Bergamini, F.Heisig, C.E.Muller, W.Kraus, P.Comba. *Chem. – Eur. J.*, **20**, 17011 (2014)
1522. F.Braun, P.Comba, L.Grimm, D.-P.Herten, B.Pokrandt, H.Wadepohl. *Inorg. Chim. Acta*, **484**, 464 (2019)
1523. O.O.Grygorenko, D.S.Radchenko, D.M.Volochnyuk, A.A.Tolmachev, I.V.Komarov. *Chem. Rev.*, **111**, 5506 (2011)
1524. M.Breuning, M.Steiner. *Synthesis*, 2841 (2008)
1525. J.Bautz, P.Comba, C.L.De Laorden, M.Menzel, G.Rajaraman. *Angew. Chem., Int. Ed.*, **46**, 8067 (2007)
1526. P.Comba, H.Wadepohl, S.Wiesner. *Eur. J. Inorg. Chem.*, 2610 (2011)
1527. P.Barman, A.K.Vardhaman, B.Martin, S.J.Wörner, C.V.Sastri, P.Comba. *Angew. Chem., Int. Ed.*, **54**, 2095 (2015)
1528. W.J.Ang, Y.S.Chng, Y.Lam. *RSC Adv.*, **5**, 81415 (2015)
1529. P.Barman, P.Upadhyay, A.S.Faponle, J.Kumar, S.S.Nag, D.Kumar, C.V.Sastri, S.P.de Visser. *Angew. Chem., Int. Ed.*, **55**, 11091 (2016)
1530. F.G.C.Reinhard, P.Barman, G.Mukherjee, J.Kumar, Deep Kumar, Dev.Kumar, C.V.Sastri, S.P.De Visser. *J. Am. Chem. Soc.*, **139**, 18328 (2017)
1531. S.S.Nag, G.Mukherjee, P.Barman, C.V.Sastri. *Inorg. Chim. Acta*, **485**, 80 (2019)
1532. L.A.Bulygina, N.D.Kagramanov, N.S.Khrushcheva, K.A.Lyssenko, A.S.Peregudov, V.I.Sokolov. *J. Organomet. Chem.*, **846**, 169 (2017)
1533. N.Simpson, K.Maaijen, Y.Roelofsen, R.Hage. *Catalysts*, **9**, 825 (2019)
1534. M.Křižan, J.Vinklárek, M.Erben, Z.Růžičková, J.Honzíček. *Inorg. Chim. Acta*, **486**, 636 (2019)
1535. X.Liu, S.Dong, L.Lin, X.Feng. *Chin. J. Chem.*, **36**, 791 (2018)
1536. J.Liu, Z.Yang, X.Liu, Z.Wang, Y.Liu, S.Bai, L.Lin, X.Feng. *Org. Biomol. Chem.*, **7**, 4120 (2009)
1537. D.Scharnagel, A.Müller, F.Prause, M.Eck, J.Goller, W.Milius, M.Breuning. *Chem. – Eur. J.*, **21**, 12488 (2015)
1538. A.Rossetti, S.Landoni, F.Meneghetti, C.Castellano, M.Mori, G.Colombo Dugoni, A.Sacchetti. *New J. Chem.*, **42**, 12072 (2018)
1539. C.Castellano, A.Sacchetti, F.Meneghetti. *Chirality*, **28**, 332 (2016)
1540. B.Over, S.Wetzel, C.Grütter, Y.Nakai, S.Renner, D.Rauh, H.Waldmann. *Nat. Chem.*, **5**, 21 (2013)
1541. B.Parrino, S.Cascioferro, D.Carbone, G.Cirrincione, P.Diana. In *Advances in Heterocyclic Chemistry*. Vol. 133. (Elsevier, 2021) (in the press); https://doi.org/10.1016/bs.aihch.2020.11.001
1542. Y.N.Nosova, I.V.Zenin, V.P.Maximova, E.M.Zhidkova, K.I.Kirsanov, E.A.Lesovaya, A.A.Lobas, M.V.Gorshkov, O.N.Kovaleva, E.R.Milaeva, M.Galanski, B.K.Keppler, A.A.Nazarov. *Bioinorg. Chem. Appl.*, Art. ID 4736321 (2017)
1543. H.Cui, R.Goddard, K.R.Pörschke, A.Hamacher, M.U.Kassack. *Inorg. Chem.*, **53**, 3371 (2014)
1544. H.Cui, R.Goddard, K.Po, A.Hamacher, M.U.Kassack, K.-R.Pörschke, A.Hamacher, M.U.Kassack. *Inorg. Chem.*, **55**, 2986 (2016)
1545. R.Mitra, R.Goddard, K.-R.Pörschke. *Inorg. Chem.*, **56**, 6712 (2017)
1546. A.A.Mazurov, D.C.Kombo, S.Akireddy, S.Murthy, T.A.Hauser, K.G.Jordan, G.J.Gatto, D.Yohannes. *Bioorg. Med. Chem. Lett.*, **23**, 3927 (2013)
1547. S.O.Bachurin, E.V.Bovina, A.A.Ustyugov. *Med. Res. Rev.*, **37**, 1186 (2017)
1548. D.C.Kombo, A.A.Mazurov, J.P.Strachan, M.Bencherif. *Bioorg. Med. Chem. Lett.*, **23**, 5105 (2013)
1549. M.I.Lavrov, D.S.Karlov, T.A.Voronina, V.V.Grigoriev, A.A.Ustyugov, S.O.Bachurin, V.A.Palyulin. *Mol. Neurobiol.*, **57**, 191 (2020)
1550. Y.Shi, S.P.O'Connor, D.Sitkoff, J.Zhang, M.Shi, S.N.Bisaha, Y.Wang, C.Li, Z.Ruan, R.M.Lawrence, H.E.Klei, K.Kish, E.C.-K.Liu, S.M.Seiler, L.Schweizer, T.E.Steinbacher, W.A.Schumacher, J.A.Robl, J.E.Macor, K.S.Atwal, P.D.Steinl. *Bioorg. Med. Chem. Lett.*, **21**, 7516 (2011)
1551. K.V.Kudryavtsev, D.A.Shulga, V.I.Chupakhin, E.I.Sinauridze, F.I.Ataullakhanov, S.Z.Vatsadze. *Tetrahedron*, **70**, 7854 (2014)
1552. S.Z.Vatsadze, D.A.Shulga, Y.D.Loginova, I.A.Vatsadze, L.Wang, H.Yu, K.V.Kudryavtsev. *Mendeleev Commun.*, **26**, 212 (2016)
1553. V.Haridas, K.S.Rajgokul, S.Sadanandan, T.Agrawal, V.Sharvani, M.V.S.Gopalakrishna, M.B.Bijesh, K.L.Kumawat, A.Basu, G.R.Medigeshi. *PLoS Negl. Trop. Dis.*, **7**, e2005 (2013)
1554. S.Norrehed, M.Erdélyi, M.E.Light, A.Gogoll. *Org. Biomol. Chem.*, **11**, 6292 (2013)
1555. V.Haridas, S.Sadanandan, Y.K.Sharma, S.Chinthalapalli, A.Shandilya. *Tetrahedron Lett.*, **53**, 623 (2012)
1556. V.Haridas, S.Sadanandan, M.V.S.Gopalakrishna, M.B.Bijesh, R.P.Verma, S.Chinthalapalli, A.Shandilya. *Chem. Commun.*, **49**, 10980 (2013)
1557. H.Yamashita, Y.Demizu, T.Misawa, T.Shoda, M.Kurihara. *Tetrahedron*, **71**, 2241 (2015)
1558. S.V.Shinde, P.Talukdar. *Angew. Chem., Int. Ed.*, **56**, 4238 (2017)
1559. A.Roy, D.Saha, P.S.Mandal, A.Mukherjee, P.Talukdar. *Chem. – Eur. J.*, **23**, 1241 (2017)
1560. P.N.Veremeeva, I.V.Grishina, V.L.Lapteva, A.A.Yaroslavov, A.V.Sybachin, V.A.Palyulin, N.S.Zefirov. *Mendeleev Commun.*, **24**, 152 (2014)
1561. P.N.Veremeeva, V.L.Lapteva, V.A.Palyulin, A.V.Sybachin, A.A.Yaroslavov, N.S.Zefirov. *Tetrahedron*, **70**, 1408 (2014)
1562. P.N.Veremeeva, I.V.Grishina, O.V.Zaborova, A.D.Averin, V.A.Palyulin. *Tetrahedron*, **75**, 4444 (2019)
1563. *Handbook of Anticancer Drugs from Marine Origin*. (Ed. S.K.Kim). (Berlin: Springer, 2014)
1564. Y.Matsuda, I.Abe. *Nat. Prod. Rep.*, **33**, 26 (2016)
1565. M.Daniel. *Medicinal Plants: Chemistry and Properties*. (Boca Raton, FL: CRC Press, 2016)
1566. V.V.Plemenkov, D.N.Shurpik, A.A.Akhmedov, J.B.Puplampu, I.I.Stoikov. In *Bioactive Natural Products*. (*Ser. Studies in Natural Products Chemistry*. Vol. 64). (Ed. Atta-ur Rahman). (Elsevier, 2020). P. 181
1567. A.R.Carroll, B.R.Copp, R.A.Davis, R.A.Keyzers, M.R.Prinsep. *Nat. Prod. Rep.*, **36**, 122 (2019)
1568. M.Menna, C.Imperatore, F.D'Aniello, A.Aiello. *Mar. Drugs*, **11**, 1602 (2013)
1569. V.Kulcitki, P.Harghel, N.Ungur. *Nat. Prod. Rep.*, **31**, 1686 (2014)
1570. K.T.Mortensen, T.J.Osberger, T.A.King, H.F.Sore, D.R.Spring. *Chem. Rev.*, **119**, 10288 (2019)

1571. C.T.Walsh, B.S.Moore. *Angew. Chem., Int. Ed.*, **58**, 6846 (2019)
1572. A.Jagels, Y.Hövelmann, A.Zielinski, M.Esselen, J.Köhler, F.Hübner, H.-U.Humpf. *Mycotoxin Res.*, **34**, 179 (2018)
1573. P.L.-G.Chong. *Chem. Phys. Lipids*, **163**, 253 (2010)
1574. S.Götze, P.Stallforth. *Org. Biomol. Chem.*, **18**, 1710 (2020)
1575. H.-Y.Tang, J.-M.Gao, Q.Zhang. *RSC Adv.*, **5**, 72433 (2015)
1576. G.Zhang, W.Zhang, Q.Zhang, T.Shi, L.Ma, Y.Zhu, S.Li, H.Zhang, Y.-L.Zhao, R.Shi, C.Zhang. *Angew. Chem., Int. Ed.*, **53**, 4840 (2014)
1577. B.Jeon, S.-A.Wang, M.W.Ruszczycky, H.Liu. *Chem. Rev.*, **117**, 5367 (2016)
1578. M.-H.Yang, M.-L.Gu, C.Han, X.-J.Guo, G.-P.Yin, P.Yu, L.-Y.Kong. *Org. Lett.*, **20**, 3345 (2018)
1579. C.-J.Li, J.Ma, H.Sun, D.Zhang, D.-M.Zhang. *Org. Lett.*, **18**, 168 (2015)
1580. Q.Chen, J.Gao, C.Jamieson, J.Liu, M.Ohashi, J.Bai, D.Yan, B.Liu, Y.Che, Y.Wang, K.N.Houk, Y.Hu. *J. Am. Chem. Soc.*, **141**, 14052 (2019)
1581. C.T.Walsh. *Nat. Chem. Biol.*, **11**, 620 (2015)
1582. D.W.Carney, K.R.Schmitz, J.V.Truong, R.T.Sauer, J.K.Sello. *J. Am. Chem. Soc.*, **136**, 1922 (2014)
1583. R.Singh, B.R.Glick, D.Rathore. *Pedosphere*, **28**, 170 (2018)
1584. T.Schneider, A.Müller, H.Miess, H.Gross. *Int. J. Med. Microbiol.*, **304**, 37 (2014)
1585. J.Hu, J.Wu, J.Lu, Y.Ju. *Tetrahedron Lett.*, **53**, 6705 (2012)
1586. V.Paquet, A.Zumbuehl, E.M.Carreira. *Bioconjug. Chem.*, **17**, 1460 (2006)
1587. H.Guo, F.Yang, W.Liu, J.Lai. *Tetrahedron Lett.*, **56**, 866 (2015)
1588. C.Yao, Q.Sun, W.Xia, J.Zhang, C.Lin, L.Wang. *J. Organomet. Chem.*, **847**, 68 (2017)
1589. J.Varshosaz, F.Hassanzadeh, H.S.Aliabadi, M.Banitalebi, M.Rostami, M.Nayebsadrian. *Colloid Polym. Sci.*, **292**, 2647 (2014)
1590. S.Xiao, Q.Wang, L.Si, X.Zhou, Y.Zhang, L.Zhang, D.Zhou. *Eur. J. Med. Chem.*, **124**, 1 (2016)
1591. S.Xiao, Q.Wang, L.Si, Y.Shi, H.Wang, F.Yu, Y.Zhang, Y.Li, Y.Zheng, C.Zhang, C.Wang, L.Zhang, D.Zhou. *ChemMedChem*, **9**, 1060 (2014)
1592. V.Balzani, A.Credi, M.Venturi. *Molecular Devices and Machines. A Journey into the Nano World*. (Weinheim: Wiley-VCH, 2003)
1593. *From Non-Covalent Assemblies to Molecular Machines*. (Eds J.-P.Sauvage, P.Gaspard). (Weinheim: Wiley-VCH, 2010)
1594. S.Erbas-Cakmak, D.A.Leigh, C.T.McTernan, A.L.Nussbaumer. *Chem. Rev.*, **115**, 10081 (2015)
1595. G.Barin, A.Coskun, M.M.G.Fouda, J.F.Stoddart. *ChemPlusChem*, **77**, 159 (2012)
1596. S.Kassem, T.van Leeuwen, A.S.Lubbe, M.R.Wilson, B.L.Feringa, D.A.Leigh. *Chem. Soc. Rev.*, **46**, 2592 (2017)
1597. V.A.Bren. *Russ. Chem. Rev.*, **70**, 1017 (2001)
1598. V.I.Minkin. *Russ. Chem. Bull., Int. Ed.*, **57**, 687 (2008)
1599. R.N.Dsouza, U.Pischel, W.M.Nau. *Chem. Rev.*, **111**, 7941 (2011)
1600. *Supramolecular Chemistry: from Molecules to Nanomaterials*. Vol. 5. (Eds J.W.Steed, P.A.Gale). (Chichester: Wiley, 2012)
1601. M.F.Budyka. *Russ. Chem. Bull., Int. Ed.*, **63**, 1656 (2014)
1602. T.L.Mako, J.M.Racicot, M.Levine. *Chem. Rev.*, **119**, 322 (2019)
1603. *Molecular Switches. Vol. 1*. 2nd Edn. (Eds B.L.Feringa, W.R.Browne). Wiley-VCH, Weinheim, 2011
1604. V.I.Minkin. *Russ. Chem. Rev.*, **82**, 1 (2013)
1605. T.Mirkovic, E.E.Ostroumov, J.M.Anna, R.van Grondelle, Govindjee, G.D.Scholes. *Chem. Rev.*, **117**, 249 (2017)
1606. I.Tochitsky, M.A.Kienzler, E.Isacoff, R.H.Kramer. *Chem. Rev.*, **118**, 10748 (2018)
1607. H.Bouas-Laurent, H.Dürr. *Pure Appl. Chem.*, **73**, 639 (2001)
1608. W.-C.Geng, H.Sun, D.-S.Guo. *J. Incl. Phenom. Macrocycl. Chem.*, **92**, 1 (2018)
1609. A.Bianchi, E.Delgado-Pinar, E.García-España, C.Giorgi, F.Pina. *Coord. Chem. Rev.*, **260**, 156 (2014)
1610. M.Baroncini, G.Ragazzon, S.Silvi, M.Venturi, A.Credi. *Pure Appl. Chem.*, **87**, 537 (2015)
1611. B.Dinda. *Essentials of Pericyclic and Photochemical Reactions. (Ser. Lecture Notes in Chemistry*. Vol. 93). (Switzerland: Springer International Publishing, 2017). P. 215
1612. S.Poplata, A.Tröster, Y.-Q.Zou, T.Bach. *Chem. Rev.*, **116**, 9748 (2016)
1613. Y.Sonoda. *Molecules*, **16**, 119 (2011)
1614. *Host Guest Complex Chemistry Macrocycles. Synthesis, Structures, Applications*. (Eds F.Vögtle, E.Weber). (Berlin, Heidelberg: Springer-Verlag, 1985)
1615. S.P.Gromov. *Russ. Chem. Bull., Int. Ed.*, **57**, 1325 (2008)
1616. A.Mishra, R.K.Behera, P.K.Behera, B.K.Mishra, G.B.Behera. *Chem. Rev.*, **100**, 1973 (2000)
1617. W.Sbliwa, G.Matusiak, B.Bachowska. *Croat. Chem. Acta*, **79**, 513 (2006)
1618. O.A.Gerasko, E.A.Kovalenko, V.P.Fedin. *Russ. Chem. Rev.*, **85**, 795 (2016)
1619. S.J.Barrow, S.Kasera, M.J.Rowland, J.del Barrio, O.A.Scherman. *Chem. Rev.*, **115**, 12320 (2015)
1620. D.Wang, W.Zhao, Q.Wei, C.Zhao, Y.Zheng. *ChemPhotoChem*, **2**, 403 (2018)
1621. B.Roy, A.Depaix, C.Périgaud, S.Peyrottes. *Chem. Rev.*, **116**, 7854 (2016)
1622. S.P.Gromov, M.V.Alfimov. *Russ. Chem. Bull., Int. Ed.*, **46**, 611 (1997)
1623. E.N.Ushakov, M.V.Alfimov, S.P.Gromov. *Russ. Chem. Rev.*, **77**, 39 (2008)
1624. M.V.Alfimov, O.A.Fedorova, S.P.Gromov. *J. Photochem. Photobiol. A*, **158**, 183 (2003)
1625. S.P.Gromov. *Rev. J. Chem.*, **1**, 1 (2011)
1626. E.N.Ushakov, S.P.Gromov. *Russ. Chem. Rev.*, **84**, 787 (2015)
1627. E.N.Ushakov, S.P.Gromov, A.V.Buevich, I.I.Baskin, O.A.Fedorova, A.I.Vedernikov, M.V.Alfimov, B.Eliasson, U.Edlund. *J. Chem. Soc., Perkin Trans. 2*, 601 (1999)
1628. M.V.Rusalov, B.M.Uzhinov, M.V.Alfimov, S.P.Gromov. *Russ. Chem. Rev.*, **79**, 1099 (2010)
1629. E.N.Ushakov, M.V.Alfimov, S.P.Gromov. *Macroheterocycles*, **3**, 189 (2010)
1630. S.P.Gromov, A.I.Vedernikov, N.A.Lobova, L.G.Kuz'mina, S.N.Dmitrieva, Y.A.Strelenko, J.A.K.Howard. *J. Org. Chem.*, **79**, 11416 (2014)
1631. S.P.Gromov, V.B.Nazarov, V.G.Avakyan, M.V.Fomina, A.I.Vedernikov, L.G.Kuz'mina, T.G.Vershinnikova, N.A.Lobova, V.Y.Rudyak, M.V.Alfimov, J.A.K.Howard. *J. Photochem. Photobiol. A*, **217**, 87 (2011)
1632. N.K.Petrov, D.A.Ivanov, Y.A.Shandarov, I.V.Kryukov, A.A.Ivanov, M.V.Alfimov, N.A.Lobova, S.P.Gromov. *Chem. Phys. Lett.*, **647**, 157 (2016)
1633. L.G.Kuz'mina, A.I.Vedernikov, N.A.Lobova, J.A.K.Howard, Y.A.Strelenko, V.P.Fedin, M.V.Alfimov, S.P.Gromov. *New J. Chem.*, **30**, 458 (2006)

1634. S.P.Gromov, A.I.Vedernikov, L.G.Kuz'mina, D.V.Kondratuk, S.K.Sazonov, Y.A.Strelenko, M.V.Alfimov, J.A.K.Howard. *Eur. J. Org. Chem.*, 2587 (2010)
1635. S.P.Gromov, A.I.Vedernikov, E.N.Ushakov, M.V.Alfimov. *Russ. Chem. Bull., Int. Ed.*, **57**, 793 (2008)
1636. L.G.Kuz'mina, A.I.Vedernikov, S.P.Gromov, M.V.Alfimov. *Crystallogr. Rep.*, **64**, 691 (2019)
1637. P.A.Angaridis, T.Lazarides, A.C.Coutsolelos. *Polyhedron*, **82**, 19 (2014)
1638. L.Cabau, C.V.Kumar, A.Moncho, J.N.Clifford, N.López, E.Palomares. *Energy Environ. Sci.*, **8**, 1368 (2015)
1639. T.Hasobe. *J. Phys. Chem. Lett.*, **4**, 1771 (2013)
1640. M.G.Walter, A.B.Rudine, C.C.Wamser. *J. Porphyrins Phthalocyanines*, **14**, 759 (2010)
1641. C.Ruthard, M.Maskos, U.Kolb, F.Gröhn. *J. Phys. Chem. B*, **115**, 5716 (2011)
1642. C.Ruthard, M.Maskos, H.Yildiz, F.Gröhn. *Macromol. Rapid Commun.*, **32**, 523 (2011)
1643. C.Ruthard, M.Schmidt, F.Gröhn. *Macromol. Rapid Commun.*, **32**, 706 (2011)
1644. F.Helmich, C.C.Lee, A.P.H.J.Schenning, E.W.Meijer. *J. Am. Chem. Soc.*, **132**, 16753 (2010)
1645. H.Sakae, H.Nagatani, K.Morita, H.Imura. *Langmuir*, **30**, 937 (2014)
1646. J.V.Hollingsworth, A.J.Richard, M.G.H.Vicente, P.S.Russo. *Biomacromolecules*, **13**, 60 (2011)
1647. C.Toncelli, J.P.Pino-Pinto, N.Sano, F.Picchioni, A.A.Broekhuis, H.Nishide, I.Moreno-Villoslada. *Dyes Pigm.*, **98**, 51 (2013)
1648. W.-S.Li, T.Aida. *Chem. Rev.*, **109**, 6047 (2009)
1649. Y.-H.Jeong, H.-J.Yoon, W.-D.Jang. *Polym J.* **44**, 512 (2012)
1650. F.Figueira, P.M.R.Pereira, S.Silva, J.A.S.Cavaleiro, J.P.C.Tome. *Curr. Org. Synth.*, **11**, 110 (2014)
1651. J.Tian, W.Zhang. *Prog. Polym. Sci.*, **95**, 65 (2019)
1652. G.Spataro, F.Malecaze, C.-O.Turrin, V.Soler, C.Duhayon, P.-P.Elena, J.-P.Majoral, A.-M.Caminade. *Eur. J. Med. Chem.*, **45**, 326 (2010)
1653. M.Ethirajan, Y.Chen, P.Joshi, R.K.Pandey. *Chem. Soc. Rev.*, **40**, 340 (2011)
1654. F.Setaro, R.Ruiz-González, S.Nonell, U.Hahn, T.Torres. *J. Inorg. Biochem.*, **136**, 170 (2014)
1655. M.Qian, W.Hou, D.Chen, X.Li, Q.Chen, C.Wu. *J. Photochem. Photobiol. A*, **383**, 111988 (2019)
1656. P.G.Mahajan, N.C.Dige, B.D.Vanjare, S.-H.Eo, S.-Y.Seo, S.J.Kim, S.-K.Hong, C.-S.Choi, K.H.Lee. *J. Photochem. Photobiol. A*, **377**, 26 (2019)
1657. E.G.Morales-Espinoza, I.V.Lijanova, O.G.Morales-Saavedra, V.Torres-Zuñiga, S.Hernandez-Ortega, M.Martínez-García. *Molecules*, **16**, 6950 (2011)
1658. T.Nyokong. In *Functional Phthalocyanine Molecular Materials*. (Ed. J.Jiang). Springer-Verlag, Berlin; Heidelberg, 2009. P. 45
1659. M.V.Mart'inez-D'iaz, G.de la Torre, T.Torres. *Chem. Commun.*, **46**, 7090 (2010)
1660. V.Garg, G.Kodis, P.A.Liddell, Y.Terazono, T.A.Moore, A.L.Moore, D.Gust. *J. Phys. Chem. B*, **117**, 11299 (2013)
1661. J.Fujimoto, S.Hayashi, H.Kainuma, K.Manseki, T.Udagawa, H.Miyaji. *Chem. – Asian J.*, **14**, 2567 (2019)
1662. A.F.R.Cerqueira, V.A.S.Almodôvar, M.G.P.M.S.Neves, A.C.Tomé. *Molecules*, **22**, 994 (2017)
1663. J.F.Maturano, J.G.D.Chavez, C.M.A.P.Carreón, M.G.Nava, I.Lijanova, T.Klimova, M.M.Garcìa. *Supramol. Chem.*, **19**, 485 (2007)
1664. B.Gao, Y.Liu, H.Yin, Y.Li, Q.Bai, L.Zhang. *New J. Chem.*, **36**, 28 (2012)
1665. S.Shinoda, M.Ohashi, H.Tsukube. *Chem. – Eur. J.*, **13**, 81 (2007)
1666. M.Kimura, Y.Nakano, N.Adachi, Y.Tatewaki, H.Shirai, N.Kobayashi. *Chem. – Eur. J.*, **15**, 2617 (2009)
1667. N.T.Nguyen, J.Hofkens, I.G.Scheblykin, M.Kruk, W.Dehaen. *Eur. J. Org. Chem.*, 1766 (2014)
1668. K.Albrecht, Y.Kasai, Y.Kuramoto, K.Yamamoto. *Chem. Commun.*, **49**, 865 (2013)
1669. R.E.H.Ramirez, I.V.Lijanova, N.V.Likhanova, O.O.Xometl. *J. Incl. Phenom. Macrocycl. Chem.*, **84**, 49 (2015)
1670. R.E.H.Ramirez, I.V.Lijanova, N.V.Likhanova, O.O.Xometl, A.H.Herrera, J.F.C.Alcalá, O.T.Chavero. *Arab. J. Chem.*, **13**, 27 (2020)
1671. U.Boas, P.M.H.Heegaard. *Chem. Soc. Rev.*, **33**, 43 (2004)
1672. H.Zhou, L.Baldini, J.Hong, A.J.Wilson, A.D.Hamilto. *J. Am. Chem. Soc.*, **128**, 2421 (2006)
1673. X.-H.Dai, W.-H.Yang, W.-L.Yan, J.-M.Hu, Y.-R.Dai, J.-M.Pan, Y.-S.Yan. *Colloids Surf., A*, **520**, 222 (2017)
1674. D.-D.Chang, W.-H.Yang, X.-H.Dai, J.-X.Wang, L.Chen, J.-M.Pan, Y.-S.Yan, Y.-R.Dai. *J. Polym. Res.*, **25**, 257 (2018)
1675. Z.-J.Wang, B.Chauvin, P.Maillard, F.Hammerer, D.Carez, A.Croisy, C.Sandré, S.Chollet-Martin, P.Prognon, J.-L.Paul, J.Blais, A.Kasselouri. *J. Photochem. Photobiol. B*, **115**, 16 (2012)
1676. S.Silva, P.M.R.Pereira, P.Silva, F.A.Almeida Paz, M.A.F.Faustino, J.A.S.Cavaleiro, J.P.C.Tomé. *Chem. Commun.*, **48**, 3608 (2012)
1677. S.Shinoda, H.Tsukube. *Chem. Sci.*, **2**, 2301 (2011)
1678. M.Fathalla, S.-C.Li, U.Diebold, A.Alb, J.Jayawickramarajah. *Chem. Commun.*, 4209 (2009)
1679. M.Fathalla, A.Neuberger, S.-C.Li, R.Schmehl, U.Diebold, J.Jayawickramarajah. *J. Am. Chem. Soc.*, **132**, 9966 (2010)
1680. R.P.Brias, T.Troxler, R.M.Hochstrasser, S.A.Vinogradov. *J. Am. Chem. Soc.*, **127**, 11851 (2005)
1681. Y.Liu, J.Jin, H.Deng, K.Li, Y.Zheng, C.Yu, Y.Zhou. *Angew. Chem., Int. Ed.*, **55**, 7952 (2016)
1682. A.Concellón, M.Marcos, P.Romero, J.L.Serrano, R.Termine, A.Golemme. *Angew. Chem., Int. Ed.*, **56**, 1259 (2016)
1683. M.Mao, Q.-H.Song. *Dyes Pigm.*, **92**, 975 (2012)
1684. K.Maurer, K.Hager, A.Hirsch. *Eur. J. Org. Chem.*, 3338 (2006)
1685. A.Concellón, M.Bucoş, J.L.Serrano, P.Romero, M.Marcos. *RSC Adv.*, **6**, 65179 (2016)
1686. M.Gómez-Tardajos, J.P.Pino-Pinto, C.Diaz-Soto, M.E.Flores, A.Gallardo, C.Elvira, H.Reinecke, H.Nishide, I.Moreno-Villoslada. *Dyes Pigm.*, **99**, 759 (2013)
1687. M.Kabiri, I.Bushnak, M.T.McDermot, L.D.Unsworth. *Biomacromolecules*, **14**, 3943 (2013)
1688. M.E.Flores, N.Sano, R.Araya-Hermosilla, T.Shibue, A.F.Olea, H.Nishide, I.Moreno-Villoslada. *Dyes Pigm.*, **112**, 262 (2015)
1689. H.He, A.Gurung, L.Si. *Chem. Commun.*, **48**, 5910 (2012)
1690. A.Hagfeldt, G.Boschloo, L.Sun, L.Kloo, H.Pettersson. *Chem. Rev.*, **110**, 6595 (2010)

1691. M.A.Green, Y.Hishikawa, W.Warta, E.D.Dunlop, D.H.Levi, J.Hohl-Ebinger, A.W.H.Ho-Baillie. *Prog. Photovolt. Res. Appl.*, **25**, 668 (2017)
1692. G.Richhariya, A.Kumar, P.Tekasakul, B.Gupta. *Renew. Sustain. Energy Rev.*, **69**, 705 (2017)
1693. N.T.Nguyen, G.Mamardashvili, M.Gruzdev, N.Mamardashvili, W.Dehaen. *Supramol. Chem.*, **25**, 180 (2013)
1694. G.M.Mamardashvili, O.V.Maltceva, N.Z.Mamardashvili, N.T.Nguyen, W.Dehaen. *RSC Adv.*, **5**, 44557 (2015)
1695. G.Mamardashvili, N.Mamardashvili, W.Dehaen. *WASET*, **3**, 450 (2017)
1696. K.Albrecht, Y.Kasai, Y.Kuramoto, K.Yamamoto. *Chem. Commun.*, **49**, 6861 (2013)
1697. K.Tashiro, T.Aida. *Chem. Soc. Rev.*, **36**, 189 (2007)
1698. H.Ozawa, M.Kawao, H.Tanaka, T.Ogawa. *Langmuir*, **23**, 6365 (2007)
1699. A.Uetomo, M.Kozaki, S.Suzuki, K.Yamanaka, O.Ito, K.Okada. *J. Am. Chem. Soc.*, **133**, 13276 (2011)
1700. A.Krieger, J.P.F.Werner, G.Mariani, F.Gröhn. *Macromolecules*, **50**, 3464 (2017)
1701. Y.-H.Jeong, M.Son, H.Yoon, P.Kim, D.-H.Lee, D.Kim, W.-D.Jang. *Angew. Chem., Int. Ed.*, **53**, 6925 (2014)
1702. J.Zhou, G.Yu, F.Huang. *Chem. Soc. Rev.*, **46**, 7021 (2017)
1703. D.Ma, Z.-H.Liu, Q.-Q.Zheng, X.-Y.Zhou, Y.Zhang, Y.-F.Shi, J.-T.Lin, W.Xue. *Macromol. Rapid Commun.*, **34**, 548 (2013)
1704. X.-H.Dai, Z.-M.Wang, L.-Y.Gao, J.-M.Pan, X.-H.Wang, Y.-S.Yan, D.-M.Liu. *New J. Chem.*, **38**, 3569 (2014)
1705. F.Portilho, C.Cavalcanti, A.Miranda-Vilela, L.Estevanato, J.Longo, M.A.Santos, A.Bocca, O.Martins, A.R.Simioni, P.Morais, R.Azevedo, A.Tedesco, Z.Lacava. *J. Nanobiotechnol.*, **11**, 41 (2013)
1706. L.Zhao, R.Qu, A.Li, R.Ma, L.Shi. *Chem. Commun.*, **52**, 13543 (2016)
1707. N.Nishiyama, Y.Nakagishi, Y.Morimoto, P.-S.Lai, K.Miyazaki, K.Urano, S.Horie, M.Kumagai, S.Fukushima, Y.Cheng, W.-D.Jang, M.Kikuchi, K.Kataoka. *J. Control. Release*, **133**, 245 (2009)
1708. S.Herlambang, M.Kumagai, T.Nomoto, S.Horie, S.Fukushima, M.Oba, K.Miyazaki, Y.Morimoto, N.Nishiyama, K.Kataoka. Springer-Verlag, *J. Control. Release*, **155**, 449 (2011)
1709. T.Uchiyama, K.Ishii, T.Nonomura, N.Kobayashi, S.Isoda. *Chem. – Eur. J.*, **9**, 5757 (2003)
1710. A.Y.Lebedev, T.Troxler, S.A.Vinogradov J.Porphyrins. *Phthalocyanines*, **12**, 1261 (2008)
1711. O.Finikova, A.Galkin, V.Rozhkov, M.Cordero, C.Hägerhäll, S.Vinogradov. *J. Am. Chem. Soc.*, **125**, 4882 (2003)
1712. C.-Y.Hsu, M.-P.Nieh, P.-S.Lai. *Chem. Commun.*, **48**, 9343 (2012)
1713. M.-J.Shieh, C.-Y.Hsu, L.-Y.Huang, H.-Y.Chen, F.-H.Huang, P.-S.Lai. *J. Control. Release*, **152**, 418 (2011)
1714. K.J.Son, H.-J.Yoon, J.-H.Kim, W.-D.Jang, Y.Lee, W.-G.Koh. *Angew. Chem., Int. Ed.*, **50**, 11968 (2011)